PORT & COASTAL SOLUTIONS

File Name:
EPBC Referral Report No. 5 - Boskalis Cambridge Gulf - FULL MODELLING

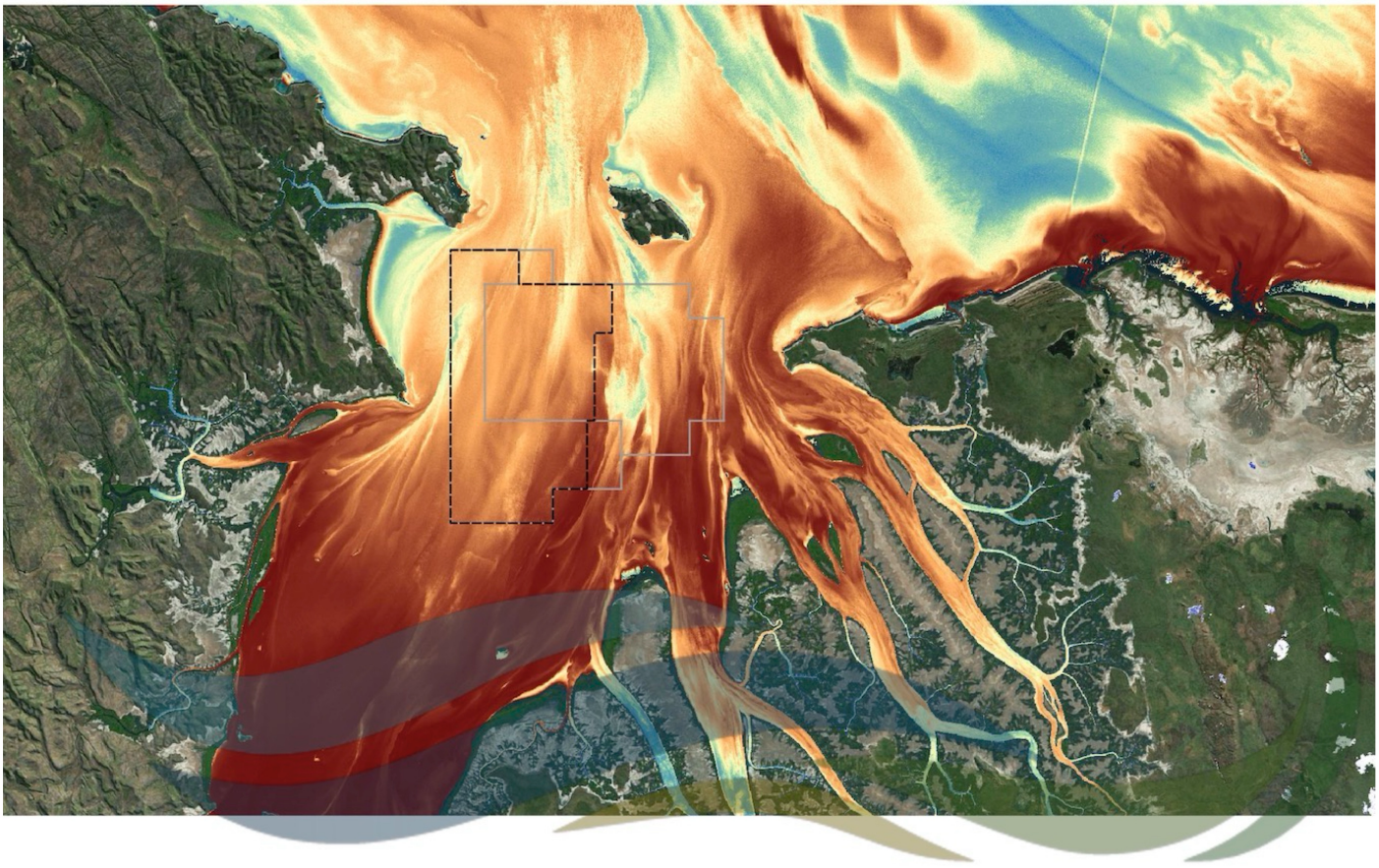
Cambridge Gulf Marine Sand Proposal

Metocean & Sediment Dynamics

Data Analysis and Numerical Modelling Report

P076_R03v1.2

PCS Output 4 – Final



Boskalis

Technical Report

January 2025

PORT & COASTAL
SOLUTIONS

Cambridge Gulf Marine Sand Proposal

Metocean & Sediment Dynamics

Data Analysis and Numerical Modelling Report

Report No. P076_R03v1.2

PCS Output 4 – Final

January 2025

For Boskalis Australia Pty Ltd

Version	Details	Authorised By	Date
1.0	Draft	Andy Symonds	26/11/2024
1.1	Second Draft	Andy Symonds	16/12/2024
1.2	Final	Andy Symonds	20/01/2025

Document Authorisation		Signature	Date
Project Manager	Andy Symonds		20/01/2025
Author(s)	Andy Symonds, Claire Conning		20/01/2025
Reviewer	Rachel White		20/01/2025

Disclaimer

No part of these specifications/printed matter may be reproduced and/or published by print, photocopy, microfilm or by any other means by any party other than the persons by whom it was commissioned, without the prior written permission of Port and Coastal Solutions Pty Ltd.; nor may they be used, without such permission, for any purposes other than that for which they were produced. Port and Coastal Solutions Pty Ltd. accepts no responsibility or liability for these specifications/printed matter to any party other than the persons by whom it was commissioned and as concluded under that Appointment.

PORT AND COASTAL SOLUTIONS PTY LTD
ABN 66 630 775 423

A | 46 Elanora Drive, Burleigh Heads, QLD, 4220
E | info@portandcoastalsolutions.com.au
W | www.portandcoastalsolutions.com.au
M | +61 (0)458 735 747

PORT & COASTAL SOLUTIONS

CONTENTS

EXECUTIVE SUMMARY xv

1. INTRODUCTION, OBJECTIVES & GUIDELINES 1
   1.1. Overview of the Marine Sand Proposal 3
   1.2. Overview of Cambridge Gulf & System Understanding 6
   1.3. Report Structure 9

2. DATA ANALYSIS 13
   2.1. Hydrodynamics 18
   2.1.1. Water Levels 18
   2.1.2. Currents 23
   2.2. Waves 46
   2.3. Water Quality 67
   2.3.1. Turbidity & Suspended Solid Concentration 67
   2.3.2. Benthic Light 78

3. NUMERICAL MODELLING APPROACH 83
   3.1. Software 83
   3.2. Model Mesh 83
   3.3. Bathymetry 84
   3.4. Hydrodynamic Model 89
   3.4.1. Model Configuration 89
   3.4.2. Calibration and Validation 89
   3.4.3. Scheme Simulations 106
   3.5. Spectral Wave Model 109
   3.5.1. Model Configuration 109
   3.5.2. Calibration and Validation 109
   3.5.3. Scheme Simulations 114
   3.6. Sediment Transport Model 115
   3.6.1. Model Configuration 115
   3.6.2. Calibration and Validation 115
   3.6.3. Scheme Simulations 123
   3.7. Sediment Plume Model 123
   3.7.1. Model Configuration 123
   3.7.2. Sand Sourcing Conceptualisation 124
   3.7.3. Scheme Simulations 127
   3.8. Beach Processes Model 127
   3.8.1. Model Configuration 127
   3.8.2. Scheme Simulations 128

4. RESULTS: HYDRODYNAMICS AND WAVES 130
   4.1. Existing Conditions 130
   4.1.1. Hydrodynamics 130
   4.1.2. Waves 138
   4.2. Scenario Changes 147
   4.2.1. Hydrodynamics 147
   4.2.2. Waves 180
   4.3. Summary Findings & Implications for the Proposal 200

5. RESULTS: SEDIMENT TRANSPORT AND BEACH PROCESSES 202
5.1. Existing Conditions 202
5.1.1. Suspended Sediment 202
5.1.2. Bedload Transport 212
5.1.3. Sedimentation 222
5.1.4. Beach Processes 225
5.2. Scenario Impacts 235
5.2.1. Suspended Sediment 235
5.2.2. Bedload Transport 254
5.2.3. Sedimentation 269
5.2.4. Beach Processes 273
5.3. Summary Findings & Implications for the Proposal 273
6. RESULTS: SEDIMENT PLUME MODELLING 276
6.1. SPV Sediment Plumes 276
6.1.1. Modelled SSC from SPV Plumes 276
6.1.2. Modelled Sedimentation from SPV Plumes 322
6.2. Summary Findings & Implications for the Proposal 329
7. ASSESSMENT AGAINST STUDY OBJECTIVES & EPA GUIDELINES 330
8. REFERENCES 354

APPENDICES

Appendix A – Model Calibration and Validation Plots
Appendix B – Hydrodynamic and Wave Impact Plots
Appendix C – Sediment Transport Impact Plots
Appendix D – Sediment Plume Modelling Results

ANNEXES

Annex A – Independent Expert Review
Annex B – Updated Factual Data Report

FIGURES

Figure 1. Location of the proposal in Cambridge Gulf near Wyndham in the northeast of Western Australia.. 5
Figure 2. The most significant coastal ecosystems and values in CG that are formed and influenced by hydrodynamics and coastal processes 10
Figure 3. Location of rivers and dams that influence CG along with West Arm and East Arm..... 11
Figure 4. Updated conceptual sediment transport and coastal processes system understanding for CG. .. 12
Figure 5. Sites where BKA have deployed self-logging instruments and measured hydrodynamics and waves and water quality parameters long with the POA..... 16
Figure 6. Annotated photograph of the instruments attached to a frame at the AWAC sites. 17
Figure 7. Annotated photograph of the instruments attached to a frame at the Pos sites..... 17
Figure 8. Water level residual in the POA along with hindcast modelled wind, hindcast modelled offshore H_s and measured river discharge from March to May 2024..... 20
Figure 9. Water level residual in the POA along with hindcast modelled wind, hindcast modelled offshore H_s and measured river discharge in June and July 2024. 21
Figure 10. Water level residual at the False Mouths of the Ord along with hindcast modelled wind, hindcast modelled offshore H_s and measured river discharge from October 2023 to March 2024. 22
Figure 11. Measured water level, current speed and direction over a 14-day spring-neap cycle at AWAC-09 during the wet season..... 24
Figure 12. Measured water level, current speed and direction over a 14-day spring-neap cycle at AWAC-01 during the wet season..... 25
Figure 13. Measured water level, current speed and direction over a 14-day spring-neap cycle at AWAC-11 during the wet season..... 26
Figure 14. Measured water level, current speed and direction over a 14-day spring-neap cycle at AWAC-08 during the wet season..... 27
Figure 15. Measured water level, current speed and direction over a 14-day spring-neap cycle at AWAC-10 during the dry season. 28
Figure 16. Measured water level, current speed and direction over a 14-day spring-neap cycle at AWAC-01 during the dry season. 29
Figure 17. Measured water level, current speed and direction over a 14-day spring-neap cycle at AWAC-11 during the dry season. 30
Figure 18. Measured vertical current profile at peak flood and peak ebb on a large spring tide in the wet season at a site offshore of CG and within the POA..... 31
Figure 19. Measured vertical current profile at peak flood and peak ebb on a large spring tide in the wet season at a site upstream of the POA and at the entrance to West Arm..... 31
Figure 20. Measured vertical current profile at peak flood and peak ebb on a large spring tide in the dry season at a site offshore of CG and within the POA 32
Figure 21. Measured vertical current profile at peak flood and peak ebb on a large spring tide in the dry season at a site upstream of the POA. 32
Figure 22. Current residuals at AWAC-01 for depth-averaged currents along with hindcast modelled wind over a 10-day period..... 35
Figure 23. Current residuals at AWAC-09 for surface (top) and depth-averaged (second) currents, hindcast modelled wind and measured river discharge during the wet season. 36
Figure 24. Current residuals at AWAC-01 for surface (top) and depth-averaged (second) currents, hindcast modelled wind and measured river discharge during the wet season. 37
Figure 25. Current residuals at AWAC-11 for surface (top) and depth-averaged (second) currents, hindcast modelled wind and measured river discharge during the wet season. 38
Figure 26. Current residuals at AWAC-01 for surface (top) and depth-averaged (second) currents, hindcast modelled wind and measured river discharge during the dry season. 39
Figure 27. Periods used to assess net transport during the wet season relative to predicted water level at Cape Domett (top), hindcast modelled wind conditions within CG (middle) and measured river discharge (bottom)..... 40
Figure 28. Periods used to assess net transport during the dry season relative to predicted water level at Cape Domett (top) and hindcast modelled wind conditions within CG (bottom). 41
Figure 29. Progressive vector diagrams showing the net transport based on measured currents in the wet season at AWAC-09 over a 14-day spring-neap tidal cycle (top) and 3-days of spring/neap tides with varying wind conditions (bottom). 42

Figure 30. Progressive vector diagrams showing the net transport based on measured currents in the wet season at AWAC-01 over a 14-day spring-neap tidal cycle (top) and 3-days of spring/neap tides with varying wind conditions (bottom). 43
Figure 31. Progressive vector diagrams showing the net transport based on measured currents in the wet season at AWAC-11 over a 14-day spring-neap tidal cycle (top) and 3-days of spring/neap tides with varying wind conditions (bottom). 44
Figure 32. Progressive vector diagrams showing the net transport based on measured currents in the dry season at AWAC-10 over a 14-day spring-neap tidal cycle. 45
Figure 33. Progressive vector diagrams showing the net transport based on measured currents in the dry season at AWAC-01 over a 14-day spring-neap tidal cycle. 45
Figure 34. Progressive vector diagrams showing the net transport based on measured currents in the dry season at AWAC-11 over a 14-day spring-neap tidal cycle. 46
Figure 35. Timeseries of predicted water level, hindcast wind within CG, hindcast offshore wave height and measured wave height offshore of CG (AWAC-09) and within CG (AWAC-01). 50
Figure 36. Comparison between measured H_s within CG (AWAC-01) and measured water level, over 56 days of the wet season. 51
Figure 37. Comparison between measured H_s within CG (AWAC-01) and measured water level over 28 days of the wet season. 51
Figure 38. Comparison between measured H_s within CG (AWAC-01) and measured water level over 28 days at the end of the wet season. 51
Figure 39. Comparison between measured H_s within CG (AWAC-01) and hindcast modelled H_s at the entrance to JBG during the wet season. 52
Figure 40. Comparison between measured wave height and hindcast modelled wind speed and measured wave direction and modelled wind direction within CG during the wet season. 52
Figure 41. Comparison between measured H_s offshore of CG (AWAC-09) and measured water level over 31 days of the dry season. 53
Figure 42. Comparison between measured wave height and hindcast modelled wind speed and measured wave direction and modelled wind direction within CG during the dry season. 53
Figure 43. Comparison between measured H_s offshore of CG (AWAC-09) and hindcast modelled H_s at the entrance to JBG (~150 km north of CG) (CSIRO, 2024) during the dry season. 54
Figure 44. Timeseries plots of measured wave conditions at a site offshore of CG (AWAC-09) during the wet season. 55
Figure 45. Timeseries plots of measured wave conditions at a site in the East Entrance of CG (AWAC-06) during the wet season. 56
Figure 46. Timeseries plots of measured wave conditions in the POA (AWAC-01) during the wet season. 57
Figure 47. Timeseries plots of measured wave conditions upstream (south) of the POA (AWAC-11) during the wet season. 58
Figure 48. Timeseries plots of measured wave conditions offshore of CG during the dry season. 59
Figure 49. Timeseries plots of measured wave conditions in the POA during the dry season. 60
Figure 50. Timeseries plots of measured wave conditions upstream (south) of the POA (AWAC-11) during the dry season. 61
Figure 51. Full directional energy spectra at multiple sites in the CG region during a large wave event on 24/03/2024. 62
Figure 52. Full directional energy spectra at multiple sites in the CG region during a wave event at the end of April 20204 (30/04/2024). 63
Figure 53. Full directional energy spectra at multiple sites in the CG region during a dry season wave event (04/07/2024). 64
Figure 54. Energy density spectra at AWAC-09 during a small wave height, low wave period wave event in the wet season (30/03/2024). 65
Figure 55. Energy density spectra at AWAC-06 during a small wave height, low wave period wave event in the wet season (30/03/2024). 65
Figure 56. Energy density spectra at AWAC-01 during a small wave height, low wave period wave event in the wet season (30/03/2024). 66
Figure 57. Energy density spectra at AWAC-11 during a small wave height, low wave period wave event in the wet season (30/03/2024). 66
Figure 58. Measured benthic turbidity at sites AWAC-02 and AWAC-06 during the dry/transitional seasons in 2023. 71
Figure 59. Measured benthic turbidity at AWAC-01, AWAC-05, AWAC-06 and AWAC-07 between March and August 2024 (wet and dry seasons). 72

Figure 60. Measured benthic turbidity at AWAC-08, AWAC-09/Pos-12, AWAC-10 and AWAC-11 between March and August 2024 (wet and dry seasons). 73
Figure 61. Measured benthic turbidity at Pos-13, Pos-14 and Pos-15 between March and August 2024 (wet and dry seasons). 74
Figure 62. An interpretive sign by the Balanggarra Indigenous Rangers at the Port of Wyndham public jetty, with reference to the area as 'Brown Water Country' and the 'muddy waters' of CG 75
Figure 63. Photographs taken during BKA's environmental survey work showing variability in SSC and turbidity in CG, with the bottom right image showing a tidal front with mixing of higher SSC upstream water with lower SSC offshore water in the outer area of CG 75
Figure 64. Predicted water level, measured river discharge, measured wave conditions and measured benthic turbidity offshore (AWAC-09), with the POA (AWAC-01) and south of the POA (AWAC-11) during the wet season. 76
Figure 65. Predicted water level, measured river discharge, measured wave conditions (AWAC-09) and measured benthic turbidity offshore (AWAC-09), at the False Mouths of the Ord (AWAC-07) and south of the POA (AWAC-11) during the dry season. 77
Figure 66. Predicted water level, measured turbidity and measured benthic irradiance at Pos-14 from March to June 2024. 80
Figure 67. Predicted water level, measured turbidity and measured benthic irradiance at AWAC-05 from June to August 2024. 81
Figure 68. Measured turbidity and measured benthic irradiance at Pos-14 over 7 days of neap tides in March 2024 82
Figure 69. Measured turbidity and measured benthic irradiance at AWAC-05 over 10 days around neap tides in July 2024. 82
Figure 70. The full extent of the numerical model mesh along with Blocks 4 and 4A (grey polygons) and the proposed operational area (black dashed polygon). 85
Figure 71. Close up of the numerical model mesh in CG along with Blocks 4 and 4A (grey polygons) and the proposed operational area (black dashed polygon). 86
Figure 72. Model bathymetry for the full model domain with Blocks 4 and 4A also shown (grey polygons) and the proposed operational area (black dashed polygon). 87
Figure 73. Model bathymetry for CG with Blocks 4 and 4A also shown (grey polygons) and the proposed operational area (black dashed polygon). 88
Figure 74. Modelled and measured water level at AWAC-01 over the model calibration period and selected calibration spring / neap cycle period. 93
Figure 75. Modelled and measured water level at AWAC-08 over the model calibration period and selected calibration spring / neap cycle period. 93
Figure 76. Modelled and measured water level at AWAC-09 over the model calibration period and selected calibration spring / neap cycle period. 94
Figure 77. Modelled and measured surface, mid and bed layer currents speed and direction at AWAC-01 over the selected calibration spring / neap cycle period. 95
Figure 78. Modelled and measured surface, mid and bed layer currents speed and direction at AWAC-08 over the selected calibration spring / neap cycle period. 96
Figure 79. Modelled and measured surface, mid and bed layer currents speed and direction at AWAC-09 over the selected calibration spring / neap cycle period. 97
Figure 80. Modelled and measured depth-averaged residual current speed at AWAC-01 over 2 months of the wet season. 98
Figure 81. Modelled and measured depth-averaged residual current speed at AWAC-09 over 2 months of the wet season. 98
Figure 82. Modelled and measured depth-averaged residual current speed at AWAC-11 over 2 months of the wet season. 99
Figure 83. Modelled and measured water level at AWAC-01 over the model validation period and selected validation spring / neap cycle period. 103
Figure 84. Modelled and measured water level at AWAC-10 over the model validation period and selected validation spring / neap cycle period. 103
Figure 85. Modelled and measured surface, mid and bed layer currents speed and direction at AWAC-01 over the selected validation spring / neap cycle period. 104
Figure 86. Modelled and measured surface, mid and bed layer currents speed and direction at AWAC-10 over the selected validation spring / neap cycle period. 105
Figure 87. The 70 km^2 area (pink dashed region) within the POA where suitable sand is present for the sand sourcing. 108

Figure 88. Modelled and measured significant wave height, peak wave period and mean wave direction at AWAC-01 over the model calibration period. 110
Figure 89. Modelled and measured significant wave height, peak wave period and mean wave direction at AWAC-08 over the model calibration period. 111
Figure 90. Modelled and measured significant wave height, peak wave period and mean wave direction at AWAC-09 over the model calibration period. 112
Figure 91. Modelled and measured significant wave height, peak wave period and mean wave direction at AWAC-01 over the model validation period. 113
Figure 92. Modelled and measured significant wave height, peak wave period and mean wave direction at AWAC-10 over the model validation period. 114
Figure 93. Measured and modelled SSC for clay/silt and sand particles at AWAC-01. 117
Figure 94. Measured and modelled SSC for clay/silt and sand particles at AWAC-05. 118
Figure 95. Measured and modelled SSC for clay/silt and sand particles at AWAC-11. 118
Figure 96. Modelled bedload transport rate at the three sites over the 27-day period between the repeat bathymetric surveys. 120
Figure 97. Modelled and measured SSC at AWAC-01 over the model calibration period. 121
Figure 98. Modelled and measured SSC at AWAC-09 over the model calibration period. 121
Figure 99. Modelled and measured SSC at AWAC-11 over the model calibration period. 122
Figure 100. Modelled and measured SSC at Pos-15 over the model calibration period. 122
Figure 101. Modelled and measured SSC at AWAC-01 over the model validation period. 122
Figure 102. Modelled and measured SSC at AWAC-09 over the model validation period. 122
Figure 103. Modelled and measured SSC at AWAC-11 over the model validation period. 123
Figure 104. Modelled and measured SSC at Pos-15 over the model validation period. 123
Figure 105. Two sand sourcing track scenarios adopted in the sediment plume modelling. 126
Figure 106. Locations of the beach cross-shore profiles adopted for the longshore and cross-shore sediment transport and beach profile modelling. 129
Figure 107. Modelled depth-averaged current speed in CG at peak flood (left) and high water (right) during a spring tide in the wet season. 132
Figure 108. Modelled depth-averaged current speed in CG at peak ebb (left) and low water (right) during a spring tide in the wet season. 133
Figure 109. Modelled depth-averaged residual current speed in CG during a spring tide (left) and a neap tide (right) in the wet season. 134
Figure 110. Modelled depth-averaged residual current speed in CG over a 14-day spring-neap tidal cycle with a high river discharge event in the wet season. 135
Figure 111. Modelled water level at AWAC-01 (top) and modelled flux of water through the West and East entrances to CG (bottom) over 15 days. 136
Figure 112. Modelled water level at AWAC-01 (top) and current speed (middle) and direction (bottom) at AWACs 01, 09 and 11 over 15 days. 137
Figure 113. Modelled wave conditions at AWACs 01, 09 and 11 over the two-month (61 days) wet season period. 139
Figure 114. Modelled wave conditions at AWACs 01, 09 and 11 over the two-month (61 days) dry season period. 140
Figure 115. Modelled wave conditions at AWACs 01, 09 and 11 over the two-month (61 days) transitional season period. 141
Figure 116. Peak H_s over the two-month (61 days) wet season simulation (21/02/2024). 142
Figure 117. Peak H_s over the two-month (61 days) transitional season simulation (01/11/2023). 143
Figure 118. Peak H_s over the two-month (61 days) dry season simulation (18/07/2024). 144
Figure 119. Modelled wave conditions at AWACs 01, 09 and 11 during TC Marcus. 145
Figure 120. Peak H_s during TC Marcus (18/03/2018). 146
Figure 121. Modelled change (compared to existing case) in water level at peak flood (left) and high water (right) after 5 years (23 million m^3) of sand sourcing during a spring tide in the wet season. 149
Figure 122. Modelled change (compared to existing case) in water level at peak ebb (left) and low water (right) after 5 years (23 million m^3) of sand sourcing during a spring tide in the wet season. 150
Figure 123. Modelled change (compared to existing case) in water level at peak flood (left) and high water (right) after 15 years (70 million m^3) of sand sourcing during a spring tide in the wet season. 151
Figure 124. Modelled change (compared to existing case) in water level at peak ebb (left) and low water (right) after 15 years (70 million m^3) of sand sourcing during a spring tide in the wet season. 152

Figure 125. Modelled change (compared to existing case) in water level at peak flood (left) and high water (right) in 100 years after 15 years of sand sourcing during a spring tide in the wet season. 153
Figure 126. Modelled change (compared to existing case) in water level at peak ebb (left) and low water (right) in 100 years after 15 years of sand sourcing during a spring tide in the wet season. 154
Figure 127. Modelled difference (compared to existing case) in water level at peak flood (left) and high water (right) for the Pre-European Settlement scenario during a spring tide in the wet season during a high discharge event. 155
Figure 128. Modelled difference (compared to existing case) in water level at peak ebb (left) and low water (right) for the Pre-European Settlement scenario during a spring tide in the wet season during a high discharge event. 156
Figure 129. Modelled difference (compared to existing case) in water level at peak flood (left) and high water (right) for the Pre-European Settlement scenario during a spring tide in the dry season. 157
Figure 130. Modelled difference (compared to existing case) in water level at peak ebb (left) and low water (right) for the Pre-European Settlement scenario during a spring tide in the dry season. 158
Figure 131. Timeseries showing the modelled change (compared to Existing case) in water level during the wet season from neap to spring tides due to 15 years (70 million m^3) of sand sourcing (Scheme). 159
Figure 132. Timeseries showing the modelled difference (compared to existing case) in water level during the wet season from neap to spring tides for the Pre-European settlement scenario (Scheme). 160
Figure 133. Modelled change in current speed at peak flood (left) and high water (right) after 5 years (23 million m^3) of sand sourcing during a spring tide in the wet season. 165
Figure 134. Modelled change in current speed at peak ebb (left) and low water (right) after 5 years (23 million m^3) of sand sourcing during a spring tide in the wet season. 166
Figure 135. Modelled change in current speed at peak flood (left) and high water (right) after 15 years (70 million m^3) of sand sourcing during a spring tide in the wet season. 167
Figure 136. Modelled change in current speed at peak ebb (left) and low water (right) after 15 years (70 million m^3) of sand sourcing during a spring tide in the wet season. 168
Figure 137. Modelled change in current speed at peak flood (left) and high water (right) in 100 years after 15 years of sand sourcing during a spring tide in the wet season. 169
Figure 138. Modelled change in current speed at peak ebb (left) and low water (right) in 100 years after 15 years of sand sourcing during a spring tide in the wet season. 170
Figure 139. Modelled difference (compared to existing case) in current speed at peak flood (left) and high water (right) for the Pre-European Settlement scenario during a spring tide in the wet season during a high discharge event. 171
Figure 140. Modelled difference (compared to existing case) in current speed at peak ebb (left) and low water (right) for the Pre-European Settlement scenario during a spring tide in the wet season during a high discharge event. 172
Figure 141. Modelled difference (compared to existing case) in current speed at peak flood (left) and high water (right) for the Pre-European Settlement scenario during a spring tide in the dry season. 173
Figure 142. Modelled difference (compared to existing case) in current speed at peak ebb (left) and low water (right) for the Pre-European Settlement scenario during a spring tide in the dry season. 174
Figure 143. Timeseries showing the modelled change in current speed and direction at AWAC-08 during the wet season from neap to spring tides due to 15 years (70 million m^3) of sand sourcing. 175
Figure 144. Timeseries showing the modelled change in current speed and direction at AWAC-11 during the wet season from neap to spring tides due to 15 years (70 million m^3) of sand sourcing. 175
Figure 145. Timeseries showing the modelled change in current speed and direction at AWAC-01 during the wet season from neap to spring tides due to 15 years (70 million m^3) of sand sourcing. 176
Figure 146. Timeseries showing the modelled change in current speed and direction at AWAC-09 during the wet season from neap to spring tides due to 15 years (70 million m^3) of sand sourcing. 176
Figure 147. Timeseries showing the modelled difference in current at AWAC-08 during the wet season from neap to spring tides between the Pre-European scenario and the existing case. 177
Figure 148. Timeseries showing the modelled difference in current at AWAC-11 during the wet season from neap to spring tides for the between the Pre-European scenario and the existing case. 177
Figure 149. Timeseries showing the modelled difference in current at AWAC-01 during the wet season from neap to spring tides between the Pre-European scenario and the existing case. 178
Figure **150**. Timeseries showing the modelled difference in current at AWAC-09 during the wet season from neap to spring tides between the Pre-European scenario and the existing case. 178
Figure 151. Modelled change in H_s during the largest wave event in the wet season period due to 5 years (23 million m^3) of sand sourcing (left) and 15 years (70 million m^3) of sand sourcing (right). 182

Figure 152. Modelled change in T_p during the largest wave event in the wet season period due to 5 years (23 million m^3) of sand sourcing and 15 years (70 million m^3) of sand sourcing. 183
Figure 153. Modelled change in wave direction during the largest wave event in the wet season period due to 5 years (23 million m^3) of sand sourcing and 15 years (70 million m^3) of sand sourcing 184
Figure 154. Modelled change in H_s during the peak of TC Marcus due to 5 years (23 million m^3) of sand sourcing and 15 years (70 million m^3) of sand sourcing 185
Figure 155. Modelled change in T_p during the peak of TC Marcus in the wet season period due to 5 years (23 million m^3) of sand sourcing and 15 years (70 million m^3) of sand sourcing 186
Figure 156. Modelled change in wave direction during the peak of TC Marcus in the wet season period due to 5 years (23 million m3) of sand sourcing and 15 years (70 million m^3) of sand sourcing..... 187
Figure 157. Timeseries showing the modelled change in H_s over the two-month wet season simulation due to 15 years of sand sourcing (Scheme) at sites AWAC-01 to AWAC-03. 188
Figure 158. Timeseries showing the modelled change in H_s over the two-month wet season simulation due to 15 years of sand sourcing (Scheme) at sites AWAC-04, AWAC-07 to AWAC-11. 189
Figure 159. Timeseries showing the modelled change in H_s over the two-month dry season simulation due to 15 years of sand sourcing (Scheme) at sites AWAC-01 to AWAC-03. 190
Figure 160. Timeseries showing the modelled change in H_s over the two-month dry season simulation due to 15 years of sand sourcing (Scheme) at sites AWAC-04, AWAC-07 to AWAC-11. 191
Figure 161. Timeseries showing the modelled change in H_s over the two-month transitional season simulation due to 15 years of sand sourcing (Scheme) at sites AWAC-01 to AWAC-03. 192
Figure 162. Timeseries showing the modelled change in H_s over the two-month transitional season simulation due to 15 years of sand sourcing (Scheme) at sites AWAC-04, AWAC-07 to AWAC-11. 193
Figure 163. Timeseries showing the modelled change in H_s over the TC Marcus simulation due to 15 years (70 million m^3) of sand sourcing (Scheme) at sites AWAC-01 to AWAC-03. 194
Figure 164. Timeseries showing the modelled change in H_s over the TC Marcus simulation due to 15 years (70 million m^3) of sand sourcing (Scheme) at sites AWAC-04, AWAC-07 to AWAC-11. 195
Figure 165. Modelled existing case SSC percentiles over the two-month wet season period. 204
Figure 166. Modelled existing case SSC percentiles over the two-month dry season period. 205
Figure 167. Modelled existing case SSC percentiles over the two-month transitional season period. 206
Figure 168. Modelled existing case SSC percentiles over TC Marcus. 207
Figure 169. Modelled SSC at AWACs 01, 09 and 11 over the two-month wet season period. 208
Figure 170. Modelled SSC at AWACs 01, 09 and 11 over the two-month dry season period. 208
Figure 171. Modelled SSC at AWACs 01, 09 and 11 over the two-month transitional season period. 208
Figure 172. Modelled SSC at AWACs 01, 09 and 11 over TC Marcus. 209
Figure 173. Modelled existing case bedload transport at peak flood and peak ebb during a spring tide in the wet season. 214
Figure 174. Modelled existing case bedload transport at peak flood and peak ebb during a spring tide in the dry season. 215
Figure 175. Modelled existing case bedload transport at peak flood and peak ebb during TC Marcus. 216
Figure 176. Modelled existing case bedload transport at peak flood and peak ebb during a high river discharge event in the wet season. 217
Figure 177. Annotated plot showing the primary sediment transport pathway for sand (large black arrows) on top of the bedload transport rate at peak ebb during a spring tide in the wet season. 218
Figure 178. Modelled water level at AWAC-01 (top) and bedload transport rate (middle) and direction (bottom) at AWACs 01, 09 and 11 over a 15-day period in the wet season. 219
Figure 179. Modelled water level at AWAC-01 (top) and bedload transport rate (middle) and direction (bottom) at AWAC 08 over a 15-day period in the wet season. 220
Figure 180. Modelled water level at AWAC-01 (top) and bedload transport rate (middle) and direction (bottom) at AWACs 01, 09 and 11 during TC Marcus. 221
Figure 181. Modelled change in bed thickness due to bedload transport for the existing case over the two-month (60/61 days) wet and dry season periods. 223
Figure 182. Modelled change in bed thickness due to bedload transport for the existing case over the two-month (61 days) transitional period and the 5-day TC Marcus period. 224
Figure 183. Cross-shore profiles at Turtle Beach West. 228
Figure 184. Cross-shore profiles at Cape Domett Seaward Beach. 229
Figure 185. Cross-shore profiles at Turtle Bay, Lacrosse Island. 230
Figure 186. Modelled annual longshore and cross-shore transport at the profiles at Turtle Beach West. 231

Figure 187. Modelled annual longshore and cross-shore transport at the three profiles at Cape Domett Seaward Beach and at the profile at Turtle Bay on Lacrosse Island. 231
Figure 188. Spatial variation in cross-shore transport along the TB1_WP beach profile over four month (121/123 days) wet and dry season periods. 232
Figure 189. Annual variation in cross-shore transport at the TB1_WP beach profile from 2015 to 2019. 232
Figure 190. Spatial variation in longshore transport along the TB1_WP beach profile over four month (121/123 days) wet and dry season periods. 233
Figure 191. Annual variation in longshore transport at the TB1_WP beach profile from 2015 to 2019. 233
Figure 192. Modelled annual longshore and cross-shore transport assuming 0.9 m of sea level rise in 100 years at the three profiles at Turtle Beach West. 234
Figure 193. Modelled annual longshore and cross-shore transport assuming 0.9 m of sea level rise in 100 years at the three profiles at Cape Domett Beach and at the profile at Turtle Bay on Lacrosse Island. 234
Figure 194. Spatial variation in cross-shore transport along the TB1_WP beach profile over four month (121/123 days) wet and dry season periods assuming 100 years of sea level rise. 235
Figure 195. Spatial variation in longshore transport along the TB1_WP beach profile over four month (121/123 days) wet and dry season periods assuming 100 years of sea level rise. 235
Figure 196. Modelled existing case and 5 years of sand sourcing scenario 50th percentile SSC over the two-month (60 days) wet season period. 238
Figure 197. Modelled existing case and 15 years of sand sourcing scenario 50th percentile SSC over the two-month (60 days) wet season period. 239
Figure 198. Modelled existing case and the pre-European settlement scenario 50th percentile SSC over the two-month (60 days) wet season period. 240
Figure 199. Modelled existing case and 5 years of sand sourcing scenario 95th percentile SSC over the two-month (60 days) wet season period. 241
Figure 200. Modelled existing case and 15 years of sand sourcing scenario 95th percentile SSC over the two-month (60 days) wet season period. 242
Figure 201. Modelled existing case and the pre-European settlement scenario 95th percentile SSC over the two-month (60 days) wet season period. 243
Figure 202. Timeseries showing the modelled change in SSC during the wet season due to 15 years (70 million m^3) of sand sourcing (Scheme). 244
Figure 203. Timeseries showing the modelled change in SSC during the dry season due to 15 years (70 million m^3) of sand sourcing (Scheme). 245
Figure 204. Timeseries showing the modelled change in SSC during the transitional season due to 15 years (70 million m^3) of sand sourcing (Scheme). 246
Figure 205. Timeseries showing the modelled change in SSC during TC Marcus due to 15 years (70 million m^3) of sand sourcing (Scheme). 247
Figure 206. Timeseries showing the modelled difference in SSC during the wet season for the pre-European settlement scenario (Scheme). 248
Figure 207. Modelled change in bedload transport rate during a spring tide at peak flood and peak ebb in the wet season due to the 5-year (23 million m^3) sand sourcing scenario. 256
Figure 208. Modelled change in bedload transport rate during a spring tide at peak flood and peak ebb in the wet season due to the 15-year (70 million m^3) sand sourcing scenario. 257
Figure 209. Modelled change in bedload transport rate at peak flood and peak ebb during TC Marcus due to the 15-year (70 million m^3) sand sourcing scenario. 258
Figure 210. Modelled difference in bedload transport rate during a spring tide at peak flood and peak ebb in the wet season for the pre-European scenario compared to existing case 259
Figure 211. Timeseries showing the modelled change in bedload transport rate (top) and direction (bottom) at AWAC-08 during the wet season due to 15 years (70 million m^3) of sand sourcing (Scheme). 260
Figure 212. Timeseries showing the modelled change in bedload transport rate (top) and direction (bottom) at AWAC-11 during the wet season due to 15 years (70 million m^3) of sand sourcing (Scheme). 260
Figure 213. Timeseries showing the modelled change in bedload transport rate (top) and direction (bottom) at AWAC-01 during the wet season due to 15 years (70 million m^3) of sand sourcing (Scheme). 261
Figure 214. Timeseries showing the modelled change in bedload transport rate (top) and direction (bottom) at AWAC-09 during the wet season due to 15 years (70 million m^3) of sand sourcing (Scheme). 261
Figure 215. Timeseries showing the modelled difference in bedload transport rate (top) and direction (bottom) at AWAC-08 during a high river discharge event in the wet season in the pre-European scenario (Scheme) compared to the existing case. 262

Figure 216. Timeseries showing the modelled difference in bedload transport rate (top) and direction (bottom) at AWAC-11 during a high river discharge event in the wet season in the pre-European scenario (Scheme) compared to the existing case. 262
Figure 217. Timeseries showing the modelled difference in bedload transport rate (top) and direction (bottom) at AWAC-01 during a high river discharge event in the wet season in the pre-European scenario (Scheme) compared to the existing case. 263
Figure 218. Timeseries showing the modelled difference in bedload transport rate (top) and direction (bottom) at AWAC-09 during a high river discharge event in the wet season in the pre-European scenario (Scheme) compared to the existing case. 263
Figure 219. Modelled difference in bed thickness between the existing case and the 5 and 15 years of sand sourcing scenarios over the two-month (60 days) wet season period. 270
Figure 220. Modelled difference in bed thickness between the existing case and the 15 years of sand sourcing scenario over the two-month (61 days) dry and transitional season periods. 271
Figure 221. Modelled difference in bed thickness between the existing case and the pre-European settlement scenario over the two-month (60/61 days) wet and dry season periods. 272
Figure 222. Modelled 50th percentile natural SSC and 50th percentile sand sourcing SSC for the near-bed layer when sand sourcing during neap tides over two-months in the wet season for Scenario 1. 280
Figure 223. Modelled 50th percentile natural SSC and 50th percentile sand sourcing SSC for the mid-depth layer when sand sourcing during neap tides over two-months in the wet season for Scenario 1. 281
Figure 224. Modelled maximum natural SSC and maximum sand sourcing SSC for the near-bed layer when sand sourcing during neap tides over two-months in the wet season for Scenario 1. 282
Figure 225. Modelled maximum natural SSC and maximum sand sourcing SSC for the mid-depth layer when sand sourcing during neap tides over two-months in the wet season for Scenario 1. 283
Figure 226. Modelled maximum natural SSC and maximum sand sourcing SSC for the near-bed layer when sand sourcing during spring tides over two-months in the wet season for Scenario 1. 284
Figure 227. Modelled maximum natural SSC and maximum sand sourcing SSC for the near-bed layer when sand sourcing during neap tides over two-months in the wet season for Scenario 2. 285
Figure 228. Modelled maximum natural SSC and maximum sand sourcing SSC for the near-bed layer when sand sourcing during spring tides over two-months in the wet season for Scenario 2. 286
Figure 229. Modelled maximum natural SSC and maximum sand sourcing SSC for the near-bed layer when sand sourcing during neap tides over two-months in the dry season for Scenario 1. 287
Figure 230. Modelled maximum natural SSC and maximum sand sourcing SSC for the near-bed layer when sand sourcing during spring tides over two-months in the dry season for Scenario 1. 288
Figure 231. Modelled maximum natural SSC and maximum sand sourcing SSC for the near-bed layer when sand sourcing during neap tides over two-months in the dry season for Scenario 2. 289
Figure 232. Modelled maximum natural SSC and maximum sand sourcing SSC for the near-bed layer when sand sourcing during spring tides over two-months in the dry season for Scenario 2. 290
Figure 233. Modelled maximum natural SSC and maximum sand sourcing SSC for the near-bed layer when sand sourcing during neap tides over two-months in the transitional season for Scenario 1. 291
Figure 234. Modelled maximum natural SSC and maximum sand sourcing SSC for the near-bed layer when sand sourcing during spring tides over two-months in the transitional season for Scenario 1. 292
Figure 235. Modelled maximum natural SSC and maximum sand sourcing SSC for the near-bed layer when sand sourcing during neap tides over two-months in the transitional season for Scenario 2. 293
Figure 236. Modelled maximum natural SSC and maximum sand sourcing SSC for the near-bed layer when sand sourcing during spring tides over two-months in the transitional season for Scenario 2. 294
Figure 237. Modelled 50th percentile natural SSC and 50th percentile natural plus sand sourcing SSC for the near-bed layer when sand sourcing during spring tides over two-months in the dry season for Scenario 2. 295
Figure 238. Modelled maximum natural SSC and maximum natural plus sand sourcing SSC for near-bed layer when sand sourcing during spring tides over two-months in the dry season for Scenario 2. 296
Figure 239. Locations of model output points for the SPV plume modelling along with the POA 297
Figure 240. Timeseries showing the modelled natural SSC and sand sourcing SSC at P01 to P04 during the dry season for Scenario 1 with releases during neap tides. 298
Figure 241. Timeseries showing the modelled natural SSC and sand sourcing SSC at P05 to P07 during the dry season for Scenario 1 with releases during neap tides. 299
Figure 242. Timeseries showing the modelled natural SSC and sand sourcing SSC at P08 to P10 during the dry season for Scenario 1 with releases during neap tides. 300
Figure 243. Timeseries showing the modelled natural SSC and sand sourcing SSC at P01 to P04 during the dry season for Scenario 1 with releases during spring tides. 301

Figure 244. Timeseries showing the modelled natural SSC and sand sourcing SSC at P05 to P07 during the dry season for Scenario 1 with releases during spring tides. 302
Figure 245. Timeseries showing the modelled natural SSC and sand sourcing SSC at P08 to P10 during the dry season for Scenario 1 with releases during spring tides. 303
Figure 246. Timeseries showing the modelled natural SSC and sand sourcing SSC at P01 to P04 during the dry season for Scenario 2 with releases during neap tides. 304
Figure 247. Timeseries showing the modelled natural SSC and sand sourcing SSC at P05 to P07 during the dry season for Scenario 2 with releases during neap tides. 305
Figure 248. Timeseries showing the modelled natural SSC and sand sourcing SSC at P08 to P10 during the dry season for Scenario 2 with releases during neap tides. 306
Figure 249. Timeseries showing the modelled natural SSC and sand sourcing SSC at P01 to P04 during the dry season for Scenario 2 with releases during spring tides. 307
Figure 250. Timeseries showing the modelled natural SSC and sand sourcing SSC at P05 to P07 during the dry season for Scenario 2 with releases during spring tides. 308
Figure 251. Timeseries showing the modelled natural SSC and sand sourcing SSC at P08 to P10 during the dry season for Scenario 2 with releases during spring tides. 309
Figure 252. Modelled sedimentation resulting from 2 months of sand sourcing in the wet season for Scenario 1 when sand sourcing activity coincided with spring (left) and neap (right) tides. 323
Figure 253. Modelled sedimentation resulting from 2 months of sand sourcing in the wet season for Scenario 2 when sand sourcing activity coincided with spring (left) and neap (right) tides. 324
Figure 254. Modelled sedimentation resulting from 2 months of sand sourcing in the dry season for Scenario 1 when sand sourcing activity coincided with spring (left) and neap (right) tides. 325
Figure 255. Modelled sedimentation resulting from 2 months of sand sourcing in the dry season for Scenario 2 when sand sourcing activity coincided with spring (left) and neap (right) tides. 326
Figure 256. Modelled sedimentation resulting from 2 months of sand sourcing in the transitional season for Scenario 1 when sand sourcing activity coincided with spring (left) and neap (right) tides. 327
Figure 257. Modelled sedimentation resulting from 2 months of sand sourcing in the transitional season for Scenario 2 when sand sourcing activity coincided with spring (left) and neap (right) tides. 328

TABLES

Table 1. BKA CG in-situ data collection program - types of equipment, data collected and deployment periods for each site. 14
Table 2. Comparison between the reported AHO tidal planes at Cape Domett and tidal planes calculated based on measured water level data at AWAC-01 and AWAC-07. 19
Table 3. Percentile turbidity and SSC values at each site based on all measured data between 7th September 2023 and 14th August 2024. 70
Table 4. Statistics for comparison of modelled and measured water levels (WLs) at AWAC-01, AWAC-06, AWAC-08, AWAC-09 and AWAC-11 during the calibration period. 91
Table 5. Statistics for comparison of modelled and measured currents through the water column at AWAC-01, AWAC-06, AWAC-08, AWAC-09 and AWAC-11 during the calibration period. 92
Table 6. Statistics for comparison of modelled and measured water levels (WLs) at AWAC-01, AWAC-05, AWAC-10 and AWAC-11 during the validation period. 101
Table 7. Statistics for comparison of modelled and measured currents through the water column at AWAC-01, AWAC-05, AWAC-10 and AWAC-11 during the validation period. 102
Table 8. Comparison of RMSE for modelled and measured significant wave height data at AWAC-01, AWAC-06, AWAC-08, AWAC-09 and AWAC-11 during the calibration period. 110
Table 9. Comparison of RMSE for modelled and measured significant wave height data at AWAC-01, AWAC-05, AWAC-10 and AWAC-11 during the validation period. 113
Table 10. Comparison between mean near-bed measured and modelled clay/silt SSC and sand SSC during the February 2024 13 hour vertical profile measurements. 117
Table 11. OSPAR Cost Function values for comparison of modelled and measured total SSC during the calibration and validation period. 121
Table 12. Summary of spill rates for the relevant SPV parameters for this assessment. 125
Table 13. Dredge cycle adopted for the modelling. 125
Table 14. Statistics of the modelled change in water level during the wet season due to the 15 years of sand sourcing scenario and the pre-European settlement scenario relative to the existing case at the 11 AWAC sites. 161
Table 15. Percent change in tidal range due to 15 years of sand sourcing and pre-European settlement during a spring tide with a high river discharge relative to the existing case. 162
Table 16. Statistics of the modelled change in current speed due to the 15 years (70 million m^3) of sand sourcing scenario and the pre-European settlement scenario relative to the existing case at the 11 AWAC sites. 179
Table 17. Percent change in peak flood and ebb current speed relative to the existing case due to 15 years (70 million m^3) of sand sourcing and pre-European settlement during a spring tide with a high river discharge. 180
Table 18. Statistics of the modelled change in H_s during the wet season due to 5 years (23 million m^3) and 15 years (70 million m^3) of sand sourcing relative to the existing case. 196
Table 19. Statistics of the modelled change in H_s during the dry season due to (23 million m^3) and 15 years (70 million m^3) of sand sourcing relative to the existing case. 197
Table 20. Statistics of the modelled change in H_s during the transitional season due to (23 million m^3) and 15 years (70 million m^3) of sand sourcing relative to the existing case. 198
Table 21. Statistics of the modelled change in H_s during TC Marcus due to (23 million m^3) and 15 years (70 million m^3) of sand sourcing relative to the existing case. 199
Table 22. Statistics of the modelled existing case SSC over two months (60/61 days) of wet and dry season conditions at the 11 AWAC sites. 210
Table 23. Statistics of the modelled existing case SSC over two months (61 days) of the transitional season and 5 days during TC Marcus at the 11 AWAC sites. 211
Table 24. Statistics of the modelled change in SSC during the wet and dry seasons due to 15 years (70 million m^3) of sand sourcing relative to the existing case. 249
Table 25. Statistics of the modelled change in SSC during the transitional season and during TC Marcus due to 15 years (70 million m^3) of sand sourcing relative to the existing case. 250
Table 26. Statistics of the modelled change in SSC during the wet season for the pre-European settlement scenario relative to the existing case and the cumulative change of the pre-European settlement scenario and the 15 years (70 million m^3) of sand sourcing scenario. 251

Table 27. Statistics of the modelled change in SSC during the dry season for the pre-European settlement scenario relative to the existing case and the cumulative change of the pre-European settlement scenario and the 15 years (70 million m^3) of sand sourcing scenario. 252
Table 28. Statistics of the modelled change in SSC during the transitional season for the pre-European settlement scenario relative to the existing case and the cumulative change of the pre-European settlement scenario and the 15 years (70 million m^3) of sand sourcing scenario. 253
Table 29. Statistics of the modelled change in bedload transport during the wet and dry seasons due to 15 years (70 million m^3) of sand sourcing relative to the existing case. 264
Table 30. Statistics of the modelled change in bedload transport during the transitional season and during TC Marcus due to 15 years (70 million m^3) of sand sourcing relative to the existing case. 265
Table 31. Statistics of the modelled change in bedload transport during the wet season for the pre-European scenario relative to the existing case and the cumulative change of the pre-European scenario and the 15 years of sand sourcing scenario. 266
Table 32. Statistics of the modelled change in bedload transport during the dry season for the pre-European scenario relative to the existing case and the cumulative change of the pre-European scenario and the 15 years of sand sourcing scenario. 267
Table 33. Statistics of the modelled change in bedload transport during the transitional season for the pre-European scenario relative to the existing case and the cumulative change of the pre-European scenario and the 15 years of sand sourcing scenario. 268
Table 34. Statistics of the modelled natural and sand sourcing SSC during the wet season for sand sourcing scenario 1 with neap releases. 310
Table 35. Statistics of the modelled natural and sand sourcing SSC during the wet season for sand sourcing scenario 1 with spring releases. 311
Table 36. Statistics of the modelled natural and sand sourcing SSC during the wet season for sand sourcing scenario 2 with neap releases. 312
Table 37. Statistics of the modelled natural and sand sourcing SSC during the wet season for sand sourcing scenario 2 with spring releases. 313
Table 38. Statistics of the modelled natural and sand sourcing SSC during the dry season for sand sourcing scenario 1 with neap releases. 314
Table 39. Statistics of the modelled natural and sand sourcing SSC during the dry season for sand sourcing scenario 1 with spring releases. 315
Table 40. Statistics of the modelled natural and sand sourcing SSC during the dry season for sand sourcing scenario 2 with neap releases. 316
Table 41. Statistics of the modelled natural and sand sourcing SSC during the dry season for sand sourcing scenario 2 with spring releases. 317
Table 42. Statistics of the modelled natural and sand sourcing SSC during the transitional season for sand sourcing scenario 1 with neap releases. 318
Table 43. Statistics of the modelled natural and sand sourcing SSC during the transitional season for sand sourcing scenario 1 with spring releases. 319
Table 44. Statistics of the modelled natural and sand sourcing SSC during the transitional season for sand sourcing scenario 2 with neap releases. 320
Table 45. Statistics of the modelled natural and sand sourcing SSC during the transitional season for sand sourcing scenario 2 with spring releases. 321
Table 46. Summary of how this report meets the Study Objectives 331
Table 47. Summary of how this report meets the relevant WA EPA Guidelines 340

ACRONYMS

3D	Three-dimensional
ADCP	Acoustic Doppler Current Profiler
AHD	Australian Height Datum
AHO	Australian Hydrographic Office
AWAC	Acoustic Wave and Current Profiler
BCH	Benthic communities and habitats
BK	Boskalis
BKA	Boskalis Australia
BM	Benchmark
BoM	Bureau of Meteorology
CAWCR	Centre for Australian Weather and Climate Research
CF	Cost Function
CG	Cambridge Gulf
CSIRO	Commonwealth Scientific and Industrial Research Organisation
DEA	Digital Earth Australia
DHI	Danish Hydraulic Institute
DSN	Dredging Science Node
DWER	(WA) Department of Water and Environmental Regulation
EFG	(WA EPA) Environmental Factor Guideline
EIA	Environmental Impact Assessment
EP	East Profile
EPA	(WA) Environmental Protection Authority
EQP	Environmental Quality Plan
FM	Flexible Mesh
GA	Geoscience Australia
GBRMPA	Great Barrier Reef Marine Park Authority
HAT	Highest Astronomical Tide
HD	Hydrodynamic
HW	High Water
IPCC	Intergovernmental Panel on Climate Change
JBG	Joseph Bonaparte Gulf
LAT	Lowest Astronomical Tide
LiDAR	Light Detection and Ranging
LW	Low Water
MEQ	Marine Environmental Quality
MHWN	Mean High Water Neaps
MHWS	Mean High Water Springs
MLWN	Mean Low Water Neaps
MLWS	Mean Low Water Springs
MSL	Mean Sea Level
MSQ	Maritime Safety Queensland
NTU	Nephelometric Turbidity Unit
PCS	Port and Coastal Solution
POA	Proposed operational area
PSD	Particle size distribution
RFP	Request for Proposal
RMS	Root Mean Square
RMSE	Root Mean Square Error
SPV	Sand Production Vessel
SSC	Suspended solids concentration
ST	Sediment Transport
SW	Spectral Wave
TC	Tropical Cyclone
TSHD	Trailer Suction Hopper Dredger
WA	Western Australia
WAMSI	Western Australian Marine Science Institution
WL	Water level
WP	West Profile

Executive Summary

In 2023 Boskalis Australia Pty Ltd (BKA) commissioned Port and Coastal Solutions (PCS) to undertake metocean and sediment data analysis and numerical modelling for the Cambridge Gulf (CG) Marine Sand Proposal (the proposal). The primary aim of this study is to analyse and interpret metocean and sediment data and then undertake detailed numerical modelling to support the environmental impact assessment and regulatory approval applications for the proposal. The study has three objectives as detailed in Section 1, which relate to assessing potential effects of the proposal on:

a) hydrodynamics and waves,

b) sediment dynamics and coastal processes, and

c) suspended sediment and turbidity.

The study in turn informs the assessment of whether any potential changes to the above three processes will affect the Key Environmental Factors of the area as defined by relevant guidelines of the WA Environmental Protection Authority (EPA), these being:

a) benthic communities and habitats (BCH) (which are quite depauperate in CG due to the extreme environmental conditions, as reported in BKA 2024b).

b) coastal processes, and the environmental resources and values of the CG area that are influenced by coastal processes (primally mangrove communities around the internal coasts of CG, including the Ord River Floodplain Ramsar site, and turtle-nesting beaches on the seaward coasts of CG and at Barnett Point).

c) marine environmental quality (MEQ), and the environmental resources and values of the CG area that are influenced by MEQ (primarily marine ecosystem health).

All work has been undertaken in accordance with relevant EPA guidelines as listed in Section 1.

The study is supported by an unprecedented volume of field data, including *inter alia* since June 2023:

- in-situ seabed-mounted ADCPs / AWACS at 11 sites throughout CG, deployed for various periods depending on the site (up to 142 days per site and a total combined deployment of 918 days or 30 months), to provide data across a very wide range of hydrodynamic conditions.
- in-situ seabed light meters and multi-sonde sensors at 14 sites throughout CG, to collect long-term benthic light (irradiance), turbidity, temperature, salinity and pH data (up to 142 days per site and a total combined deployment of 1,402 days or 46 months).

The volume of data generated as part of this in-situ data collection program provides for comprehensive process understanding and numerical model calibration and validation, which in turn supports an extremely high level of confidence in the numerical modelling results.

A previous report by PCS (2024a), titled 'System Understanding, Conceptual Model & Initial Modelling', was prepared, which provides a review and analysis of a wide range of pre-existing data relating to CG, new field data collected by BKA from June 2023 to June 2024, the setup and results from initial numerical modelling and a system understanding and conceptual model of CG.

Two supplementary appendices to PCS (2024a) were also developed, these being PCS (2024b) titled 'Supplementary Technical Note' (which analyses additional field data collected since PCS (2024a) was drafted) and PCS (2024c) titled 'Factual Data Report' (which presents all data used for the study up to the end of June 2024, this has been updated to include all data up to 14th August 2024 in Annex B).

This current report (PCS, 2025a) should be read in light of the three previous reports (PCS 2024a, 2024b & 2024c), as it is very much informed by them. This report provides additional analysis of the field data collected by BKA, including the additional data collected since June 2024 up to 14th August 2024, providing measured in-situ hydrodynamic, wave and water quality data from June 2023 to mid-August 2024, and presents results from the full numerical modelling to inform the three study objectives.

The data analysis in this report was specifically focused on data which are directly relevant to the numerical modelling, with hydrodynamic, wave, turbidity and benthic light data all being analysed. The analysis showed the following.

- Current speeds in CG can be very high (up to 2.9 m/s or 5.6 knots at the northern entrance to West Arm) due to the 8 m tidal range.

- Similar temporal patterns in residual current speeds were present between different sites in CG and between the surface and depth-averaged currents. The data indicate that wind conditions could influence the residual currents, but that the influence is only likely to be significant in terms of changes to the net drift during neap tides.

- There was a strong correlation between the measured H_s around CG and the offshore hindcast modelled wave data in Joseph Bonaparte Gulf (JBG), and a very strong correlation between the measured significant wave height (H_s) around CG and the hindcast modelled wind data within CG. Both hindcast modelled waves and winds were shown to represent the diurnal variability in the measured wave height, providing confidence that the hindcast modelled data are able to represent important mesoscale processes such as the sea-breeze.

- On occasion, wave conditions also showed a very slight variation over a semi-diurnal tidal cycle. Close inspection of the data showed that this was associated with adverse and following tidal currents, with peaks occurring at mid flood under southerly winds, and mid ebb under northerly winds.

- Measured wave spectra showed that multiple different wave conditions are often present within CG, with a combination of old sea waves from offshore and locally generated fetch-limited waves from within CG.

- Suspended Solids Concentrations (SCC) and turbidity in CG can be extremely high, with 99th percentile values of 1,057 mg/L and 470 NTU respectively, due to the strong tidal currents causing constant resuspension of sediment, and significant inputs of terrestrial sediments during wet season rainfall events.

- The SSC and turbidity were shown to be variable both spatially and temporally, with higher SSC and turbidity upstream and lower values offshore. The SSC and turbidity varied over multiple time scales, with lower SSC and turbidity at high tide and higher SSC and turbidity at low tide and lower SSC and turbidity in the dry season and higher SSC and turbidity in the wet season. As outlined above, SSC and turbidity within CG was predominantly influenced by the astronomical tide, although high river discharge events were also shown to result in elevated SSC and turbidity, while the SSC and turbidity offshore of CG and within CG close to the entrances, were more influenced by offshore wave conditions than the astronomical tide.

- The very high SSC and turbidity in CG prevent sunlight penetrating through the water column to the seabed and the in-situ data showed a permanent aphotic zone with zero to almost zero benthic light throughout CG. As per the analysis in PCS (2024b), detectable benthic light was only measured at sites shallower than 15 m (sites AWAC-05 and Pos 14), at very low levels and only during occasional periods of lower turbidity (less than 10 NTU). At these sites, periods of lower turbidity and thus some detectable benthic light only occurred during neap tides, with no benthic light being measured at any of the sites during spring tides.

A system understanding of the CG region in terms of coastal processes and sediment transport is presented, this is based on information from the literature combined with data analysis and the results of the numerical modelling as presented in this report and the previous PCS reports (PCS, 2024a & 2024b). For context, the system understanding is summarised below:

- Bathymetric data provided by Geoscience Australia (2023) show that depths through the main body of CG are deeper than -15 m lowest astronomical tide (LAT), with depths of more than -50 m LAT at the West Entrance and in the West Arm.

- The large tidal range in CG results in high tidal current speeds, which in turn result in regular sediment suspension and transport and naturally very high SSC and turbidity in CG overall.

- The region experiences significant seasonal variability in the wind, wave and rainfall conditions. The wind and wave conditions are typically from the northwest to north from December to April (wet season), from north to east between April and September (dry season) and from the northwest to northeast from September to December (transitional season).

- Waves within CG are sheltered by King Shoals and Medusa Bank offshore of CG and Lacrosse Island in the middle of the entrance to CG, resulting in variable wave exposure in CG depending on the offshore wave direction. The influence of wave action in CG on sediment transport processes is limited to very large wave events during the wet season (e.g. during tropical

cyclones and tropical lows). These wave events can result in erosion of areas of mudflats and mangroves and also in the formation and landward migration of features such as stranded beach ridges. The influence of waves on sediment transport within the POA will be small compared to the influence of tidal currents.

- Multiple rivers flow into CG, including the Ord River, Pentecost River, Durack River, King River and the Forrest River. High river flows only occur occasionally and only during the wet season. The catchment for the Ord River has been subject to extensive land clearing for cattle and irrigated agriculture, and it also has two dams, the lower Kununurra Diversion Dam (referred to as the Lower Ord Dam) and the upper Ord River Dam (referred to as the Ord River Dam), built to develop the Ord River Irrigation Scheme. The extensive land clearing for cattle commenced around the start of the 20th Century, while the dams were constructed between 1969 and 1972 (Wolanski *et al.*, 2001). The Ord River flows were noted to have experienced significant variability in discharge prior to the construction of the dams, but since the construction the river discharge is now almost constant. The seasonal variability and large floods still occur in the other rivers that flow into CG.

- The supply of sediment from the rivers to CG will vary significantly due to the high variability in the river discharge. Peaks in sediment supply from the rivers will occur in the wet season, with limited supply of sediment during the dry season. The rivers supply a mixture of sand-sized sediment and fine-grained silt and clay. Results from numerical modelling indicate that the construction of the Ord River Dam, which suppressed the wet season flood flows in the Ord River, resulted in a significant reduction in the peak SSC which can occur in CG during the wet season. Sediment sampling undertaken as part of the project has also shown that the sediment in both West and East Arms is predominantly sand with high percentages of quartz and feldspar which are also the dominant elements in the sand present in the POA (PCS 2024a). It is therefore likely that there is an ongoing supply of sand to CG from the West and East Arms, although the supply from East Arm will be significantly lower compared to prior to the construction of the Ord River dam.

- Sediment present within CG will be subject to regular reworking by the strong tidal currents that occur in the region, resulting in well-sorted sandy sediment being present where stronger currents occur. Sediment sampling results have shown that there is an abundance of sediment available for transport within CG, with a combination of sand, silt and clay all present in CG and an estimated minimum of 300 million m^3 of sand present in the POA.

- There is significant variability in the sediment transport which occurs in the region, with the tide being the dominant process which influences sediment transport in CG. Measured data have shown that the sediment which is regularly transported in suspension is predominantly made up of fine-grained silt and clay, with some very fine sand also present, while the coarser sand is predominantly transported as bedload (PCS 2024a). The sediment transport varies between the flood and ebb stages of the tide and between spring and neap tides. Relatively low SSC and transport rates only occur for short durations on small neap tides, while higher SSC and transport rates occur more often during larger range tides which regularly influence CG. The measured data showed peaks in SSC typically on the ebb tide and at low water, indicating a net export of fine-grained silt and clay from CG, while changes in bedforms present in CG also showed a dominant net export of sand from CG.

- Due to the regular high SSC in the region, the benthic light availability is zero to very low throughout CG. The only sites where regular benthic light was measured were in water depths of less than 15 m (relative to mean sea level (MSL), equivalent to -11 m LAT) and the benthic light was only measured during the smallest range neap tides when the turbidity was very low (typically less than 10 NTU).

The setup of the final hydrodynamic, spectral wave, sediment transport, beach processes and sediment plume models are presented. The MIKE software suite developed by Danish Hydraulic Institute (DHI) was applied for all of the modelling, with a flexible mesh approach adopted for the hydrodynamic, wave, sediment transport and plume models. The model mesh extends ~200 km north to south and 280 km east to west, with the triangular element side lengths varying from 4 km in the offshore areas to 200 m in CG. The hydrodynamic and wave models were subject to a detailed calibration and validation exercise, with the models calibrated at five sites around CG during wet season conditions and validated at four sites during dry season conditions. The sediment transport model was calibrated to ensure it was able to represent the composition of the sediment in suspension and the bedload transport rates. The SSC was calibrated and validated over two month (60/61 days) wet season and dry season conditions at nine and eight sites, respectively.

The numerical modelling has been used to better understand the existing conditions in CG and how they vary spatially and temporally, and to assess the potential changes from:

- the proposed sourcing of 23 million m^3 of sand after 5 years.
- the proposed sourcing of 70 million m^3 after 15 years.
- the potential changes in 100-years after the 15-years sourcing of 70 million m^3.

In order to assist in assessing potential cumulative impacts of the proposed sand sourcing, as required by WA EPA guidelines, the modelling also assessed potential changes to hydrodynamics, waves, sediment transport, SSC and turbidity that have occurred in CG since European settlement (primarily from the construction of two dams on the Ord River in 1969 and 1971), which have created the existing conditions in CG today. This allowed any additional changes that might be caused by the proposed sand sourcing to be assessed in the context of the historical changes since European settlement.

A summary of the key results from the different aspects of the modelling is provided below.

- Hydrodynamics: Overall, the modelling indicated that potential changes to hydrodynamics from the proposed sourcing of 23 million m^3 of sand after 5 years and 70 million m^3 of sand after 15-years, and 100-years after the 15-years sand sourcing, will be negligible. The modelled changes were similar for the different metocean conditions considered (wet, dry and transitional seasons and a tropical cyclone).

  The modelling results indicated that the sourcing of 70 million m^3 of sand after 15-years could potentially result in a very minor change in phase of the tidal wave propagation in CG of up to 30 seconds (s). This change results in very minor apparent modelled changes in water level of up to ± 0.05 m (50 mm) during the peak flood and peak ebb stages of the tide, while modelled changes to the tidal range were insignificant (less than 0.05%). The modelled changes in tidal range were further reduced in 100-years time after the 15-years sourcing, with changes of less than 0.025%.

  The modelling assessed that building the two dams on the Ord River may have increased the tidal range in CG by up to 0.55% during a high river discharge event compared to pre-European settlement conditions. While this is a minor change, it is an order of magnitude higher than the very minor <0.05% modelled for the proposed sand sourcing.

  Modelled changes to currents resulting from the sand sourcing were insignificant and localised within and adjacent to the proposed operational area (POA). Modelled changes in current speed were up to ± 0.05 m/s after 15 years (70 million m^3) of sand sourcing, resulting in changes in the peak flood and ebb currents within the POA of a maximum of -2.1% and less than ± 0.5% outside of the POA. Modelled changes to currents in 100-years after the 15-years sourcing of 70 million m^3 were lower than after 15 years of sand sourcing for existing water levels, with changes of up to ± 0.03 m/s and maximum changes in peak flood and ebb currents outside of the POA remaining at less than ± 0.5%.

  The modelling assessed that building the two dams on the Ord River may have caused changes to currents throughout CG and in the West and East Arms upstream of CG, with a modelled increase in peak flood current speeds of up to 11.7% and a reduction in the peak ebb current speed of up to -6.3% during a high river discharge event.

  Overall, the modelled potential changes to hydrodynamics from the proposed sand sourcing under all scenarios are so minor that there are no mechanisms whereby they could in turn cause changes to the environmental resources and values of the CG area that are influenced by hydrodynamics (primarily mangrove communities around the internal shoreline of CG, including the Ord River Floodplain Ramsar site, and turtle nesting beaches on the seaward coasts of CG and at Barnett Point inside CG).

- Waves: The modelling indicated that potential changes to wave conditions resulting from the sand sourcing after both 5 years (23 million m^3) and 15 years (70 million m^3) were very minor and localised. The modelling assessed that the sand sourcing would only influence the wave conditions in CG during specific wave conditions, typically during larger wave events. The modelled changes during the largest wave event over the simulation period were up to ± 0.01 m in H_s, up to ± 0.05 s in peak wave period (T_p) and less than 0.5º in wave direction. The largest (but still minor) changes occurred during the wet season when the wave climate is more energetic.

The modelling assessed that building the two dams on the Ord River has not changed wave conditions in CG compared to pre-European settlement conditions.

Overall, the modelled potential changes to waves from the proposed sand sourcing under all scenarios are so minor that there are no mechanisms whereby they could in turn cause changes to the environmental resources and values of the CG area that are influenced by waves (primarily mangrove communities around the internal shoreline of CG, including the Ord River Floodplain Ramsar site, and turtle nesting beaches on the seaward coasts of CG and at Barnett Point inside CG).

- Suspended Sediment: The modelling indicated that the deepening due to the sand sourcing will not significantly change the SSC within CG, with very little change to the spatial pattern of the SSC and the main (but minor) change in SSC being due to the minor change in phase of the tidal propagation. Due to the deepening of the POA associated with the sand sourcing, the modelling indicated a reduction in SSC within the POA of up to 8%, while outside of the POA, the changes were still predominantly reductions with changes of ± 3%. These changes are likely to be due to the minor changes in tidal current speed (predominantly reductions) resulting from the deepening of the POA. These changes in SSC are not expected to impact the supply of fine-grained sediment to mangroves and mudflats in the region or to measurably change the benthic light in the region, which is already permanently zero to near-zero throughout CG.

  The modelling assessed that building the two dams on the Ord River may have significantly reduced SSC in CG during a large river discharge event in the wet season compared to pre-European settlement conditions. Reductions in peak SSC throughout CG and offshore of up to 87% were modelled during high river discharge events in the wet season, due to the dams reducing wet season river discharges into to CG. During the dry season the SSC was modelled to have increased since European settlement within CG by up to 16% due to the increase in dry season river discharge associated with controlled releases from the dams. The cumulative changes in SSC due to the Ord River dams and 15 years of sand sourcing show that the relative contribution of the sand sourcing to the cumulative changes are negligible.

- Bedload Transport: The modelled changes in bedload transport due to the sand sourcing were similar in spatial pattern to the changes in current speed. The model indicated very minor reductions in bedload transport within and to the west and east of the POA and minor increases in bedload transport directly to the north and south of the POA. Reductions in peak modelled bedload transport rates were between 3.1% and 10.5% within the POA, while outside of the POA modelled changes in bedload transport were between a 1.8% reduction to a 2.6% increase. As the sand sourcing will leave most of the existing sand resource present throughout the POA (the proposal will only take a maximum of 23% of the existing sand resource), the changes to the bedload transport are relatively small and localised and are not assessed to influence the wider sediment transport processes in CG and offshore.

  Modelled changes in bed thickness due to the sand sourcing (in addition to the deepening of an average of just under 1 m over 75 km^2 of the POA by the activity itself), showed that changes of more than 0.01 m and up to 0.05 m over 2 months (60/61 days) only occurred in localised areas within and adjacent to the POA. The largest changes within the POA over the two-month simulation period were very minor at up to ± 0.05 m. The modelling also identified an area of minor erosion within the POA directly adjacent to its northern boundary for all metocean conditions simulated. The modelled erosion of sand in this area will provide a source meaning that the modelled small reduction in bedload transport within the POA due to the deepening does not change the supply of sand offshore.

  Overall, the modelled potential changes to sediment transport are so minor that there are no mechanisms whereby they could in turn cause changes to the environmental resources and values of the CG area that are influenced by sediment transport (primarily mangrove communities around the internal shoreline of CG, including the Ord River Floodplain Ramsar site, and turtle nesting beaches on the seaward coasts of CG and at Barnett Point inside CG).

- Beach Processes: Wave modelling of the sand sourcing scenarios indicated that they would not result in any changes to the wave conditions offshore of CG, and so would not result in any direct changes to the longshore or cross-shore sediment transport at the three turtle nesting beaches on the seaward coasts of CG. Results from the hydrodynamic, wave and sediment transport modelling indicated that there would not be any direct or indirect impacts from the sand sourcing on the supply or transport of sand to any of these beaches or the turtle nesting beach at East Bank Point (Barnett Point) inside CG.

- Sediment Plumes: The modelling showed that the SSC resulting from sediment plumes generated by the Sand Production Vessel (SPV) was consistently low for all model simulations, with only the 99th percentile modelled depth-averaged SSC exceeding 1 mg/L for short periods at localised sites both within and near the POA, with negligible changes at King Shoals offshore from CG (which is a Sanctuary Zone in the State Marine Park). Comparing the modelled sand sourcing SSC with the very high modelled natural SSC in CG shows that the relative contribution of the sand sourcing SSC is less than 1.5% of the natural SSC and that the increases to the natural SSC only occur in localised areas for restricted periods. These very minor variations will not cause changes to the BCH or MEQ of CG. It should also be noted that there are no sensitive benthic communities in CG that could potentially be impacted even if SSC was significantly elevated by the sand-sourcing operation.

  There are several key factors that contribute to keeping SSC from the proposed operation at low levels, in localised areas and for short durations, including the facts that:

  – the operation will target coarser sand and not fine-grained silts and clays.

  – the operation will not be continuous, as the SPV will only operate in CG for one to two days (average 30 hours) every 14 days, as, in between loading cycles, the SPV will deliver the sand to Asia and return to CG.

  – the operation will not include any dumping of sediment in CG (as the loaded sand will be exported).

  – the SPV will be fitted with best-practice turbidity reduction measures, including a 'green valve' in the water overflow discharge and placing the discharge at the keel (~19 m below the water line).

  The modelling showed that the sedimentation rates resulting from the sediment plumes generated by the SPV were less than 0.0005 g/cm^2/day over two-months (60/61 days) of sand sourcing activity for the majority of CG. The only localised areas with higher (but still minor) sedimentation rates outside of the POA were directly to the north of the POA where sedimentation rates of very fine sand of up to 0.0025 g/cm^2/day over two-months (60/61 days) was modelled. Detailed bathymetric survey undertaken by BKA in 2024 showed that sand waves are present in this area and so the very fine sand from the sand sourcing activity will mix with the existing sand present in the area. In addition, the natural bedform and morphological changes in this area are likely to be significantly larger than the sedimentation resulting from the sand sourcing. These very minor variations will not cause changes to the BCH or MEQ of CG. It should also be noted that there are no sensitive benthic communities in CG that could potentially be impacted even if sedimentation was significantly elevated by the sand-sourcing operation.

Overall, based on the results from the modelling presented in this report, the potential changes to all factors that were modelled from the proposed sand sourcing under all scenarios are so minor that there are no mechanisms whereby they could in turn cause changes to the environmental resources and values of the CG area (primarily mangrove communities around the internal shoreline of CG, including the Ord River Floodplain Ramsar site, and turtle nesting beaches on the seaward coasts of CG and at Barnett Point inside CG).

Potential impacts are assessed further in BKA (2024d) (Referral Report No. 4 - *Impact Assessments*).

In order to address the study objectives and the specific requirements of the relevant EPA guidelines, as outlined in Section 1, Section 7 of this report presents an assessment of how the data analysis and numerical modelling answers each of the questions set by the study objectives and the relevant EPA guidelines.

An independent expert review of this technical report has been undertaken by Steve Buchan from MetOcean Consulting, this is included in Annex A.

1. INTRODUCTION, OBJECTIVES & GUIDELINES

In 2023 Boskalis Australia Pty Ltd (BKA) commissioned Port and Coastal Solutions (PCS) to undertake metocean and sediment data analysis and numerical modelling for the Cambridge Gulf (CG) Marine Sand Proposal (the proposal). The primary aim of this study is to analyse and interpret metocean and sediment data and then undertake detailed numerical modelling to support the environmental impact assessment and regulatory approval applications for the proposal, with three objectives as follows.

Objective 1: Hydrodynamics and waves.

a) Define the existing hydrodynamic conditions in the subject areas, under the seasonal range of natural conditions, including any changes since European colonization.

b) Predict potential impacts of the proposal on the hydrodynamics of the subject areas, including during the operation (after five years), at the end of the operation (approximately 15 years) and in 100 years-time.

c) Predict likely 'worst-case' and 'best-case' impacts and also potential 'cumulative' impacts of the proposal on hydrodynamics (with 'worst-case' and 'best-case' being consistent with meanings in relevant Western Australian (WA) Environmental Protection Authority (EPA) guidance as listed below, and 'cumulative' meaning in addition to those that may have been caused by previous developments in the area, such as the Ord River dams).

d) Provide hydrodynamics data analysis and modelling to support the other objectives below.

Objective 2: Sediment transport and coastal processes.

a) Define existing sediment transport and coastal processes in the subject areas, including natural sediment sources and pathways, sediment sizes on the seabed and in transport under the seasonal range of natural conditions, and any changes since European colonization.

b) Predict potential impacts of the proposal on sediment transport and coastal processes of the subject areas, including during the operation (after five years), at the end of the operation (15 years) and in 100 years, with particular focus on predicting:

- potential for natural replenishment of sand in dredged areas of the tenements, including likely timeframes for replenishment.
- potential for coastal erosion and accretion.
- potential impacts on turtle nesting beaches both inside and immediately outside CG, including potential changes in sand grain size and beach geomorphology.
- potential impacts on mangroves and other coastal and intertidal communities and impacts on the Ord River Floodplain Ramsar site as a result of the sand extraction.

c) This should include prediction of likely 'worst-case' and 'best-case' impacts and also 'cumulative' impacts of the proposal on sediment transport and coastal processes (with 'worst-case' and 'best-case' being consistent with meanings in relevant WA EPA guidance as listed below, and 'cumulative' meaning in addition to those that may have been caused by previous developments in the area, such as the Ord River dams).

Objective 3: Suspended sediment and turbid plume dispersal and potential impacts on benthic habitats & communities (see note below).

a) Define the existing suspended sediment and turbidity regime in the subject areas, under the seasonal range of natural conditions.

b) Predict potential dispersal of sediment and turbidity plumes from the proposed operation, under the seasonal range of natural conditions, in particular towards King Shoals and the State Marine Park Sanctuary Zone (although noting that benthic surveys in this area have not identified any sensitive benthic communities (BKA, 2024d)).

The study in turn informs the assessment of whether any potential changes to the processes listed in the three objectives above, will affect the Key Environmental Factors (KEFs) of the area as defined by relevant guidelines of the WA Environmental Protection Authority (EPA), with the KEFs being:

a) benthic communities and habitats (BCH) (which are quite depauperate in CG due to the extreme environmental conditions, see BKA 2024b).

b) coastal processes, and the environmental resources and values of the CG area that are influenced by coastal processes (primally mangrove communities around the internal coasts of CG, including the Ord River Floodplain Ramsar site, and turtle-nesting beaches on the seaward coasts of CG and at Barnett Point inside CG, see Figure 2).

c) marine environmental quality (MEQ), and the environmental resources and values of the CG area that are influenced by MEQ (primally marine ecosystem health).

The inclusion of any changes since European colonization in Objectives 1 and 2 is to assist in assessing any potential cumulative impacts of the proposal, over and above any such historical changes, as required by EPA guidelines.

The time-frame adopted for assessing potential changes during the sand sourcing operation under Objectives 1 and 2 was five years from commencement of the operation, when it is assumed that up to 23 million m^3 of sand would be sourced. Fifteen years is used as the predicted end of the operation, when up to 70 million m^3 of sand would be sourced, according to the proposal specifications advised by BKA.

In addressing these objectives, all work has been undertaken in accordance with all relevant guidelines of the WA EPA as follows:

a) Western Australia (WA) Environmental Protection Authority (EPA) 2021 *Technical Guidance for EIA of Marine Dredging Proposals.*

b) WAMSI/CSIRO 2020 *Guideline for Dredge Plume Modelling for EIA* (Sun *et al.*, 2020).

c) WA EPA 2016 *Environmental Factor Guideline - Coastal Processes.*

d) WA EPA 2016 *Environmental Factor Guideline - Marine Environmental Quality.*

e) WA EPA 2016 *Technical Guidance - Protecting the Quality of Western Australia's Marine Environment.*

Section 7 describes how each of these EPA guidelines have been applied and addressed.

This study is supported by an unprecedented volume of field data, including *inter alia* since June 2023:

- in-situ seabed ADCPs / AWACS at 11 sites throughout CG, deployed for various periods depending on the site (up to 142 days), to provide data across a very wide range of hydrodynamic conditions.

- in-situ seabed light meters and multi-sonde sensors at 14 sites throughout CG, to collect long-term near-seabed light (irradiance), turbidity, temperature, salinity and pH data.

The volume of data generated through the in-situ data collection program provides an extremely high level of confidence in the numerical modelling results.

A previous report by PCS (2024a), titled 'System Understanding, Conceptual Model & Initial Modelling', was prepared, which provides a review and analysis of a wide range of pre-existing data relating to CG, new field data collected by BKA in CG from June 2023 to June 2024, the setup and results from initial numerical modelling and a system understanding and conceptual model of CG.

Two supplementary appendices to PCS (2024a) were also developed, these being PCS (2024b) titled 'Supplementary Technical Note' (which analyses additional filed data collected since PCS 2024a was drafted) and PCS (2024c) titled 'Factual Data Report' (which presents all data used for the study up to the end of June 2024, this has been updated to include all data up to 14th August 2024 in Annex B).

This current report (PCS, 2025a) should be read in light of the three previous reports (PCS, 2024a, b & c), as it is very much informed by them. This report provides additional analysis of the field data collected by BKA, including the additional data collected since June 2024 up to 14th August 2024 and presents results from the full numerical modelling to inform the three study objectives.

IMPORTANT NOTE ON OBJECTIVE 3

The WA EPA 2021 *Technical Guidance for EIA of Marine Dredging Proposals* requires prediction of potential impacts of sediment and turbidity plumes on benthic communities and habitats (BCH), including, if applicable, definition of Zones of High Impact (ZoHI), Zones of Moderate Impact (ZoMI) and Zones of Influence (ZoI), and likely 'worst-case' and 'best-case' impacts, as defined in the guidance.

However, as part of environmental assessment studies, Boskalis has undertaken comprehensive surveys of BCH in CG, including at King Shoals, and no potential sensitive BCH have been identified (see Referral Report 2 - *Setting & Existing Environment* (BKA, 2024d)). Due to extreme tidal currents (up to 4 knots on spring tides), constant seabed sediment suspension and naturally very high turbidity and lack of sunlight near the seabed, there appear to be no seagrass meadows, coral communities, sponge-beds, macro-algae communities or similar inter-tidal and sub-tidal benthic communities in CG.

Additionally, the nature of the proposed operation, using a Sand Production Vessel (SPV) similar to a Trailer Suction Hopper Dredge (TSHD), will not cause significant elevation of suspended sediments and turbidity above natural background levels. This is because the operation will only target sand and avoid areas of fine sediment, will not involve any dumping (the sand will be retained on the SPV and exported, with the SPV also being the export vessel), the SPV will only be on site for one or two days every two weeks each cycle (it will not be a continuous, turbidity-generating operation), and it will include best-practice turbidity control measures (e.g. 'green valve' on the SPV, water overflow discharge at keel etc).

Never-the-less, in order to address Objective 3, modelling of predicted plume dispersal and changes above natural background levels has been carried out. However, it has not been feasible or necessary to assess ZoHI, ZoMI and ZoI as defined in the EPA guidance, as there are no potentially sensitive benthic communities to model these zones and set biological response triggers for.

1.1. Overview of the Marine Sand Proposal

Boskalis Australia Pty Ltd (BKA) is assessing the feasibility of developing a marine sand sourcing and export operation in Cambridge Gulf (CG) near Wyndham in the northeast of Western Australia (WA) (Figure 1). The sand in CG is derived from natural terrestrial sources via river inputs.

The proposal is subject to the WA *Mining Act* including the comprehensive environmental assessment and management framework under that Act. BKA currently holds two exploration tenements in CG, E80/5655 (Block 4) and E80/6009 (Block 4A) (Figure 1). Based on sand distribution, the proposed operational area (POA) where BKA proposes to apply for a mining tenement is the western part of Block 4 and all of Block 4A (Figure 1). Key facts relating to the proposal are as follows.

a) Project lifespan: Up to 15 years from commencement of operations.

b) Zero coastal or land-based development: The proposal does not involve the construction and operation of any shore-based facilities and does not involve the alteration of the coastline in any way. It will be a 100% vessel-based operation.

c) Marine area: The POA is located in the central part of CG where there is a significant seabed sand resource, covering an area of ~100 km^2 as shown on Figure 1. The area of sand within the POA is estimated at 75.3 km^2. Water depths within the area average -25 m MSL (-21 m LAT). The seabed within and around the POA comprises highly-dynamic sand-waves with very little benthic biota and no significant benthic communities, due to the constantly moving substrate, strong tidal currents (>2 m/s), constantly high suspended sediments and permanent lack of benthic light.

d) Single vessel: The proposed operation will involve a Sand Production Vessel (SPV) based generally on the design of a large Trailer Suction Hopper Dredger (TSHD). Indicative specifications are Length Overall ~350 m, draft ~19 m and sand capacity 75,000 m^3 to 125,000 m^3.

e) Zero activity in CG for 86% of time: The SPV will self-load sand in CG for one to two days every two weeks. It will then sail to the sand delivery port in Asia and return two weeks later to repeat the cycle. This means that the SPV will only operate in CG for 52 days per year, or 14% of the time. There will be zero operational activity in CG for 86% of the time.

f) Sand volumes: Exploration surveys indicate a minimum of 300 million m^3 of sand in the POA and likely several times more. There are several orders of magnitude higher volumes of sand throughout CG overall. It is proposed to export up to 70 million m^3 of sand. This is a maximum of only 23% of the minimum volume of 300 million m^3 of sand estimated to occur in the POA, and a much smaller percentage of the volume of sand throughout CG overall.

g) Low footprint each loading cycle: During each one- to two-day sand loading cycle, the SPV will work over an area of ~0.5 km^2 within the POA, with a draghead width of ~6 m. The SPV will remove a layer of approximately 40 cm of sand from the seabed during each loading cycle.

h) End of project seabed condition: At the end of the 15-year project timeframe, if the proposed 70 million m^3 of sand is exported, the area within the POA will be on average <1m deeper than the pre-project seabed. It will still comprise sand with similar seabed morphology, dynamics and habitat features as before sand sourcing.

To support its feasibility assessment BKA has undertaken a wide range of studies since 2018. These studies find that the proposal is feasible and viable and unlikely to cause significant environmental impacts, as defined under the WA *Environmental Protection Act* (EP Act) and the Commonwealth *Environmental Protection & Biodiversity Conservation Act* (EPBC Act). Despite the low likelihood of significant impacts, as a responsible company with stringent environmental and social policies, BKA has self-referred the proposal under section 38 of the EP Act, and to the Commonwealth under Part 7 of the EPBC Act, for their determination of what further environmental assessments might be required, if any. This report has been developed by PCS for BKA as part of boarder set of referral reports.

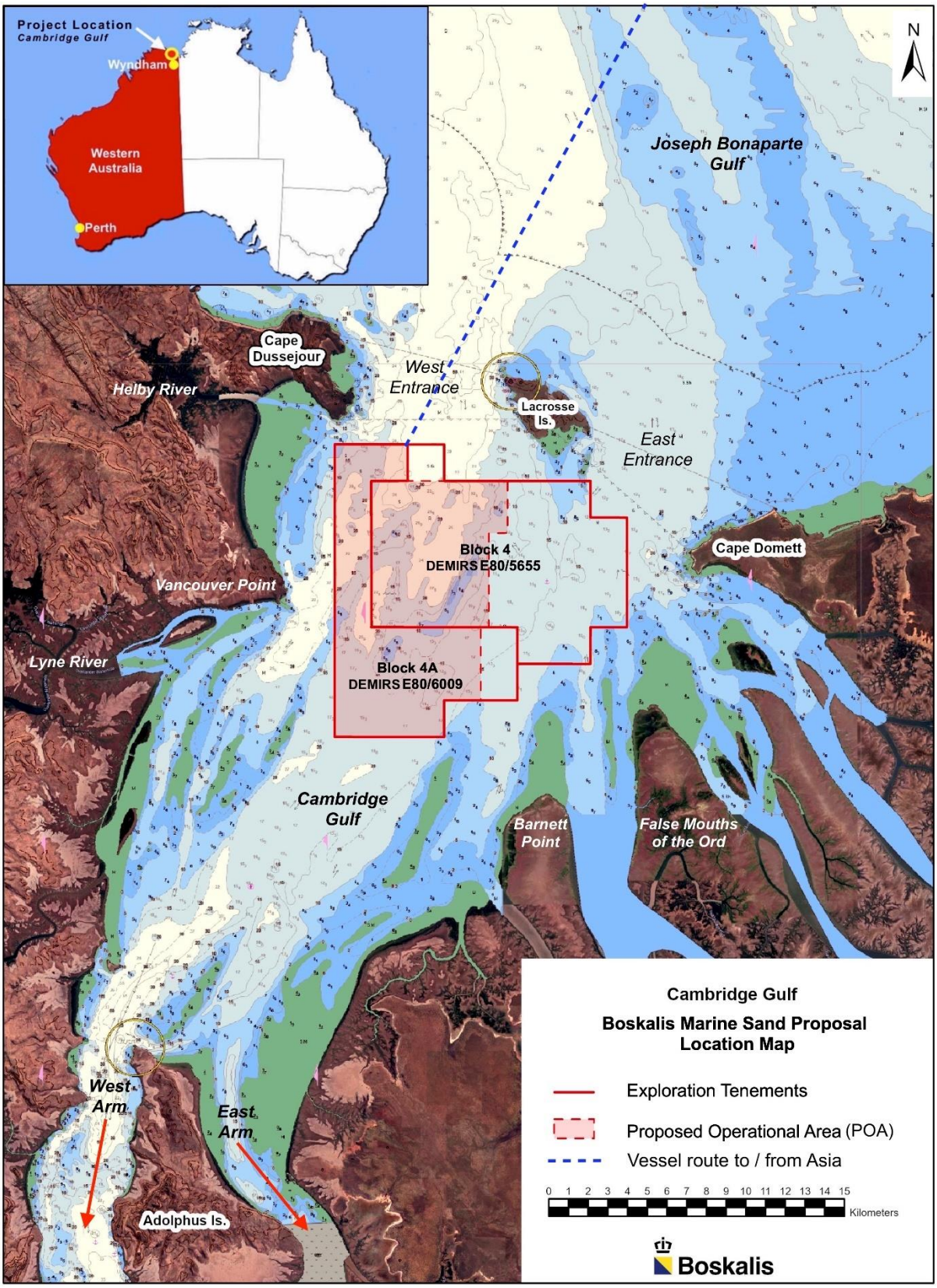


Figure 1. **Location of the proposal in Cambridge Gulf near Wyndham in the northeast of Western Australia.**

1.2. Overview of Cambridge Gulf & System Understanding

This section presents an overview of CG along with an updated system understanding of the CG region in terms of coastal processes and sediment transport (further to that presented in PCS (2024a)), based on information from the literature combined with data analysis and the results of the numerical modelling as presented in this report.

CG is a large, highly dynamic and highly turbid embayment located on the tropical northeast coast of WA, centred on 14° 52.00' S and 128° 16.00' E, facing northwards and seawards to the larger Joseph Bonaparte Gulf (JBG). Some of the main features are shown on Figures 1 and 2. The seaward mouth of CG is bounded to the west by Cape Dussejour and to the east by Cape Domett, with Lacrosse Island located centrally, dividing the mouth into a West Entrance and an East Entrance. Large sand banks at King Shoals and Medusa Bank are located outside CG in JBG offshore of Lacrosse Island. The main body of CG extends 40 km from its seaward mouth upstream to Adolphus Island, with the widest point being 20 km (Figure 2). Bathymetric data provided by Geoscience Australia (2023) show that depths through the main body of CG are deeper than -15 m LAT, with depths of more than -50 m LAT at the West Entrance and in the West Arm. Based on multibeam survey undertaken by BKA in February 2024 the average depth in the POA is approximately -21 m LAT.

To the east of Adolphus Island is East Arm of CG, which is the mouth of the Ord River. To the west of Adolphus Island is West Arm of CG, forming a channel between Adolphus Island and the west coast of CG, which extends southwards and widens towards the Port of Wyndham located ~ 40km to the south of Adolphus Island, as shown on Figure 3.

The marine environment of CG is macrotidal, with semi-diurnal tides with a spring tidal range of 8 m. Measured data and numerical modelling results have shown that the large tidal range in CG results in high tidal current speeds, with up to 2.9 m/s or 5.6 knots measured at the northern entrance to West Arm. The strong currents in turn result in regular sediment suspension and transport and naturally very high SSC and turbidity, with 99th percentile values of 1,057 mg/L and 470 NTU respectively in CG overall. Net tidal currents in CG have been shown to typically be in a northerly direction, indicating an ebb dominance. Current speeds are higher in West Entrance to CG compared to the East Entrance. The large tidal range is likely to have been the dominant process in the formation of CG in its current form (Thom *et al.*, 1975).

The region experiences significant seasonal variability in the wind, wave and rainfall conditions. The wind and wave conditions are typically from the northwest to north from December to April (wet season), from north to east between April and September (dry season) and from the northwest to northeast from September to December (transitional season).

The wave conditions directly offshore from CG are relatively calm, with the shallow King Shoals and Medusa Bank acting to limit the wave height which can reach the entrance to CG and the adjacent seaward beaches to the west and east. There is a strong seasonal variability in wave conditions in the region, with larger wave events predominantly from the west-northwest occurring during the wet season and calmer wave conditions from the northeastern quadrant occurring during the dry season. The wave conditions result in a combination of cross-shore and longshore transport influencing the beaches adjacent to the entrance to CG. Modelling has shown that at most of the beach profiles, sand is transported onshore to the beaches through cross-shore transport and then transported alongshore in the intertidal area.

Waves within CG are further sheltered by the presence of Lacrosse Island in the middle of the entrance to CG, resulting in variable wave exposure in CG depending on the offshore wave direction. The influence of wave action in CG on sediment transport processes is limited to very large wave events during the wet season (e.g. during tropical cyclones and tropical lows). These wave events can result in erosion of areas of mudflats and mangroves and also in the formation and landward migration of features such as stranded beach ridges. The influence of waves on sediment transport within the POA will be small compared to the influence of tidal currents. Waves with an H_s of more than 1 m were calculated to occur for less than 1% of the time in the POA. Based on an average water depth of 20 m in the area, the peak near bed velocities of a wave with an H_s of 1 m (and corresponding typical peak wave period of 6 s) based on the linear wave theory would be 0.3 m/s (van Rijn, 1993). This is almost three times lower than the measured peak near-bed spring tidal current speeds in the area (around 0.8 m/s).

The region is semi-arid, with annual rainfall in the region of 500 mm, mainly occurring in the wet season. Multiple rivers flow into CG, including the Ord River, Pentecost River, Durack River, King River and the Forrest River (Thom *et al.*, 1975; Wolanski *et al.*, 2001) (Figure 3). High river flows only occur

occasionally and only during the wet season. The wet season river discharge has been noted to have considerable inter-annual variability, with order of magnitude variations from year to year. There is also significant daily variability in river flows during flood events, with very high flows following a tropical cyclone only lasting a few days (Wolanksi *et al.*, 2001).

As outlined above at the upstream (southern) end of the main body of CG, there are two arms either side of Adolphus Island, the West and East Arms. The Pentecost, Forrest, King and Durack Rivers drain into West Arm, while the Ord River drains into East Arm, as shown on Figure 3. The total catchment area for CG is approximately 87,000 km^2 and 62% of this area is the Ord River catchment, while the catchments for the Pentecost and Durack Rivers combined represent approximately 27% (the remaining 11% is made up of smaller rivers and creeks and coastal areas) (dataWA, 2023). There are also three small rivers on the west coast of the main body of CG, from north to south; the Helby, Lyne and Thompson Rivers, as shown on Figures 1 and 2. These are all highly estuarine and are lined with mangroves well into their upper-most reaches.

The catchments for all of the rivers except the Ord are not dammed and the land remains largely uncleared. In contrast, the catchment for the Ord River has been subject to extensive land clearing for cattle and irrigated agriculture, and it also has two dams, the lower Kununurra Diversion Dam (referred to as the Lower Ord Dam) and the upper Ord River Dam (referred to as the Ord River Dam), built to develop the Ord River Irrigation Scheme. The Ord River dam is the largest of these and it created Lake Argyle which is the largest artificial lake in the southern hemisphere. The extensive land clearing for cattle commenced around the start of the 20th Century, while the dams were constructed between 1969 and 1972 (Wolanski *et al.*, 2001). The Ord River flows were noted to have experienced significant variability in discharge prior to the construction of the dams, but since the construction the river discharge is now almost constant. The seasonal variability and large floods still occur in the other rivers that flow into CG (Wolanksi *et al.*, 2001).

The rivers that drain into CG all discharge sediment into the Gulf. Over time, this has resulted in the formation of multiple small deltas and tidal flats, with these Quaternary deposits alternating with ancient rock outcrops (Wright *et al.*, 1973). The supply of sediment from the rivers to CG will vary significantly due to the high variability in the river discharge. Peaks in sediment supply from the rivers will occur in the wet season, with limited supply of sediment during the dry season. The rivers supply a mixture of sand-sized sediment and fine-grained silt and clay. It is likely that the relative contribution of sand and fine-grained sediment supplied by the rivers varies depending on the river discharge, with lower discharge events likely to supply a higher proportion of fine-grained sediment while higher discharge events have the potential to supply a higher proportion of sand.

Sediment present within CG will be subject to regular reworking by the strong tidal currents that occur in the region, resulting in well-sorted sandy sediment being present where stronger currents occur. Sediment sampling results have shown that there is an abundance of sediment available for transport within CG, with a combination of sand, silt and clay all present in CG and an estimated minimum of 300 million m^3 of sand present in the POA (and likely orders of magnitude more than this within the entire CG and King Shoals) (BKA 2024b - Annex 1: Sand Assessment Report). Since the damming of the Ord River significant sedimentation of East Arm of the CG (which is downstream of the dam) has been observed, with average siltation depths of 3 m (Wolanski *et al.*, 2004).

There is significant variability in the sediment transport which occurs in the region, with the tide being the dominant process which influences sediment transport in CG. Measured data have shown that the sediment which is regularly transported in suspension is predominantly made up of fine-grained silt and clay, with some very fine sand also present, while the coarser sand is predominantly transported as bedload (PCS 2024a). The sediment transport varies between the flood and ebb stages of the tide and between spring and neap tides. Relatively low SSC and transport rates only occur for short durations on small neap tides, while higher SSC and transport rates occur more often due to the larger neap and spring tides which regularly influence CG. The measured data showed peaks in SSC typically on the ebb tide and at low water, indicating a net export of fine-grained silt and clay from CG, while changes in bedforms present in CG also showed a dominant net export of sand from CG.

Water quality monitoring and results from numerical modelling have shown that SSC within CG is typically higher during the wet season compared to the dry season. Due to the regular high SSC in the region, the benthic light availability is zero to very low throughout CG. The only sites where regular benthic light was measured were in water depths of less than 15 m (relative to mean sea level (MSL), equivalent to -11 m LAT) and the benthic light was only measured during neap tides when the turbidity was typically less than 10 NTU.

Results from numerical modelling indicate that the construction of the Ord River Dam, which suppressed the wet season flood flows in the Ord River, resulted in a significant reduction in the peak SSC which can occur in CG during the wet season. Wolanski *et al.* (2004) previously estimated that since

completion of the Ord River Dam, the majority of the sediment transported downstream along West Arm was subsequently imported into East Arm, with almost no fine-grained sediment being transported into CG from either West or East Arm. However, data measured at the northern entrance to West Arm as part of this project consistently showed higher turbidity at this location compared to the sites within CG itself and also showed elevated turbidity following a large river discharge event. In addition, satellite-derived SSC data presented by PCS (2024a) consistently showed high SSC in both West and East Arms, which extended into the southern half of the open bay area of CG, indicating an ongoing supply of suspended sediment from West Arm.

Therefore, it can be concluded that although sedimentation has occurred in East Arm following construction of the Ord River dam, fine-grained sediment from West and East Arms is still being transported into CG and providing an ongoing supply of fine-grained sediment for the mudflats and mangroves in the region.

Sediment sampling undertaken as part of the project has also shown that the sediment in both West and East Arms is predominantly sand with high percentages of quartz and feldspar which are also the dominant elements in the sand present in the POA (PCS 2024a). It is therefore likely that there is an ongoing supply of sand to CG from the West and East Arms, although the supply from East Arm will be significantly lower compared to prior to the construction of the Ord River dam.

The modelling results presented in this report are designed to assist in assessing potential impacts of the proposed sand sourcing operation on the main coastal and marine environmental resources and values of the CG area, so it is important to consider what these are. The main coastal and marine environmental resources and values of the CG area that are influenced by hydrodynamics, sediment transport and coastal processes are shown on Figure 2 and include the following.

- **The King Shoals Sanctuary Zone of the State North Kimberley Marine Park:** This comprises three large sand banks located offshore from the West Entrance of CG. Comprehensive benthic surveys at King Shoals in both the dry- and wet seasons found very little benthic biota and no significant benthic communities, the seabed mainly comprised highly dynamic sand-substrate (BKA 2024b).

- **Benthic biota and communities:** Very little benthic biota and no significant sub-tidal benthic communities have been found throughout CG during extensive dry- and wet season benthic surveys (BKA 2024b). The low benthic light, strong tidal currents and dynamic seabed sediment are expected to be the major inhibitors on benthic biota. The surveys indicate that there are no seagrass meadows, coral communities, sponge-beds, macro-algae communities or similar intertidal and subtidal benthic communities in CG or at King Shoals. The main benthic community in CG is mangroves, as outlined below.

- **Mangrove communities:** The main intertidal benthic community in CG is the relatively narrow band of mangroves along most of the coast, especially on the eastern side, which is part of the Ord River Floodplain Ramsar site (see below), backed by intertidal salt flats and mudflats (BKA 2024b). Evidence of mangrove destruction and coastal erosion was observed within CG during BKA's July-August 2023 and February 2024 environmental surveys, assumed to have been caused by a large wave event, storm surge and high winds, probably during a tropical cyclone (TC) (PCS, 2024a) (BKA 2024b). The last tropical cyclone to pass over or near CG was TC Ellie in December 2022.

- **False Mouths of the Ord / Ord River Floodplain Ramsar site:** The False Mouths of the Ord comprise a series of very large tidal inlets located on the eastern side of the main body of CG. They form part of the Ord River Floodplain Ramsar site, which is protected as the State-designated Ord River Nature Reserve. The main ecological community in this area is a relatively narrow band of mangroves backed by intertidal salt flats and mudflats, as described for CG overall above.

- **Flatback Turtle Nesting Beaches:** There is a globally important nesting beach for Flat Back Turtles *(Natator depressus)* on the seaward side of Cape Domett (Cape Domett Seward Beach), and three other turtle nesting beaches with lesser numbers at Turtle Beach West (west of Cape Dussejour), Turtle Bay at Lacrosse Island and Barnett Point inside CG, south east of the POA (BKA, 2024b) (Figure 2). The beach at Barnett Point comprises stranded sand ridges (cheniers) located behind a mangrove fringe. Assessment by PCS (2024a) found that Turtle Beach West and Cape Domett Seaward Beach have advanced slightly over the last 30 years, while the beach at Turtle Bay on Lacrosse Island was shown to have remained stable over the period. This suggests that any changes to the sediment transport processes in CG that may have been caused by the Ord River dam have not reduced the supply of sand to these beaches. The western and eastern ends of the beach ridge at Barnett Point was shown to have historically

migrated landward over the last thirty years. This is a common response of stranded beach ridges as a result of the limited supply of sand due to their location perched on top of mudflats.

A conceptual sediment transport and coastal processes system understanding for CG, which summarises the text detailed in this section, is shown in Figure 4.

1.3. Report Structure

The report herein is set out as follows:

- an introduction to the study is provided in **Section 1**;
- analysis of relevant data is presented in **Section 2**;
- the modelling approach, setups and calibration and validation are detailed in **Section 3**;
- results from the hydrodynamic and wave modelling are included in **Section 4**;
- results from the sediment transport and beach processes modelling are provided in **Section 5**;
- results from the plume modelling are detailed in **Section 6**; and
- details of how the study addresses each project objective and relevant EPA guidelines is provided in **Section 7**.

The following conventions have been adopted throughout:

- volumes are in-situ cubic metres;
- depths are provided relative to Australian Height Datum (AHD) unless stated otherwise;
- current directions are quoted as directions to; and
- wave and wind directions are quoted as directions from.

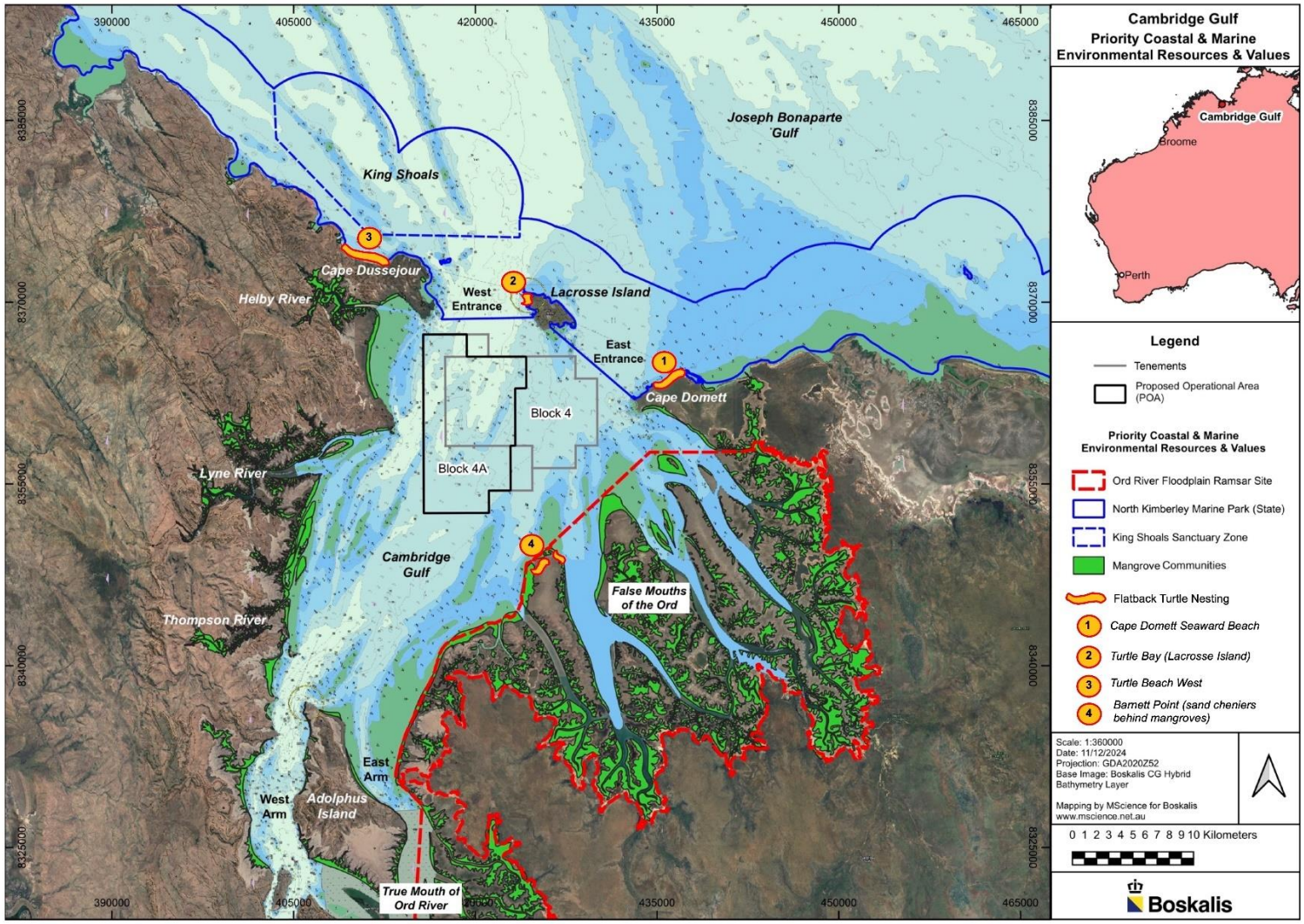


Figure 2. **The most significant coastal ecosystems and values in CG that are formed and influenced by hydrodynamics and coastal processes comprise the King Shoals offshore West Entrance, the mangroves around the coast of CG marked in bright green, including the mangrove-lined inlets in the Ord River Floodplain Ramsar Wetland on the eastern side of CG; and the four Flatback Turtle nesting sites marked in orange.**

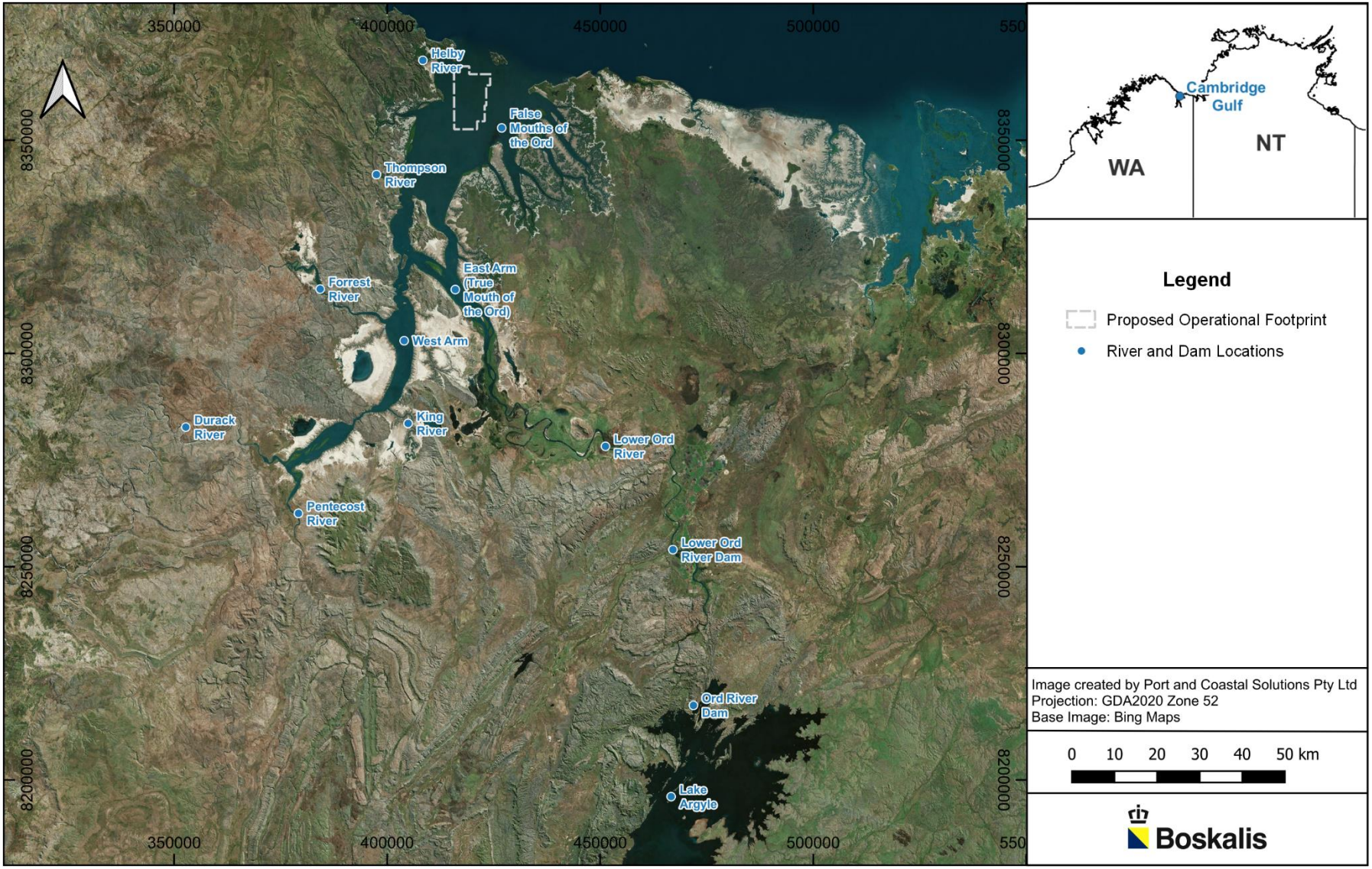


Figure 3. **Location to of rivers and dams that influence CG along with West Arm and East Arm.**

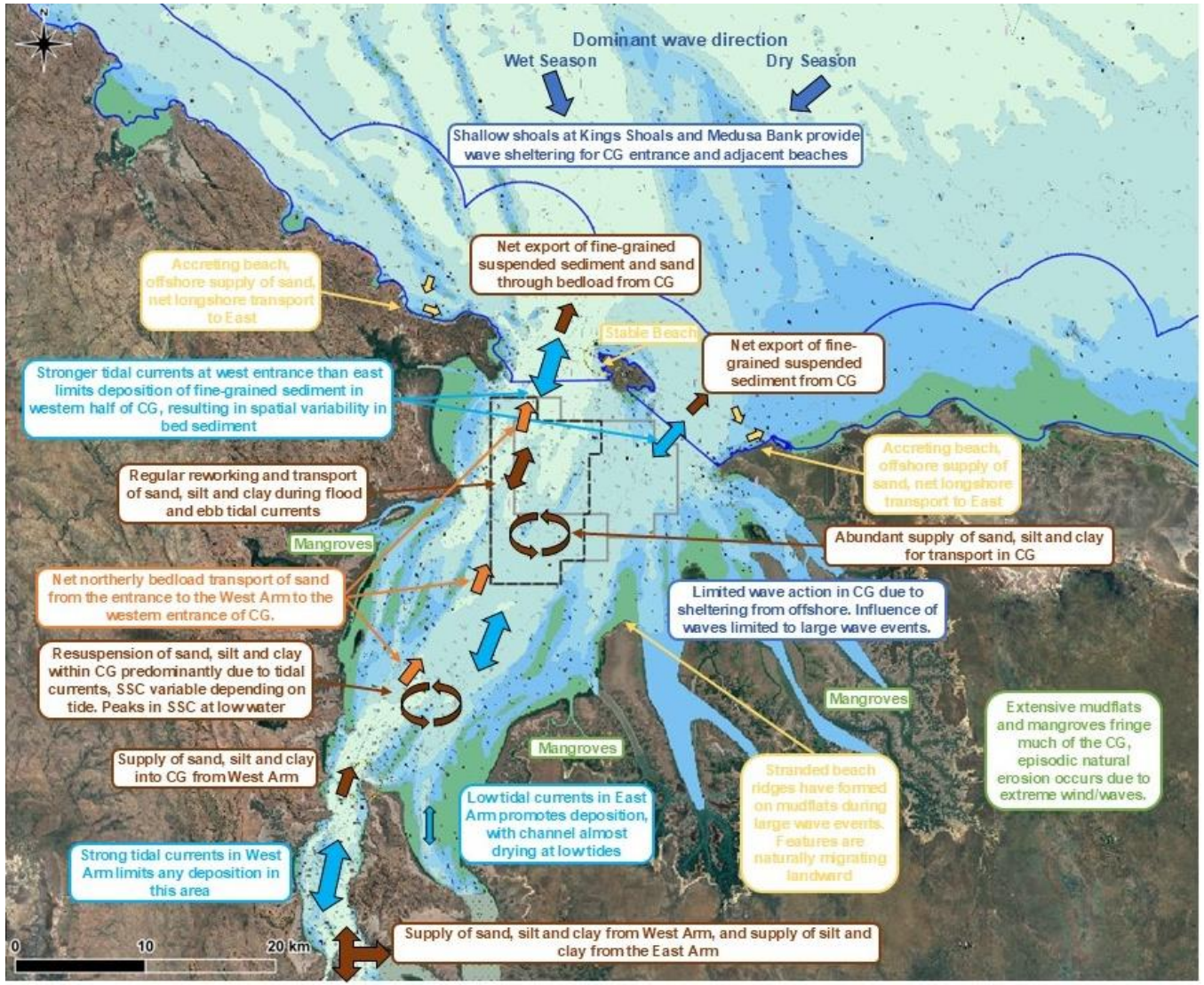


Figure 4. **Updated conceptual sediment transport and coastal processes system understanding for the CG.** *Note: text and arrows in dark blue relate to waves, pale blue relates to tidal currents, brown relates to suspended sediment transport, orange relates to bedload transport, yellow relates to beach changes and local sand supply and green relates to mangroves.*

2. DATA ANALYSIS

As outlined in Section 1, this study is supported by an unprecedented volume of field data, including data sourced from previous studies in CG and new data collected by BKA since June 2023. The volume of data obtained from existing sources and generated through BKA's in-situ data collection program provides for comprehensive process understanding and numerical model calibration and validation, which in turn supports an extremely high level of confidence in the numerical modelling results.

A previous report by PCS (2024a), titled 'Referral Report No. 5 - *System Understanding, Conceptual Model & Initial Modelling'*, was prepared, which provides a review and analysis of a wide range of pre-existing data relating to CG, new field data collected by BKA in CG from June 2023 to June 2024, the setup and results from initial numerical modelling and a system understanding and conceptual model of CG.

Two supplementary appendices to PCS (2024a) were also developed, these being PCS (2024b) titled *Supplementary Technical Note* (which analyses additional field data collected since PCS (2024a) was drafted), and PCS (2024c) titled *Factual Data Report* (which presents all data used for the study up to the 21st June 2024).

This current report (PCS, 2025a) should be read in light of the three previous reports (PCS 2024a, b & c), as it is very much informed by them. This report provides additional analysis of the field data collected by BKA, to support the full numerical modelling to inform the three study objectives.

The data analysed in this section were collected from June 2023 to 14th August 2024. The data analysed in this section are from in-situ, seabed-mounted sensors and loggers deployed by BKA at 14 sites in the CG region (Figure 5).

At the 11 sites marked 'AWAC' on Figure 5 (AWAC-01 to AWAC-11) the seabed frames included an Acoustic Wave & Current Profiler (AWAC) or another type of Acoustic Doppler Current Profiler (ADCP) (an AWAC is a type of ADCP), to measure current speed and direction, water level and waves. Depending on the site and the deployment, some of the AWAC sites also had a co-mounted light meter and/or a multi-sonde for turbidity, temperature, salinity and pH.

At the four sites marked 'Pos' on Figure 5 (Pos 12 to Pos 15) the seabed frames did not have an AWAC or ADCP and were fitted with a light meter and a multi-sonde for turbidity, temperature, salinity and pH. It should be noted that sites AWAC 09 and Pos 12 are the same site, as shown on Figure 5, and both an AWAC frame and a separate non-AWAC frame were deployed at this site, but for different periods.

Table 1 lists the types of equipment, data collected and deployment periods for each site. Figure 6 shows an example of the AWAC frames and Figure 7 an example of the non-AWAC frames at the Pos sites as deployed in CG.

An update to the Factual Data Report (PCS, 2024c) including all data analysed in this report (up to 14th August 2024) is submitted in support of this report and included in Annex B.

Table 1. BKA CG in-situ data collection program - types of equipment, data collected and deployment periods for each site.

Site	Location		Time Coverage			Data Collection	
	Longitude [deg]	Latitude [deg]	Start	End	Time period [days]	Equipment	Data Collected
AWAC-01	128.268	-14.807	09/06/2023[1] 03/03/2024 29/06/2024	21/07/2023[1] 08/05/2024 09/08/2024	41.7 66.2 41.1	Nortek AWAC/Signature 500 LI-COR LI-1500 light sensor/Odyssey Xtreem Logger Manta/WiMo multi-sonde probe	Hydrodynamics/Waves Benthic Light Temperature, salinity, pressure, turbidity
AWAC-02	128.300	-14.788	07/09/2023	08/09/2023	1.2	Nortek Signature 1000 LI-COR LI-1500 light sensor Manta multi-sonde probe	Hydrodynamics/Waves Benthic Light Temperature, salinity, pressure, turbidity
AWAC-03	128.277	-14.848	13/10/2023	15/10/2023	1.9	Nortek Signature 1000 LI-COR LI-1500 light sensor Manta multi-sonde probe[2]	Hydrodynamics/Waves Benthic Light Temperature, salinity, pressure, turbidity
AWAC-04	128.225	-14.812	07/09/2023	08/09/2023	0.8	Nortek AWAC LI-COR LI-1500 light sensor	Hydrodynamics Benthic Light
AWAC-05	128.224	-14.756	20/06/2024	12/08/2024	53.0	Nortek Signature 500 Odyssey Logger WiMo multi-sonde probe	Hydrodynamics/Waves Benthic Light Temperature, salinity, pressure, turbidity
AWAC-06	128.348	-14.789	08/09/2023 06/03/2024	13/10/2023 10/05/2024	35.1 64.6	Nortek Signature 1000 LI-COR LI-1500 light sensor WiMo multi-sonde probe	Hydrodynamics/Waves Benthic Light Temperature, salinity, pressure, turbidity
AWAC-07	128.332	-14.914	15/10/2023 10/05/2024	05/03/2024 25/06/2024[2]	142.0 45.9	Nortek Signature 1000 LI-COR LI-1500 light sensor Manta multi-sonde probe[3]	Hydrodynamics/Waves Benthic Light Temperature, salinity, pressure, turbidity
AWAC-08	128.109	-15.044	02/03/2024	18/06/2024	108.3	Nortek AWAC LI-COR LI-1500 light sensor WiMo multi-sonde probe	Hydrodynamics/Waves Benthic Light Temperature, salinity, pressure, turbidity
AWAC-09	128.176	-14.853	04/03/2024	21/06/2024	109.2	Nortek Signature 500 Odyssey Logger WiMo multi-sonde probe	Hydrodynamics/Waves Benthic Light Temperature, salinity, pressure, turbidity
AWAC-10	128.363	-14.734	26/06/2024	13/08/2024	48.3	Nortek Signature 1000 Odyssey Logger Manta multi-sonde probe	Hydrodynamics/Waves Benthic Light Temperature, salinity, pressure, turbidity
AWAC-11	128.214	-14.914	02/03/2024 10/05/2024 24/06/2024	08/05/2024 23/06/2024 11/08/2024	66.8 43.9 48.0	Nortek Signature 500 LI-COR LI-1500 light sensor/Odyssey Xtreem Logger Manta/WiMo multi-sonde probe	Hydrodynamics/Waves Benthic Light Temperature, salinity, pressure, turbidity
Pos-12 (same location as AWAC-09)	128.224	-14.662	04/03/2024 28/06/2024	21/06/2024 14/08/2024	109.3 47.1	LI-COR LI-1500 light sensor/Odyssey Xtreem Logger WiMo multi-sonde probe	Benthic Light Temperature, salinity, pressure, turbidity
Pos-13	128.176	-14.853	03/03/2024 23/06/2024	12/05/2024 12/08/2024	69.9 49.9	LI-COR LI-1500 light sensor/Odyssey Xtreem Logger WiMo multi-sonde probe	Benthic Light Temperature, salinity, pressure, turbidity

Site	Location		Time Coverage			Data Collection	
	Longitude [deg]	Latitude [deg]	Start	End	Time period [days]	Equipment	Data Collected
Pos-14	128.311	-14.772	03/03/2024 21/06/2024	20/06/2024 10/08/2024	109.4 50.0	LI-COR LI-1500 light sensor/Odyssey Xtreem Logger WiMo multi-sonde probe	Benthic Light Temperature, salinity, pressure, turbidity
Pos-15	128.364	-14.826	04/03/2024 27/06/2024	26/06/2024 11/08/2024	114.0 44.7	Odyssey Xtreem Logger WiMo multi-sonde probe	Benthic Light Temperature, salinity, pressure, turbidity

[1] *only the Nortek AWAC was deployed for the June to July 2023 deployment.*
[2] *due to an issue with the logger no turbidity data were measured.*
[3] *due to an issue with the logger no turbidity data were measured during the October 2023 to March 2024 deployment.*

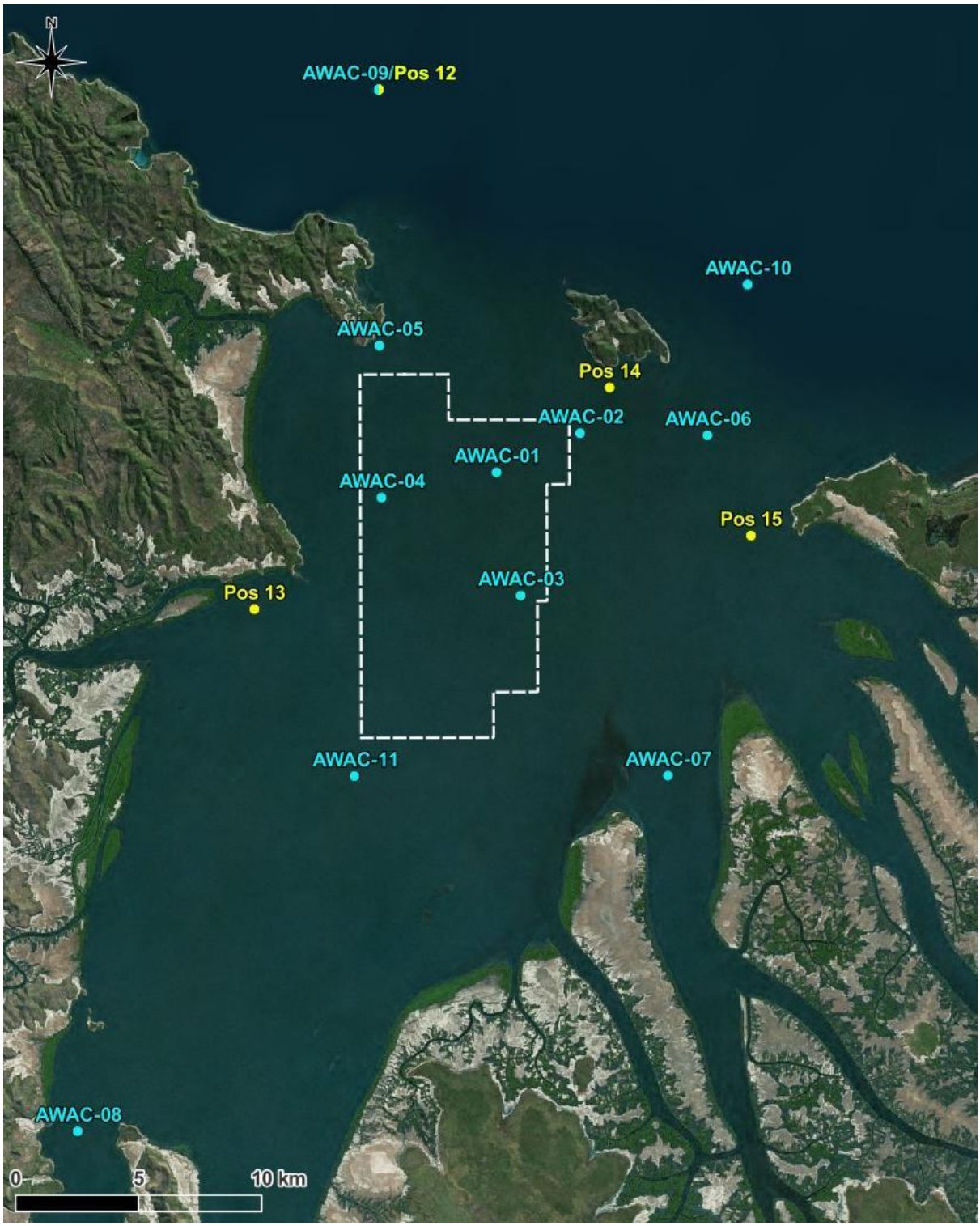


Figure 5. **Sites where BKA have deployed self-logging instruments and measured hydrodynamics and waves (blue sites) and water quality parameters (all sites) along with the POA (white dashed lines).**

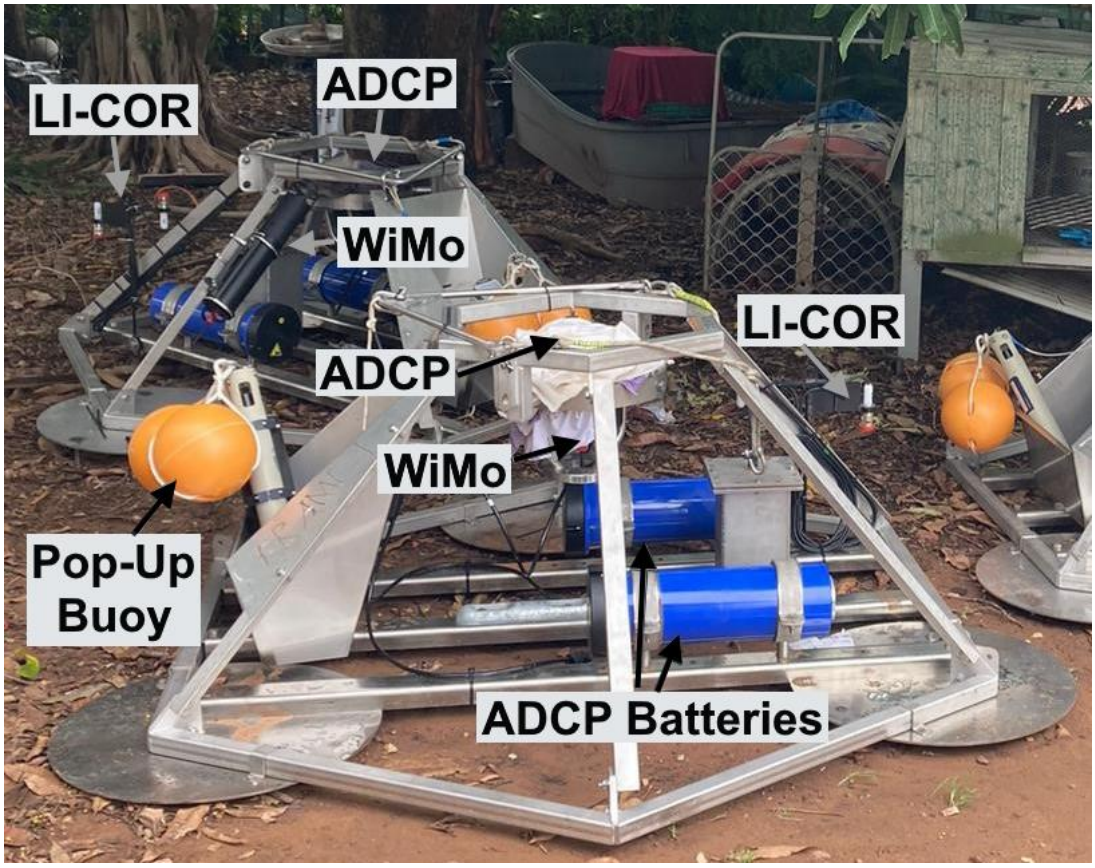


Figure 6. Annotated photograph of the instruments attached to a frame at the AWAC sites.

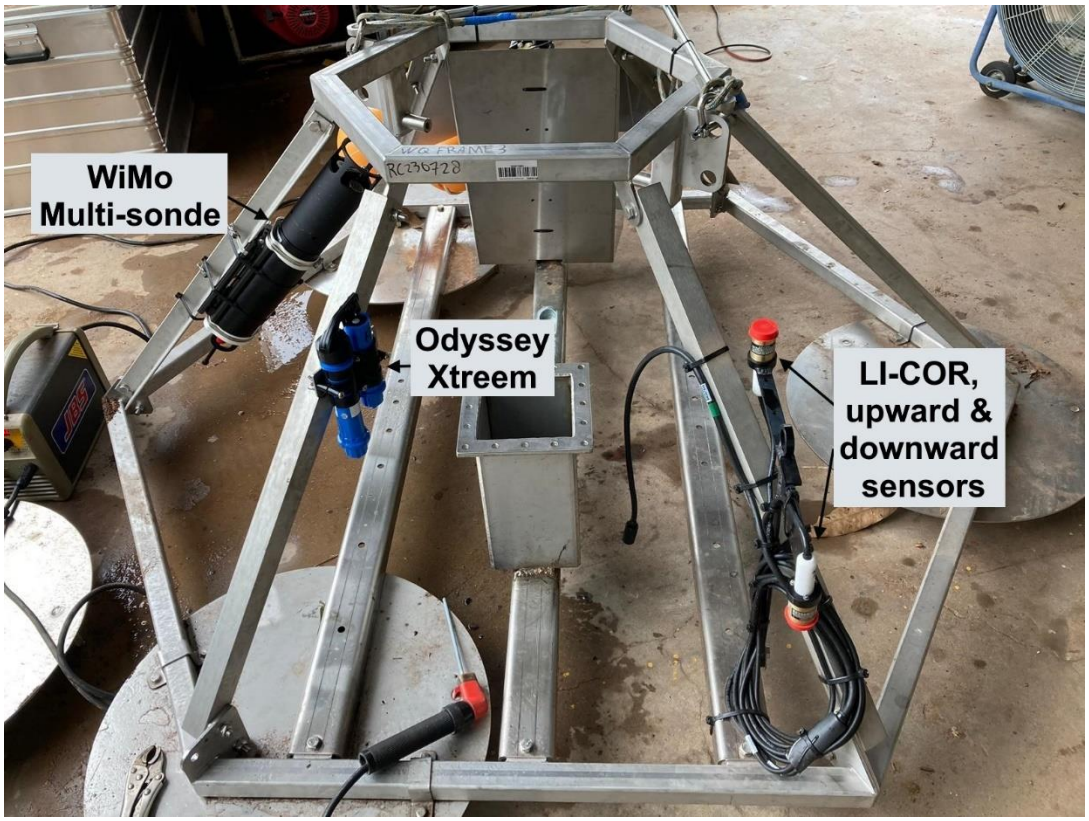


Figure 7. Annotated photograph of the instruments attached to a frame at the Pos sites.

2.1. Hydrodynamics

Analysis of measured water level and current data collected by the AWACs/ADCPs is presented in the following sections.

2.1.1. Water Levels

To better understand the water levels in CG and how they are influenced by different drivers including tides, wind, waves, atmospheric pressure and river discharge, measured water level data collected at two selected AWAC sites were analysed using the Danish Hydraulic Institute (DHI) Tide Analysis Toolbox. Data from the two AWAC sites within and close to the POA with the longest duration measured data have been analysed for water level, rather than combine data from all 11 AWAC sites, as the constituents will be slightly different at different sites. The following water level data were analysed for the two key sites:

- Proposed operational area (POA) (AWAC-01): Measured water level data were available from two separate deployments, from 03/03/2024 to 08/05/2024 (66 days) and from 29/06/24 to 09/08/24 (41 days). This site was selected as it is representative of water levels in the POA and it is the closest monitoring site within CG to where the Australian Hydrographic Office's (AHO) Cape Domett tide gauge was located over 116 days in 1972 (AHO, 2023) (close to Pos-15 in Figure 5), with both wet and dry season data available.

- False Mouths of the Ord (AWAC-07): Measured water level data were available from a single deployment from 15/10/2023 to 05/03/2024 (142 days). This site was selected as it represents the longest single measured water level dataset available, and it is also one of the closest monitoring sites to where the Cape Domett tide gauge referenced above was located. The False Mouths of the Ord are also a high priority area for protection as they are part of the Ord River Floodplain Ramsar wetland (Figure 2).

A harmonic analysis of the measured water level data at these two sites was undertaken, with the outputs being the predicted and residual water levels along with the calculated tidal constituents. Residual water levels are the contribution to the measured water level by drivers other than the astronomical tide and it is useful to understand these in order to determine the relative influence of these drivers along with the astronomical tide in influencing hydrodynamic conditions in the region.

To help understand the longer-term trends in residual water levels, a daily moving mean was applied to the residual water level and is presented along with the residual water level. The measured, predicted and residual water levels at AWAC-01 over the wet and dry season periods and at AWAC-07 over the transitional and wet seasons, along with the hindcast modelled wind within CG, the hindcast modelled offshore significant wave height (H_s) in JBG and the measured river discharge are shown in Figure 8 to Figure 10. The plots show the following:

- Larger residuals occurred in the wet season compared to the dry season. In the wet season the semi-diurnal residual fluctuations were ± 0.8 m while during the dry season they were ± 0.2 m. The daily moving mean residual provides a good indication of the long-term trend in residual water level, with values ranging from ± 0.25 m in the wet season to ± 0.1 m in the dry season.

- In the wet season there are clear peaks and troughs in the residual water level, while in the dry season the changes are relatively small.

- During both seasons there is no clear correlation between the calculated residual water level and the potential drivers. An additional check on the measured atmospheric pressure at the Bureau of Meteorology (BoM) Wyndham Weather Station was also undertaken. This did not show any significant changes during either of the periods and so the residual was not due to a change in atmospheric pressure in the region. This indicates that residual water levels in the region are typically small compared to the astronomical tide.

- During both the wet and dry seasons there are residuals with a semi-diurnal signal present, this suggests that some of the constituents are not fully represented (some require up to 18.6 years of measured data to accurately represent). However, the data are suitable to indicate the relative magnitude of the residuals which are relevant to this proposal.

The tidal constituents calculated as part of the analysis were used to estimate tidal planes at the two stations. The planes for Mean High Water Springs (MHWS), Mean High Water Neaps (MHWN), Mean Sea Level (MSL), Mean Low Water Neaps (MLWN) and Mean Low Water Springs (MLWS) were all calculated based on the derived constituents and the approach detailed by AHO (2024). To calculate

the Lowest Astronomical Tide (LAT) the tidal constituents were used to predict water levels at both sites over the 20-year Tidal Datum Epoch from 1992 to 2011 (inclusive) as detailed by MSQ (2024), and LAT was taken as the lowest predicted water level over this period.

The calculated tidal planes at AWAC-01 and AWAC-07 are shown along with the tidal planes for Cape Domett defined by AHO in Table 2. The tidal planes are shown relative to the existing LAT reported at Cape Domett, which is 7.628 m below the Cape Domett BM1972 (AHO, 2023). Australian Height Datum (AHD) is reported to be 3.508 m below the Cape Domett BM1972 (AHO, 2023). The table shows that the elevation of LAT based on the data measured as part of this project is calculated to be 0.09 to 0.13 m higher than the LAT reported by AHO at Cape Domett. This could be due to differences in how LAT was calculated or differences in the tidal conditions (and therefore constituents represented) captured by the measurements.

The other AHO reported tidal planes agree well with the values derived from AWAC-01 and AWAC-07, with MLWS and MHWS being within 0.01 m. For neap tides (i.e. MLWN and MHWN) the planes based on data measured at AWAC-01 underestimate the tidal range, while the planes based on data measured at AWAC-07 overestimate the tidal range relative to the AHO tidal planes at Cape Domett. Given the relative difference in neap tidal levels between AWAC-01 and AWAC-07 this is likely to be due to differences in the tidal conditions (and therefore constituents represented) captured by the measurements (with AWAC-07 measuring transitional and wet season conditions and AWAC-01 measuring predominantly dry season conditions). The similarity of the tidal plane values at the AHO and two BKA sites suggests that the AHO tidal planes at Cape Domett are likley to be representative for the area and that the conversion between MSL and AHD at Cape Domett is still applicable.

In summary, the implications of these findings for the proposed operation and for the numerical modelling are:

- The astronomical tide is the dominant driver for water levels in CG, with residual water levels from other drivers only resulting in small variations in longer-term water levels and with none of these variations clearly corresponding to a specific driver. This shows that the modelling should not focus on accurately representing residual water levels resulting from specific drivers. This was addressed in the model (see Section 3.4).
- Comparison between the tidal planes derived at Cape Domett by the AHO and tidal planes based on measured data collected by BKA indicates that the tidal planes at Cape Domett can be considered to be representative for the area and that the conversion between MSL and AHD at Cape Domett is unlikely to have changed significantly. Based on this, AHD can be considered to be approximately 0.07 m lower than MSL in the region.

Table 2. Comparison between the reported AHO tidal planes at Cape Domett and tidal planes calculated based on measured water level data at AWAC-01 and AWAC-07.

Tidal Plane	AHO Cape Domett (m LAT)*	AWAC-01 (m LAT)	AWAC-07 (m LAT)
MHWS	6.90	6.90	6.89
MHWN	5.20	5.09	5.24
MSL	4.19	4.19	4.19
AHD	4.12	4.12	4.12
MLWN	3.20	3.29	3.15
MLWS	1.50	1.49	1.50
LAT	0.00	0.13	0.09

**The AHO Cape Domett data are sourced from AHO (2023).*

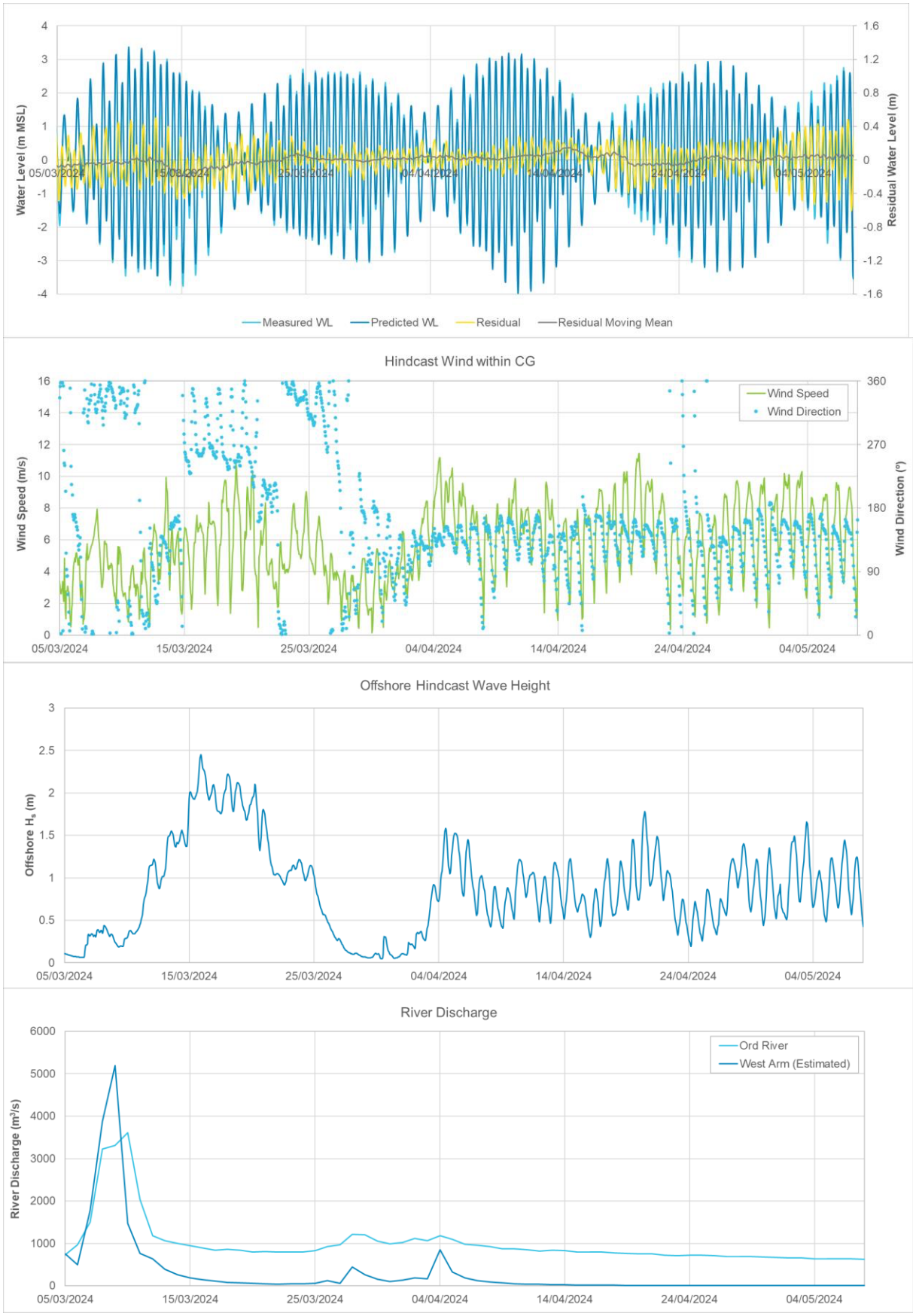


Figure 8. Water level residual in the POA (AWAC-01) (top) along with hindcast modelled wind (second from top), hindcast modelled offshore H_s and measured river discharge from March to May 2024.

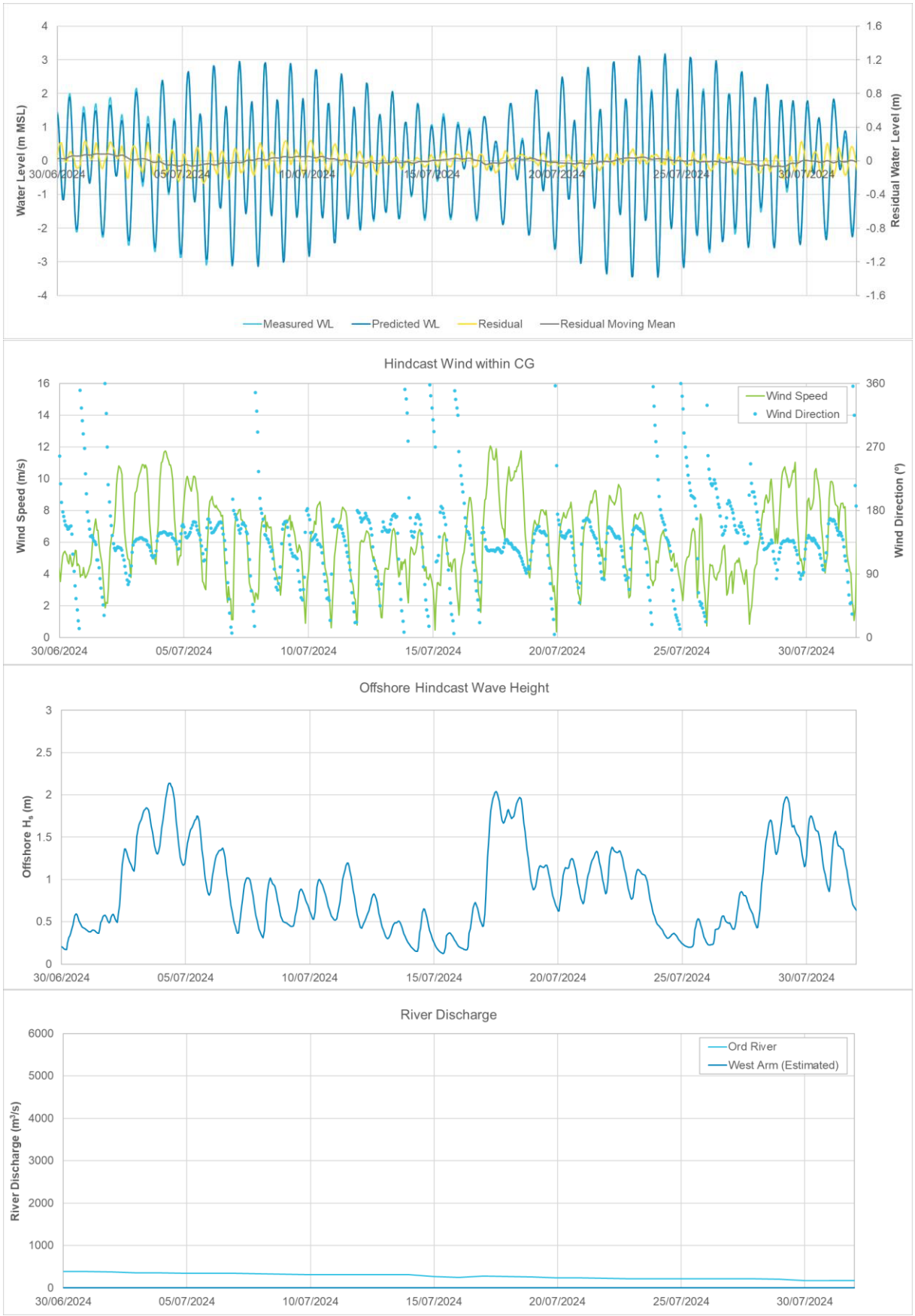


Figure 9. **Water level residual in the POA (AWAC-01) (top) along with hindcast modelled wind (second from top), hindcast modelled offshore H_s and measured river discharge in June and July 2024.**

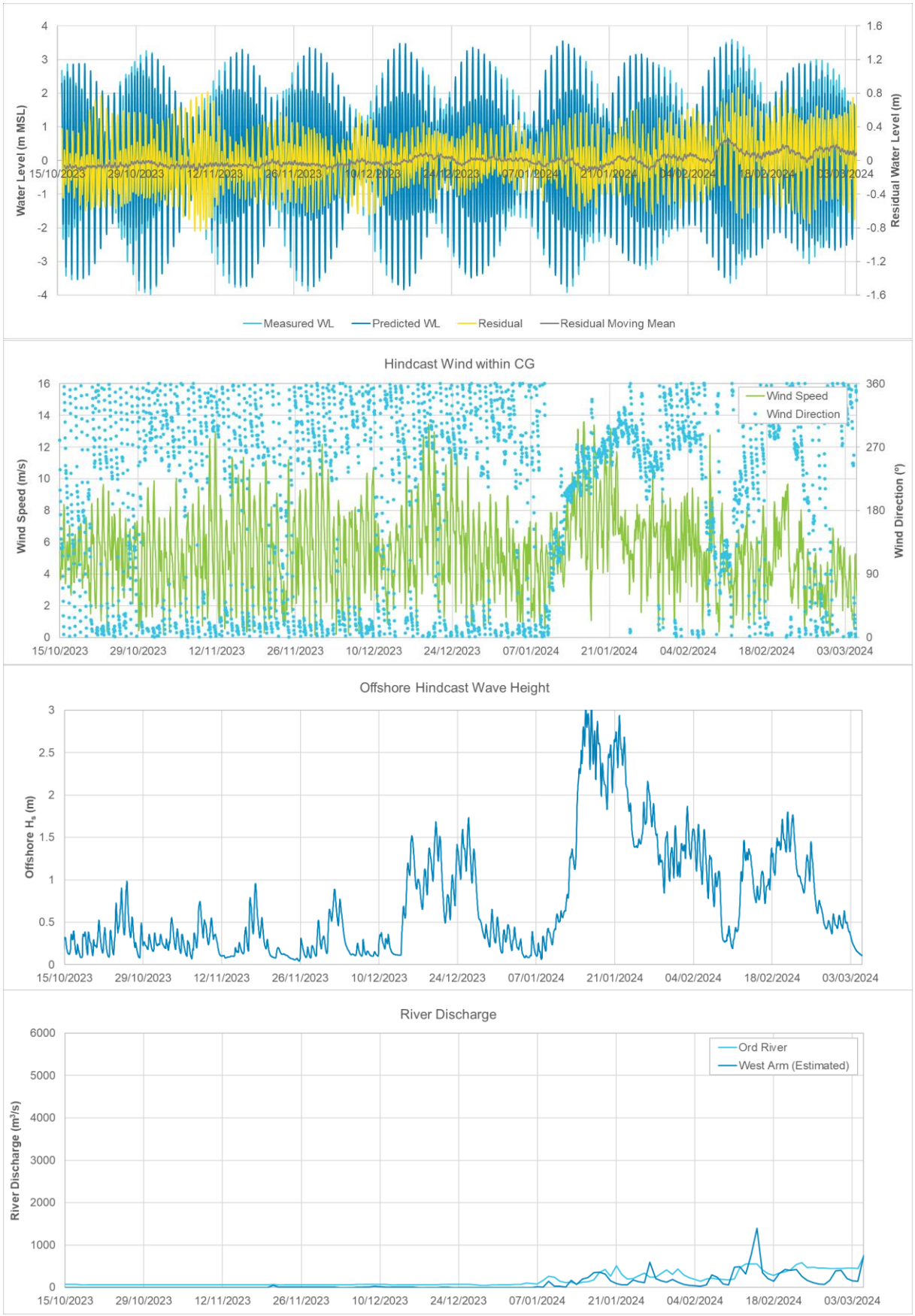


Figure 10. Water level residual at the False Mouths of the Ord (AWAC-07) (top) along with hindcast modelled wind (second from top), hindcast modelled offshore H_s and measured river discharge from October 2023 to March 2024.

2.1.2. Currents

2.1.2.1. Current Speed and Direction through the Water Column

To provide an understanding of the temporal and spatial variability, timeseries plots of the measured water level and the current speed and direction through the water column over a 14-day spring-neap cycle are shown at selected sites in the wet and dry seasons in Figure 11 to Figure 17. To understand how the currents vary spatially in the CG region, the measured data are shown at sites located offshore of CG (AWAC-09 in the wet season and AWAC-10 in the dry season), within the POA (AWAC-01 in both seasons), upstream of the POA (AWAC-11 in both seasons) and at the entrance to West Arm (AWAC-08, only in the wet season).

The plots show a strong tidal signal at all sites, with peak current speeds increasing as the tidal range increases from neaps to springs, as would be expected. The current speed increases from the bed layer to the surface layer at all sites, while the current direction remains relatively consistent through the water column with some variation during periods of low current speed when the current direction switches.

The peak current speeds vary between the sites, with the lowest peak speeds (bed = 0.8 m/s, mid = 1.0 m/s, surface = 1.1 m/s) offshore of the East Entrance to CG (AWAC-10) and the highest peak speeds (bed = 1.6 m/s, mid = 2.2 m/s, surface = 2.5 m/s) at the northern entrance to West Arm (AWAC-08). The highest current speed over all the measured data was recorded at the northern entrance to West Arm (AWAC-08) with a surface current speed of 2.9 m/s (5.6 knots). The current speeds and directions are generally similar during the wet and dry seasons. The plots show similar flood and ebb current speeds at most sites except within the POA (AWAC-01) and directly upstream of the POA (AWAC-11) where there is asymmetry in the current speeds, with ebb current speeds consistently higher than the flood current speeds (this asymmetry is most noticeable at AWAC-11) and with the difference between the two being largest in the surface layer and smallest in the bed layer.

Vertical profiles of the measured current speed through the water column during a spring tide at peak flood and peak ebb, in the wet and dry seasons are shown at the same locations as the timeseries data in Figure 18 to Figure 21. The plots show a relatively consistent increase in current speed through the water column, with the lowest recorded current speed (ranging from 0.7 to 1.4 m/s) close to the seabed and the highest recorded current speed (ranging from 1.3 to 2.9 m/s) near the surface, as would be expected due to friction effects closer to the seabed.

The plots indicate that the peak current speeds and the increase in current speed through the water column is typically higher in the wet season compared with the dry season, this could be partially due to the higher river discharge in the wet season but is also at least partially due to the tidal characteristics over the plotted timeframe as the timeseries plots indicated similar current speeds between the two seasons. The plots indicate similar flood and ebb current speeds through the water column at the sites except for the site directly upstream of the POA (AWAC-11), where the peak ebb current speeds are significantly higher and increase faster up through the water column compared with the peak flood current speeds.

In summary, the implications of these findings for the proposed operation and for the numerical modelling are:

- There is significant spatial and temporal variability in current speeds in the CG region. It will therefore be important for the hydrodynamic model to use the extensive measured dataset available to determine how reliably it can represent both the spatial and temporal variability in tidal currents in the region. It is important for the model to be able to represent the variability in the currents in order to be able to assess changes due to the sand sourcing and represent sediment transport processes. This was addressed in the model (see Section 3.4).
- There is a consistent increase in current speed through the water column during peak flood and peak ebb on spring tides, with the lowest current speed close to the seabed and the highest current speed near the surface. Flood and ebb current speeds through the water column were similar at most sites, except for the site directly upstream of the POA, where the peak ebb current speeds were significantly higher compared with the peak flood current speeds (i.e. there is a clear ebb tide dominance in this area). It will be important for the hydrodynamic model to represent variations between flood and ebb currents in the region as these will strongly influence net sediment transport patterns (both suspended and bedload transport). This was addressed in the model (see Section 3.4).

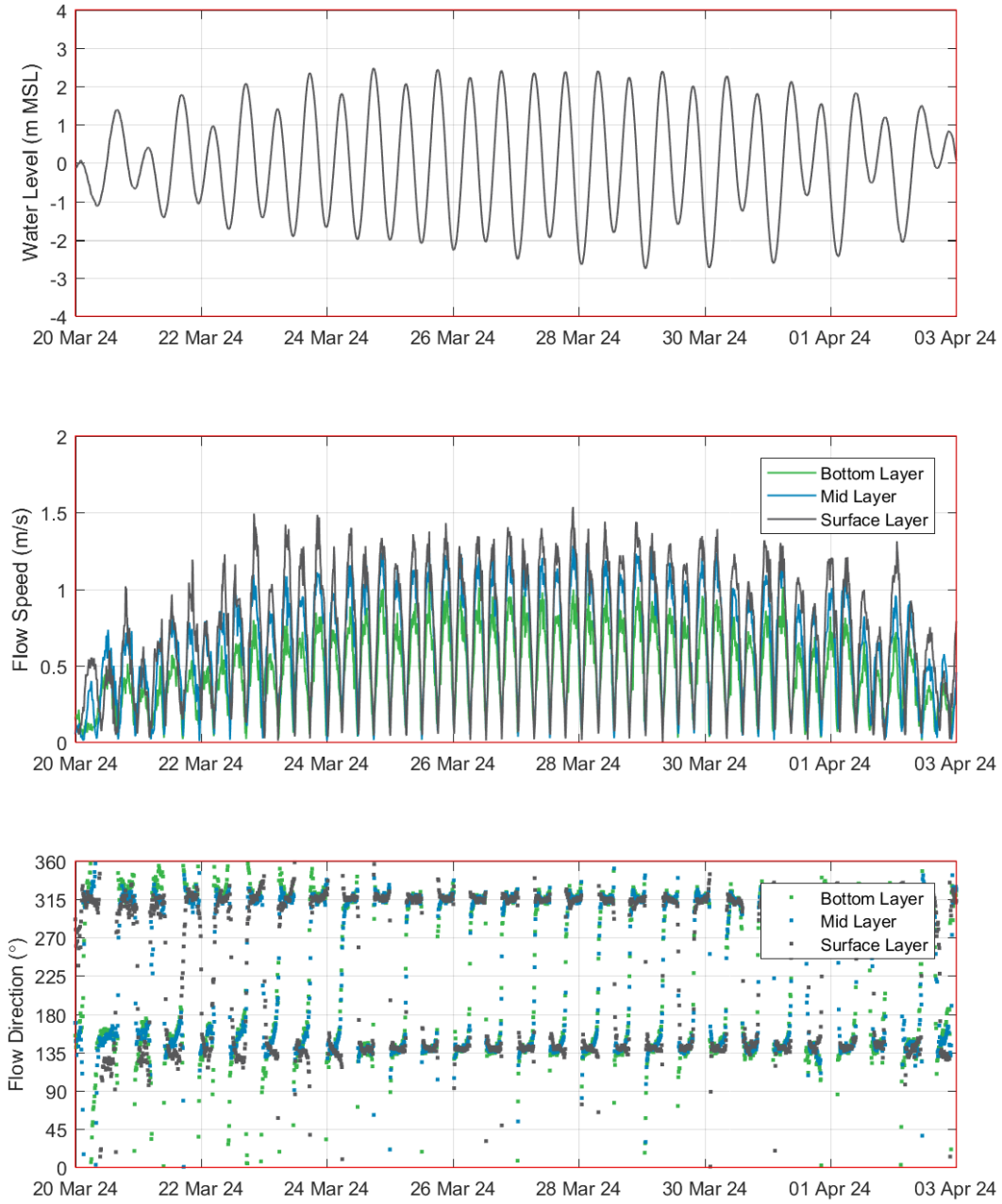


Figure 11. Measured water level, current speed and direction over a 14-day spring-neap cycle at AWAC-09 during the wet season.

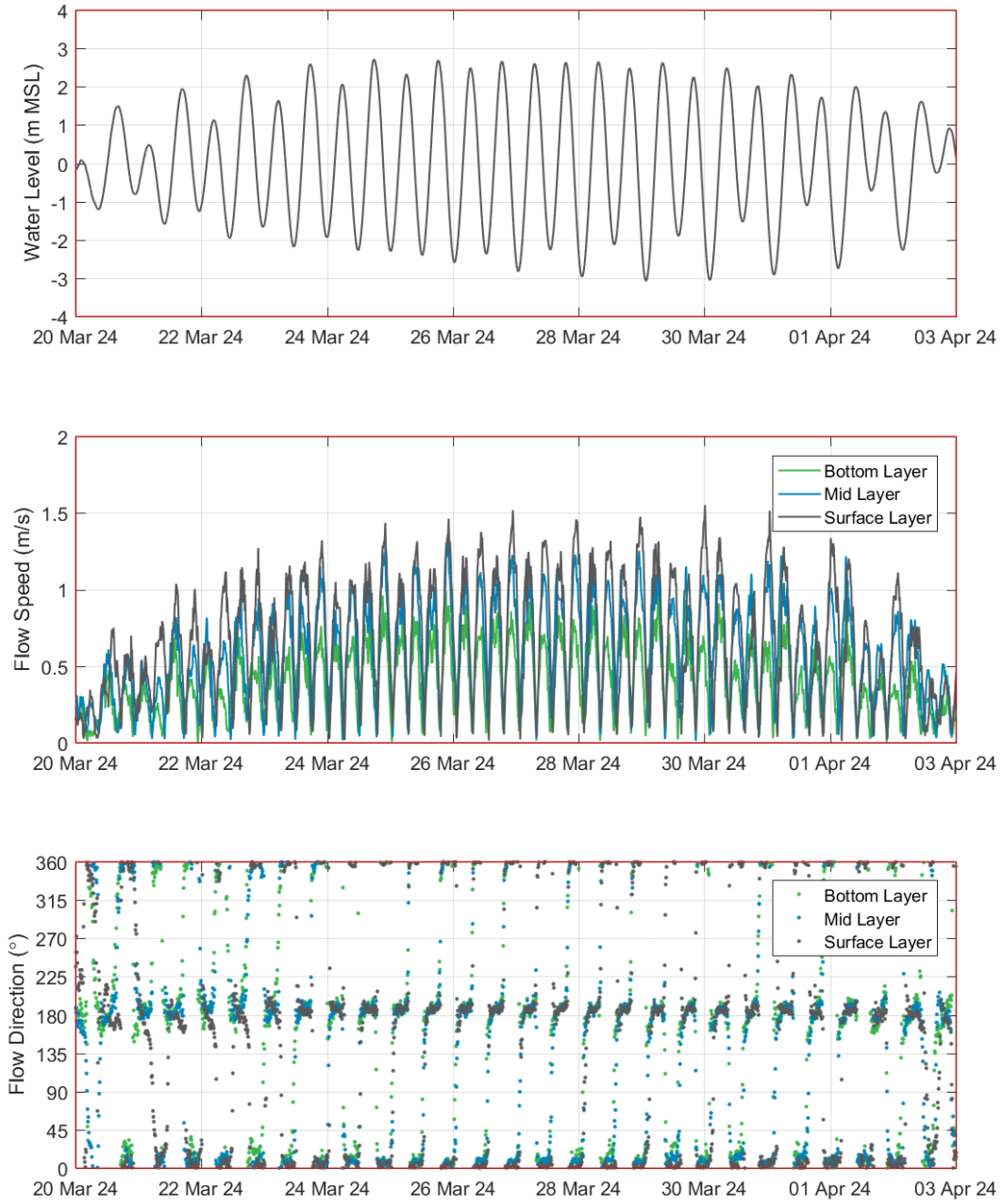


Figure 12. Measured water level, current speed and direction over a 14-day spring-neap cycle at AWAC-01 during the wet season.

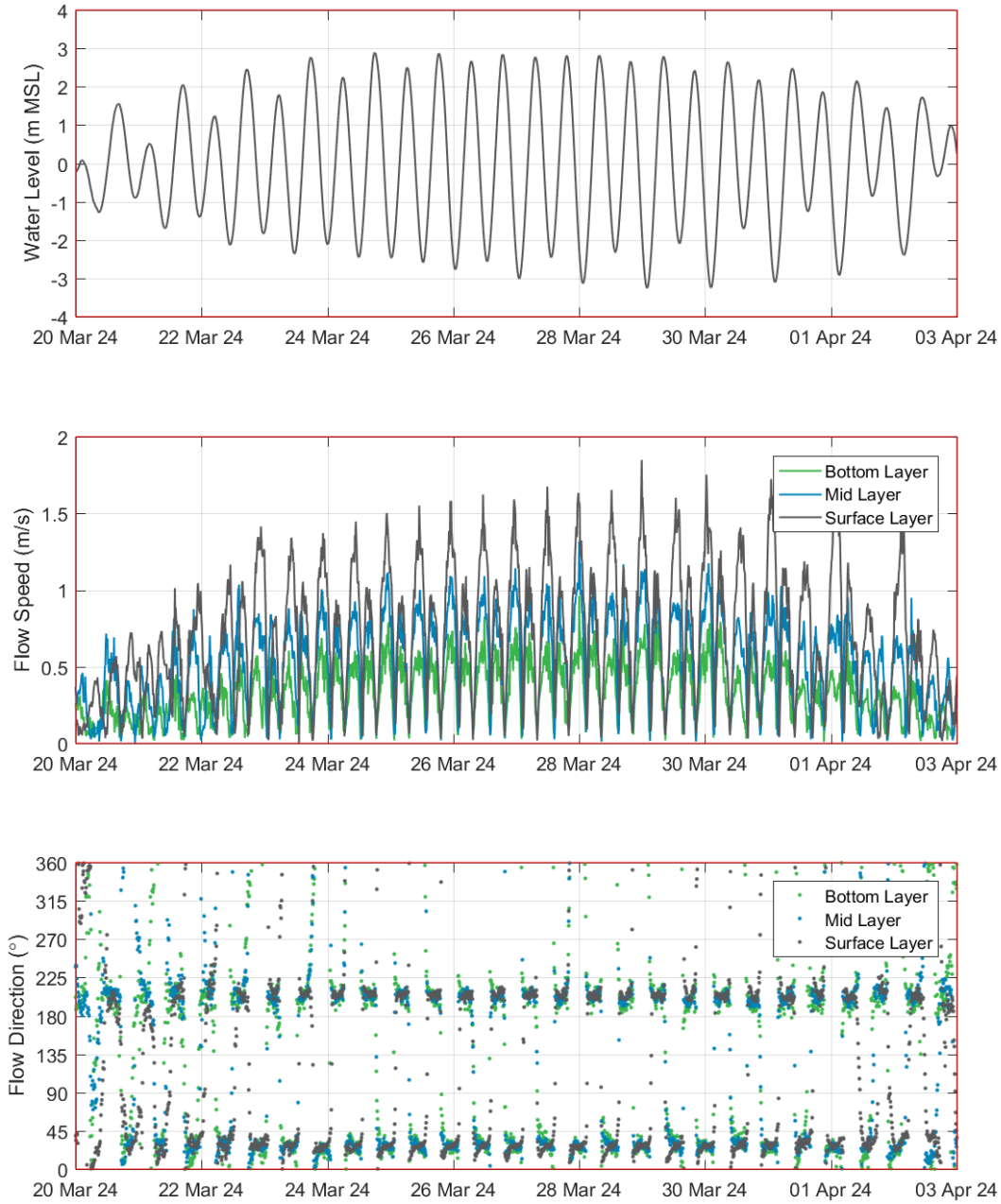


Figure 13. Measured water level, current speed and direction over a 14-day spring-neap cycle at AWAC-11 during the wet season.

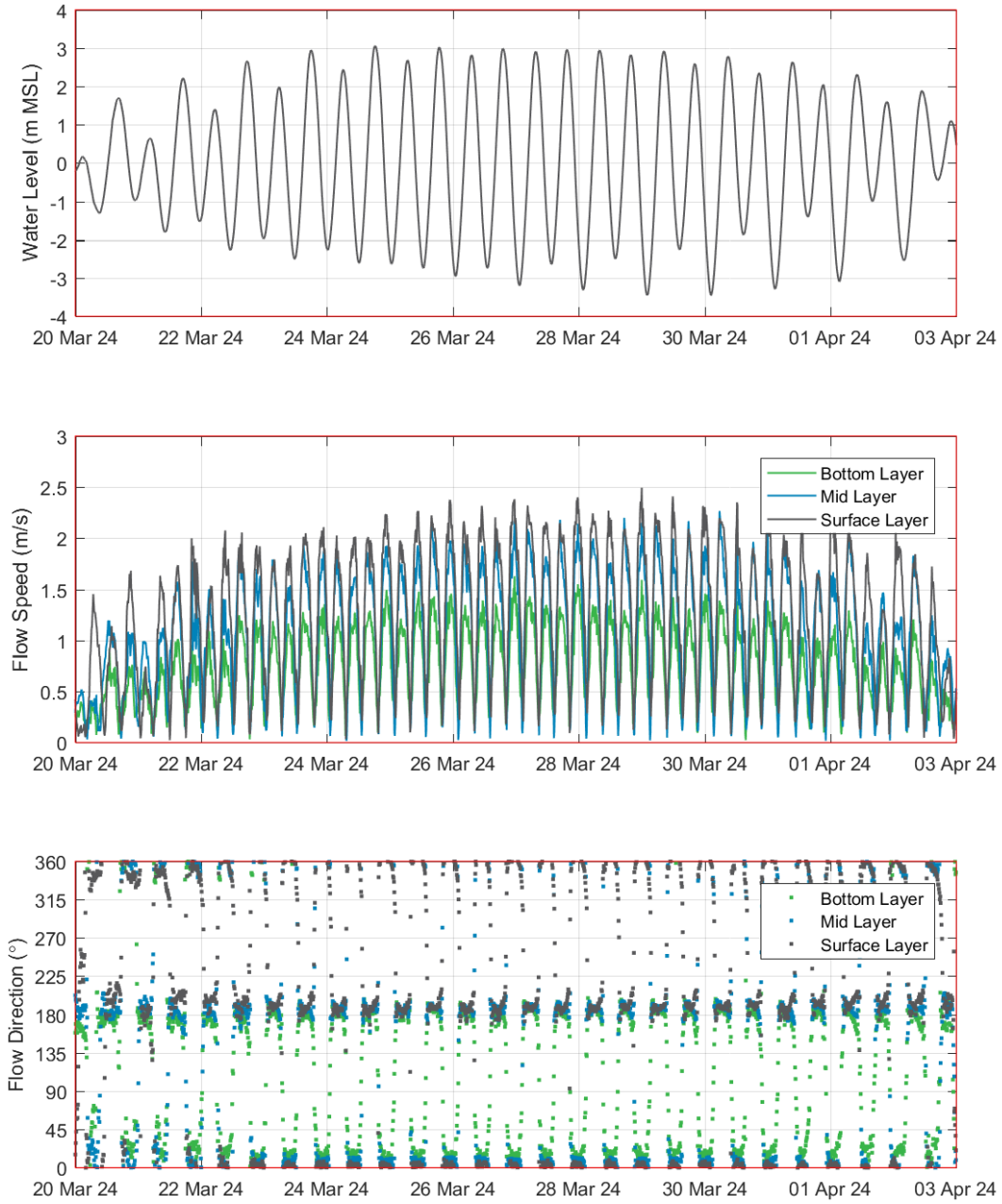


Figure 14. Measured water level, current speed and direction over a 14-day spring-neap cycle at AWAC-08 during the wet season.

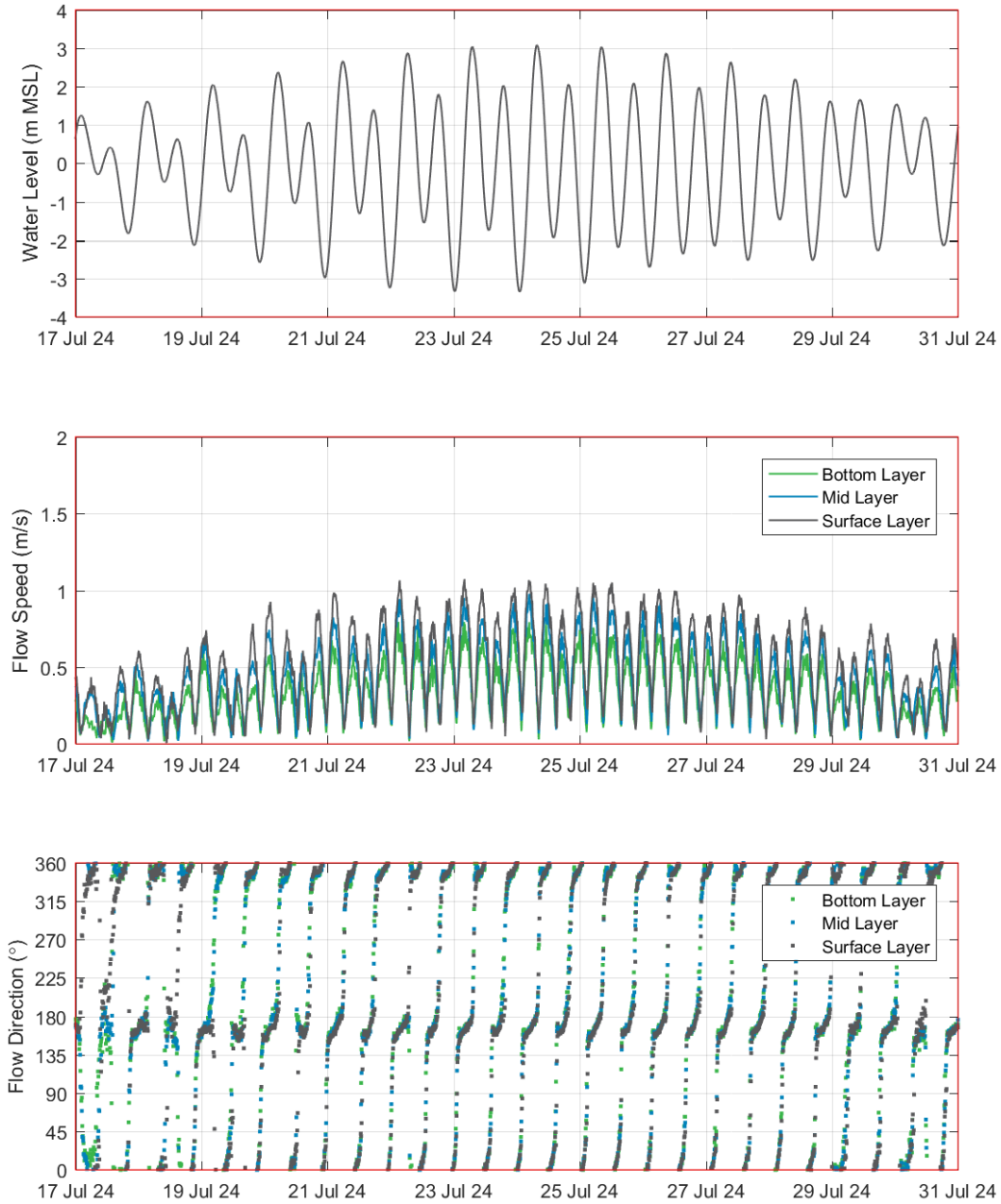


Figure 15. Measured water level, current speed and direction over a 14-day spring-neap cycle at AWAC-10 during the dry season.

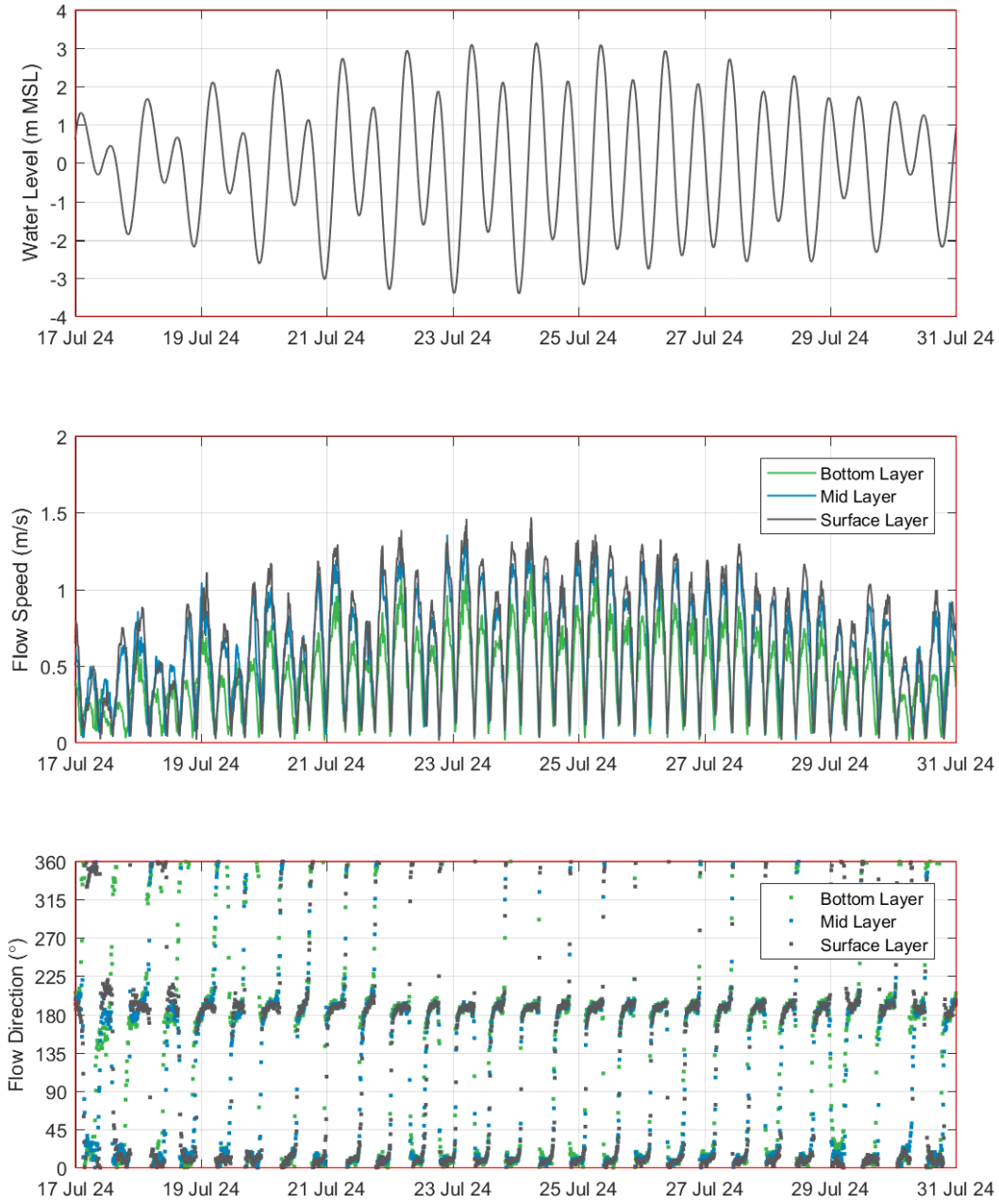


Figure 16. Measured water level, current speed and direction over a 14-day spring-neap cycle at AWAC-01 during the dry season.

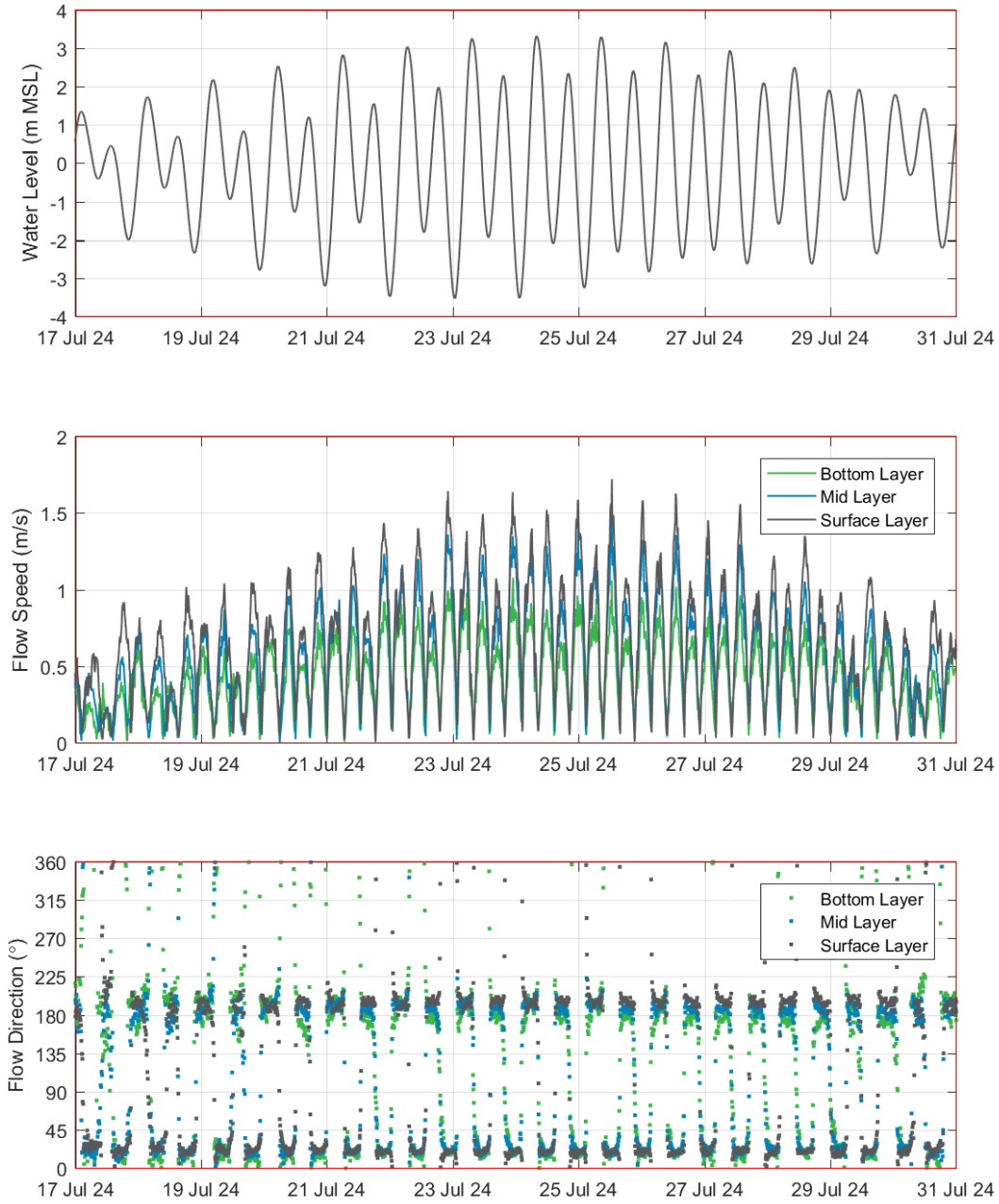


Figure 17. Measured water level, current speed and direction over a 14-day spring-neap cycle at AWAC-11 during the dry season.

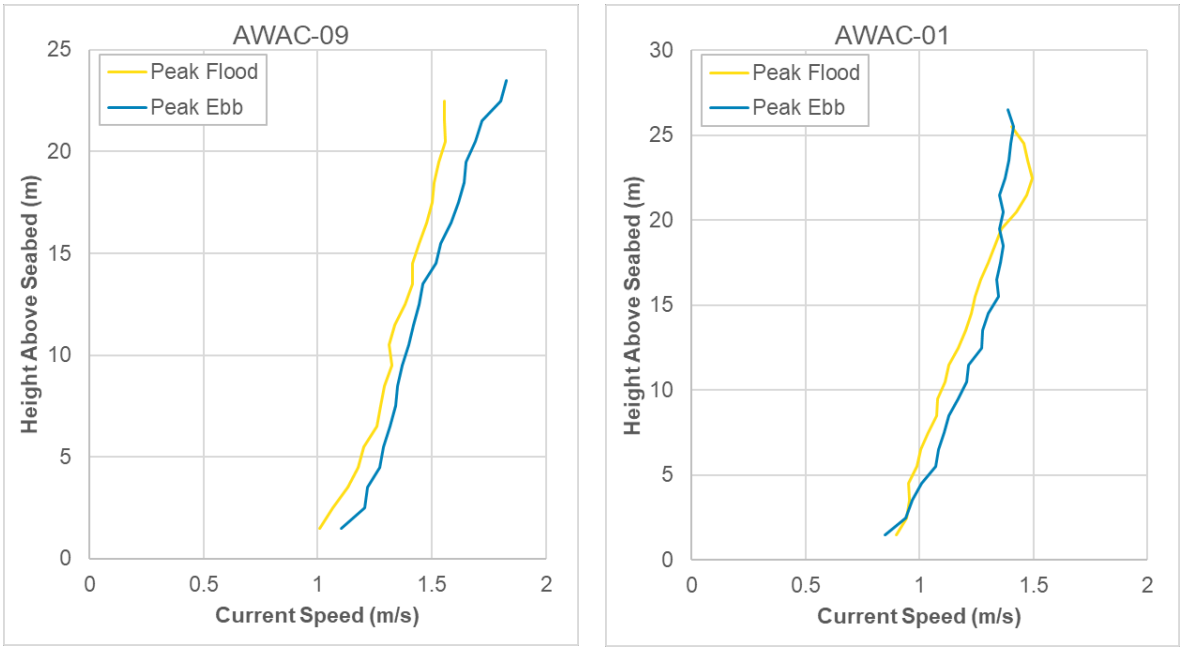


Figure 18. **Measured vertical current profile at peak flood and peak ebb on a large spring tide in the wet season at a site offshore of CG (AWAC-09) and within the POA (AWAC-01).**

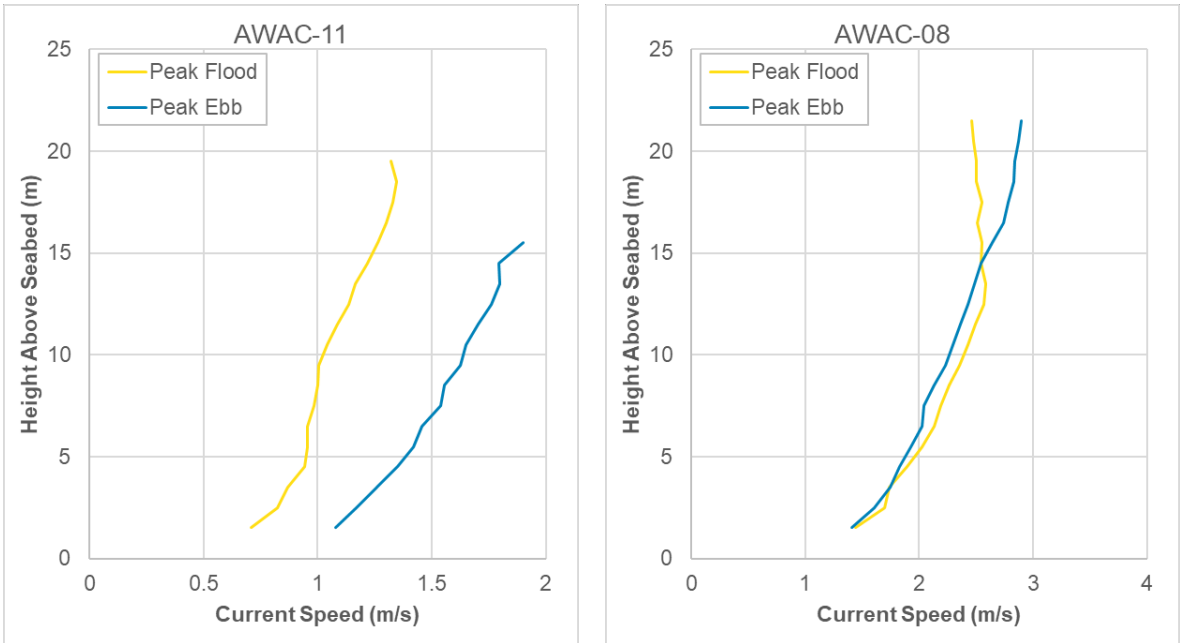


Figure 19. **Measured vertical current profile at peak flood and peak ebb on a large spring tide in the wet season at a site upstream of the POA (AWAC-11) and at the entrance to West Arm (AWAC-08).**

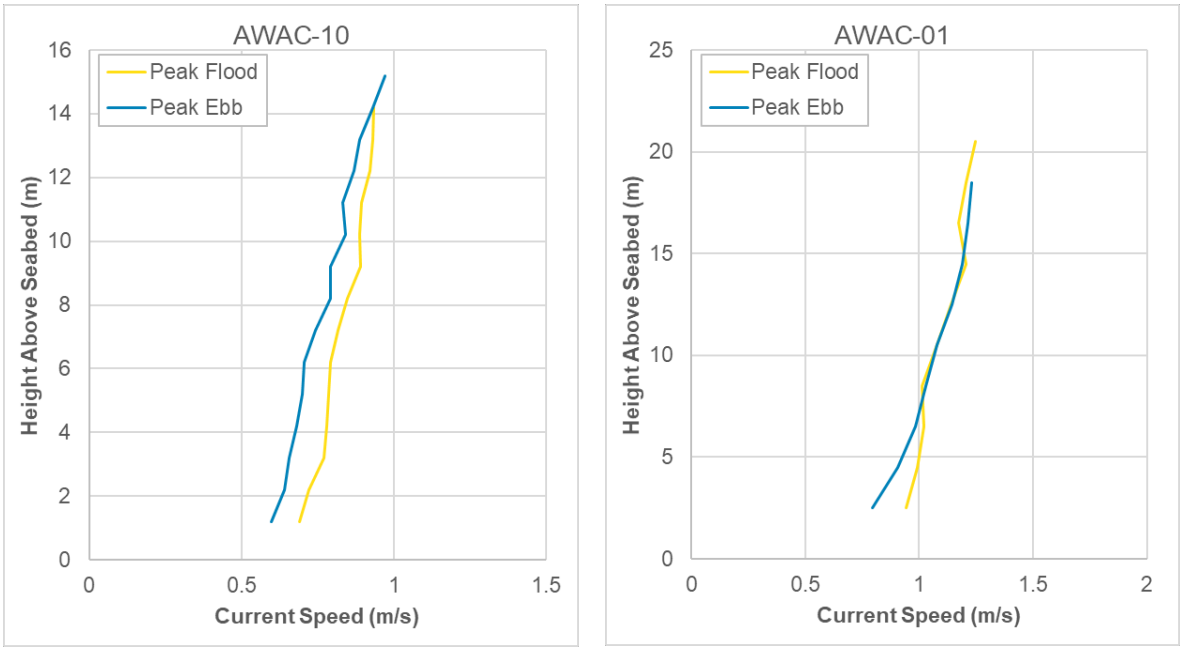


Figure 20. **Measured vertical current profile at peak flood and peak ebb on a large spring tide in the dry season at a site offshore of CG (AWAC-10) and within the POA (AWAC-01).**

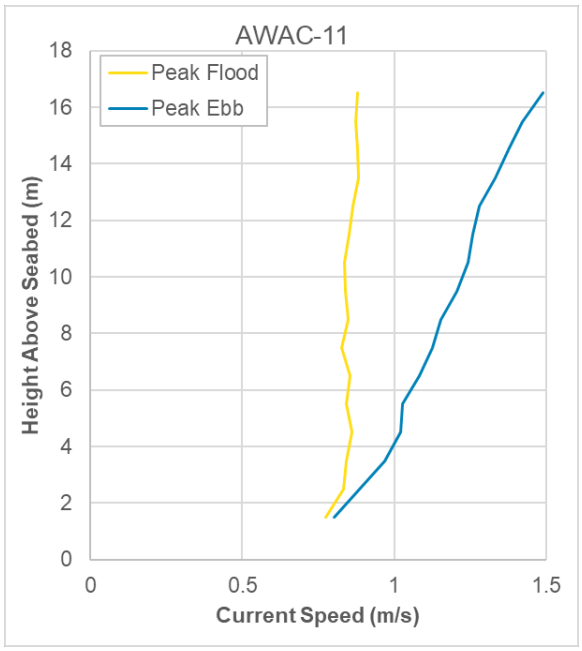


Figure 21. **Measured vertical current profile at peak flood and peak ebb on a large spring tide in the dry season at a site upstream of the POA (AWAC-11).**

2.1.2.2. Residual Currents

To better understand how the currents around CG are influenced by different drivers and how this varies spatially and temporally, the measured current data collected at selected sites between March 2024 and August 2024 (the period when the most concurrent data were collected throughout the region) were analysed using the Danish Hydraulic Institute (DHI) Tide Analysis Toolbox. A harmonic analysis of the measured surface current data (calculated based on the top three layers with reliable data, with layers adopted varying over time) and measured depth-averaged current data, was undertaken.

Based on this analysis the predicted and residual current speeds were calculated. To help understand the longer-term trends in residual currents, a daily moving mean was applied to the residual current and is presented along with the residual current.

The depth-averaged measured, predicted and residual current speeds at AWAC-01 over 10 days of the wet season along with the hindcast modelled wind within CG are shown in Figure 22. The plot shows a semi-diurnal signal in the derived residual current, with two peaks and two troughs per day, with the peaks and troughs representing both positive and negative residual current speeds. The semi-diurnal signal suggests as with the water level data that some of the constituents are not fully represented.

The short-term fluctuations in the residual current speed does not correspond with the mesoscale variations in the wind speed, suggesting that these fluctuations are more likely to be due to some constituents not being fully resolved. However, the duration of data available for the analysis ensure that the calculated residuals provide a reliable representation of the longer-term trends in residual currents and allow for analysis of the potential for wind conditions to influence these, this is considered below.

Residual currents were calculated for the surface and depth-averaged layers at locations offshore of CG (AWAC-09), within the POA (AWAC-01) and upstream of the POA (AWAC-11) over a 64-day period in the wet season are shown in Figure 22 to Figure 25. In addition, residual current results within the POA (AWAC-01) are shown for a 32-day period of the dry season in Figure 26. The results show the following:

- The pattern in the calculated residual current is similar between the surface layers and depth-averaged currents, but with the residual current in the surface layers typically being of greater magnitude compared with the depth-averaged currents.
- Over the wet season period the temporal variability and magnitude of the residual current was similar at the three sites.
- There was a large river discharge event towards the start of the 64-day wet season period and immediately after this there was a positive residual current speed which lasted for approximately 10 days. However, the residual current speed at the site offshore of CG (AWAC-09) was generally larger than the residual current speed upstream of CG, suggesting that the residual current was not due to the river discharge.
- There is some variability in the residual current speeds which correspond with the spring-neap tidal cycle. Around neap tides there appears to typically be low or negative current residual speeds, while during the period when the tidal range is increasing from neaps to springs and during spring tides there is a greater chance of higher positive residual current speeds.
- Some of the peaks in residual current speed approximately correlate with periods of higher wind speed (e.g. 05/04/2024 and 20/04/2024), although these typically also coincide with periods when the tidal range is increasing from neaps to springs. There are also periods with higher wind speeds when a negative residual current speed occurred (e.g. 19/03/2024), although the wind direction was from the west for this event and it coincided with neap tides while for the periods which correlated with increased residual current speeds the wind was from the south-southeast and coincided with the tidal range in increasing from neaps to springs. The results therefore indicate that during the wet season there is the potential that the wind conditions can influence the current speed residual, but the relationship appears to be complex with factors such as the wind direction and tidal stage potentially influencing the residual current speed.
- The calculated residual current speed during the dry season within the POA was significantly lower than during the wet season, with peak daily moving averages of less than ± 0.05 m/s for the depth-averaged currents compared to ± 0.15 m/s in the wet season. The peak wind speeds during the dry season were lower than the peak wind speeds during the wet season, this provides further evidence that the wind speed can influence the residual current speed.

The analysis of the residual currents indicates that the tidal processes are dominant in the area but that there is the potential for the wind conditions to influence the residual currents, but the relationship appears to be complex and dependent on factors such as the wind direction and tidal state. To understand the combined influence of the astronomical tide and the wind conditions on the currents, the measured surface layer current velocity data were integrated over time to provide a notional net drift.

Progressive vector diagrams of the notional net drift have been calculated over 14-day spring-neap cycles for both the wet season and the dry season. During the wet season measurement period the wind was variable which allowed the net drift to be calculated over 14-day spring-neap cycles with different dominant wind conditions, and over three-day spring and neap periods with different wind conditions (Figure 27). During the dry season the wind was relatively consistent and so the net drift was calculated over two different 14-day spring-neap cycles to understand the variability over different spring-neap cycles (Figure 28). The wet season progressive vector plots are shown in Figure 29 to Figure 31 and the dry season plots are shown in Figure 31 to Figure 34. The plots show the following:

- The net drift at the two offshore sites (AWAC-09 and AWAC-10) differ from 120 km to the west at the site at King Shoals (AWAC-09) during the wet season to 60 km to the northeast at the site in Medusa Bank (AWAC-10) during the dry season. However, at both sites the net drift shows similar spatial patterns and magnitudes for the two 14-day periods, with differences in the final net drift position of 10 to 20 km.

- During the wet season at King Shoals the net drift over the 14-day period with winds from the southeast was calculated to be ~20 km further west (~15% increase in total drift distance) compared with the period of northerly winds, indicating that the southeasterly winds could have increased the westerly net drift.

- The drift over the three-day periods in the wet season showed similar net drift except for the neap period with northwesterly winds, with the net drift to the north being more than doubled (increased by 20 km) for these conditions. The peak wind speeds over this period corresponded with predominantly westerly wind conditions which could have reduced the net westerly drift and instead increased the net northerly drift.

- The results within the POA show a net drift to the north of 40 to 70 km during wet season conditions and a net drift to the north-northeast of 20 to 50 km during dry season conditions. During the wet season the change in net drift relative to the wind conditions for both the 14-day periods and the three-day periods is the opposite of what would be expected if the winds were influencing the currents (i.e. the net drift is further to the north during a period of northerly winds compared to a period of southeasterly winds). This suggests that the wind is not a significant driver in terms of the net drift at this site.

- Upstream (south) of the POA the net drift is indicated to be to the northeast for both the wet and dry seasons. The net drift in the wet season over the 14-day periods is indicated to be further compared with the net drift in the dry season, with 200 to 240 km during the wet season compared with 100 to 140 km during the dry season. In the wet season the net drift is shown to be fairly consistent in direction, but with the net drift distance being double with northerly winds compared with southeasterly winds during spring tides. To the site within the POA, this change in net drift is the opposite of what would be expected if the winds were influencing the currents, which suggests that river outflow, and not wind, is the more significant driver in terms of the net drift at this site.

Overall, the residual current and net drift plots indicate that the influence of winds on currents is relatively small within CG. The results indicate the potential for the winds to have a larger influence on the currents directly offshore of CG, but the changes remain relatively small and are only likely to be significant in terms of net drift during neap tidal conditions.

In summary, the implications of these findings for the proposed operation and for the numerical modelling are:

- The currents in the CG are predominantly controlled by the astronomical tide, with residual currents only resulting in relatively small increases and decreases in current speed. As a result, the currents in the region can be considered to be relatively consistent and predictable, which supports accurate and reliable modelling of currents.
- Residual current speeds were shown to vary temporally, with higher residual current speeds during wet season conditions compared with dry season conditions. During the wet season the residual currents had similar temporal variability and magnitudes at sites offshore of CG, within the POA and upstream (south) of the POA. The data indicate the potential for the wind and river

outflow conditions to influence the residual currents, but the influence is relatively small within CG. There is the potential for the winds to have a larger influence on the currents directly offshore of CG, but the changes remain relatively small and are only likely to be significant in terms of net drift during neap tidal conditions. Although residual currents only result in a relatively small contribution to the overall current speed, the ability of the model to represent them during wet season conditions was assessed to understand the relative accuracy for plume dispersion modelling. This was addressed in the hydrodynamic model which was subsequently used to drive the plume model (see Sections 3.4 and 3.7).

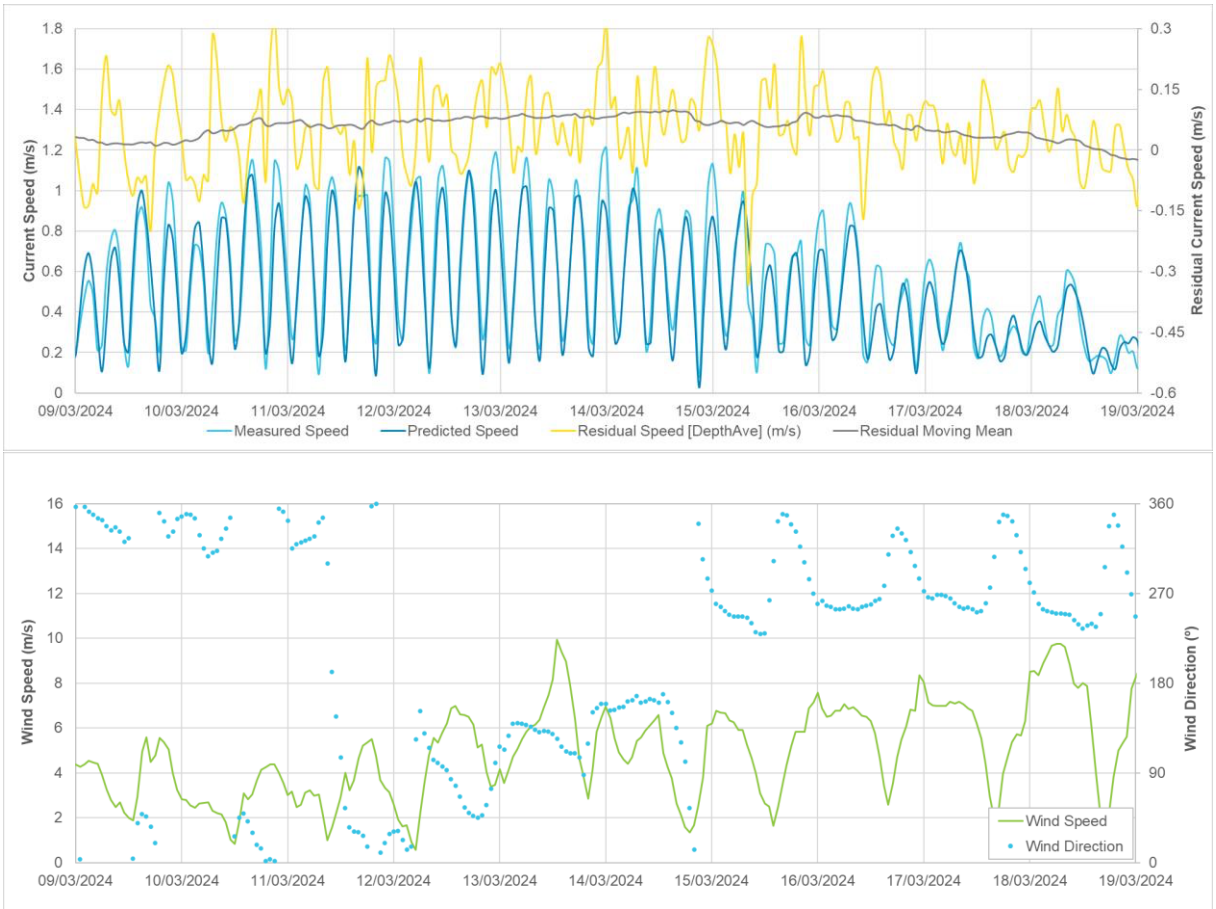


Figure 22. Current residuals at AWAC-01 for depth-averaged currents along with hindcast modelled wind over a 10-day period.



Figure 23. Current residuals at AWAC-09 for surface (top) and depth-averaged (second) currents, hindcast modelled wind and measured river discharge during the wet season.



Figure 24. Current residuals at AWAC-01 for surface (top) and depth-averaged (second) currents, hindcast modelled wind and measured river discharge during the wet season.

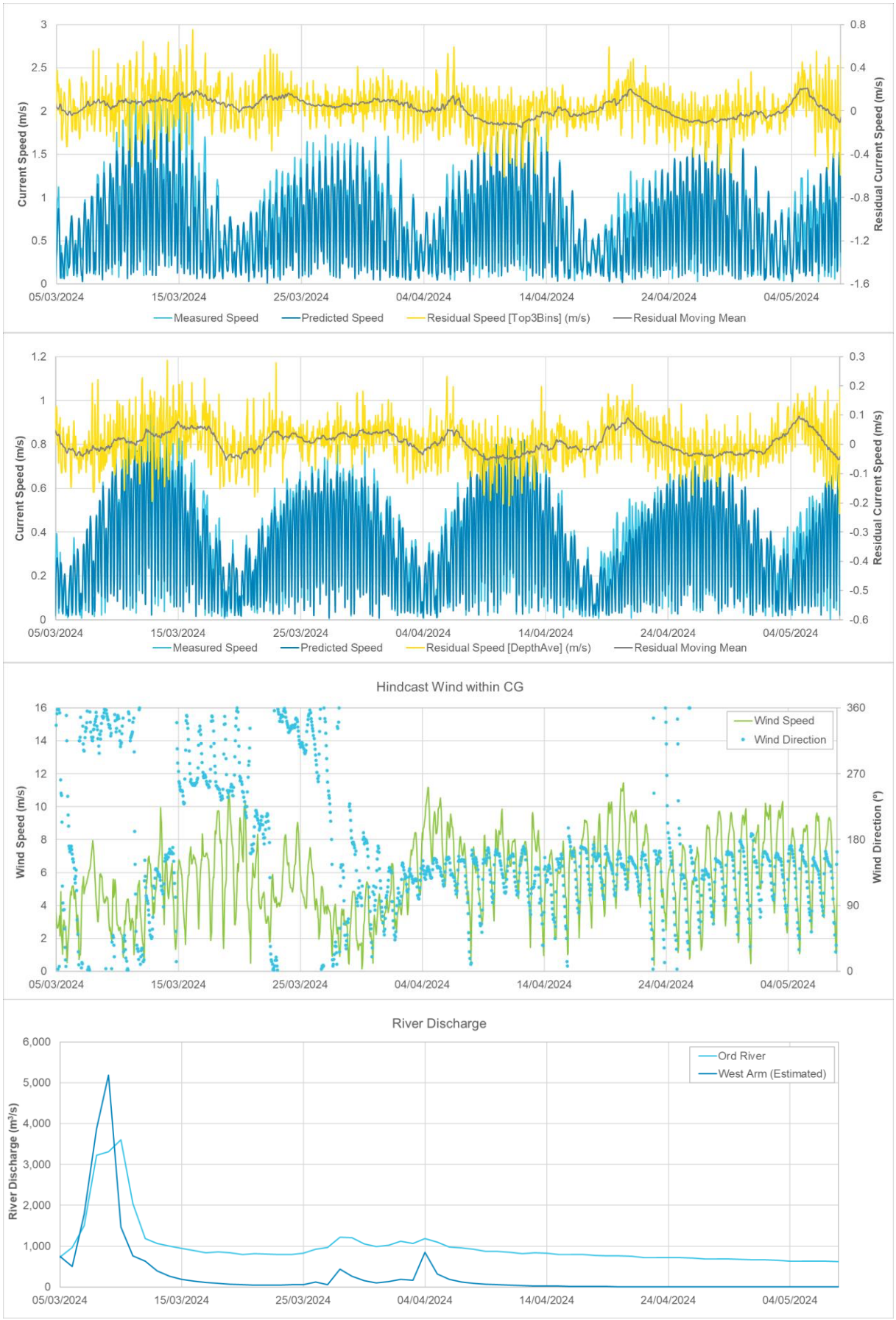


Figure 25. Current residuals at AWAC-11 for surface (top) and depth-averaged (second) currents, hindcast modelled wind and measured river discharge during the wet season.

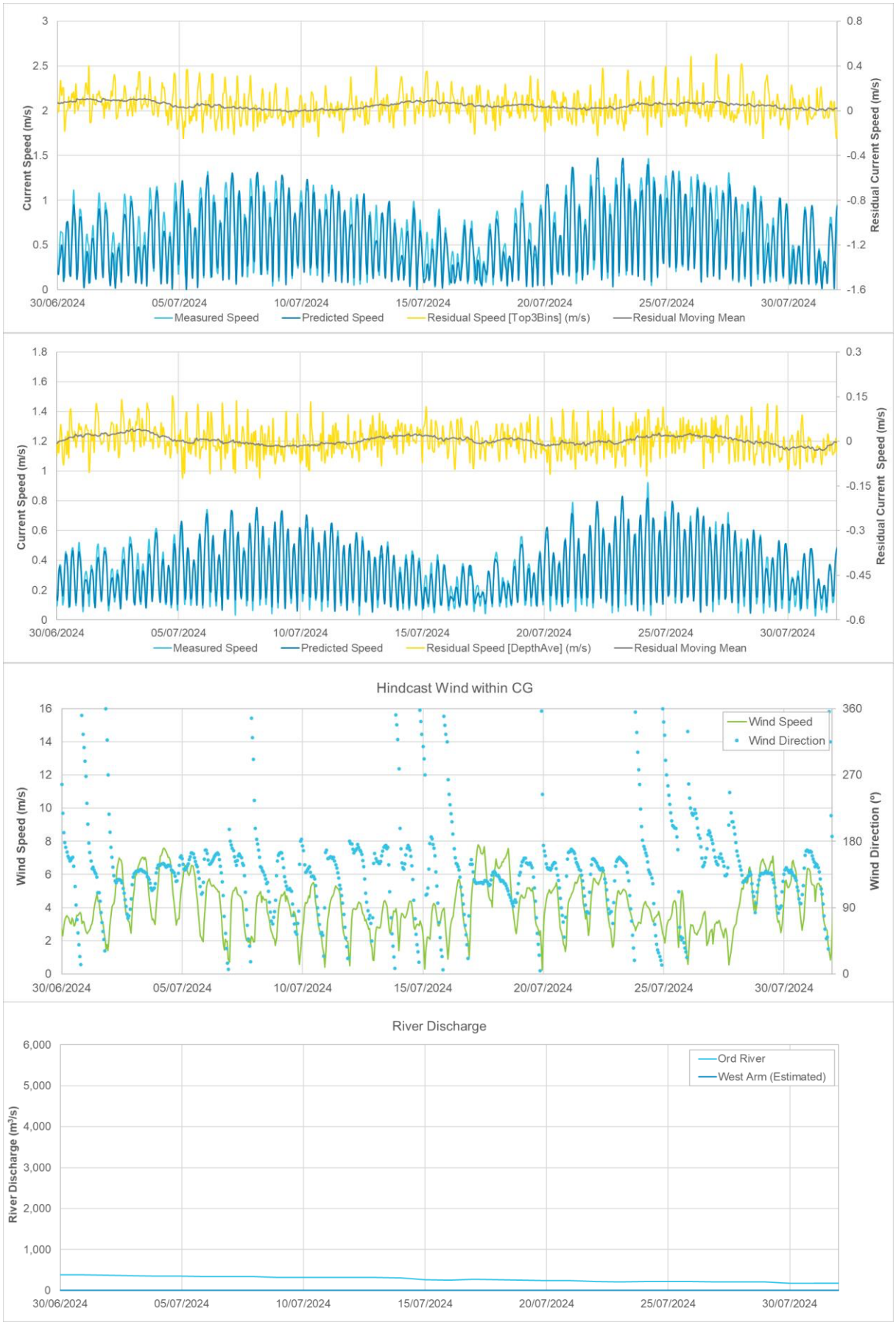


Figure 26. Current residuals at AWAC-01 for surface (top) and depth-averaged (second) currents, hindcast modelled wind and measured river discharge during the dry season.

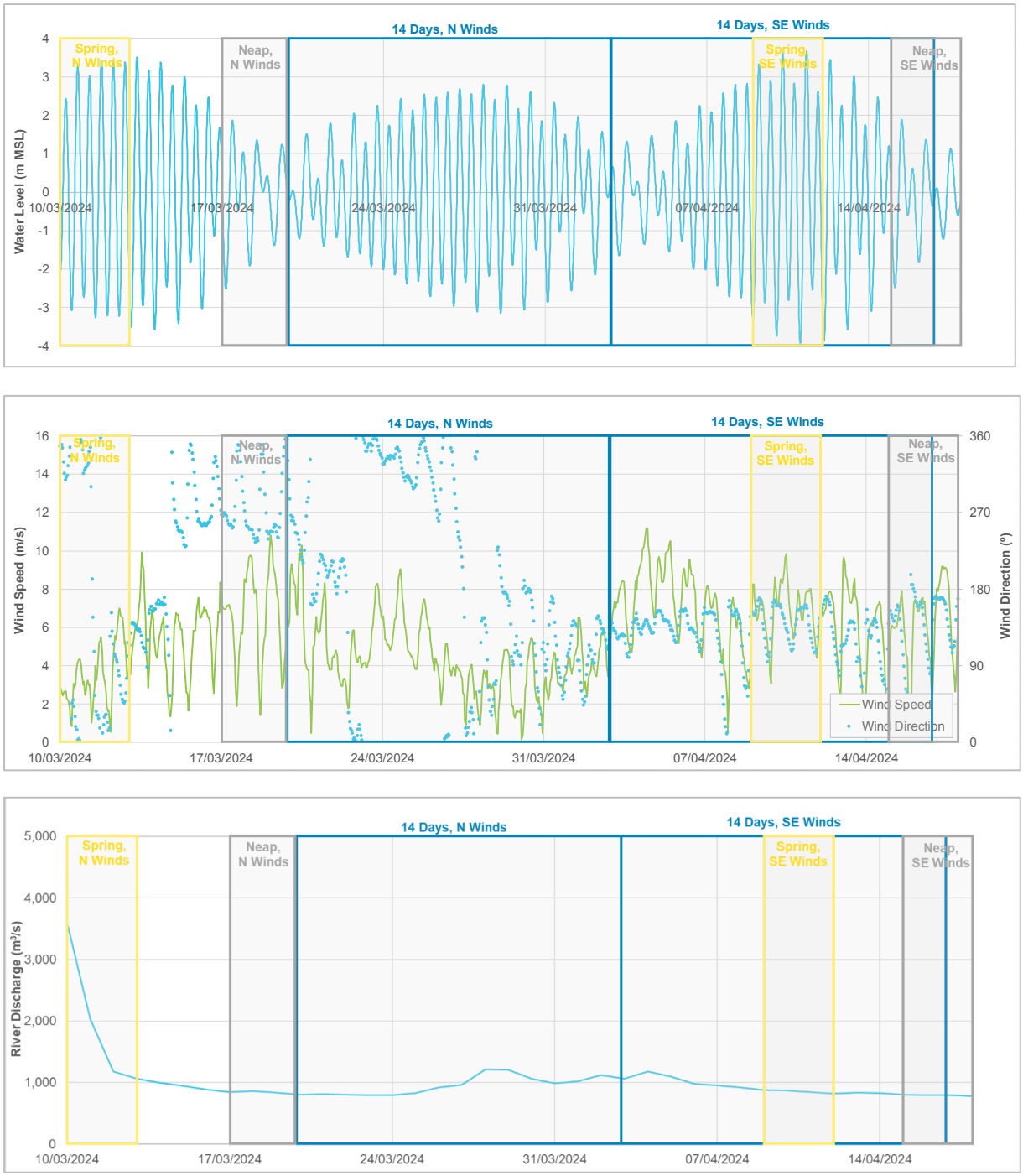


Figure 27. **Periods used to assess net transport during the wet season relative to predicted water level at Cape Domett (top), hindcast modelled wind conditions within CG (middle) and measured river discharge (bottom).**

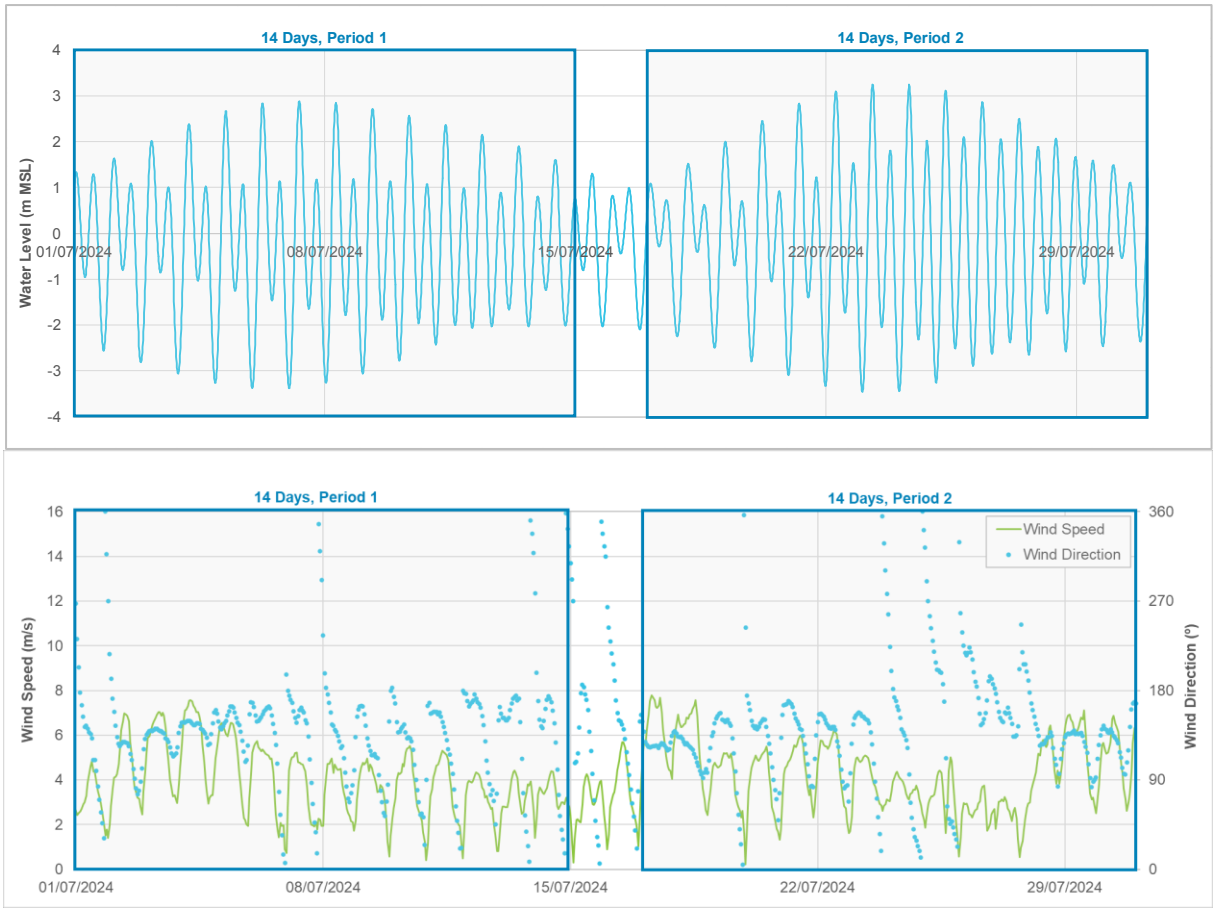


Figure 28. Periods used to assess net transport during the dry season relative to predicted water level at Cape Domett (top) and hindcast modelled wind conditions within CG (bottom).

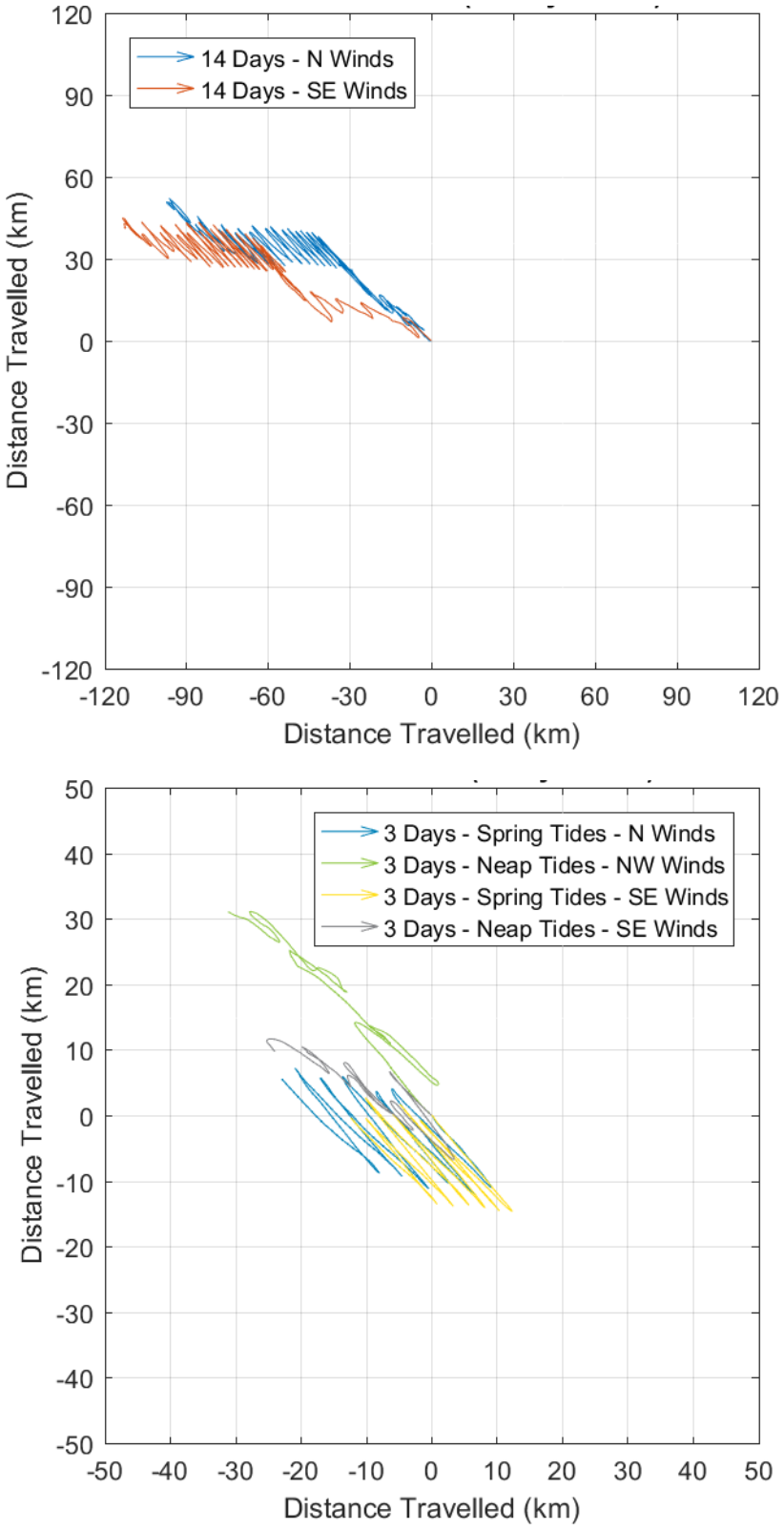
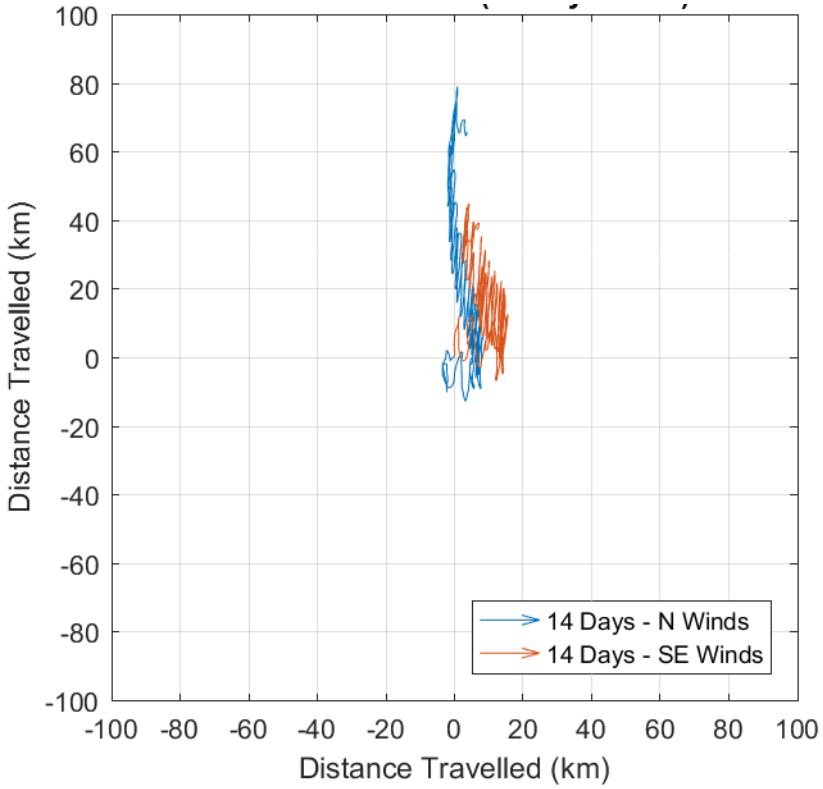


Figure 29. **Progressive vector diagrams showing the net transport based on measured currents in the wet season at AWAC-09 over a 14-day spring-neap tidal cycle (top) and 3-days of spring/neap tides with varying wind conditions (bottom).**



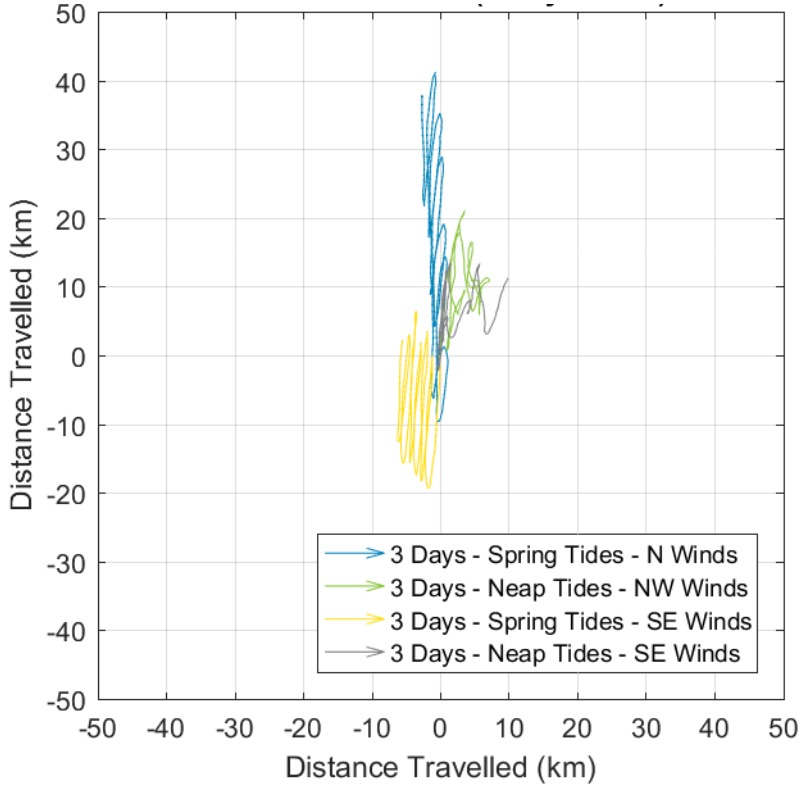


Figure 30. **Progressive vector diagrams showing the net transport based on measured currents in the wet season at AWAC-01 over a 14-day spring-neap tidal cycle (top) and 3-days of spring/neap tides with varying wind conditions (bottom).**

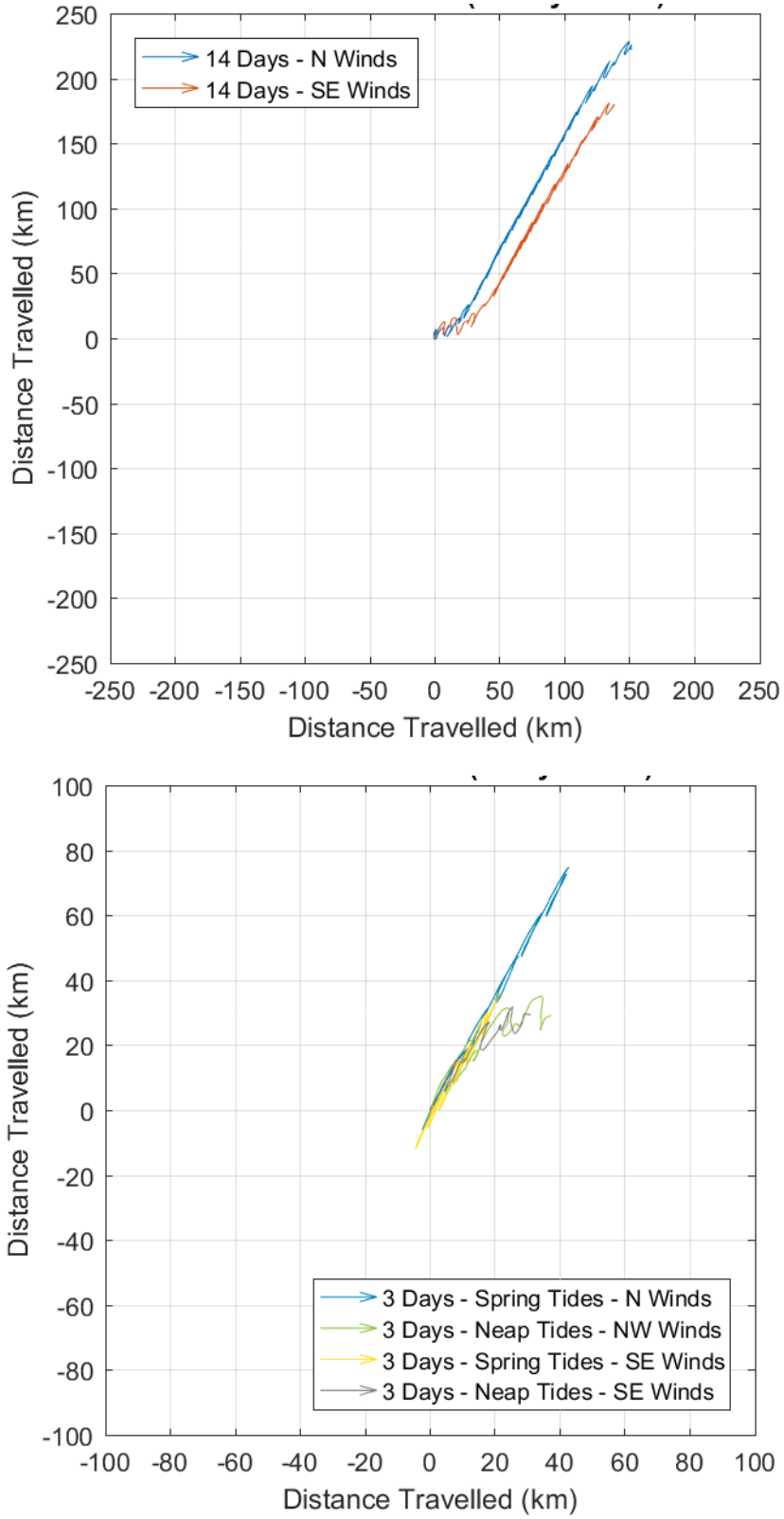


Figure 31. **Progressive vector diagrams showing the net transport based on measured currents in the wet season at AWAC-11 over a 14-day spring-neap tidal cycle (top) and 3-days of spring/neap tides with varying wind conditions (bottom).**

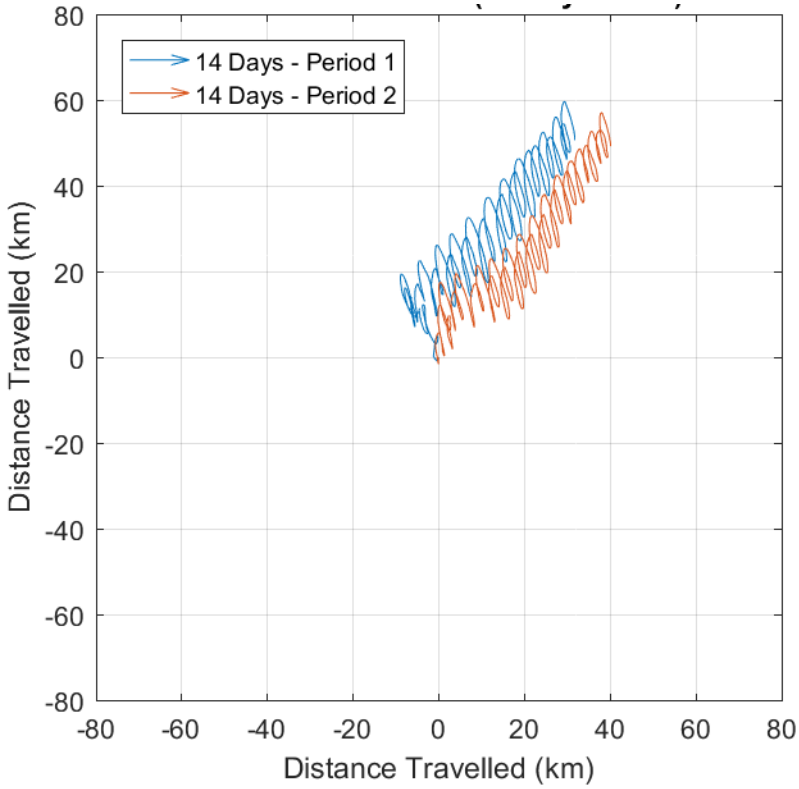


Figure 32. **Progressive vector diagrams showing the net transport based on measured currents in the dry season at AWAC-10 over a 14-day spring-neap tidal cycle.**

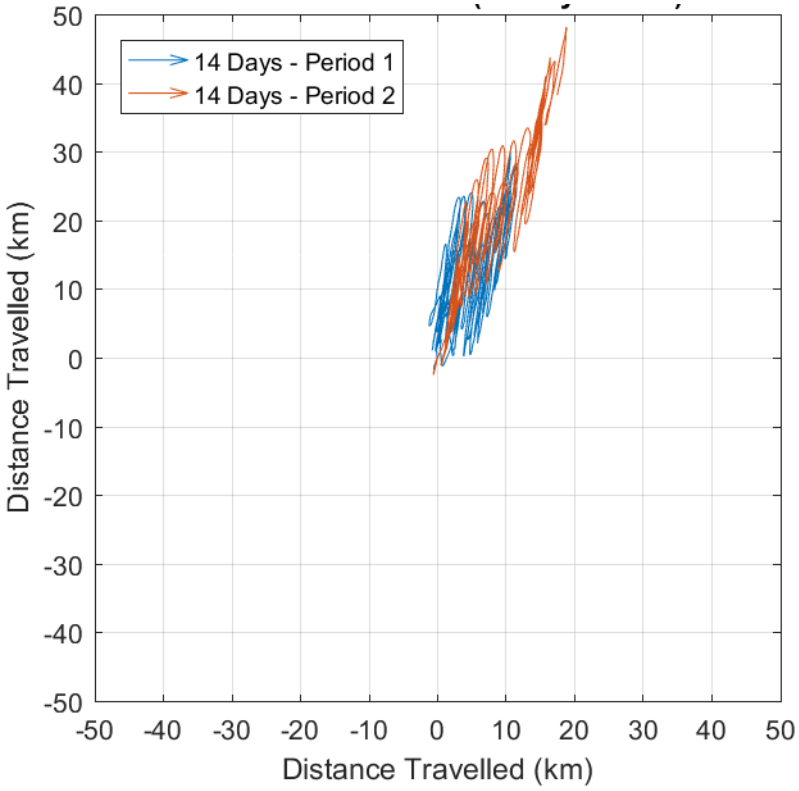


Figure 33. **Progressive vector diagrams showing the net transport based on measured currents in the dry season at AWAC-01 over a 14-day spring-neap tidal cycle.**

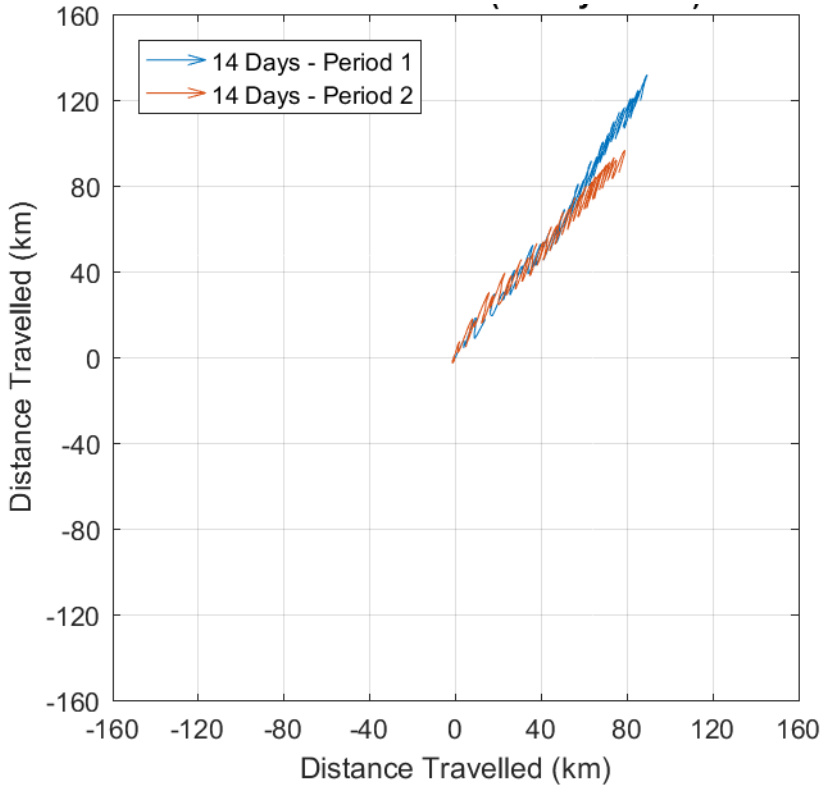


Figure 34. Progressive vector diagrams showing the net transport based on measured currents in the dry season at AWAC-11 over a 14-day spring-neap tidal cycle.

2.2. Waves

Previous analysis by PCS (2024b & 2024c) considered how the wave height varied between the AWAC sites, but did not consider how the wave conditions are influenced by other metocean conditions. Therefore, the analysis presented in this section is aimed to provide a better understanding as to how the waves directly offshore and within CG are influenced by other metocean conditions and how in turn this influences their spatial and temporal variability.

Timeseries plots of the measured H_s offshore of CG (AWAC-09) and within the POA (AWAC-01) along with the predicted water level at Cape Domett (AHO, 2023), hindcast modelled wind speed and direction within CG from the Centre for Australian Weather and Climate Research (CAWCR) (CSIRO, 2024) and the hindcast modelled offshore H_s in JBG from CAWCR (CSIRO, 2024) over 56 days of the wet season are shown in Figure 35.

In addition, plots from these two AWAC sites comparing the measured wave height to the specific metocean parameters are also shown for wet season conditions in Figure 36 to Figure 40 and for dry season conditions in Figure 41 to Figure 43. The plots show the following:

- The measured H_s offshore from CG and in the POA within CG are similar, with both experiencing the same temporal variability. The H_s offshore from CG are typically larger than those within CG except for periods with very small waves, when H_s is similar in both locations. These periods correlate with low offshore H_s and relatively low wind speeds from the east to south, meaning that H_s will be the result of the local fetch-limited winds.

- There is no sustained correlation between the spring-neap tidal cycle and the measured wave height. Occasionally, a small semi-diurnal signal is evident in the wave heights (e.g. 7th to 14th April in Figure 38). Close inspection of these data shows that this is due to adverse tidal currents causing the southerly waves to peak at mid flood tide.

- During the first month of the wet season period shown (March), there is no obvious correlation with the semi-diurnal water level variations, with peaks in H_s often occurring at low water rather than high water. This seasonal variation in water level influence indicates that the wave conditions during the wet season differed to the wave conditions at the end of the wet season (April) and in the dry season.

- The wave conditions during the wet season were predominantly due to offshore waves, while at the end of the wet season (April) and in the dry season the waves were predominantly due to local fetch-limited wind waves within CG.

- There is a strong correlation between the hindcast modelled offshore H_s in JBG and the measured H_s around CG during both the wet and dry seasons. This indicates that the waves in CG can be influenced by waves generated in JBG and that the waves in both JBG and CG are influenced by the local wind conditions in the region.

- The local wind speed has a very strong correlation with H_s within CG during both the wet and dry seasons. The peaks in H_s correspond with the diurnal peaks in wind speed and the varying magnitude of the wind speed approximately correlates with the variability in H_s. This gives confidence that the hindcast modelled wind conditions represent the mesoscale wind processes in the CG region and that they can be used to drive a wave model which will include the temporal variability in H_s around CG.

- The correlation between H_s and wind speed is strongest towards the end of the wet season (April) and in the dry season, when the wind direction is predominantly from the south to southeast and so the waves within CG are predominantly local fetch-limited wind waves. The measured H_s over the first month (March) of the wet season period can be larger relative to the wind speed compared to measured H_s over the second month (April). The times when the measured H_s appears to be larger coincide with times when the offshore H_s in JBG is also larger, this shows that the offshore wave conditions also influence the H_s offshore and within CG during wet season periods.

- The hindcast modelled wind direction does not correlate with the measured wave direction. This is especially the case towards the end of the wet season (April) and in the dry season when the wind is typically from the southeast while the waves from the north through to east. The reason for this is likely to be related to limitations in the AWACs/ADCPs in reliably calculating short period wave direction during smaller wave conditions due to the hydrodynamic filtering effect. This will be assessed in more detail through the measured wave spectra, which is discussed below.

To understand how the wave conditions varied spatially and temporally through the CG region, timeseries plots of the measured H_s, T_p and wave direction in the wet and dry seasons at locations offshore of CG (AWAC-09 during wet season and AWAC-10 during dry season), at the East Entrance to CG (AWAC-06) (wet season only), within the POA (AWAC-01) and upstream (south) of the POA (AWAC-11) are shown in Figure 44 to Figure 50. The plots show the following:

- Offshore of CG the H_s during the wet season can be larger than during the dry season, with the H_s regularly exceeding 1 m in the wet season while during the dry season it typically remains below 1 m.

- Periods with larger wave heights during the wet season are typically from the north to northeast and associated with T_p of 5 to 6 s indicating old sea waves (i.e. wind waves generated within JBG which then propagated to CG, arriving at a direction no longer coincident with the forcing wind). During the dry season the periods with larger wave heights are typically from the northeast and associated with a T_p of 3 to 5 s, indicating wind waves. For this assessment old sea waves are considered to be waves with a T_p of 5 to 8 s, which are no longer aligned with the forcing wind direction, while wind waves are waves with a T_p of less than 5 s and swell waves are waves with a T_p of more than 8 s.

- During the dry season the T_p can be up to 9 s (i.e. old sea and swell waves), but these periods with higher wave periods typically correlate with low H_s (< 0.5 m). These waves are likely to be a result of small, longer period old sea and swell waves propagating into CG during periods of low wind speed resulting in limited locally generated wind waves. Due to the small H_s of these waves, they are considered unlikely to be important in terms of sediment transport. The larger H_s events (> 0.7 m) during the dry season correspond with waves from the northeast and a T_p of 3 to 5 s, indicating wind waves.

- During the wet season there is a noticeable reduction in H_s between the site offshore of CG and the sites within CG, but during the dry season the H_s is similar offshore and within CG. This again suggests that the wave conditions during the wet season are more influenced by the southward propagation of old sea from JBG, while during the dry season, the waves are more influenced by local winds.

The timeseries plots have a series of vertical lines to represent when wave spectra have been extracted from the measured data to allow a more detailed analysis of the wave conditions. During the wet season, full directional energy spectra have been extracted to represent a large old sea wave event (Figure 51) and a wind wave event (Figure 52), while during the dry season, wave conditions to represent a typical wind wave event (Figure 53) have been extracted. To better understand the wave periods during a small H_s and low T_p wave event during the wet season, the energy density spectra have been extracted and are shown in Figure 54 to Figure 57 (the wave energy was too low during this event for the full directional energy spectra). The plots show the following:

- Large wet season wave event: The frequency of the peak wave energy is similar at all sites, with a peak wave period of around 5 s at all sites, indicating old sea waves. At the offshore site there are two peaks in wave energy, with waves from the north-northeast and northwest. At the East Entrance to CG there is limited energy for waves from the northwest (due to sheltering of the site from this direction by Lacrosse Island), with the dominant wave energy being from the north-northeast. Within the POA, the wave energy is from a single wave direction, the north, this is likely to be due to sheltering from north-northeast waves at this site. Upstream (south) of the POA, the wave energy is from two directions again, the north and northeast, showing that this location is exposed to offshore waves from both the north-northeast and northwest.

- End of wet season wave event: The frequency of the peak wave energy is similar at all sites, with a peak wave period of around 4 s, indicating wind waves. At the offshore site the peak wave energy is from the east, but there is also some wave energy from other directions. At the East Entrance to CG to main peak in wave energy is from northeast, which indicates that the offshore easterly waves have refracted into CG, but there is also a smaller peak in energy from the west-southwest, which indicates some influence from locally generated wind waves in CG. At the sites within the POA and upstream from it (to the south) the main peak in energy remains from the north-northeast to northeast, while a secondary peak in wave energy from the west-southwest is also present. This suggests that during this event there is a combination of wave conditions in CG, with waves from offshore of CG along with wind waves generated within CG.

- Dry season wave event: The frequency of the peak wave energy varies between the sites, with a peak wave period of around 5 s at the offshore site and peak wave period of 3 to 4 s at the sites within CG. The energy spectra is very localised at the offshore site, with a peak direction from the east-northeast. In the POA the dominant peak in wave energy is from the west-northwest, but there are also peaks from the north and east-northeast. This shows that the offshore wave is not dominant at this site, which is due to the site being sheltered from waves from the east-northeast by Lacrosse Island. At the site upstream of the POA the peak wave energy is from the east-northeast again, showing that the offshore waves are dominant at this site, but there are also peaks in wave energy from the west to north-west. The plots therefore show that the relative influence of offshore old sea waves in CG is variable and is dependent on the wave direction, with some areas being sheltered from certain directions.

- Wet season small wave event: The energy density spectra show that the lowest wave energy is at the offshore site, with much higher wave energy at the sites within CG. At the offshore site there is almost equivalent wave energy in the swell wave frequencies as there is in the wind waves frequency, while within CG, the swell wave frequency is much lower than the wind wave frequency. At all sites, the peak in wave energy is between 2.5 to 3s, but the bimodal energy distribution at the offshore site demonstrates how longer period waves can be measured during periods of low wave energy.

In summary, the implications of these findings for the proposed operation and for the numerical modelling are:

- There was a strong correlation between the measured H_s in and just offshore from CG and the offshore hindcast modelled wave data in JBG and a very strong correlation between the measured H_s in and just offshore from CG and the hindcast modelled wind data in CG. Both hindcast modelled waves and winds were shown to represent the diurnal variability in the measured wave height. This gives confidence that the hindcast modelled wind conditions represent the mesoscale wind processes in the CG region, that they can be used to drive the wave model for this assessment and that the wave model will still include the temporal variability in H_s in CG.

- The measured wave data show that waves within CG are typically relatively calm, with the potential for the largest waves to occur during the wet season. During the wet season the larger waves were shown to correspond with old sea waves propagating from JBG, while in the dry season the larger waves were shown to correspond with wind waves generated within CG. Overall, the wave data has shown that the waves within CG are unlikely to be a dominant driver

in terms of sediment transport, but they should still be included in the sediment transport modelling as moderate and large wave events could still increase the near-bed shear stresses and therefore influence the transport rates. This was addressed in the sediment transport model (see Section 3.6).

- The influence of waves from offshore of CG varies spatially within CG and is also dependent on the wave direction, with some areas being sheltered from certain wave directions by Lacrosse Island. This highlights how the wave model needs to be calibrated and validated at multiple sites within CG to ensure it represents the spatial variability in wave conditions within CG. This was addressed in the wave model (see Section 3.5.2).

- Wave spectra have shown that wave energy from multiple directions are often present within CG, with a combination of old sea waves from offshore and locally generated fetch-limited waves from within CG. The timeseries data have shown that the measured wave directions within CG during calmer periods in the dry and transitional seasons did not correlate with the wind directions, this is likely to be related to limitations associated with measuring wave directions for smaller, short period waves. Therefore, the model should focus on being able to represent the spatial variability in wave height in the region and if this can be achieved the model can be considered to be providing a reasonable representation of the wave conditions. This was addressed in the wave model (see Section 3.5.2).

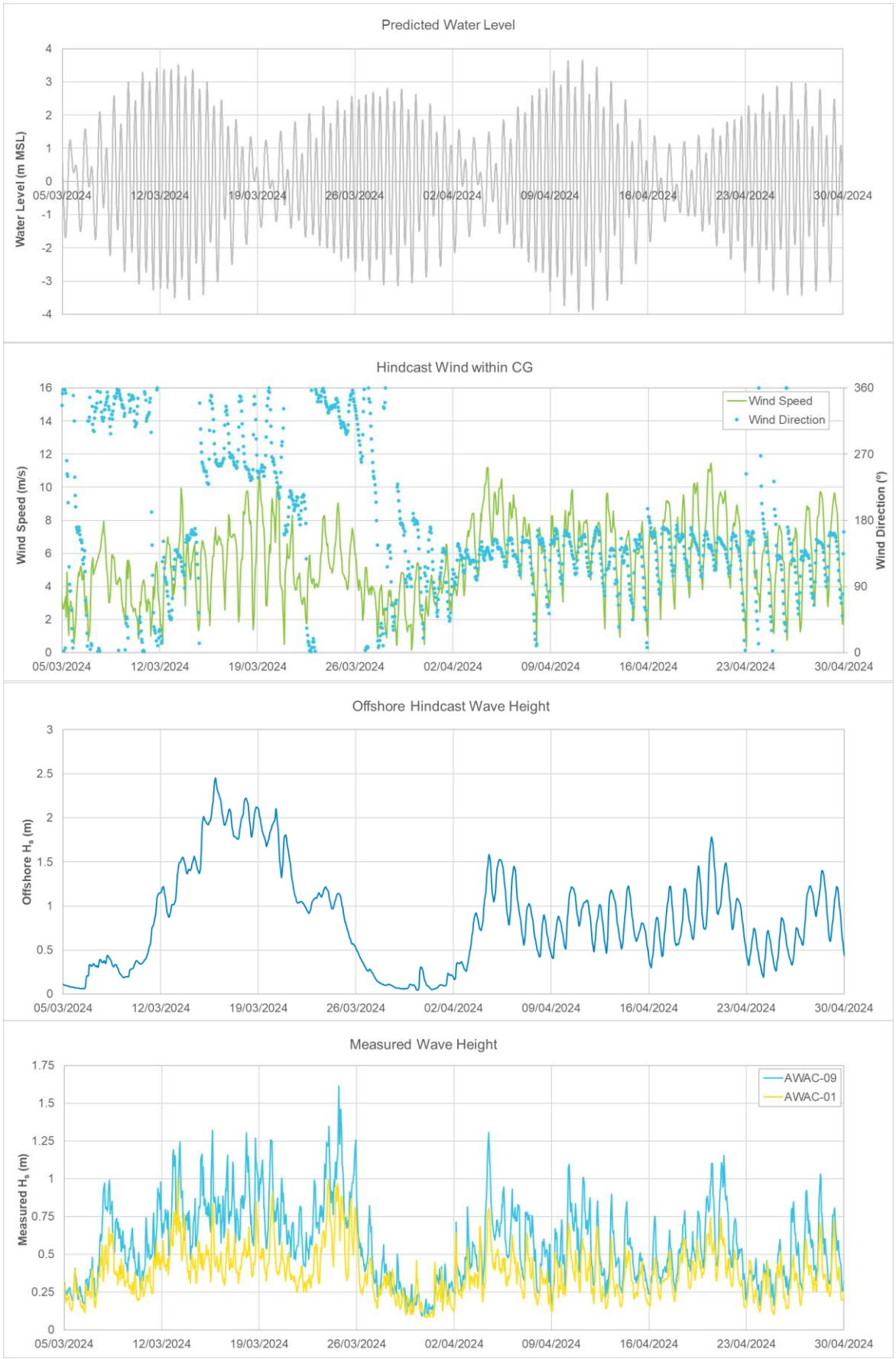


Figure 35. Timeseries of predicted water level (AHO, 2023), hindcast wind within CG (CSIRO, 2024), hindcast offshore wave height (CSIRO, 2024) and measured wave height offshore of CG (AWAC-09) and within CG (AWAC-01).

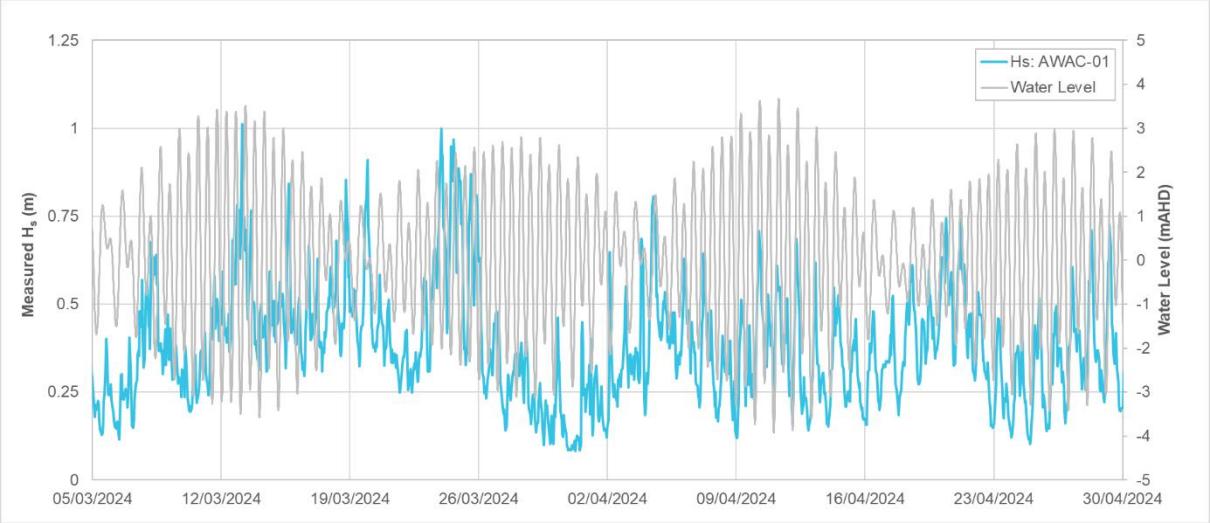


Figure 36. **Comparison between measured H_s within CG (AWAC-01) and measured water level, over 56 days of the wet season.**

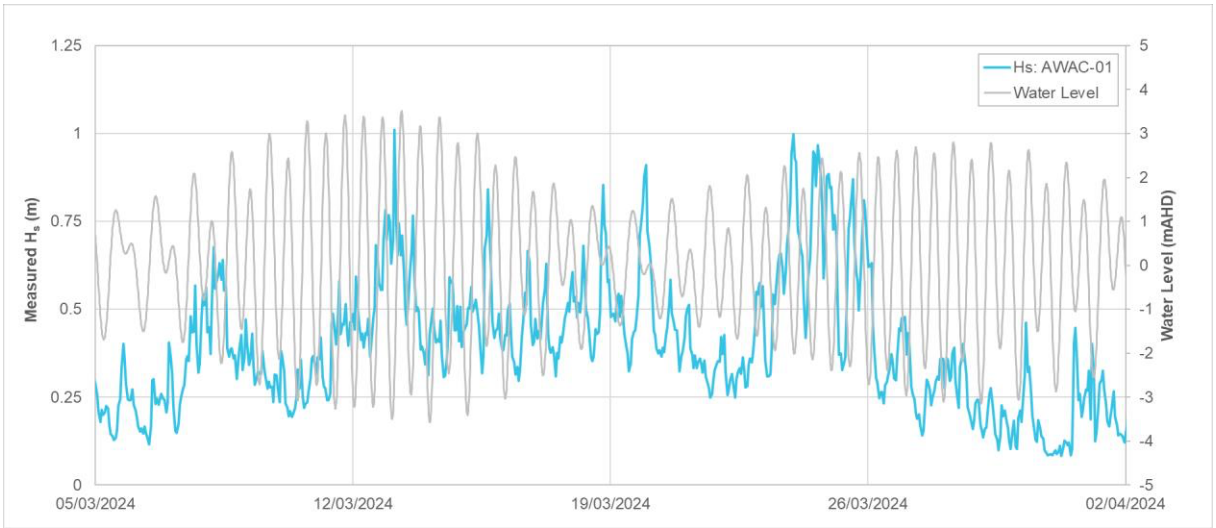


Figure 37. **Comparison between measured H_s within CG (AWAC-01) and measured water level over 28 days of the wet season.**

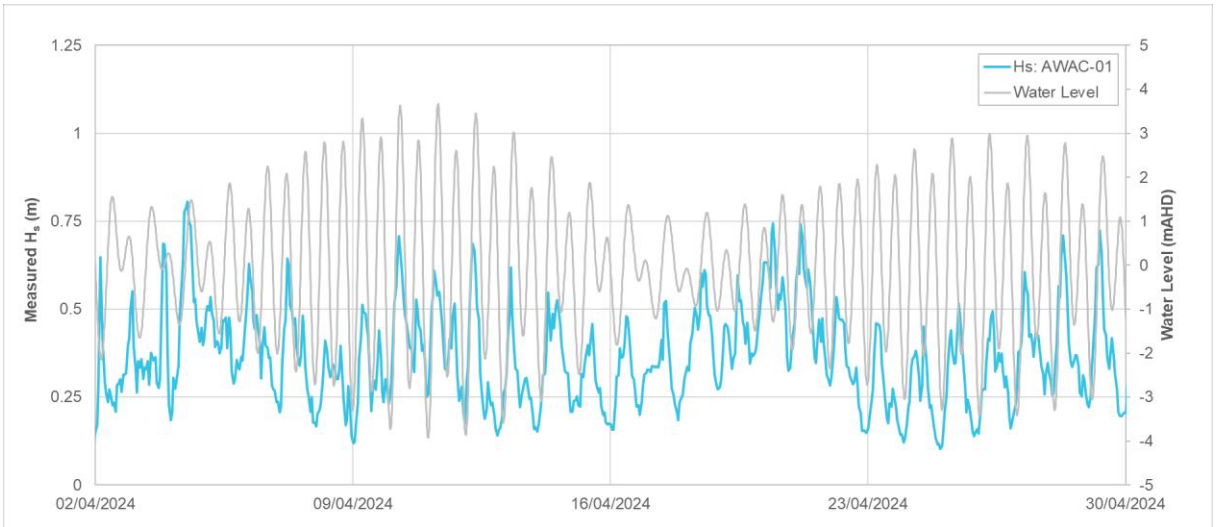


Figure 38. **Comparison between measured H_s within CG (AWAC-01) and measured water level over 28 days at the end of the wet season.**

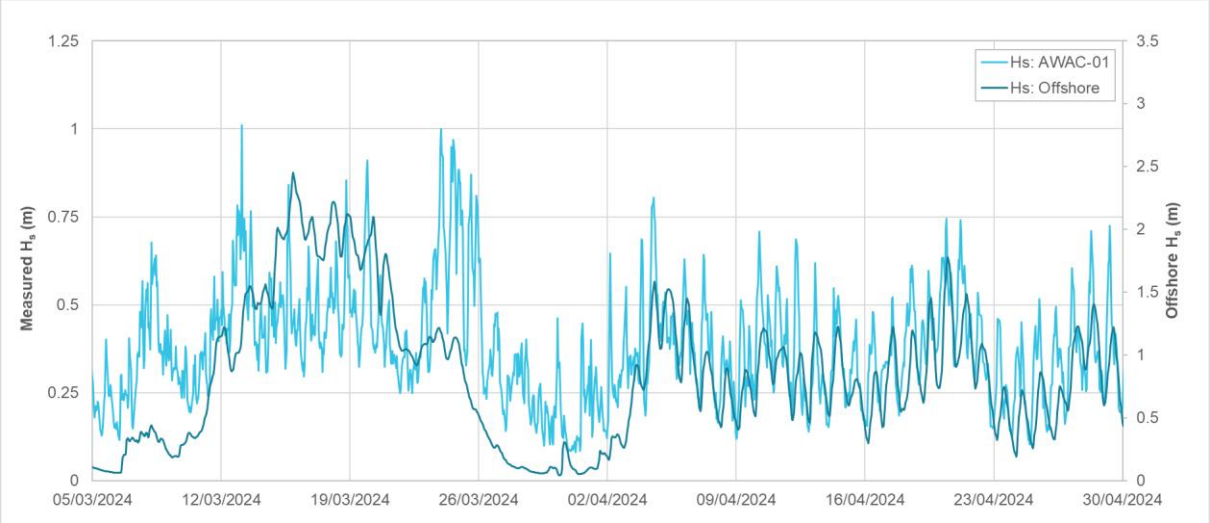


Figure 39. **Comparison between measured H_s within CG (AWAC-01) and hindcast modelled H_s at the entrance to JBG (~150 km north of CG) (CSIRO, 2024) during the wet season.**

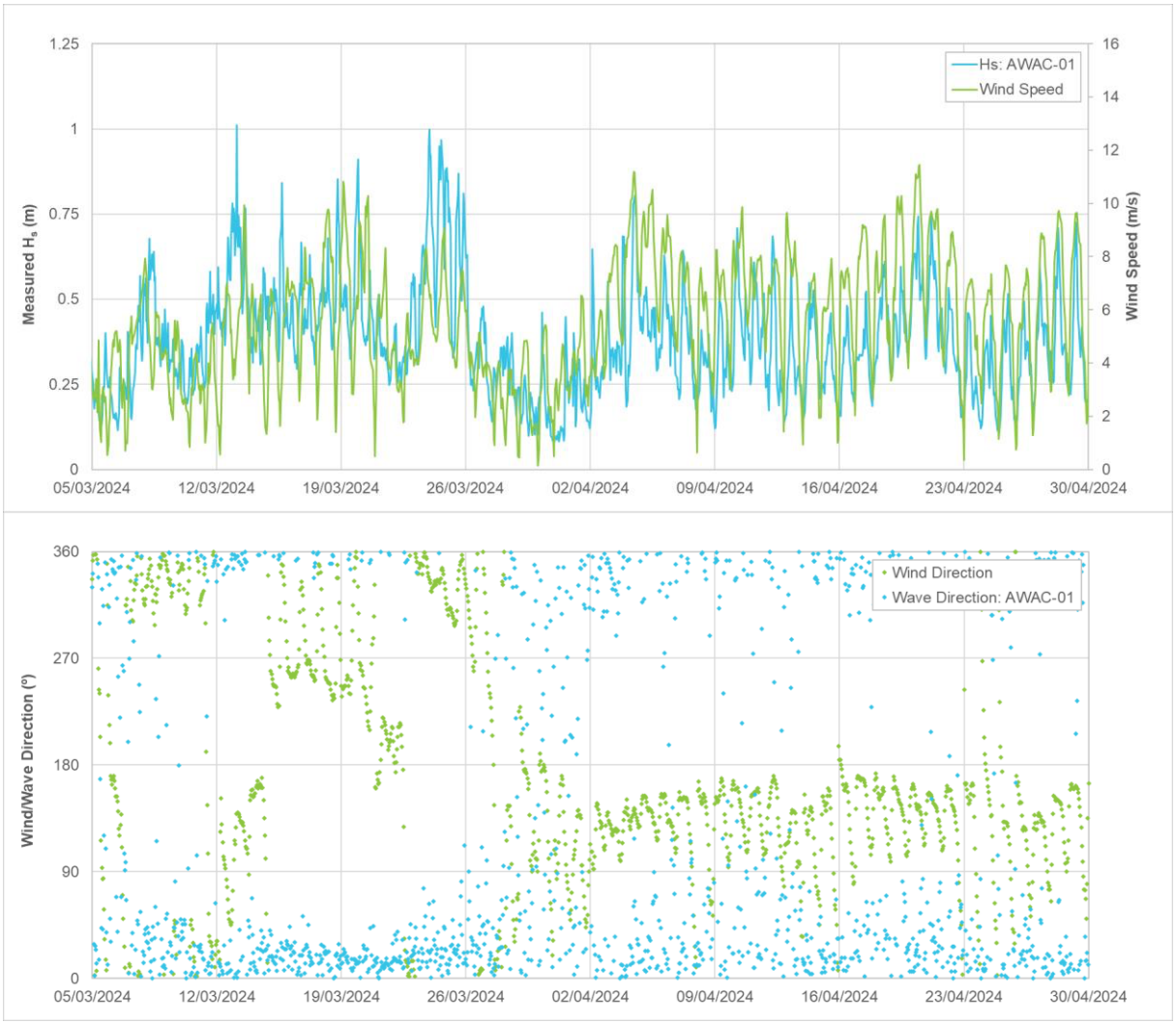


Figure 40. **Comparison between measured wave height and hindcast modelled wind speed (CSIRO, 2024) (upper) and measured wave direction and modelled wind direction (CSIRO, 2024) (lower) within CG during the wet season.**

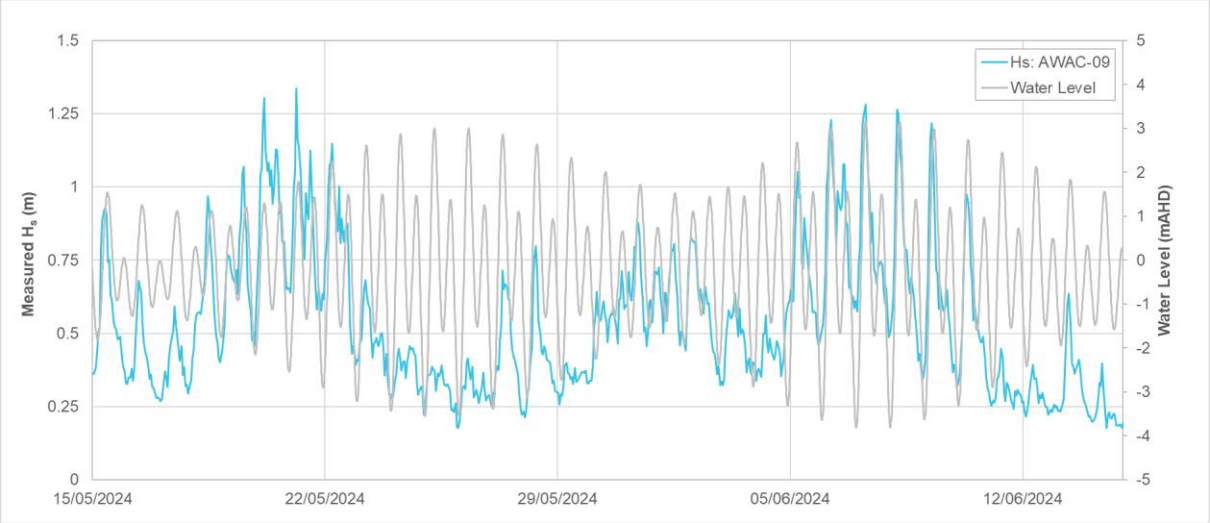


Figure 41. **Comparison between measured H_s offshore of CG (AWAC-09) and measured water level over 31 days of the dry season.**



Figure 42. **Comparison between measured wave height and hindcast modelled wind speed (CSIRO, 2024) (upper) and measured wave direction and modelled wind direction (CSIRO, 2024) (lower) within CG during the dry season.**

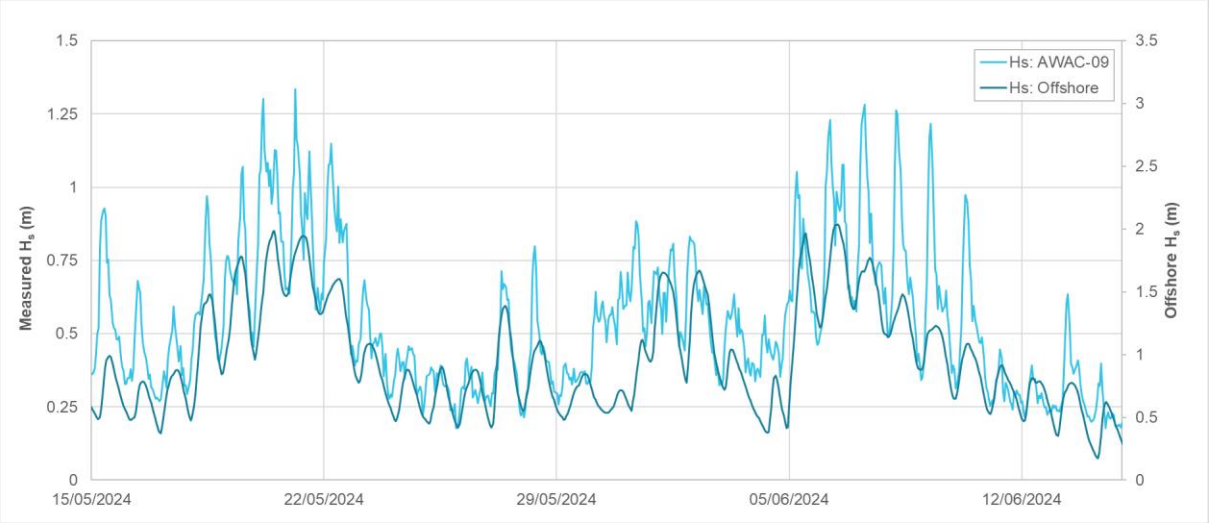


Figure 43. Comparison between measured H_s offshore of CG (AWAC-09) and hindcast modelled H_s at the entrance to JBG (~150 km north of CG) (CSIRO, 2024) during the dry season.

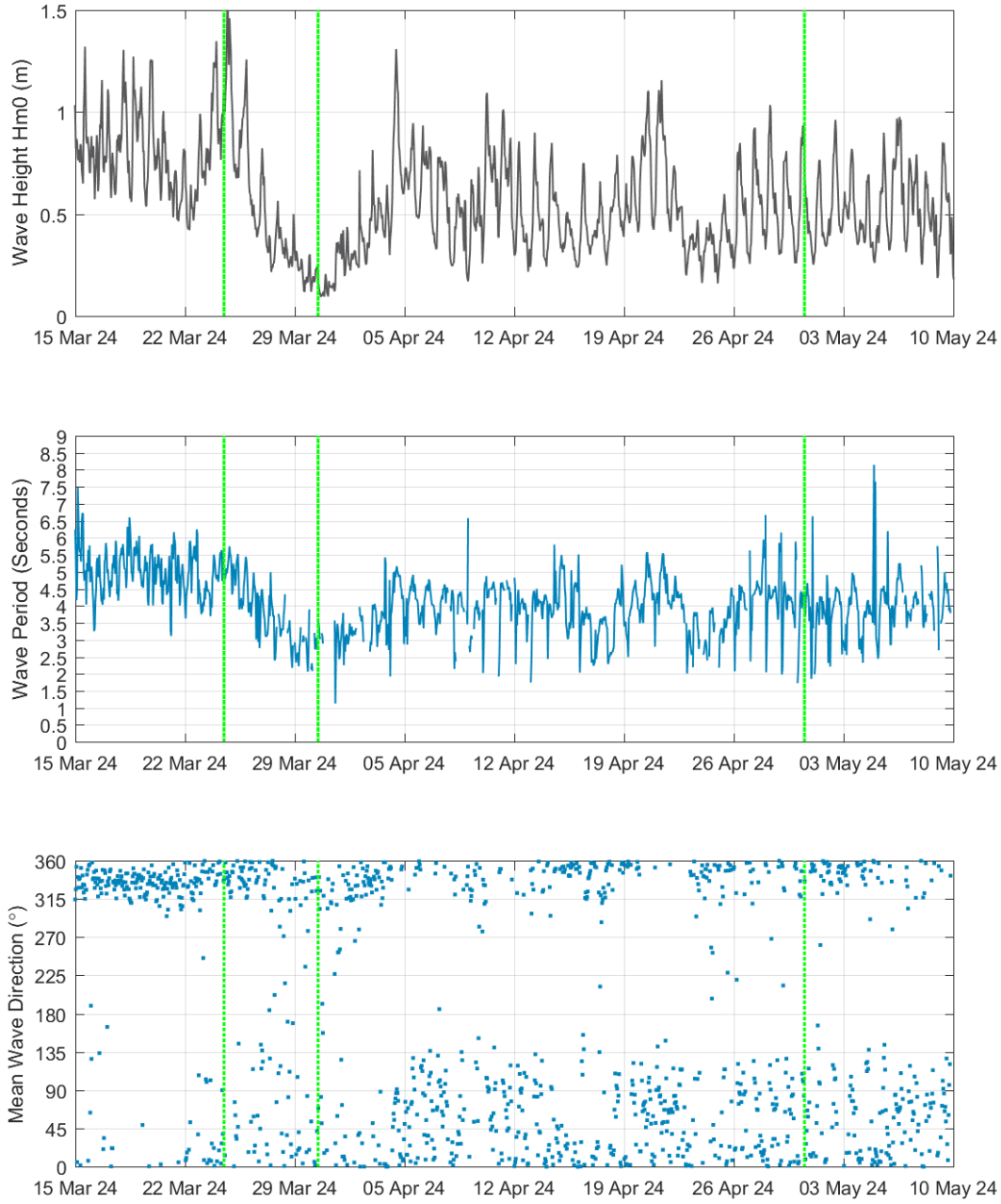


Figure 44. Timeseries plots of measured wave conditions at a site offshore of CG (AWAC-09) during the wet season. *Note: the green lines show times when wave spectra have been extracted.*

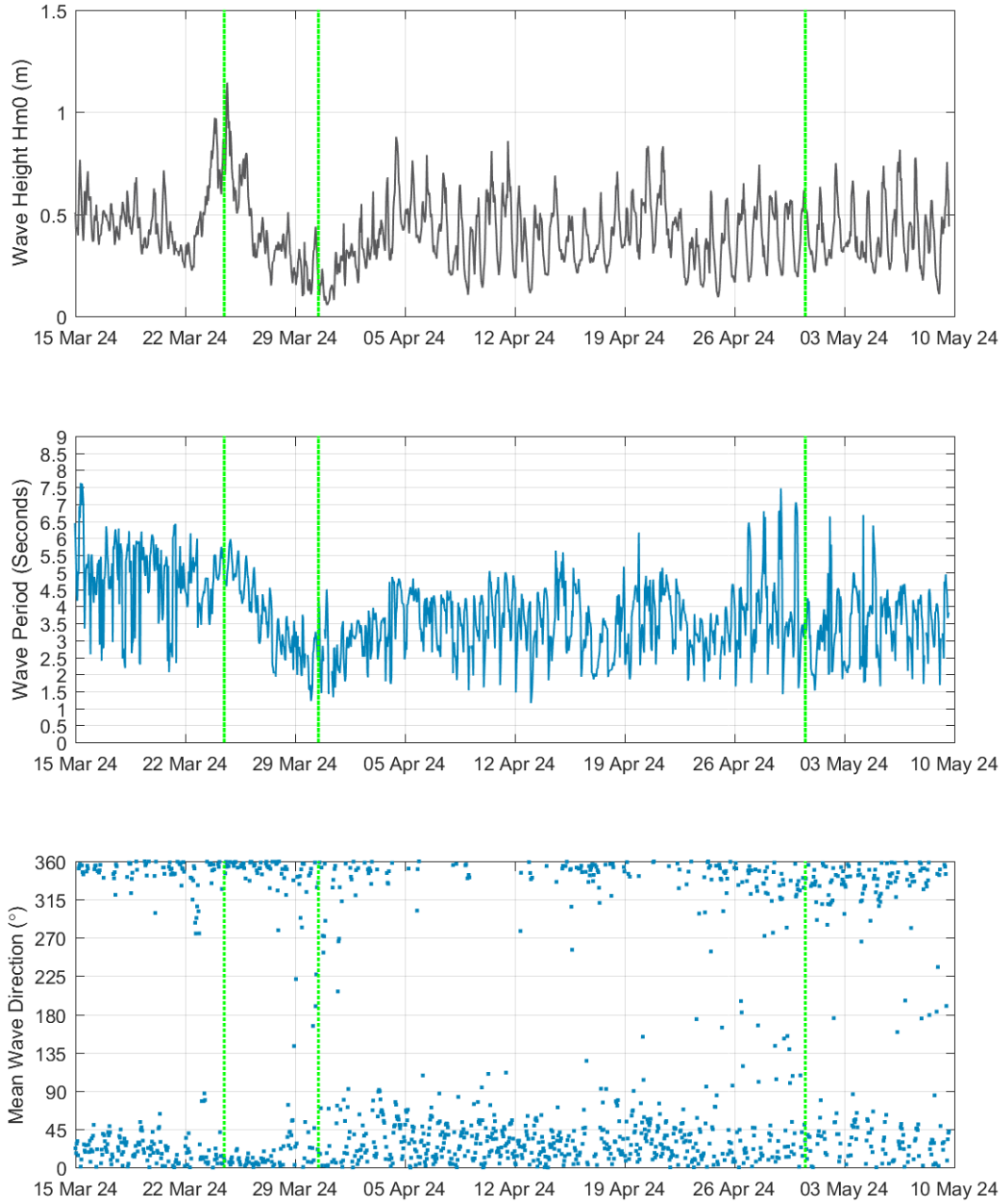


Figure 45. Timeseries plots of measured wave conditions at a site in the East Entrance of CG (AWAC-06) during the wet season. *Note: the green lines show times when wave spectra have been extracted.*

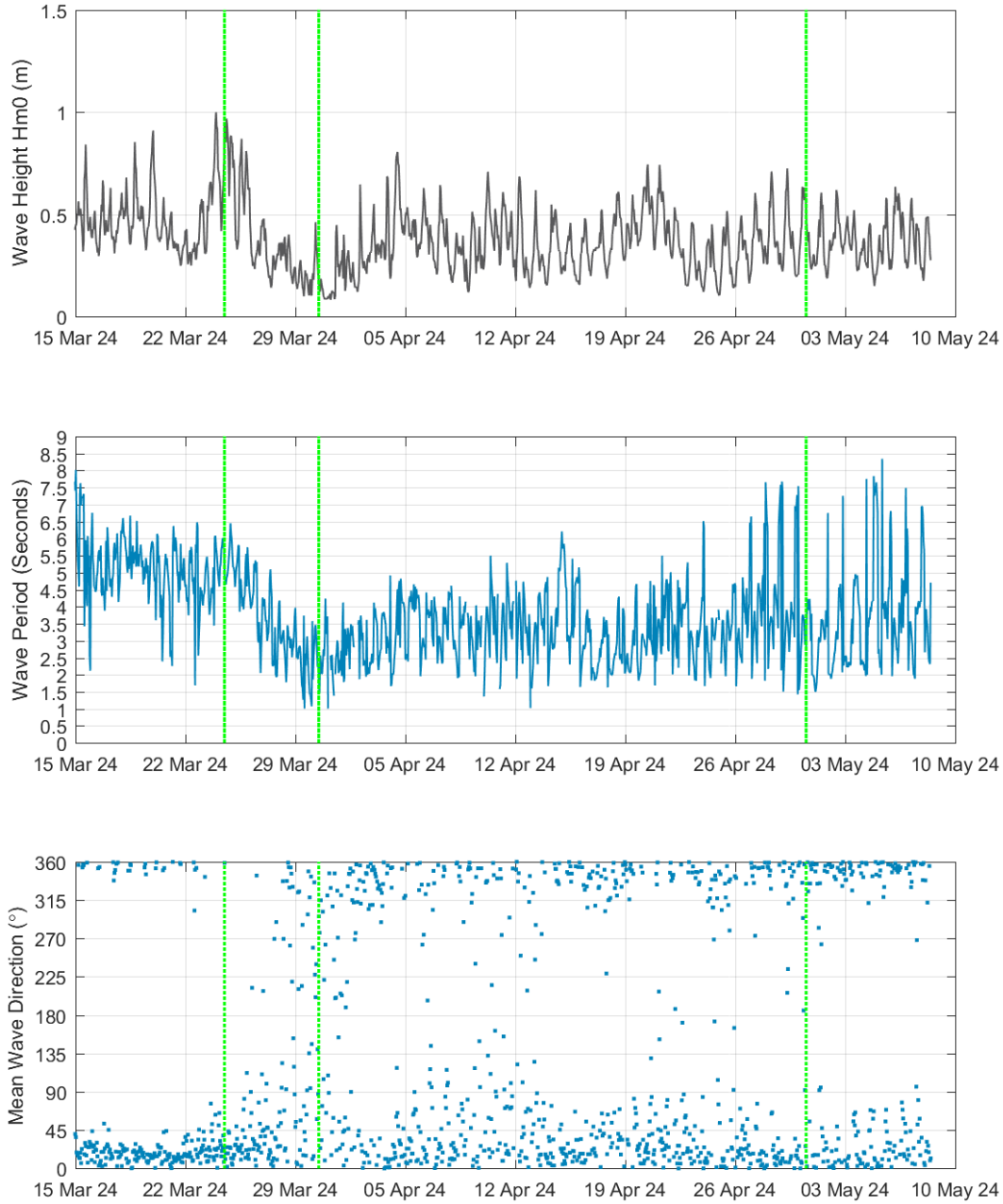


Figure 46. Timeseries plots of measured wave conditions in the POA (AWAC-01) during the wet season. *Note: the green lines show times when wave spectra have been extracted.*

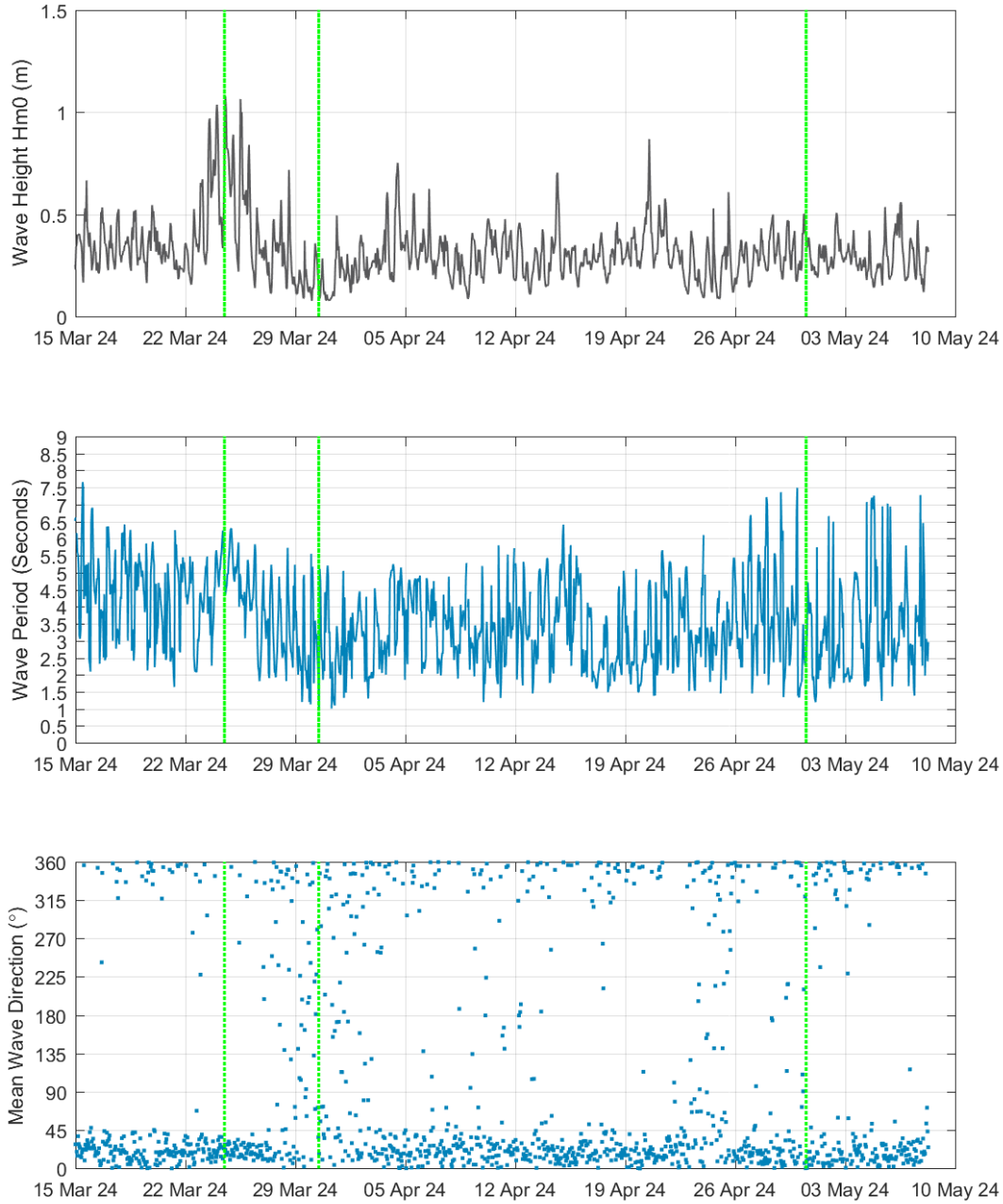


Figure 47. Timeseries plots of measured wave conditions upstream (south) of the POA (AWAC-11) during the wet season. *Note: the green lines show times when wave spectra have been extracted.*

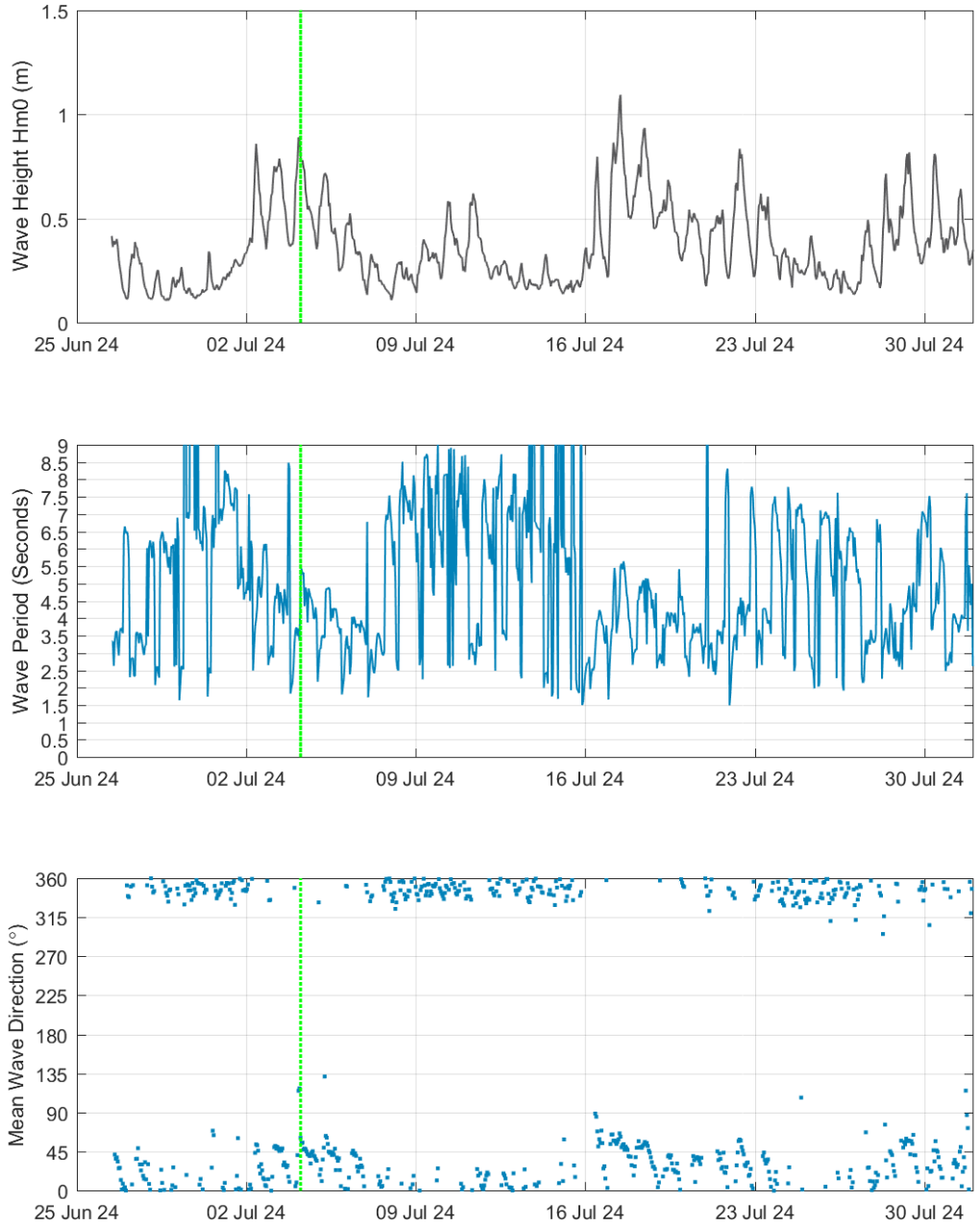


Figure 48. Timeseries plots of measured wave conditions offshore of CG (AWAC-10) during the dry season. *Note: the green line shows the time when wave spectra have been extracted.*

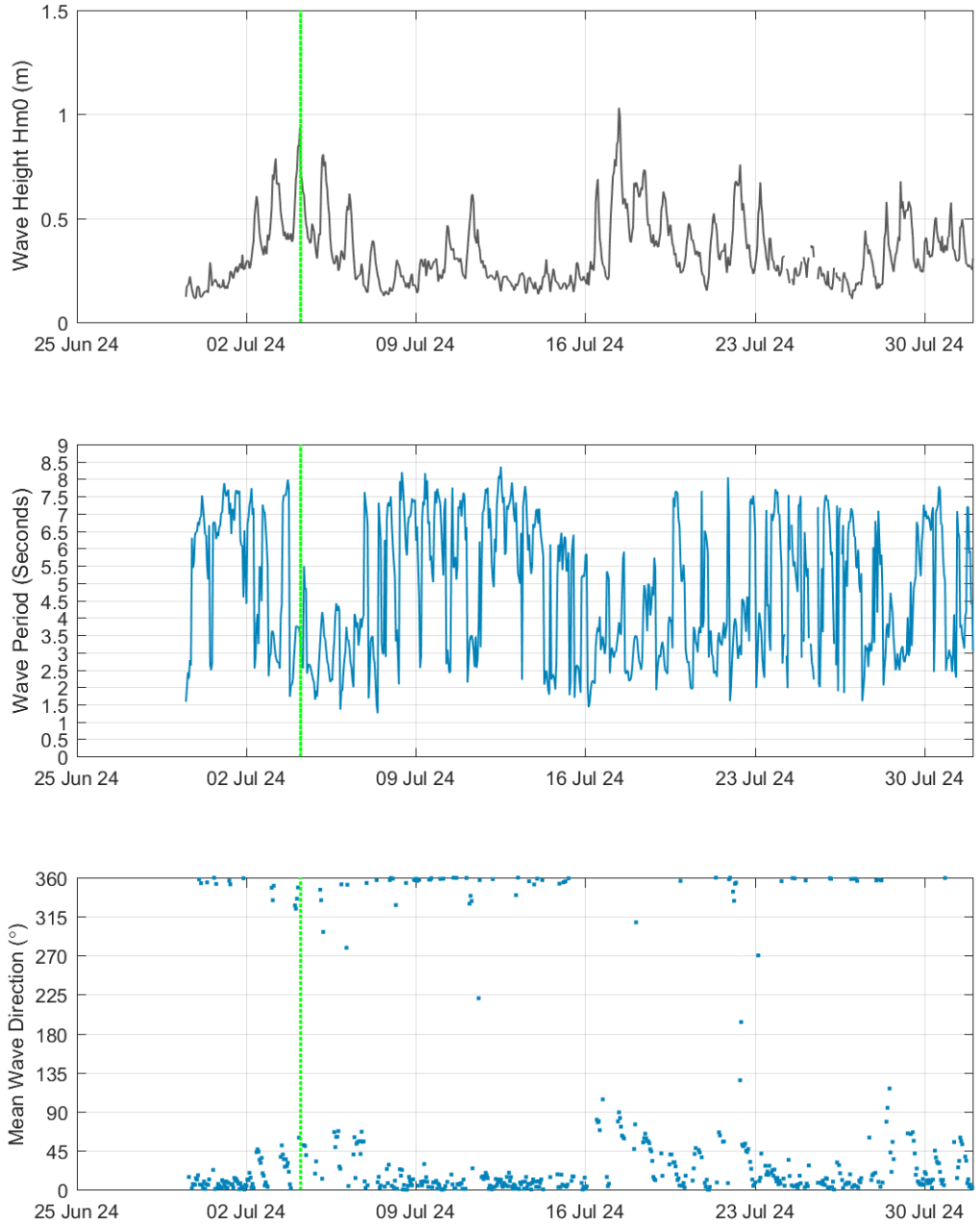


Figure 49. Timeseries plots of measured wave conditions in the POA (AWAC-01) during the dry season. *Note: the green line shows the time when wave spectra have been extracted.*

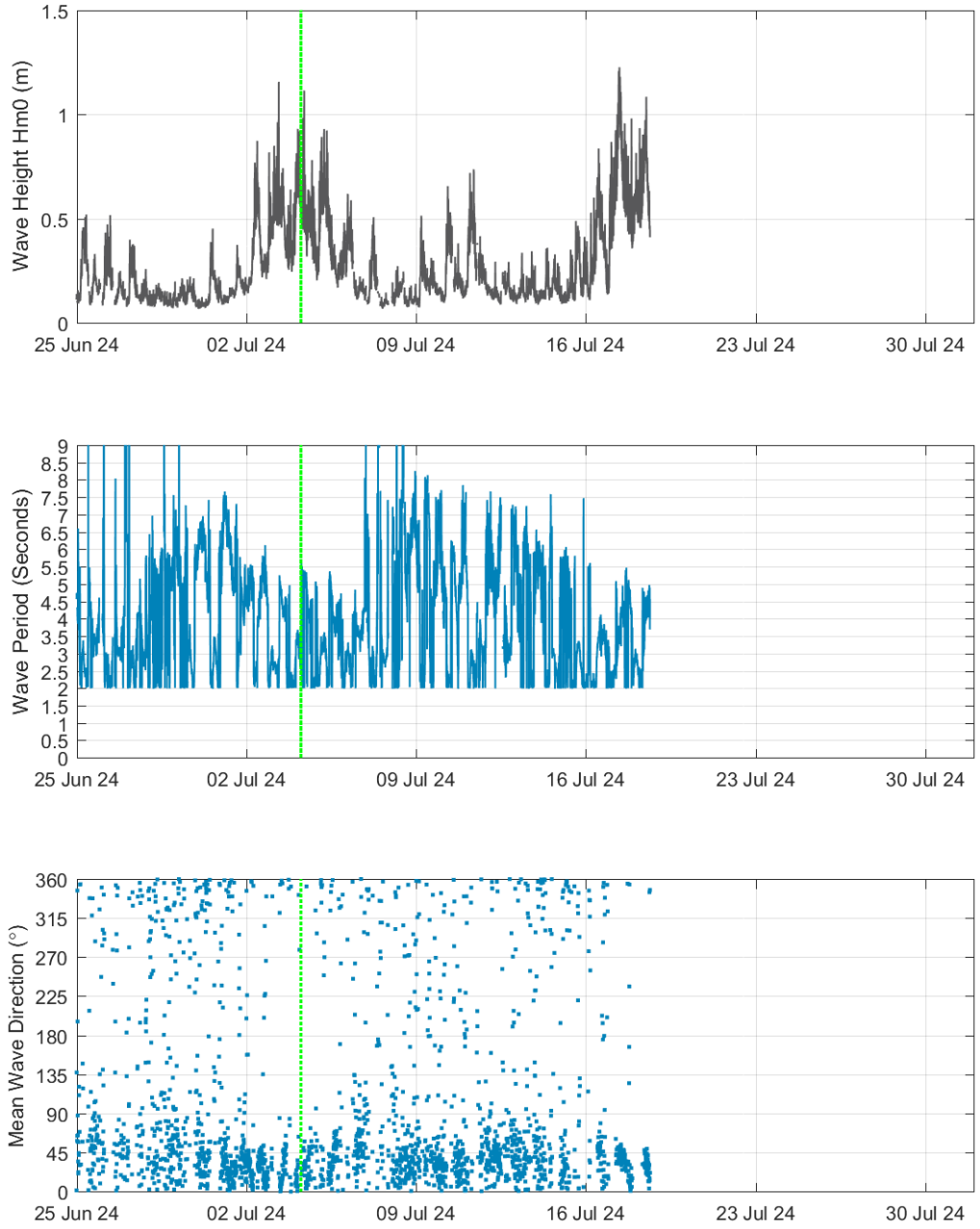
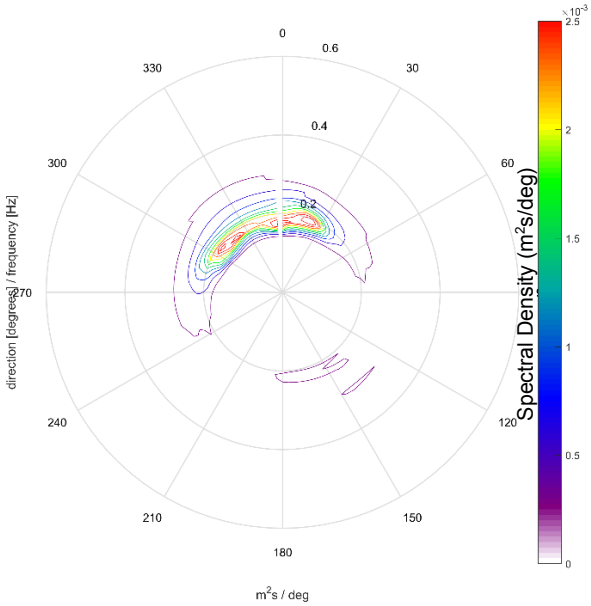
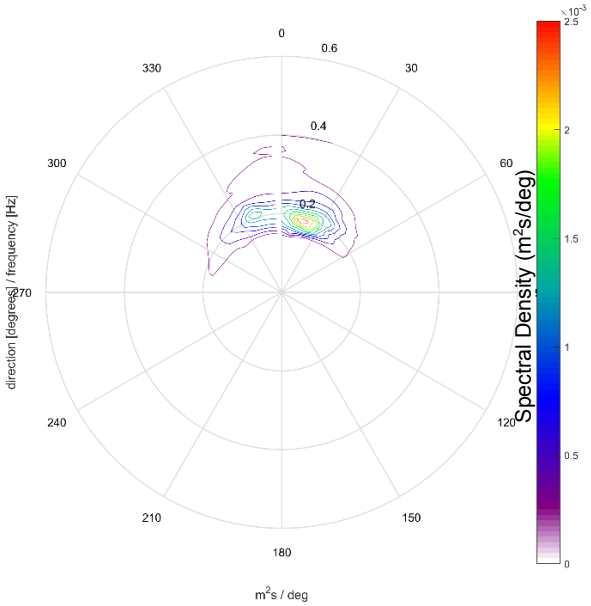


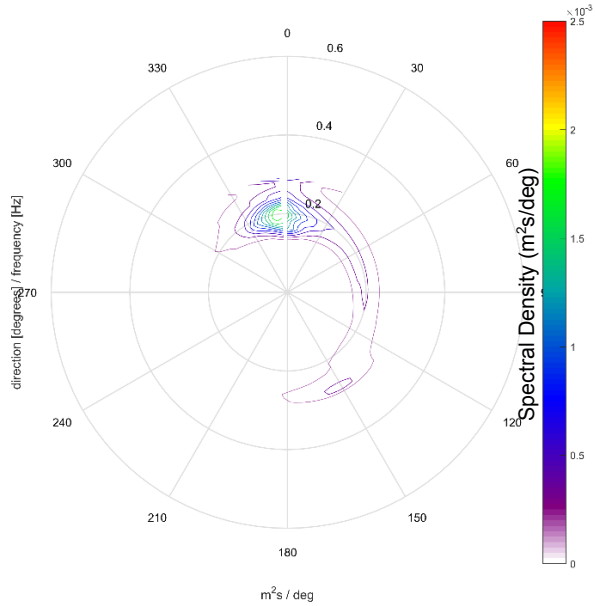
Figure 50. Timeseries plots of measured wave conditions upstream (south) of the POA (AWAC-11) during the dry season. *Note: the green line shows the time when wave spectra have been extracted.*



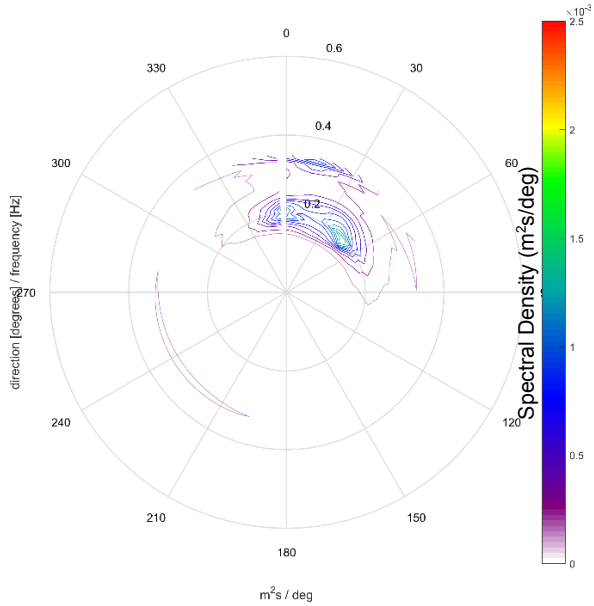
AWAC-09 (Offshore)



AWAC-06 (East Entrance)

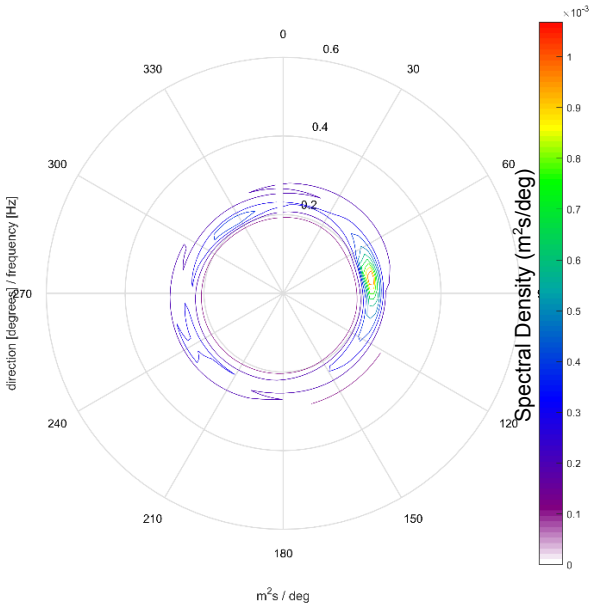


AWAC-01 (Proposed Operational Area)

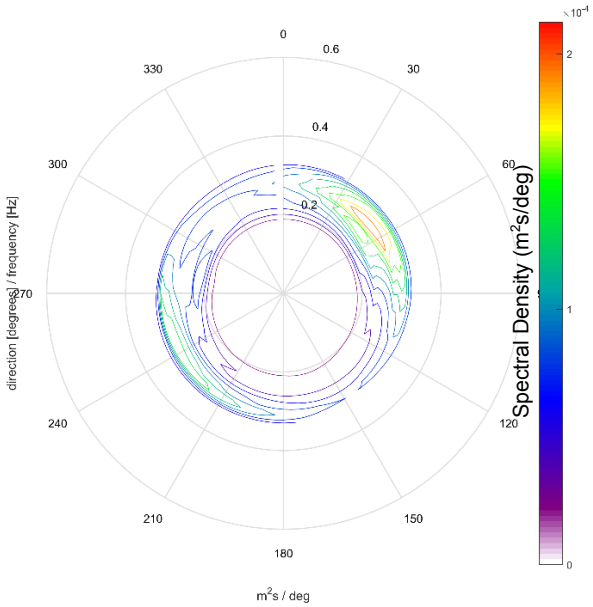


AWAC-11 (Upstream)

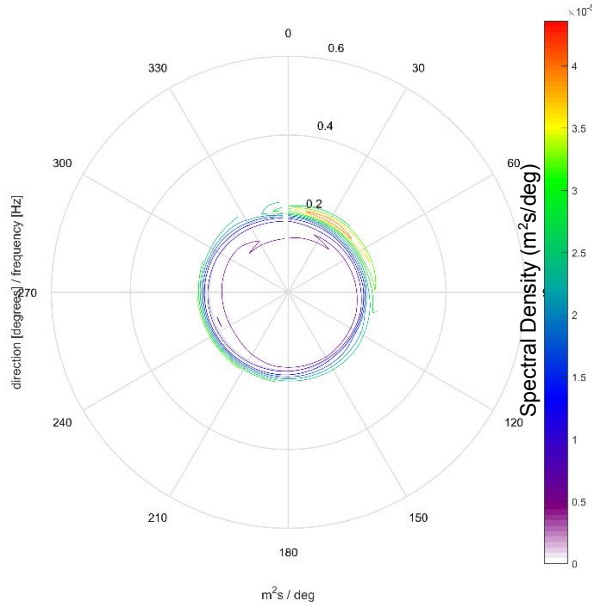
Figure 51. Full directional energy spectra at multiple sites in the CG region during a large wave event on 24/03/2024.



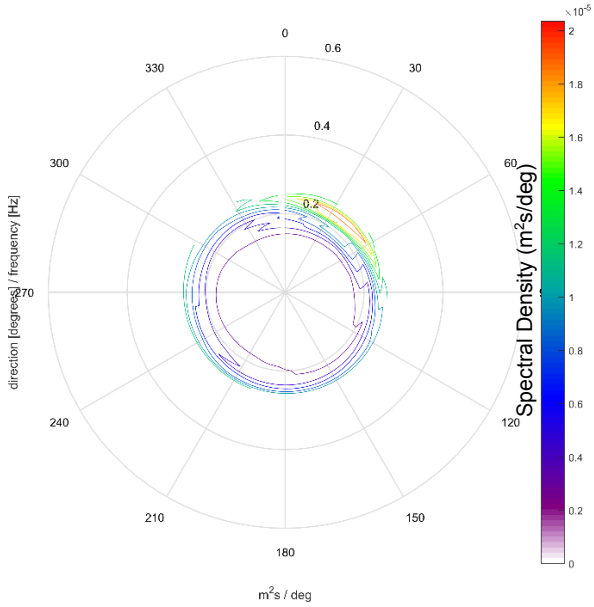
AWAC-09 (Offshore)



AWAC-06 (East Entrance)

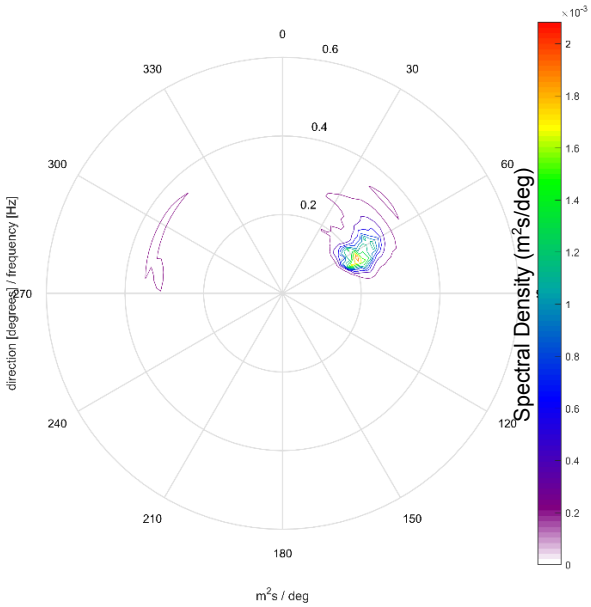


AWAC-01 (Proposed Operational Area)

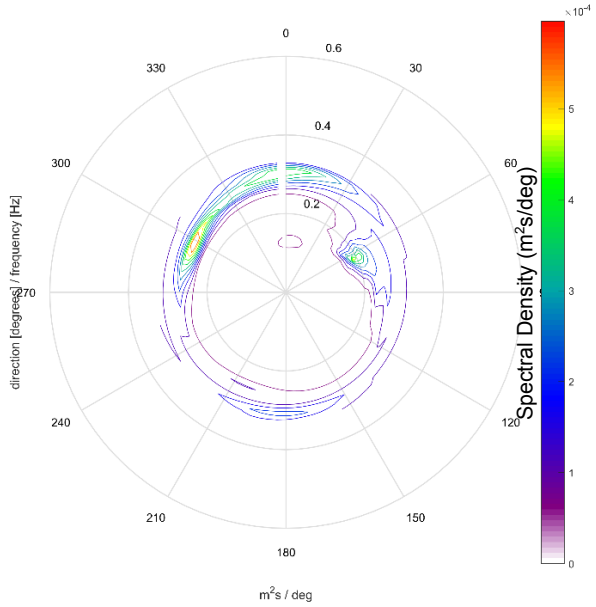


AWAC-11 (Upstream)

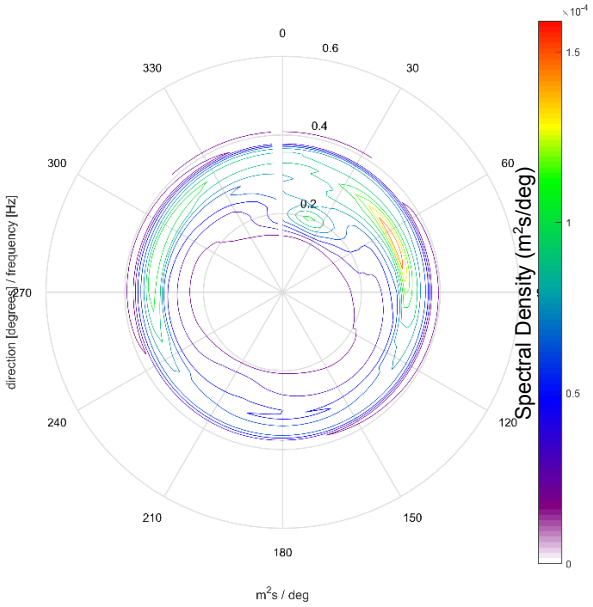
Figure 52. Full directional energy spectra at multiple sites in the CG region during a wave event at the end of April 2024 (30/04/2024).



AWAC-10 (Offshore)



AWAC-01 (Proposed Operational Area)



AWAC-11 (Upstream of POA)

Figure 53. Full directional energy spectra at multiple sites in the CG region during a dry season wave event (04/07/2024).

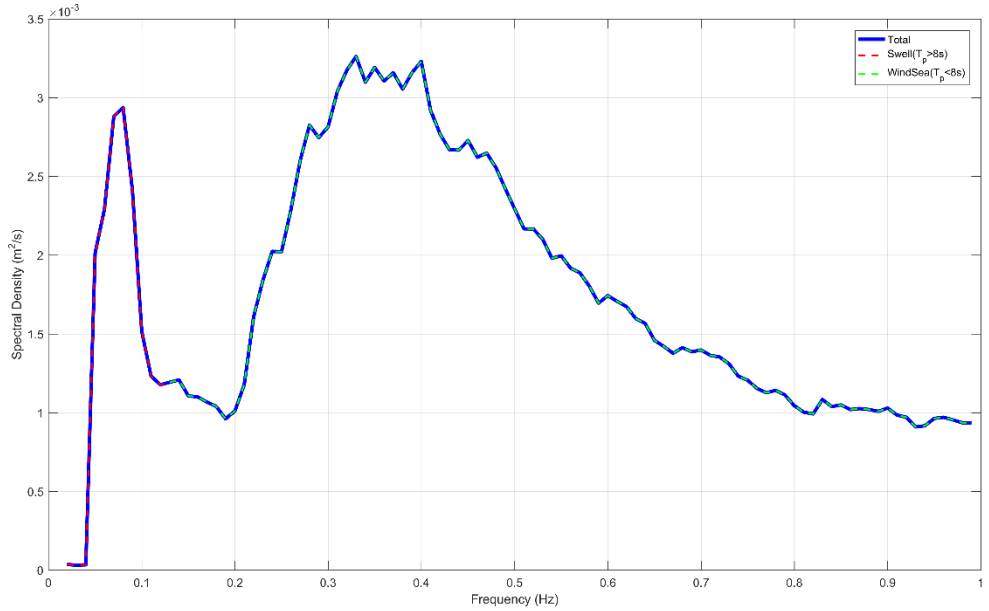


Figure 54. Energy density spectra at AWAC-09 during a small wave height, low wave period wave event in the wet season (30/03/2024).

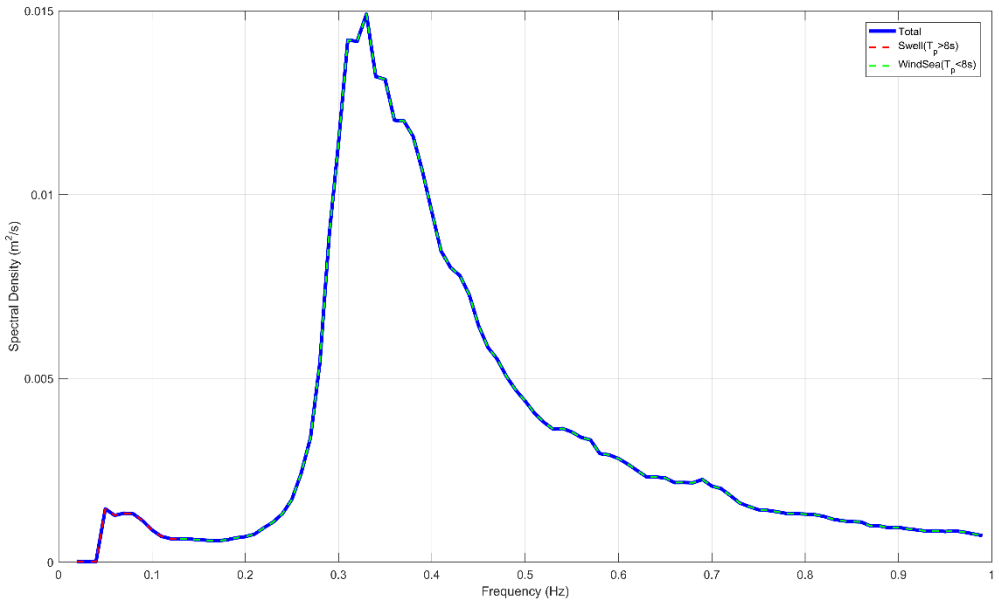


Figure 55. Energy density spectra at AWAC-06 during a small wave height, low wave period wave event in the wet season (30/03/2024).

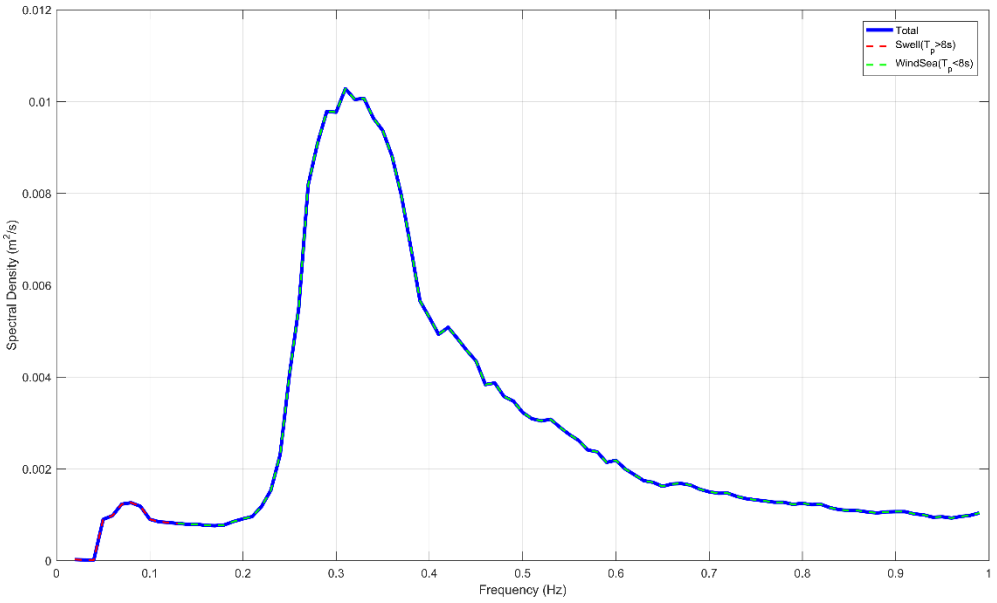


Figure 56. Energy density spectra at AWAC-01 during a small wave height, low wave period wave event in the wet season (30/03/2024).

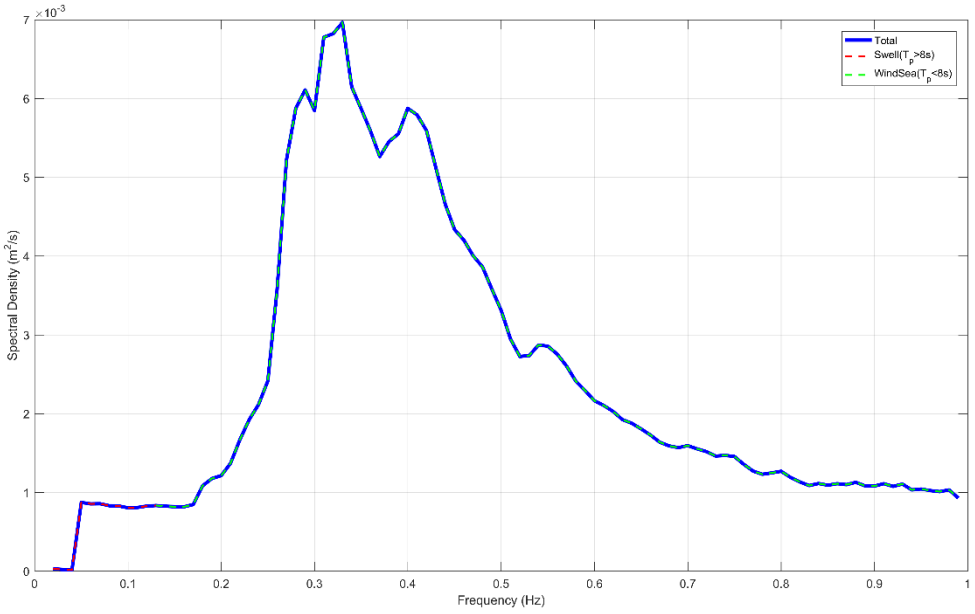


Figure 57. Energy density spectra at AWAC-11 during a small wave height, low wave period wave event in the wet season (30/03/2024).

2.3. Water Quality

BKA has put significant effort into collecting in-situ benthic light and turbidity data at most of the 14 AWAC and Pos sites shown on Figure 3, for the periods listed in Table 1, in section 2. This is in order to provide reliable baseline data on natural benthic light and turbidity conditions in the CG area, over the full range of both wet and dry season conditions. Because benthic communities are dependent on benthic light and are affected by changes in turbidity, it is important to have reliable baseline data on these parameters, in order to assist the assessment of potential impacts on benthic communities from any changes to these parameters that might be caused by the proposed operation (although it should be noted that benthic communities are depauperate in CG - BKA 2024b).

It is also important to establish the relationship between turbidity and Suspended Solids Concentrations (SSC) under local conditions in both the wet and dry season, to inform the sediment transport and plume modelling. This relationship has been established for CG as described in section 2.3.1.

An initial analysis of the available water quality data collected by BKA up to June 2024 was undertaken by PCS (2024b). This report provides a more detailed analysis of the measured turbidity and benthic light data, including the significant volume of additional data collected from the AWAC and Pos sites since June 2024, to better understand the range of near-seabed light and turbidity values and ranges and measured spatial and temporal variability.

As outlined in section 2 the turbidity sensors attached to the frames at the AWAC and Pos sites were part of multi-sonde units also equipped with temperature, salinity and pH sensors. However, these parameters are not analysed in this report, as they do not relate to the objectives of this report, which are to assess and model hydrodynamics, sediment dynamics and coastal processes and sediment plumes and turbidity.

The separate Factual Data Report (PCS (2024c) covers all relevant data, including data sourced from previous studies by others and all data collected by BKA, including the temperature, salinity and pH data.

As outlined in section 2, an update to the Factual Data Report (PCS, 2024c) including all data analysed in this report (up to 14th August 2024) is submitted in support of this report.

2.3.1. Turbidity & Suspended Solid Concentration

This section analyses all available in-situ near-seabed turbidity data collected from all of the AWAC and Pos sites shown on Figure 3 from 7th September 2023 (when the first turbidity data were collected) to 14th August 2024.

In order to establish the relationship between turbidity and TSS under local conditions, BKA collected concurrent turbidity data in Nephelometric Turbidity Units (NTUs) and water samples for SSC analysis via vertical profile sampling with Niskin bottles, at various locations and depths throughout CG and offshore, in both the dry season (July 2023) and wet season (February 2024) (PCS, 2024a & 2024b). The water samples were analysed in the laboratory to measure SSC in mg/L, and a correlation was then developed between the measured NTU values and mg/L values for both wet and dry season conditions, as follows:

- Dry season: 1 NTU = 1.72 mg/L.
- Wet season: 1 NTU = 2.77 mg/L.

It should be noted that the relationship between turbidity and SSC in an environment such as CG, where mixed sediment types can be in suspension, can be complex due to potential variability in the type and mass of suspended sediments, both spatially and temporally. In order to address this, a wide range of locations and conditions was sampled and represented in the relationships. However, it is still possible that the relationships could over- or under-estimate SSC at some locations and times. Never-the-less, the relationships are considered to be suitable to allow the measured turbidity data to be converted to SSC to allow calibration and validation of the sediment transport model (Section 3.6).

To show how the turbidity range and typical values vary in the region, the 1st, 50th and 99th percentile turbidity values based on all measured data at each of the AWAC and Pos sites are presented in Table 3, along with the correlated TSS values. All available measured turbidity data at each site are shown as timeseries plots in Figure 58 to Figure 61.

Table 3 and Figure 58 to Figure 61 show that the natural near-seabed turbidity and correlated TSS values in CG can be extremely high compared to other coastal areas of northern WA, most likely due to

regular resuspension of seabed sediments by the strong tidal currents. This was also observed by BKA during the 2023 and 2024 environmental survey work in CG, with the Traditional Owners of the area referring to CG as 'Brown Water Country' and the water throughout much of CG consistently being very turbid (Figure 62 and Figure 63).

The highest 99th percentile recorded between all AWAC and Pos sites throughout the monitoring period were 470 NTU and 1,057 mg/L, at AWAC-08, with the highest values having been recorded mid-March 2024. The lowest 1st percentile recorded between all sites throughout the monitoring period were 4 NTU and 9 mg/L, at AWAC-05 and Pos 14, with low values consistently occurring during neap tides. The median values for the data from the sites throughout the monitoring period ranged from 16 to 143 NTU and 27 to 323 mg/L.

Of particular relevance to the environmental assessment of the proposed operation are the turbidity and SSC values at the following locations:

a) Within the POA (site AWAC-01), as this is where the sand-sourcing operation is proposed.

b) At King Shoals (site AWAC-09 and Pos 12) offshore from CG, which is a Sanctuary Zone within the State Kimberley Marine Park, and therefore a high priority for protection, and which represents open-water conditions outside of CG.

c) At the False Mouths of the Ord (site AWAC-07), on the eastern side of CG, which is part of the Ord River Floodplain Ramsar wetland, and therefore a high priority for protection, and which represents more estuarine conditions.

d) At West Arm well upstream (south of) the POA (site AWAC-08), to assess how upstream conditions might differ from within the POA and from the other sites.

The key turbidity and SSC values for each of these sites are presented below:

a) Within the POA (site AWAC-01) the 99th percentile values over the monitoring period were 160 NTU and 361 mg/L, with higher turbidity during the wet season. The 1st percentile values over the monitoring period were 6 NTU and 11 mg/L, with lowest turbidity during neap tides in the dry season. The median values at the site throughout the monitoring period were 28 NTU and 64 mg/L.

b) At King Shoals (site AWAC-09 and Pos 12) the 99th percentile values over the monitoring period were 114 NTU and 256 mg/L, with higher turbidity during wave events in the wet season. The 1st percentile values over the monitoring period were 5 NTU and 10 mg/L, with the lowest turbidity measured during neap tides in the dry season. The median values for all data at the site throughout the monitoring period were 22 NTU and 49 mg/L.

c) At the False Mouths of the Ord (site AWAC-07), the 99th percentile values over the monitoring period were 240 NTU and 413 mg/L, with elevated turbidity consistently occurring during spring tides. The 1st percentile values over the monitoring period were 7 NTU and 12 mg/L, with low turbidity occurring during the smallest range neap tides. The median values for all data from this site throughout the monitoring period were 55 NTU and 94 mg/L.

d) At West Arm (site AWAC-08), the 99th percentile values over the monitoring period were 470 NTU and 1,057 mg/L, with the highest turbidity measured in mid-March 2024. The 1st percentile values over the monitoring period were 51 NTU and 114 mg/L, with lower turbidity occurring during the neap tides. The median values for all data from this site throughout the monitoring period were 143 NTU and 323 mg/L.

It is clear from the values presented above and from further analysis of the measured turbidity data from all of the AWAC and Pos sites that turbidity and correlated SSC varied spatially and temporally in and offshore from CG.

The turbidity was generally lower close to the two entrances to CG and in offshore waters outside of CG and higher further upstream (south) within CG. The turbidity was higher in the wet season compared with the dry season at sites within CG, while at sites offshore of CG the turbidity was fairly similar for the wet and dry season. Within CG the turbidity was typically highest around low water due to the ebb stage of the tide transporting higher turbidity water from upstream into CG, and lower around high water as a result of the flood stage of the tide transporting lower turbidity water from offshore into CG. This was the case within the POA (AWAC-01), in the East Entrance to CG (AWAC-06) and upstream (south) of the POA (sites AWAC-11). The measured turbidity data (and correlated TSS values) therefore suggest

a net import of fine-grained suspended sediment from West and East Arms into CG, with this sediment then either being redistributed within CG or exported out through the West and East Entrances.

At most sites there was a clear spring-neap tidal signal with higher turbidity coinciding with the spring tides and lower turbidity coinciding with the neap tides. This would have been due to increased resuspension of seabed sediments by stronger tidal currents during spring tides along with the increased transport distance of suspended sediment from West and East Arms into CG due to the stronger tidal currents during spring tides.

At the offshore site at King Shoals (AWAC-09 and Pos 12), the spring-neap tidal pattern was not as clear, suggesting that the turbidity at this location may not be as strongly influenced by tidal currents, but possibly influenced more by the wave conditions. In contrast, the site offshore of the East Entrance to CG (AWAC-10) experiences a clear spring-neap tidal variability and is more similar to the sites within CG than to the other offshore site at King Shoals (AWAC-09 and Pos 12). These differences are likely to be at least partially related to the sediment composition at the sites, with very little fine-grained silt and clay present at King Shoals or in the POA around AWAC-01, while around Medusa Bank at AWAC-10, there is a higher percentage of fine-grained silt and clay due to the area being less energetic both in terms of currents and waves.

To better understand the relative influence of potential drivers on turbidity and SSC in the wet season, the measured turbidity at an offshore site (AWAC-09), a site in the POA (AWAC-01) and a site upstream (south) of the POA (AWAC-11) are plotted along with the water level, river discharge and offshore measured wave conditions (AWAC-09) in Figure 64. The plots show the following:

- There is strong spring-neap tidal signal in the turbidity at the site upstream of the POA, while the turbidity at the offshore site does not exhibit a clear spring-neap signal while the site in the POA has similar turbidity to the offshore site but does experience a small spring-neap tidal signal.
- The highest turbidity at the offshore and POA sites coincided with a large wave event, but other large wave events did not appear to result in increased turbidity which suggests that other parameters are also important, potentially such as the duration of the wave event and the wave direction.
- The turbidity at the site upstream (south) of the POA (AWAC 11) was significantly higher over the first two sets of spring tides compared with the subsequent two spring tides despite the tidal range of the latter two spring tides being larger. The reason for this is due to the high river discharge event which peaked on 09/03/2024 resulting in increased suspended sediment being discharged from both West and East Arms. This resulted in the turbidity remaining elevated for at least 1 month in the upstream (southern) half of CG. This period of elevated river discharge did not influence the turbidity at the site within the POA or located offshore of CG.

To better understand the relative influence of potential drivers on turbidity and SSC in the dry season, the measured turbidity at an offshore site (AWAC-09), a site in in the False Mouths of the Ord (AWAC-07) and a site upstream (south) of the POA (AWAC-11) are plotted along with the water level, river discharge and offshore measured wave conditions (AWAC-09) in Figure 64. The plots show the following:

- Similar to the site upstream of the POA, the site at the False Mouths of the Ord shows a strong spring-neap tidal signal in turbidity. Both sites experience similar magnitude peaks in turbidity during spring tides (200 to 300 NTU), while the turbidity at the site in the False Mouths of the Ord are lower during neap tides.
- The timing of the peaks in turbidity at the sites upstream of the POA and at the False Mouths of the Ord do not directly correlate. The highest peaks in turbidity upstream of the POA coincide with the lower of the two daily low waters while the highest peaks in turbidity at the False Mouths of the Ord coincide with the higher of the two daily low waters (which is immediately after the higher of the two daily high waters). This suggests that the source of the turbidity differs, with the turbidity upstream of the POA due to higher turbidity water from West and East Arms flowing into CG, while the turbidity at the False Mouths of the Ord are due to local sediment resuspended from within these creeks as a result of inundation of the mudflats, mangroves and saltpans during the higher spring tides.
- The turbidity at the offshore site typically remained between 20 and 70 NTU over the whole period, with short duration peaks in turbidity of 100 to 180 NTU occurring during periods with larger waves.

In summary, the implications of these findings for the proposed operation and for the numerical modelling are:

- The turbidity is variable in the region, with higher turbidity upstream and lower turbidity offshore. The turbidity also varies over multiple time scales, with lower turbidity at high tide, higher turbidity at low tide, and lower turbidity in the dry season and higher turbidity in the wet season. This shows how important it is for the modelling to consider a range of different time scales, including simulating sediment transport during different seasons. This was addressed in the model (see Section 3.6.2).
- The turbidity within CG is predominantly influenced by the astronomical tide, although high river discharge events can also result in elevated turbidity, while the turbidity offshore of CG is more influenced by offshore wave conditions than the astronomical tide. The turbidity within the southern half of the POA was shown to correlate more with the offshore turbidity than the turbidity at other sites within CG. This is likely to be related to the small percentage of fine-grained silt and clay present within the sediment in the POA. The results therefore demonstrate that the modelling needs to include a range of drivers (including offshore waves and upstream river discharges) to be able to represent the temporal and spatial variability in turbidity. This was addressed in the model (see Section 3.6).
- Extensive turbidity data have been collected by BKA in the CG region, allowing a detailed understanding of the variability in turbidity in the region and how different drivers can influence the turbidity. These data were used to allow an extensive calibration and validation of the sediment transport model to determine whether the model can represent the temporal and spatial variability in SSC, and in turn whether it sufficiently resolves the driving forcing which influences the transport.
- The natural near-seabed turbidity and correlated SSC values in CG are considered to be high due to regular resuspension of seabed sediments by the strong tidal currents. It is important that any changes resulting from the sand sourcing (either the deepening of the POA or sediment suspended by the activity) are considered relative to the high natural turbidity/SSC in the region.

Table 3. Percentile turbidity and SSC values at each site based on all measured data between 7th September 2023 and 14th August 2024.

Site	1st Percentile		50th Percentile (Median)		99th Percentile	
	NTU	SSC (mg/L)	NTU	SSC (mg/L)	NTU	SSC (mg/L)
AWAC-01	6	14	28	64	160	361
AWAC-02	6	10	29	49	67	116
AWAC-03	-	-	-	-	-	-
AWAC-04	-	-	-	-	-	-
AWAC-05	4	9	16	27	45	102
AWAC-06	5	11	27	59	193	434
AWAC-07	7	12	55	94	240	413
AWAC-08	51	114	143	323	470	1057
AWAC-09/ Pos-12	5	10	22	49	114	256
AWAC-10	9	16	30	52	112	193
AWAC-11	12	27	52	116	268	604
Pos-13	8	18	40	90	203	457
Pos-14	4	9	25	55	116	261
Pos-15	11	24	55	123	317	712

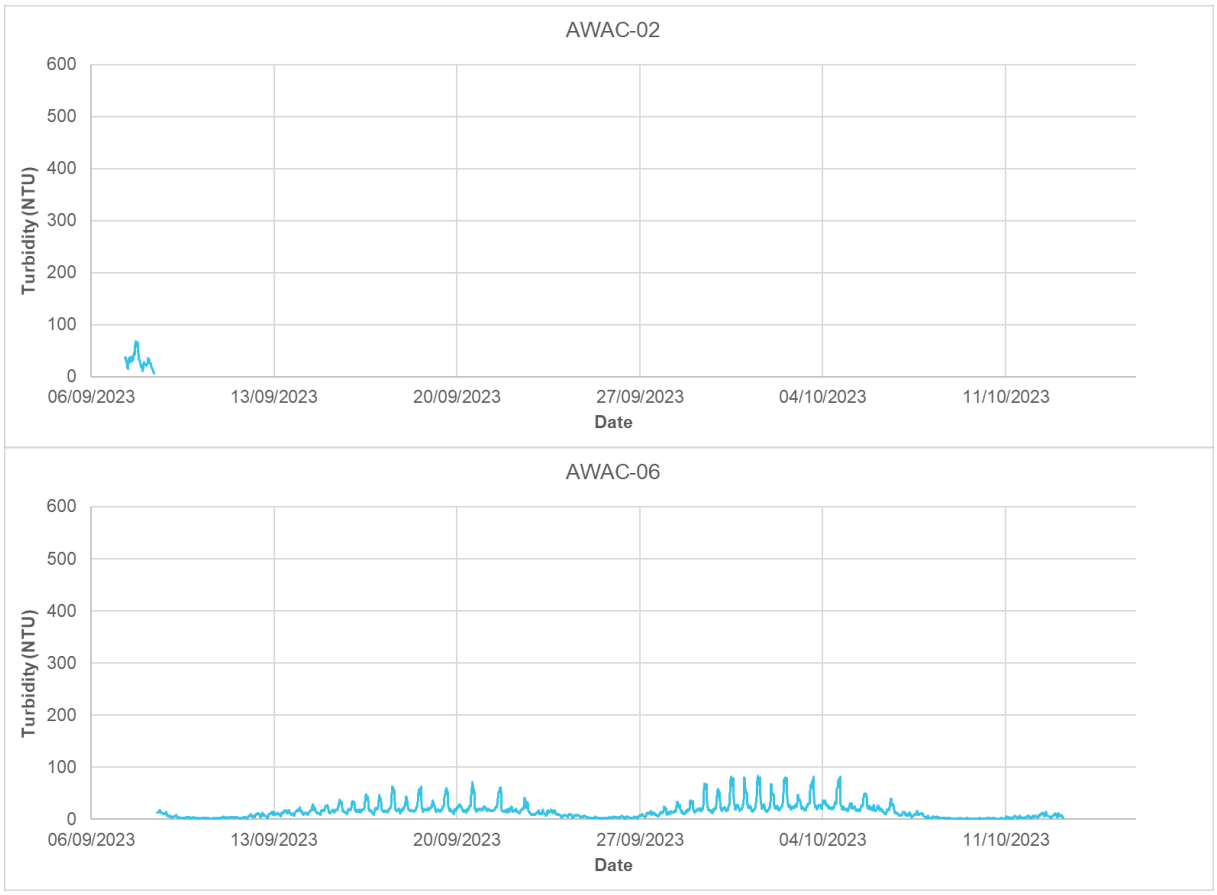


Figure 58. Measured benthic turbidity at sites AWAC-02 and AWAC-06 during the dry/transitional seasons in 2023.

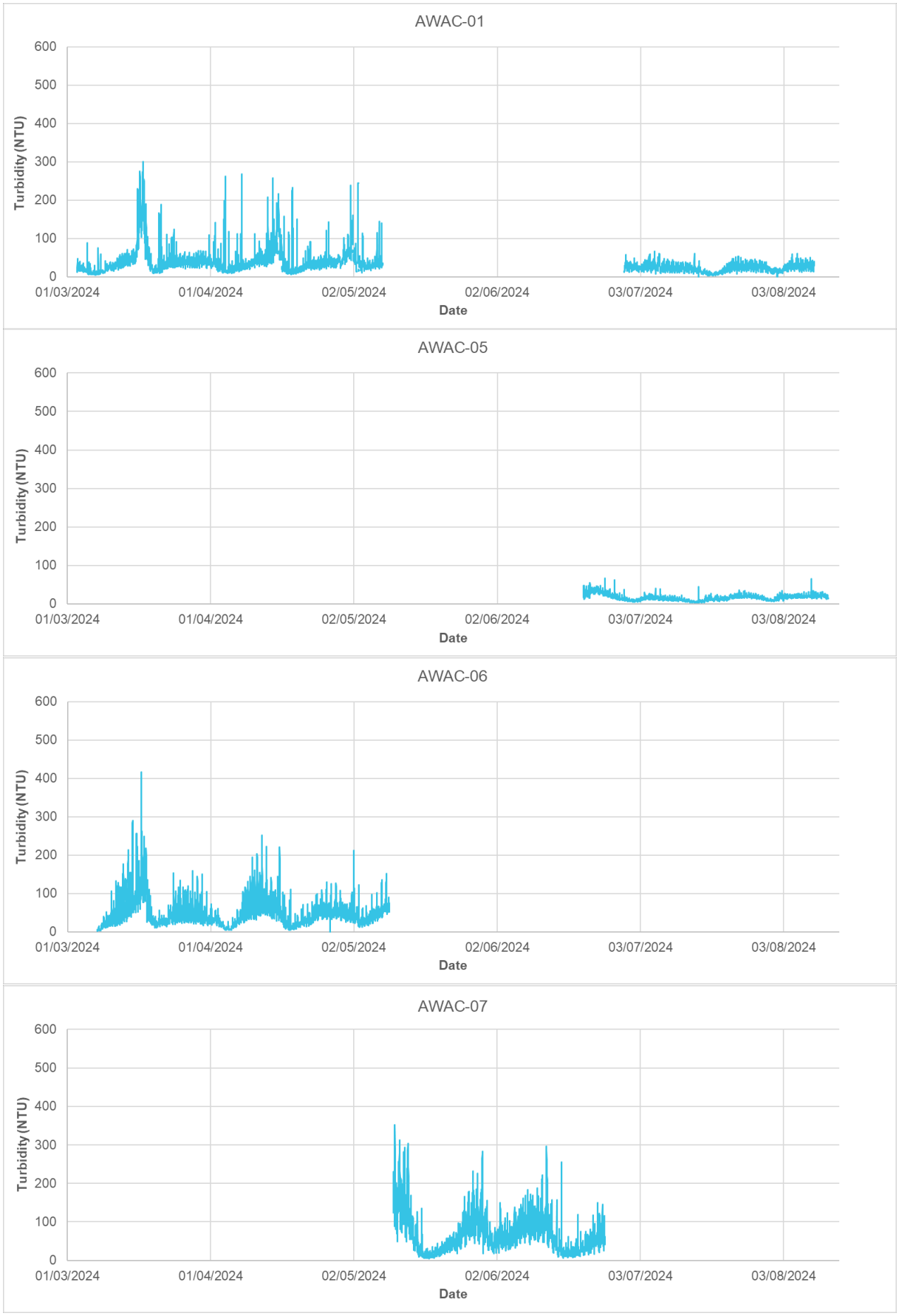


Figure 59. Measured benthic turbidity at AWAC-01, AWAC-05, AWAC-06 and AWAC-07 between March and August 2024 (wet and dry seasons).

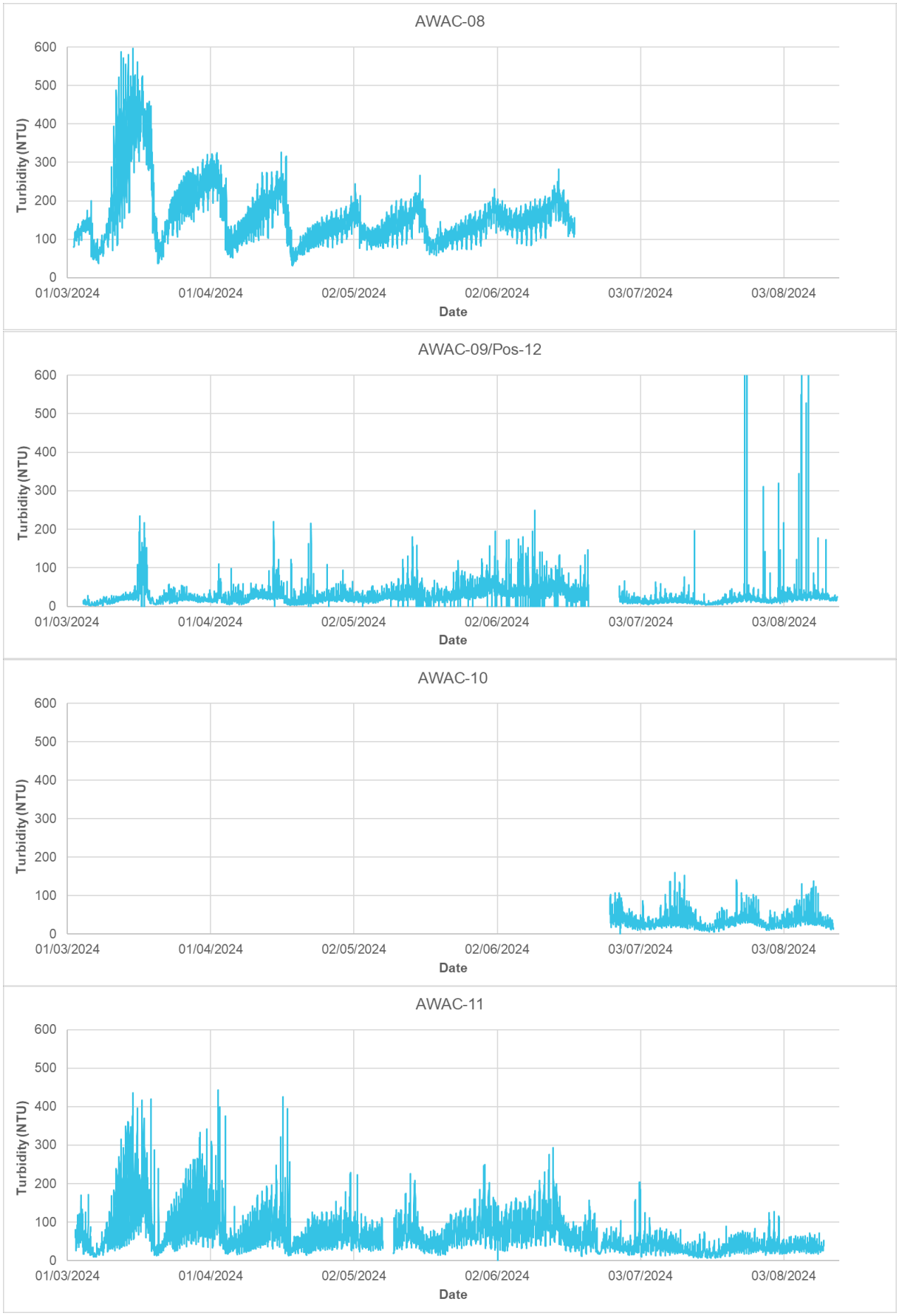


Figure 60. Measured benthic turbidity at AWAC-08, AWAC-09/Pos-12, AWAC-10 and AWAC-11 between March and August 2024 (wet and dry seasons).

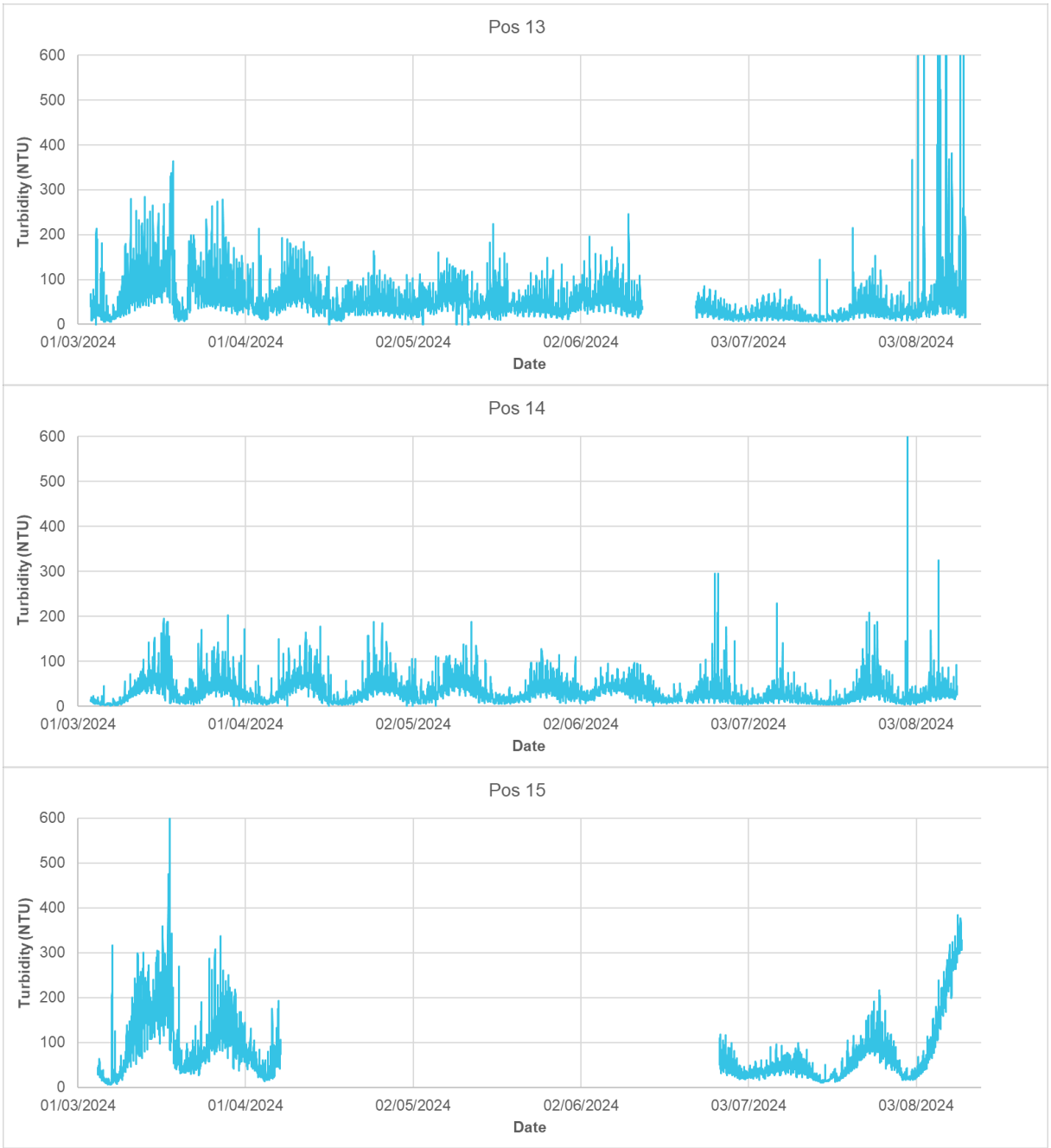


Figure 61. Measured benthic turbidity at Pos-13, Pos-14 and Pos-15 between March and August 2024 (wet and dry seasons).

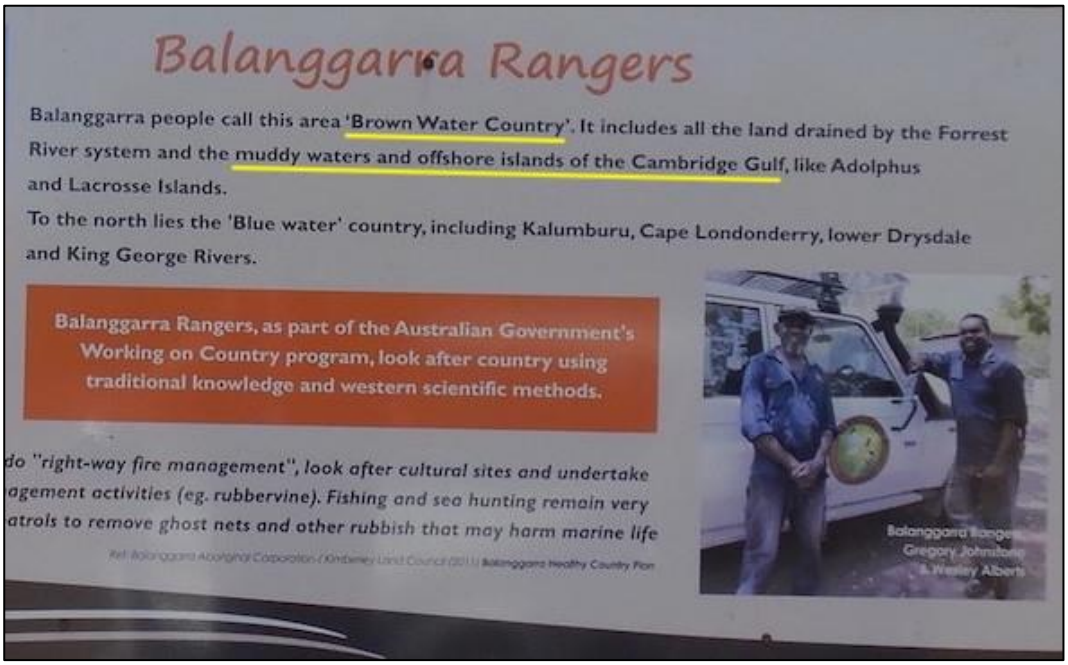


Figure 62. **An interpretive sign by the Balanggarra Indigenous Rangers at the Port of Wyndham public jetty, with reference to the area as 'Brown Water Country' and the 'muddy waters' of CG (BKA, 2024d).**



Figure 63. **Photographs taken during BKA's environmental survey work showing variability in SSC and turbidity in CG, with the bottom right image showing a tidal front with mixing of higher SSC upstream water with lower SSC offshore water in the outer area of CG (images: Raaymakers).**

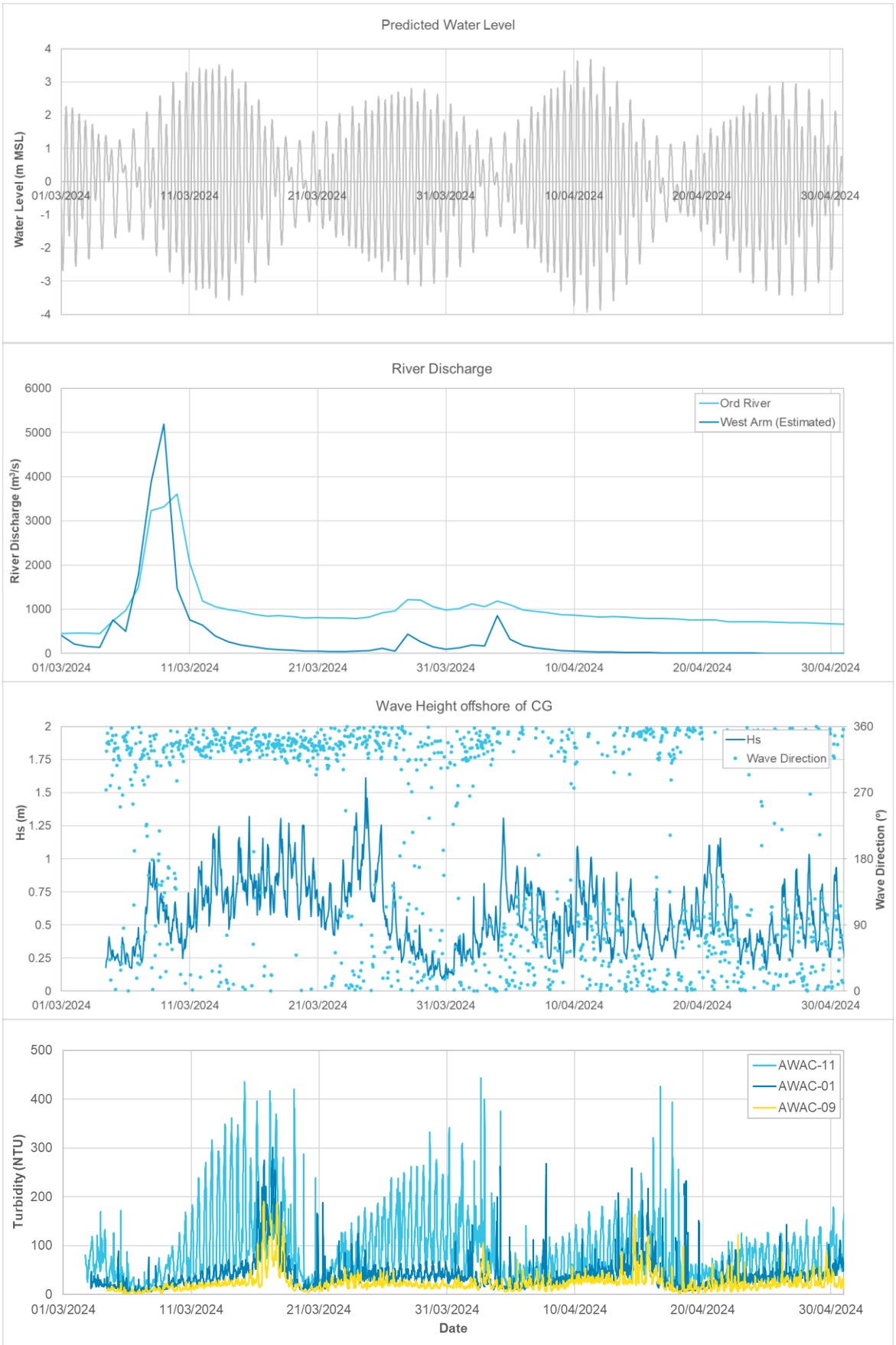


Figure 64. Predicted water level, measured river discharge, measured wave conditions and measured benthic turbidity offshore (AWAC-09), with the POA (AWAC-01) and south of the POA (AWAC-11) during the wet season.

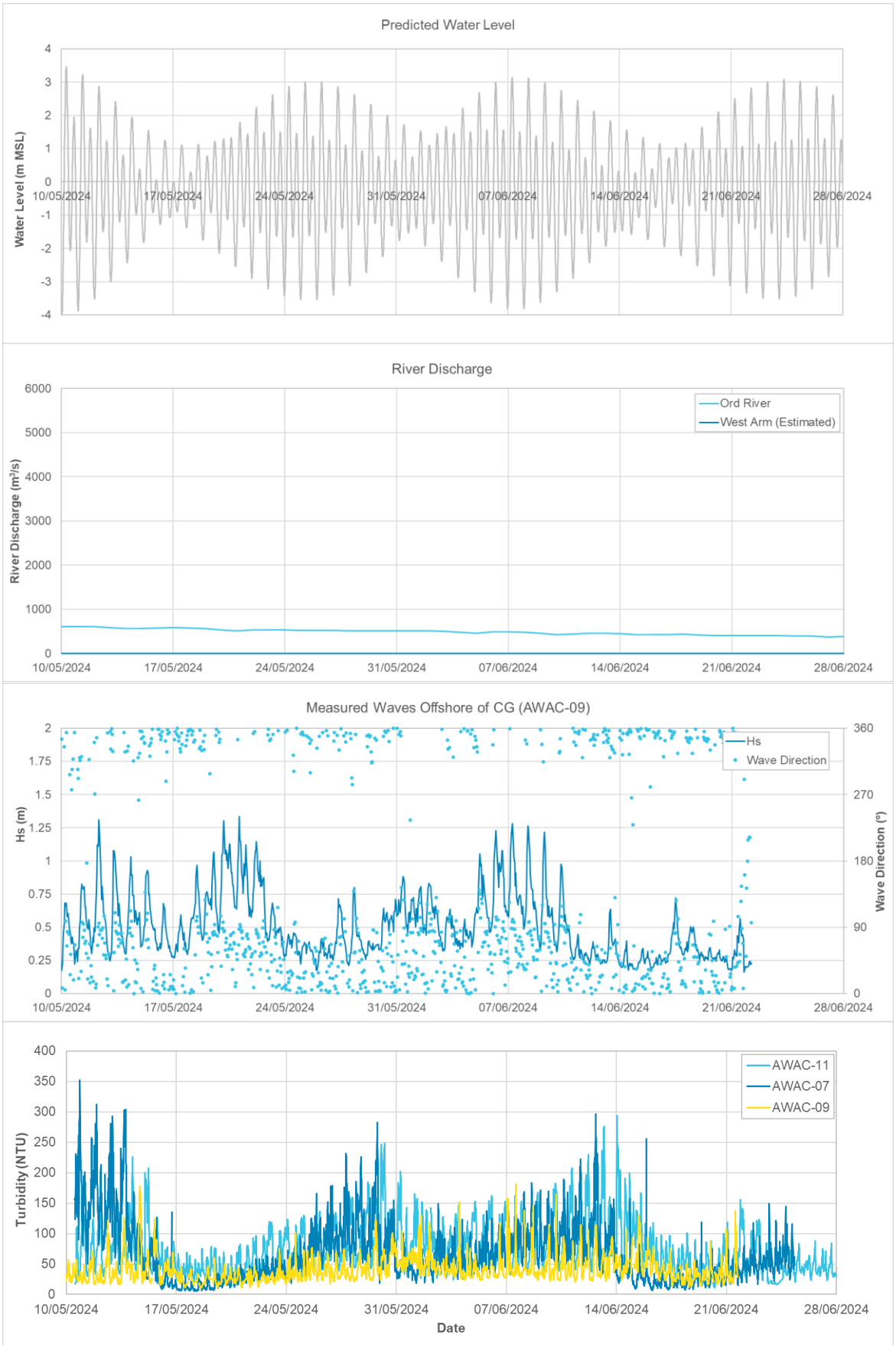


Figure 65. Predicted water level, measured river discharge, measured wave conditions (AWAC-09) and measured benthic turbidity offshore (AWAC-09), at the False Mouths of the Ord (AWAC-07) and south of the POA (AWAC-11) during the dry season.

2.3.2. Benthic Light

As outlined in Section 2.3, BKA has put significant effort into collecting in-situ benthic light data because benthic biota and communities are dependent on benthic light, and to assist the assessment of potential impacts on benthic communities from any changes to benthic light that might be caused by the proposed operation (although it should be noted that benthic communities are deficient in both quantity and diversity of species in CG (BKA, 2024b)). Benthic light is strongly influenced by turbidity and SSC, with higher turbidity and SSC values resulting in lower benthic light values, as the suspended solids prevent sunlight from penetrating to the seabed.

Benthic light was measured by purpose-built underwater light meters as 'irradiance' – the radiant flux received by a surface per unit area per unit time, expressed as µmol/m^2/s. Use of the simple term 'light' below refers to irradiance.

Previous analysis by PCS (2024b) of the measured benthic light data collected at nine sites within CG showed very low benthic light, with virtually no light at the measurement sites. The data showed that there was no benthic light at the sites in CG with water depths of more than 20 m (sites AWAC-02, AWAC-04, AWAC-06, AWAC-07, AWAC-08, AWAC-11 and Pos 12), and at the shallower sites (sites Pos 13 and Pos 14) benthic light was only present during neap tides when the turbidity was at its lowest, albeit still at very low levels with daily peaks ranging from 0.25 to 4.5 µmol/m^2/s.

Since the previous analysis, additional benthic light data have been collected using Odyssey light meters, with data collected from 3rd March 2024 to 14th August 2024 being analysed here. Data have been collected at the following sites over this period:

- AWAC-09/Pos 12 (offshore at King Shoals), water depth of 20 m: Data have been collected from 4th March to 14th August 2024 (163 days). The data show no benthic light for the majority of the time, with the only exception being a very small peak of less than 0.4 µmol/m^2/s in mid-July 2024.
- Pos 13 (western side of CG), water depth of 13.5 m: Data have been collected from 3rd March to 12th August 2024 (162 days). The data show no benthic light for the majority of the time, with the only exception being a very small peak of less than 0.5 µmol/m^2/s in mid-July 2024.
- Pos 14 (south coast of Lacrosse Is.), water depth of 13.7 m: Data have been collected from 3rd March to 21st June 2024 (110 days) (there was an issue with the logger during the second deployment from 21st June to 10th August). The data show regular periods with benthic light values of more than 1 µmol/m^2/s, with the highest value recorded being 470 µmol/m^2/s, making this the site with the highest benthic light (see below).
- Pos 15 (near Cape Domett), water depth of 14.0 m: Data have been collected from 4th March to 12th August 2024 (161 days). The data show no benthic light for the majority of the time, with the only exception being a very small peak of less than 0.1 µmol/m^2/s in mid-July 2024.
- AWAC-01 (inside the POA), water depth of 21.9 m: Data have been collected from 29th June to 9th August 2024 (41 days). The data show no benthic light over the period.
- AWAC-05 (near Cape Dussejour), water depth of 9.8 m: Data have been collected from 20th June to 12th August 2024 (53 days). The data show regular periods with benthic light values of more than 1 µmol/m^2/s, with a highest value of 6 µmol/m^2/s (which is still very low).
- AWAC-10 (offshore from East Entrance, in JBG), water depth of 18.0 m: Data have been collected from 26th June to 13th August 2024 (48 days). The data show no benthic light over the period.
- AWAC-11 (central CG just south of POA), water depth of 22.2 m: Data have been collected from 24th June to 4th August 2024 (41 days). The data show no benthic light over the period.

The data at the majority of the sites shows no benthic light for the majority of the time, and for the very few periods with some benthic light, the values were very low (less than 0.5 µmol/m^2/s). At two sites benthic light of more than 1.0 µmol/m^2/s was measured during multiple tides, with these sites being the shallowest at 9.8 m (AWAC-05) and third shallowest at 13.7 m (Pos 14).

The measured benthic light along with the measured turbidity and predicted water level are shown at these two sites in Figure 60 and Figure 61. The plots show that the peaks in benthic light coincide with periods of neap tides when the turbidity was at its lowest. The benthic light was highest at Pos 14, with values of up to 470 µmol/m^2/s measured in early April 2024. The higher values at Pos 14 relative to

AWAC-05 are expected to be partially due to seasonal variability in the available light. Peaks in benthic light measured at Pos 14 in June 2024 were of a similar magnitude to peaks measured at AWAC-05 in June to August 2024, which suggests that much higher peaks in benthic light could have occurred at AWAC-05 in early April 2024.

Plots of the measured benthic light and turbidity at both sites over a series of neap tides are shown in Figure 68 and Figure 69. The plots show that the peaks in benthic light occur during the middle of the day (when ambient light will be highest) and typically coincide with periods when the measured turbidity is less than 10 NTU.

Overall, the additional benthic light data analysed in this report agree with the data previously analysed by PCS (2024b), with most sites not measuring any benthic light at all most of the time, indicating a permanent near-seabed aphotic zone throughout CG.

As per the analysis in PCS (2024b), detectable benthic light was only measured at sites shallower than 15 m (sites AWAC-05 and Pos-14), at low levels and only during occasional periods of lower turbidity (less than 10 NTU). At these sites, periods of lower turbidity and thus some detectable benthic light only occurred during neap tides, with no benthic light being measured at any of the sites during spring tides.

In summary, the implications of these findings for the proposed operation and for the numerical modelling are:

- There is a permanent near-seabed aphotic zone throughout CG. This is most likely caused by constant suspension of seabed sediments by the strong tidal currents, causing constantly high turbidity and SSC throughout CG, which is added to by wet season inputs of sediment-laden freshwater from the catchment.
- The permanent near-seabed aphotic zone in CG is a major inhibiter of benthic biota and communities, and as a result the benthic communities in CG are depauperate (deficient in both quantity and diversity of species), with an absence of corals and coral reefs, seagrasses, macroalgae communities, sponge beds, oyster reefs and other significant primary-producer sub-tidal benthic communities, as reported in BKA (2024b).
- The permanent near-seabed aphotic zone and resulting depauperate benthic communities in CG, precludes the risk of the proposed operation causing significant impacts on such communities, as they do not exist in the area, and it is not possible to reduce light further when it is almost always naturally zero to near-zero throughout the area. This very low benthic community risk profile was one of the reasons that CG was selected during the alternative sites screening process as reported in BKA (2024c).
- In terms of sediment plume dispersal modelling, the permanent near-seabed aphotic zone and resulting depauperate benthic communities in CG, mean that it is not feasible or necessary to assess ZoHI, ZoMI and ZoI as defined in the EPA guidance (EPA 2021), as there are no potentially sensitive benthic communities to model these zones and set biological response triggers for, and the natural benthic light regime is already at the extremely low end, being zero to near-zero at most sites most of the time.

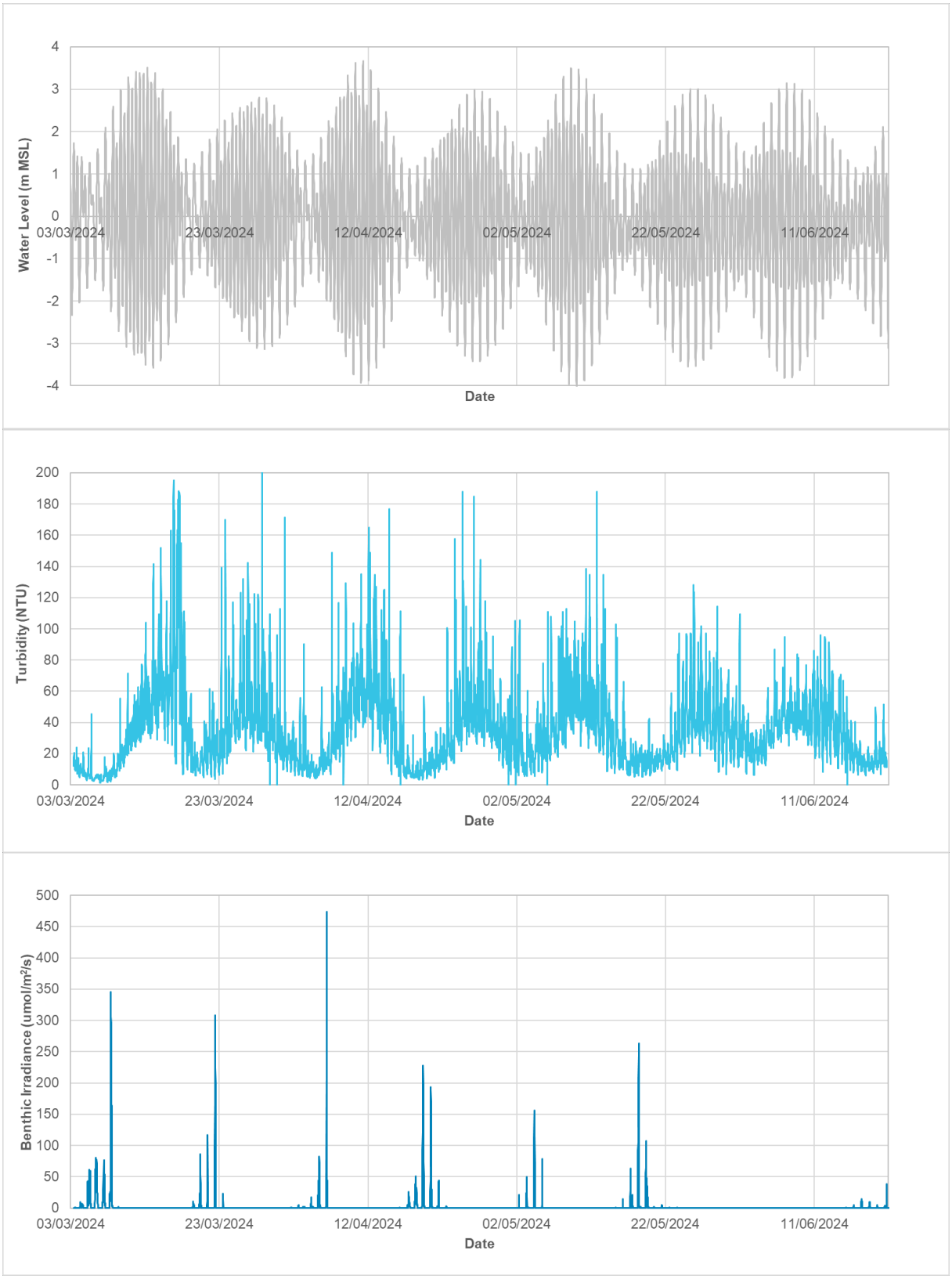


Figure 66. Predicted water level, measured turbidity and measured benthic irradiance at Pos-14 from March to June 2024.

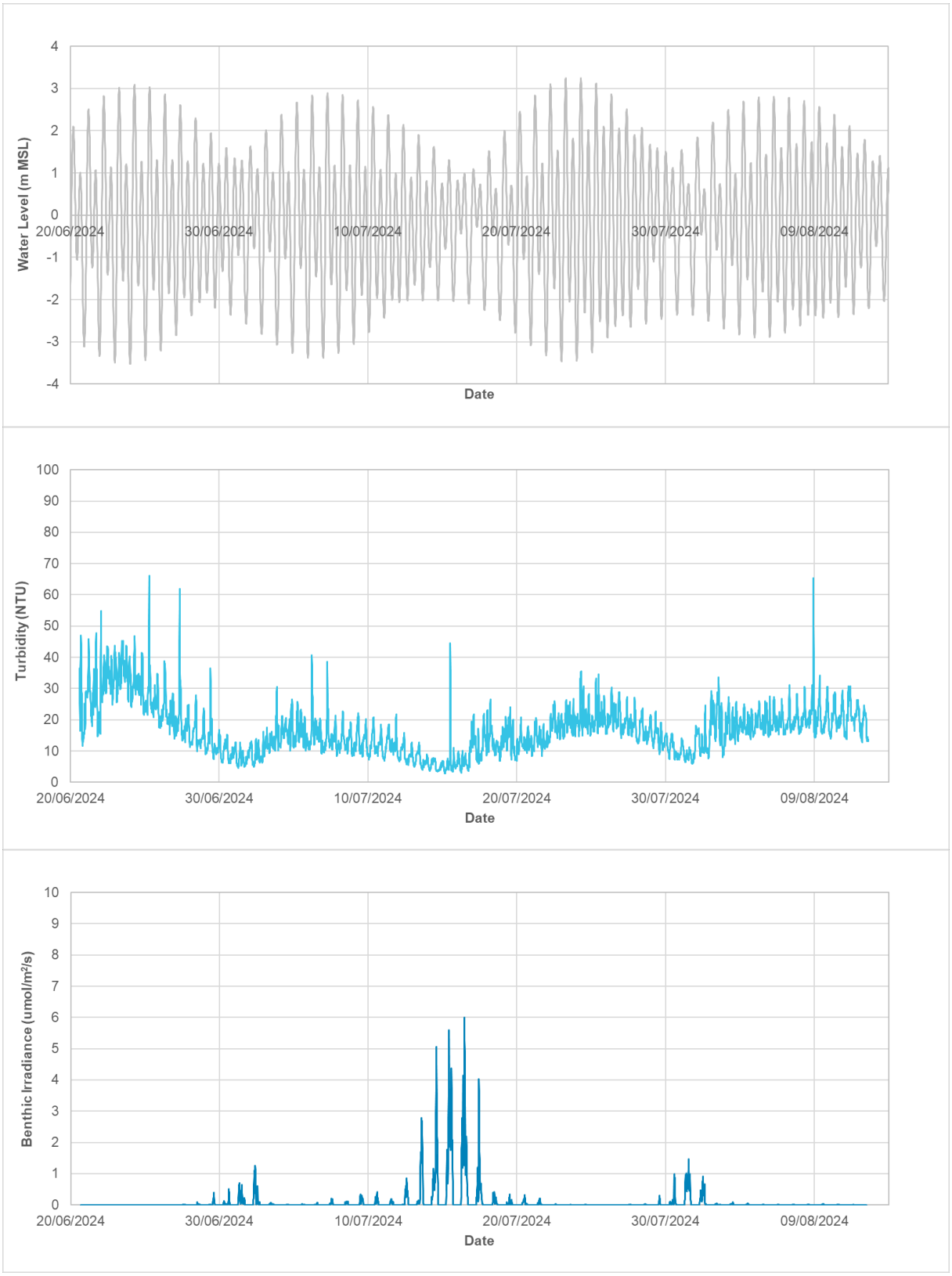


Figure 67. Predicted water level, measured turbidity and measured benthic irradiance at AWAC-05 from June to August 2024.

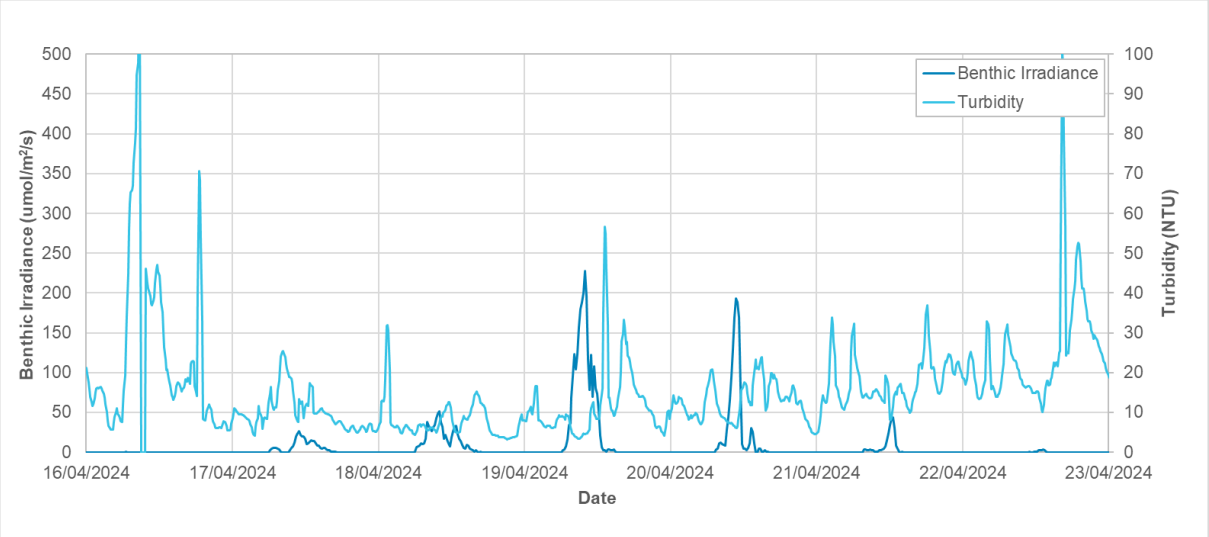


Figure 68. Measured turbidity and measured benthic irradiance at Pos-14 over 7 days of neap tides in March 2024.

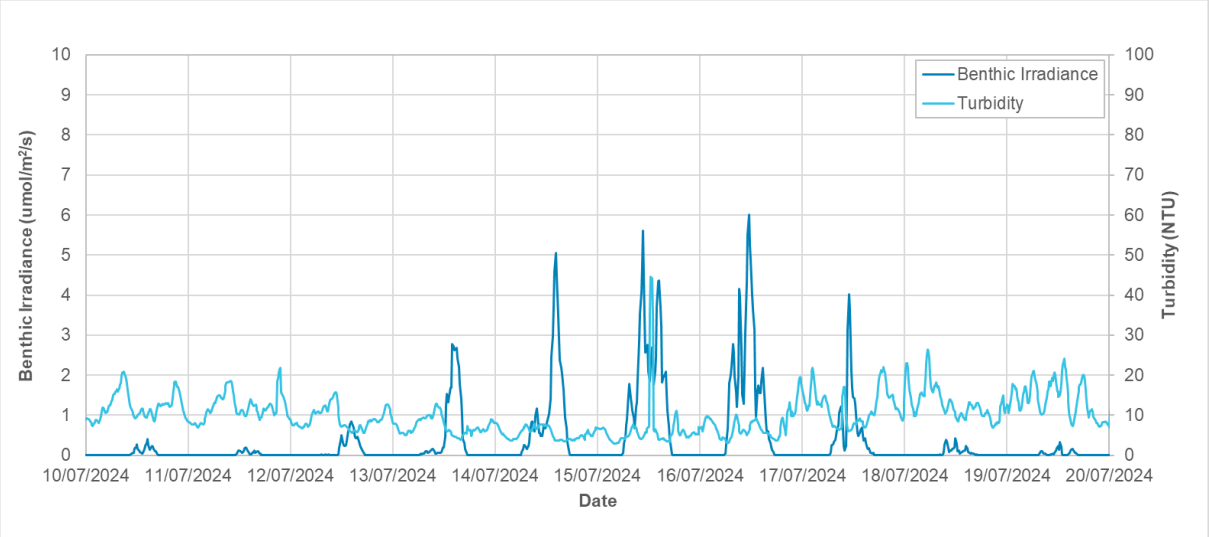


Figure 69. Measured turbidity and measured benthic irradiance at AWAC-05 over 10 days around neap tides in July 2024.

3. NUMERICAL MODELLING APPROACH

This section provides details of the numerical modelling approach adopted for the study including the hydrodynamic (HD), spectral wave (SW), sediment transport, beach processes and sediment plume models.

The initial setup and calibration of the hydrodynamic (HD), spectral wave (SW), sediment transport and beach processes models is detailed in PCS (2024a), while this report presents the final setup for the models and the full calibration and validation of those models as well as the sediment plume model, which was not addressed in PCS (2024a).

3.1. Software

In selecting the modelling software PCS has sought to apply best-practice and to meet the requirements of the WA *Technical Guidance for EIA of Marine Dredging Proposals* (EPA 2021) and the WAMSI/CSIRO *Guideline for Dredge Plume Modelling for EIA* (Sun *et al.*, 2020).

For the modelling of a complex estuarine system like CG to be considered best-practise, the model should utilise a flexible mesh approach, which allows the resolution of the mesh to vary spatially as required. The DHI MIKE Flexible Mesh (FM) software is internationally recognised as state-of-the-art and has been previously adopted by PCS elsewhere in Australia and internationally for similar projects. The MIKE suite includes HD, SW and sediment transport (ST) modules (this module includes the transport of silt and clay sized cohesive sediment, and silt and sand sized non-cohesive sediment), which allow all the necessary processes required for the CG assessment to be represented in the model.

The MIKE modules adopt a FM which allows suitable model resolutions to be adopted throughout, thus ensuring that the model accuracy and efficiency can be balanced. This means that areas of particular interest can have a higher mesh resolution (e.g. the POA and narrow channels) while a lower mesh resolution can be adopted in offshore areas and away from areas of particular interest.

For the longshore and cross-shore sediment transport modelling at the high-priority turtle nesting beaches, which are exposed to wave conditions, the MIKE Littoral Processes modelling suite has been adopted. This model can calculate the longshore and cross-shore transport at a series of beach profiles along the shoreline at each beach, with the model being driven by wave conditions extracted from the SW model.

3.2. Model Mesh

The model mesh was developed with consideration to:

- Meeting the best-practice requirements of EPA (2021) and Sun et al (2020).
- The model needing to be able to accurately represent the hydrodynamics, waves and sediment transport processes in the CG region.
- Ensuring that the majority of the sediment suspended by sand production activities remain within the model domain, with limited sediment reaching the model boundaries.
- The boundaries are located in a suitable position so that boundary conditions can be adopted to allow the hydrodynamics and waves to be accurately represented in the models.
- The model mesh extends upstream in West and East Arms of CG to locations where model boundary conditions can be adopted for the hydrodynamic model, without resulting in unnecessarily high-resolution cells to represent the narrow channels and complex bathymetry in these areas.
- Managing the overall model domain extent and mesh resolution to ensure that model simulation times are not prohibitive.

The final model domain extent and model mesh are shown in Figure 70. The model extends ~200 km north to south and 280 km east to west. The mesh extends to Cape Rulhieres to the west, which is ~140 km from Lacrosse Island, and to Cape Scott to the northeast, which is located ~150 km from Lacrosse Island. The same model mesh extent has been used for the HD and ST modelling, with the SW model adopting a slightly reduced extent in West and East Arms as waves are not important in these areas. The mesh for the HD/ST and SW modules has been designed to ensure higher resolution in the

areas where sand sourcing is proposed (the POA) and where any resultant plumes from the activity are likely to be transported (within and close to CG). The arc lengths of the triangular mesh elements range from ~4 km in the furthest offshore areas of the domain, to between 200 and 500 m in CG. A close-up of the HD/ST model mesh in CG is shown in Figure 71.

While a similar model mesh extent has been adopted for all the different modelling components of the study, in some areas the model mesh resolution in the SW model is lower than for the other models. The SW model mesh is coarser than the HD and ST model mesh in some of the smaller tidal creeks within CG as the HD and ST models require a higher resolution to allow flow connectivity in these creeks, while the SW model does not require such a high resolution to propagate the waves.

3.3. Bathymetry

The bathymetry included in the models was selected to provide the most realistic representation of the bathymetry based on the available data. Comparison within CG between the Geoscience Australia (GA) 30 m gridded data, an interpolation based on the AHO navigation chart (AUS726 & AUS32) and the multibeam data collected by BKA within the POA in February and March 2024 (as reported in PCS 2024a), showed that the GA 30 m gridded dataset did not accurately represent the bathymetry in CG, while the AHO navigation charts provided a reasonable representation. As a result, the following datasets were adopted to represent the bathymetry within CG:

- The measured multibeam bathymetric data collected by BKA in February and March 2024 within and adjacent to the POA.
- AHO navigation chart contours and spot heights.
- The measured intertidal bathymetric data from the LiDAR drone surveys undertaken by BKA in February 2024 (BKA 2024b).
- Digital Earth Australia 25 m gridded bathymetry for intertidal areas not covered by the BKA drone survey.

For the JBG region the GA 30 m gridded bathymetric data was adopted. This dataset also incorporates the Digital Earth Australia 25 m intertidal gridded bathymetry in the intertidal areas.

Data from the various sources were converted to MSL (which based on the analysis in Section 2.1.1 is 0.07 m above AHD) and then interpolated onto the model mesh. An overview of the interpolated model bathymetry covering the full extent of the model domain is shown in Figure 72 and a close-up of the CG region is shown in Figure 73.

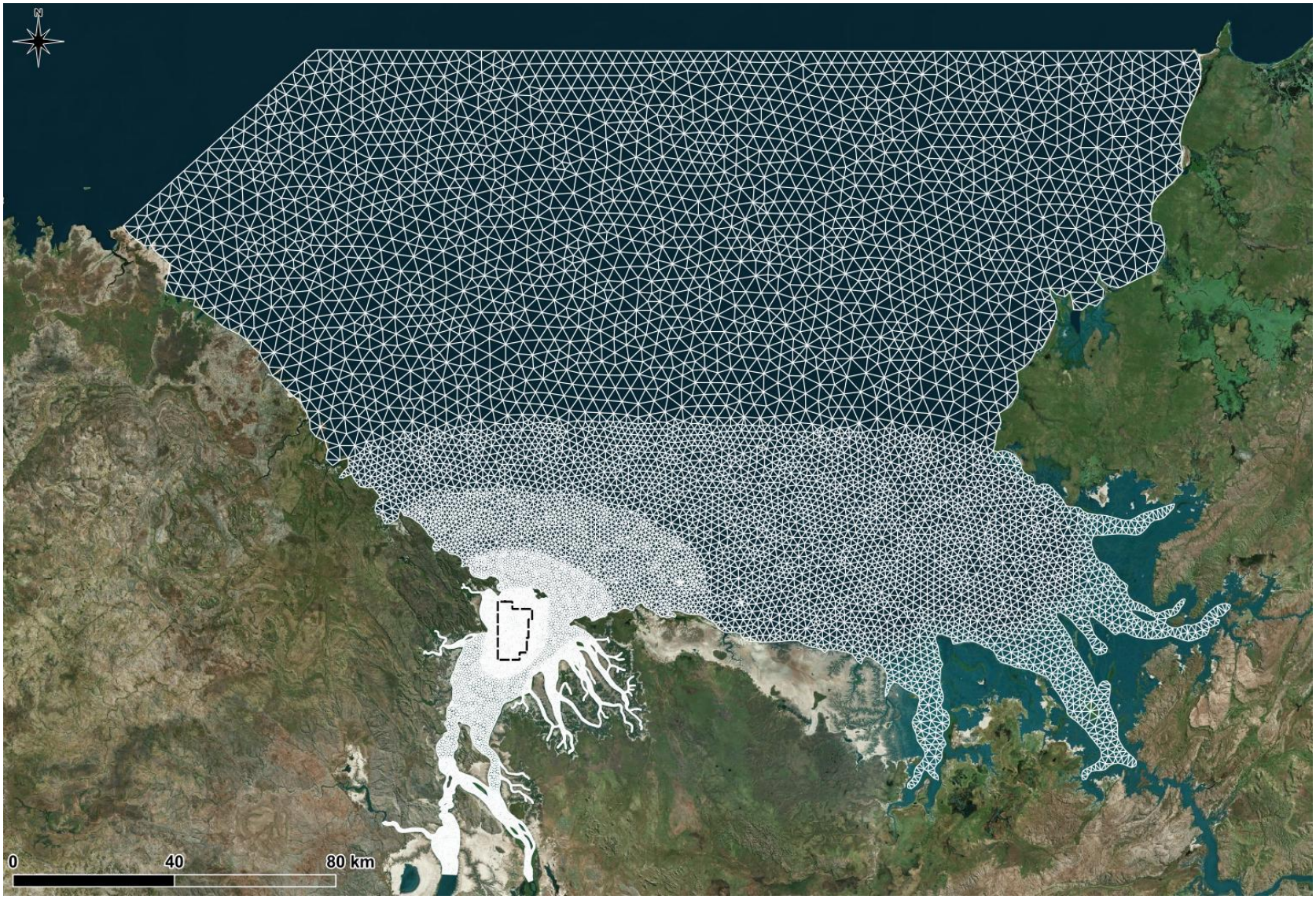


Figure 70. The full extent of the numerical model mesh along with Blocks 4 and 4A (grey polygons) and the proposed operational area (black dashed polygon).

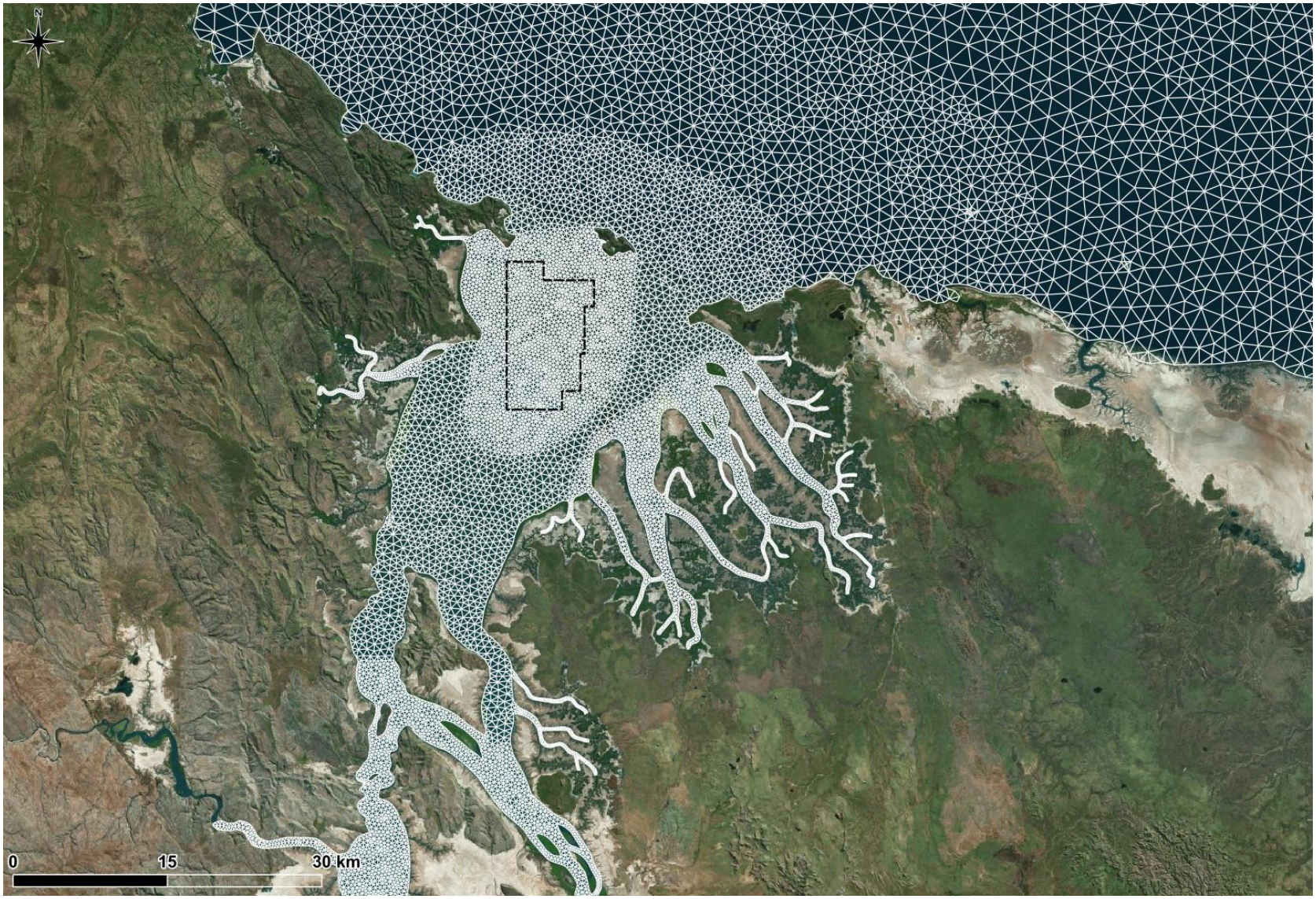


Figure 71. Close up of the numerical model mesh in CG along with Blocks 4 and 4A (grey polygons) and the proposed operational area (black dashed polygon).

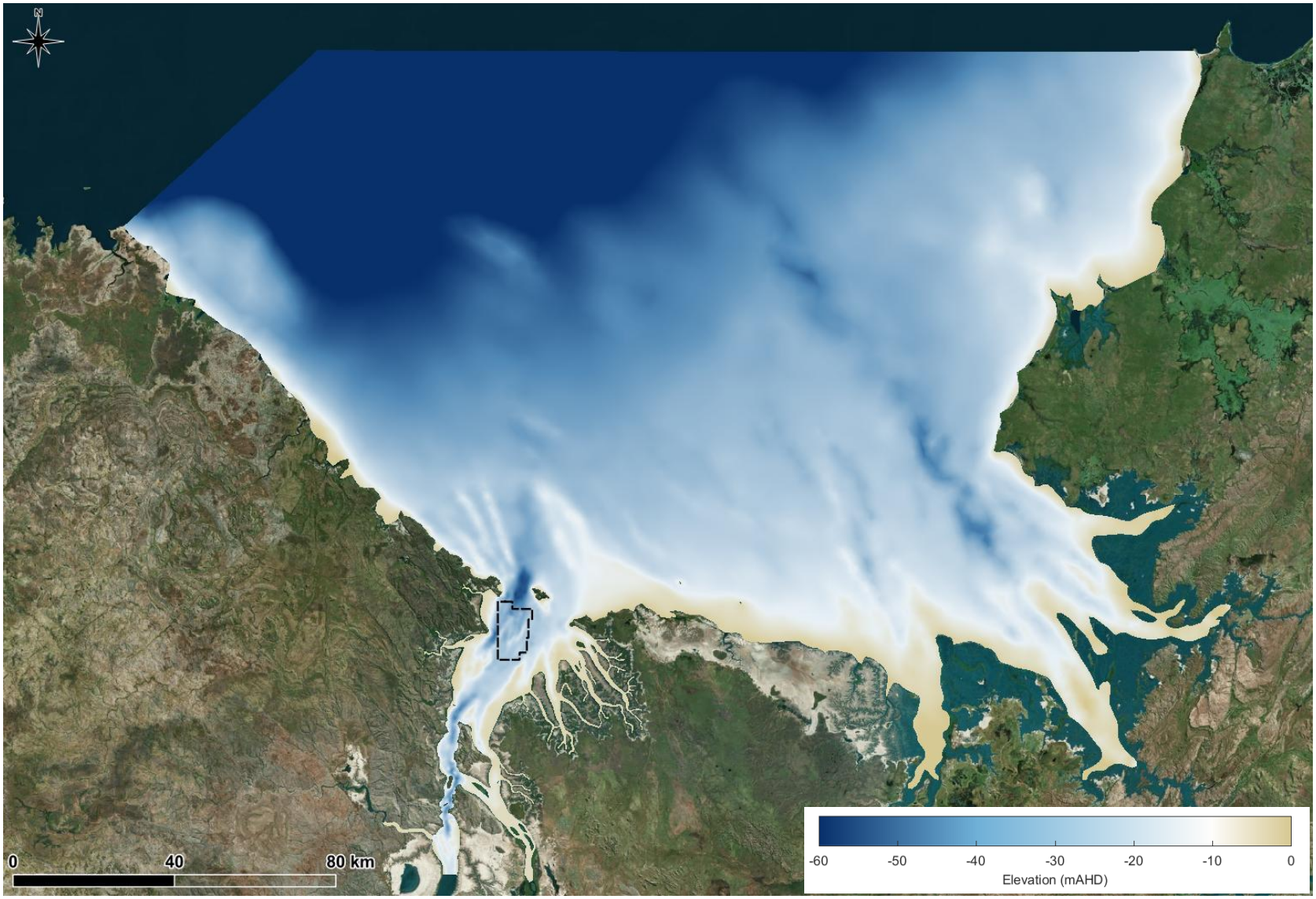


Figure 72. Model bathymetry for the full model domain with Blocks 4 and 4A also shown (grey polygons) and the proposed operational area (black dashed polygon).

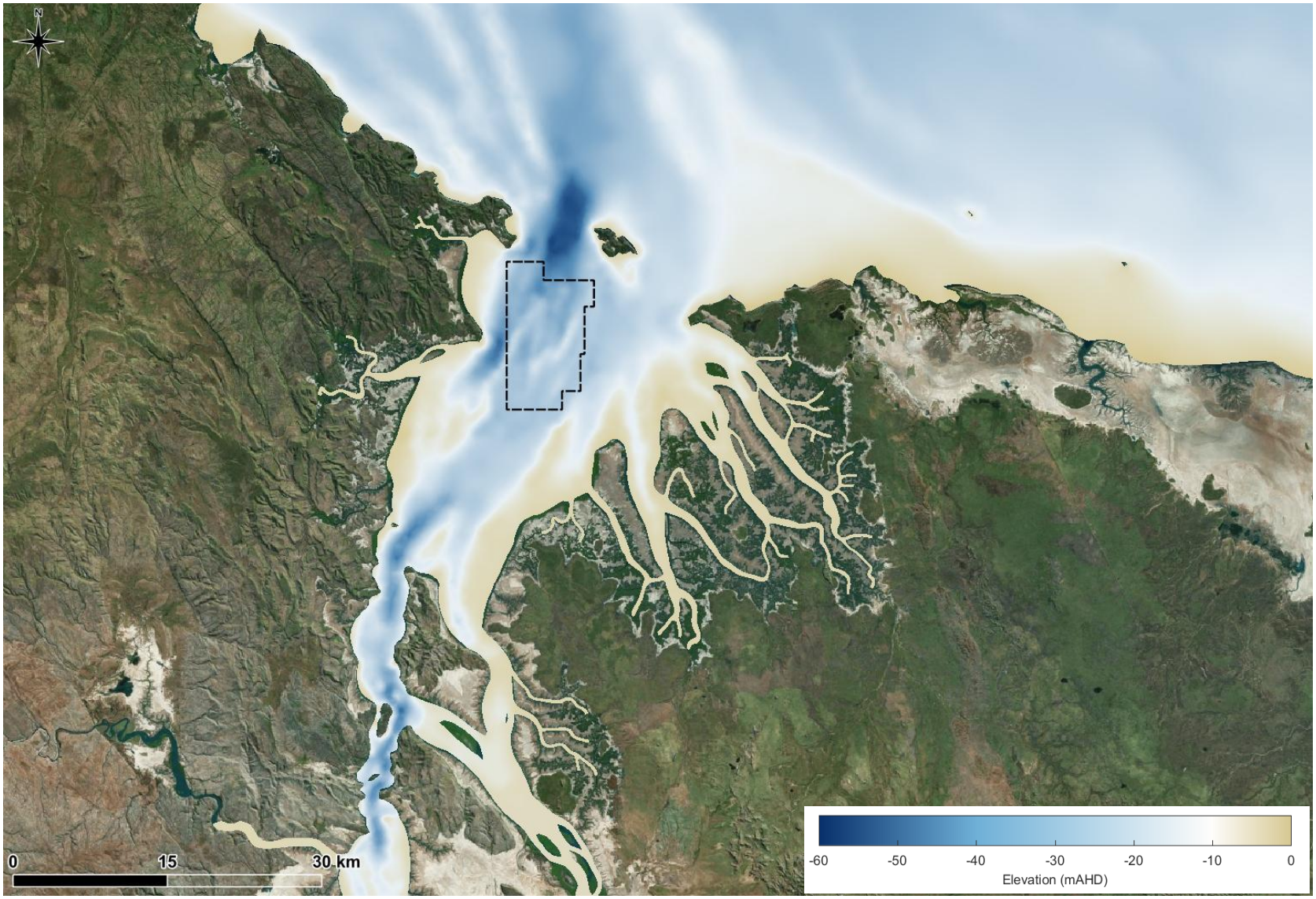


Figure 73. Model bathymetry for CG with Blocks 4 and 4A also shown (grey polygons) and the proposed operational area (black dashed polygon).

3.4. Hydrodynamic Model

The MIKE HD model simulates water level variations and flows in response to a variety of forcing functions in coastal regions and estuaries. Details of the model configuration, initial calibration and results are provided in the following sections.

3.4.1. Model Configuration

As noted previously in PCS (2024a), currents in JBG are predominantly driven by the astronomical tide, with no larger scale ocean circulation processes influencing the region. Therefore, the hydrodynamic offshore model boundaries were represented using only astronomical tidal water levels which were extracted from the DTU Space Global Tidal Model (DHI, 2007). Tidal constituents were extracted along the two open model boundaries from the 0.125° x 0.125° version of the Global Tide Model, which includes the following 10 major constituents: M2, S2, K2, N2 (semidiurnal), S1, K1, O1, P1, Q1 (diurnal) and M4 (shallow water). The water levels along the boundaries were both spatially and temporally varying.

The upstream boundary in West and East Arms of CG were represented using measured river discharge data from the WA Department of Water and Environmental Regulation (DWER) (DWER, 2024). For West Arm, data were only available for the King River, and so to approximate the combined discharge of the King River, Durack River and Pentecost River, the discharge from the King River was scaled based on the spatial areas covered by the rivers and their catchments. The model includes the influence of the wind on the currents, with winds extracted from the Centre for Australian Weather and Climate Research (CAWCR) (CSIRO, 2024) wave/wind hindcast, from a location within the POA applied in the model.

The HD model was set up as a 3-dimensional (3D) model, with 5 equally spaced sigma layers for depths of 0 to 40 m, and then an additional 5 z-layers with each representing 10 m depth bins (i.e. depths down to 90 m in total).

3.4.2. Calibration and Validation

Model calibration is the process of specifying model parameters so that the model reproduces measured data to a suitable level of accuracy. Model validation is used to confirm that the calibrated model continues to consistently represent the natural processes to the required level of accuracy in periods other than the calibration period, without any additional adjustment to the model parameters. The calibration and validation processes provide confidence in the model results and are essential to ensure the accurate representation of variations in water levels and currents.

There are no specific model calibration and validation guidelines adopted by the WA EPA and the available numerical modelling guidelines developed in WA (e.g. Sun *et al.*, 2016; and Sun *et al.*, 2020) and elsewhere in Australia (e.g. GBRMPA, 2012) only provide qualitative guidance. The lack of model performance guidelines for coastal and estuarine areas globally resulted in Williams and Esteves (2017) providing metrics of performance based on practical experience. They suggest the following metrics for HD models of estuaries, which have been used for the modelling in this study:

- Water Levels: Water level (WL) differences are calculated at high water (HW) and low water (LW) to ensure that the model captures the full tidal range. Modelled WLs should be within ±10% of the measured WLs during a neap tide and ±15% during a spring tide, in relative terms. The mean tidal phase difference should be within ±15 minutes in open coast, within ±15 minutes at the mouth of an estuary and within ±25 minutes at the head of an estuary. The calibration guideline standard will be considered to be met if it falls within the standards outlined.

- Currents: Speed and direction differences are calculated at peak flood and peak ebb to ensure that the model captures the peaks flows and any flood/ebb dominance. The average model current speed should be within ±10-20% of the average measured speed and the current direction should be within ±10-15° of the measured direction. The calibration guideline standard will be considered to be met if it falls within the standards outlined.

Although the guidelines by Williams and Esteves (2017) do not provide recommendations for the calibration of non-tidal residuals, they can be important processes which influence sediment transport and plume dispersion (although the analysis presented in Section 2.1.2 indicates the residual currents have limited influence on currents in CG). Therefore, a visual comparison of the residual currents has also been undertaken as part of the model calibration at key monitoring sites. The comparison between measured and modelled residual currents considered the depth-averaged residual currents as these are more important than the surface residual currents for this study, as the depth-averaged residual currents

can be considered to also represent the currents in the bottom half of the water column, which is more important in terms of both sediment transport and plume dispersion (overflow water released by the SPV will be in the bottom half of the water column, as in accordance with best-practice the overflow water discharge will be located at the SPV's keel ~19 m below the waterline, to minimize plume generation and dispersal).

An initial calibration of the hydrodynamic model using measured water level and current data collected at site AWAC-01 in June to July 2023 was presented in PCS (2024a). This initial model calibration showed that the HD model was able to provide a realistic representation of the water levels and currents through the water column at AWAC-01 over this period. Since this initial model calibration, additional water level and current data have been collected by BKA as part of the project, which allows an extensive model calibration and validation at multiple sites. Further details are provided below:

- Calibration period: A two-month (61 days) wet season period was selected from the 1st March 2024 to the 1st May 2024. Within this period, a spring-neap cycle (03/04/2024 – 18/04/2024) was selected to highlight tidal variability in the calibration plots and for statistical analysis. Measured water level and current data were available at five sites over the calibration period (AWAC-01, AWAC-06, AWAC-08, AWAC-09 and AWAC-11).

- Validation period: A two-month (61 days) dry season period was selected from the 1st June 2024 to 1st August 2024. Within this period, a spring-neap cycle (16/07/2024 – 30/07/2024) was selected to highlight tidal variability in the validation plots and for statistical analysis. Measured water level and current data were available at four sites over the validation period (AWAC-01, AWAC-05, AWAC-10 and AWAC-11).

3.4.2.1. Model Calibration

For conciseness, only a selection of the calibration plots are shown here to represent the general trends observed. The complete set of calibration and validation plots are included in Appendix A. The measured and modelled water level at AWAC-01, AWAC-08 and AWAC-09 are shown in Figure 74 to Figure 76, and the measured and modelled current speed and direction are shown at the surface, mid depth and near bed layers in Figure 77 to Figure 79. A statistical summary of the model calibration is shown for the water levels in Table 4 and for currents in Table 5. The calibration results meet the model performance guidelines recommended by Williams and Esteves (2017), which demonstrates that the HD model provides a realistic representation of the water levels and currents through the water column.

All modelled water levels are within 10% of the observed measurements, with HW levels consistently within ~4%, and LW levels consistently within 7% except for AWAC-08 which is 8.3%. Across all locations, the phase difference for both high and low waters is less than ±15 minutes, with an overall average difference of less than ±3 minutes across the full period at all sites. Modelled HW peaks are generally ahead by 9 minutes for sites closer to the areas of interest, whilst HW peaks at AWAC-09 and AWAC-08 (to the north and south) are ahead by ~5 minutes. Modelled LW peaks are slightly late at all calibration sites with the offshore site AWAC-09 having the smallest LW phase difference of less than 1 minute and AWAC-11 having the largest LW phase difference of -8.3 minutes.

The modelled current speeds align closely with the measured values, being within ±20% on both the flood and ebb at all sites (in line with recommended guideline standards), within ±15% at AWAC-06 and AWAC-09, and within ±10% at AWAC-01. These statistics indicate that the model consistently captures both the amplitude and timing of tidal flows across all locations.

The majority of modelled current directions are within ±10º of the measured directions demonstrating a good level of agreement in modelled and measured flow directions throughout the water column. However, the modelled directions exceed the estuarine guideline standard of ±15º at one site only (AWAC-11) on the flood stage of the tide at the surface layer (highlighted in yellow in Table 5). The timeseries plots show that in the surface layer both the flood and ebb current directions are well represented by the model during all periods except for the smaller neap tides. During these smaller neap tides when current speeds are lower there is more difference between the measured and modelled directions. However, as this difference only occurs in the surface layer and on neap tides when lower current speeds occur, it does not impact on the overall reliability of the model for the present study.

The water level and speed / direction plots across all calibration AWAC sites demonstrate a strong alignment between the modelled and measured data. The water level plots show that the model tends to slightly over-predict HW peaks and slightly under-predict LW peaks. This tendency is more pronounced during spring tides than during neap tides, however, the differences remain well within the performance guidelines recommended by Williams and Esteves (2017).

The plots for bed, mid and surface layer currents show that there is variability in the model's tendency to slightly over or under-predict peak tidal ebb / flood speeds. For example, at AWAC-08 the model tends to under-predict peak surface flows during a spring tide during the calibration period. However, as with the water levels, all discrepancies between modelled and measured current speed data remain within acceptable variation margins (Williams and Esteves 2017), demonstrating a close alignment with measured values. Overall, the plots indicate that the model is well calibrated and performs reliably at the calibration sites which are spread throughout the CG region, providing confidence in the accuracy of the modelled hydrodynamics.

The measured and modelled depth-averaged residual current speeds at sites offshore of CG (AWAC-09), within the POA (AWAC-01) and upstream (south) of the POA (AWAC-11) are shown in Figure 80 to Figure 82. It is important to note that the modelled residuals will all have been generated within the model with no residual water level or current added to the offshore water level boundaries. Therefore, the residuals within the model will have been due to local drivers included in the model, such as winds and river discharge. The plots show that the model provides a realistic representation of the semi-diurnal peaks in residual current at the site upstream of the POA, while at the site offshore from CG and within the POA it slightly underestimates these peaks. However, the model generally provides a good representation of the daily moving mean residual current at all three sites, giving confidence that it can accurately represent the longer-term residual currents in the region.

Table 4. Statistics for comparison of modelled and measured water levels (WLs) at AWAC-01, AWAC-06, AWAC-08, AWAC-09 and AWAC-11 during the calibration period.

Statistic	HW / LW	AWAC-01	AWAC-06	AWAC-08	AWAC-09	AWAC-11
Mean WL difference (m)	HW	0.14	0.14	0.12	0.11	0.11
	LW	-0.27	-0.27	-0.34	-0.25	-0.28
WL RMS (m)	HW	0.24	0.24	0.26	0.21	0.23
	LW	0.34	0.34	0.43	0.31	0.36
Mean percentage difference relative to maximum WL (%)	HW	4.3	4.4	3.4	3.6	3.3
	LW	6.9	7.0	8.3	7.0	7.0
Mean WL phase difference (mins)	HW	10	10	4	7	10
	LW	-5	-5	-5	-1	-8
	Full Period	2	3	-1	3	1

Notes: Differences are modelled minus predicted/measured so that positive values indicate that the model value is high/late relative to predicted/measured

Table 5. Statistics for comparison of modelled and measured currents through the water column at AWAC-01, AWAC-06, AWAC-08, AWAC-09 and AWAC-11 during the calibration period.

Statistic		AWAC01			AWAC06			AWAC08			AWAC09			AWAC11		
		Bed	Mid	Surface	Bed	Mid	Surface	Bed	Mid	Surface	Bed	Mid	Surface	Bed	Mid	Surface
Mean speed difference (m/s)	ebb	0.09	0.05	-0.07	0.12	0.05	-0.06	-0.02	-0.12	-0.45	0.02	0.16	0.09	0.17	0.22	-0.01
	flood	-0.09	-0.01	-0.04	0.05	0.04	0.01	0.05	-0.27	-0.38	-0.08	-0.08	-0.08	-0.02	-0.02	-0.03
Speed RMS (m/s)	ebb	0.12	0.09	0.12	0.14	0.10	0.12	0.10	0.20	0.51	0.12	0.19	0.27	0.18	0.25	0.17
	flood	0.12	0.19	0.24	0.10	0.12	0.12	0.15	0.33	0.42	0.12	0.14	0.14	0.11	0.18	0.18
Mean percentage difference relative to maximum speed (%)	ebb	8.7	3.6	-4.2	10.9	3.6	-3.8	-1.1	-5.4	-17.6	1.8	11.2	5.4	16.6	16.3	-0.6
	flood	-7.8	-0.8	-2.6	4.9	3.3	0.7	3.0	-12.5	-14.7	-7.8	-5.9	-5.4	-2.1	-1.7	-2.3
Mean direction difference (°)	ebb	-1	1	5	1	5	8	-8	1	5	-8	2	6	6	-3	0
	flood	4	3	6	4	6	-7	7	2	1	-3	1	-2	2	0	27

Notes: Differences are modelled minus measured so that positive values indicate that the model value is high relative to measured.
Values in yellow lie outside of the guideline standards

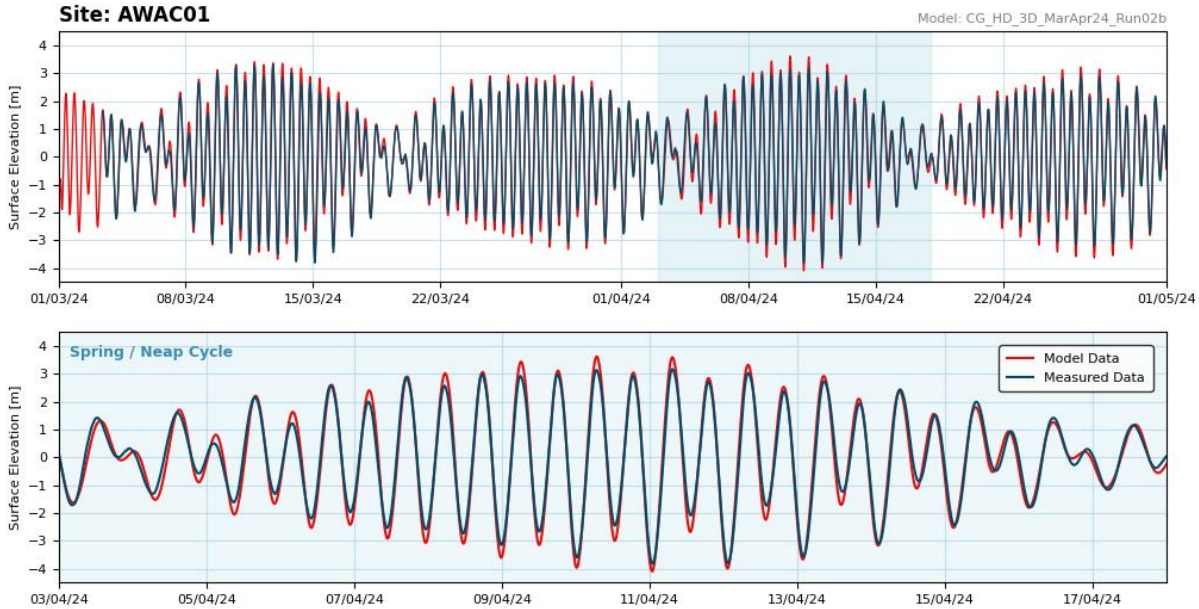


Figure 74. Modelled and measured water level at AWAC-01 over the model calibration period and selected calibration spring / neap cycle period.

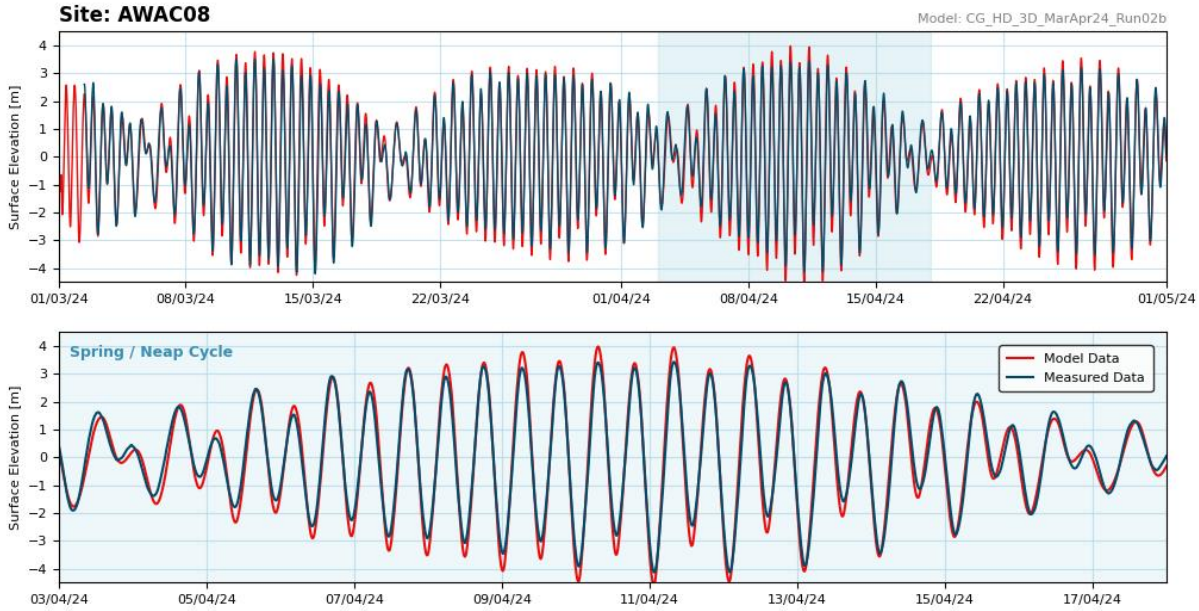


Figure 75. Modelled and measured water level at AWAC-08 over the model calibration period and selected calibration spring / neap cycle period.

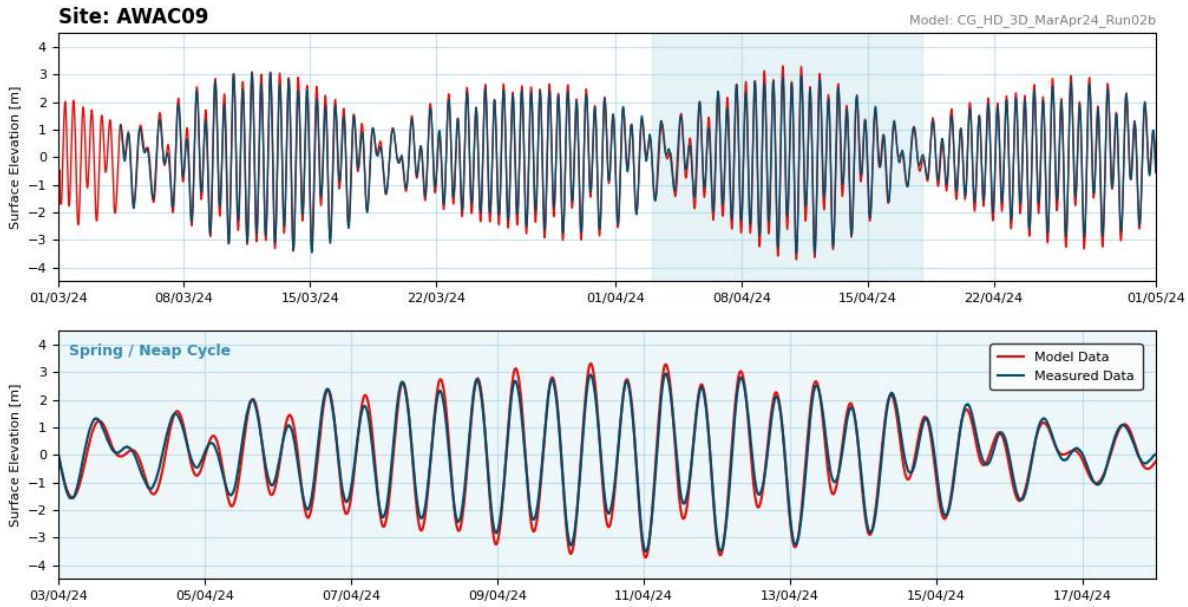


Figure 76. Modelled and measured water level at AWAC-09 over the model calibration period and selected calibration spring / neap cycle period.

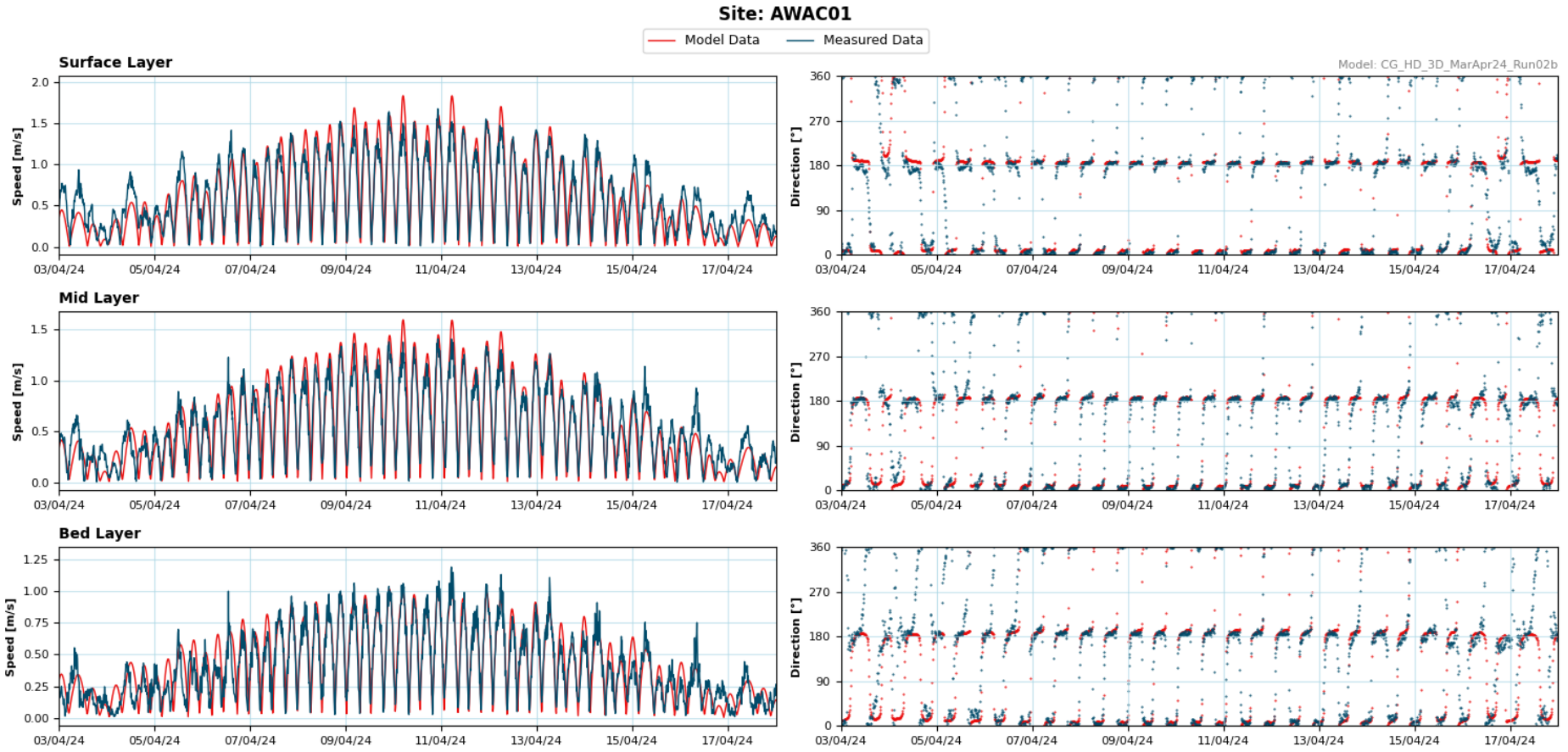


Figure 77. Modelled and measured surface, mid and bed layer currents speed and direction at AWAC-01 over the selected calibration spring / neap cycle period.

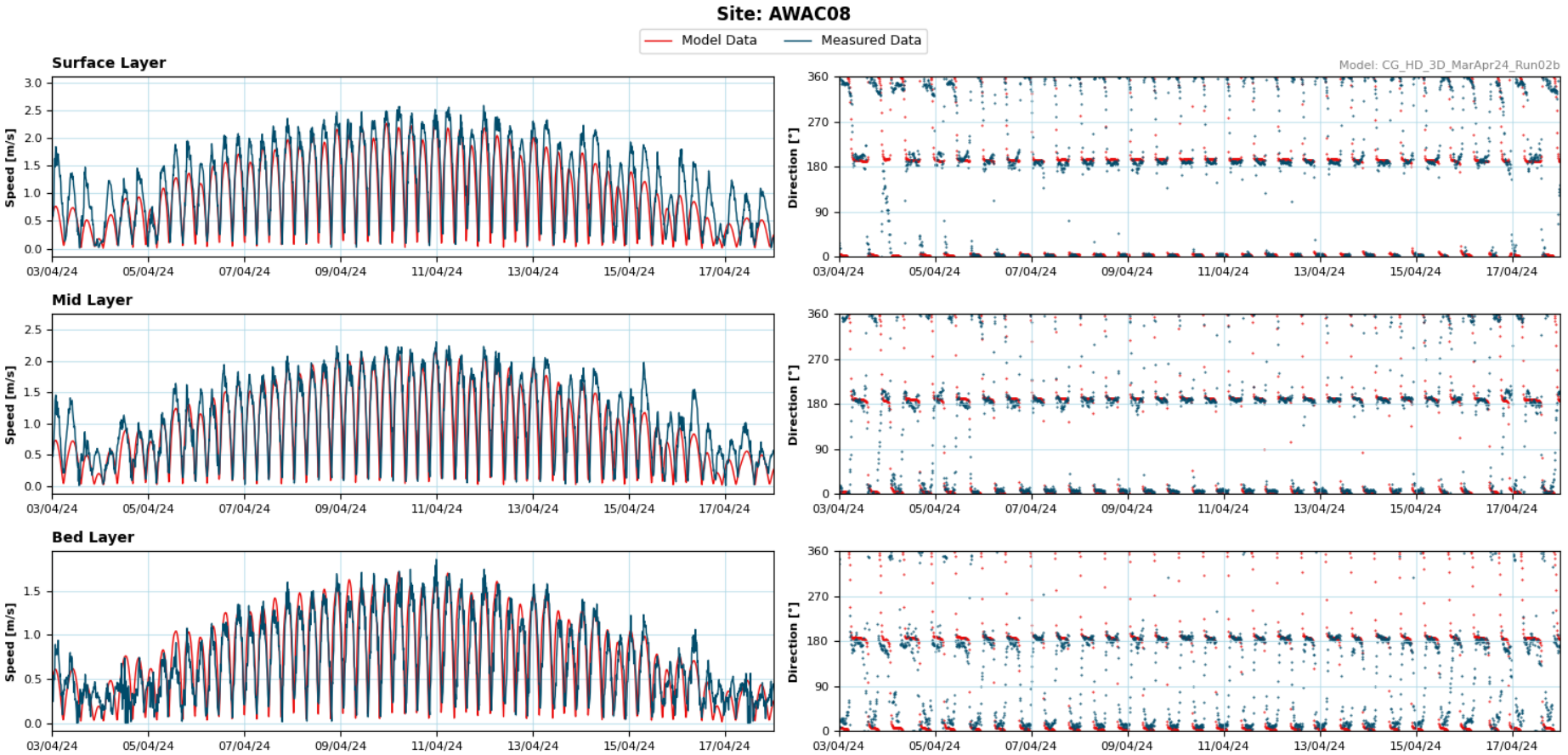


Figure 78. Modelled and measured surface, mid and bed layer currents speed and direction at AWAC-08 over the selected calibration spring / neap cycle period.

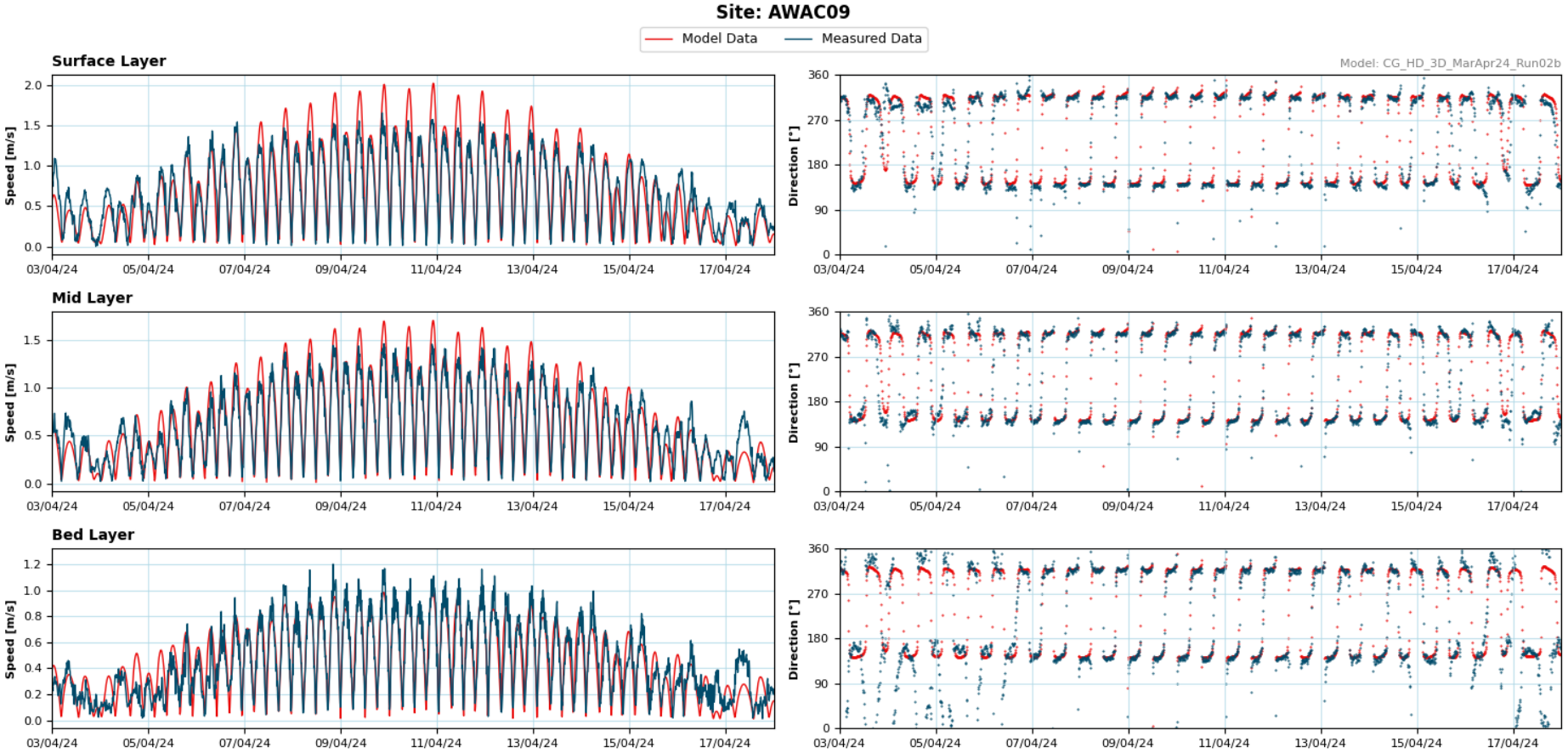


Figure 79. Modelled and measured surface, mid and bed layer currents speed and direction at AWAC-09 over the selected calibration spring / neap cycle period.

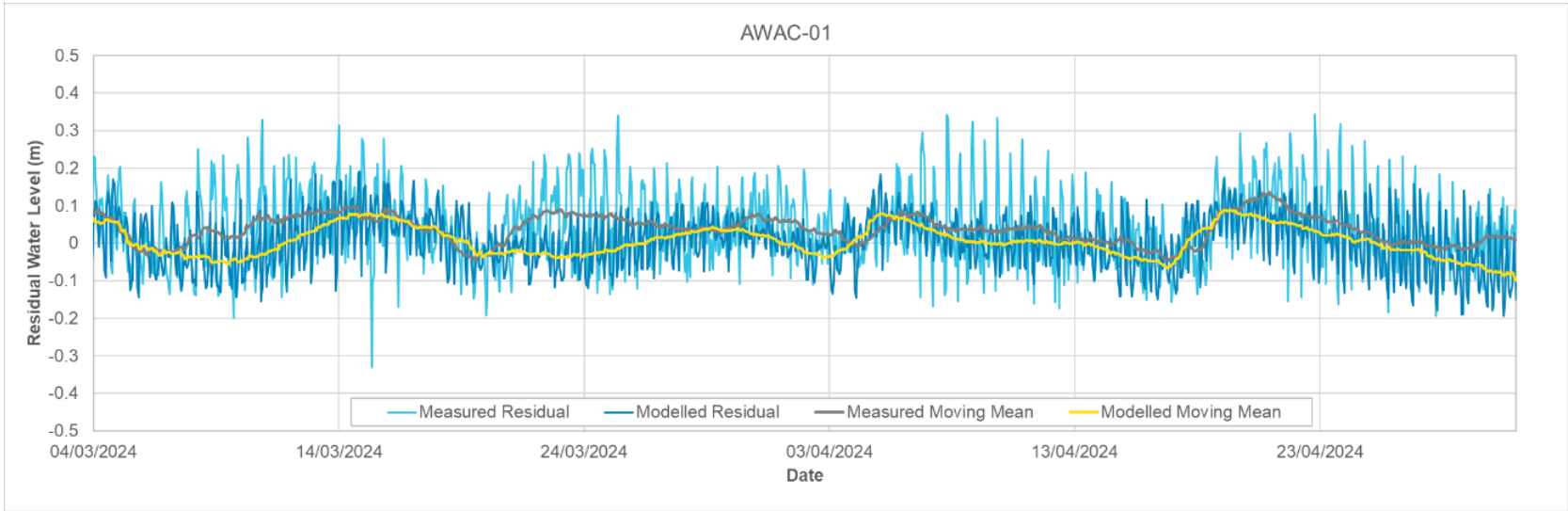


Figure 80. Modelled and measured depth-averaged residual current speed at AWAC-01 over 2 months of the wet season.

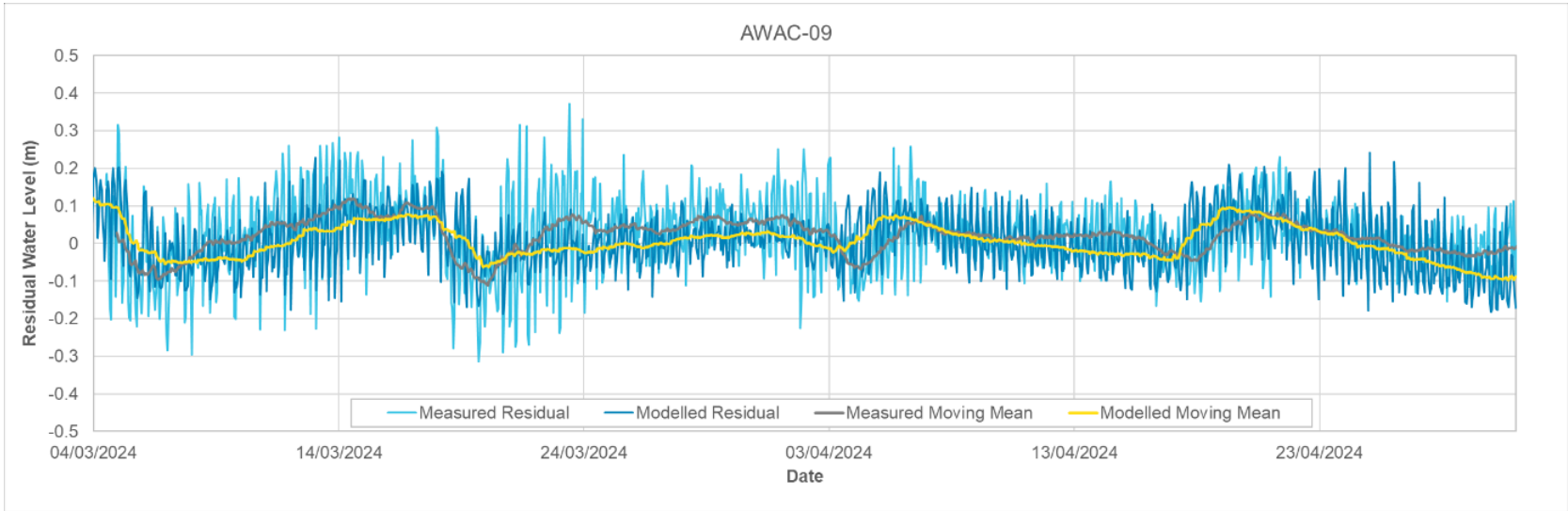


Figure 81. Modelled and measured depth-averaged residual current speed at AWAC-09 over 2 months of the wet season.

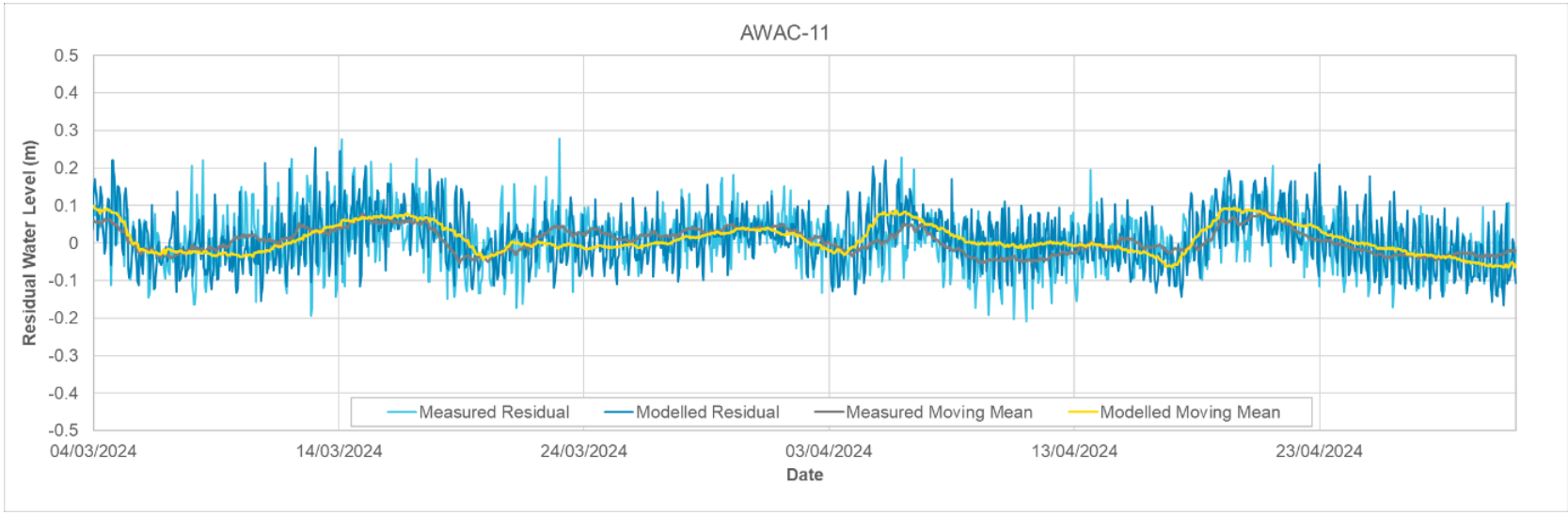


Figure 82. Modelled and measured depth-averaged residual current speed at AWAC-11 over 2 months of the wet season.

3.4.2.2. Model Validation

As with the model calibration, only a selection of the validation plots are shown to represent the general trends observed. The full set of calibration and validation plots are included in Appendix A. The measured and modelled water level at AWAC-01 and AWAC-10 are shown in Figure 83 and Figure 84 and the measured and modelled current speed and direction are shown for these sites at surface, mid and bottom depths in Figure 85 and Figure 86, respectively. A statistical summary of the model validation is shown for the water levels in Table 6 and for the currents in Table 7 . The validation results align with the model performance guidelines outlined by Williams and Esteves (2017), confirming that the HD model accurately represents water levels and currents throughout the water column.

All modelled WLs are within ±10% of the observed measurements, with HW levels consistently within ~4% and LW levels consistently within ~5%. As with the calibration period, the water level plots show that the model tends to slightly over-predict HW peaks and slightly under-predict LW peaks with more pronounced discrepancies during spring tides. However, the discrepancies remain within the calibration guideline standards of Williams and Esteves (2017), demonstrating a close alignment between modelled and measured variables.

Across all locations the overall average modelled phase difference is ~7 minutes earlier than measured, which is well within the guideline standard of ±15 minutes, applicable in open coastal waters. The modelled HW timing has a small phase difference of less than ±2 minutes, whilst modelled LW peaks are late by ~13 minutes across all sites other than AWAC-11 which is 16 minutes late. This remains within the Williams and Esteves (2017) guideline standard for tidal phasing in estuaries, which is 15 minutes at the mouth and 25 minutes at the head.

The modelled average current speeds are within 20% of measured speeds at all sites other than AWAC-05 where there are some notable discrepancies between modelled and measured flood currents. This measurement site is located in relatively shallow water (depth of 9.8 m) within 500 m of the shoreline of Cape Dussejour, where there is very complex bathymetry and a rock outcrop located ~500 m to the north, which will act to block flood currents at AWAC-05. The arc length of the model mesh elements in this area is ~400 m, and it is therefore unable to resolve the complex bathymetry and rock outcrop, resulting in the over estimation of flood current speeds at this site. All modelled directions (with the exception of AWAC-11 bed layer on the flood tide which has a difference of 19º), are within ±15º of the measured values demonstrating a good level of directional accuracy. At AWAC-11 the statistics show that the current direction is well within ±15º for all other cases and analysis of the timeseries plots show a significant change in flood current direction between the mid and bed layers, while the ebb current direction remains similar. This suggests that localised near-bed features (e.g. sand waves) could be influencing the near-bed current direction on the flood stage of the tide and as the model is not able to resolve these smaller scale features, it is not surprising that the model cannot replicate this small change. As the model has been shown to reliably represent the current direction for the other layers and for all layers during the ebb stage of the tide, the difference will not impact on the overall reliability of the model for the present study.

Overall, the model can be considered to replicate the measured tidal characteristics to a good degree of accuracy as demonstrated by both a visual assessment of water level and current speed / direction plots and by statistical assessments. Water levels are consistently within the Williams and Esteves (2017) guideline standards, closely matching observed values at both high and low tides. Similarly, the vast majority of discrepancies in current speed and direction lie within the guideline standards, while those outside of these guidelines either do not significantly impact on the overall accuracy of the model or can be attributed to specific local factors. These validation results demonstrate that the model is reliably calibrated, providing confidence in the consistency and precision of its outputs.

Table 6. Statistics for comparison of modelled and measured water levels (WLs) at AWAC-01, AWAC-05, AWAC-10 and AWAC-11 during the validation period.

Statistic	HW / LW	AWAC-01	AWAC-05	AWAC-10	AWAC-11
Mean WL difference (m)	HW	0.14	0.10	0.15	0.12
	LW	-0.16	-0.16	-0.13	-0.19
Mean percentage difference relative to maximum WL (%)	HW	4.6	3.4	4.7	3.5
	LW	4.7	4.9	4.0	5.3
WL RMS (m)	HW	0.19	0.16	0.19	0.17
	LW	0.25	0.24	0.22	0.30
Mean WL phase difference (mins)	HW	-2	-2	-1	0
	LW	-13	-13	-13	-16
	Full Period	-7	-7	-7	-8

Table 7. Statistics for comparison of modelled and measured currents through the water column at AWAC-01, AWAC-05, AWAC-10 and AWAC-11 during the validation period.

Statistic		AWAC-01			AWAC-05			AWAC-10			AWAC-11		
		Bed	Mid	Surface	Bed[1]	Mid	Surface	Bed	Mid	Surface	Bed	Mid	Surface
Mean speed difference (m/s)	**ebb**	0.08	0.01	-0.04	N/A	-0.08	-0.22	0.07	0.13	0.06	-0.02	0.11	0.02
	flood	-0.05	-0.01	-0.05	N/A	0.25	0.32	-0.04	-0.04	-0.09	-0.06	0.03	0.00
Mean percentage difference relative to maximum speed (%)	**ebb**	9.0	0.8	-3.0	N/A	-4.9	-11.5	9.4	14.3	5.5	-2.0	8.2	1.2
	flood	-4.5	-0.7	-3.4	N/A	36.5	42.2	-5.3	-4.1	-8.2	-6.8	2.3	0.0
Speed RMS (m/s)	**ebb**	0.09	0.11	0.13	N/A	0.11	0.23	0.08	0.15	0.13	0.07	0.15	0.15
	flood	0.08	0.11	0.14	N/A	0.27	0.37	0.05	0.07	0.11	0.07	0.08	0.09
Mean direction difference (°)	**ebb**	-3	-2	5	N/A	-2	-5	0	3	3	3	1	1
	flood	3	2	-0	N/A	-11	-10	8	7	4	19	11	5

Notes: Differences are modelled minus measured so that positive values indicate that the model value is high relative to measured.

[1] the measured current data at AWAC-05 only had 2 bins of reliable data, with the instrument having a vertical bin resolution of 2 m. As a result the bins were assumed to represent the mid and surface layers.

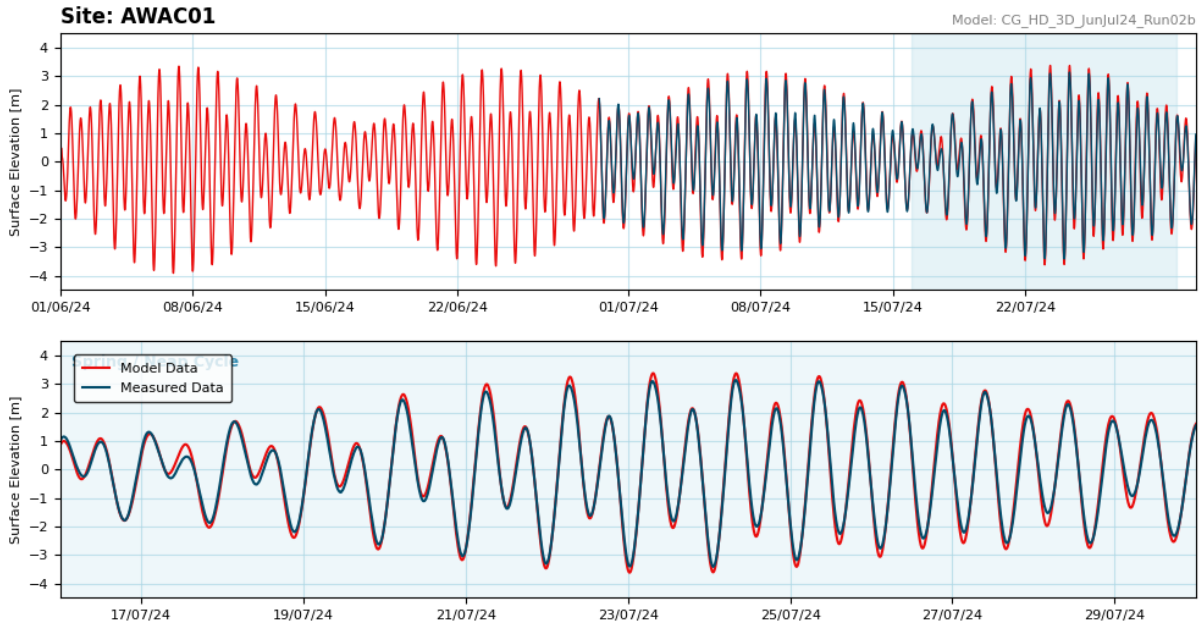


Figure 83. Modelled and measured water level at AWAC-01 over the model validation period and selected validation spring / neap cycle period.

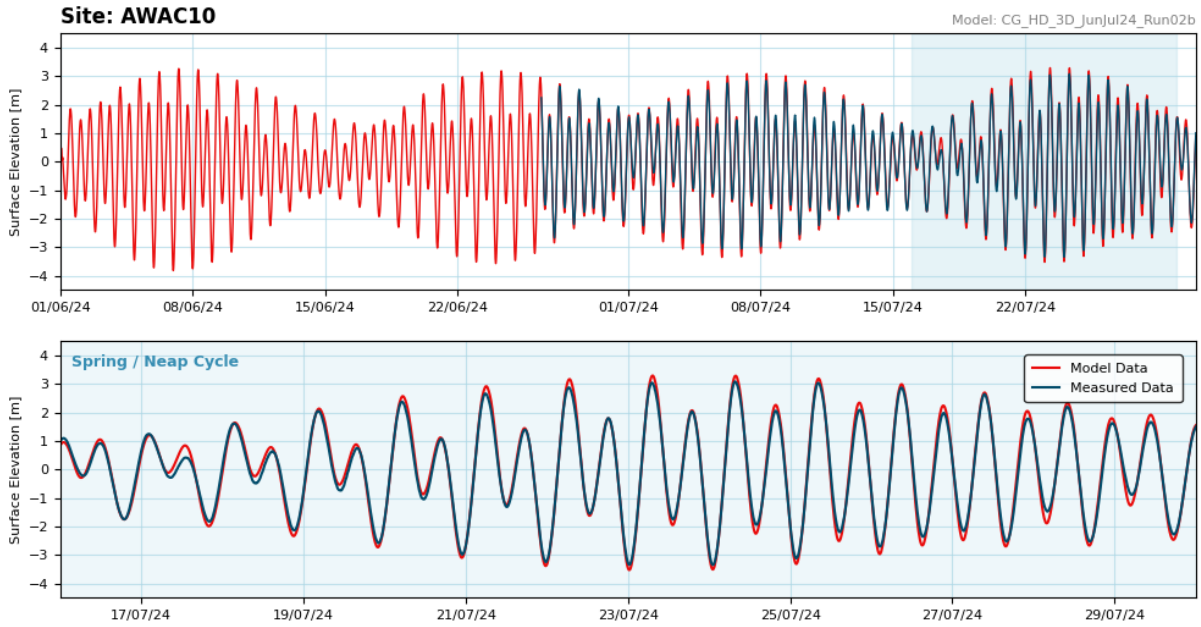


Figure 84. Modelled and measured water level at AWAC-10 over the model validation period and selected validation spring / neap cycle period.

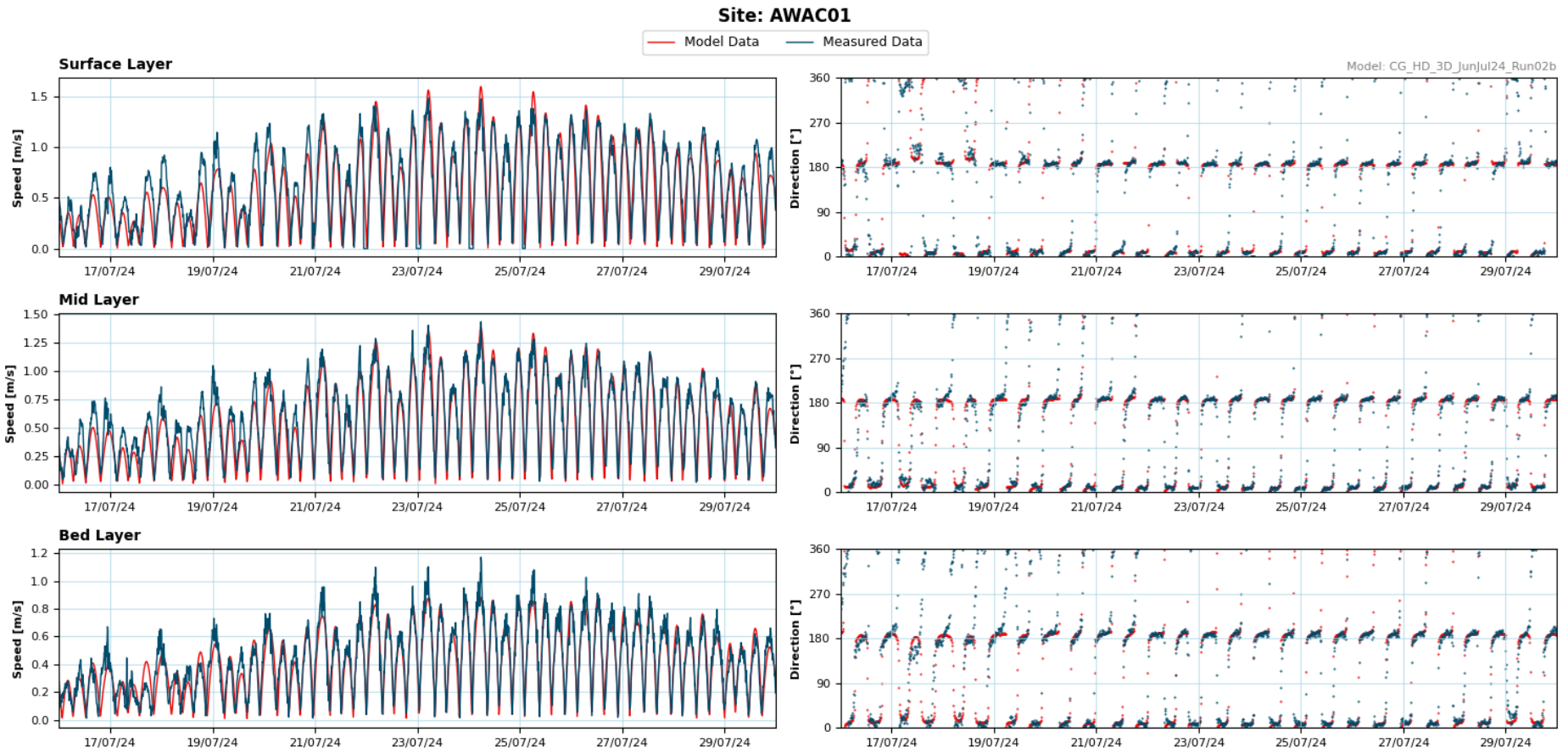


Figure 85. Modelled and measured surface, mid and bed layer currents speed and direction at AWAC-01 over the selected validation spring / neap cycle period.

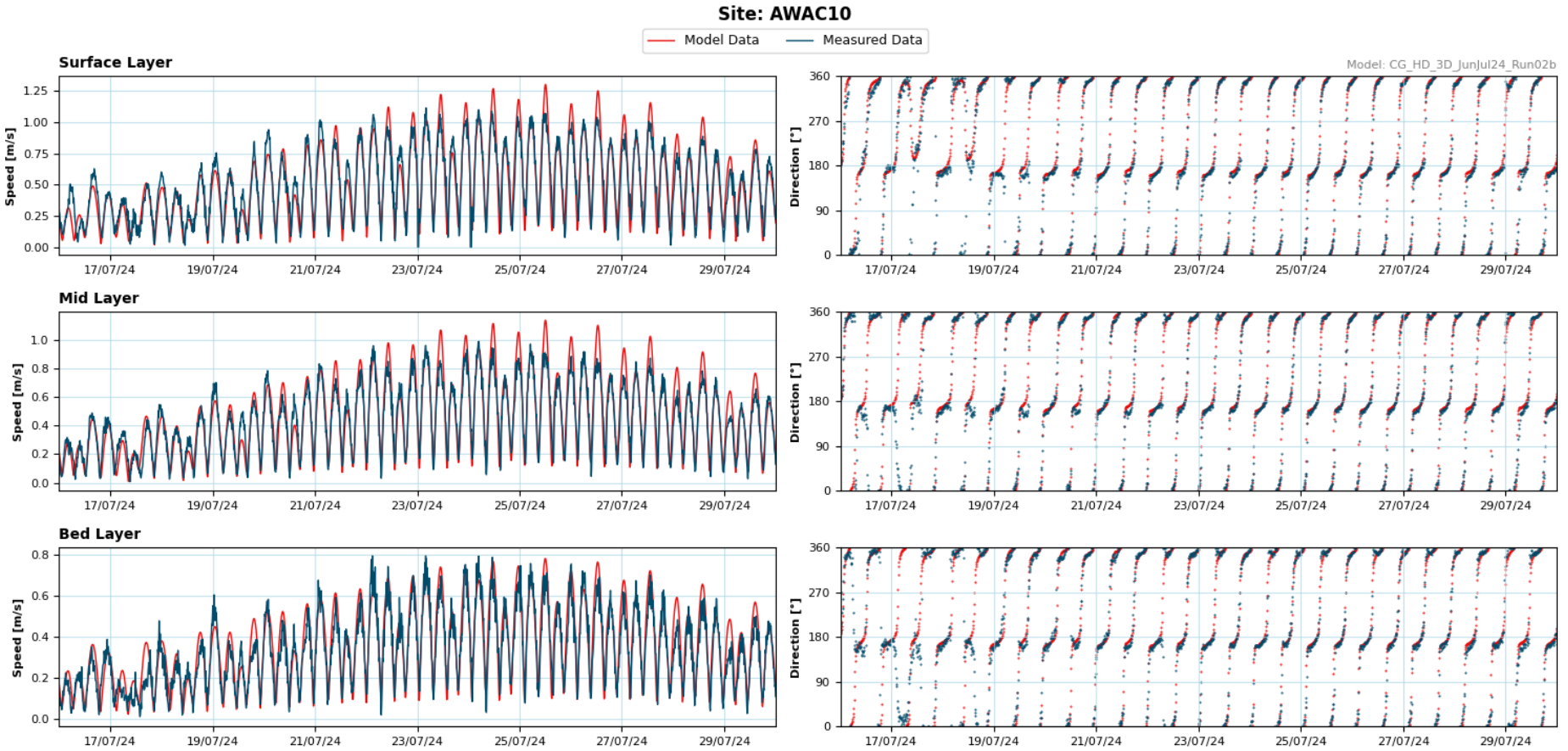


Figure 86. Modelled and measured surface, mid and bed layer currents speed and direction at AWAC-10 over the selected validation spring / neap cycle period.

3.4.3. Scheme Simulations

Following the calibration and validation of the HD model, the model setup of the existing case was modified to represent the following scenarios:

- Existing: This is the same setup as adopted for the model calibration and validation and represents the existing state of CG, with no proposed sand sourcing operation.

- Pre-European Settlement: This scenario approximately represents the conditions prior to European settlement based on the available information and data. Based on information detailed in Wolanski *et al.* (2004) during the wet season a peak river discharge for the Ord River of 30,000 m^3/s was adopted, while during the dry season no river discharge was applied for the Ord River. The discharge flowing into West Arm (from the King, Durack and Pentecost Rivers) was assumed to have stayed the same as the existing discharge. Despite Wolanski *et al.* (2004) noting that increased sedimentation had occurred in East Arm since construction of the Ord River dam, no changes were made to the model bathymetry within East Arm due to uncertainty in the location and extent of the changes.

- 5 years of sand sourcing (23 million m^3): This scenario assumes that 5 years of sand sourcing activity has been undertaken and that the total proposed maximum case of 70 million m^3 of sand sourcing over up to 15 years is undertaken at a consistent rate over time, giving 23 million m^3 after 5 years. It is also assumed that the sand sourcing will be undertaken evenly over the 75 km^2 area of the POA where sand is present (Figure 87). For this scenario, the conservative, worst case assumption that no natural sand infill occurred within the POA, was adopted. Based on this, the model bathymetry has been deepened by 0.31 m over the area where sand is present. In reality, there will be some natural replenishment of sand into the POA during this period.

- 15 years of sand sourcing (70 million m^3): This scenario assumes that the total proposed maximum case of 70 million m^3 of sand has been removed from the 75 km^2 area of the POA where sand is present (Figure 87). For this scenario, the conservative, worst case assumption that no natural sand infill occurred within the sand sourcing area, was adopted. Based on this, the model bathymetry has been deepened by 0.94 m over the area where sand is present. In reality, there will be some natural replenishment of sand into the POA during this period and so the changes presented can be considered to be conservative.

- 100 years from today, no sand sourcing: This scenario is required to provide a future (100 years from today) existing case to compare with results from the 100 years with sand sourcing scenario. This scenario assumed that no sand sourcing has been undertaken and so the existing model bathymetry was adopted. The metocean conditions have been updated to represent the conditions 100 years from today. This includes factoring in climate change predictions, including 0.9 m of sea level rise (based on Department of Transport (2010) and IPCC (2024)), an increase in river discharge of 20% during the wet season and a reduction in river discharge of 13% for the dry season (based on Department of Primary Industries and Regional Development, 2024). The river discharge for the Ord River during the dry season is assumed to remain the same as the existing dry season discharge due to the Ord River dams regulating the discharge, and assuming no changes to dams in the CG catchment over 100 years.

- 100 years from today, with sand sourcing (70 million m^3): This scenario assumes the same changes to the water level and river discharge as the 100 years with no sand sourcing scenario. This scenario also includes for the removal of 70 million m^3 of sand over 15 years. Results from the ST modelling were used to estimate the natural replenishment of sand into the POA from natural catchment sources. The results assessed ~200,000 m^3/yr of sand would be deposited at the southern end of the POA. This is approximately half of the annual deposition rate of 375,000 m^3/yr estimated based on the measured bedform migration (Section 5.2.3), and so is considered to represent a lower estimate of the future replenishment which is considered conservative in terms of modelling future changes due to the deepening from the sand sourcing. Based on this, it was conservatively estimated that 20 million m^3 of sand would have been deposited into the southern region of the POA over 100 years, and based on this, the sand over 28% of the southern region was assumed to have been filled back in for this scenario.

The HD model was set up to represent these scenarios as well as the existing case for the following conditions:

- Wet season: A two-month (60 days) period from 01/02/2024 to 01/04/2024. This period is considered representative of typical wet season conditions, with a high river discharge event

and typical wet season wind and wave conditions (predominantly from the northwest to north). All the scenarios were modelled for this condition.

- Transitional season: A two-month (61 days) period from 01/10/2023 to 01/12/2023. This period is considered representative of typical transitional season conditions with low river discharge and typical transitional season wind and wave conditions (predominantly from the northwest to northeast). All the scenarios were modelled for this condition.

- Dry season: A two-month (61 days) period from 01/06/2024 to 01/08/2024. This period is considered representative of typical dry season conditions with low river discharge and typical dry season wind and wave conditions (predominantly from the east to south). All the scenarios were modelled for this condition.

- Tropical Cyclone: A 5-day period from 15/03/2018 to 20/03/2018 was selected to simulate the strong winds and waves resulting from Tropical Cyclone (TC) Marcus, which passed east to west within the JBG with the centre of the TC passing ~80 km to the north of CG in March 2028. TC Marcus was selected for the simulation as it resulted in the largest waves directly offshore of CG over the last 10 years (based on hindcast modelled wave conditions from the CAWCR model). The track data for TC Marcus from the Bureau of Meteorology (BoM) was used to develop a TC wind and pressure field using the Holland (1980) wind field model with a 2,000 m resolution rectilinear grid. This wind and pressure field was adopted in the HD model to represent TC Marcus. All scenarios except for the pre-European settlement (as the river discharge during the event was not very high and so this scenario would have been the same as the existing scenario) were modelled for this condition.

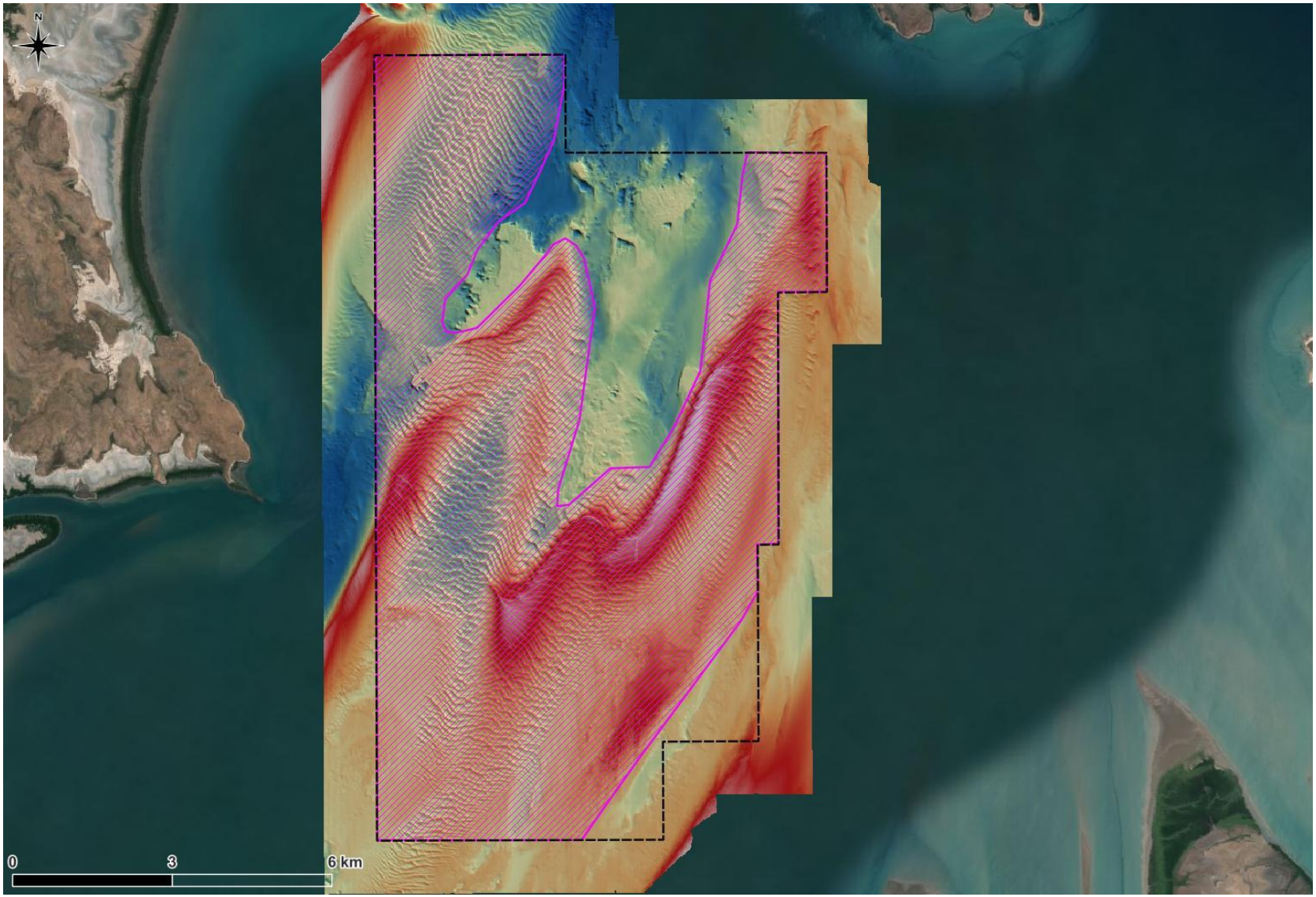


Figure 87. The 75 km^2 area (pink dashed region) within the POA where suitable sand is present for the sand sourcing.

3.5. Spectral Wave Model

The MIKE SW model is able to model the growth, decay and transformation of wind-generated and swell waves in both offshore and coastal environments. The SW model is able to represent wave processes which are expected to influence wave conditions both in JBG and CG. Details of the model configuration, calibration and validation and scheme simulations are provided in the following sections.

3.5.1. Model Configuration

Wave parameters were extracted at the offshore model boundary from the CAWCR wave/wind hindcast for Australia (Smith *et al.*, 2020). The CAWCR hindcast provides modelled wave conditions with a 4-arc minute (approximately 7.4 km) spatial resolution at an hourly temporal resolution. The extracted wave parameters from the CAWCR model were applied at the offshore boundary of the SW model. Sensitivity testing was undertaken as part of the model calibration process to determine the most appropriate approach to represent wind in the model. The modelled wind from the CAWCR wave/wind hindcast extracted from within CG resulted in the best agreement between the SW modelled wave conditions and measured wave conditions (this is discussed in more detail in the following section).

To account for the effect of the large variations in water depth occurring throughout the tide on the wave processes, a time varying water level based on predicted water levels at Cape Domett (AHO, 2023) was applied in the SW model.

3.5.2. Calibration and Validation

There are no specific model calibration and validation guidelines adopted by the WA EPA for SW models and the available numerical modelling guidelines developed in WA (e.g. Sun *et al.*, 2016; and Sun *et al.*, 2020) and elsewhere in Australia (e.g. GBRMPA, 2012) only provide qualitative guidance. The lack of model performance guidelines for coastal and estuarine areas globally resulted in Williams and Esteves (2017) providing practical wave model performance guidelines. They state that a good agreement between the model and measured data is represented by a Root Mean Square Error (RMSE) of the mean H_s that is ≤0.4 m for Type A (design) or ≤0.5 m for type B (appraisal). They also state that meeting these criteria for at least 90% of positions / time combinations is an acceptable criterion in most circumstances.

No measured wave data were available as part of the initial model calibration presented in PCS (2024a) and instead, a validation of the wave model against hindcast modelled wave conditions from CAWCR was undertaken. Since this initial model validation, additional wave data have been collected by BKA as part of the project, allowing for calibration and validation of the wave model at multiple sites in the CG region. Further details are provided below:

- Calibration period: A two-month (61 days) wet season period was selected from the 1st March 2024 to the 1st May 2024. Statistical analysis to compare the measured and modelled H_s was undertaken over the entire period of concurrent data within the 2 months. Measured wave data were available at five sites over the calibration period (AWAC-01, AWAC-06, AWAC-08, AWAC-09 and AWAC-11).
- Validation period: A two-month (61 days) dry season period was selected from the 1st June 2024 to 1st August 2024. Statistical analysis to compare the measured and modelled H_s was undertaken over the entire period of concurrent data within the 2 months. Measured wave data were available at four sites over the validation period (AWAC-01, AWAC-05, AWAC-10 and AWAC-11).

3.5.2.1. Model Calibration

For conciseness, only a selection of the calibration time series plots are shown below to represent the general trends observed. The complete set of calibration and validation plots are included in Appendix A. The measured and modelled H_s, peak wave period (T_p) and mean wave direction at AWAC-01, AWAC-08 and AWAC-09 are shown in Figure 88 to Figure 90. There are several instances of gaps (e.g. AWAC-08) and outliers (e.g. AWAC-09) within the measured data but this does not influence the model calibration.

The plots show that the model captures variations in H_s between the three sites as well as the variability over different temporal scales. For T_p, the model shows good agreement with measured data during the peaks of the wave events, whilst underestimating the measured T_p during the troughs, but due to the small wave heights during these periods this limitation in the model is not considered to affect the ability of the model for use in this study. The modelled mean wave direction shows general alignment

with the measured data up to the start of April 2024. In April 2024 the measured data shows significant variability in wave direction, while the model shows waves typically from the east to south (i.e. correlating with the wind direction). Detailed analysis of the measured wave data presented in Section 2.2 noted that there was uncertainty in the measured wave direction during smaller, low period wave conditions (such as in April 2024). As the modelled wave direction corresponds with the wind direction (which was generating the waves) and so it is considered to be able to represent the dominant wave direction resulting from the local wind conditions, which will be the most important for sediment transport. Overall, both the measured and modelled time series exhibit similar fluctuations across all wave characteristics, demonstrating that the model effectively replicates the trends and variations seen in the measured data.

A statistical summary of the wave data calibration is presented in Table 8 detailing the RMSE of the H_s at each site. The RMSE are all within ≤0.2 m which comfortably falls within the Type A band (engineering design) standards (Williams and Esteves, 2017) even though this is not an engineering design project. Overall, the calibration results align with the model performance guidelines recommended by Williams and Esteves (2017), illustrating that the SW model can accurately represent waves across the study area.

Table 8. Comparison of RMSE for modelled and measured significant wave height data at AWAC-01, AWAC-06, AWAC-08, AWAC-09 and AWAC-11 during the calibration period.

AWAC Site	H_s RMSE (m)
AWAC-01	0.15
AWAC-06	0.13
AWAC-08	0.11
AWAC-09	0.19
AWAC-11	0.12

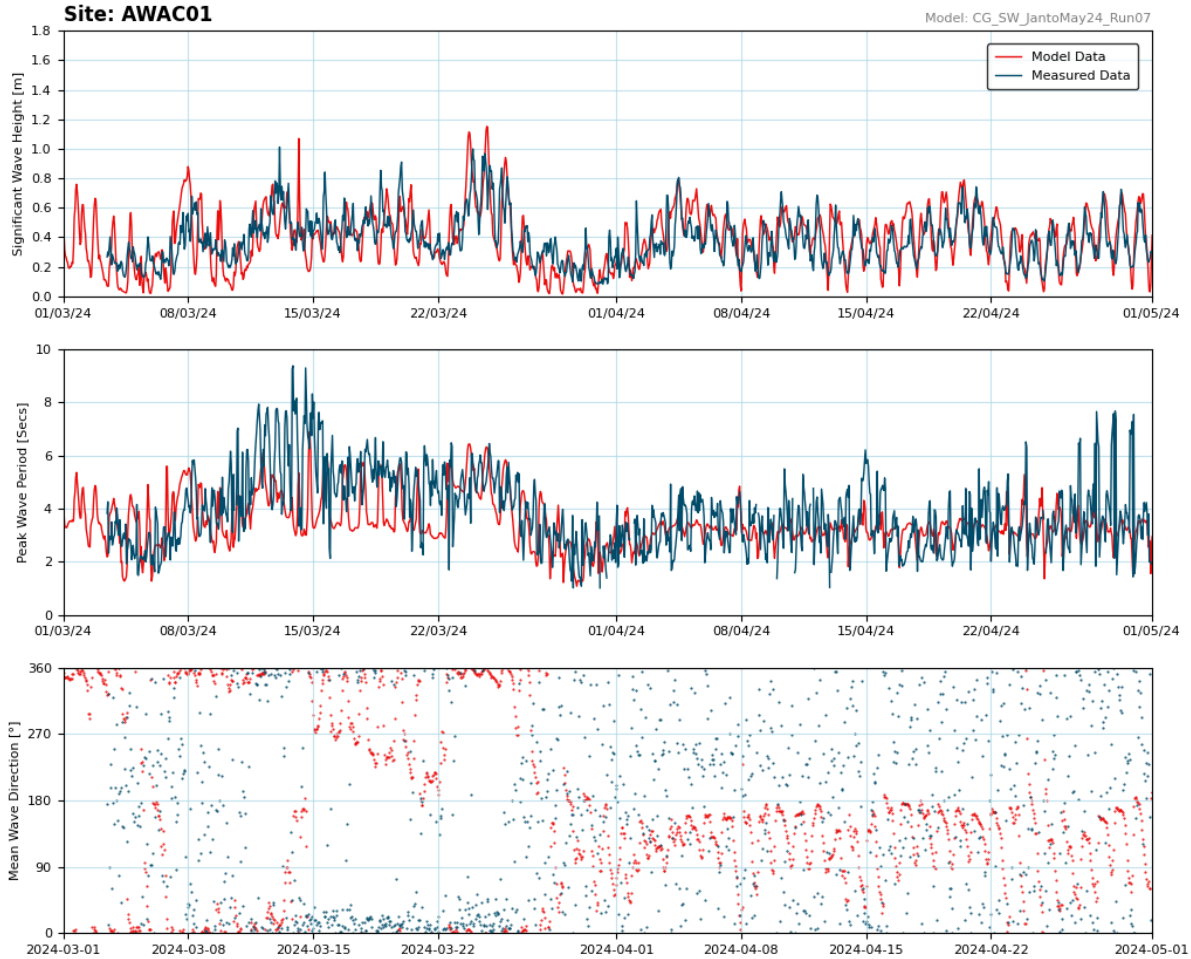


Figure 88. Modelled and measured significant wave height, peak wave period and mean wave direction at AWAC-01 over the model calibration period.

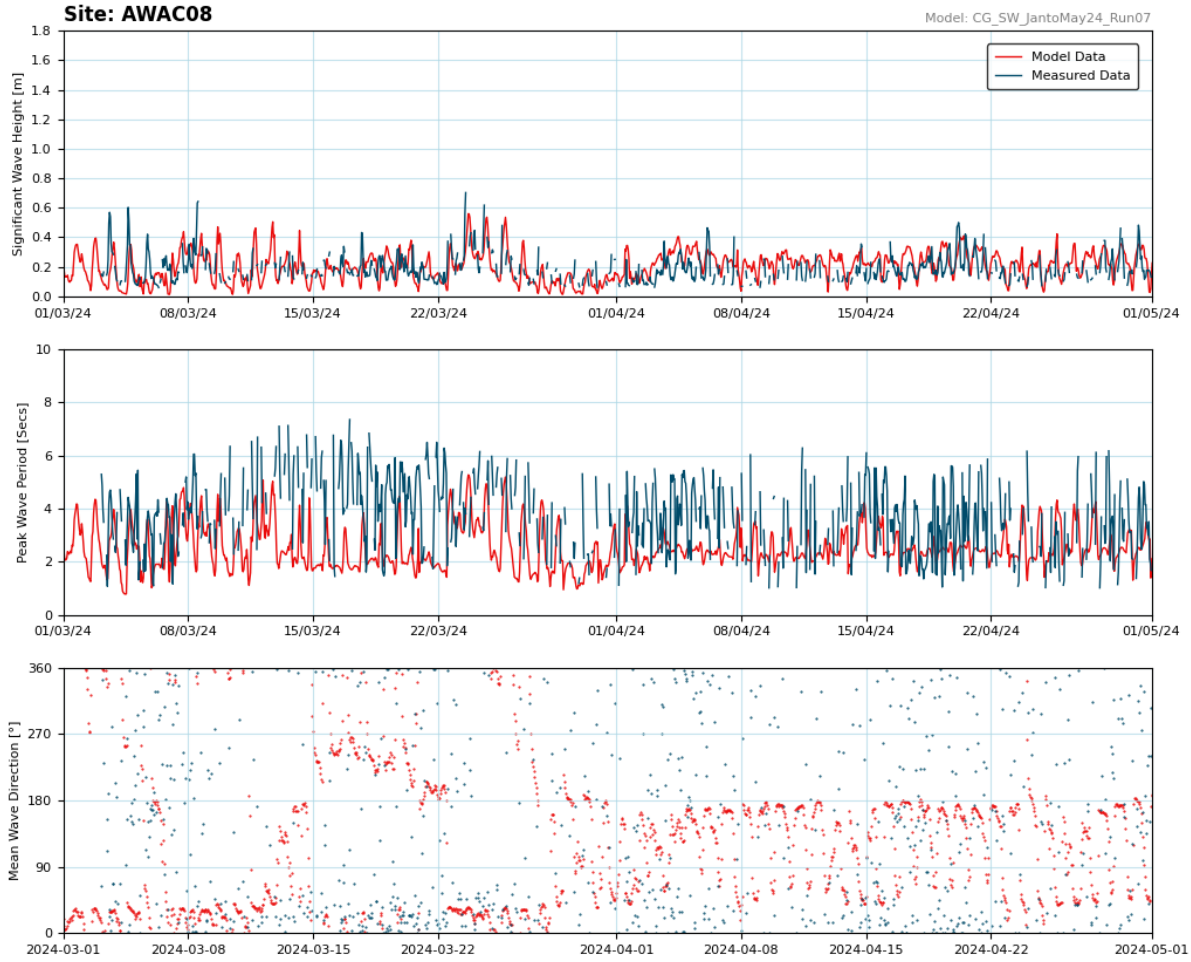


Figure 89. Modelled and measured significant wave height, peak wave period and mean wave direction at AWAC-08 over the model calibration period.

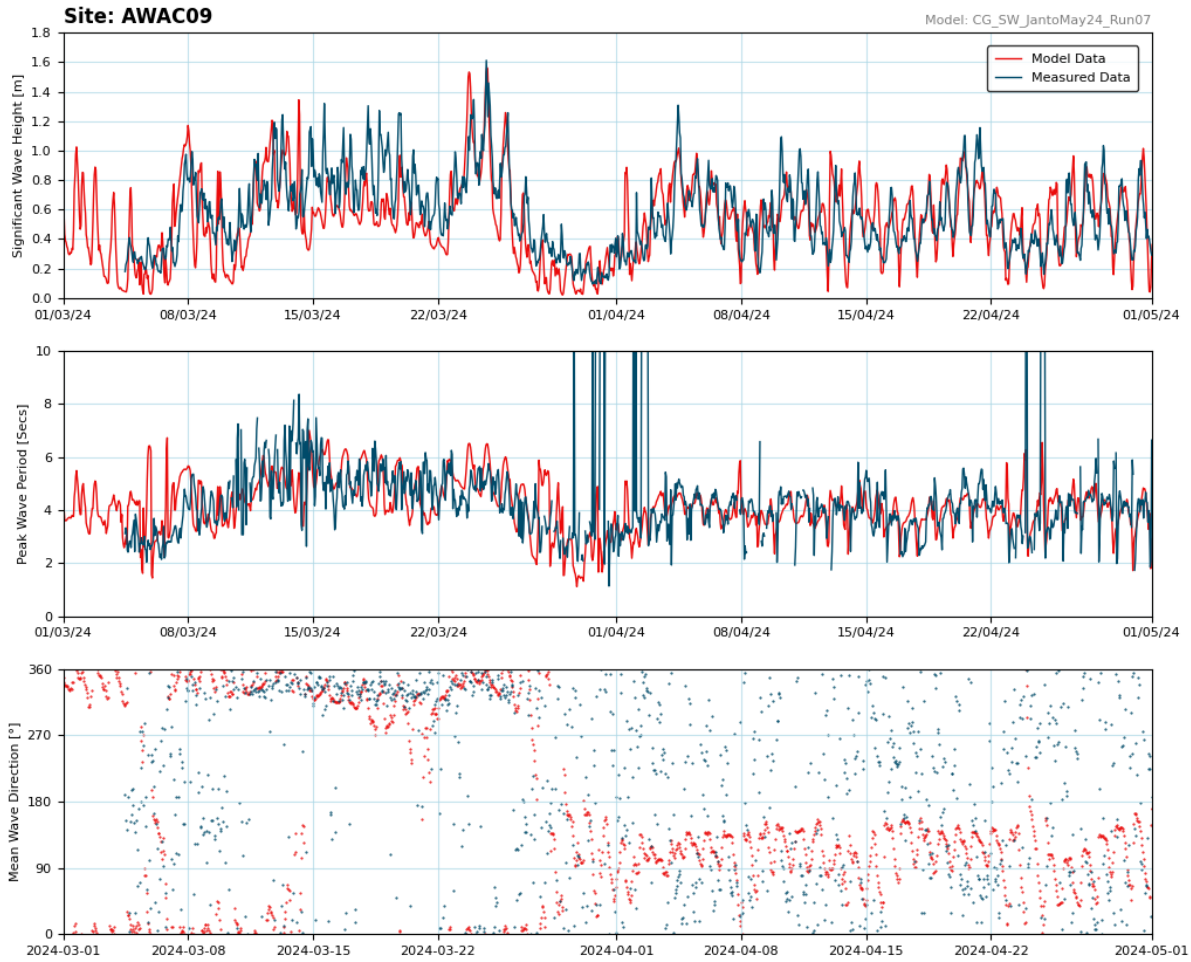


Figure 90. Modelled and measured significant wave height, peak wave period and mean wave direction at AWAC-09 over the model calibration period.

3.5.2.2. Model Validation

As with the model calibration, only a selection of the validation plots are shown below to represent the general trends observed. The full set of calibration and validation plots are shown in Appendix A. The measured and modelled H_s, T_p and mean wave direction at AWAC-01 and AWAC-10 are shown in Figure 91 and Figure 92.

Both the measured and modelled time series exhibit similar H_s fluctuations in response to diurnal and longer-term wind variability, demonstrating that the model accurately replicates the trends and variations seen in the measured data. The measured T_p exhibits significant variability, with values regularly jumping from 2 to 3 s up to 6 to 9 s and back. This indicates that the highest wave energy is varying between the low period locally generated wind waves and the longer period old sea and swell waves, although both wave components are still present. However, the periods with higher values of T_p correlate with calm periods (H_s < 0.3 m), which are not as critical for the model to accurately represent as they are unlikely to influence sediment transport in CG.

The model provides a good representation of the measured T_p at both sites during periods with a larger H_s (> 0.3 m). The measured wave direction can be seen to be predominantly from the north during the calm periods and higher T_p, while during periods with higher H_s the measured wave direction is predominantly from the east to south. During the periods with higher H_s the modelled wave direction agrees well with the measured wave direction, but during the calm periods the modelled wave direction is still dominated by locally generated wind waves while the measured wave direction is more variable. As previously noted in Section 2.2 there was uncertainty in the measured wave direction during smaller, low period wave conditions and so the measured wave directions during these periods are not considered to be reliable. Overall, the validation gives confidence in the model being able to represent the wave conditions during periods with larger wave heights which are more likely to influence sediment transport in the region.

A statistical summary of the validation is presented in Table 9 detailing the RMSE of the H_s for each site location. The RMSE are all within ≤0.4 m and the Type A band (engineering design) standards (Williams and Esteves, 2017) even though this is not an engineering design project. Overall, the validation results are within the model performance criteria outlined by Williams and Esteves (2017), confirming that the SW model accurately represents wave conditions during both wet and dry seasons.

Table 9. Comparison of RMSE for modelled and measured significant wave height data at AWAC-01, AWAC-05, AWAC-10 and AWAC-11 during the validation period.

AWAC Site	H_s RMSE (m)
AWAC-01	0.14
AWAC-05	0.19
AWAC-10	0.15
AWAC-11	0.14

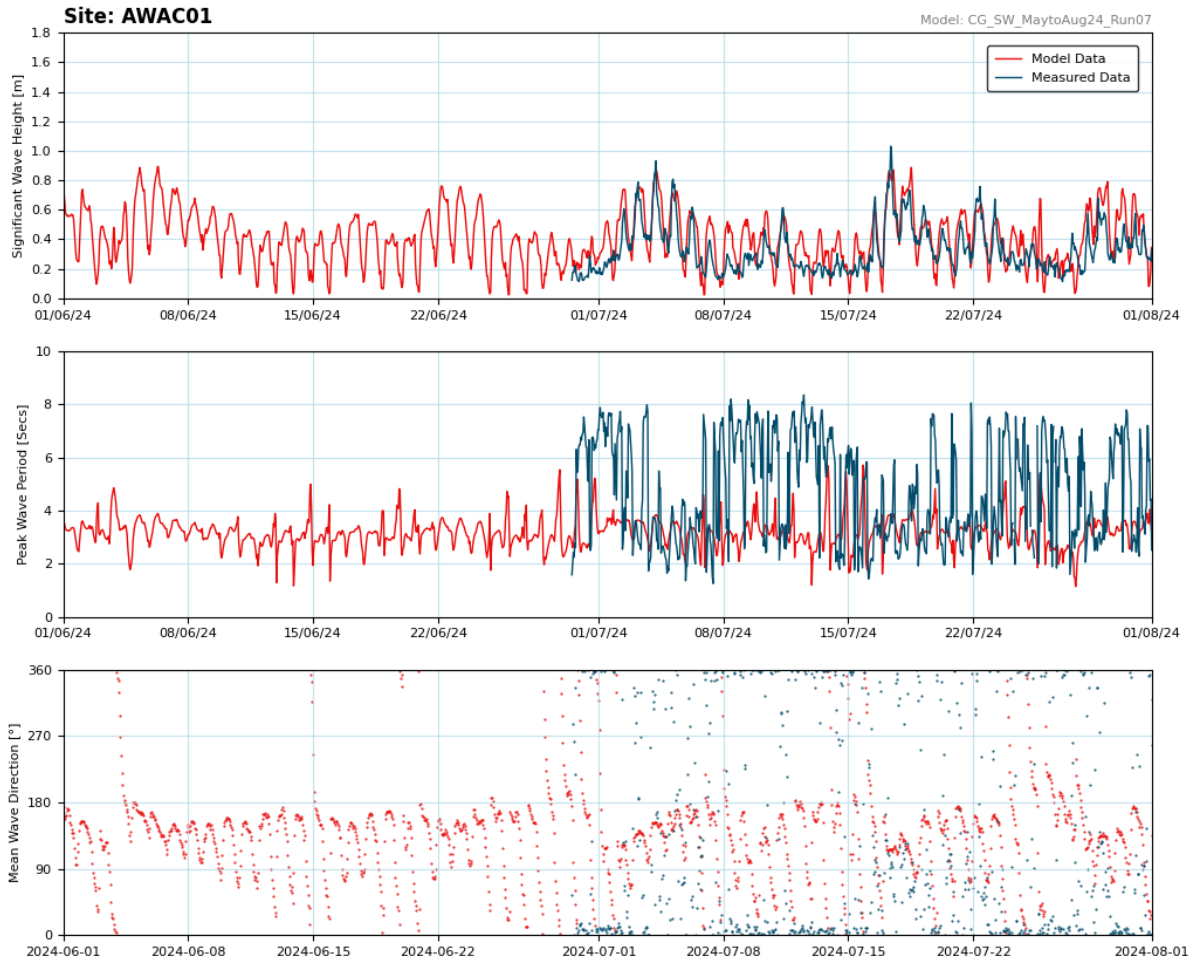


Figure 91. Modelled and measured significant wave height, peak wave period and mean wave direction at AWAC-01 over the model validation period.

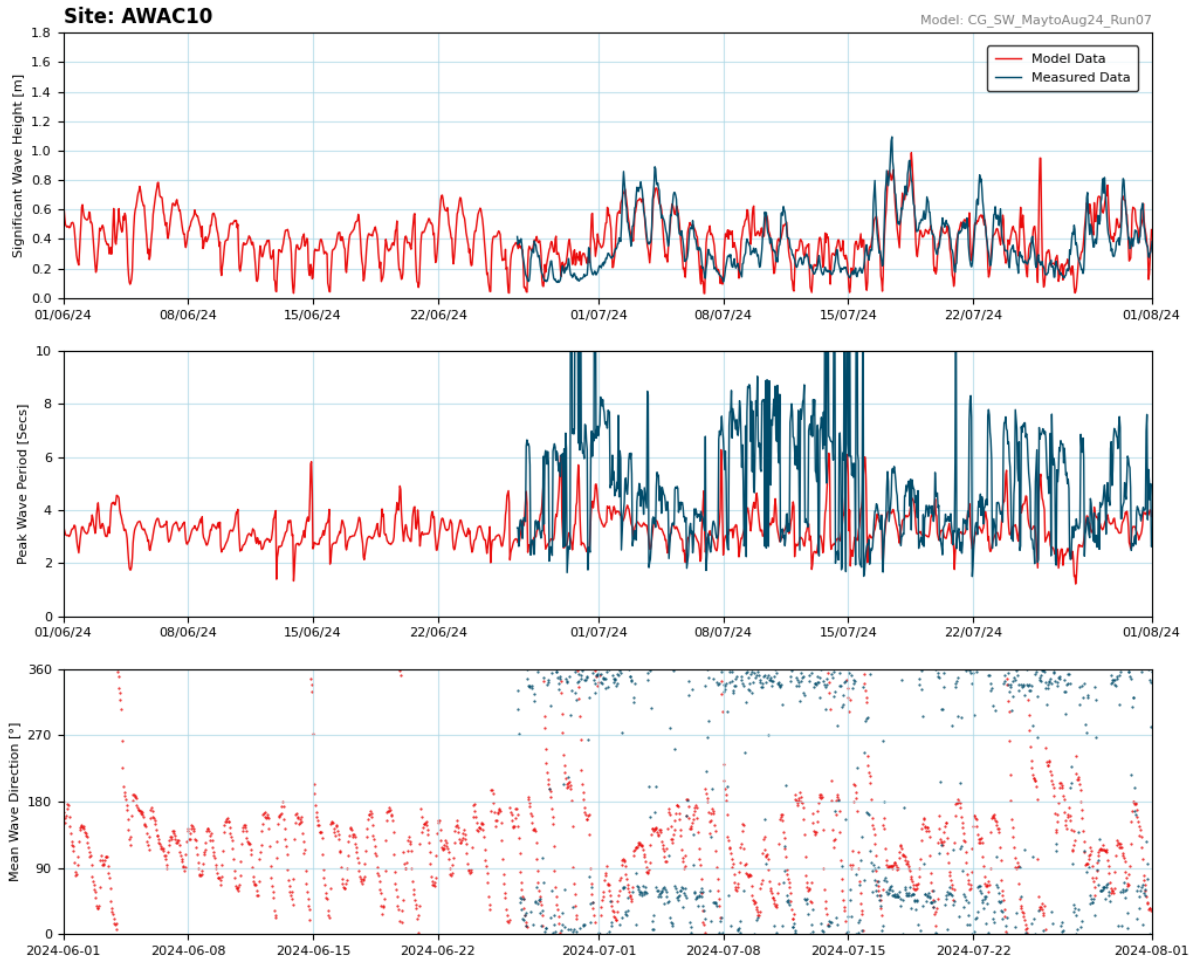


Figure 92. Modelled and measured significant wave height, peak wave period and mean wave direction at AWAC-10 over the model validation period.

3.5.3. Scheme Simulations

Following the calibration and validation of the SW model, the model setup of the existing case was modified to represent the following scenarios:

- 5 years of sand sourcing (23 million m^3 removed): This scenario was represented in the same way as for the HD model, with the model bathymetry deepened by 0.31 m over the area of the proposed operational area where sand is present.
- 15 years of sand sourcing (70 million m^3 removed): This scenario was represented in the same way as for the HD model, with the model bathymetry deepened by 0.94 m over the area of the proposed operational area where sand is present.
- 100 years from today, no sand sourcing: To represent this scenario in the SW model the water levels were increased by 0.9 m to represent predicted climate-change related sea level rise (based on Department of Transport (2010) and IPCC (2024)). No change to the wave climate was assumed based on the findings from National Environmental Science Programme (2024).
- 100 years from today, with sand sourcing (70 million m^3 removed): This scenario assumes the same increase in water level as the 100 years with no sand sourcing scenario. The scenario also includes for the sourcing of 70 million m^3, but with some sedimentation also assumed to have occurred within the POA (for further detail see Section 3.4.3).

The SW model was set up to represent these scenarios as well as the existing case for the same wet season, transitional season, dry season and TC Marcus periods as the HD model. In addition, the SW model was also set up for the existing case to simulate the wave conditions over a five-year period from 2015 to 2020 to provide wave conditions to inform the Beach Processes model (see below).

3.6. Sediment Transport Model

The ST model describes the erosion, transport and deposition of sediment, including clay, silt and sand, due to currents and waves. The module is designed specifically for sediment transport studies in coastal and estuarine environments with fine-grained and sand-sized sediment, and for dredging studies. Details of the model configuration, calibration and validation and scheme simulations are provided in the following sections.

3.6.1. Model Configuration

The MIKE ST model is driven by the hydrodynamic and wave conditions from the HD and SW models. The configuration of the ST model has been developed with consideration to all relevant sediment and sediment transport data collected as part of the project, including bed sediment properties, suspended sediment properties and bedform migration rates, as reported in PCS (2024a & 2024b). The ST model is a 3D model with the same 10 layers adopted as in the HD model. The model has been set up to represent the transport of clay, silt and sand in suspension and the transport of sand as bedload.

Based on the sediment data collected by BKA's field studies the model has been set up with four sediment types/sizes, reflecting the predominant sediment types/sizes found in CG, as reported in PCS (2024a, b & c). These were clay (D_{50} = 4 μm), medium silt (D_{50} = 30 μm), very fine sand (D_{50} = 80 μm, with sediment grading ((D_{84}/D_{16})$^{0.5}$) of 1.3) and a medium sand (D_{50} = 300 μm, with sediment grading of 1.45). The predominant sediment type/size found in the POA was medium sand (i.e. the sand that is the subject of the BKA proposal) with an average D_{50} of 303 μm based on the 2024 wet season sediment sampling.

The model has a single bed layer which has a spatially varying distribution of the sediment types informed by the bed sediment samples from CG reported in PCS (2024a, b & c). For the simulations a bed sediment thickness of 4 m was adopted, this was based on the average thickness of sand present within the POA from vibro-cores collected by BKA. This average bed thickness of 4 m is a conservative underestimate, and in some areas the thickness of sand in the POA may be up to approximately 15 m (on top of the sand waves), as outlined in section 5 of BKA (2024b). The model was then set up to simulate sediment transport over a 6-month period, and areas where erosion of more than 1 m was modelled over this period were assumed to indicate that clay, silt and sand-sized sediment are not likely to remain in these areas, with the bed likely to be made up of rock or gravel. The bed sediment thickness in these areas was set to a 0 m bed thickness.

The resultant bed thickness was then applied as the initial bed thickness for the simulations. The upstream input of clay and silt-sized sediment released in East and West Arms was variable depending on the river discharge, with 300 mg/L released during periods of low discharge and 1,000 mg/L released during periods of high discharge (with discharge of more than 400 m^3/s). These concentrations were selected during the model calibration stage to achieve the measured SSC values at the site at the northern entrance to West Arm (AWAC-08).

3.6.2. Calibration and Validation

The extensive data which have been collected by BKA as part of the project, as reported in PCS (2024a, b & c) allow the following to be considered as part of the sediment transport model calibration and validation:

- Composition of the suspended sediment: Results of the Particle Size Distribution (PSD) of suspended sediment from vertical profiling every hour over a 13-hour spring tidal cycle at each of three sites in CG in February 2024 were used to calibrate the SSC of clay/silt- and sand-sized particles in suspension.
- Bedload transport rates: The dimensions of the sand waves and their migration rates based on repeat bathymetric surveys of the POA over a full lunar-tidal cycle in February 2024 were used to estimate the net bedload transport rate for the areas where the sand waves are present based on the approach detailed by Cilli *et al.* (2021). This has been used to calibrate the bedload transport rates calculated by the model.
- SSC in the near-bed layer of the water column: Timeseries of the in-situ measured turbidity data collected at multiple sites within CG were converted to SSC based on the turbidity-TSS relationships described in Section 2.3.1, which are considered suitable to allow calibration and validation of the sediment transport model, as described in that section.

As with the HD and SW models, there are no specific model calibration and validation guidelines for sediment transport (ST) models adopted by the WA EPA and the available numerical modelling guidelines developed in WA (e.g. Sun *et al.*, 2016; and Sun *et al.*, 2020) and elsewhere in Australia (e.g. GBRMPA, 2012) only provide qualitative guidance. Typically, a qualitative calibration and validation process is undertaken for ST models to demonstrate that the numerical model can approximately replicate the spatial and temporal patterns in SSC. Demonstrating that the model can replicate the spatial and temporal patterns in SSC provides confidence that the model is representing the key processes which mobilise the sediment as well as the processes which transport the sediment once it is suspended.

However, despite the inherent complexities associated with ST modelling (such as having to accurately represent the hydrodynamic and wave conditions and the properties of the sediment on the bed and in the water column), it is possible to provide a quantitative measure of the performance of a ST model. By calculating the normalised mean absolute error between the model and measured data the performance of the model can be categorised as detailed by Los and Blaas (2010). The OSPAR cost function (CF) as described in Los and Blaas (2010) was used to provide a measure of the level of calibration of the SSC for this study. The normalisation expresses the goodness of fit in terms of the standard deviation, with the following classifications:

- CF of less than 1 being ‘very good’;
- CF between 1 and 2 being ‘good’;
- CF between 2 and 3 being ‘reasonable’; and
- CF of more than 3 being ‘poor’.

Despite these classifications it was noted in Los and Blaas (2010) that the OSPAR CF indicate good or reasonable agreement despite there being clear and consistent differences between the modelled and measured data. Therefore, it is proposed that an OSPAR CF of less than 1 should be achieved at the majority of the sites. The different aspects of the model calibration and validation are detailed in the following sections.

3.6.2.1. Suspended Sediment Composition

The ST model was set up to simulate the sediment transport conditions from the 8th February 2024 to the 6th March 2024 for the initial calibration of the suspended sediment composition and the bedload transport. This represents the time between the two bathymetric surveys of Target Areas 1 and 2 within the POA as reported in PCS (2024a), whilst also covering the times when the hourly 13-hour vertical profiling was undertaken at three sites in CG in February 2024, as also reported in PCS (2024a). The sites were AWAC-01 within the POA, AWAC-05 in West Entrance north of the POA and AWAC-11 south of the POA.

Water samples collected as part of the hourly 13-hour vertical profiling were analysed in the laboratory to determine both the SSC and the PSD of the suspended sediment. The measured data have been processed to calculate the SSC of the clay/silt- and sand-sized particles in suspension. The measured near-bed SSC data for clay/silt and sand were then compared with the modelled near-bed SSC results for these sediment types (the clay and medium silt in the model were combined to represent the clay/silt sediment and the very fine sand and medium sand in the model were combined to represent the sand sediment) at the three vertical profile sites (Figure 93 to Figure 95). The plots show that the model consistently provides a good representation of the SSC for the clay/silt- and sand-sized sediment at the three sites, with the model able to represent the difference in SSC between the two fractions as well as providing a reasonable representation of the temporal variability.

The mean measured and modelled SSC for clay/silt and sand are compared in Table 10. The results shows that the modelled mean SSC for the silt/clay is within 30% of the measured mean SSC at all three sites, while the modelled mean SSC for sand was within 45% of the measured mean SSC. However, the largest difference between the measured and modelled sand-sized SSC was 1.6 mg/L, which is a very small difference and therefore the comparison demonstrates that the model can replicate the low SSC of sand-sized sediment.

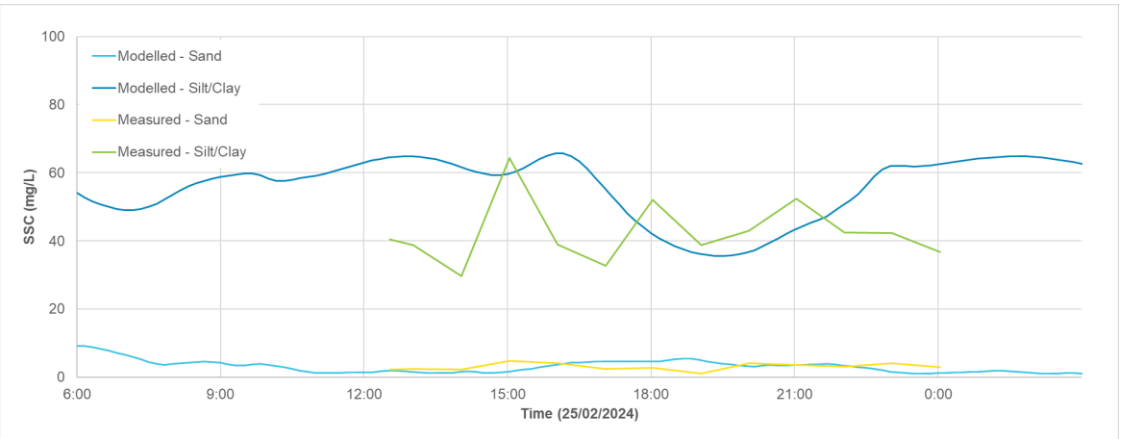
The calibration demonstrates that the model provides a reliable representation of the SSC of both clay/silt- and sand-sized particles in suspension at locations within the POA and to the immediate north and south of the POA.

Table 10. Comparison between mean near-bed measured and modelled clay/silt SSC and sand SSC during the February 2024 13 hour vertical profile measurements.

Location	Clay/Silt Suspended Sediment			Sand Suspended Sediment		
	Measured SSC (mg/L)	Modelled SSC (mg/L)	Difference (%)	Measured SSC (mg/L)	Modelled SSC (mg/L)	Difference (%)
AWAC-01	39.3	46.5	18%	1.7	2.4	42%
AWAC-05	42.5	53.1	25%	3.1	3.1	0%
AWAC-11	91.5	102.9	12%	4.0	2.4	-40%



Figure 93. Measured and modelled SSC for clay/silt and sand particles at AWAC-01.



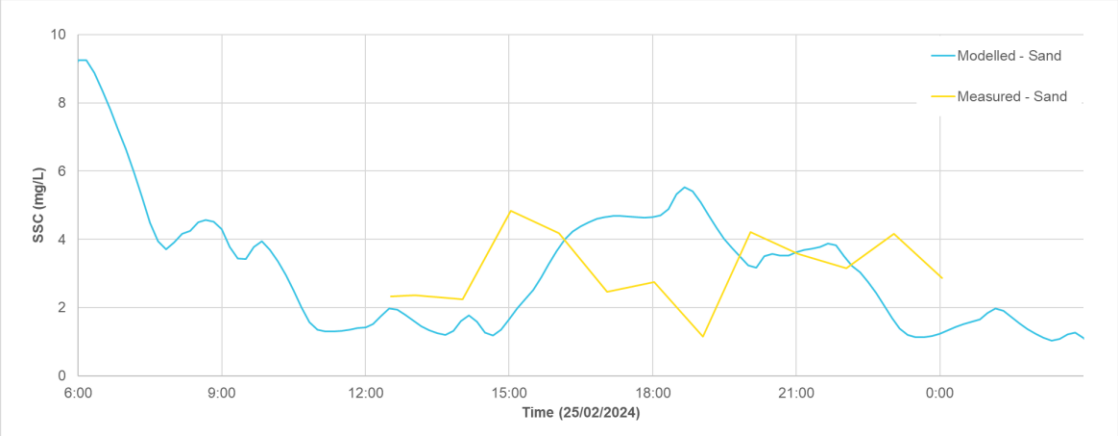


Figure 94. Measured and modelled SSC for clay/silt and sand particles at AWAC-05.

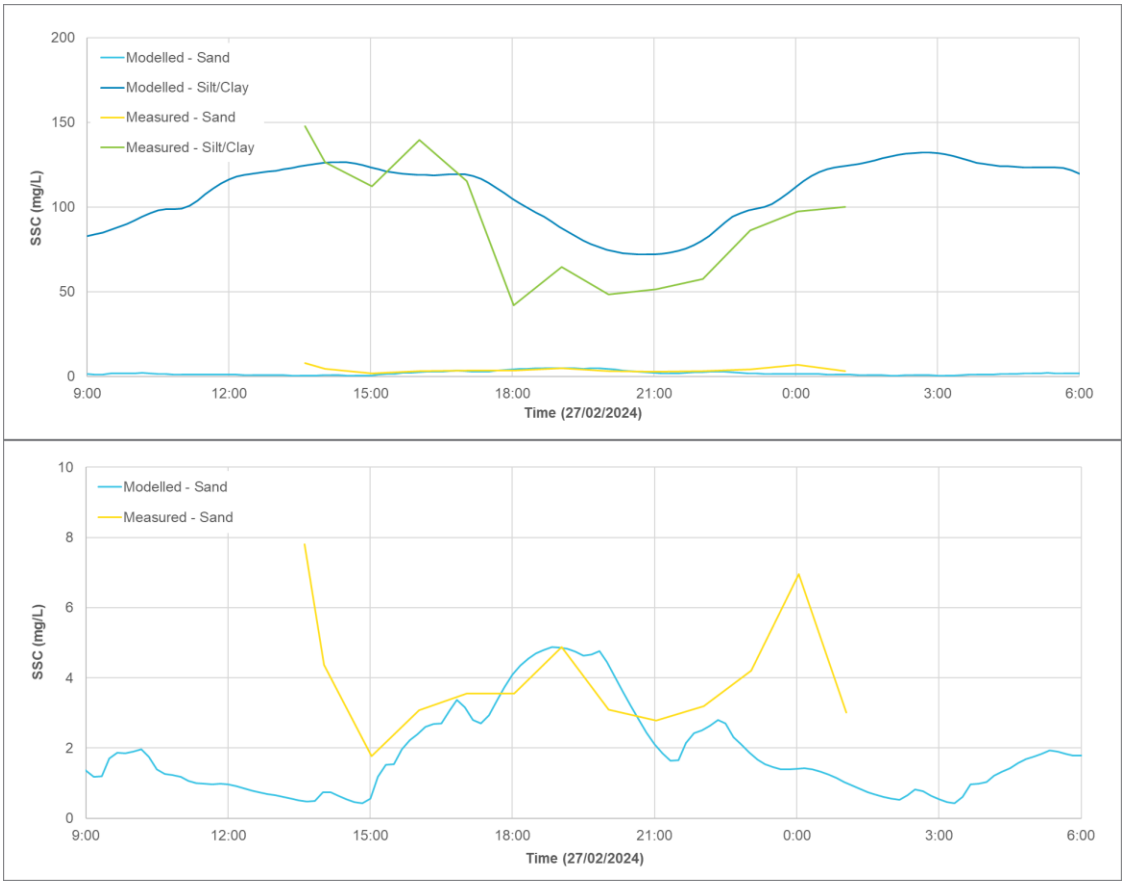


Figure 95. Measured and modelled SSC for clay/silt and sand particles at AWAC-11.

3.6.2.2. Bedload Transport

It is not realistic in terms of model simulation times and computational requirements for the mesh of the ST model to be of sufficient resolution to represent the sand waves present within the POA, which have vertical heights from trough to peak up to 8 m and horizontal lengths from peak to peak ranging from 50 m to 200 m, as measured by the bathymetric survey undertaken by BKA in February-March 2024 (PCS 2024a). Therefore, the model is not able to replicate the horizontal migration of the sand waves measured by the repeat bathymetric surveys undertaken by BKA, which was 5 to 10 m over 27 days (PCS 2024a). However, the surveyed dimensions of the sand waves and their migration rates can be used to estimate the net bedload transport rates, which can be compared with the modelled bedload transport rates. The following equation was used to estimate the net bedload transport rates in the POA (Cilli *et al.*, 2021):

$$q_b = (1-p)U_d \frac{h}{2}$$

where:

q_b = volumetric net bedload transport per metre

p = bed porosity (0.3 was adopted for sand based on Holmes (2010))

h = mean dune height (m)

U_d = dune celerity (m/s)

The resultant volumetric net bedload transport rate was converted to a mass bedload transport rate by assuming a dry sediment density of 1,600 kg/m^3, which is representative of sediment made up of predominantly sand (~95%) based on Van Rijn (1993).

The surveyed sand wave migration was predominantly in a northerly direction, with only localised areas where a southerly migration occurred. The bathymetric survey of the entire POA was used to calculate the sand wave sizes at the three monitoring sites where the calibration of the suspended sediment composition was undertaken (AWAC-01, AWAC-05 and AWAC-11), as there is confidence that the model is accurately representing the transport of fine sand in suspension at these sites and the sites represent conditions within the POA and to the north and south of the POA (i.e. where sand could be transported to or from). At AWAC-05, the average sand wave height was 4 m. At AWAC-11, the average sand wave height was estimated to be 5 m (based on the sand waves in the area of the survey closest to AWAC-11, as the survey didn't extend out to AWAC-11). At AWAC-01 there were no sand waves present. At AWAC-05 and AWAC-11 an average migration rate of 8 m over 27 days was determined from the repeat bathymetric survey, and based on this, the following net bedload transport rates were calculated:

- AWAC-05: 0.0074 kg/m/s.
- AWAC-11: 0.0092 kg/m/s.

Due to the lack of sand waves at AWAC-01 it is not possible to calculate a net bedload transport rate, but it can be inferred that it will be significantly lower than at the other two sites.

The modelled bedload transport rates were extracted from the ST model at the three monitoring sites for the period from the 8th February 2024 to the 6th March 2024 (the time between the repeat bathymetric surveys of Target Areas 1 and 2 within the POA). The bedload transport rate was processed so transport in a southerly direction (during the flood stage of the tide) was negative and transport in a northerly direction (during the ebb stage of the tide) was positive (Figure 96). The bedload transport rates show a strong tidal signal, with higher transport rates coinciding with spring tides and lower transport rates coinciding with neap tides.

The timeseries plot also shows that the bedload transport rates were higher at AWAC-05 and AWAC-11 compared to AWAC-01 and that the bedload transport in a northerly direction (i.e. positive bedload transport rates) was greater than the transport in a southerly direction (i.e. negative bedload transport rates). The bedload transport rates were used to calculate the net bedload transport at the three sites over the 27-day period between the repeat bathymetric surveys:

- AWAC-01: 0.0025 kg/m/s.
- AWAC-05: 0.0078 kg/m/s.
- AWAC-11: 0.0091 kg/m/s.

The modelled net bedload transport rates were all positive, indicating a net northerly bedload transport at these locations in the model. The net bedload transport rates calculated by the model at AWAC-05 and AWAC-11 are very similar to the net bedload transport rates calculated based on the measured sand wave dimensions and migration rates. At AWAC-01, where no sand waves were present, the net bedload migration rate was more than three times lower, which is as expected given the lack of bedforms in this area.

Overall, the modelled bedload transport rates can be considered to provide a good representation of the bedload transport rates calculated based on the sand wave migration, giving confidence that the model is able to represent the transport of medium-sized sand (i.e. the dominant type of sediment present within the POA) as bedload around the POA.

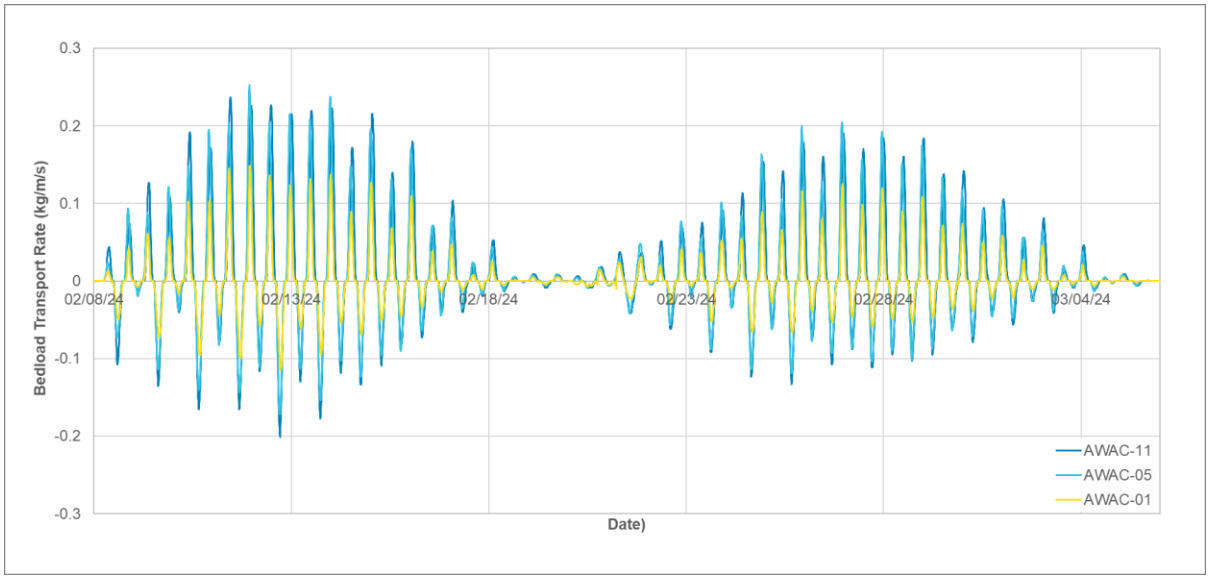


Figure 96. Modelled bedload transport rate at the three sites over the 27-day period between the repeat bathymetric surveys. *Note: positive transport is in a northerly direction, negative transport is in a southerly direction.*

3.6.2.3. SSC

The inferred SSC and modelled SSC are compared to determine whether the model effectively replicates the observed sediment dynamics. This comparison provides insights into the model's ability to capture temporal patterns, magnitudes and variability in the SSC across the different sites. By analysing both statistical metrics and graphical outputs, the model's performance is assessed during the following calibration and validation periods:

- Calibration period: The same calibration period as for the HD and SW models was selected, from the 1st March 2024 to the 1st May 2024. Measured turbidity data were available at eight sites over the calibration period (AWAC-01, AWAC-06, AWAC-08, AWAC-09, AWAC-11, Pos 13, Pos 14 and Pos 15).
- Validation period:Tthe same validation period as for the HD and SW models was selected, from the 1st June 2024 to the 31st July 2024. Measured turbidity data were available at eight sites over the calibration period (AWAC-01, AWAC-05, AWAC-09, AWAC-10, AWAC-11, Pos 13, Pos 14 and Pos 15).

For conciseness, only a selection of the calibration timeseries plots are shown below to represent the general trends observed. The full set of calibration and validation plots are included in Appendix A. The inferred and modelled SSC timeseries at AWAC-01, AWAC-09, AWAC-11 and Pos 15 are shown in Figure 97 to Figure 100 for the calibration period and Figure 101 to Figure 104 for the validation period.

The OSPAR CF values for the calibration and validation periods are detailed in Table 11. In the calibration period, OSPAR CF values remained below 1 at all sites, indicating that they meet the proposed standard, indicating a 'very good' model performance. Pos 13 had the highest CF of 0.74. The validation plots show some discrepancies between the magnitude of modelled and inferred SSC, particularly in capturing peak events.

Additionally, the model is not able to replicate all of the periods of elevated SSC, with the peak SSC at AWAC-01 and AWAC-09 from 15th to 19th March not being represented by the model. This peak was due to an offshore wave event resulting in elevated SSC offshore of CG which the model did not replicate, but the model did replicate the consistent semi-diurnal and spring-neap tidal signals in the SSC data for the remainder of the calibration period and as noted, the model performs well at all sites, providing confidence that the model accurately represents the resuspension and transport of suspended sediment in CG.

During the validation period all of the OSPAR CF values were below 1, indicating 'very good' performance at all sites, demonstrating a high degree of consistency between modelled and inferred SSC during the validation period. Whilst the validation plots show some discrepancies between the magnitude of modelled and inferred SSC, particularly in representing peak events, the model

successfully captures the temporal and spatial variability and fluctuations in SSC, demonstrating that the model provides a good representation of the sediment transport processes in CG during both wet and dry season conditions.

Table 11. OSPAR Cost Function values for comparison of modelled and inferred total SSC during the calibration and validation period.

AWAC Site	Calibration	Validation
AWAC-01	0.58	0.06
AWAC-05	No measured data	0.49
AWAC-06	0.69	No measured data
AWAC-08	0.43	No measured data
AWAC-09	0.23	0.55
AWAC-10	No measured data	0.14
AWAC-11	0.37	0.38
Pos 13	0.74	0.06
Pos 14	0.42	0.6
Pos 15	0.47	0.33

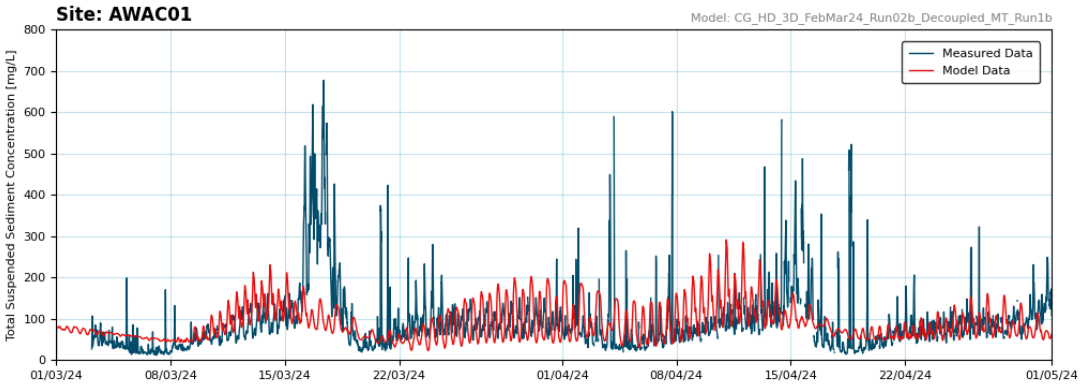


Figure 97. Modelled and inferred SSC at AWAC-01 over the model calibration period.

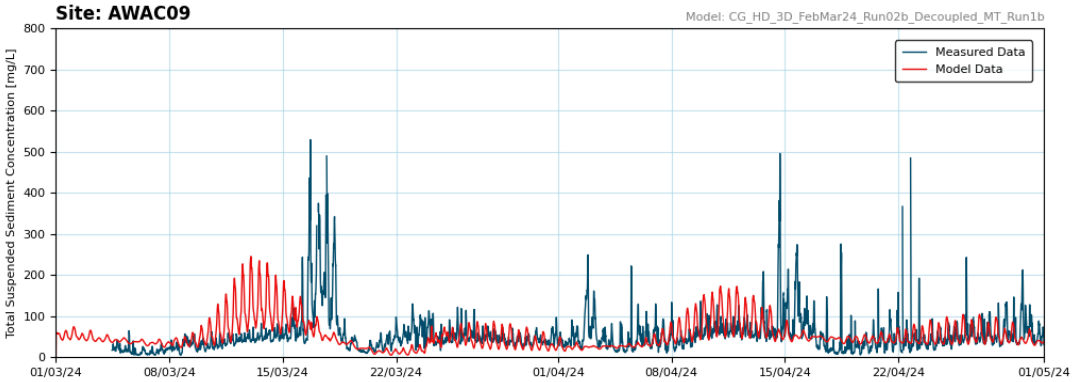


Figure 98. Modelled and inferred SSC at AWAC-09 over the model calibration period.

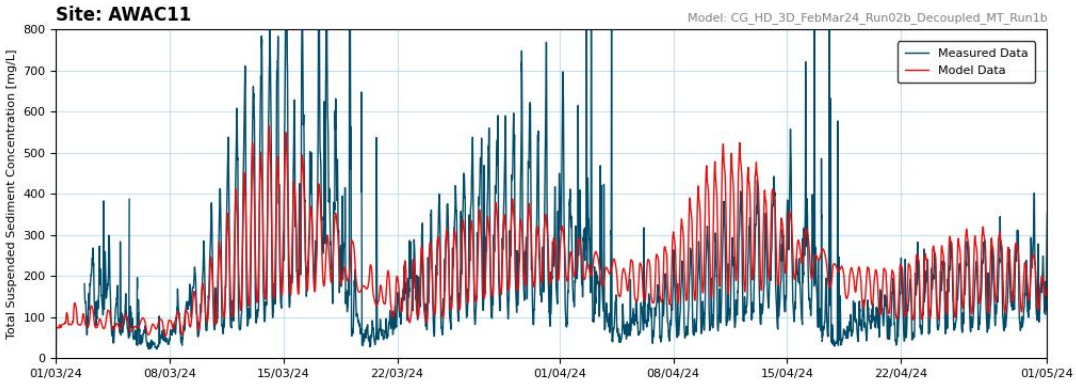


Figure 99. Modelled and inferred SSC at AWAC-11 over the model calibration period.

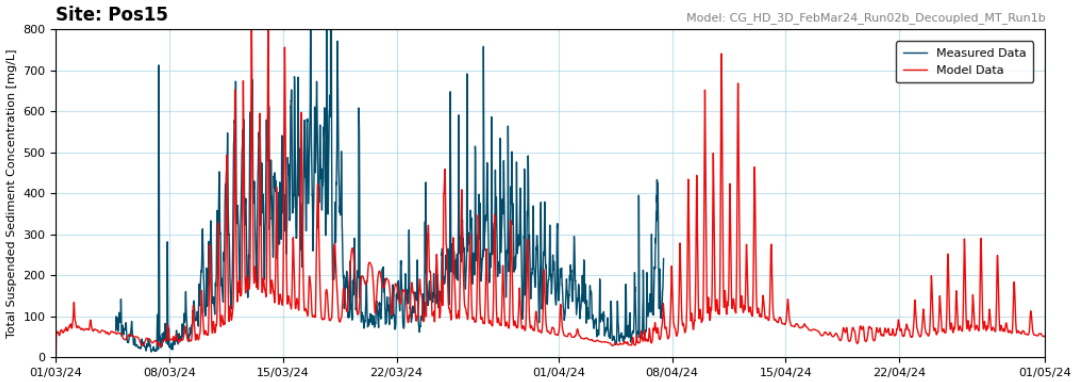


Figure 100. Modelled and inferred SSC at Pos-15 over the model calibration period.

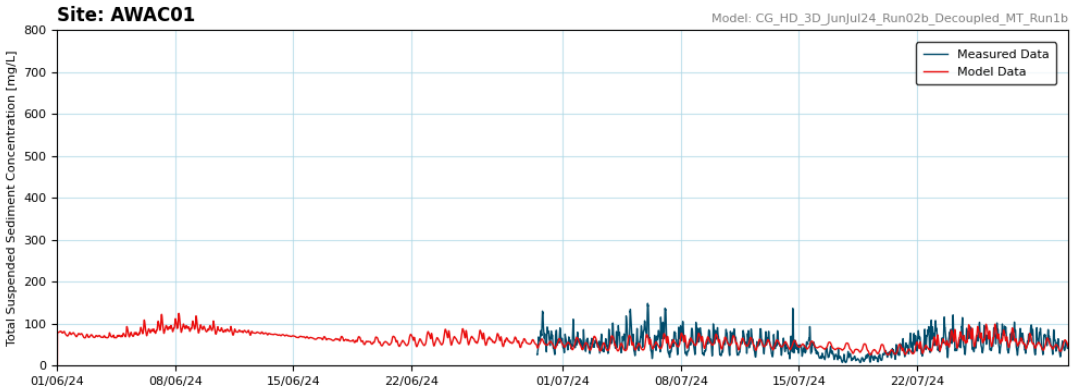


Figure 101. Modelled and inferred SSC at AWAC-01 over the model validation period.

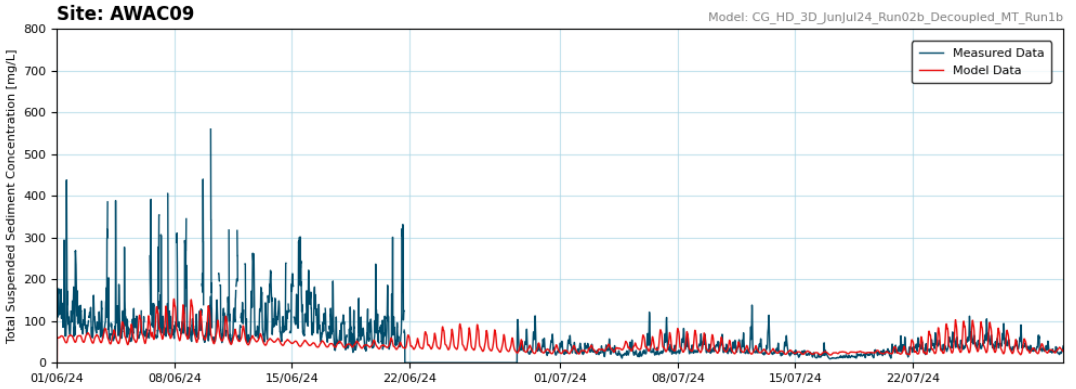


Figure 102. Modelled and inferred SSC at AWAC-09 over the model validation period.

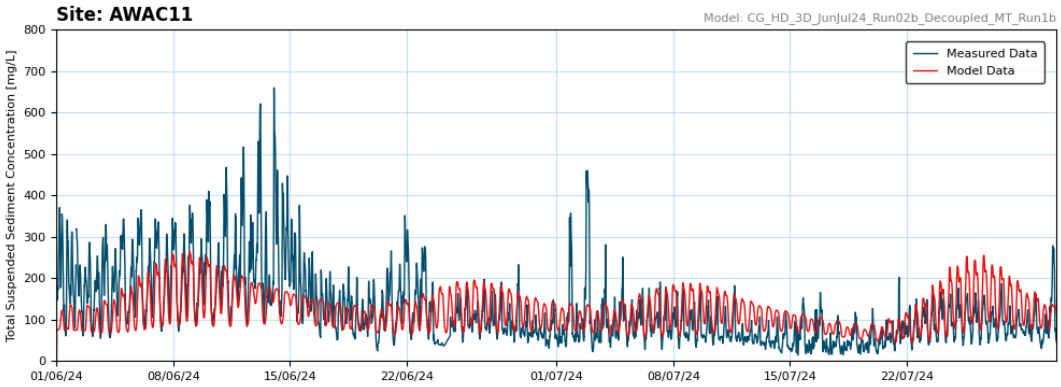


Figure 103. Modelled and inferred SSC at AWAC-11 over the model validation period.

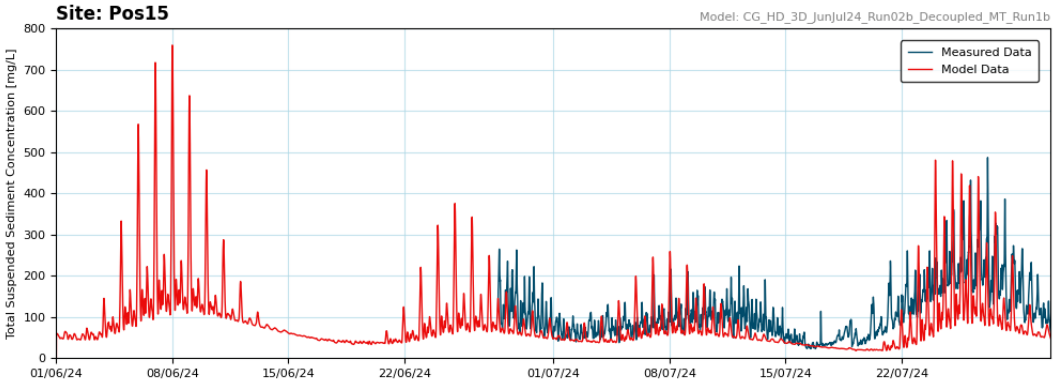


Figure 104. Modelled and inferred SSC at Pos-15 over the model validation period.

3.6.3. Scheme Simulations

Following the calibration and validation of the ST model, the model was set up to represent the same scenarios as the HD model (see Section 3.4.3). The sand sourcing scenarios were represented as a deepening of the bathymetry which influenced the HD, SW and ST models. The proposed sand sourcing will only remove a proportion of the sand present within the POA (up to 23% only, and likely significantly less, after 15 years). Significant sand will remain in the POA at the end of the project (a minimum of 77% and possibly more of the pre-sourcing resource) (PCS, 2024a) (BKA 2024b). As a result, to represent the sand sourcing scenarios, the modelling has assumed that the thickness of the bed sediment layer has been reduced in line with the deepening adopted in the HD and SW models (0.31 m after 5 years of sand sourcing and 0.94 m after 15 years of sand sourcing) over the 75 km^2 where sand is present within the POA.

The only change to the ST model setup to represent the pre-European settlement scenario relative to the existing scenario was a change to the SSC of the water being discharged from Ord River. The SSC of the discharged water was set based on the Ord River pre-European settlement discharge (detailed in Section 3.4.3) with an SSC of 300 mg/L during periods of low discharge (less than 400 m^3/s) and 1,000 mg/L during periods of higher discharge (more than 400 m^3/s).

The ST model was set up to represent the same scenarios as the HD model (wet season, transitional season, dry season and tropical cyclone based on TC Marcus).

3.7. Sediment Plume Model

The plume modelling has been undertaken using the ST model. Details of the model configuration and the scheme representation are provided in the following sections.

3.7.1. Model Configuration

The ST model is driven by the hydrodynamic and wave conditions from the HD and SW models. The ST model also adopts the same 3D vertical layers as the HD model, with 5 equally spaced sigma layers for depths of 0 to 40 m, and then an additional 5 z-layers with each representing 10 m depth bins. This

approach allows the modelling to specify where in the water column the plumes will be generated, ensuring that any 3D structure which may form in the plumes, as noted by Sun *et al.* (2020), can be represented in the modelling.

To represent potential sediment plumes resulting from the sand sourcing operation, the MIKE MT model was set up with no natural sediment present, so that the only sediment in the model was the sediment suspended by the sand sourcing. The properties of the sediment released by the sand sourcing were the same as the properties adopted in the calibrated ST model, as recommended by Sun *et al.* (2020), and the model considers clay, silt and very fine sand particles, as these have all been shown to have the potential to naturally be transported in suspension and are present in CG. This approach aligns with the recommendations by Sun *et al.* (2020) who suggest that two fine-grained sediment fractions should be adopted to represent the sediment released by an SPV.

3.7.2. Sand Sourcing Conceptualisation

To represent the proposed sand sourcing operation in the ST model it is necessary to conceptualise it, whilst ensuring that the timings and overflow-water release rates assumed in the model are realistic based on the operational parameters provided by BKA.

As noted in Section 1.1, the sand sourcing is proposed to be undertaken by a single SPV. The vessel will have a hopper capacity of 75,000 to 125,000 m^3 and will pump ~5,000 m^3 of sand per hour. The under-keel hopper water overflow will be at ~19 m draft and will commence after the initial 6.5 hours of sand loading and the time to fill the hopper with sand will be in the order of 25 to 30 hours. During sand sourcing the SPV will sail at a speed of 1.5 to 2 knots and will cover a track of 60 to 70 km to fill the hopper. Once the hopper is full, the SPV will depart CG and return with an empty hopper ~14 days later, to repeat the cycle.

To understand how potential increases in SSC due to the sand sourcing varies depending on the route taken by the SPV, two different scenarios have been simulated, based on two possible operational variations as advised by BKA (Figure 105):

- Scenario 1: Repeat sand sourcing concentrated along a fixed 500 m wide track which extends the length of the POA (~14 km); and
- Scenario 2: Targeted sand sourcing occurring at locations throughout the POA where sand is present.

During each cycle the sand sourcing activity was assumed to occur continuously over 30 hours, with 30 minutes of downtime at the end of each line to allow time to reposition the SPV for the next line. Overflow of the hopper was assumed to occur after 6.5 hours of sand sourcing and continue until the end of the 30-hour cycle.

Extensive monitoring of the far-field plumes resulting from Trailer Suction Hopper Dredgers (TSHDs), which the SPV will be based on, have shown that a proportion of the sediment disturbed by the activity can remain in suspension as part of a passive plume which is available for transport (Becker *et al.*, 2015; Mills and Kemps, 2016, Sun *et al.*, 2020). The major sources of sediment released by a TSHD are noted by Kemps and Masini (2017) and those which are relevant to this project are:

- the SPV draghead(s) disturbing fine-grained sediment on the seabed during the activity;
- resuspension of fine-grained sediment on the seabed from the propeller wash of the SPV (this source is typically combined with the draghead); and
- fine-grained sediment released as part of the water overflow from the hopper during sand sourcing.

Table 12 provides a summary of the typical ranges of source terms which are defined by Sun *et al.* (2020) based on data specified by Becker *et al.* (2015). The spill rate is defined as the percentage of the fine-grained sediment present in the sourced sediment which is resuspended into a plume. Table 12 shows that the spill rates vary from 0 to 3% for the draghead and propeller wash and from 0 to 20% for the hopper water overflow. For this assessment a precautionary, conservative approach has been adopted, with the highest spill rate defined in the literature adopted for the modelling. However, it should be noted that the BKA operation will target sand above a certain grain size that is present in the POA and which the export market requires, and will not target silts and clays that are often present in other areas such as commercial ports that are dredged by TSHDs.

As previously noted by PCS (2024b), the sediment to be dredged within the POA is predominantly made up of sand, although some fine-grained silt and clay are present along with some very fine-grained sand which can be transported in suspension. PSD data from a total of 17 sediment samples collected by BKA within the POA during the 2024 wet season (February to March 2024) and the 2023 sand exploration survey (February to March 2023) were used to calculate the average percentage of clay, silt and very fine sand present. Based on the PSD data it was calculated that 0.6% of the sediment was clay particles, 1.4% of the sediment was silt particles and 2.5% of the sediment was very fine sand (up to 125 µm). Based on this, the SPV details and the percent spill rates the source term for the draghead and propeller wash was calculated to be 2.6 kg/s and the source term for the overflow was calculated to be 17.3 kg/s. These source terms were adopted in the modelling, with the draghead and the propeller wash term included in the near-bed layer for the entire period that sand sourcing was undertaken while the overflow term was included in the mid water column layer for the period that sand sourcing was undertaken after the initial 6.5 hours. The dredge cycle, along with the source terms included in the model, is shown in Table 13. This cycle will be repeated when the SPV returns to CG 14 days later, after transporting the sand to Asia.

Table 12. Summary of spill rates for the relevant SPV parameters for this assessment.

Source Type	Spill Rate (% of fines in sediment)	
	Literature Range	Adopted Values for this Study
Draghead and Propeller Wash	0–3%	3%
Hopper Water Overflow	0–20%	20%

Table 13. Dredge cycle adopted for the modelling.

Details	Time (hours)	Source Term (kg/s)
Sand Sourcing, No Overflow	6.5	2.6
Sand Sourcing, With Overflow	23.5	19.9 (2.6 + 17.3)
Total	**30**	**-**

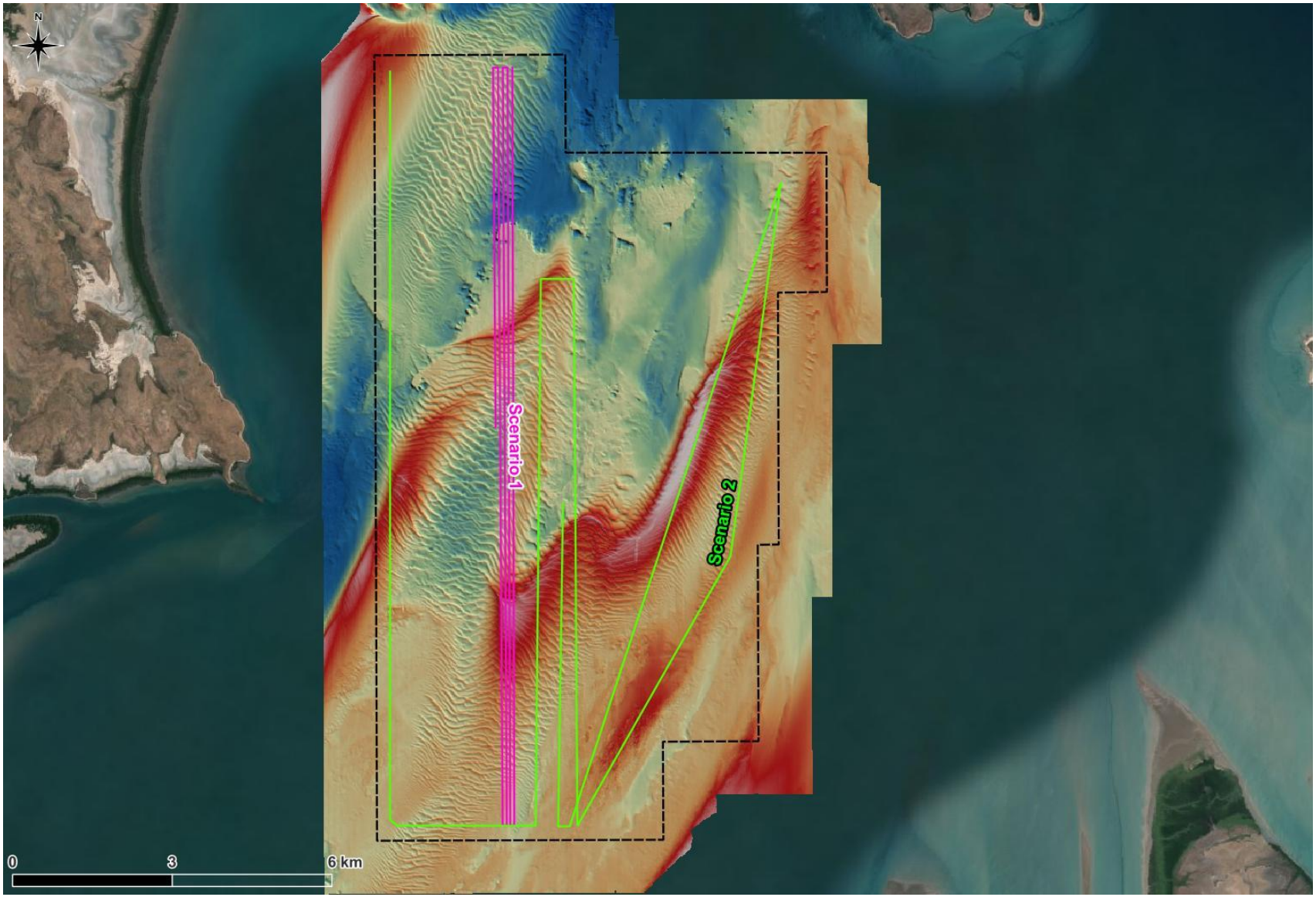


Figure 105. Two sand sourcing track scenarios adopted in the sediment plume modelling.

3.7.3. Scheme Simulations

The ST model was used to represent both the natural SSC in the area (the setup for this is detailed in Section 3.6.1) and the SSC resulting from the sand sourcing operation. Simulating the natural SSC as well as the SSC from the sand sourcing allows any plumes from the sand sourcing to be put into context with the natural environment to help understand the modelled increases in SSC.

The ST model was set up to simulate the SSC resulting from the sand sourcing operation during the same two-month (60/61 days) duration wet, transitional and dry season periods as simulated by the HD model. The sediment plume model was not set up to simulate the plume during a tropical cyclone as sand-sourcing would not be undertaken during these conditions. This means that for each 60/61 days duration simulation there will be a total of four periods of sand sourcing activity.

As the time between when the SPV will be operating in CG (14 days) is approximately the same as the duration of a spring-neap cycle (14.75 days), the modelling has been set up to simulate the plumes when the sand sourcing commences during neap tides and when it commences during spring tides. This therefore covers the range of conditions in tidal currents for the activity and allows the relative influence of the tidal currents on the plumes to be better understood.

3.8. Beach Processes Model

The MIKE Littoral Processes LITDRIFT and LITPROF modules have been adopted to model the longshore and cross-shore transport of sediment at the three high-priority turtle-nesting beaches on the seaward coast outside of CG (Figure 2) The LITDRIFT and LITPROF modules calculate the propagation, shoaling and breaking of waves, the momentum balance for cross-shore and longshore currents and the resultant longshore and cross-shore sediment transport.

3.8.1. Model Configuration

Beach processes modelling at multiple beach profiles at the three high-priority turtle-nesting beaches was presented by PCS (2024a) (Figure 106). Since the previous modelling was undertaken the following additional data have become available:

- Measured wave data have been collected by BKA at the 11 AWAC sites, which has allowed the SW model to be calibrated and validated, therefore improving the confidence in the wave conditions which drive the beach processes model.
- Detailed intertidal and supratidal topographic data were collected using drone-based high-resolution LiDAR for the three beaches by BKA in February 2024 (BKA 2024b - Annex 10: Aerial Drone LiDAR Report).
- The data were shown by PCS (2024b) to generally be similar to the DEA intertidal elevation data, which were previously used to represent the intertidal area up to 1 to 2.5 m AHD (the highest elevation that the dataset extends). However, differences in elevation above 0 m AHD between the GA 30 m depth model and the 2024 LiDAR data were typically at least 2 m and could be more than 5 m. Therefore, the updated modelling presented in this report which adopts the 2024 LiDAR topographic data is more accurate than the modelling previously presented in PCS (2024a).
- As part of the February 2024 aerial drone survey photogrammetry data were also collected for the three beaches. These data allow areas where rock is present to be defined and included in the cross-shore beach profiles.
- Due to high crocodile risk, it was not possible to collect sand samples across the profiles at each beach and so the sediment properties from the previous modelling were adopted (median grain size of 200 µm).

The cross-shore profiles adopted in the LITDRIFT and LITPROF modules were updated so that they included the drone-based LiDAR data and so that areas with surface rock were represented in the model. The wave conditions at the seaward ends of the cross-shore profiles were extracted from the calibrated and validated SW model. The modules were then used to simulate the potential longshore and cross-shore transport of sediment at each of the cross-shore profiles shown in Figure 106 over a 5 year period. The 5 year period selected is not related to the sand sourcing time periods being considered as part of the proposal, but rather a suitable period of time to represent seasonal and annual variability in wave conditions to understand how the longshore and cross-shore sediment transport rates vary.

3.8.2. Scheme Simulations

The beach processes modelling has been undertaken over a 5 year period (this duration was selected to represent a suitable range in wave conditions to understand seasonal and annual variability) for the present-day conditions and for conditions in 100 years from today (sea level rise of 0.9 m, no change to the wave climate).

As expected, results from the SW modelling show no change in wave conditions offshore of CG (see Section 4.2.2) and so the model results will remain the same regardless of whether the sand sourcing is included or not. In addition, the pre-European Settlement scenario does not influence wave conditions and so this scenario will also not influence the beach processes modelling results and so has not been considered.

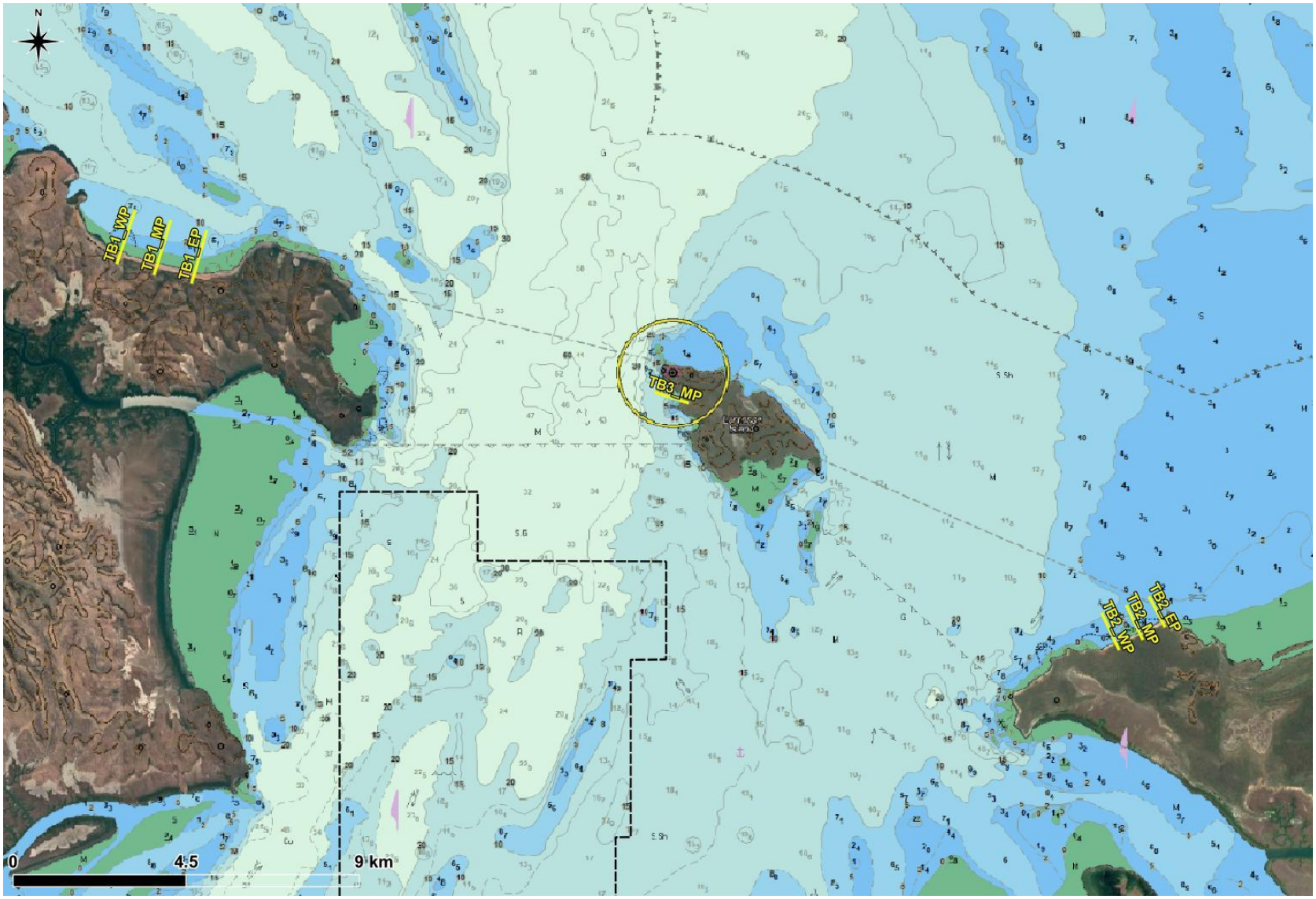


Figure 106. Locations of the beach cross-shore profiles adopted for the longshore and cross-shore sediment transport and beach profile modelling.

4. RESULTS: HYDRODYNAMICS AND WAVES

This section provides details of the results from the HD and SW modelling. Results from the modelling showing the existing conditions, presented along with modelled changes to water levels, currents and waves due to the various scenarios considered as part of this assessment.

4.1. Existing Conditions

Results from the existing case scenario are presented in the following sections to provide an overview of the existing hydrodynamic and wave conditions in and offshore from CG.

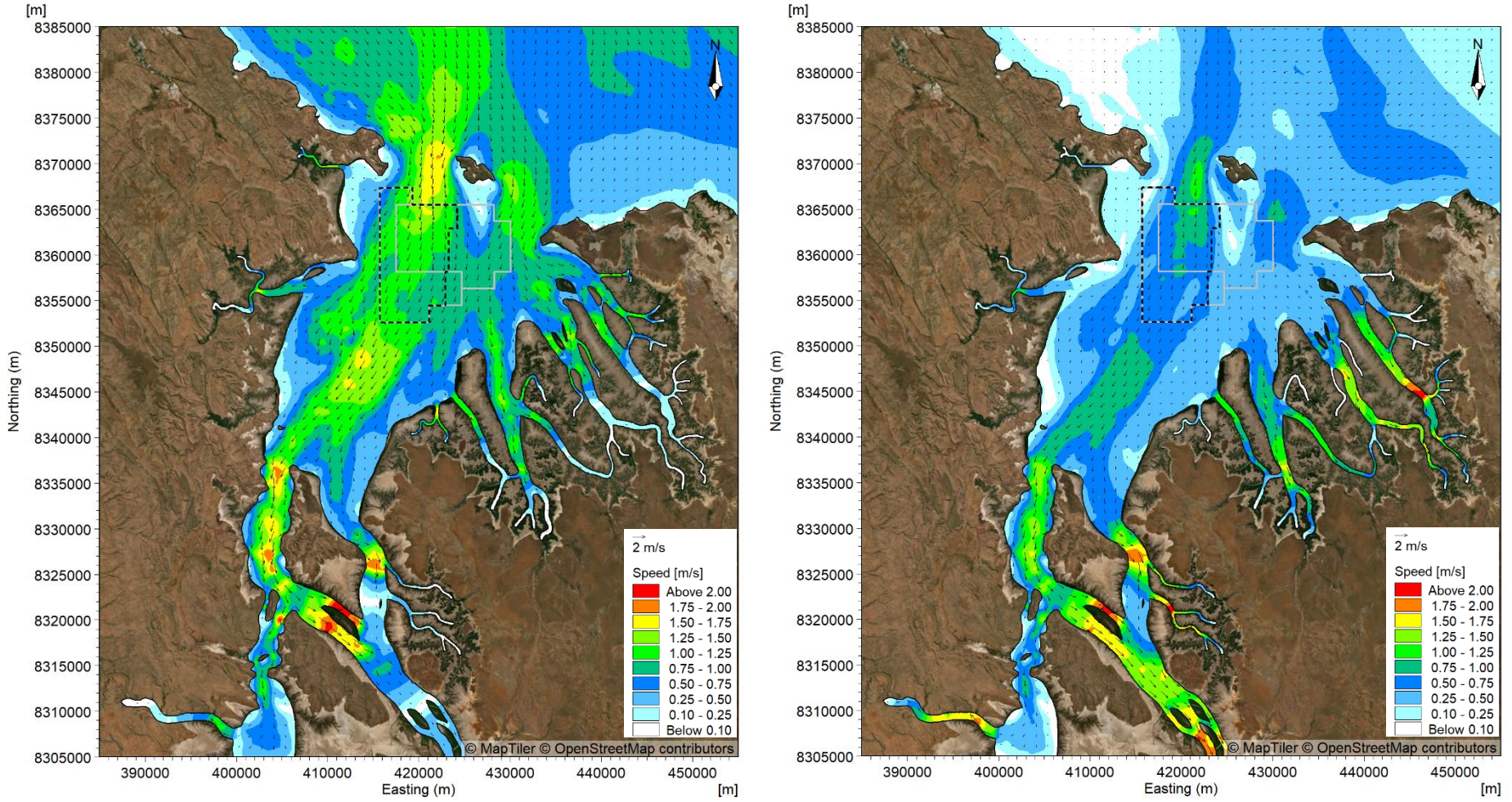
4.1.1. Hydrodynamics

Spatial maps from the HD model of the depth-averaged current speed and flow vectors at peak flood, high water, peak ebb and low water during a spring tide in the wet season are shown in Figure 107 and Figure 108. Modelled currents during the transitional and dry season conditions were very similar due to the strong dominance in the astronomical tide on the tidal currents, and so are not presented.

Spatial maps showing the modelled tidal residual current over a spring and neap tide are shown in Figure 109. The modelled tidal residual current over a 14-day spring-neap cycle during the wet season over a period with elevated river discharge is shown in Figure 110. In addition, a timeseries plot of the flux of water through the West and East Entrances to CG is shown in Figure 111 and timeseries of the current speed and direction at a site offshore of CG (AWAC-09), within the POA (AWAC-01) and upstream (south) of the POA (AWAC-11) are shown in Figure 112. The plots show the following:

- Offshore from CG the tide floods and ebbs from/to the northwest, with the highest flows occurring through the deeper channel to the east of King Shoals. Relatively high current speeds also occur around King Shoals and to the west of CG, while the current speeds around Medusa Bank to the north and northeast of CG were consistently lower during both the flood and ebb stages of the tide.
- Higher current speeds occurred in the West Entrance to CG compared to the East Entrance, with peak depth-averaged speeds in the West Entrance of around 1.7 m/s during spring tides compared to 1.2 m/s in the East Entrance. The timing of the peak flood and peak ebb currents was the same in the two entrances. The flux of water flowing through the West Entrance during both the flood and ebb stages of the tide was in the order of three times larger than the flux of water through the East Entrance.
- Current speeds within CG were similar on the flood and ebb stages of the tide, while flood current speeds were higher than ebb speeds in West and East Arms although this dominance varied spatially through CG and temporally between spring and neap tides.
- The modelled tidal residual current speeds during both spring and neap tides were relatively low, with speeds less than 0.1 m/s over the majority of CG during neap tides and less than 0.2 m/s over the majority of CG during spring tides. During spring tides the tidal residual currents were highest around Lacrosse Island and in the West Entrance to CG. Tidal residual currents at the western side of the West Entrance were in a northerly direction, while at the eastern side of the entrance they were in a southerly direction. This indicates that the current speeds in the West Entrance were stronger on the west side during the ebb stage of the tide and stronger on the east side during the flood stage of the tide.
- The tidal residual currents over a 14-day spring-neap tidal cycle during the wet season were lower than the tidal residual currents during a spring tide, with currents less than 0.1 m/s throughout the majority of CG. This indicates that the stronger tidal residual currents during spring tides were partially balanced out over a 14-day spring-neap cycle. Over this duration the tidal residual currents still showed a residual current speed of up to 0.3 m/s flowing out of CG at the western side of the West Entrance and a tidal residual current speed of up to 0.3 m/s flowing into CG at the eastern side of the West Entrance.
- Overall, the tidal residual currents showed that despite some variability in current speeds on the flood and ebb stages of the tide, the flows around CG were relatively balanced over a 14-day spring-neap tidal cycle.
- Modelled currents at the sites located offshore from CG, within the POA and upstream of the POA were similar, with peak depth-averaged speeds of 1 to 1.4 m/s during spring tides and 0.4

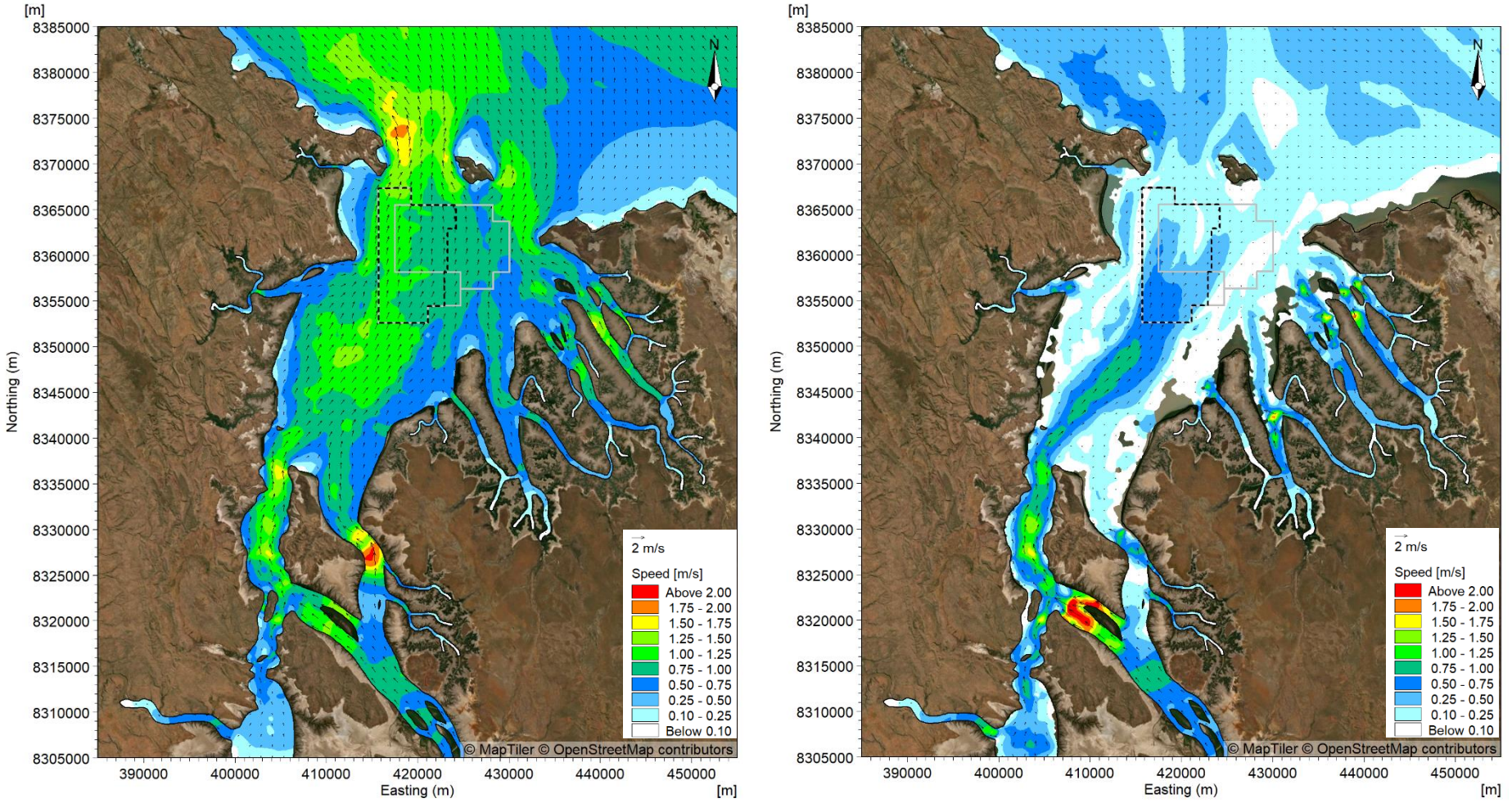
to 0.6 m/s during neap tides. Current directions were similar at the two sites within CG (AWAC-01 and AWAC-11), with flood currents in a southerly direction and ebb currents in a northerly direction, while at the offshore site in King Shoals the flood currents were to the southeast and the ebb currents were to the northwest.



Peak Flood

High Water

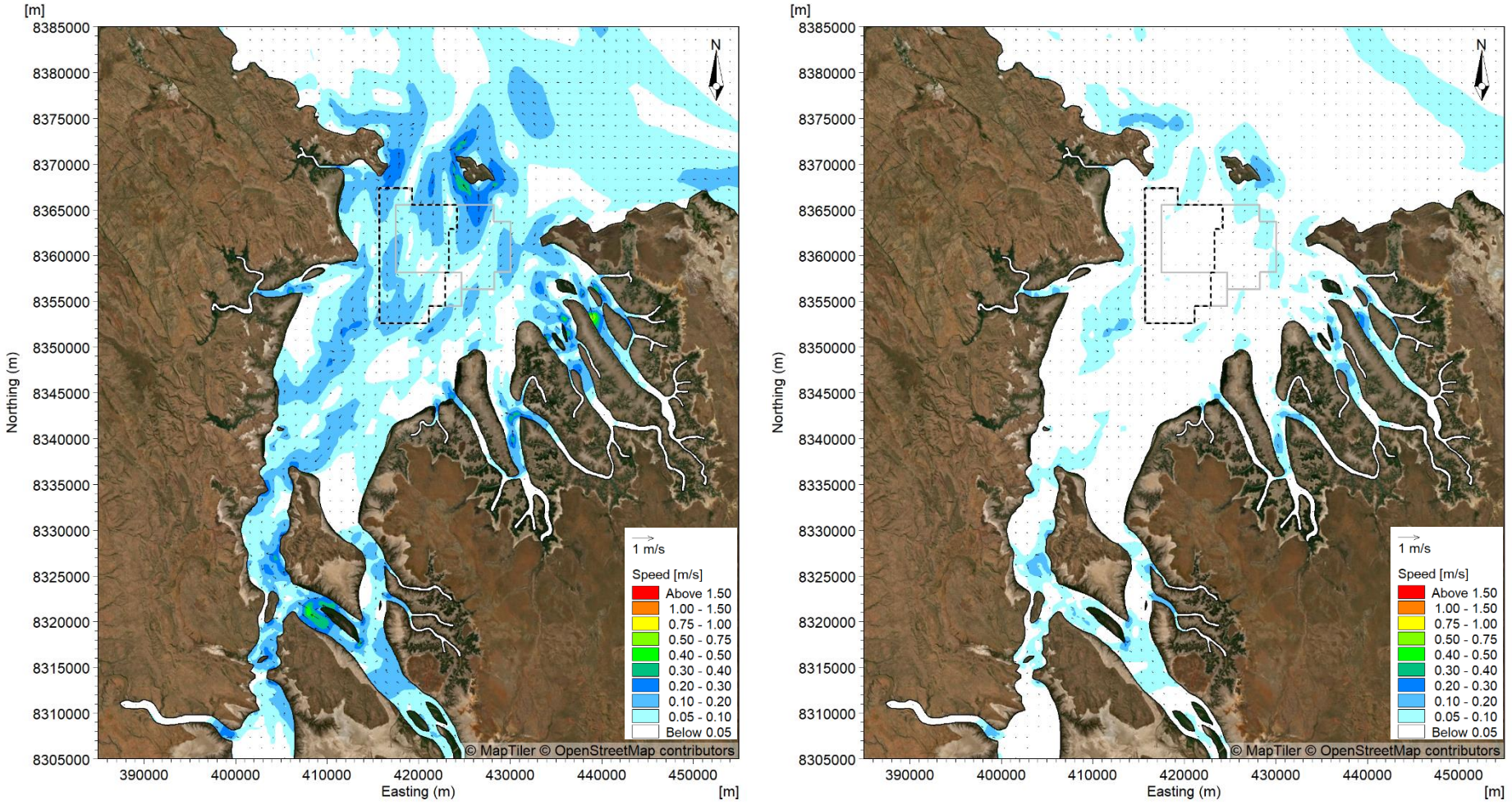
Figure 107. Modelled depth-averaged current speed in CG at peak flood (left) and high water (right) during a spring tide in the wet season.



Peak Ebb

Low Water

Figure 108. Modelled depth-averaged current speed in CG at peak ebb (left) and low water (right) during a spring tide in the wet season.



Spring Tide

Neap Tide

Figure 109. Modelled depth-averaged residual current speed in CG during a spring tide (left) and a neap tide (right) in the wet season.

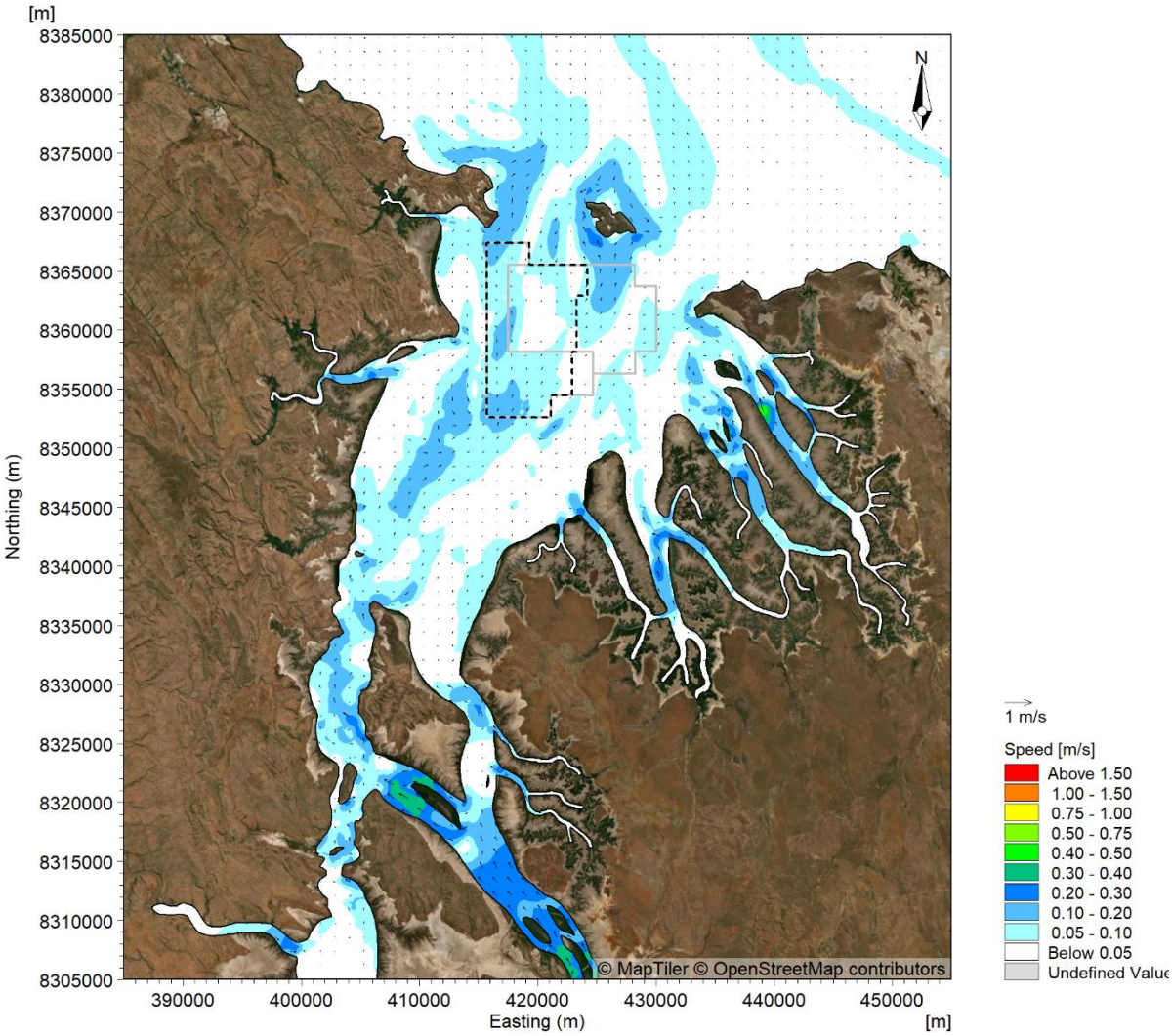


Figure 110. Modelled depth-averaged residual current speed in CG over a 14-day spring-neap tidal cycle with a high river discharge event in the wet season.

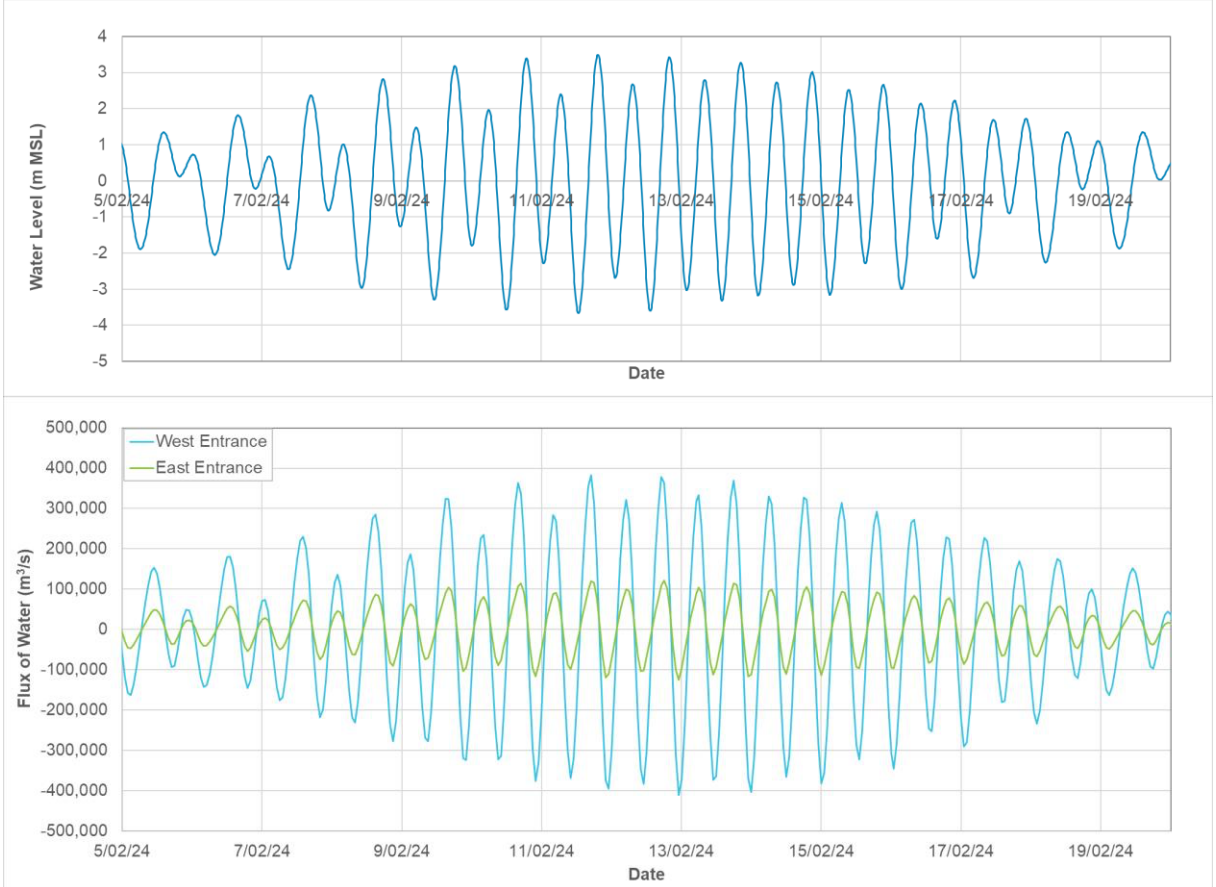
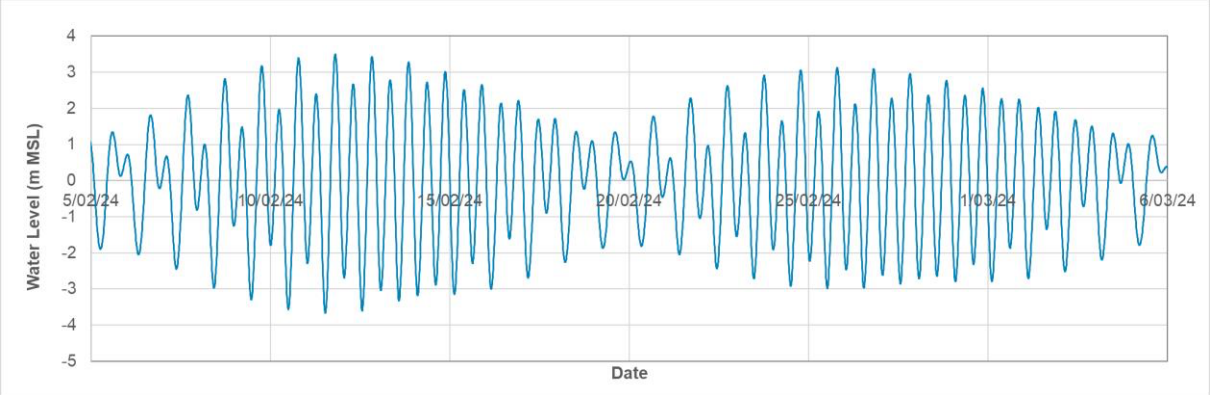
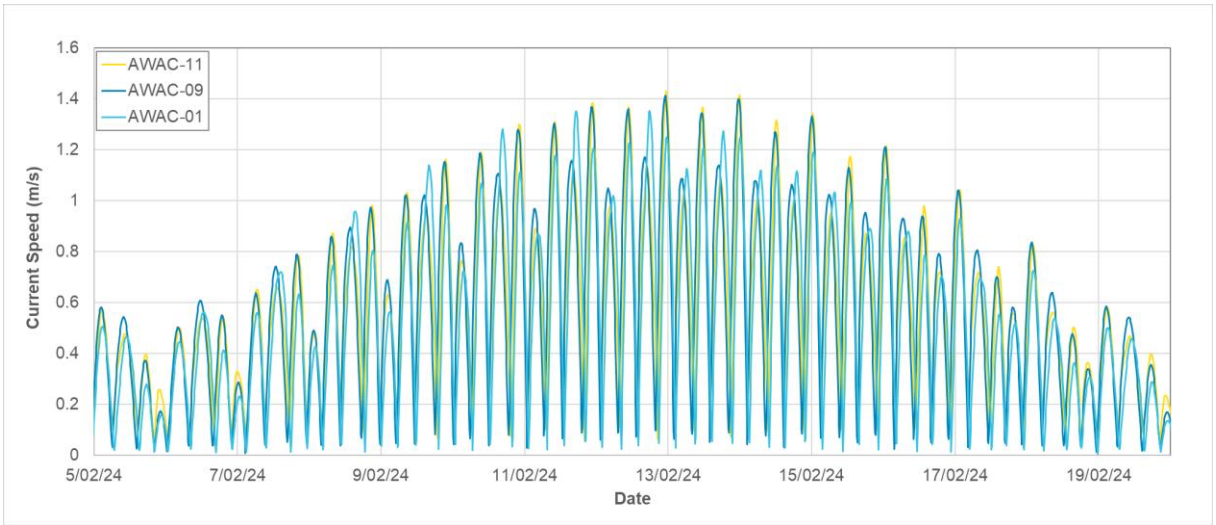


Figure 111. Modelled water level at AWAC-01 (top) and modelled flux of water through the West and East entrances to CG (bottom) over 15 days. *Note: positive flux is flowing into CG, negative flux is flowing out of CG.*





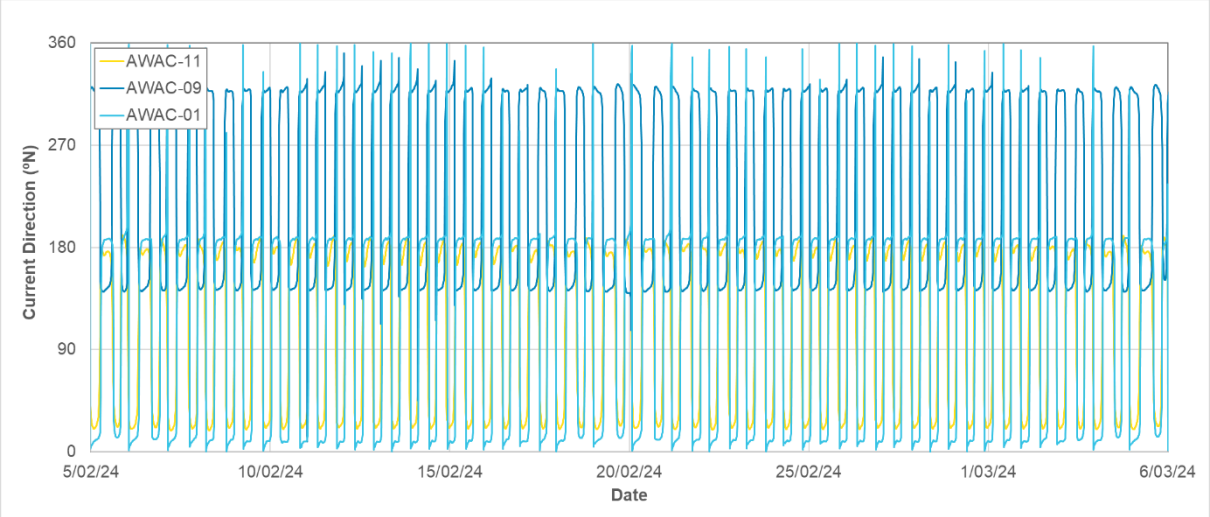


Figure 112. Modelled water level at AWAC-01 (top) and current speed (middle) and direction (bottom) at AWACs 01, 09 and 11 over 15 days.

4.1.2. Waves

Timeseries plots of the modelled wave conditions for the existing case during the three seasonal periods (wet, transitional and dry) at sites located offshore (AWAC-09), within the POA (AWAC-01) and upstream (south) of the POA (AWAC-11) are shown in Figure 113 to Figure 118. The plots show that the largest waves occurred during the wet season, with the H_s at the offshore site regularly exceeding 1 m, while during the dry and transitional seasons, the H_s at the offshore site was predominantly less than 1 m due to fetch limitation during the prevailing southeasterly winds.

During all three seasons a diurnal variability in H_s was evident due to the land/sea breeze, with a higher H_s during the day and lower H_s during the night. The diurnal variability was strongest during the transitional season and weakest during the wet season.

Throughout all three seasons the T_p typically varied between 2 and 6 s, with the T_p on average being highest during the wet season and lowest during the dry season.

The modelled wave direction varied between the three seasons but was similar between the three sites, with directions during the wet season predominantly from the northwest to north, directions during the dry season predominantly from the east to southeast and directions during the transitional period predominantly from the north to northeast.

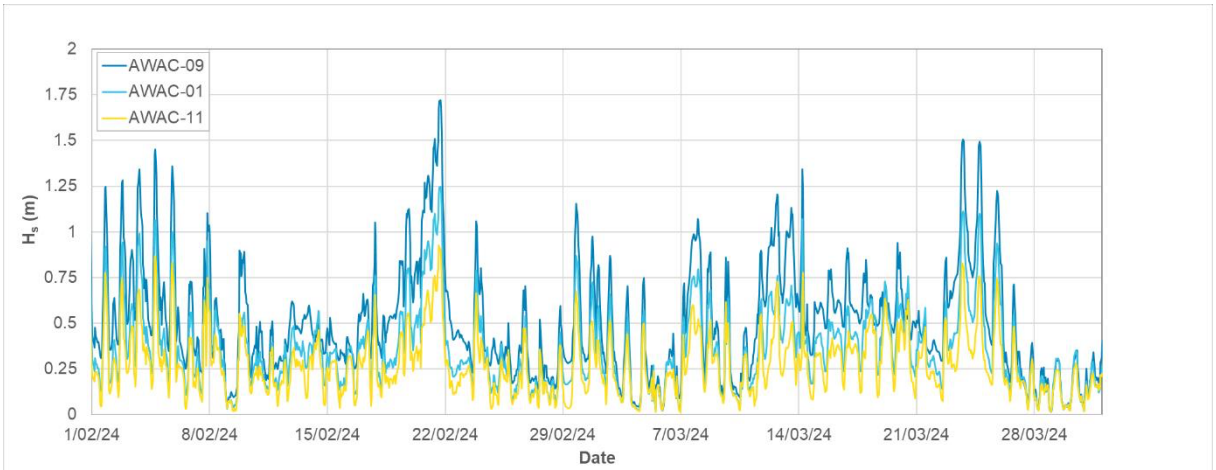
As expected, the H_s varied between the sites with the largest waves at the offshore site and the smallest waves at the upstream site. The difference in H_s between the sites varied between the seasons, with the largest difference during the wet season when the waves were predominantly from the northwest and the smallest difference during the transitional season when the waves were predominantly from the north to northeast.

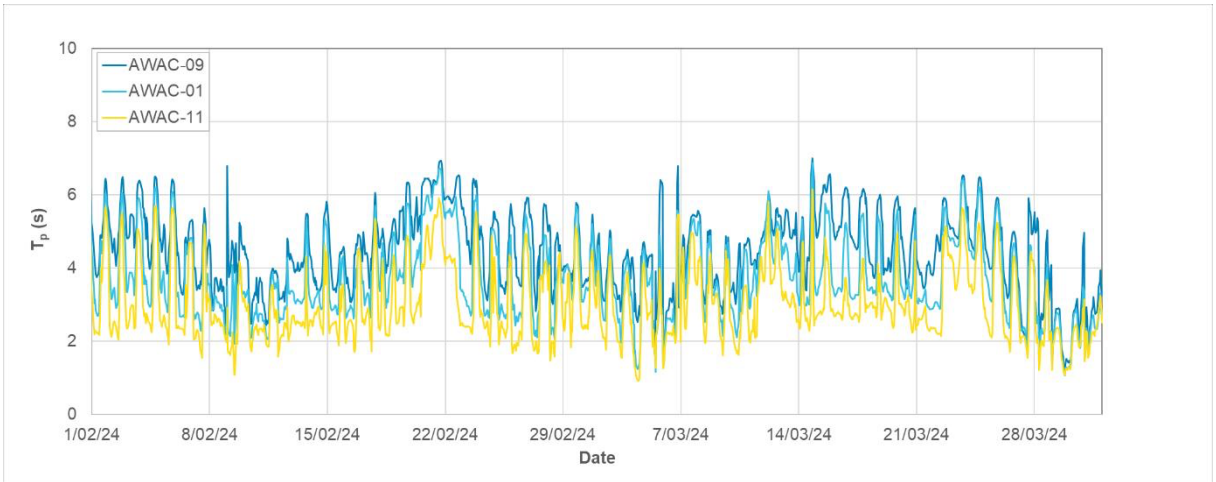
Spatial maps of the peak H_s over the two-month (61 days) simulation period for each season are shown in Figure 116 to Figure 118. The plots show how the H_s within CG was lower than the offshore H_s for the different wave directions experienced in the different seasons, with Lacrosse Island consistently providing sheltering in its lee. The plots show the following:

- The dominant wave direction varied between the three seasons, with waves from a northerly direction during both the wet and transitional seasons and waves from the east during the dry season. The easterly wave direction during the dry season meant that offshore waves did not propagate into CG, with the waves within CG being generated by local winds.
- During the peak wave event during the wet season the H_s offshore from CG exceeded 1.75 m, while during both the dry and transitional seasons the offshore H_s was predominantly below 1.25 m. Within the POA the H_s during the peak wave event was between 1.0 and 1.25 m during the wet season, while during the transitional season it was between 0.75 and 1.0 m and during the dry season it was between 0.5 and 1.0 m. Throughout the remainder of CG, the H_s during these peak wave events were predominantly between 0.25 and 0.5 m, with an H_s of less than 0.25 m in the tidal creeks.
- Due to northerly wave directions, the H_s was modelled to be larger along the eastern shoreline in CG during the wet and transitional season, and due to the east to southeast wave direction during the dry season, the H_s was modelled to be larger along the western shoreline in CG.
- Considering that the plots show the peak in H_s over two-month (61 days) periods, the results show that the overall wave conditions within CG were relatively calm.

To understand the wave conditions that can occur due to tropical cyclones, the SW model was set up to simulate the wave conditions resulting from TC Marcus, which passed east to west across JBG with the centre of the cyclone passing ~80 km to the north of CG. TC Marcus was selected as it resulted in the largest waves directly offshore from CG over the last 10 years. Timeseries plots of the modelled wave conditions at sites located offshore (AWAC-09), within the POA (AWAC-01) and upstream (south) of the POA (AWAC-11) are shown in Figure 119 and a spatial map of the H_s at the peak of the event is shown in Figure 120.

The plots show that the event resulted in a peak H_s offshore of CG of just under 3.5 m, while the peak H_s at the site in the proposed operational area was just over 2 m and the peak H_s upstream of the proposed operational area had reduced to 1.8 m. The peak T_p during the event was 8.6 s and the wave direction varied from east to north-northeast, with the direction from the northeast at the peak of the event. The spatial map shows how waves with an H_s of 1 to 1.75 m can occur within CG adjacent to the western shoreline while waves with an H_s of 0.75 to 1.25 m can occur adjacent to the eastern shoreline.





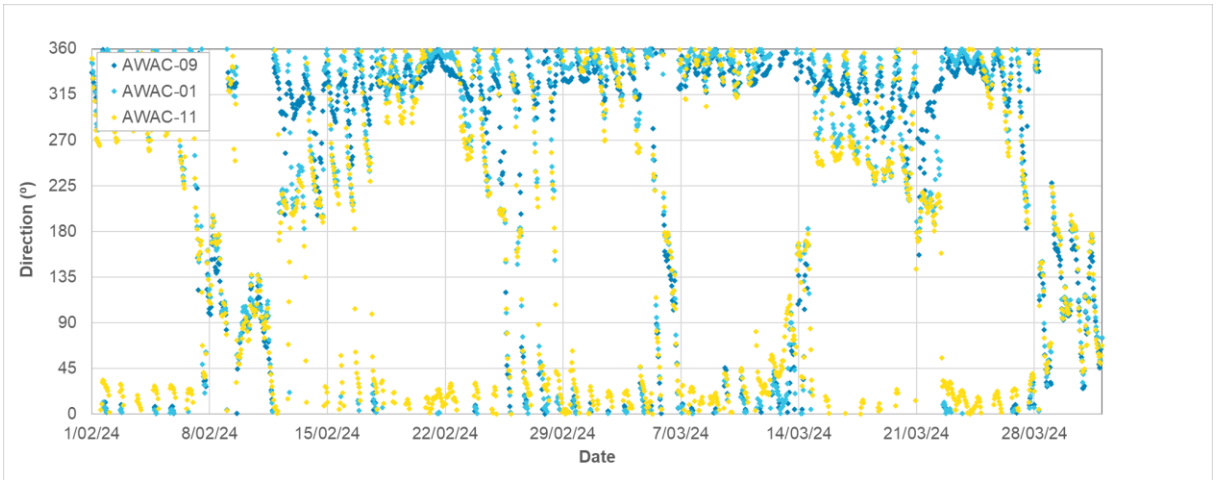
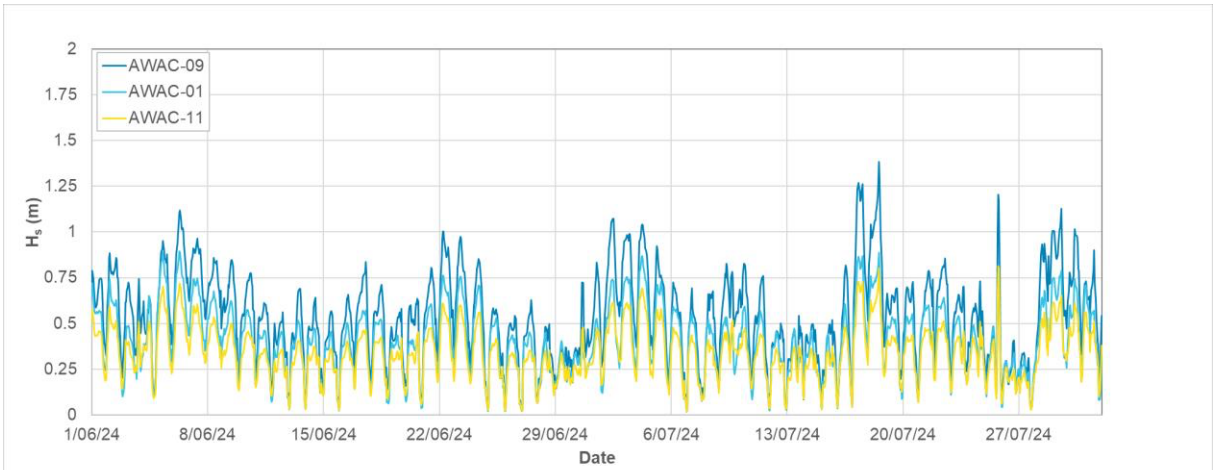
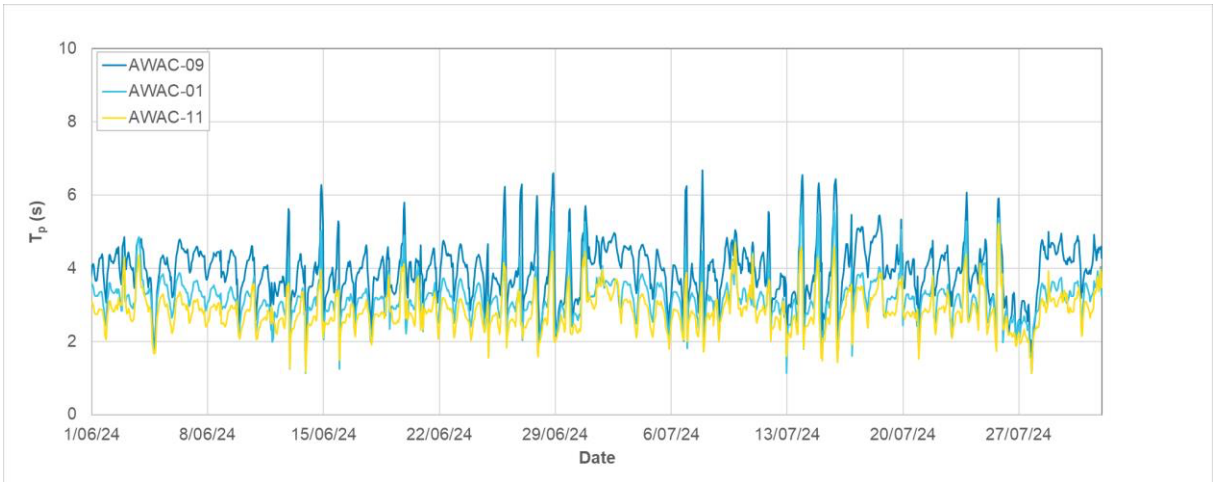


Figure 113. Modelled wave conditions at AWACs 01, 09 and 11 over the two-month (61 days) wet season period.





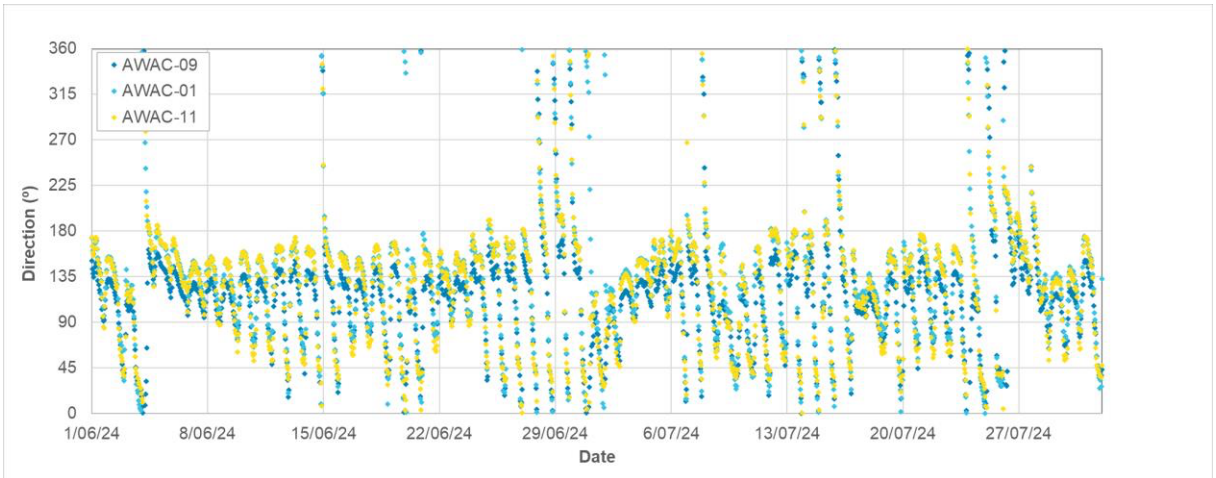


Figure 114. Modelled wave conditions at AWACs 01, 09 and 11 over the two-month (61 days) dry season period.



Figure 115. Modelled wave conditions at AWACs 01, 09 and 11 over the two-month (61 days) transitional season period.

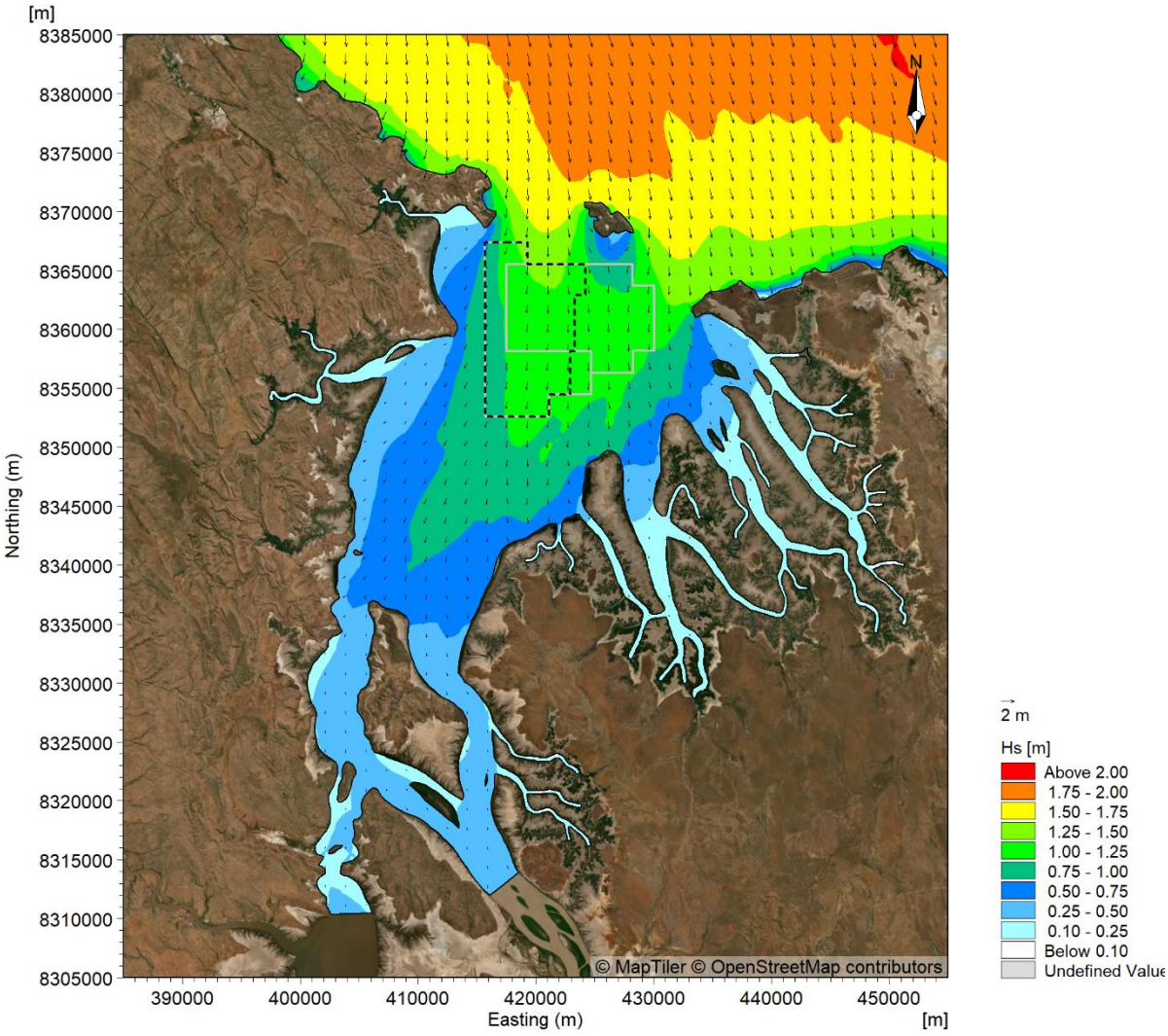


Figure 116. Peak H_s over the two-month (61 days) wet season simulation (21/02/2024).

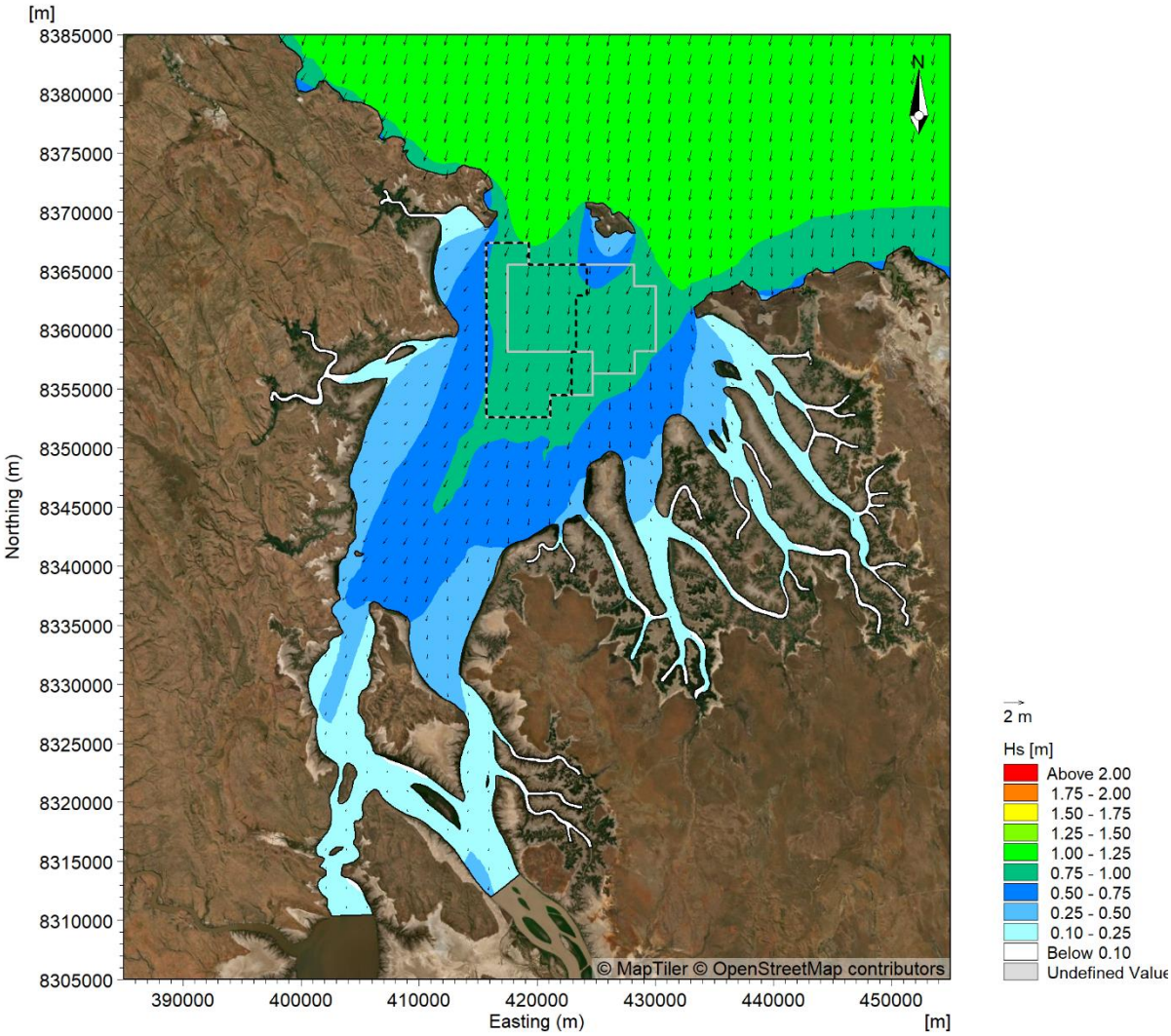


Figure 117. Peak H_s over the two-month (61 days) transitional season simulation (01/11/2023).

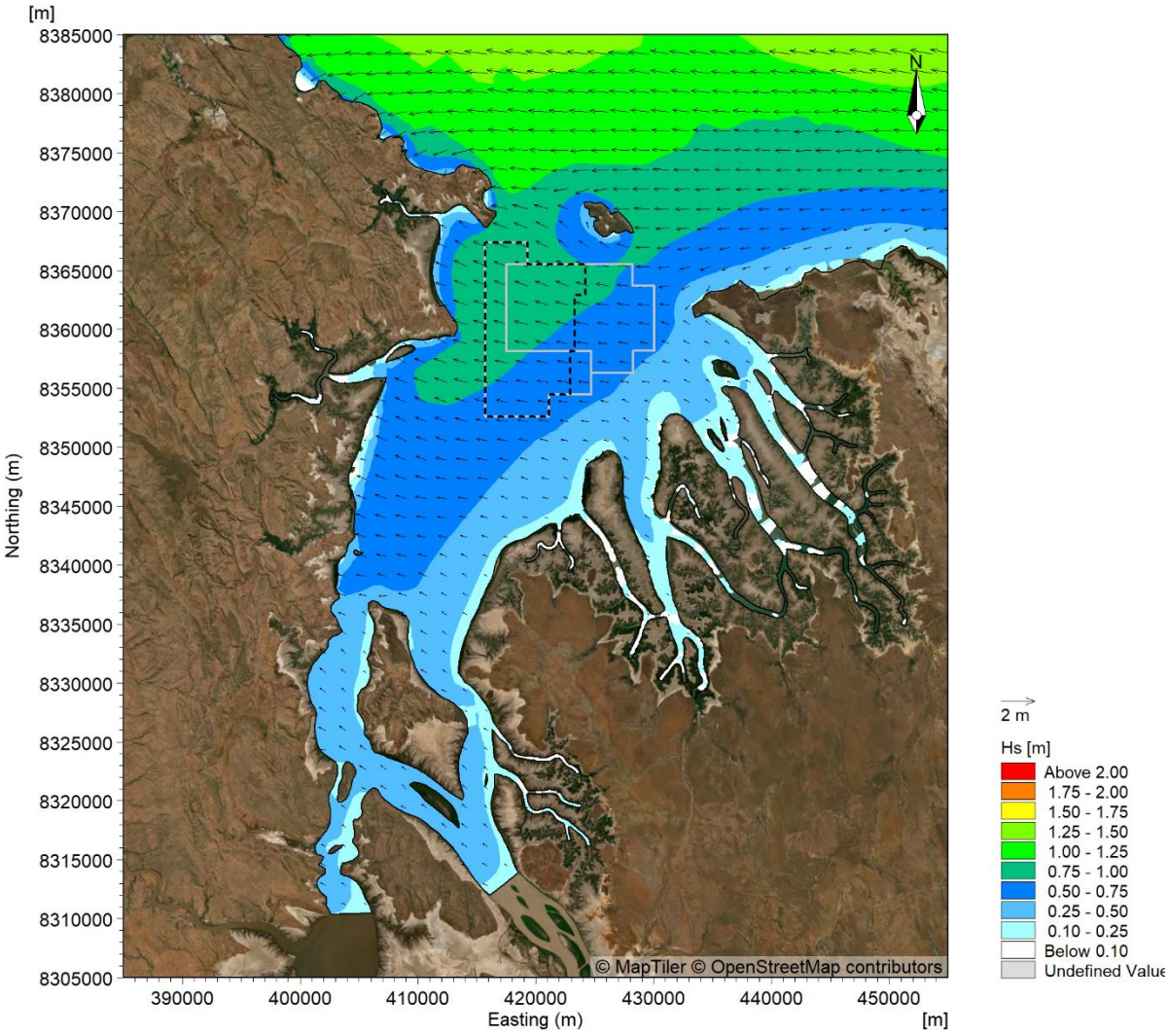


Figure 118. Peak H_s over the two-month (61 days) dry season simulation (18/07/2024).

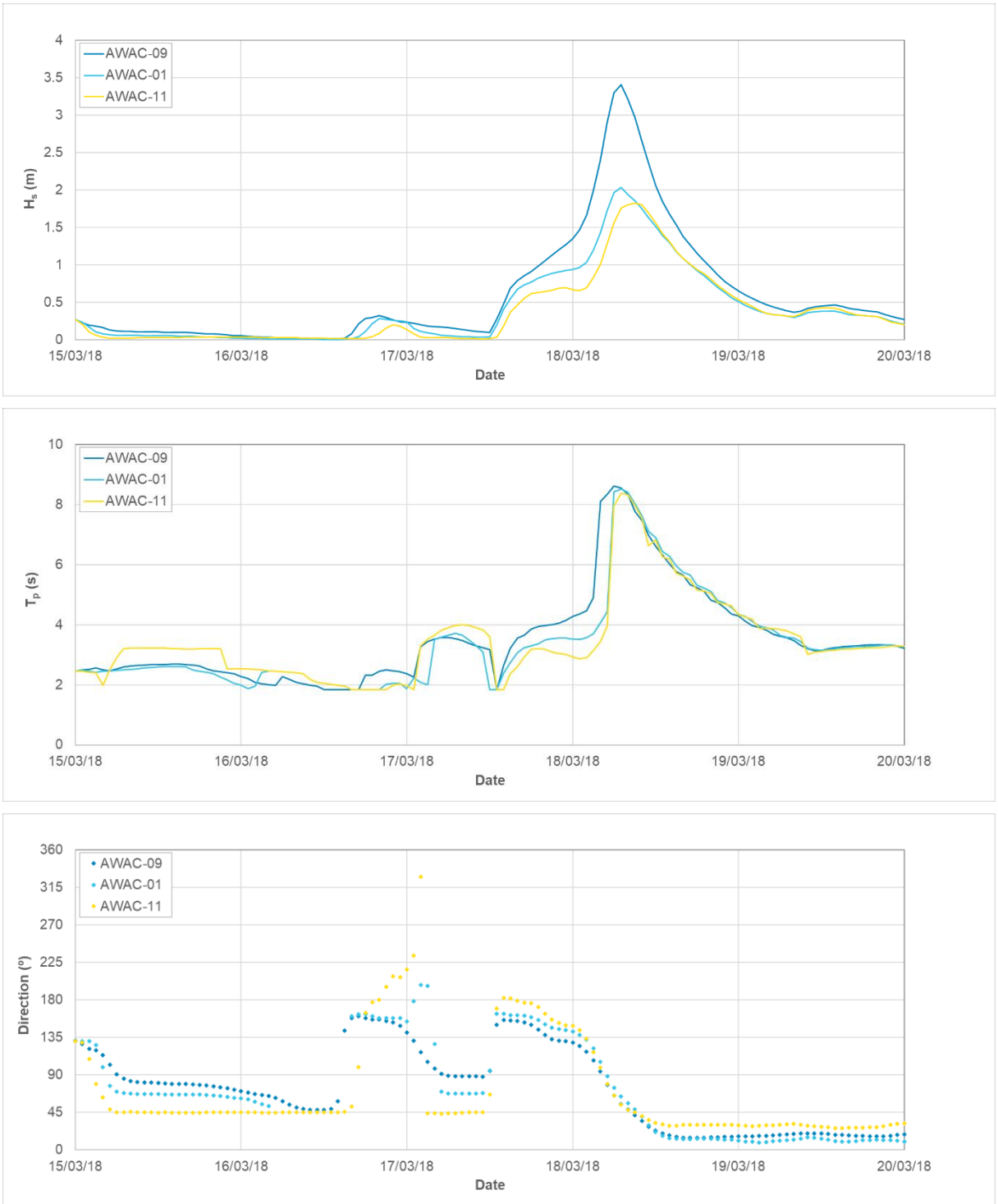


Figure 119. Modelled wave conditions at AWACs 01, 09 and 11 during TC Marcus.

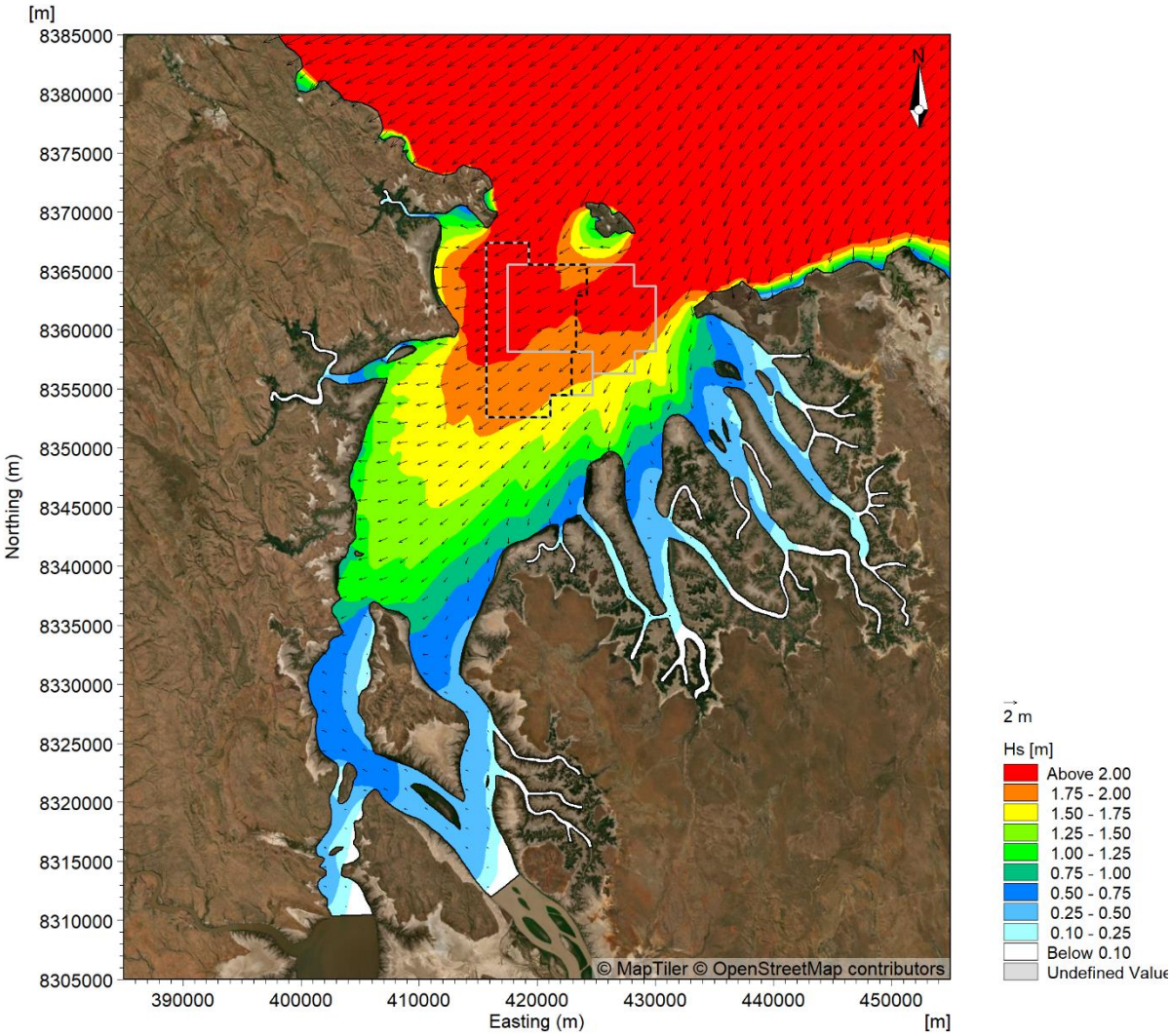


Figure 120. Peak H_s during TC Marcus (18/03/2018).

4.2. Scenario Changes

To assess the potential changes of the pre-European, 5 years of sand sourcing and 15 years of sand sourcing scenarios, results from the HD and SW simulations for the four metocean conditions (dry season, transitional season, wet season and tropical cyclone) have been compared with the existing case. In addition, results from the scenario 100 years from today with sand sourcing have been compared with the scenario of no sand sourcing 100 years from today to determine the potential future changes.

4.2.1. Hydrodynamics

This section presents a summary of the modelled changes for specific scenarios and metocean conditions, to provide an overview of the changes. Plots of the changes for all the scenarios and during all metocean conditions are provided in Appendix B.

4.2.1.1. Water Levels

Spatial maps showing the modelled change in water level at peak flood, high water, peak ebb and low water during a spring tide in the wet season due to the sand sourcing after 5 years, after 15 years and 100 years from today are shown in Figure 121 to Figure 126. During the dry season, transitional season and the tropical cyclone the modelled changes in water level due to the sand sourcing were similar to the wet season and so plots for these cases are not shown here, but are included in Appendix B.

Due to the similarity in the results for the metocean conditions between the three seasons it is not possible to define best-case and worst-case changes for the water levels. Plots of the modelled difference in water level between the existing case and the pre-European settlement scenario for a spring tide in the wet season during a period with high river discharge are shown in Figure 127 to Figure 128, and plots for a spring tide in the dry season are shown in Figure 129 and Figure 130. The plots show the following:

- The sand sourcing was assessed to result in a very small increase in water level at peak flood and high water and a very small decrease in water level at peak ebb and low water. The modelled changes were up to ± 0.005 m (5 mm) after 5 years of sand sourcing and up to ± 0.05 m (50 mm) after 15 years of sand sourcing. The modelled changes were predominantly constrained within CG, but do extend just offshore of the entrance, with the magnitude of the changes decreasing offshore. The combination of very small increases and decreases at different stages of the tide suggests that the changes are due to a change in the phase of the tidal propagation into CG as opposed to a change in the magnitude of the tide. This will be further assessed using timeseries results below.

- The modelled changes in water level in 100 years from today after 15 years of sand sourcing were smaller than the changes after 15 years of sand sourcing. This shows that the increase in water depth due to sea level rise over 100 years combined with the ongoing sedimentation in the POA will reduce the already small changes to water levels over time.

- The modelling results indicate that pre-European settlement, during a high river discharge event in the wet season (peak discharge of 30,000 m^3/s for pre-European settlement case and 3,500 m^3/s for existing case), water levels in CG were higher relative to the existing case. This is due to the Ord River dams being built post-European settlement, which limits the river discharge for the existing case, meaning that much higher discharges occurred pre-European settlement. The results indicate that water levels during a high river discharge event pre-European settlement were more than 0.1 m (10 cm) higher than the existing case in East and West Arms throughout all stages of the tide. Within CG itself and in the POA, the model indicates that the water level would have been higher by 0.01 to 0.1 m (1 to 10 cm) during all stages of the tide, except for peak ebb when the water level would have been reduced by 0.01 to 0.05 m (1 to 5 cm). This is due to the higher river discharge from the undammed Ord River increasing water levels throughout CG during both low and high water.

- The modelling results indicate that pre-European settlement, during the dry season the water levels were generally lower in East Arm by 0.01 m (1 cm) to more than 0.1 m (10 cm) relative to the existing case. This is due to the Ord River dams regulating the Ord River flows during the dry season in the existing case, providing a consistent river discharge over the dry season, while pre-European settlement the Ord River discharge during the dry season would have been much lower. As well as the reduction in water level in East Arm, the model also indicated that pre-European settlement water levels were both higher (at low water) and lower (at high water) by ± 0.005 m (5 mm) in the main area of CG relative to the existing case.

To better understand the modelled changes in water level relative to the existing case due to the sand sourcing after 15 years and the pre-European settlement scenario, timeseries plots of the change in water level during the wet season at sites from the upstream end of CG (AWAC-08) to offshore in CG at King Shoals (AWAC-09) are shown in Figure 131 and Figure 132. It is important to note that the plots show results for both the existing case and the scenarios (15 years or sand sourcing and pre-European settlement) but generally they are almost identical, so it is not possible to differentiate between the two. A statistical summary of the modelled change in water level due to the two scenarios is provided in Table 14 and the change in total tidal range is summarised in Table 15. The results show the following:

- For both scenarios the largest (but still very minor) changes were assessed to be at the furthest upstream sites (AWAC-08 and AWAC-11), with minor changes at these upstream sites of up to ± 0.012 m (1.2 cm) for the 15 years of sand sourcing and larger changes of ± 0.2 m (20 cm) for the pre-European settlement scenario.

- For both scenarios there was generally a very minor increase in water level during the flood stage of the tide and a decrease during the ebb stage of the tide at all the sites, suggesting that the scenarios are changing the tidal propagation.

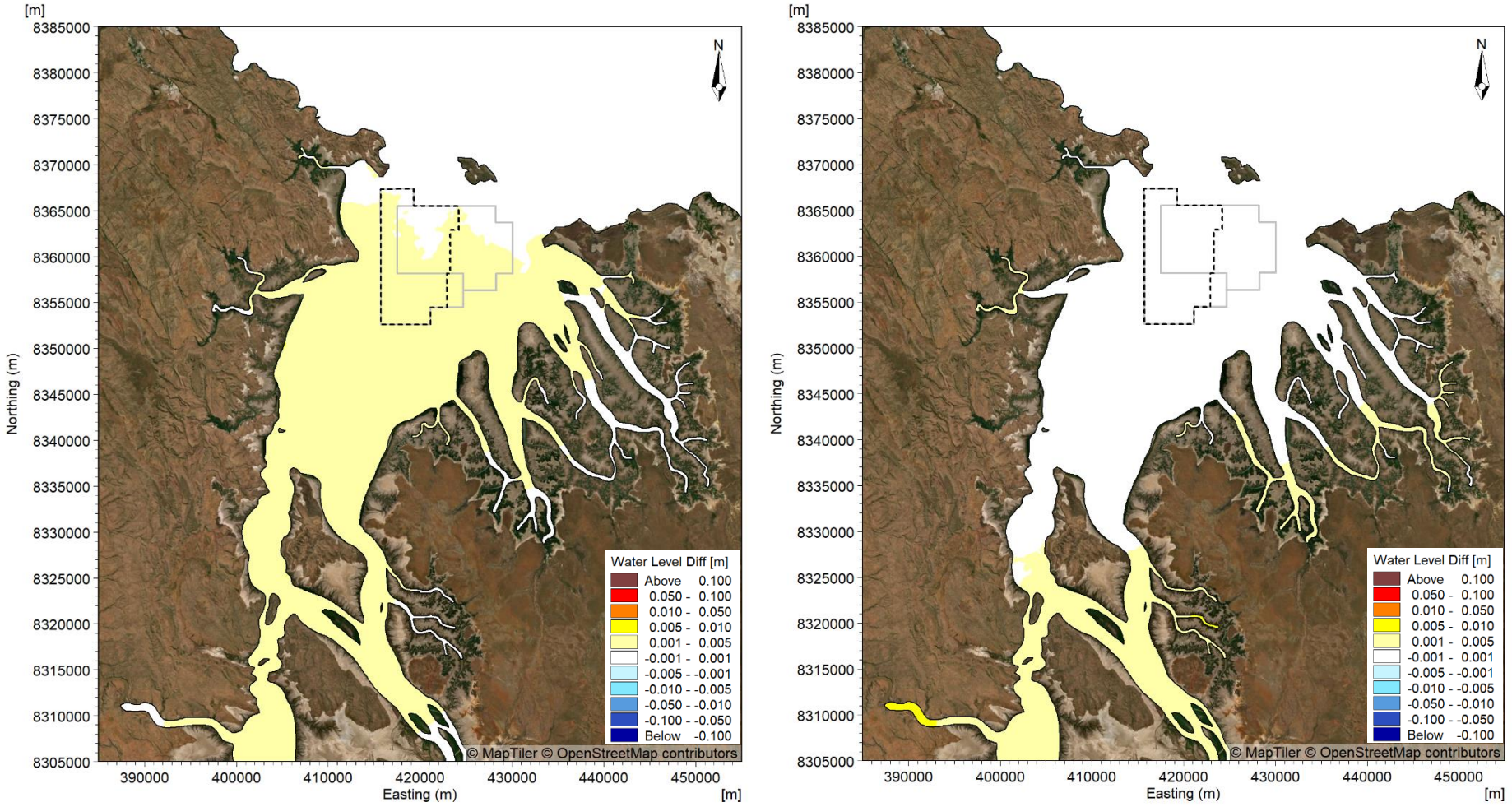
- For the 15 years of sand sourcing the largest (but still very minor) changes at the upstream sites coincide with the flood and ebb stages of the tides, with changes at high and low water close to zero. Within the POA and further offshore there was assessed to be a very minor reduction in water level at low water, but this was less than 0.003 m (3 mm). The modelled changes in water level during the flood and ebb stages of the tide were predominantly due to a change in the phase of the tidal propagation, with the deepening of the POA by 1 m due to the 15 years of sand sourcing resulting in the tidal wave propagating into and out of CG being up to 30 seconds earlier than during the existing case.

- The 15 years of sand sourcing was assessed to result in a maximum increase in water level of 0.01 m (1 cm) and a maximum reduction in water level of 0.015 m (1.5 cm). As the changes occur during the flood and ebb stages of the tide respectively, overall, they do not change the maximum or minimum water levels. The change in tidal range for the 15 years of sand sourcing scenario was modelled to be less than 0.05% of the existing tidal range over a large spring tide.

- The pre-European settlement results show that prior to construction of the Ord River dams both high water and low water levels within CG during a wet season high discharge event were higher than the existing case, with increases of more than 0.2 m (20 cm) at high water and more than 0.1 m (10 cm) at low water at the entrance to West Arm (AWAC-08). The increases in high water and low water levels reduce with distance downstream, with increases of around 0.03 m (3 cm) at high water and low water in King Shoals (AWAC-09), compared to the existing case.

- The tidal water levels pre-European settlement were up to 0.22 m higher and up to 0.12 m lower than existing levels, with some of the changes relative to existing levels coinciding with high water and low water and so resulting in a change to maximum and minimum water levels. The modelling results indicated that the pre-European settlement tidal range could have been up to 0.55% larger than the existing tidal range during a high discharge event.

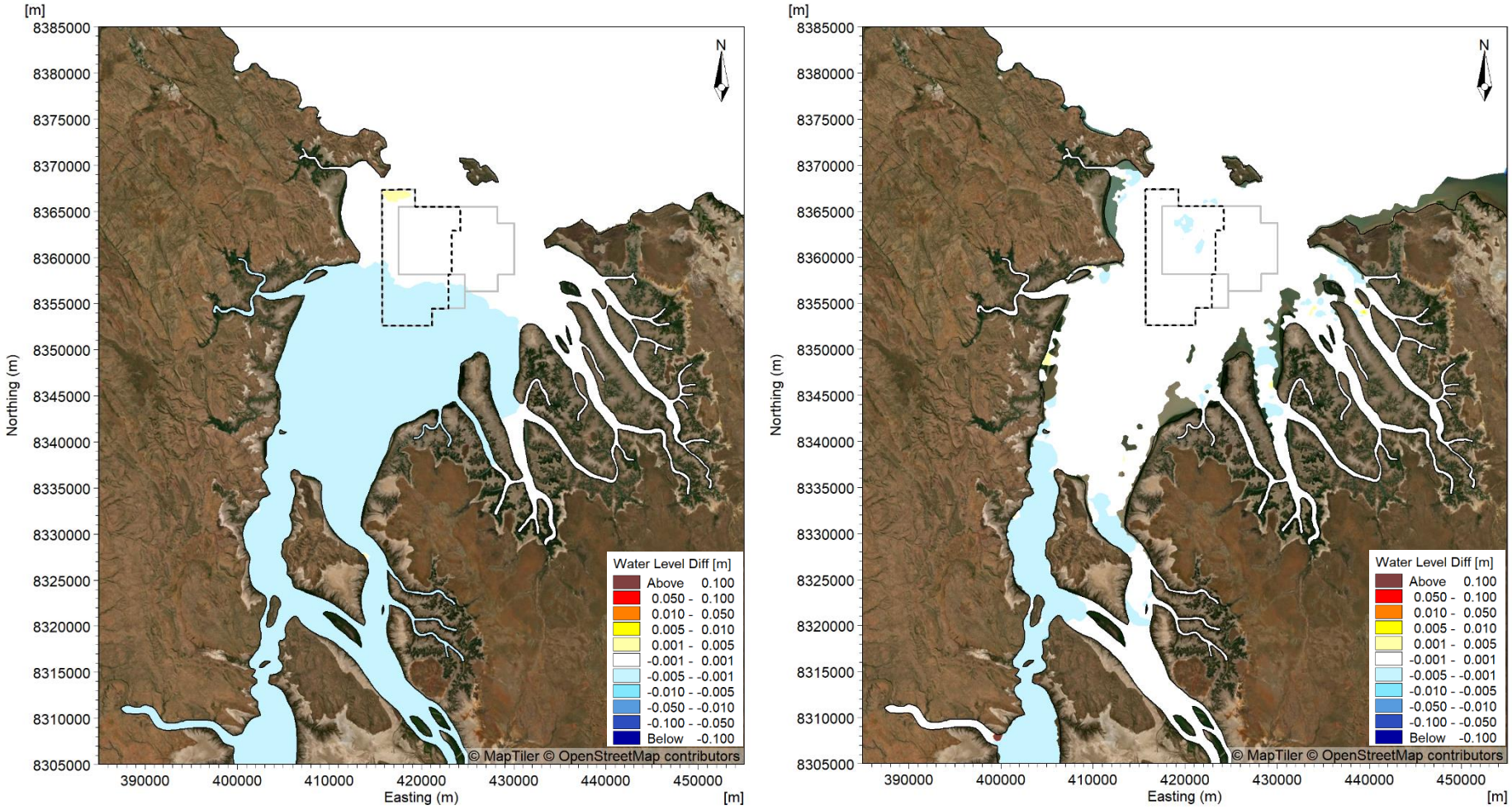
- The pre-European settlement results indicate that prior to construction of the Ord River dams the tidal range in CG was larger during a large river discharge event relative to existing conditions by up to 0.55% (i.e. the existing case water levels are 0.55% lower than they were pre-European settlement). The 15 years of sand sourcing was modelled to result in a very minor increase in tidal range of up to 0.05%, and so the cumulative changes from the two scenarios are opposite, meaning that the very minor changes in water level due to the sand sourcing will act to reduce the impacts that the Ord River dams had on water levels in CG.



Peak Flood

High Water

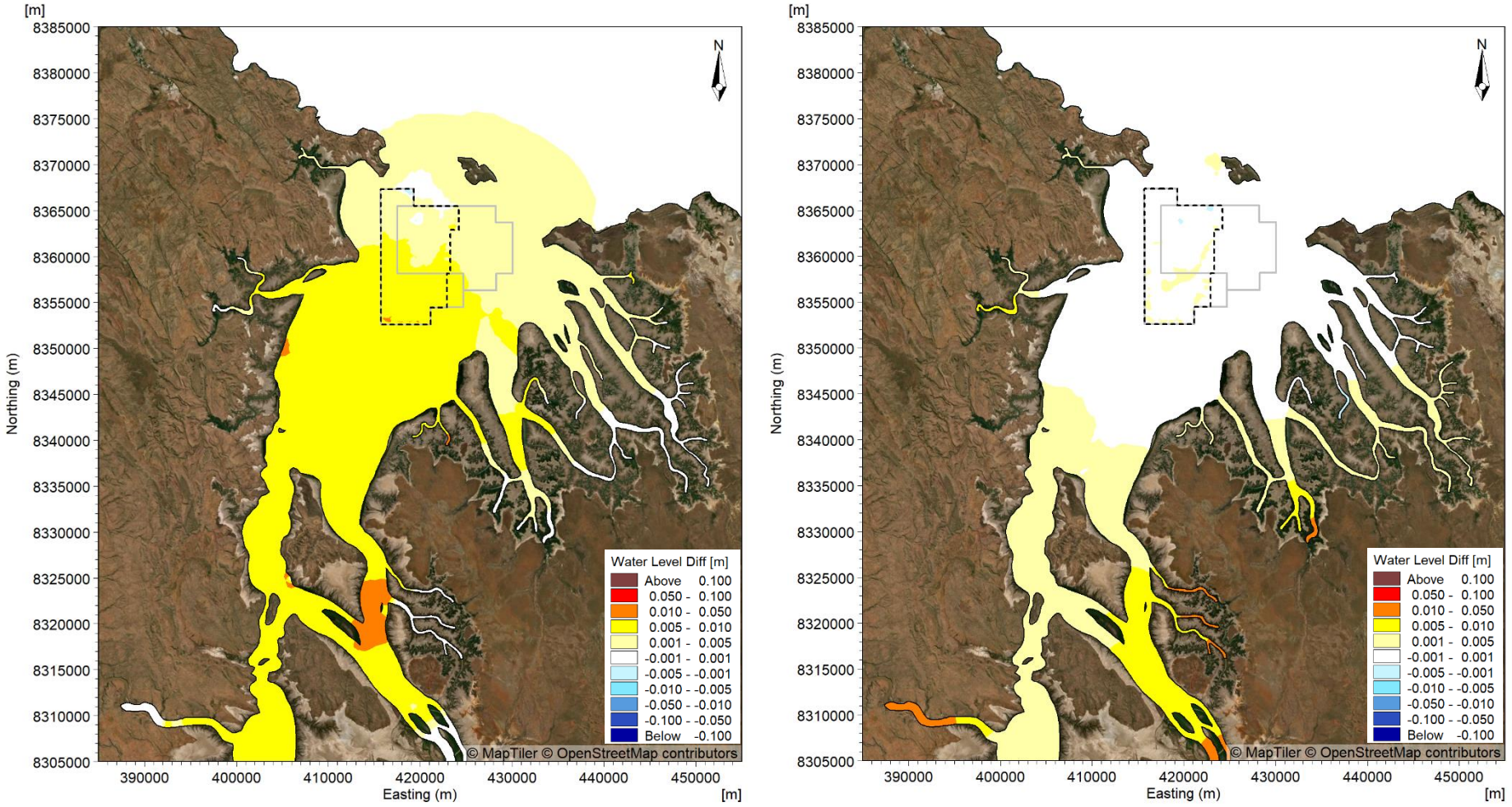
Figure 121. Modelled change (compared to existing case) in water level at peak flood (left) and high water (right) after 5 years (23 million m^3) of sand sourcing during a spring tide in the wet season.



Peak Ebb

Low Water

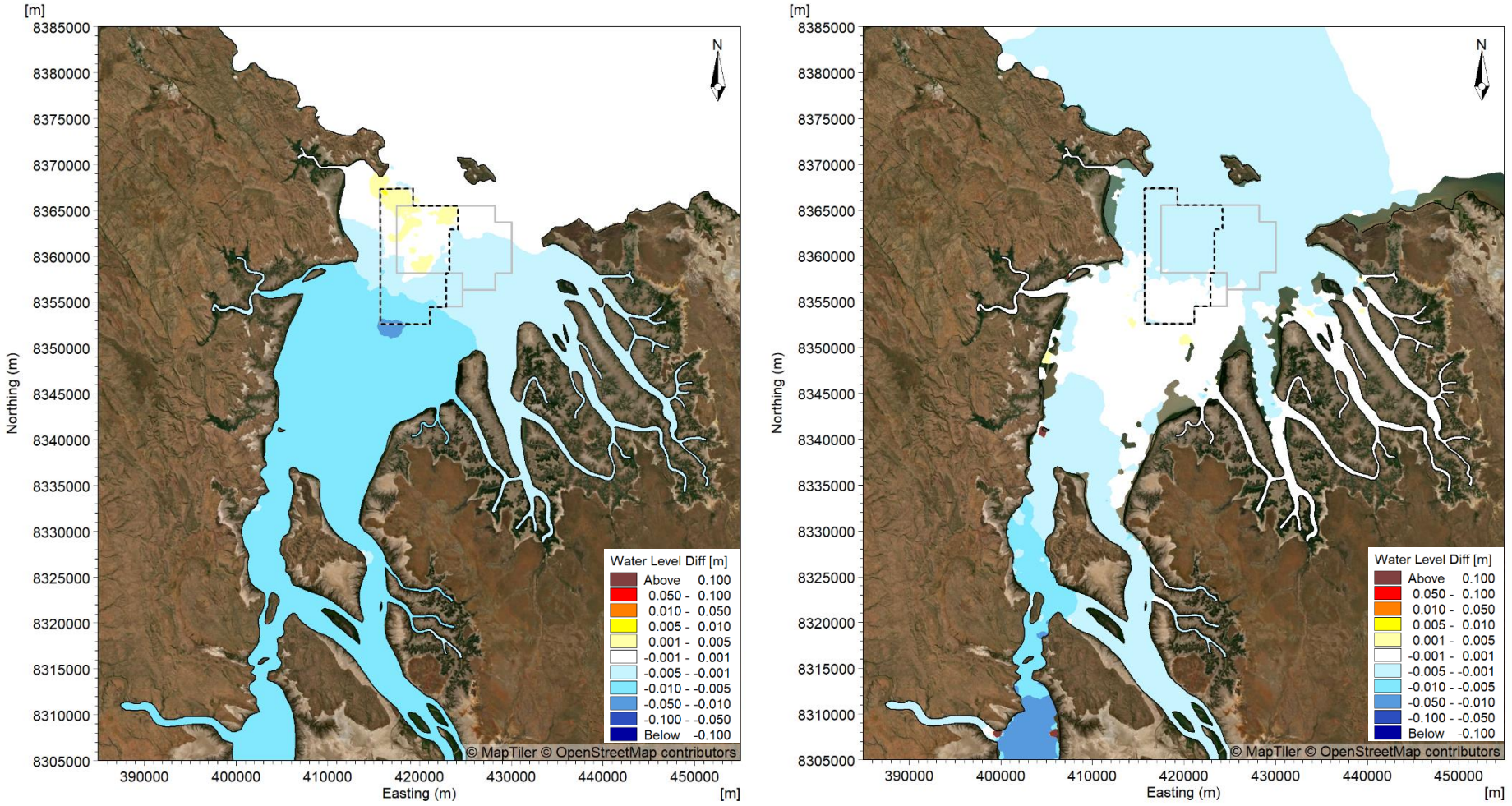
Figure 122. Modelled change (compared to existing case) in water level at peak ebb (left) and low water (right) after 5 years (23 million m^3) of sand sourcing during a spring tide in the wet season.



Peak Flood

High Water

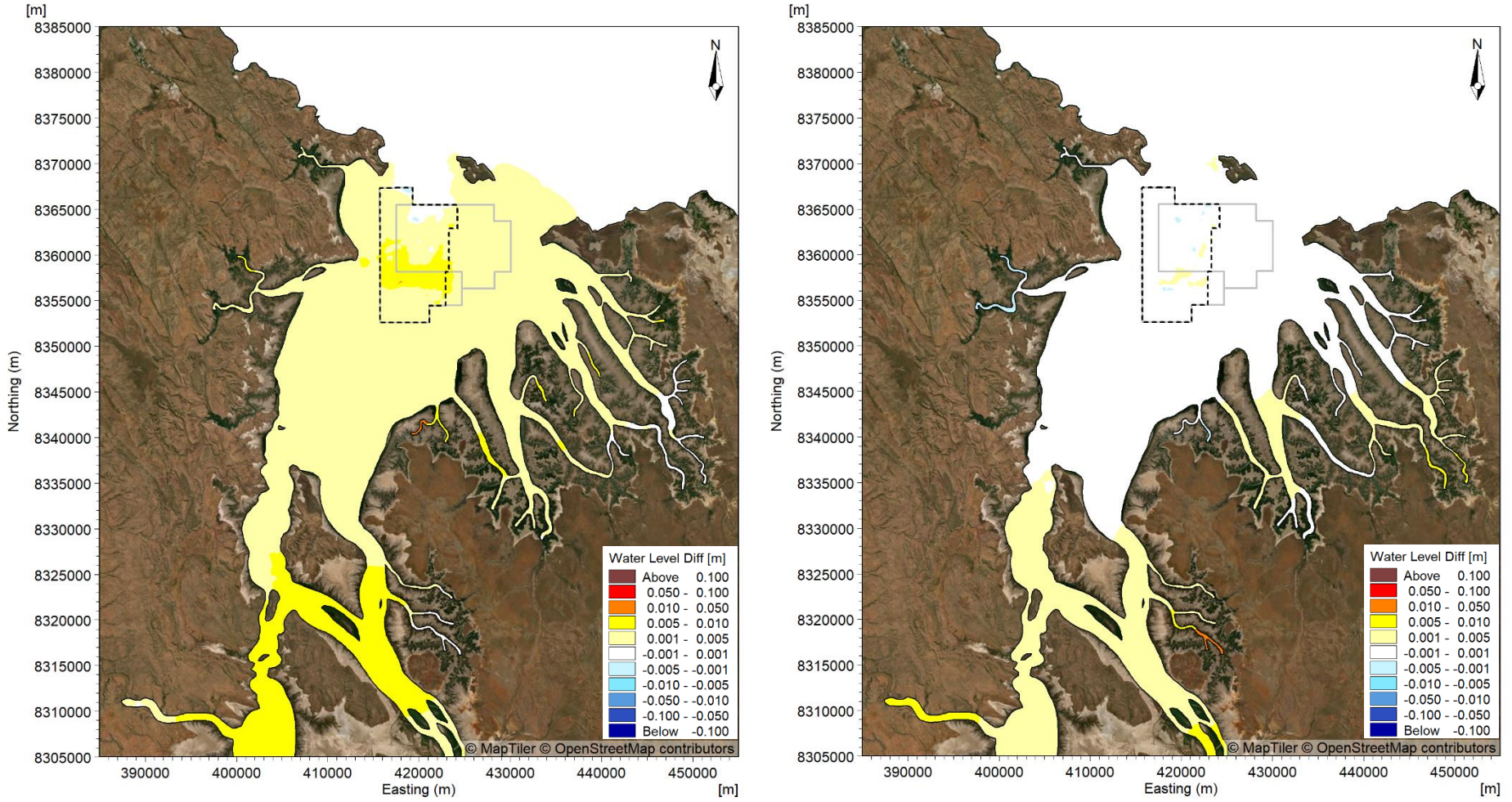
Figure 123. Modelled change (compared to existing case) in water level at peak flood (left) and high water (right) after 15 years (70 million m^3) of sand sourcing during a spring tide in the wet season.



Peak Ebb

Low Water

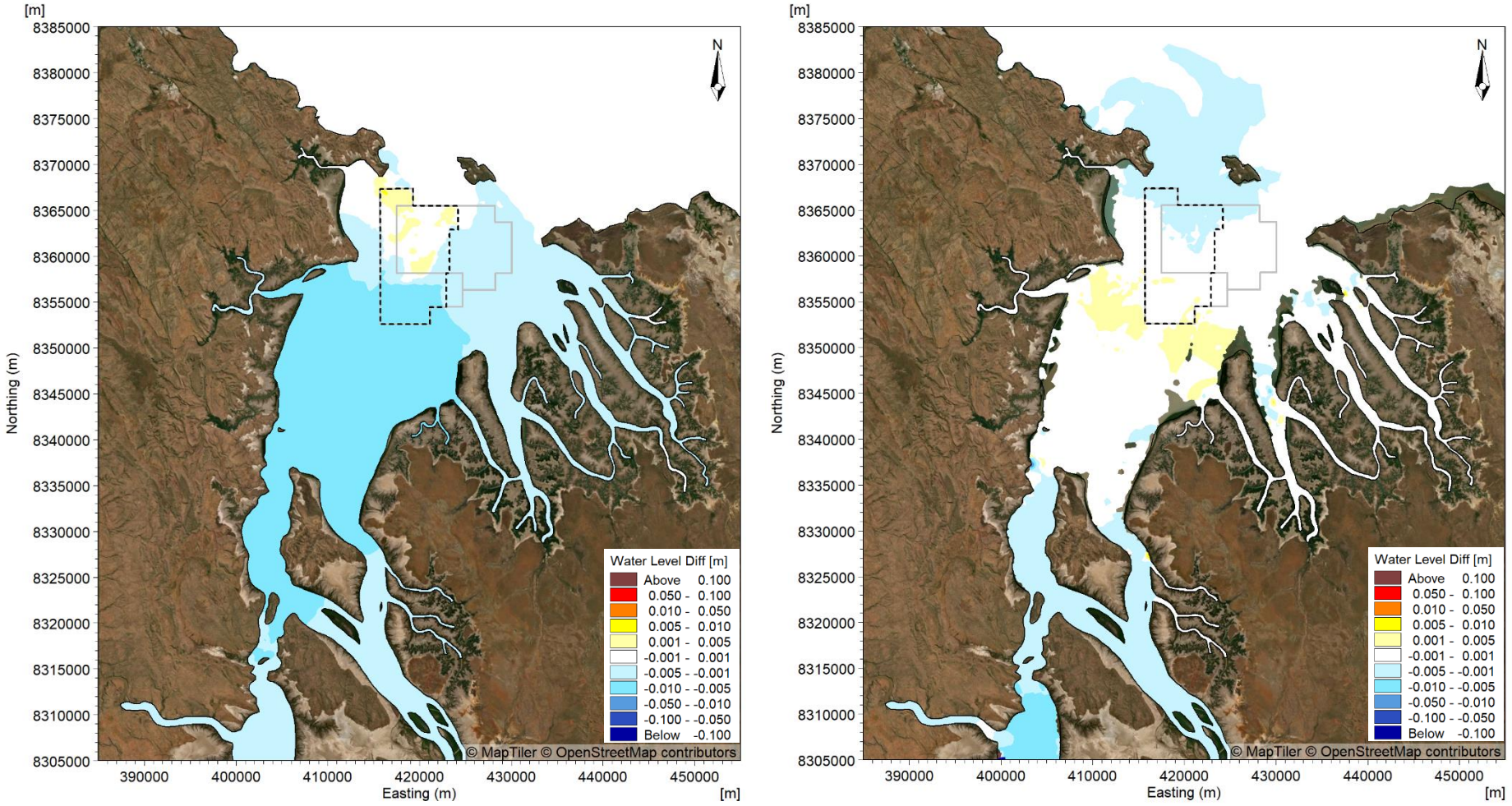
Figure 124. Modelled change (compared to existing case) in water level at peak ebb (left) and low water (right) after 15 years (70 million m^3) of sand sourcing during a spring tide in the wet season.



Peak Flood

High Water

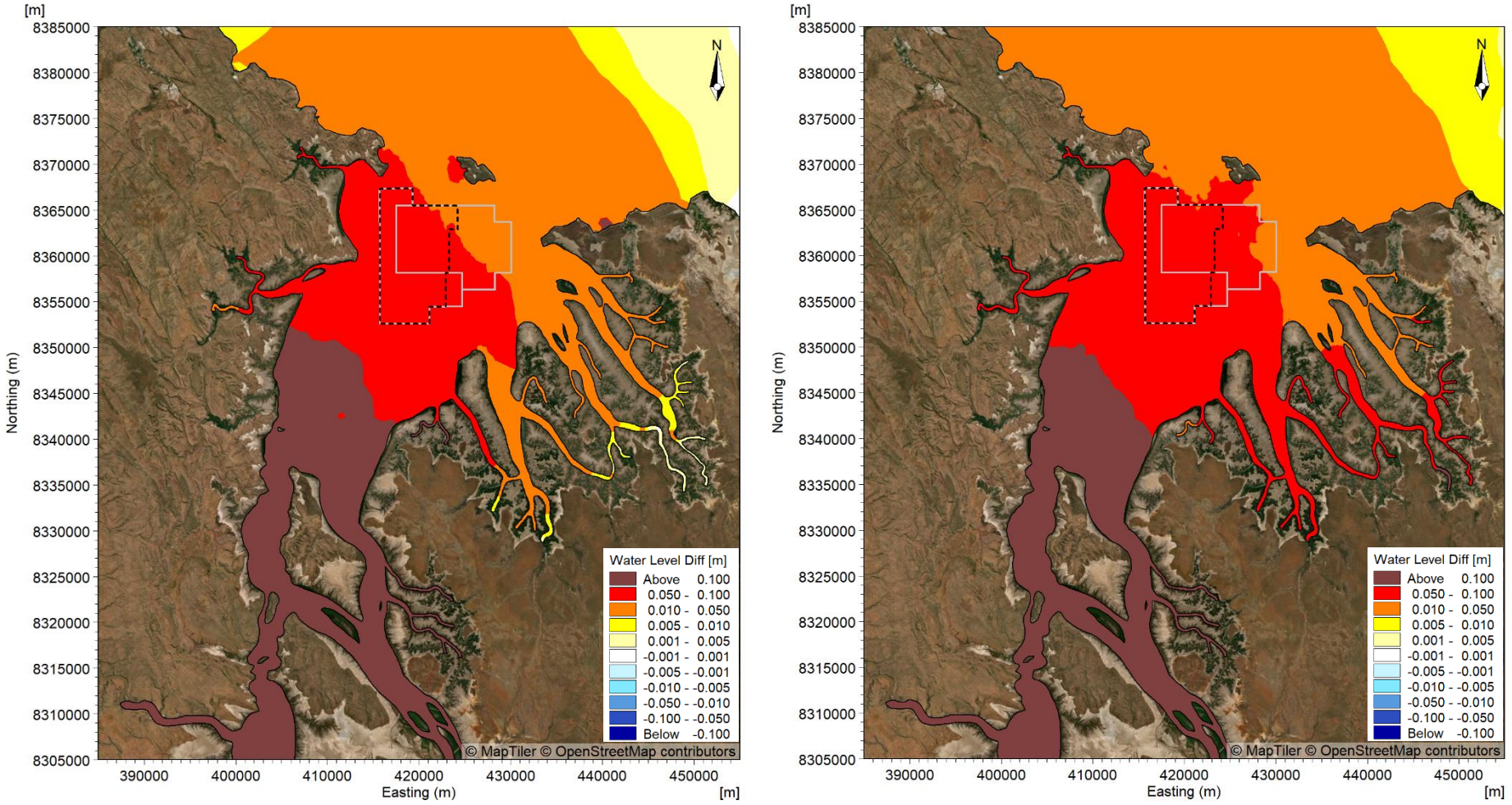
Figure 125. Modelled change (compared to existing case) in water level at peak flood (left) and high water (right) in 100 years from today after 15 years (70 million m^3) of sand sourcing during a spring tide in the wet season.



Peak Ebb

Low Water

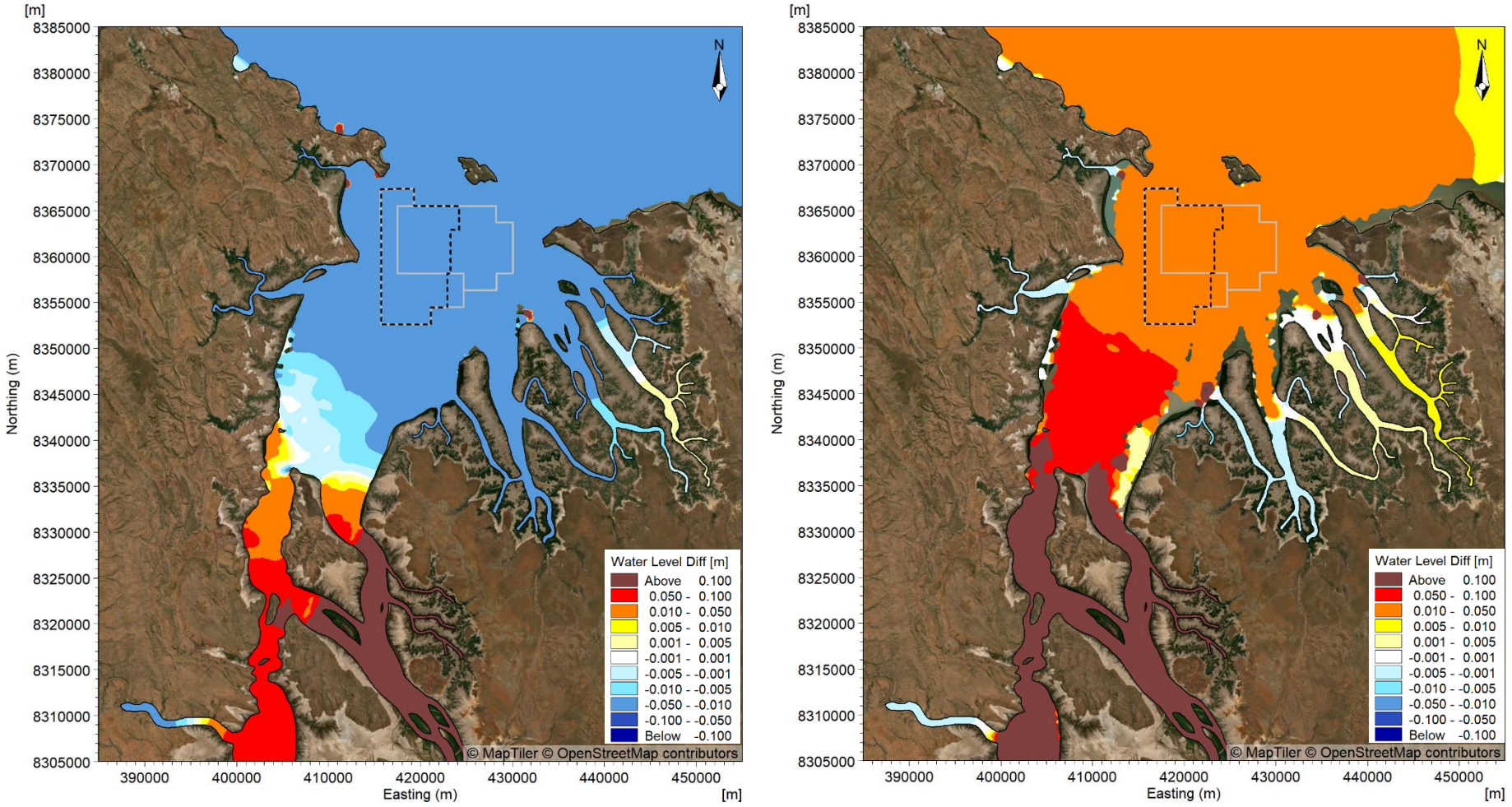
Figure 126. Modelled change (compared to existing case) in water level at peak ebb (left) and low water (right) in 100 years from today after 15 years (70 million m^3) of sand sourcing during a spring tide in the wet season.



Peak Flood

High Water

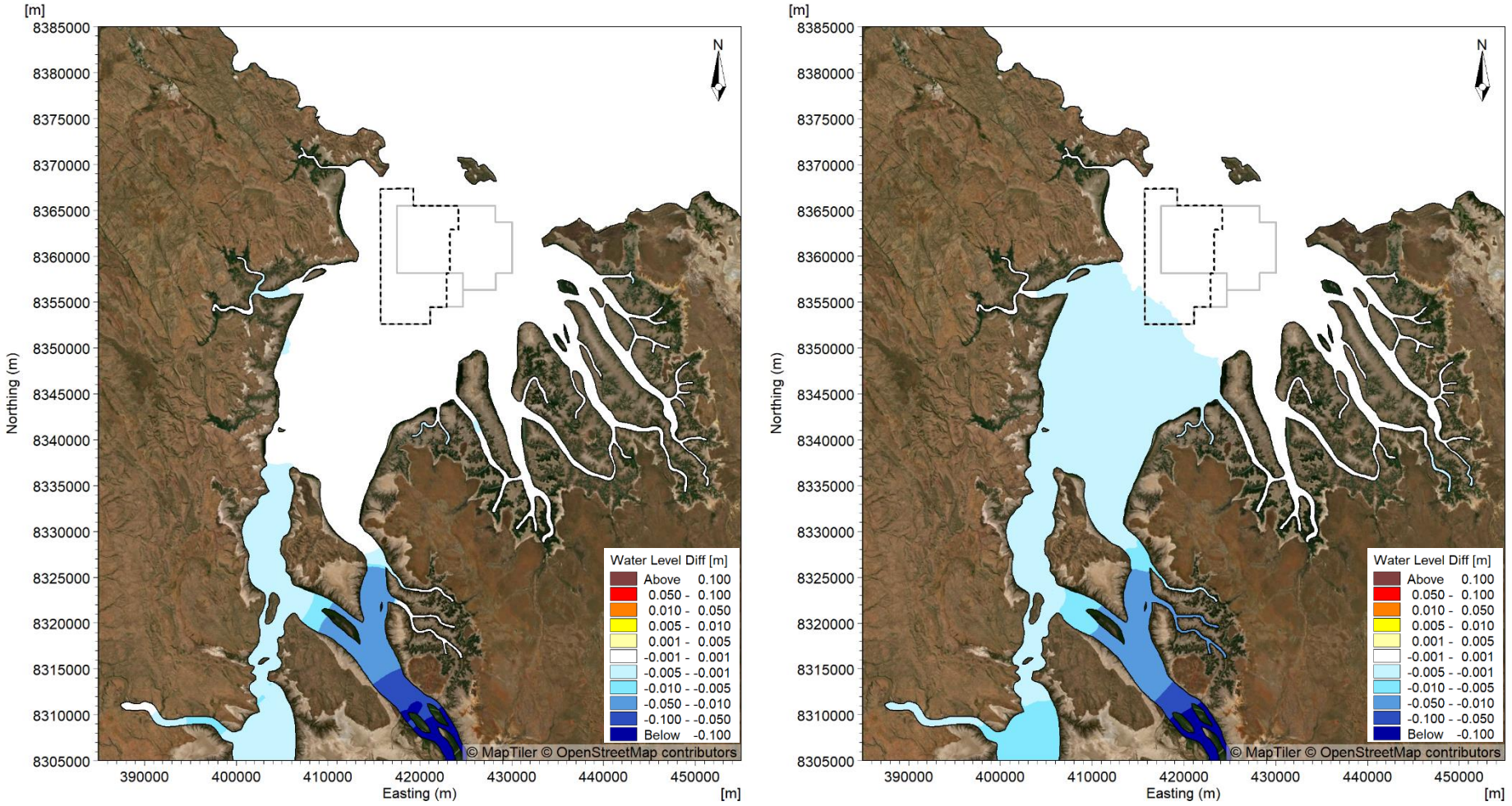
Figure 127. Modelled difference (compared to existing case) in water level at peak flood (left) and high water (right) for the Pre-European Settlement scenario during a spring tide in the wet season during a high discharge event.



Peak Ebb

Low Water

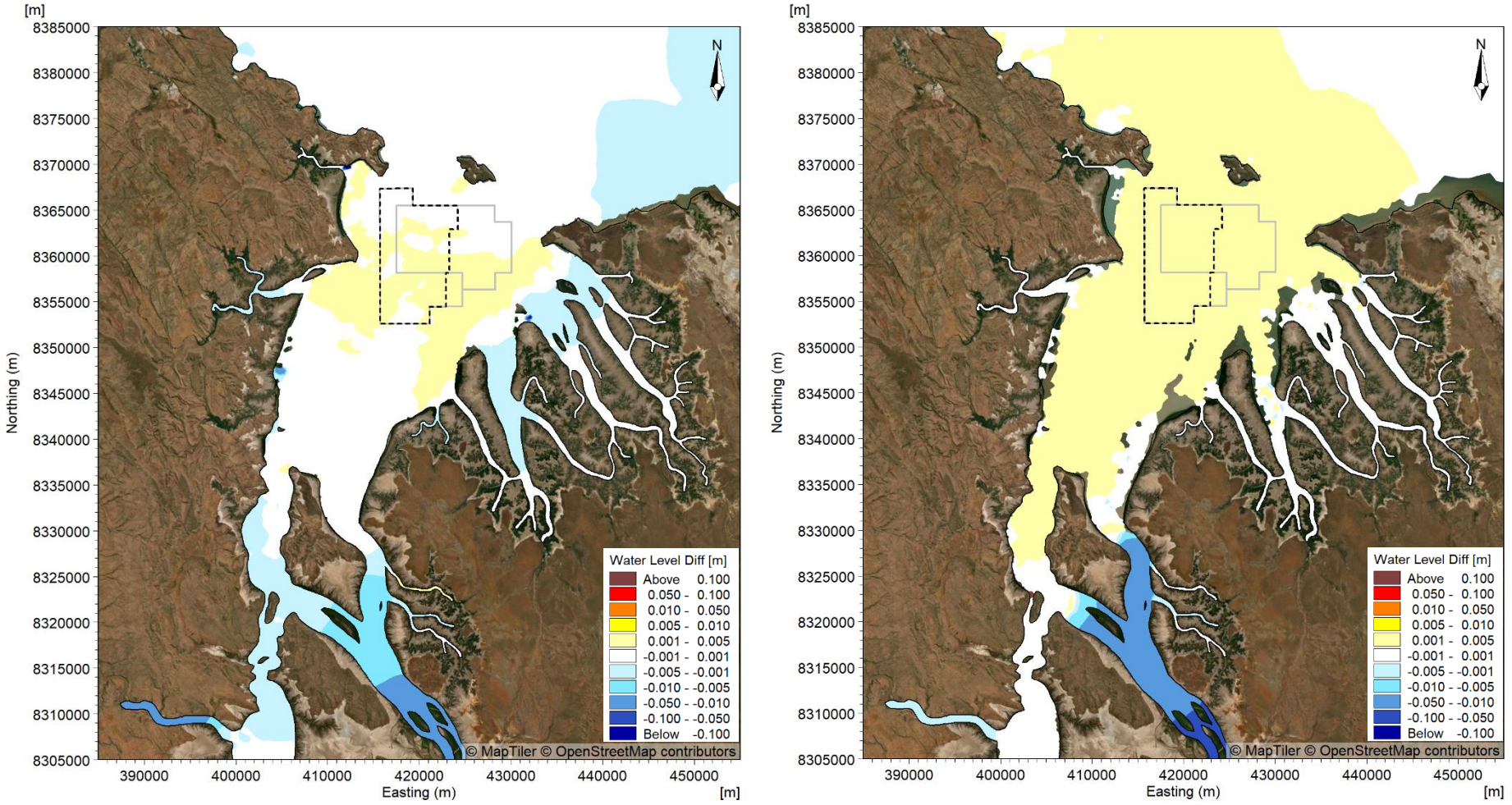
Figure 128. Modelled difference (compared to existing case) in water level at peak ebb (left) and low water (right) for the Pre-European Settlement scenario during a spring tide in the wet season during a high discharge event.



Peak Flood

High Water

Figure 129. Modelled difference (compared to existing case) in water level at peak flood (left) and high water (right) for the Pre-European Settlement scenario during a spring tide in the dry season.



Peak Ebb

Low Water

Figure 130. Modelled difference (compared to existing case) in water level at peak ebb (left) and low water (right) for the Pre-European Settlement scenario during a spring tide in the dry season.

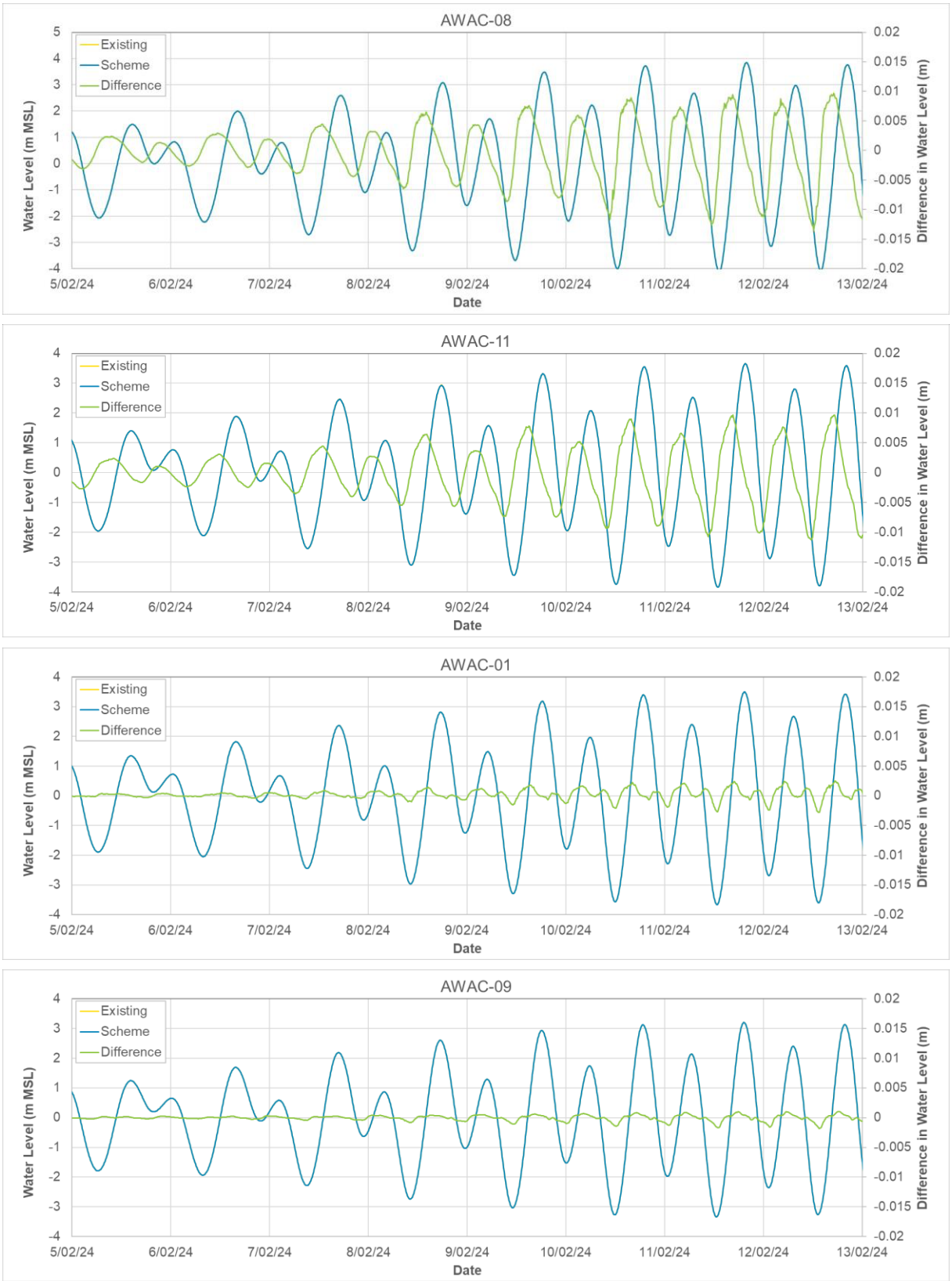


Figure 131. Timeseries showing the modelled change (compared to Existing case) in water level during the wet season from neap to spring tides due to 15 years (70 million m^3) of sand sourcing (Scheme). *The plots show the change from the furthest upstream site (AWAC-08, top) to the furthest offshore site (AWAC-09, bottom).*

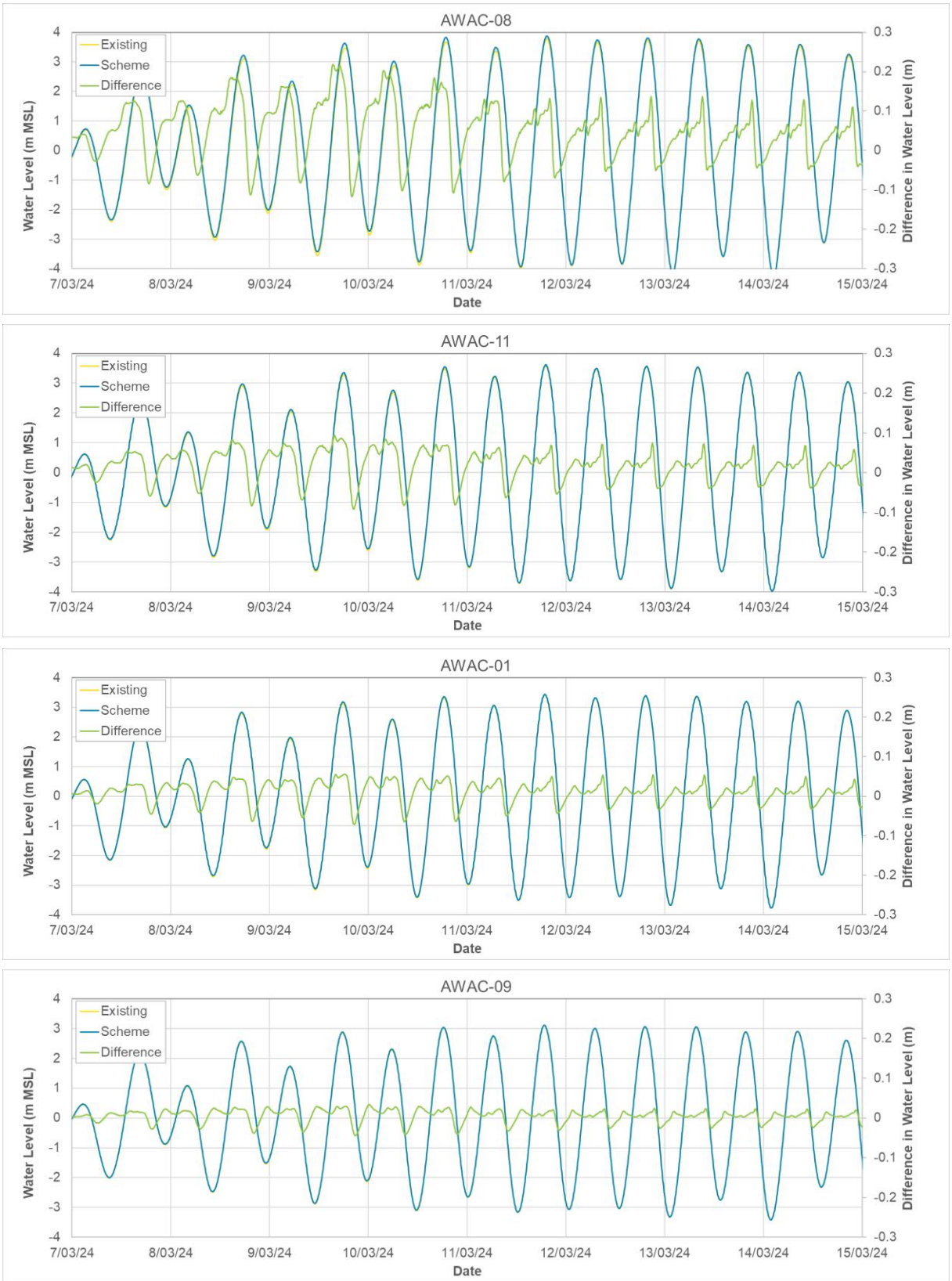


Figure 132. Timeseries showing the modelled difference (compared to existing case) in water level during the wet season from neap to spring tides for the Pre-European settlement scenario (Scheme). *The plots show the change from the furthest upstream site (AWAC-08, top) to the furthest offshore site (AWAC-09, bottom). Note: the difference in water level scale is different to Figure 131.*

Table 14. Statistics of the modelled change in water level during the wet season due to the 15 years of sand sourcing scenario and the pre-European settlement scenario relative to the existing case at the 11 AWAC sites.

Site	AWAC-01 (in POA)	AWAC-02 (in POA)	AWAC-03 (in POA)	AWAC-04 (in POA)	AWAC-05	AWAC-06	AWAC-07	AWAC-08	AWAC-09	AWAC-10	AWAC-11
15 years of Sand Sourcing Scenario Water Level Change (m)											
Maximum	0.003	0.003	0.007	0.005	0.003	0.003	0.006	0.010	0.002	0.002	0.010
99th %ile	0.002	0.003	0.006	0.004	0.002	0.002	0.005	0.009	0.001	0.001	0.009
90th %ile	0.001	0.002	0.004	0.002	0.001	0.001	0.003	0.006	0.000	0.001	0.006
80th %ile	0.001	0.001	0.002	0.002	0.001	0.001	0.002	0.004	0.000	0.001	0.004
50th %ile	0.000	0.000	0.000	0.000	0.000	0.000	0.000	0.000	0.000	0.000	0.000
20th %ile	0.000	0.000	-0.002	0.000	0.000	-0.001	-0.002	-0.005	0.000	-0.001	-0.004
10th %ile	-0.001	-0.001	-0.002	-0.001	-0.001	-0.001	-0.003	-0.008	-0.001	-0.001	-0.006
1st %ile	-0.002	-0.002	-0.003	-0.002	-0.002	-0.003	-0.005	-0.012	-0.002	-0.002	-0.011
Minimum	-0.004	-0.003	-0.004	-0.002	-0.003	-0.003	-0.006	-0.015	-0.002	-0.002	-0.013
Water Level Change since European Settlement (m)											
Maximum	0.056	0.053	0.060	0.061	0.055	0.048	0.063	0.219	0.033	0.039	0.094
99th %ile	0.043	0.041	0.046	0.047	0.042	0.037	0.047	0.155	0.024	0.029	0.067
90th %ile	0.017	0.016	0.018	0.018	0.016	0.015	0.018	0.056	0.010	0.012	0.025
80th %ile	0.009	0.008	0.009	0.010	0.009	0.007	0.009	0.034	0.005	0.005	0.015
50th %ile	0.000	0.000	0.000	0.000	0.000	0.000	0.000	0.000	0.000	0.000	0.000
20th %ile	0.000	0.000	0.000	0.000	0.000	0.000	0.000	0.000	0.000	0.000	0.000
10th %ile	-0.005	-0.004	-0.005	-0.005	-0.004	-0.004	-0.006	-0.011	-0.004	-0.004	-0.007
1st %ile	-0.035	-0.033	-0.036	-0.035	-0.032	-0.033	-0.038	-0.055	-0.025	-0.029	-0.044
Minimum	-0.072	-0.067	-0.076	-0.075	-0.065	-0.067	-0.082	-0.118	-0.045	-0.055	-0.091

Note: AWAC-02 is actually located 450 m to the east of the POA, but as it is so close to the POA boundary the changes are representative of changes within the POA.
The inverse of the pre-European Settlement changes reflect the changes that European settlement (i.e. construction of the Ord River dams) had on the water levels.

Table 15. Percent change in tidal range due to 15 years of sand sourcing and pre-European settlement during a spring tide with a high river discharge relative to the existing case.

Location	Change in Tidal Range (%)	
	Sand Sourcing (15yrs)	Pre-European Settlement
AWAC-01 (in POA)	0.04%	0.24%
AWAC-02 (in POA)	0.03%	0.18%
AWAC-03 (in POA)	0.02%	0.22%
AWAC-04 (in POA)	0.02%	0.32%
AWAC-05	0.04%	0.24%
AWAC-06	0.03%	0.15%
AWAC-07	0.00%	0.16%
AWAC-08	0.00%	0.55%
AWAC-09	0.03%	0.02%
AWAC-10	0.03%	0.00%
AWAC-11	0.00%	0.42%

Note: AWAC-02 is actually located 450 m to the east of the POA, but as it is so close to the POA boundary the changes are representative of changes within the POA.
The inverse of the pre-European Settlement changes reflect the changes that European settlement (i.e. construction of the Ord River dams) had on the water levels.

4.2.1.2. Currents

Spatial maps showing the modelled change in current speed at peak flood, high water, peak ebb and low water during a spring tide in the wet season due to the sand sourcing after 5 years, after 15 years and 100 years from today after 15 years are shown in Figure 133 to Figure 138. During the dry season, transitional season and the tropical cyclone, the modelled changes in current speed due to the sand sourcing were similar to those for the wet season and so plots for these cases are not shown here but are included in Appendix B.

Due to the similarity in the results for the metocean conditions, it is not possible to define best-case and worst-case changes for the currents. Plots of the indicated difference in current speed between the existing case and the pre-European settlement scenario for a spring tide in the wet season during a period with high river discharge are shown in Figure 139 and Figure 140 and plots for a spring tide in the dry season are shown in Figure 141 and Figure 142. The plots show the following:

- As with the changes in water level, the spatial changes in current speed as a result of the 5 years and 15 years of sand sourcing were extremely minor and localised within and adjacent to the POA. The localised changes were predominantly within ±0.01 m/s as a result of 5 years of sand sourcing and within ±0.05 m/s as a result of 15 years of sand sourcing.
- The largest (but extremely minor) reduction in current speed as a result of the sand sourcing occurred at the peak flood and peak ebb stages of the tide, while at high water and low water a combination of localised extremely minor increases and decreases in current speed were modelled.
- The modelled changes in current speed 100 years from today after 15 years of sand sourcing were of a smaller spatial extent than the changes after 15 years of sand sourcing, assuming present day conditions. This indicates that over time the increase in water depth due to climate change related sea level rise predicted by IPCC (2024), combined with the ongoing sedimentation in the POA will result in the already extremely minor changes to current speeds being reduced.
- The modelled changes in current speeds since construction of the Ord River dams (i.e. the difference between pre-European settlement and the existing case in CG), during a high river discharge event in the wet season, were significantly larger than the very minor changes in current speed that were modelled from the sand sourcing.
- The modelling indicates that as a result of construction of the Ord River dams, existing currents speeds in the CG area have changed during a high river discharge event in the wet season as follows:

- During the peak flood and high-water stages of the tide, current speed has been reduced by 0.05 m/s to 0.35 m/s within the main body of CG (including the POA).
- During the peak ebb stage of the tide, current speed has increased by up to 0.08 m/s within the main body of CG (including the POA).
- During low water, current speed has increased by up to 0.14 m/s within the main body of CG (including the POA).
- During all stages of the tide, current speed has increased by up to 1.2 m/s in East Arm.

- The modelling indicates that as a result of construction of the Ord River dams, existing currents speeds in the CG area have changed in the dry season as follows:
  - During peak flood and high-water conditions, current speeds have increased by up to 0.05 m/s for most of East Arm and by up to 0.3 m/s further upstream in East Arm.
  - During peak ebb and low-water conditions, current speeds have decreased by up to 0.05 m/s in localised areas of East Arm, and have decreased by up to 0.01 m/s through West Arm and into CG and the POA.
- These modelled changes are due to the reduced (wet season) and more controlled (dry season) river discharges from the Ord River as a result of the construction of the dams.

The spatial map plots showed that the sand sourcing after 15 years resulted in the largest extent and highest magnitude changes to current speed out of the sand sourcing scenarios considered (although these changes were still very minor). Therefore, to better understand the potential changes in current speed and direction relative to the existing case due to the sand sourcing, timeseries of after-15 years sand sourcing scenario only, are considered.

To understand the relative cumulative changes due to the pre-European settlement and the sand sourcing, timeseries showing the difference between pre-European settlement and the existing case are also considered. Timeseries plots of the change in current speed and direction during the wet season (results were similar for the three seasons so just the wet season timeseries results are presented) at sites from the upstream (southern) end of CG (AWAC-08) to offshore of CG at King Shoals (AWAC-09) are shown in Figure 143 to Figure 150.

It is important to note that the plots show results for both the existing case and the two scenarios (15 years of sand sourcing and pre-European settlement), but for the sand sourcing they are almost identical to the existing case and so it may not be possible to differentiate between the two. A statistical summary of the change in current speed relative to the existing case due to the two scenarios is provided in Table 16 and the change in peak spring flood and ebb current speed relative to the existing case is summarised in Table 17. The results show the following:

- For the 15 years of sand sourcing scenario the results showed extremely minor increases and decreases in current speed at the upstream (± 0.008 m/s) and offshore (± 0.003 m/s) sites (AWAC-08 and AWAC-09) and negligible changes to the current direction. The largest (but extremely minor) changes occurred around slack water when there was a switch from an increase to a decrease compared to the existing case, which indicates that the change was predominantly due to the very slight change in phase of the tidal propagation.
- Within and adjacent to the POA the 15 years of sand sourcing resulted in larger (but still very minor) changes, with the sand sourcing assessed to predominantly result in very minor reductions in current speed, of up to 0.02 m/s, during both the flood and ebb stages of the tide. The changes in current direction were minor (less than 1º) except at the times when the current direction switches and the current speed was at its lowest, when larger changes were modelled (up to 45º within the POA). These changes were due to the small change in phase of the tidal propagation as opposed to being actual changes to the current direction.
- The statistics indicate that the modelled maximum increase in current speed due to the 15 years of sand sourcing were very minor, being up to 0.03 m/s within the POA and up to 0.01 m/s outside of the POA. The maximum modelled reduction in current speed were also minor, between 0.02 and 0.04 m/s within the POA and directly adjacent to it (including AWAC-02 and AWAC-11), while away from the POA the reductions were limited to 0.01 m/s.
- When expressed as a percentage change, the statistics indicate that the modelled changes in peak flood and ebb current speed during a spring tide represent a reduction of up to 2.1% within

and adjacent to the POA and typically less than ±0.5% away from it. The only exception to this was at AWAC-05, located on the western side of the West Entrance to CG, where the peak flood current speed was assessed to be reduced by 1.5% (this is partially due to the peak flood speed being relatively low at this site (0.4 m/s)).

- For the pre-European scenario, the results show that prior to construction of the Ord River dams the current speeds at the entrance to West Arm (AWAC-08) were up to 0.5 m/s lower during the flood stage of the tide and up to 0.15 m/s higher at the peak ebb stage of the tide. The model indicates that directly upstream of the POA (AWAC-11) and within the POA (AWAC-01) the peak flood current speed was lower prior to construction of the Ord River dams by up to 0.2 m/s, while at the offshore site (AWAC-09) they were lower by up 0.03 m/s. The modelled differences in current direction between the pre-European scenario and the existing case were relatively small (up to 12º) during the peak flood and ebb stages of the tide, and largest when the current direction switches, indicating they were predominantly due to a change in the tidal phase.

- The statistics indicate that the maximum increase in current speed since European settlement range from 0.04 to 0.57 m/s, while the maximum reduction in current speed range from 0.06 to 0.58 m/s.

- When expressed as a percentage change, the statistics indicate that since European settlement the peak flood current speed in CG during a large river discharge event has typically increased, with the maximum increase of 11.7%, while the peak ebb current speed has typically reduced, with the maximum reduction of 6.3%.

- The pre-European settlement results indicate that the construction of the Ord River dams has on average over CG increased the peak flood current speeds and reduced the peak ebb current speeds during a large river discharge event. The 15 years of sand sourcing was assessed to predominantly very slightly reduce current speeds in CG during both flood and ebb stages of the tide (with some localised areas of very minor increases). Therefore, the larger increases in current speed during the flood stage of the tide resulting from the construction of the Ord River dams would be locally reduced around the POA due to the sand sourcing, resulting in a reduction in the change in flood current speeds due to the Ord River dams. The changes due to the sand sourcing were assessed to add slightly to the changes due to the Ord River dams at the majority of the sites (6 out of 11) during the ebb stage of the tide, while at some of the sites the changes would act to slightly reduce the changes due to the Ord River dams. Overall, the relative contribution of the sand sourcing to the cumulative changes are negligible.

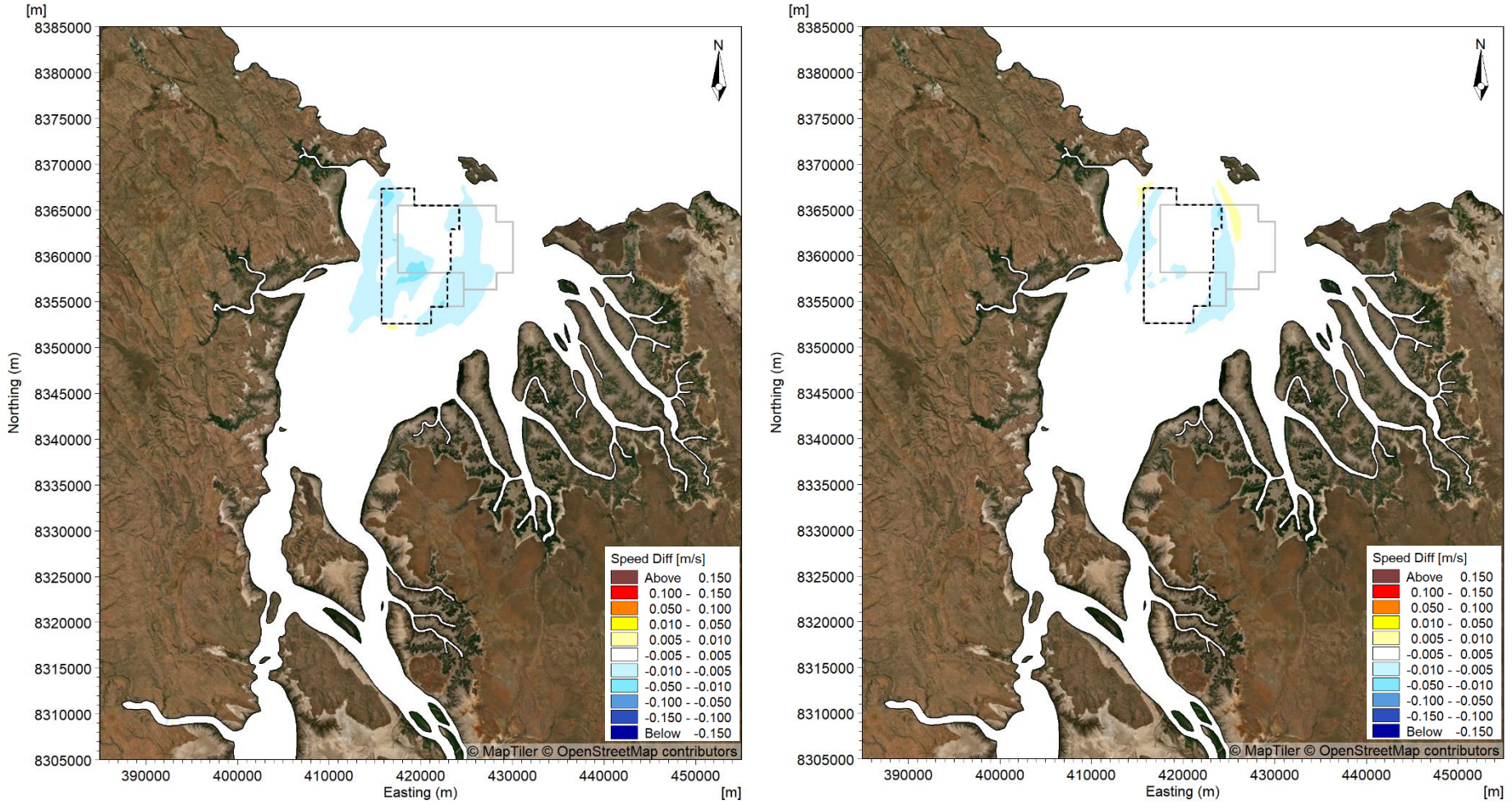
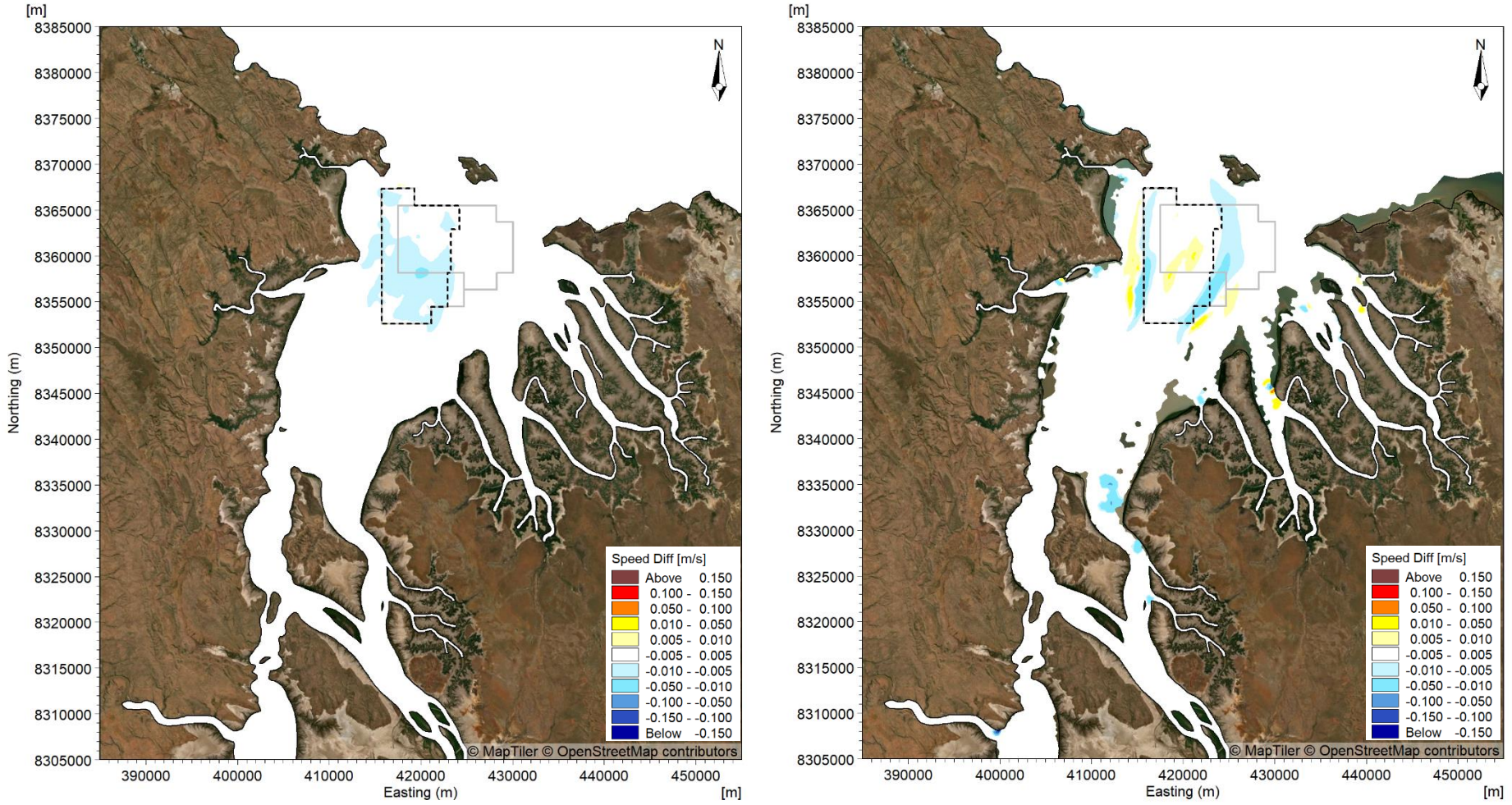


Figure 133. Modelled change in current speed at peak flood (left) and high water (right) after 5 years (23 million m^3) of sand sourcing during a spring tide in the wet season.



Peak Ebb

Low Water

Figure 134. Modelled change in current speed at peak ebb (left) and low water (right) after 5 years (23 million m^3) of sand sourcing during a spring tide in the wet season.

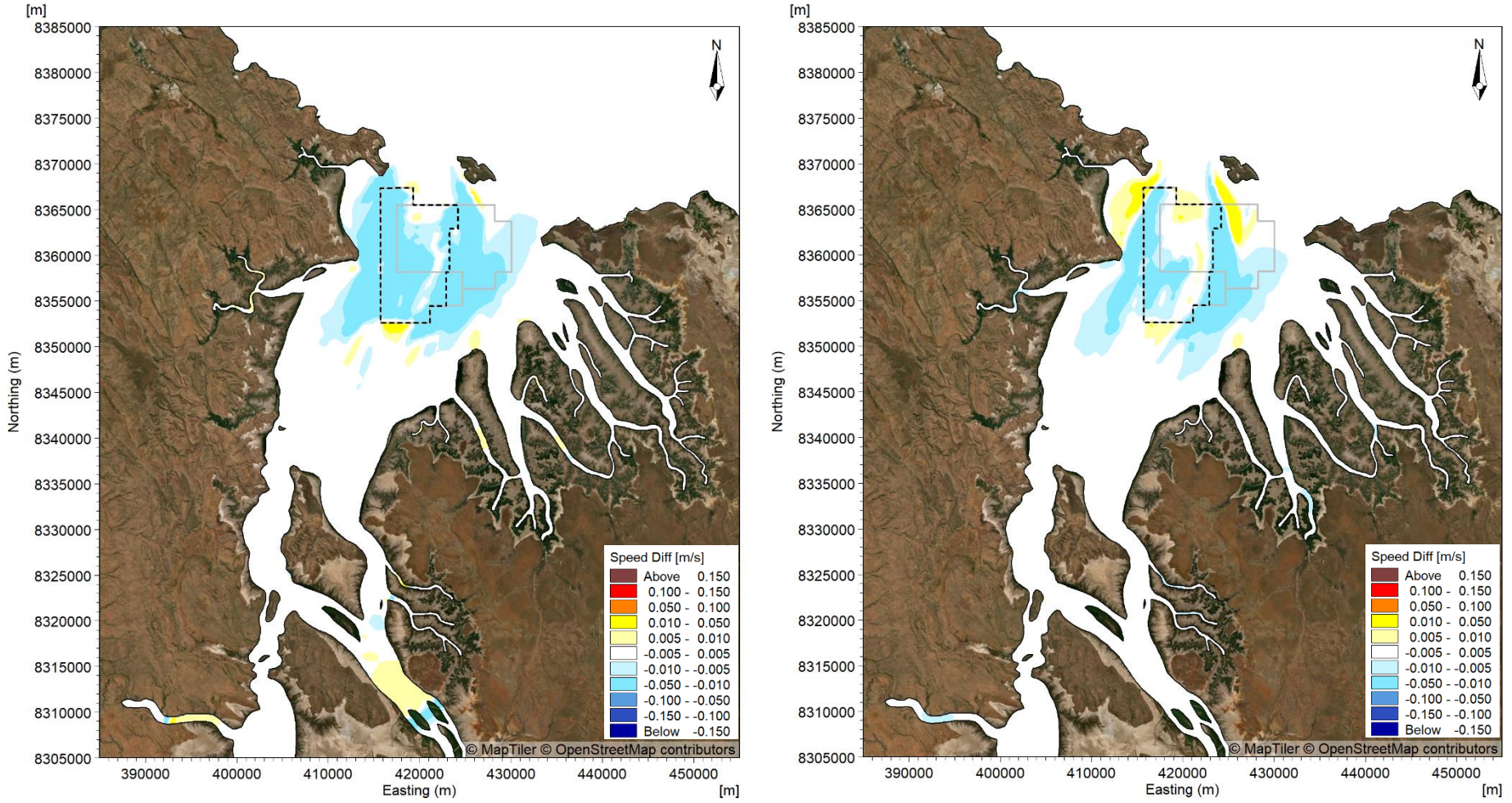
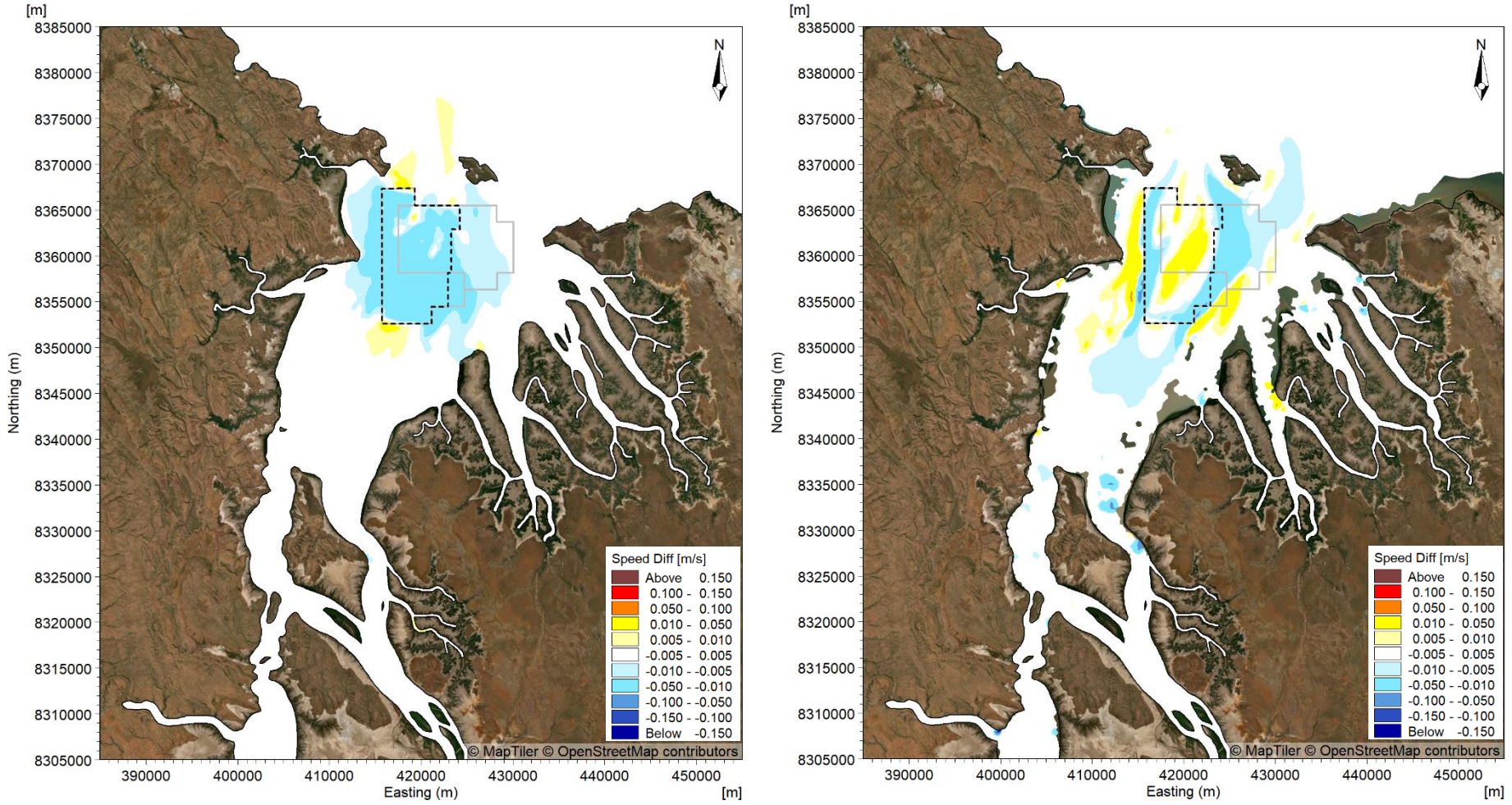


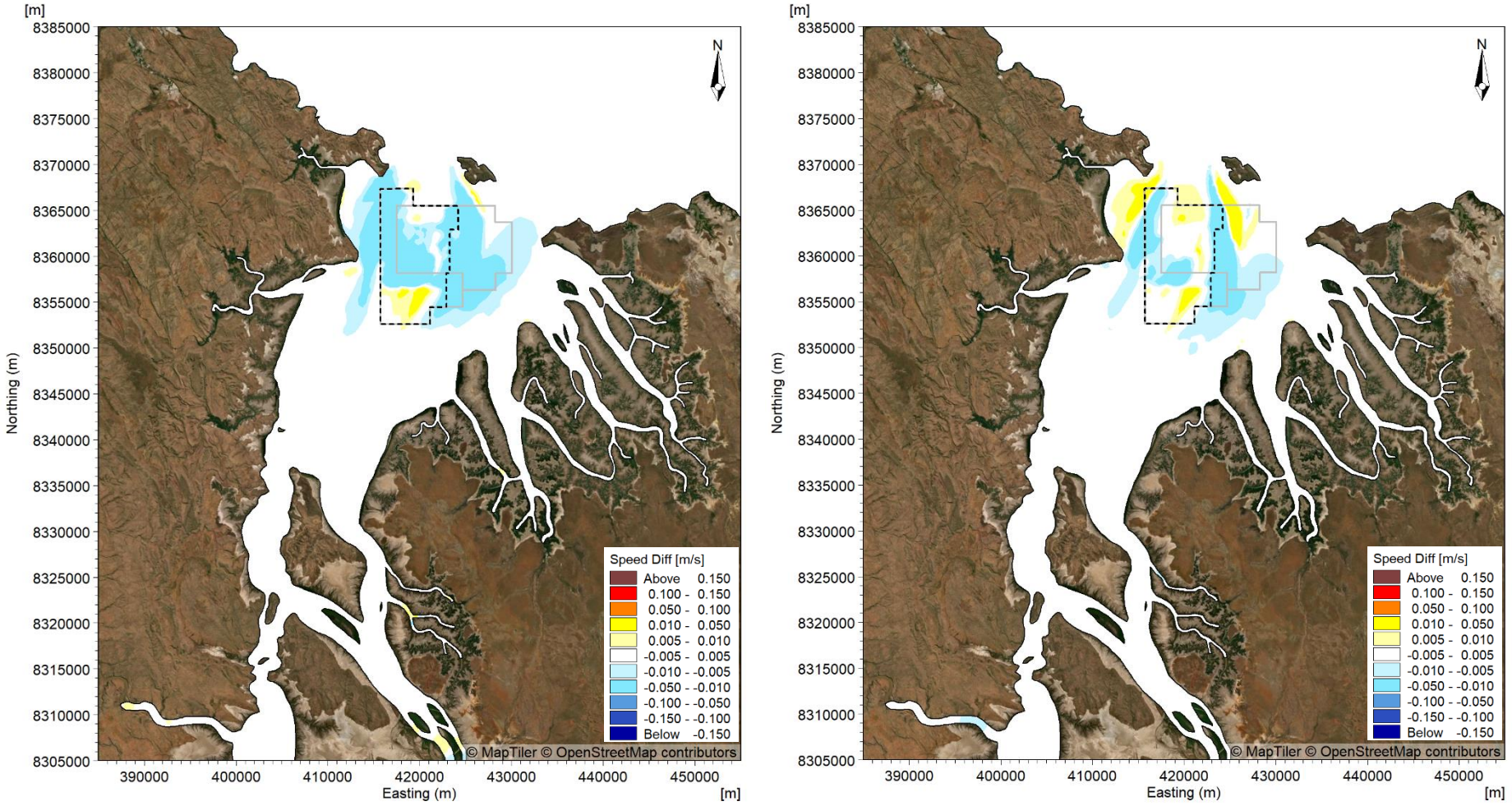
Figure 135. Modelled change in current speed at peak flood (left) and high water (right) after 15 years (70 million m^3) of sand sourcing during a spring tide in the wet season.



Peak Ebb

Low Water

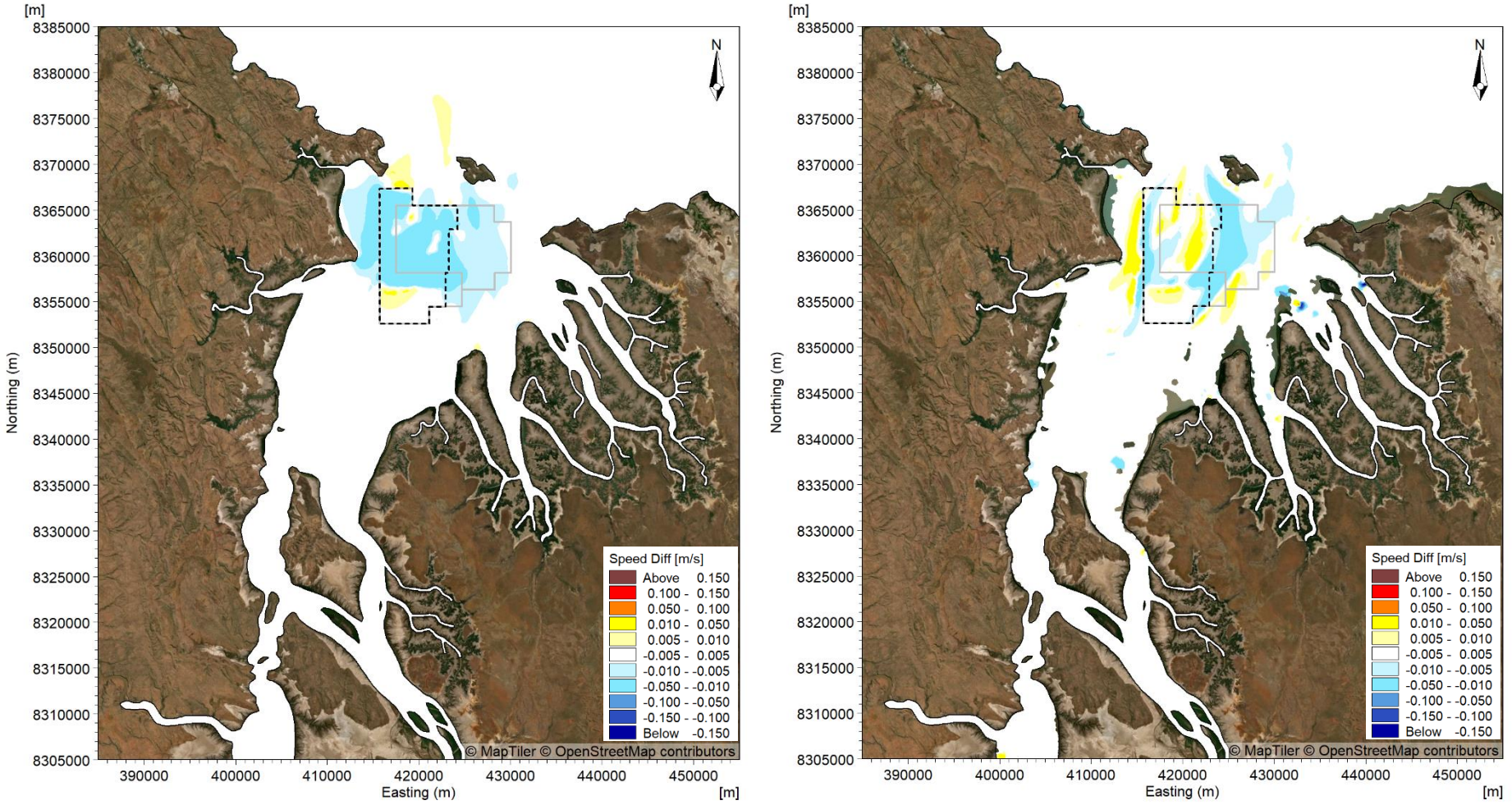
Figure 136. Modelled change in current speed at peak ebb (left) and low water (right) after 15 years (70 million m^3) of sand sourcing during a spring tide in the wet season.



Peak Flood

High Water

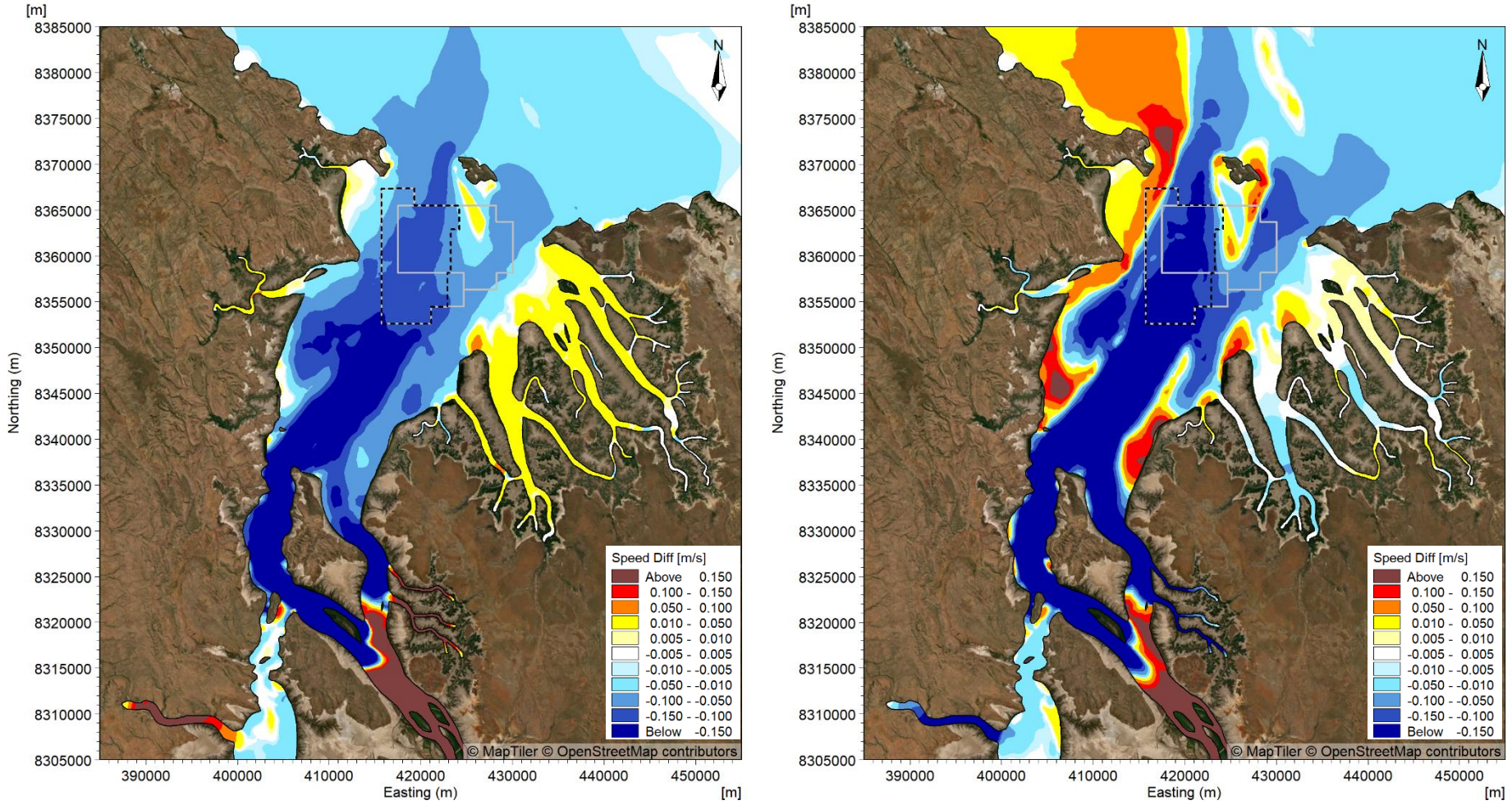
Figure 137. Modelled change in current speed at peak flood (left) and high water (right) in 100 years from today after 15 years of sand sourcing during a spring tide in the wet season.



Peak Ebb

Low Water

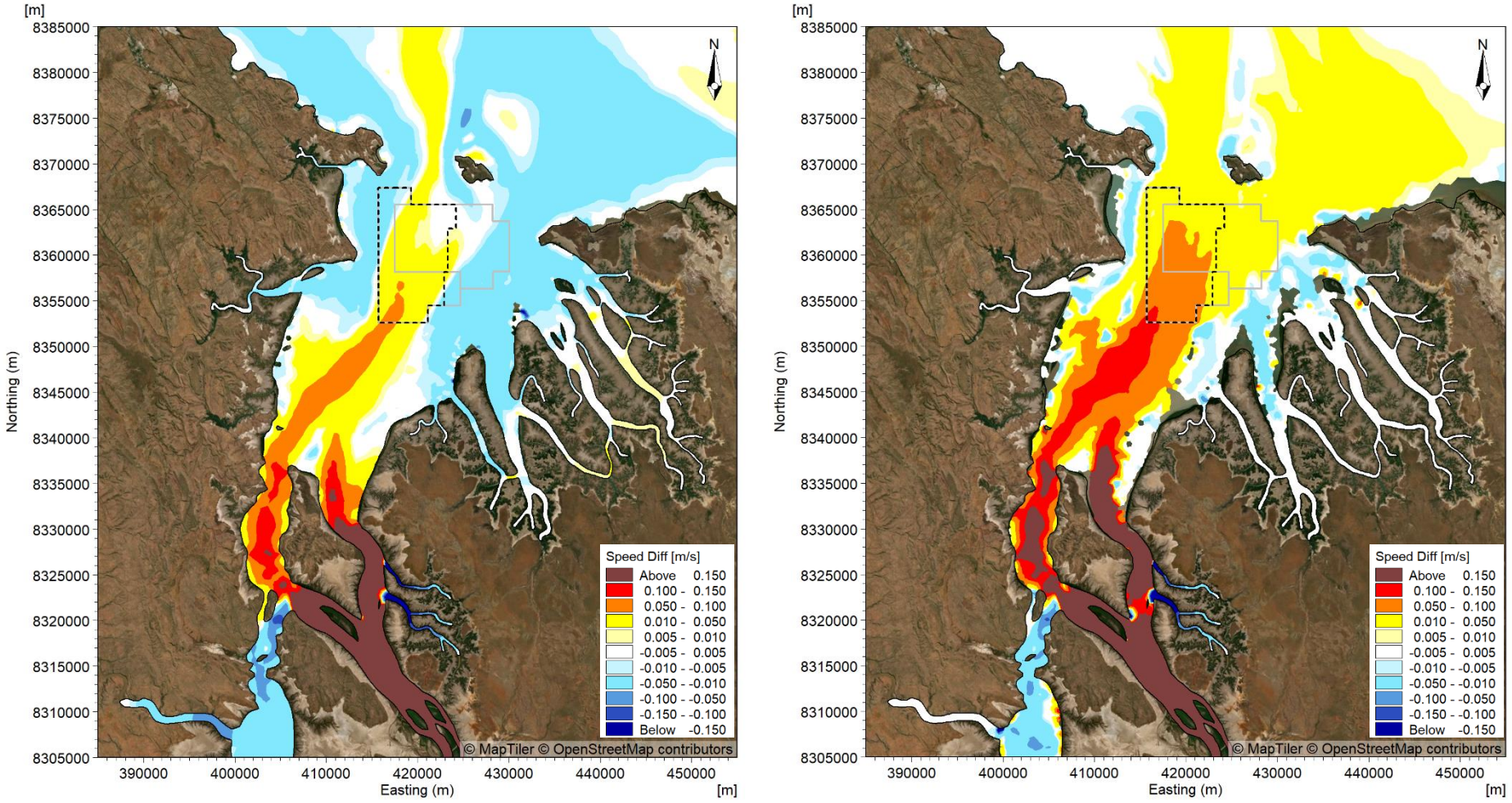
Figure 138. Modelled change in current speed at peak ebb (left) and low water (right) in 100 years from today after 15 years of sand sourcing during a spring tide in the wet season.



Peak Flood

High Water

Figure 139. Modelled difference (compared to existing case) in current speed at peak flood (left) and high water (right) for the Pre-European Settlement scenario during a spring tide in the wet season during a high discharge event.



Peak Ebb

Low Water

Figure 140. Modelled difference (compared to existing case) in current speed at peak ebb (left) and low water (right) for the Pre-European Settlement scenario during a spring tide in the wet season during a high discharge event.

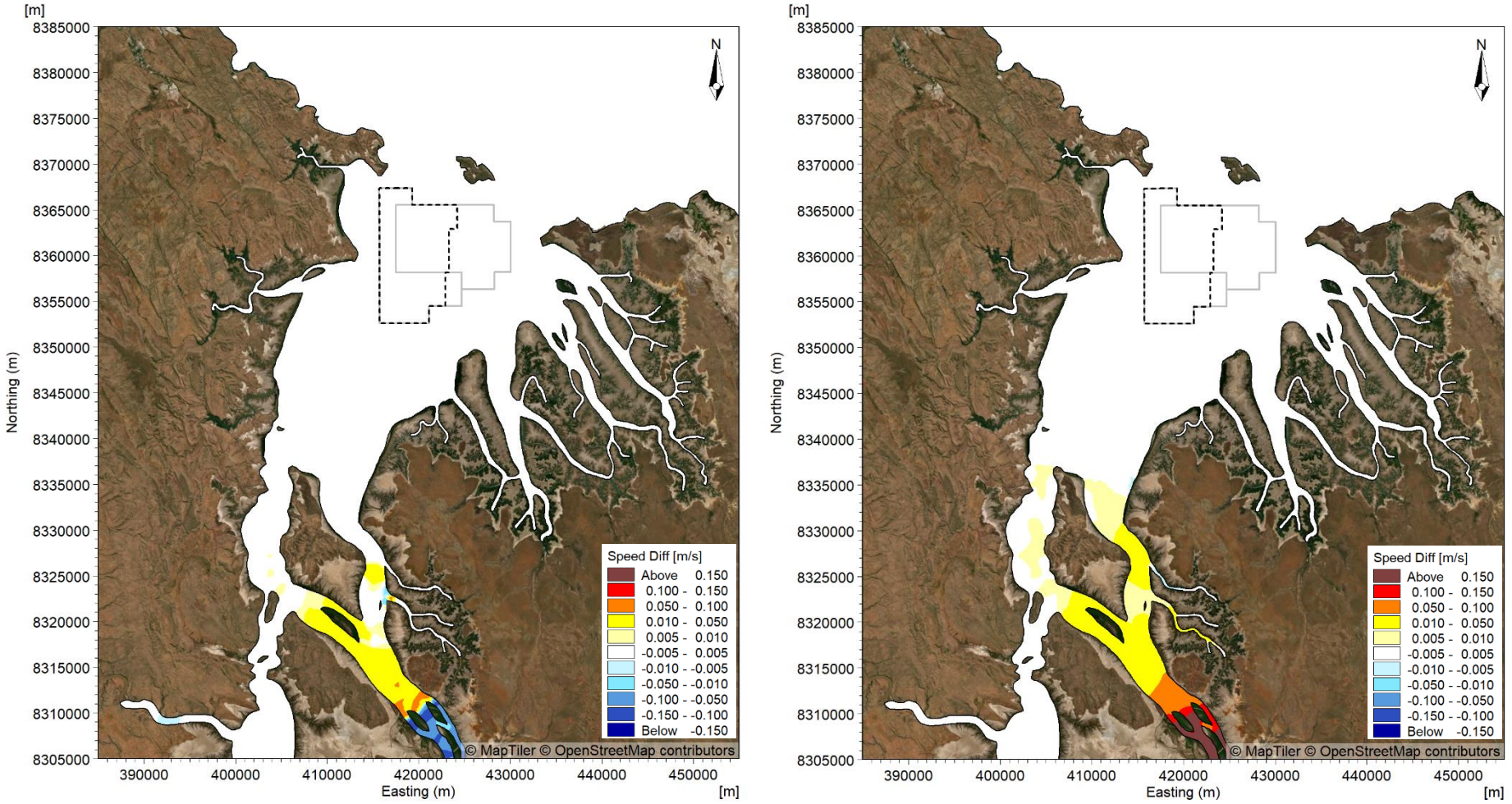
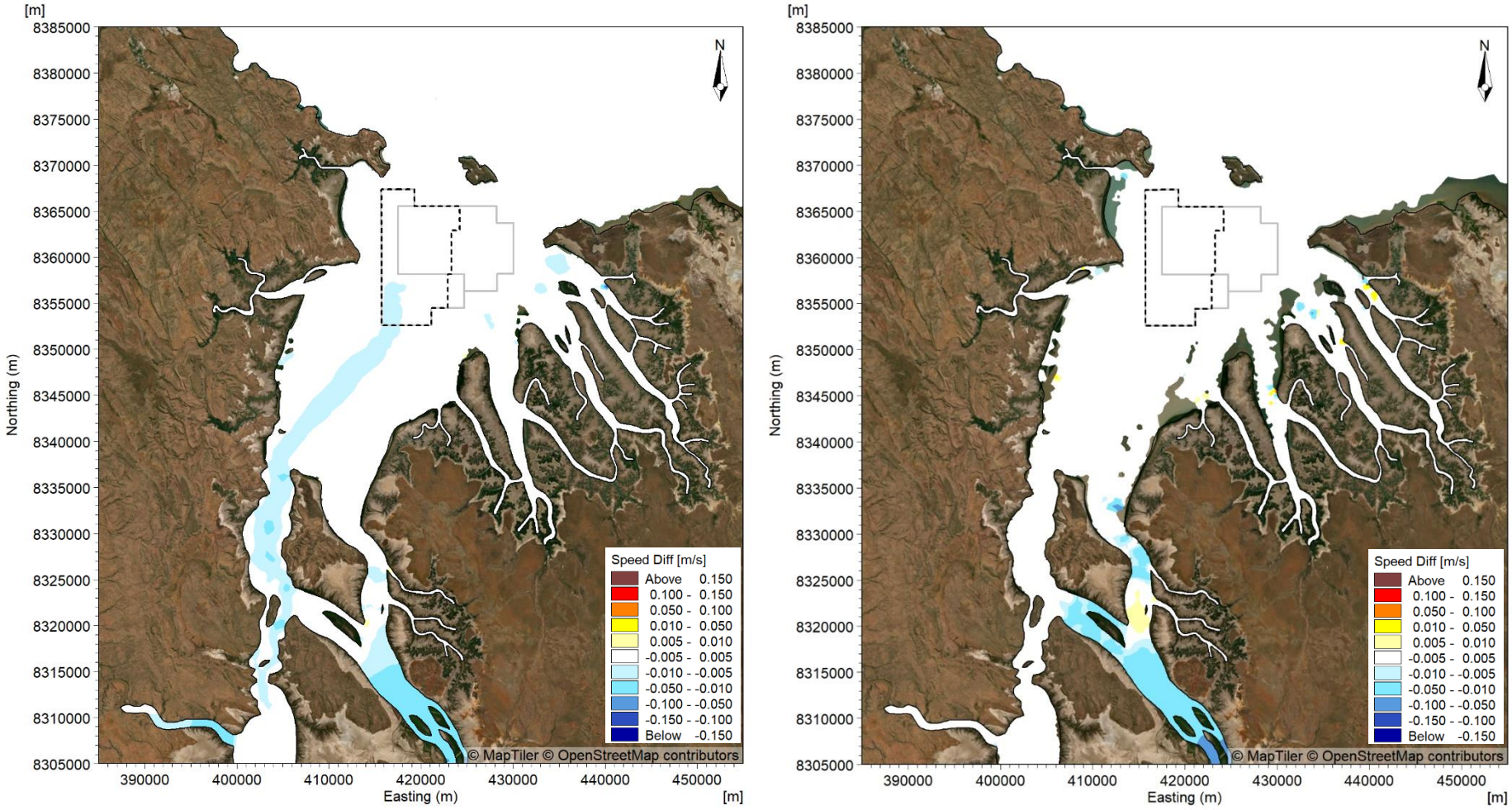


Figure 141. Modelled difference (compared to existing case) in current speed at peak flood (left) and high water (right) for the Pre-European Settlement scenario during a spring tide in the dry season.



Peak Ebb

Low Water

Figure 142. Modelled difference (compared to existing case) in current speed at peak ebb (left) and low water (right) for the Pre-European Settlement scenario during a spring tide in the dry season.

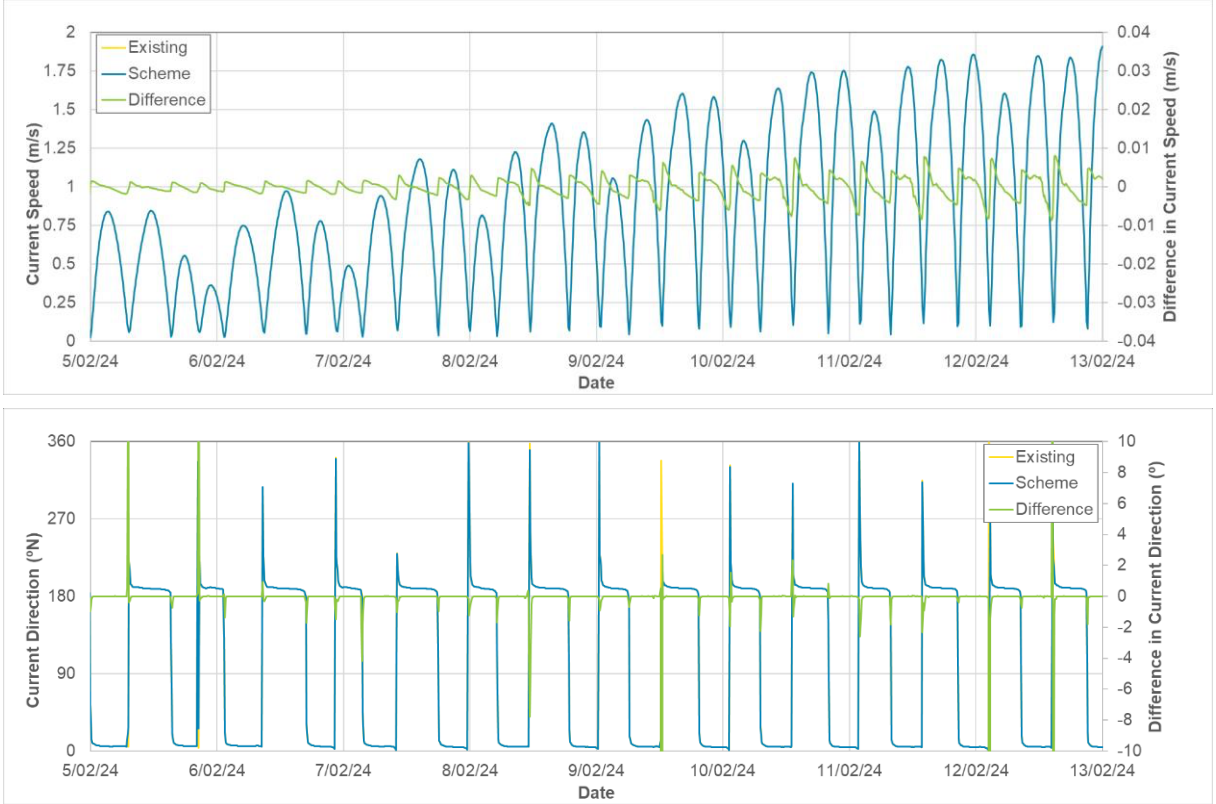


Figure 143. Timeseries showing the modelled change in current speed and direction at AWAC-08 during the wet season from neap to spring tides due to 15 years (70 million m^3) of sand sourcing (Scheme).

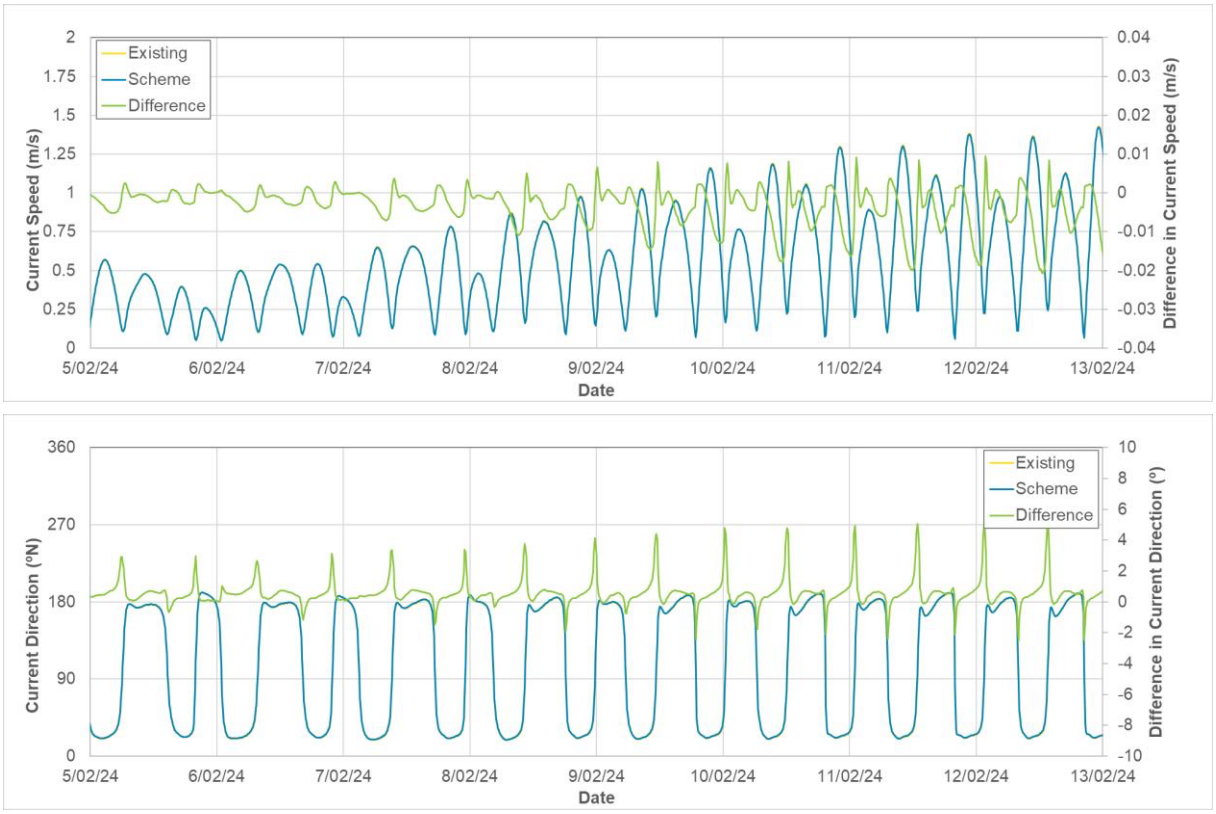


Figure 144. Timeseries showing the modelled change in current speed and direction at AWAC-11 during the wet season from neap to spring tides due to 15 years (70 million m^3) of sand sourcing (Scheme).

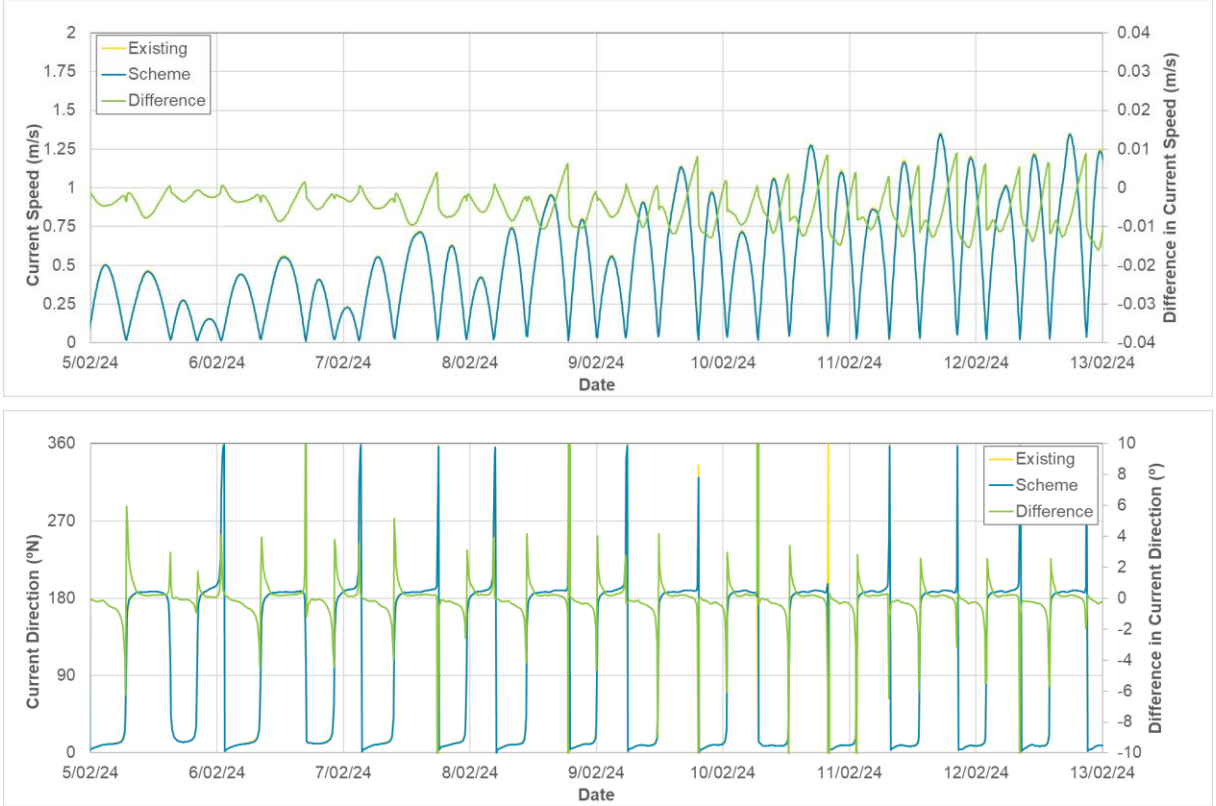


Figure 145. Timeseries showing the modelled change in current speed and direction at AWAC-01 during the wet season from neap to spring tides due to 15 years (70 million m^3) of sand sourcing (Scheme).

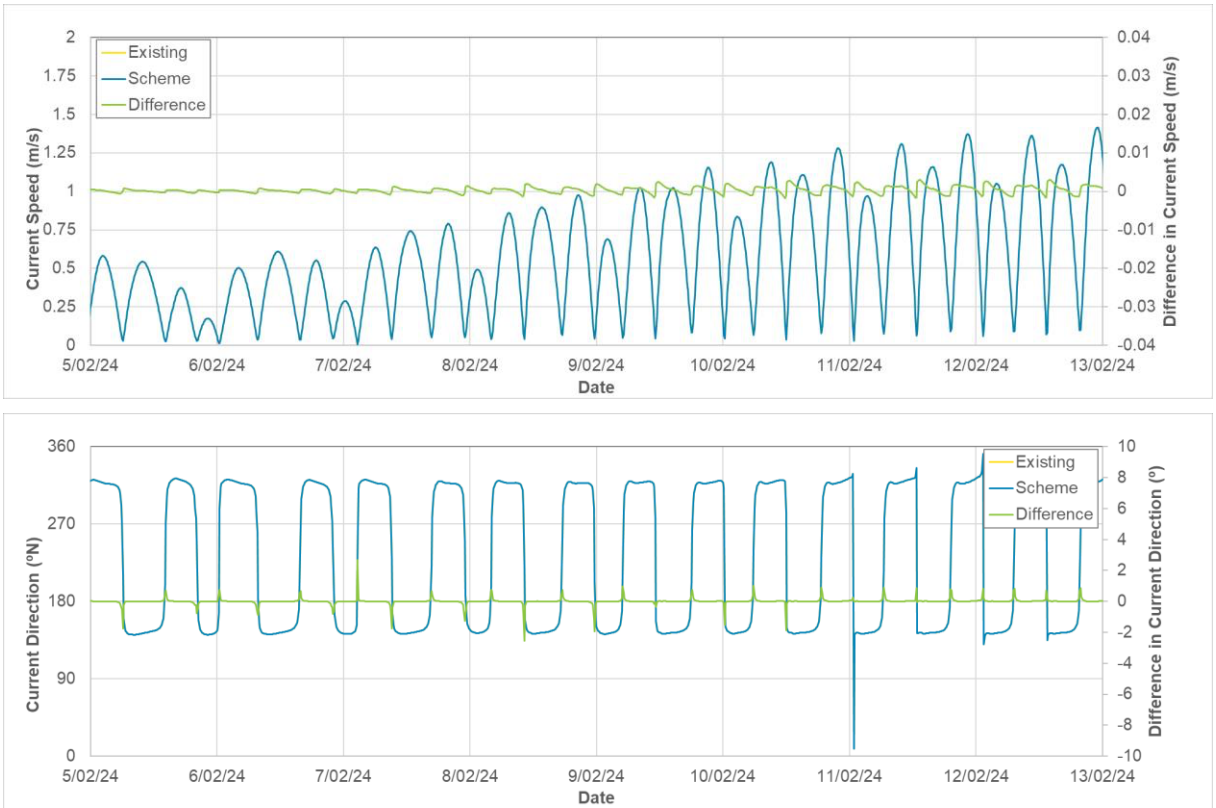
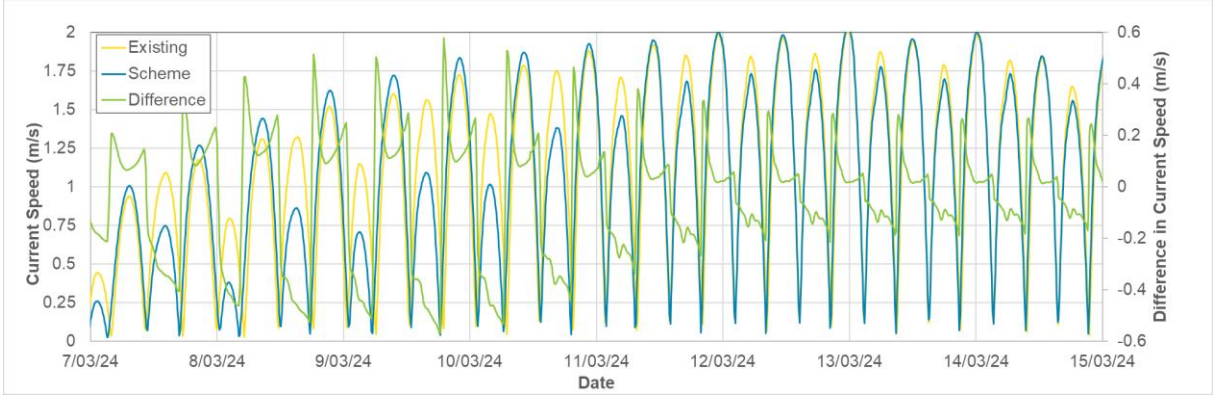


Figure 146. Timeseries showing the modelled change in current speed and direction at AWAC-09 during the wet season from neap to spring tides due to 15 years (70 million m^3) of sand sourcing (Scheme).



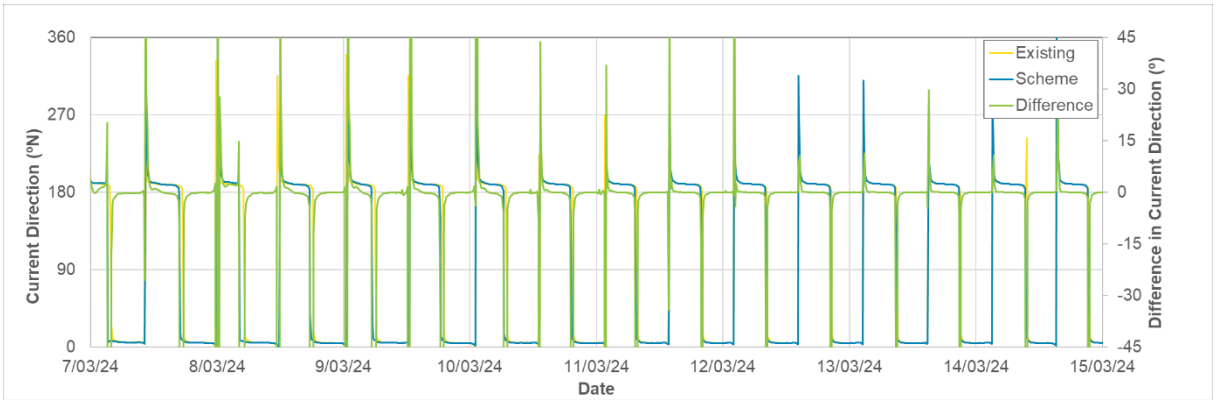
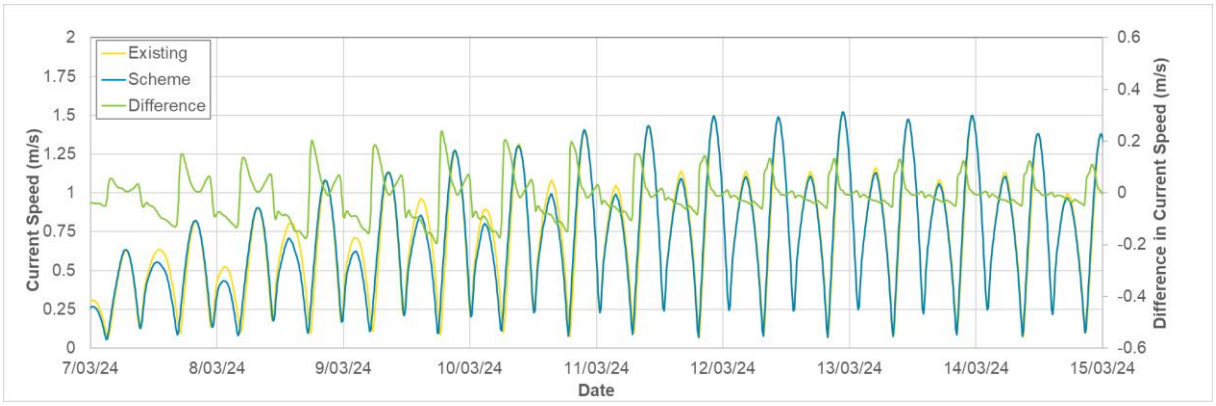


Figure 147. Timeseries showing the modelled difference in current speed and direction at AWAC-08 during the wet season from neap to spring tides between the Pre-European scenario (Scheme) and the existing case.



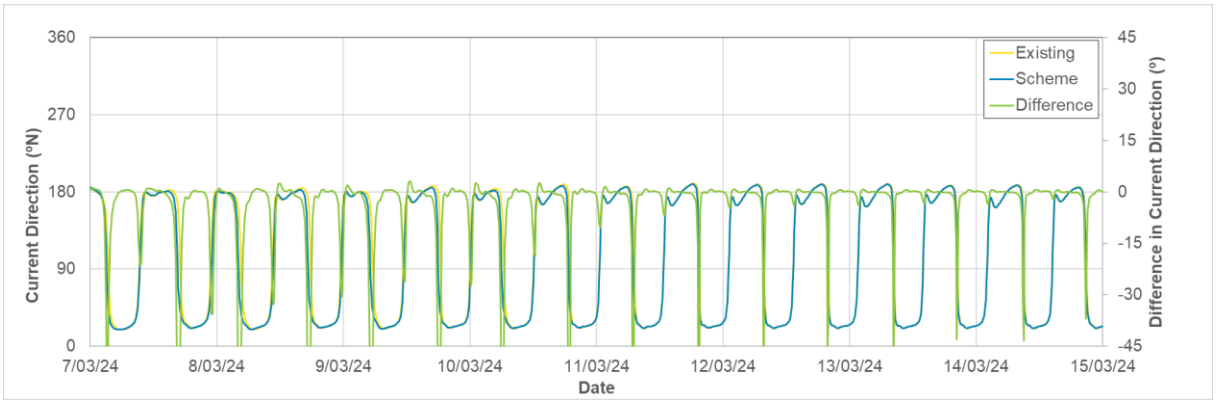


Figure 148. Timeseries showing the modelled difference in current speed and direction at AWAC-11 during the wet season from neap to spring tides for the between the Pre-European scenario (Scheme) and the existing case.

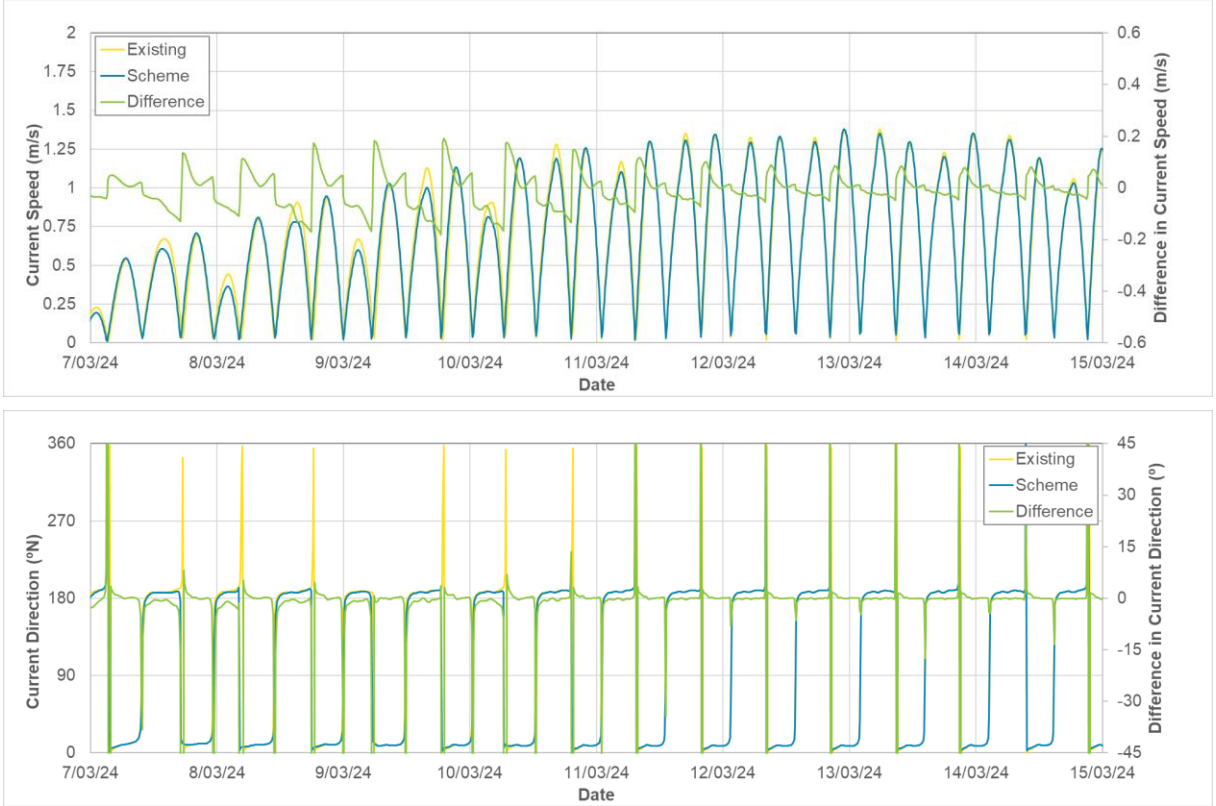


Figure 149. Timeseries showing the modelled difference in current speed and direction at AWAC-01 during the wet season from neap to spring tides between the Pre-European scenario (Scheme) and the existing case.

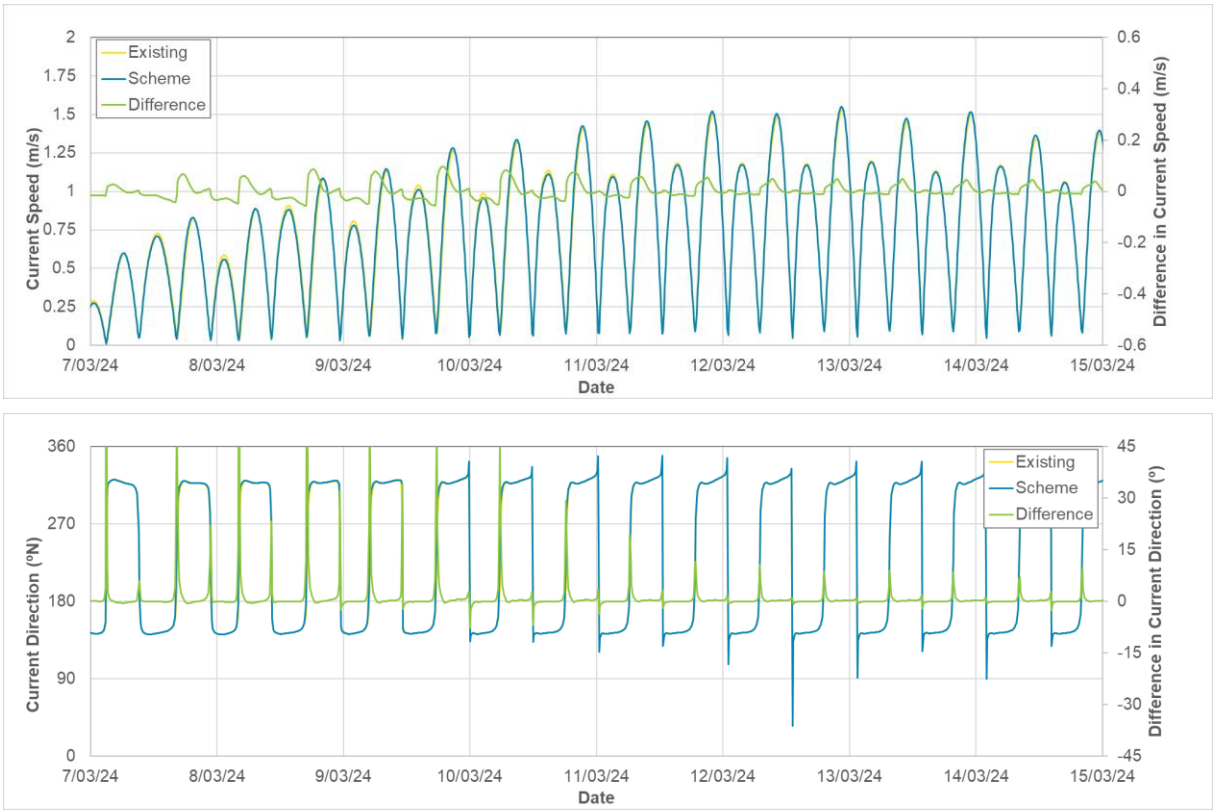


Figure **150**. Timeseries showing the modelled difference in current speed and direction at AWAC-09 during the wet season from neap to spring tides between the Pre-European scenario (Scheme) and the existing case.

Table 16. Statistics of the modelled change in current speed due to the 15 years (70 million m^3) of sand sourcing scenario and the pre-European settlement scenario relative to the existing case at the 11 AWAC sites.

Site	AWAC-01 (in POA)	AWAC-02 (in POA)	AWAC-03 (in POA)	AWAC-04 (in POA)	AWAC-05	AWAC-06	AWAC-07	AWAC-08	AWAC-09	AWAC-10	AWAC-11
15 years of Sand Sourcing Scenario Current Speed Change (m/s)											
Maximum	0.01	0.03	0.01	0.01	0.01	0.01	0.01	0.01	0.00	0.01	0.01
99th %ile	0.01	0.02	0.01	0.01	0.01	0.00	0.00	0.01	0.00	0.00	0.01
90th %ile	0.00	0.01	0.00	0.00	0.00	0.00	0.00	0.00	0.00	0.00	0.00
80th %ile	0.00	0.00	0.00	0.00	0.00	0.00	0.00	0.00	0.00	0.00	0.00
50th %ile	-0.01	-0.01	-0.01	-0.01	0.00	0.00	0.00	0.00	0.00	0.00	0.00
20th %ile	-0.01	-0.02	-0.01	-0.02	0.00	0.00	0.00	0.00	0.00	0.00	-0.01
10th %ile	-0.01	-0.02	-0.01	-0.02	-0.01	-0.01	0.00	0.00	0.00	0.00	-0.01
1st %ile	-0.01	-0.03	-0.02	-0.03	-0.01	-0.01	0.00	-0.01	0.00	-0.01	-0.02
Minimum	-0.02	-0.04	-0.02	-0.04	-0.01	-0.01	0.00	-0.01	0.00	-0.01	-0.02
Current Speed Change since European Settlement (m/s)											
Maximum	-0.19	-0.06	-0.21	-0.17	-0.08	-0.17	-0.07	-0.58	-0.10	-0.06	-0.24
99th %ile	-0.09	-0.02	-0.09	-0.08	-0.04	-0.08	-0.04	-0.26	-0.05	-0.04	-0.12
90th %ile	-0.02	-0.01	-0.02	-0.01	-0.01	-0.01	-0.01	-0.06	-0.01	-0.01	-0.02
80th %ile	0.00	0.00	-0.01	0.00	0.00	0.00	0.00	-0.02	0.00	0.00	0.00
50th %ile	0.00	0.00	0.00	0.00	0.00	0.00	0.00	0.00	0.00	0.00	0.00
20th %ile	0.01	0.00	0.01	0.01	0.00	0.01	0.00	0.05	0.01	0.00	0.01
10th %ile	0.03	0.01	0.02	0.02	0.01	0.02	0.01	0.12	0.01	0.01	0.03
1st %ile	0.10	0.04	0.09	0.09	0.02	0.08	0.02	0.43	0.03	0.04	0.12
Minimum	0.18	0.06	0.17	0.13	0.04	0.15	0.04	0.57	0.06	0.06	0.20

Note: AWAC-02 is actually located 450 m to the east of the POA, but as it is so close to the POA boundary the changes are representative of changes within the POA.
The inverse of the pre-European Settlement changes reflect the changes that European settlement (i.e. construction of the Ord River dams) has had on the current speeds.

Table 17. Percent change in peak flood and ebb current speed relative to the existing case due to 15 years (70 million m^3) of sand sourcing and pre-European settlement during a spring tide with a high river discharge.

Location	Flood Current Speed Change (%)		Ebb Current Speed Change (%)	
	Sand Sourcing (15yrs)	Pre-European Settlement	Sand Sourcing (15yrs)	Pre-European Settlement
AWAC-01 (in POA)	-0.6%	-11.3%	-1.2%	2.2%
AWAC-02 (in POA)	-2.0%	-3.8%	-1.5%	-1.4%
AWAC-03 (in POA)	-1.0%	-8.3%	-1.4%	1.9%
AWAC-04 (in POA)	-2.1%	-7.7%	-2.1%	0.1%
AWAC-05	-1.5%	-2.2%	0.3%	-1.6%
AWAC-06	-0.4%	-5.0%	-0.5%	-0.7%
AWAC-07	0.0%	0.6%	0.0%	-2.3%
AWAC-08	0.0%	-11.7%	0.1%	6.3%
AWAC-09	0.1%	-2.7%	0.1%	1.4%
AWAC-10	-0.1%	-3.2%	-0.4%	0.5%
AWAC-11	-0.5%	-11.1%	-0.5%	0.8%

Note: AWAC-02 is actually located 450 m to the east of the POA, but as it is so close to the POA boundary the changes are representative of changes within the POA.
The inverse of the pre-European Settlement changes reflect the changes that European settlement (i.e. construction of the Ord River dams) has had on the current speeds.

4.2.2. Waves

This section presents a summary of the modelled changes to wave conditions for specific scenarios and metocean conditions, to provide an overview of the changes. Plots of the modelled changes for all the scenarios and during all metocean conditions are provided in Appendix B.

Spatial maps showing the modelled change in H_s, T_p and wave direction during the peak of the largest wave event over the two-month (60 days) wet season simulation (at AWAC-01 in the POA, H_s = 1.25, T_p = 6.7 s, Direction = 358º) and during the peak of TC Marcus (at AWAC-01 in the POA, H_s = 2.04, T_p = 8.5 s, Direction = 64º) due to 5 years and 15 years of sand sourcing are shown in Figure 151 to Figure 156. During the dry season, transitional season and in 100 years from today after 15 years, the differences due to the sand sourcing were either assessed to be similar or less, and so plots for these cases are not shown here but are included in Appendix B. The plots show the following:

- The changes in H_s due to the 5 years and 15 years of sand sourcing were modelled to be relatively minor and localised to within the POA and upstream (south of), meaning that all changes are constrained within CG. The changes to H_s for both scenarios were predominantly extremely minor increases in H_s, but some extremely minor reductions were also assessed. The changes in H_s due to 5 years of sand sourcing were modelled to be less than ± 0.005 m (5 mm), while for 15 years of sand sourcing they were up to ± 0.01 m (10 mm). The changes are therefore considered to be negligible in an environmental context (i.e. they will not cause impacts on dependent environmental resources and values).

- Both 5 years and 15 years of sand sourcing were assessed to only result in very minor and localised changes to T_p, with changes of less than 0.05 s.

- Modelled changes in wave direction were less than ± 0.5º for the 5 years of sand sourcing scenario and for the 15 years of sand sourcing scenario the changes were predominantly less than ± 0.5º. For the 15 years of sand sourcing scenario the largest changes in wave direction were less than 2º (1º for TC Marcus), with these changes being in areas of shallow bathymetry, meaning that deep water changes in direction are amplified by local wave refraction.

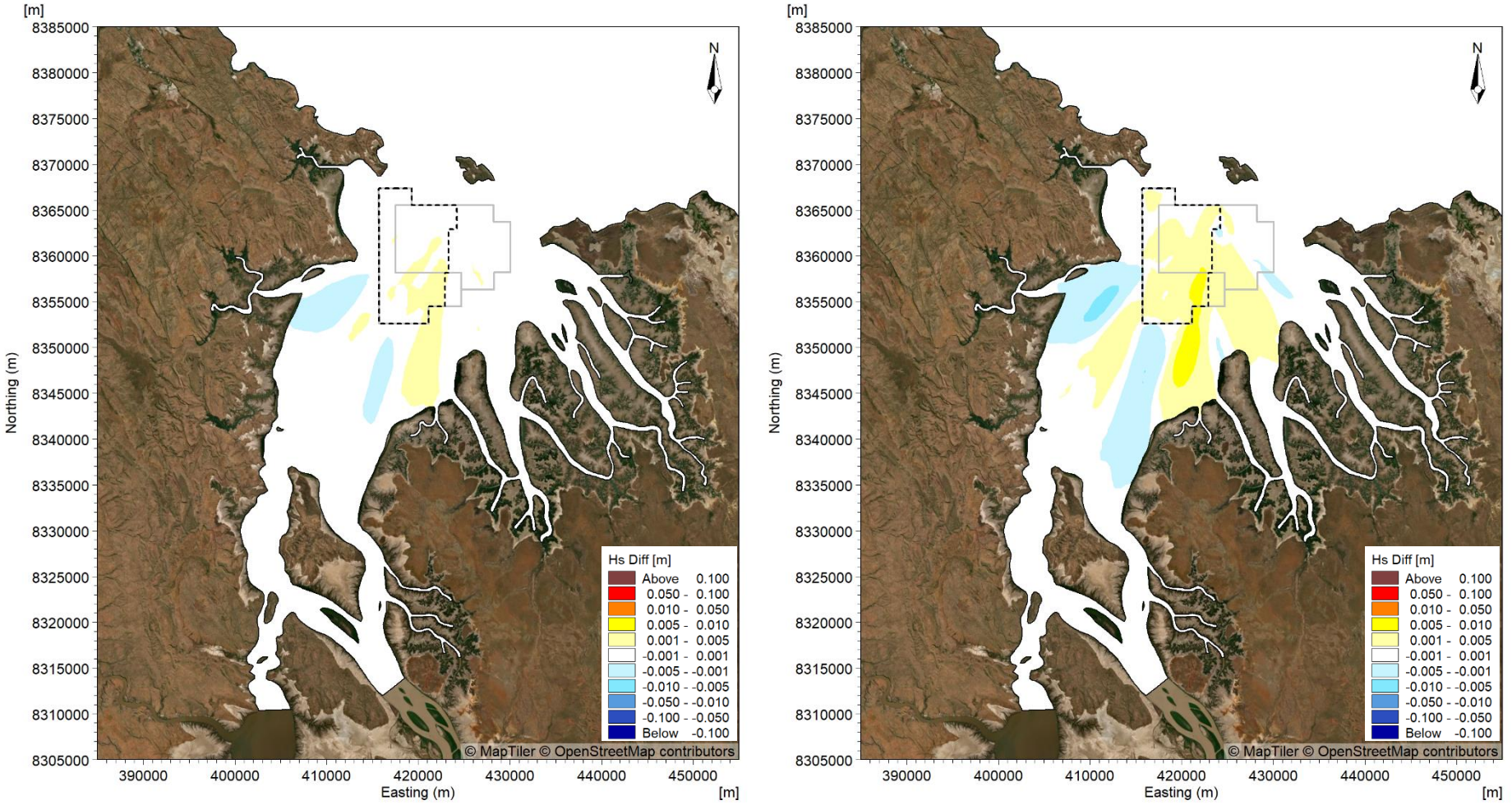
The plots show that the modelled changes to the wave conditions as a result of the 5 years and 15 years of sand sourcing were negligible, with none of the changes likely to result in a noticeable change in sediment transport within CG. However, further analysis of the changes in H_s (as this is the parameter which has the greatest potential to influence sediment transport) are presented as timeseries and statistical analysis below.

To better understand the changes in H_s due to the sand sourcing after 15 years, timeseries plots of the modelled change during the wet season, dry season, transitional season and TC Marcus are shown at the sites within the areas of changes shown by the maps in Figure 157 to Figure 164. The plots show the following:

- There was no change in H_s between the existing case and the 15 years of sand sourcing scenario for the majority of the time, but with short duration, very minor increases and decreases in H_s occurring during specific wave conditions as a result of the sand sourcing.
- During all three seasons the changes in H_s as a result of the 15 years of sand sourcing were typically less than ± 0.005 m (5 mm), although some wave conditions resulted in changes of between ± 0.005 to 0.01 m (5 mm to 10 mm).
- The largest (but still very minor) modelled changes in H_s occurred during the wet season, with increases in H_s of 0.005 to 0.01 m (5 mm to 10 mm) within the POA (AWAC-03) during larger wave events with a peak H_s of more than 0.9 m.

The modelled H_s at each site has been analysed for the existing case, 5 years of sand sourcing and 15 years of sand sourcing to calculate percentiles. The percentiles for the sand sourcing scenarios are compared with the percentiles for the existing case to show the modelled percentage change in H_s relative to the existing case for each of the metocean periods. The change in H_s due to the sand sourcing is shown at the sites where changes in H_s were modelled in Table 18 to Table 21. The tables show modelled changes in H_s outside of the POA (AWAC-02, AWAC-07 and AWAC-11) of up to 0.6% for all percentiles and less than 0.5% for the 50th percentile and above.

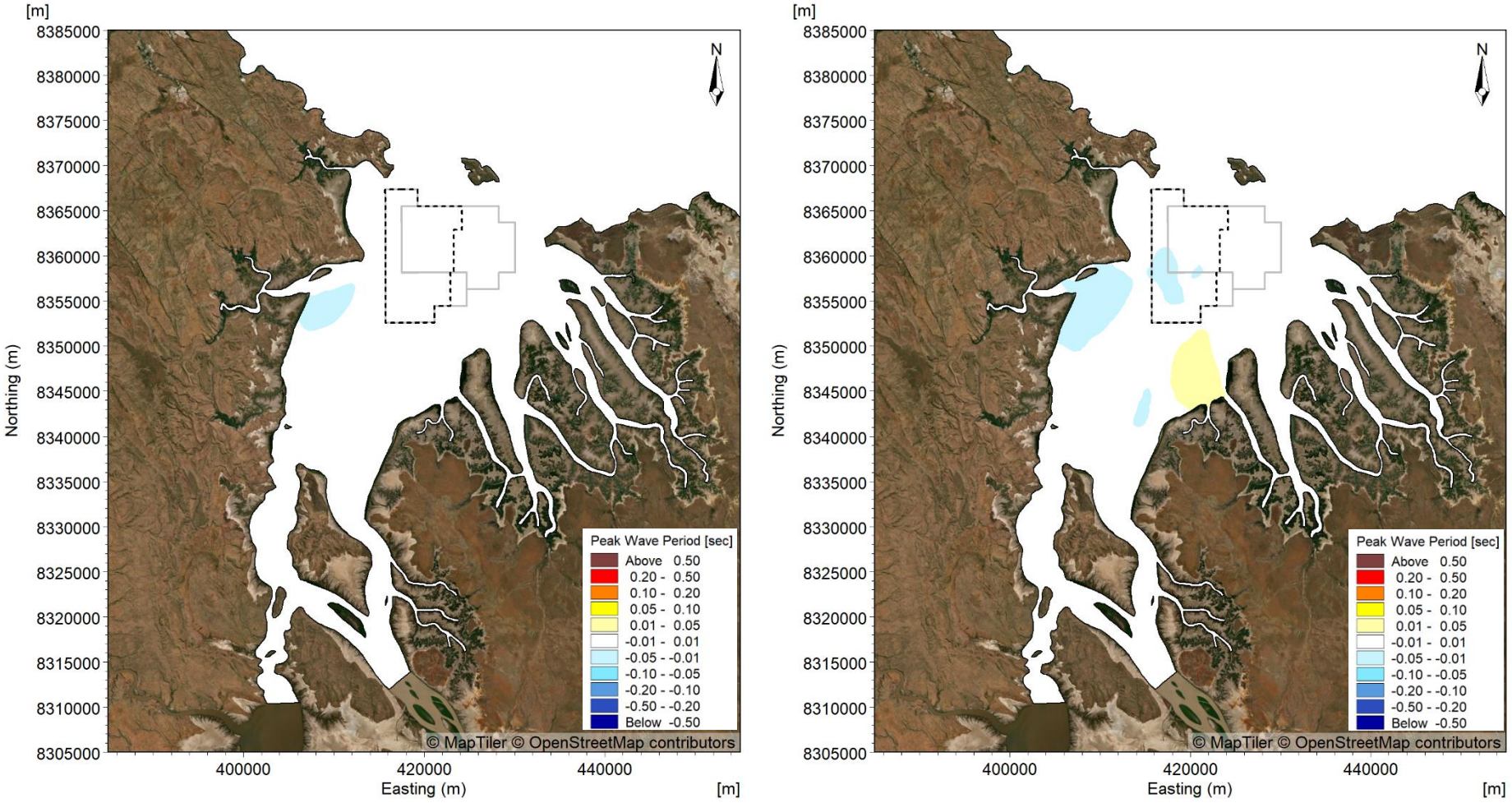
The largest (but still very minor) change in H_s was within the POA, with an increase in the 99th percentile of 0.62% at AWAC-03 during the wet season. The largest modelled increase in the 99th percentile H_s outside of the POA was 0.31% at AWAC-11 during TC Marcus. The statistics confirm that both the 5-year and 15-year sand sourcing scenarios were only assessed to result in very minor changes in H_s and that this is the case for the range in wave heights experienced during the different seasons and during tropical cyclones.



5yr Sand Sourcing

15yr Sand Sourcing

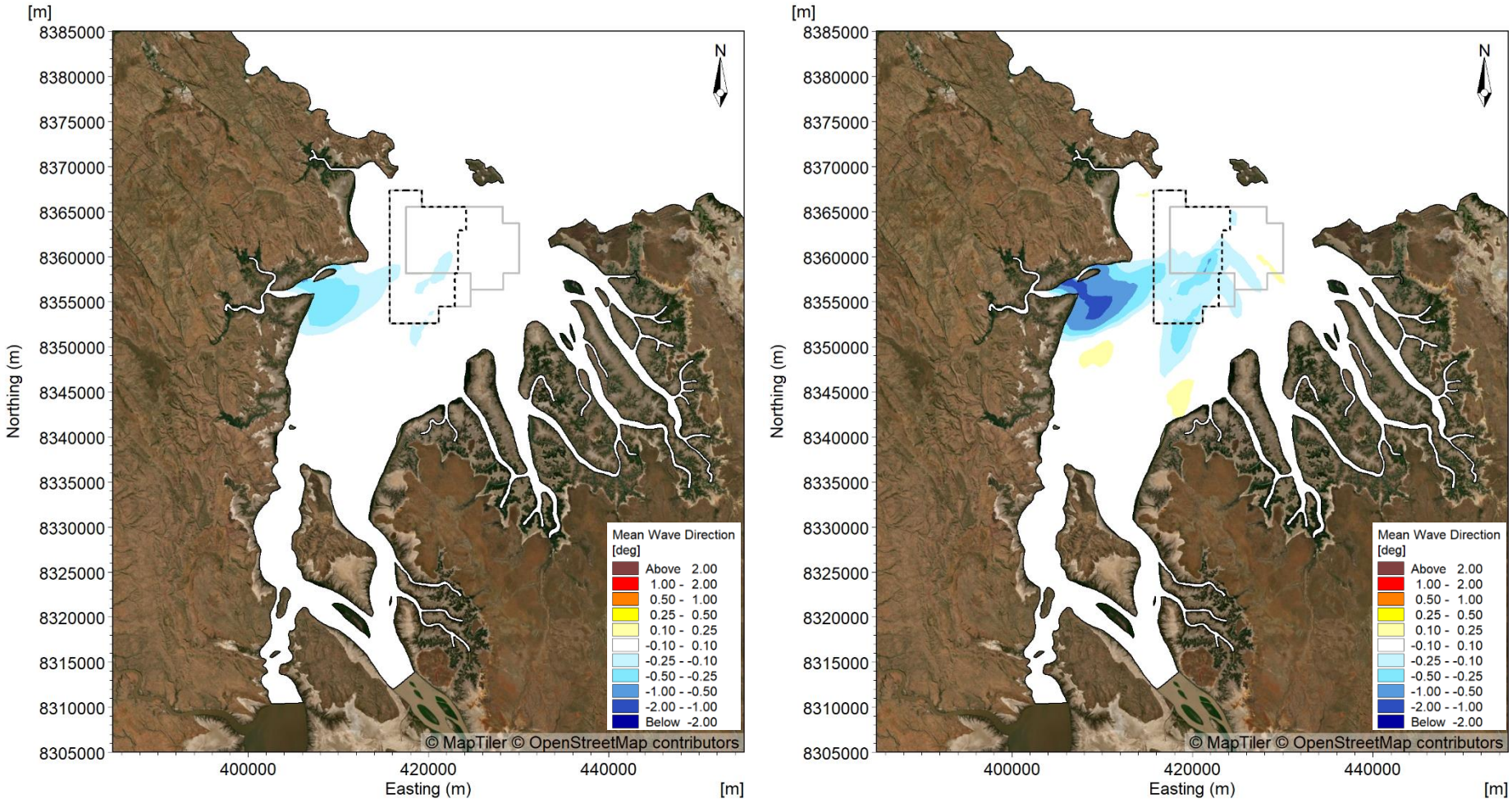
Figure 151. Modelled change in H_s during the largest wave event in the wet season period due to 5 years (23 million m^3) of sand sourcing (left) and 15 years (70 million m^3) of sand sourcing (right).



5yr Sand Sourcing

15yr Sand Sourcing

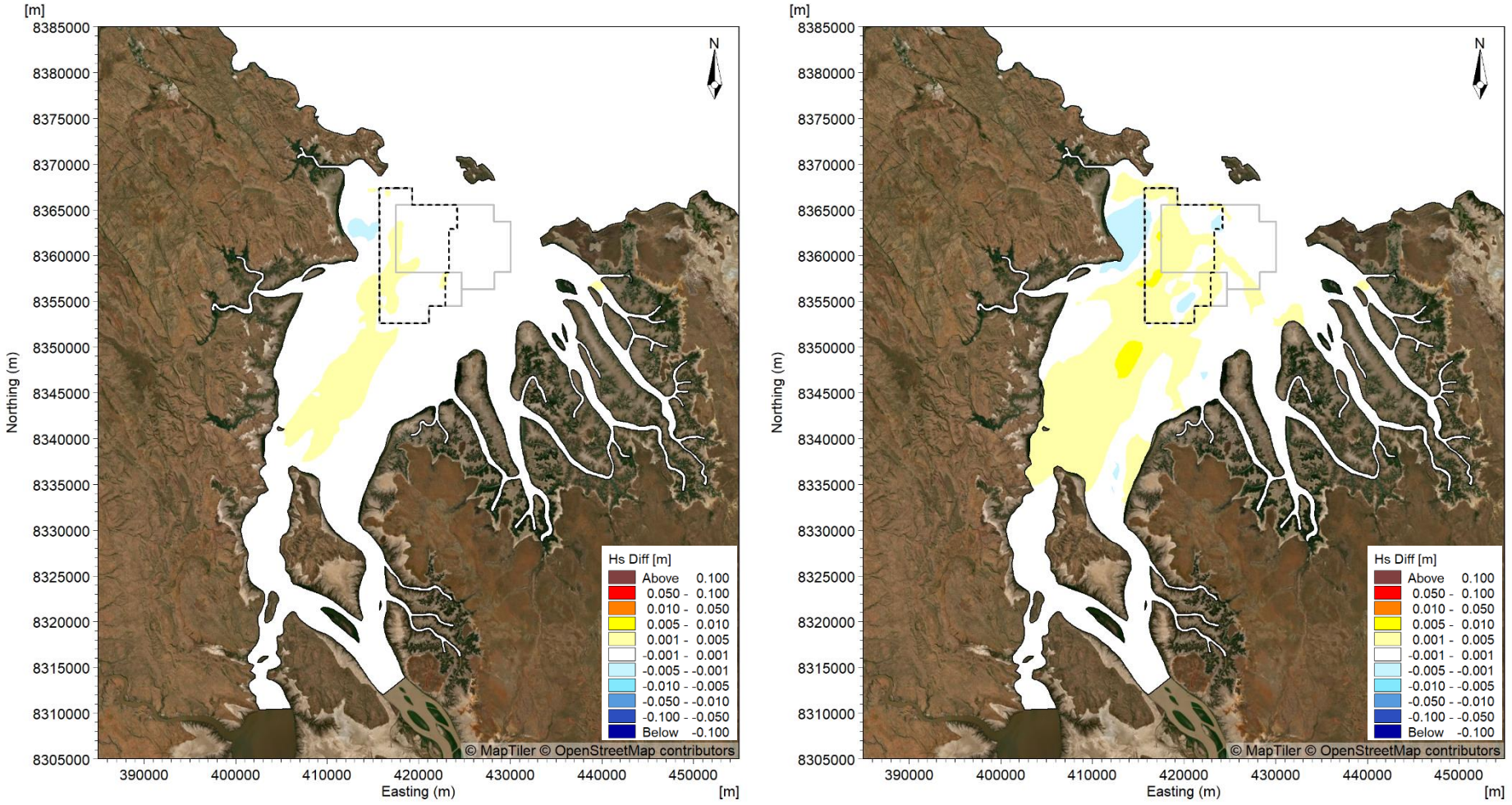
Figure 152. Modelled change in T_p during the largest wave event in the wet season period due to 5 years (23 million m^3) of sand sourcing (left) and 15 years (70 million m^3) of sand sourcing (right).



5yr Sand Sourcing

15yr Sand Sourcing

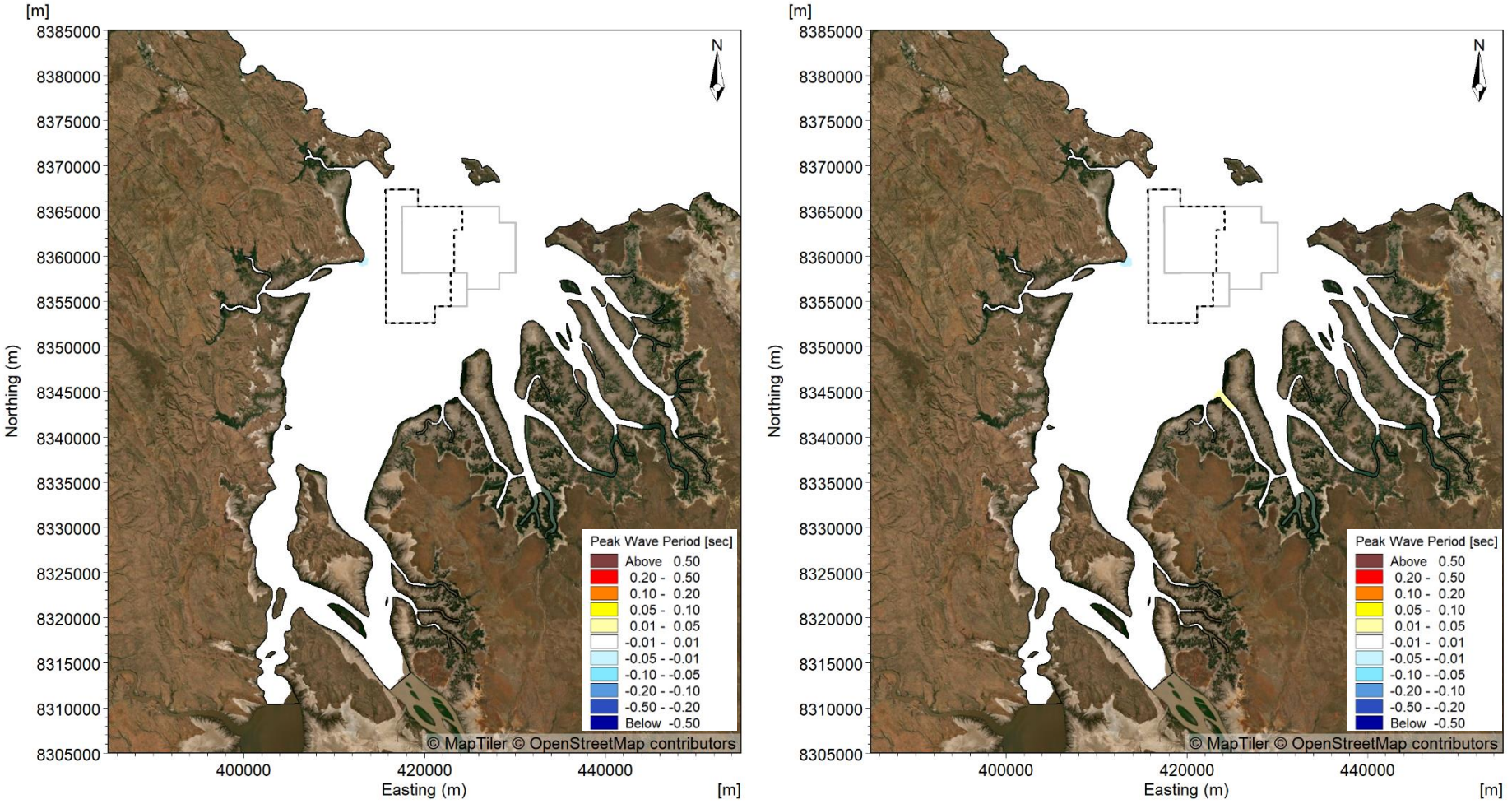
Figure 153. Modelled change in wave direction during the largest wave event in the wet season period due to 5 years (23 million m^3) of sand sourcing (left) and 15 years (70 million m^3) of sand sourcing (right).



5yr Sand Sourcing

15yr Sand Sourcing

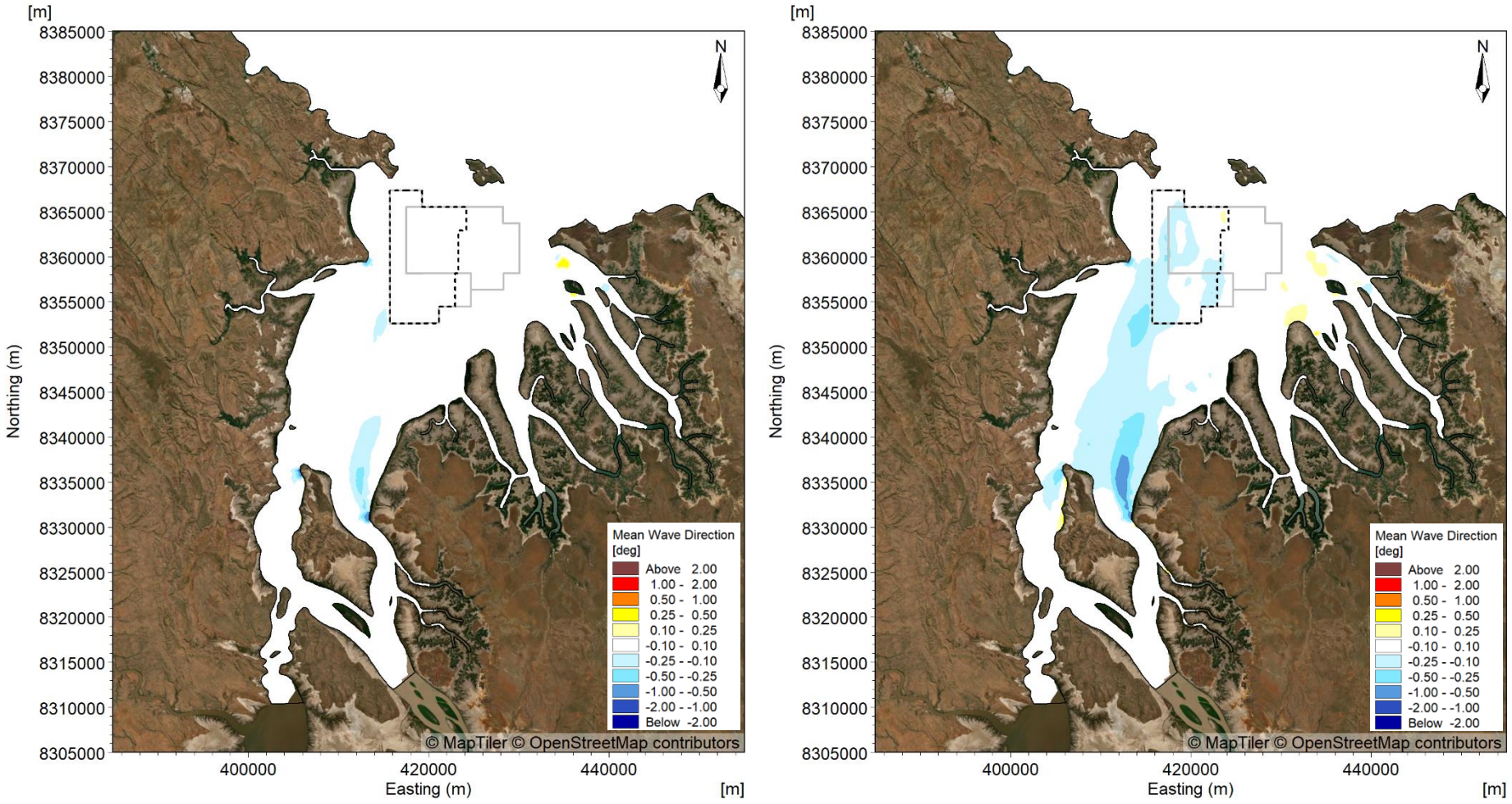
Figure 154. Modelled change in H_s during the peak of TC Marcus due to 5 years (23 million m^3) of sand sourcing (left) and 15 years (70 million m^3) of sand sourcing (right).



5yr Sand Sourcing

15yr Sand Sourcing

Figure 155. Modelled change in T_p during the peak of TC Marcus in the wet season period due to 5 years (23 million m^3) of sand sourcing (left) and 15 years (70 million m^3) of sand sourcing (right).



5yr Sand Sourcing

15yr Sand Sourcing

Figure 156. Modelled change in wave direction during the peak of TC Marcus in the wet season period due to 5 years (23 million m3) of sand sourcing (left) and 15 years (70 million m^3) of sand sourcing (right).

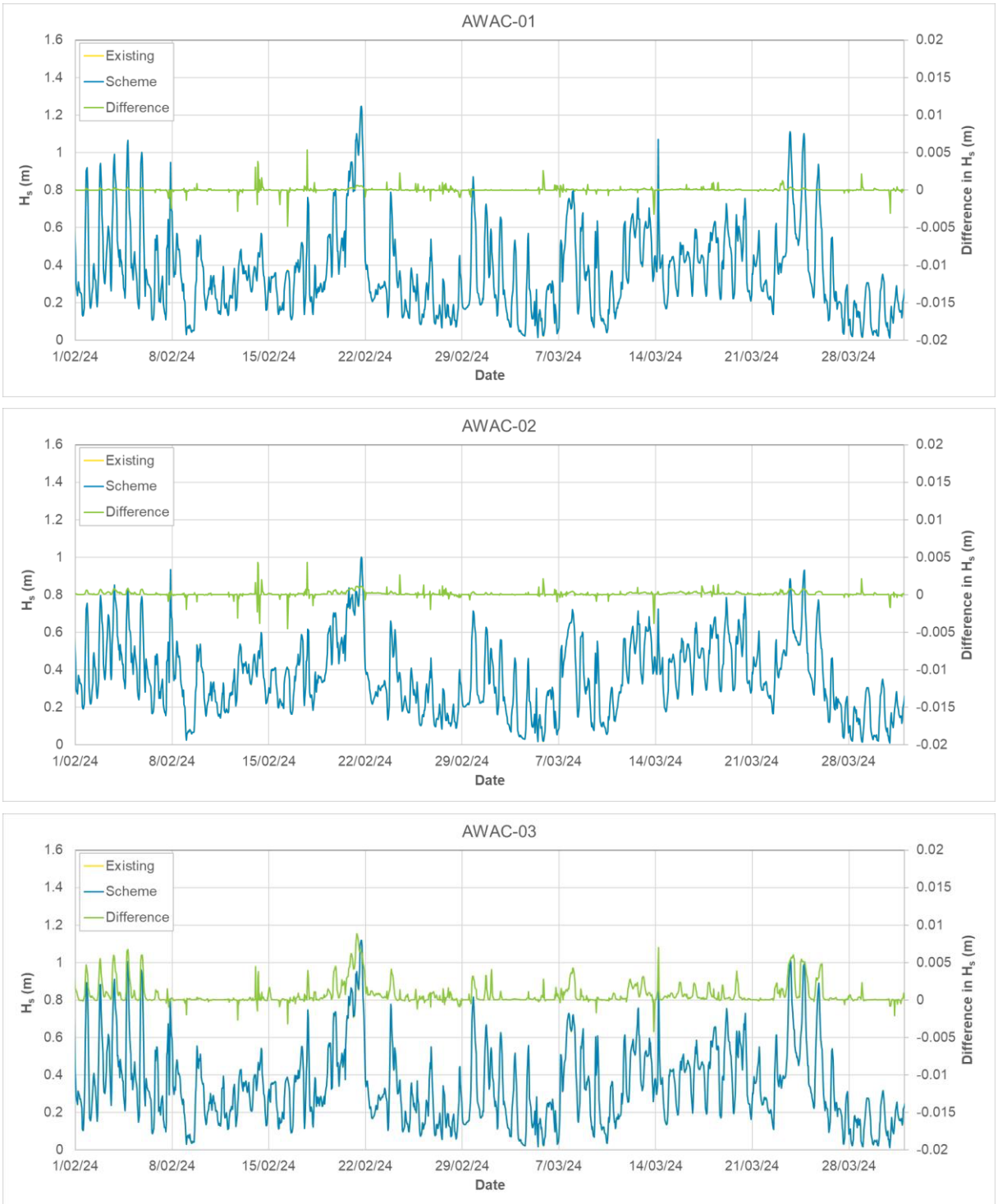


Figure 157. Timeseries showing the modelled change in H_s over the two-month (60 days) wet season simulation due to 15 years of sand sourcing (Scheme) at sites AWAC-01 to AWAC-03.



Figure 158. Timeseries showing the modelled change in H_s over the two-month (60 days) wet season simulation due to 15 years of sand sourcing (Scheme) at sites AWAC-04, AWAC-07 to AWAC-11.



Figure 159. Timeseries showing the modelled change in H_s over the two-month (61 days) dry season simulation due to 15 years of sand sourcing (Scheme) at sites AWAC-01 to AWAC-03.



Figure 160. Timeseries showing the modelled change in H_s over the two-month (61 days) dry season simulation due to 15 years of sand sourcing (Scheme) at sites AWAC-04, AWAC-07 to AWAC-11.



Figure 161. Timeseries showing the modelled change in H_s over the two-month (61 days) transitional season simulation due to 15 years of sand sourcing (Scheme) at sites AWAC-01 to AWAC-03.



Figure 162. Timeseries showing the modelled change in H_s over the two-month (61 days) transitional season simulation due to 15 years of sand sourcing (Scheme) at sites AWAC-04, AWAC-07 to AWAC-11.

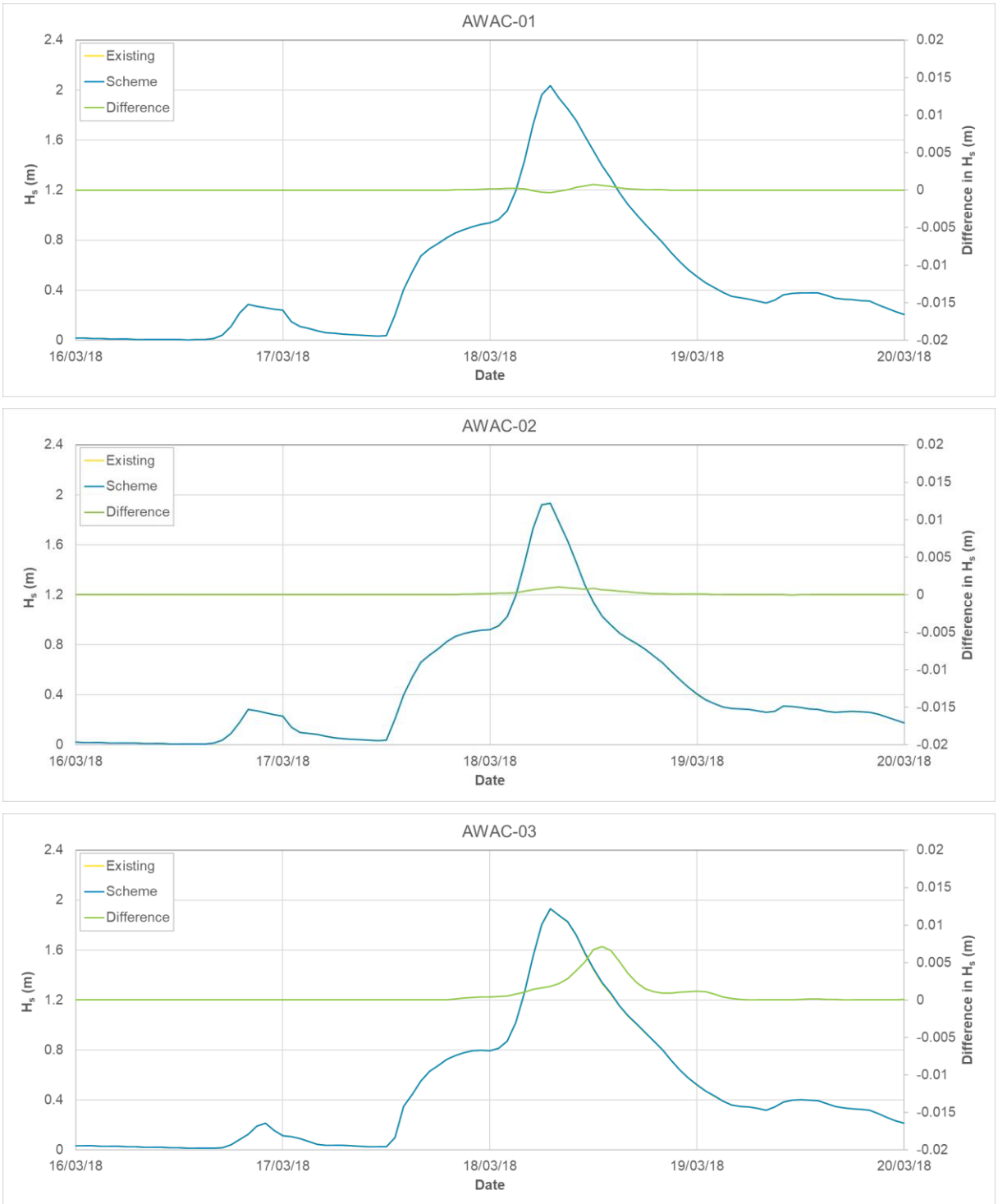


Figure 163. Timeseries showing the modelled change in H_s over the TC Marcus simulation due to 15 years (70 million m^3) of sand sourcing (Scheme) at sites AWAC-01 to AWAC-03.

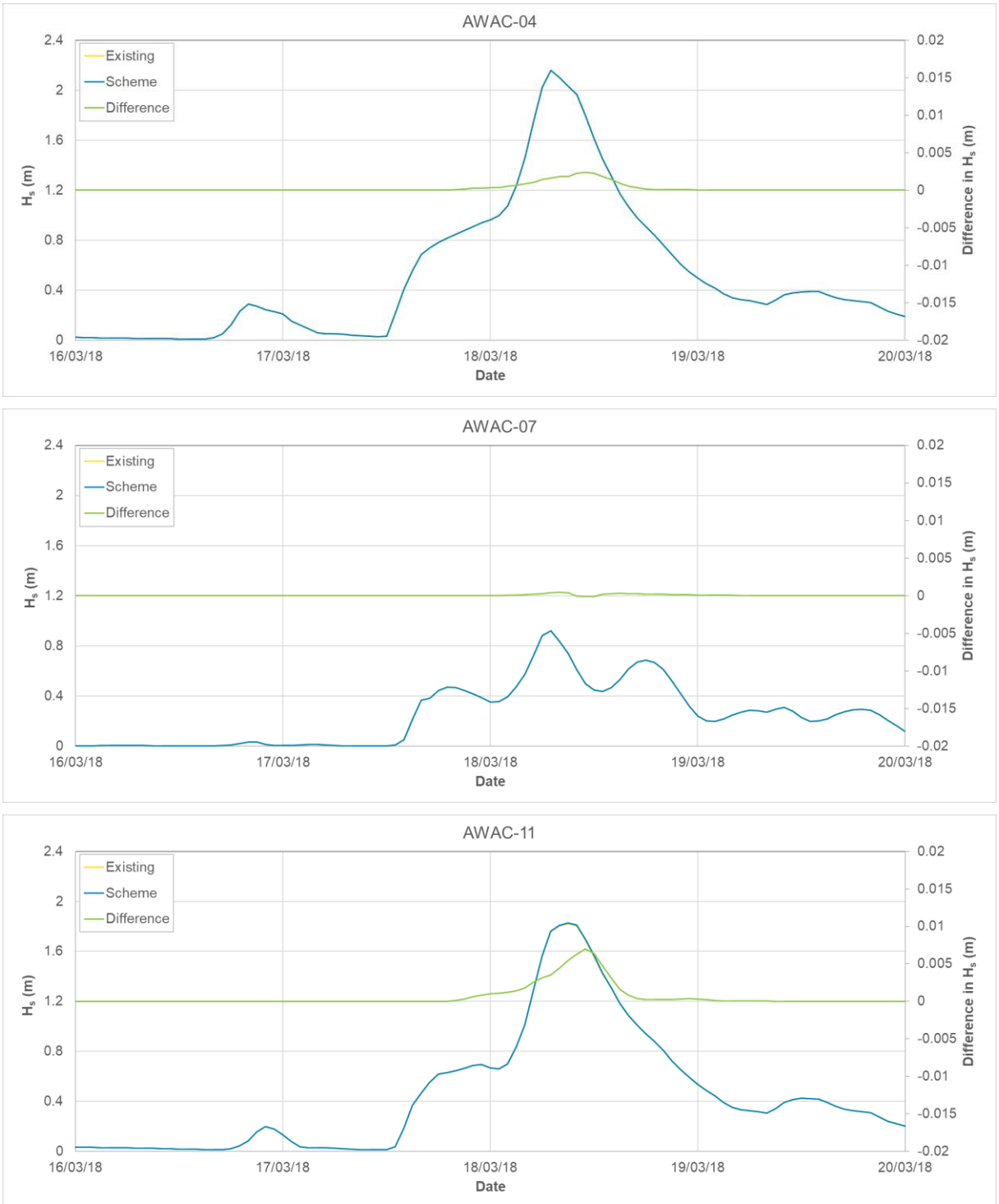


Figure 164. Timeseries showing the modelled change in H_s over the TC Marcus simulation due to 15 years (70 million m^3) of sand sourcing (Scheme) at sites AWAC-04, AWAC-07 to AWAC-11.

Table 18. Statistics of the modelled change in H_s during the wet season due to 5 years (23 million m^3) and 15 years (70 million m^3) of sand sourcing relative to the existing case.

Site	Existing Case AWAC-07 H_s (m)	Existing Case AWAC-01 H_s (m)	AWAC-01 (in POA)	AWAC-02 (in POA)	AWAC-03 (in POA)	AWAC-04 (in POA)	AWAC-07	AWAC-11
5 years of Sand Sourcing Scenario H_s Change (%)								
99th %ile	0.60	1.07	0.01%	0.03%	0.22%	0.03%	0.07%	0.06%
95th %ile	0.48	0.80	0.01%	0.01%	0.19%	0.01%	0.04%	-0.10%
90th %ile	0.42	0.67	0.01%	0.02%	0.27%	0.02%	0.09%	-0.04%
80th %ile	0.34	0.53	0.00%	0.01%	0.03%	0.00%	0.02%	0.00%
50th %ile	0.19	0.32	0.00%	0.02%	0.01%	0.11%	0.14%	-0.07%
20th %ile	0.10	0.17	-0.01%	0.01%	0.01%	0.02%	0.03%	-0.05%
10th %ile	0.07	0.12	0.05%	0.02%	-0.03%	0.02%	0.04%	0.04%
15 years of Sand Sourcing Scenario H_s Change (%)								
99th %ile	0.60	1.07	0.02%	0.09%	0.62%	0.08%	0.21%	0.09%
95th %ile	0.48	0.80	0.02%	0.04%	0.54%	0.03%	0.12%	-0.30%
90th %ile	0.42	0.67	0.02%	0.07%	0.51%	0.06%	-0.08%	-0.08%
80th %ile	0.34	0.53	0.07%	0.04%	0.10%	0.08%	0.06%	0.00%
50th %ile	0.19	0.32	0.00%	0.08%	0.01%	-0.17%	0.36%	0.01%
20th %ile	0.10	0.17	-0.01%	0.01%	0.02%	0.04%	0.03%	-0.06%
10th %ile	0.07	0.12	0.07%	0.08%	-0.09%	0.00%	0.00%	0.01%

Notes: the existing case H_s at AWAC-07 represents the smallest waves out of the sites shown in the table, while the H_s at AWAC-01 represents the largest waves.
AWAC-02 is actually located 450 m to the east of the POA, but as it is so close to the POA boundary the changes are representative of changes within the POA.

Table 19. Statistics of the modelled change in H_s during the dry season due to (23 million m^3) and 15 years (70 million m^3) of sand sourcing relative to the existing case.

Site	Existing Case AWAC-07 H_s (m)	Existing Case AWAC-01 H_s (m)	AWAC-01 (in POA)	AWAC-02 (in POA)	AWAC-03 (in POA)	AWAC-04 (in POA)	AWAC-07	AWAC-11
5 years of Sand Sourcing Scenario H_s Change (%)								
99th %ile	0.40	0.84	0.00%	0.00%	0.00%	0.00%	0.00%	0.02%
95th %ile	0.35	0.74	-0.05%	0.00%	0.01%	0.00%	0.00%	0.00%
90th %ile	0.32	0.67	0.33%	0.00%	0.00%	0.00%	0.00%	0.00%
80th %ile	0.27	0.57	0.00%	0.00%	0.05%	0.00%	0.00%	0.01%
50th %ile	0.18	0.40	-0.14%	-0.02%	-0.11%	-0.07%	0.00%	0.00%
20th %ile	0.11	0.24	-0.01%	0.00%	0.00%	-0.04%	-0.06%	0.00%
10th %ile	0.08	0.17	-0.02%	0.12%	0.00%	0.00%	0.00%	0.01%
15 years of Sand Sourcing Scenario H_s Change (%)								
99th %ile	0.40	0.84	0.01%	0.01%	0.00%	0.01%	0.00%	0.04%
95th %ile	0.35	0.74	0.01%	0.00%	0.02%	0.01%	0.00%	0.01%
90th %ile	0.32	0.67	0.13%	0.00%	0.00%	0.00%	0.00%	-0.10%
80th %ile	0.27	0.57	0.00%	0.00%	0.12%	0.00%	-0.03%	0.04%
50th %ile	0.18	0.40	0.00%	-0.02%	0.00%	-0.07%	0.00%	0.07%
20th %ile	0.11	0.24	0.07%	0.00%	0.00%	0.00%	0.20%	0.00%
10th %ile	0.08	0.17	0.06%	0.03%	0.00%	0.00%	0.00%	-0.03%

Notes: the existing case H_s at AWAC-07 represents the smallest waves out of the sites shown in the table, while the H_s at AWAC-01 represents the largest waves.
AWAC-02 is actually located 450 m to the east of the POA, but as it is so close to the POA boundary the changes are representative of changes within the POA.

Table 20. Statistics of the modelled change in H_s during the transitional season due to (23 million m^3) and 15 years (70 million m^3) of sand sourcing relative to the existing case.

Site	Existing Case AWAC-07 H_s (m)	Existing Case AWAC-01 H_s (m)	AWAC-01 (in POA)	AWAC-02 (in POA)	AWAC-03 (in POA)	AWAC-04 (in POA)	AWAC-07	AWAC-11
5 years of Sand Sourcing Scenario H_s Change (%)								
99th %ile	0.49	0.73	0.00%	0.01%	0.07%	0.00%	0.01%	-0.02%
95th %ile	0.39	0.59	0.00%	0.02%	0.16%	0.02%	0.01%	-0.01%
90th %ile	0.32	0.49	0.00%	0.01%	0.01%	-0.10%	0.03%	0.00%
80th %ile	0.23	0.35	0.01%	0.03%	0.14%	0.02%	0.03%	0.00%
50th %ile	0.13	0.18	0.00%	0.01%	0.02%	0.00%	0.12%	0.01%
20th %ile	0.06	0.10	-0.02%	-0.01%	0.00%	-0.03%	0.57%	0.00%
10th %ile	0.04	0.06	0.01%	0.03%	0.20%	-0.06%	0.00%	-0.01%
15 years of Sand Sourcing Scenario H_s Change (%)								
99th %ile	0.49	0.73	0.01%	0.02%	0.17%	0.02%	0.02%	-0.07%
95th %ile	0.39	0.59	0.00%	0.04%	0.37%	0.06%	0.04%	-0.14%
90th %ile	0.32	0.49	0.00%	0.01%	0.05%	-0.07%	0.03%	0.01%
80th %ile	0.23	0.35	0.04%	0.02%	0.30%	0.06%	0.15%	0.00%
50th %ile	0.13	0.18	0.00%	0.01%	0.06%	0.00%	0.32%	0.00%
20th %ile	0.06	0.10	-0.02%	-0.01%	0.07%	-0.29%	0.14%	0.16%
10th %ile	0.04	0.06	0.01%	-0.04%	0.56%	0.28%	0.09%	-0.05%

Notes: the existing case H_s at AWAC-07 represents the smallest waves out of the sites shown in the table, while the H_s at AWAC-01 represents the largest waves.
AWAC-02 is actually located 450 m to the east of the POA, but as it is so close to the POA boundary the changes are representative of changes within the POA.

Table 21. Statistics of the modelled change in H_s during TC Marcus due to (23 million m^3) and 15 years (70 million m^3) of sand sourcing relative to the existing case.

Site	Existing Case AWAC-07 H_s (m)	Existing Case AWAC-04 H_s (m)	AWAC-01 (in POA)	AWAC-02 (in POA)	AWAC-03 (in POA)	AWAC-04 (in POA)	AWAC-07	AWAC-11
5 years of Sand Sourcing Scenario H_s Change (%)								
99th %ile	0.91	2.15	0.00%	0.02%	0.04%	0.03%	0.01%	0.13%
95th %ile	0.69	1.79	0.00%	0.02%	0.11%	0.05%	0.01%	0.15%
90th %ile	0.57	1.22	0.01%	0.01%	0.15%	0.02%	0.01%	0.03%
80th %ile	0.42	0.83	0.00%	0.00%	0.01%	0.00%	0.01%	0.04%
50th %ile	0.05	0.23	0.00%	0.00%	0.01%	0.00%	0.00%	0.00%
20th %ile	0.00	0.04	0.00%	0.00%	0.00%	0.00%	0.00%	0.00%
10th %ile	0.00	0.02	0.00%	0.00%	0.00%	0.00%	0.00%	0.01%
5th %ile	0.00	0.01	0.00%	0.00%	0.00%	0.00%	0.00%	0.00%
15 years of Sand Sourcing Scenario H_s Change (%)								
99th %ile	0.91	2.15	-0.02%	0.05%	0.10%	0.08%	0.04%	0.31%
95th %ile	0.69	1.79	0.00%	0.06%	0.30%	0.13%	0.03%	0.39%
90th %ile	0.57	1.22	0.02%	0.03%	0.42%	0.06%	0.03%	0.08%
80th %ile	0.42	0.83	0.00%	0.01%	0.03%	0.01%	0.02%	0.09%
50th %ile	0.05	0.23	0.00%	0.00%	0.03%	0.00%	0.00%	0.00%
20th %ile	0.00	0.04	0.00%	0.00%	0.00%	0.00%	0.00%	0.00%
10th %ile	0.00	0.02	0.00%	0.00%	0.00%	0.00%	0.00%	0.03%
5th %ile	0.00	0.01	0.00%	0.00%	0.00%	0.00%	0.00%	0.00%

Notes: the existing case H_s at AWAC-07 represents the smallest waves out of the sites shown in the table, while the H_s at AWAC-01 represents the largest waves.
AWAC-02 is actually located 450 m to the east of the POA, but as it is so close to the POA boundary the changes are representative of changes within the POA.

4.3. Summary Findings & Implications for the Proposal

The numerical modelling assessed the potential changes to hydrodynamics and waves in and offshore from CG in relation to the existing baseline case (current situation), from the proposed sourcing of 23 million m^3 of sand at 5 years and 70 million m^3 of sand at 15 years, as well as potential changes 100 years from today for the 15 years sand sourcing.

Overall, the modelling assessed that changes to hydrodynamics and waves in and offshore from CG will be negligible for the 5, 15 and 100 year scenarios, with the main modelled changes summarised below.

The very small magnitude of modelled changes are unlikely to cause measurable changes to sediment transport, coastal processes and marine environmental quality (MEQ), and will thus not cause significant impacts on the environmental resources and values of the area that are influenced by these processes. In the CG area the main environmental resources and values that are influenced by hydrodynamics, waves, sediment transport, coastal processes and MEQ are the mangrove communities that line the coast within CG, the False Mouths of the Ord on the eastern side of CG (which are part of the Ord River Floodplain Ramsar site) and three turtle nesting beaches on the seaward coasts outside of CG and one at Barnett Point inside CG, southeast of the POA (see Section 1.2 and Figure 2).

The modelling also assessed the potential changes in hydrodynamics and waves in CG that may have occurred since European settlement of the area, including from the construction two dams on the Ord River (in 1967 and 1971). These changes constitute the existing baseline case in CG today, and were included in the modelling so as to allow assessment of potential cumulative impacts from the proposed sand sourcing, in addition to any changes that may have been caused by the Ord River dams, as required by EPA guidance on cumulative assessment.

This modelling found that there have been changes in water levels and currents in CG between the pre-European scenario and the existing case in CG, primarily from the construction of the two dams, and that those changes were more significant than the modelled changes from the proposed sand sourcing, with the main modelled changes summarised below.

Given that overall, the modelling indicates that changes to hydrodynamics and waves will mostly be negligible under all sand-sourcing scenarios, the cumulative changes in addition to the changes caused by the two dams was also considered to be negligible.

The main modelled changes to hydrodynamics and waves are summarised as follows:

- The modelled changes were similar for the different metocean conditions and were of the highest magnitude (although still minor) for the 15 years (70 million m^3) sand sourcing scenario, assuming present day water levels.
- The 15 years (70 million m^3) sand sourcing could result in a very minor change in phase of the tidal wave propagation in CG of up to 30 s. This change results in very small apparent changes in water level during the peak flood and peak ebb stages of the tide, with changes to the tidal range assessed to be insignificant (less than 0.05%). This compares to a modelled 0.55% reduction in tidal range in CG during a high river discharge event due to the construction of the Ord River dams.
- Changes to currents resulting from the sand sourcing were assessed to be very minor and localised within and adjacent to the POA. The deepening associated with the sand sourcing was modelled to result in a very minor reduction in current speed within and adjacent to the western and eastern sides of the POA, with some localised very minor increases in current speed adjacent to the north and south of the POA.
- The changes in current speed were modelled to be up to ± 0.05 m/s for 15 years of sand sourcing, resulting in changes in the peak flood and ebb currents within the POA of up to -2.1% and less than ± 0.5% outside of the POA.
- In contrast, the modelling indicates that since European settlement and building of the Ord River dams, there have been changes in current speeds throughout CG and in both West and East Arms south of the main body of CG, of a larger magnitude than those modelled for the sand sourcing scenarios. The modelling indicates that during a high river discharge event, the construction of the Ord River dams and resultant regulation of the river discharge has resulted in a reduction in peak flood current speeds of up to 11.7% and an increase in the peak ebb current speed of up to 6.3%.
- Changes to the current direction as a result of the Ord River dams were also modelled to be significantly larger than changes due to the sand sourcing. However, both scenarios were shown to predominantly only influence current speeds, with changes in direction only occurring during

periods of low current speed when the current direction was switching, indicating the modelled changes were due to a change in phase of the tidal wave propagation rather than an absolute change in current direction.

- Modelled changes to wave conditions resulting from the sand sourcing after both 5 years and 15 years were very small and highly localised. The modelling assessed that the sand sourcing would only influence the wave conditions in CG during specific wave conditions, typically during larger wave events, when short duration changes could occur. The modelled changes were up to ± 0.01 m in H_s, up to ± 0.05 s in T_p and less than 0.5º in wave direction. The largest (but still minor) changes occurred during the wet season when the waves are largest.
- Overall, the results from the hydrodynamic and wave modelling have identified very minor and highly localised changes in water levels, currents and waves as a result of the proposed sand sourcing. The results are similar to the changes modelled as part of the initial modelling presented by PCS (2024a), although the results presented here supersede the previous results as the models have been subject to further development and calibration, supported by a significant volume of field data.

5. RESULTS: SEDIMENT TRANSPORT AND BEACH PROCESSES

This section provides details of the results from the ST modelling of the suspended and bedload transport of clay, silt and sand, and results from the Littoral Processes modelling of longshore and cross-shore sediment transport in relation to the three turtle nesting beaches on the seaward coasts outside of CG.

Existing conditions are presented along with modelled changes to suspended and bedload transport due to the sand sourcing, as well as the differences between the existing case and pre-European settlement conditions, to assist in assessing potential cumulative changes from the proposed sand sourcing.

The sand sourcing scenarios are not assessed to result in any changes to the wave conditions offshore of CG and so will not result in any direct impacts to the longshore and cross-shore sediment transport at the turtle nesting beaches. Additionally, the modelling indicates that there have not been any changes to wave conditions offshore from CG since pre-European conditions, that could have changed longshore and cross-shore sediment transport at the turtle nesting beaches. However, in order to assess any potential indirect changes to sand supply to the turtle nesting beaches from the proposed sand sourcing, bedload transport modelling has been undertaken.

5.1. Existing Conditions

Results from the existing case scenario are presented in the following sections to provide an overview of the existing sediment transport conditions and beach processes in and offshore from CG.

5.1.1. Suspended Sediment

Spatial maps of the 50th and 95th percentile depth averaged SSC over the 2 month (60/61 days) duration wet season, dry season and transitional season periods, along with the 5-day TC Marcus period, are shown in Figure 165 to Figure 168. The plots show the following:

- Overall, SSC values in CG were very high compared to coastal waters in many other parts of northern Australia, with the 50th percentile SSC within the main body of CG ranging from 50 to 500 mg/L and the 95th percentile SSC within the main body of CG ranging from 100 to more than 3,000 mg/L.

- During all three seasons the model showed a general reduction in SSC in a northerly direction (from inshore to offshore), with highest SSC in West and East Arms and the False Mouths of the Ord, lesser SSC in the main body of CG including the POA and the lowest SSC offshore. In East and West Arms and the False Mouths of the Ord the modelled SSC was shown to typically be above 1,000 mg/L for both the 50th and 95th percentile, while in the main body of CG the SSC was predominantly between 50 and 1,000 mg/L except for some shallow areas, where the 95th percentile SSC can be above 2,000 mg/L. Offshore of CG the modelled SSC was predominantly between 10 and 250 mg/L, although the 95th percentile SSC at Medusa Bank can be above 2,000 mg/L. These are all extremely high SSC values.

- The SSC was modelled to generally be highest in the wet season and lowest in the dry season. In the POA the modelled SSC was between 100 and 250 mg/L for the 50% percentile in the wet and transitional seasons and between 250 and 500 mg/L for the 95th percentile. In the dry season the modelled SSC lower, with an SSC in the POA for the 50th percentile of 50 to 100 mg/L and the 95th percentile of between 100 and 250 mg/L.

- During TC Marcus the 50th percentile SSC indicates a relatively low SSC over the majority of the event, this is partially because the model only included winds due to TC Marcus and so is likely to under-estimate the ambient wind and waves conditions over the few days immediately before TC Marcus. The 95th percentile SSC shows that during the peak of the cyclone the SSC was higher throughout much of CG and offshore compared to during typical seasonal conditions, with an SSC of more than 3,000 mg/L throughout the majority of the shallow areas within CG and over Medusa Bank. The SSC within the POA was modelled to be lower than during the wet and transitional seasons. The modelled SSC during TC Marcus provides an indication as to how the SSC behaves during a large wave event without a coinciding large river discharge (the wet season period has a large river discharge event and so shows the influence of this on SSC), with the large waves offshore and within CG resulting in resuspension of sediment from the shallow areas.

Timeseries plots of the modelled SSC at a site offshore of CG (AWAC-09), within the POA (AWAC-01) and upstream (south) of the POA (AWAC-11) are shown for the three seasonal periods and TC Marcus in Figure 169 to Figure 172. The plots show the following:

- There was semi-diurnal and spring-neap tidal variability in the SSC. The semi-diurnal variability is a result of higher SSC in East and West Arms and in the False Mouths of the Ord and lower SSC in the offshore area, meaning that peaks in SSC occur around low water (following the ebb stage of the tide which brings higher SSC water from upstream into CG), and troughs in SSC occur around higher water (following the flood stage of the tide which brings lower SSC water from offshore into CG). The SSC at low water can be 50 to 400 mg/L higher than the SSC at high water. The spring-neap tidal variability is due to the higher current speeds during spring tides compared to neap tides, which results in higher SSC during spring tides. The peaks in SSC during spring tides can be between 50 and 300 mg/L higher than the peaks in SSC during neap tides, while the high-water troughs are typically fairly similar.

- For all three seasons the SSC was modelled to be highest at the furthest upstream site (AWAC-11) and lowest at the furthest offshore site (AWAC-09), although during the dry season the SSC at the site within the POA (AWAC-01) and offshore were similar.

- During the wet season there was a clear increase in SSC at the upstream site and within the POA from the 9th March 2024 onwards. This is due to a high river discharge event (with increased SSC associated with this, see Section 3.6.1) which commenced this day and resulted in elevated SSC within CG over the subsequent 21 days (and potentially beyond). The elevated SSC resulted in the peak SSC over this period being ~300 mg/L higher than previous spring tides at the upstream site and ~150 mg/L higher within the POA. At the offshore site the SSC appeared to have not been influenced by the event.

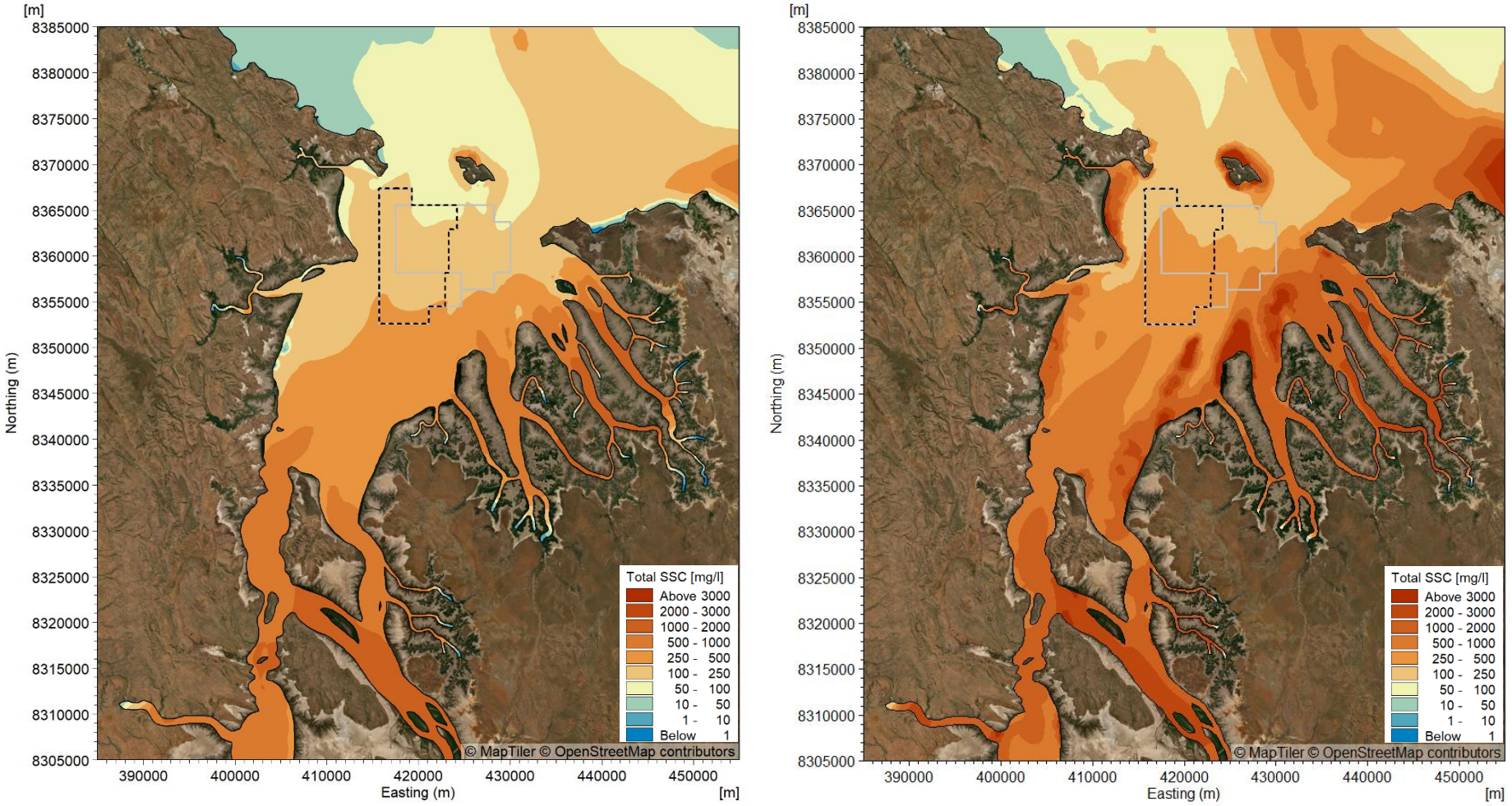
- During the wet season there was also a short duration peak in SSC at the offshore site on 21/02/2024. At this time the SSC increased by ~250 mg/L, resulting in a peak SSC of 300 mg/L which was the highest value at this site over the two-month period. This peak in SSC coincided with a large wave event, with an H_s of 1.75 m at AWAC-09 (Figure 113), indicating that the increase was driven by wave activity. The wave event did not result in an increase in SSC at the sites within CG.

- The SSC during TC Marcus showed the opposite spatial trend to the other seasonal periods, with the highest SSC at the offshore site and the lowest SSC at the furthest upstream site. This was because the tropical cyclone was associated with large wave conditions in the region but no significant river discharge. The cyclone resulted in relatively short duration (a few hours) peaks in SSC of just over 1,000 mg/L at the offshore site and ~800 mg/L at the site in the POA. The cyclone did still result in a change in SSC at the upstream site, with peaks in SSC increasing from 150 mg/L prior to the TC, to 350 mg/L after the cyclone, indicating that some of the sediment suspended by the waves remained in suspension and was then subsequently transported around CG until it settled out.

A summary of the existing case SSC percentiles for the wet, dry and transitional seasons and for TC Marcus are provided in Table 22 and Table 23. The percentiles show how the SSC varied between the sites and between the different metocean conditions, with the 99th percentile SSC at AWAC-01 in the POA varying from just over 100 mg/L in the dry season to just over 600 mg/L during TC Marcus, while the 5th percentile SSC only varied by 30 mg/L between the different periods (from 37 to 67 mg/L).

The highest SSC was consistently at AWAC-07, which is located adjacent to shallow shoals and in the False Mouths of the Ord River. The lowest SSC was typically at AWAC-09 (except during TC Marcus when the SSC was lower in CG), which is located at King Shoals, where the 99th percentile varied between the three seasons from 126 to 190 mg/L and the 5th percentile varied from 12 to 24 mg/L.

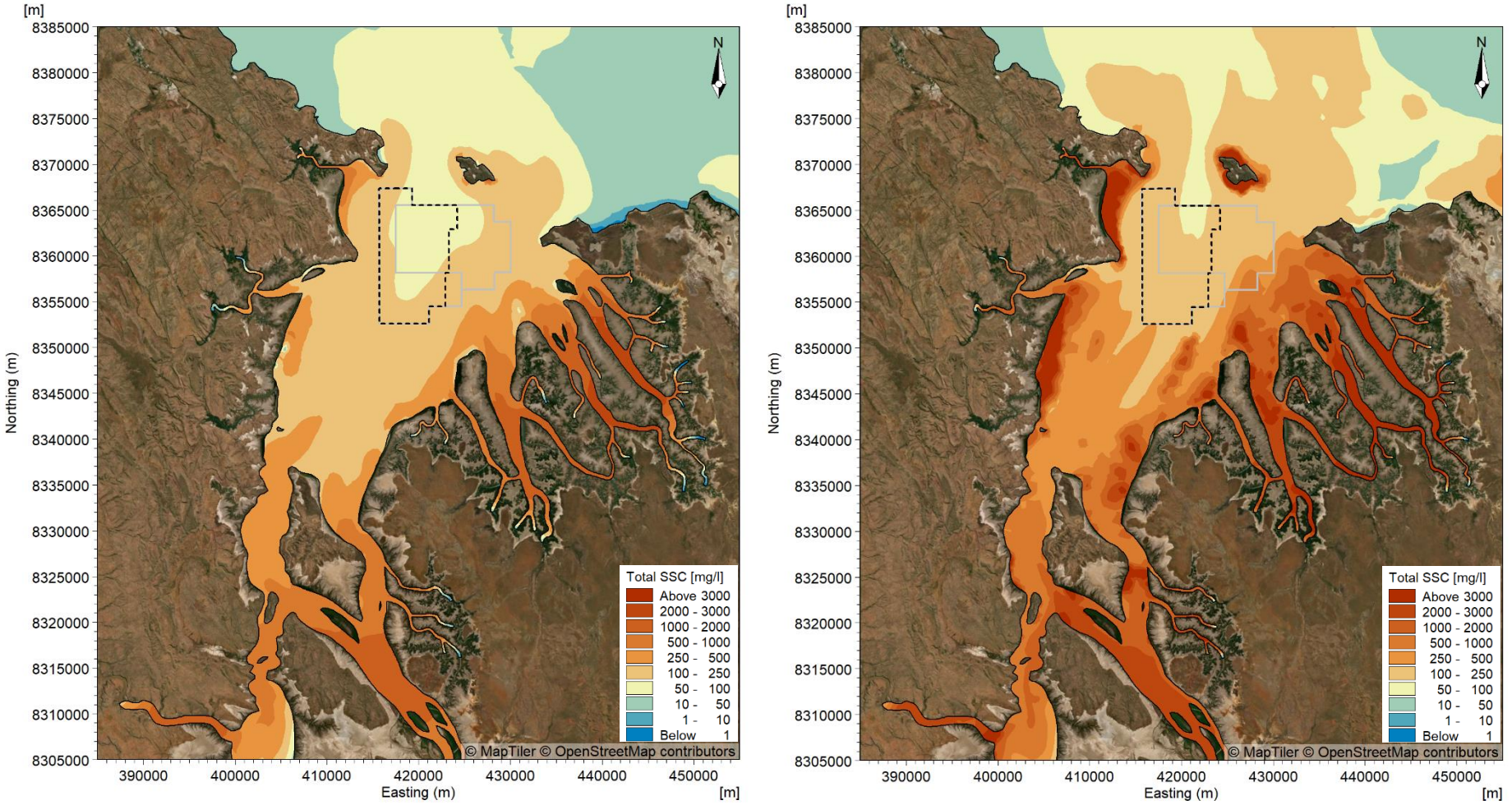
The 5th up to 50th percentile SSCs were similar at all sites over the three different seasons, indicating that during periods with calm wind and waves and low river discharge the SSC resulting from just the astronomical tide is similar.



50th Percentile SSC

95th Percentile SSC

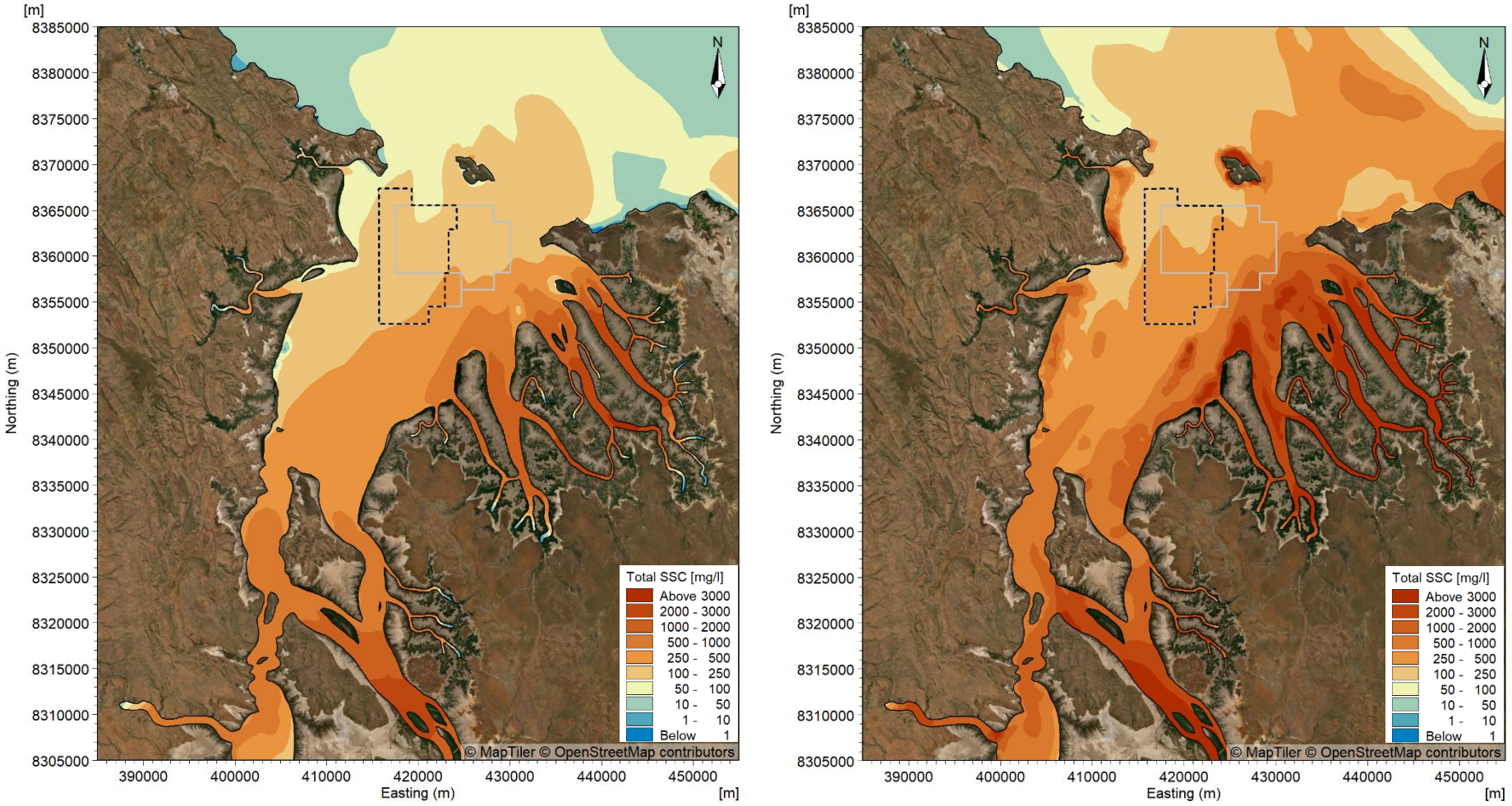
Figure 165. Modelled existing case SSC percentiles over the two-month (60 days) wet season period.



50th Percentile SSC

95th Percentile SSC

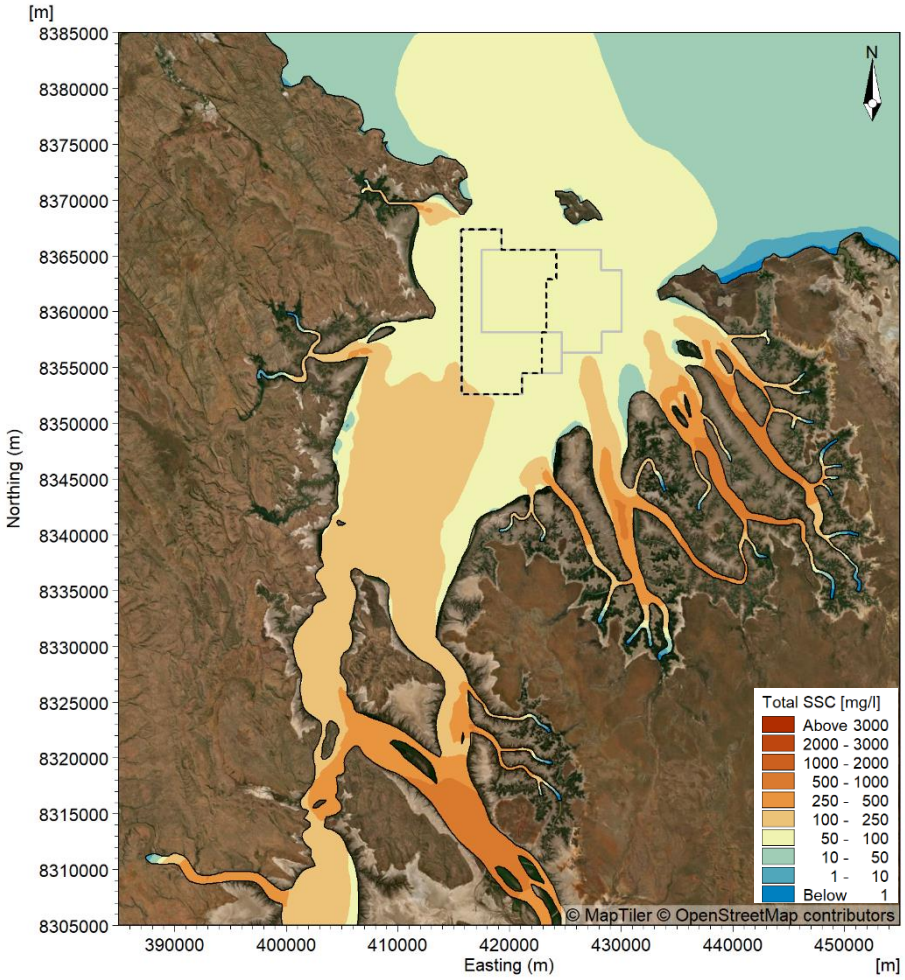
Figure 166. Modelled existing case SSC percentiles over the two-month (61 days) dry season period.



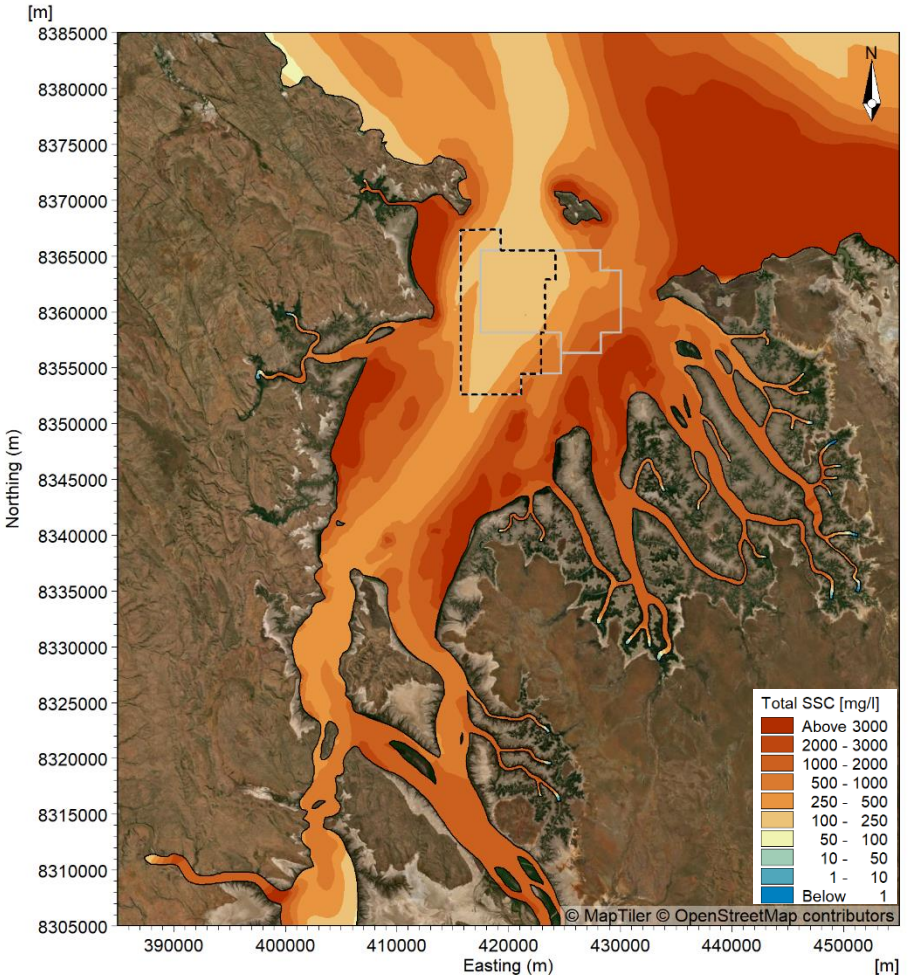
50th Percentile SSC

95th Percentile SSC

Figure 167. Modelled existing case SSC percentiles over the two-month (61 days) transitional season period.



50th Percentile SSC



95th Percentile SSC

Figure 168. Modelled existing case SSC percentiles over TC Marcus.

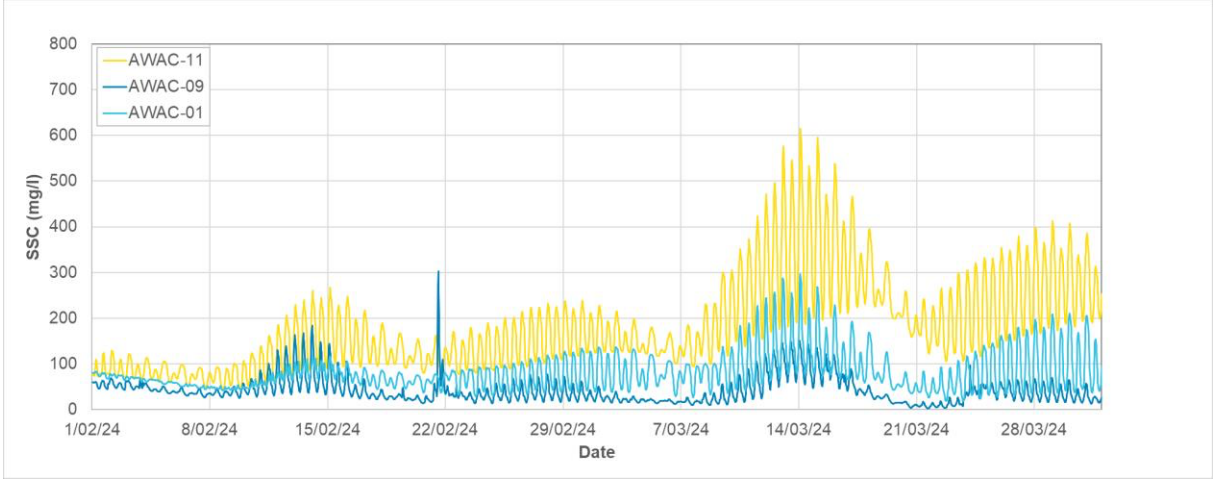


Figure 169. Modelled SSC at AWACs 01, 09 and 11 over the two-month (60 days) wet season period.

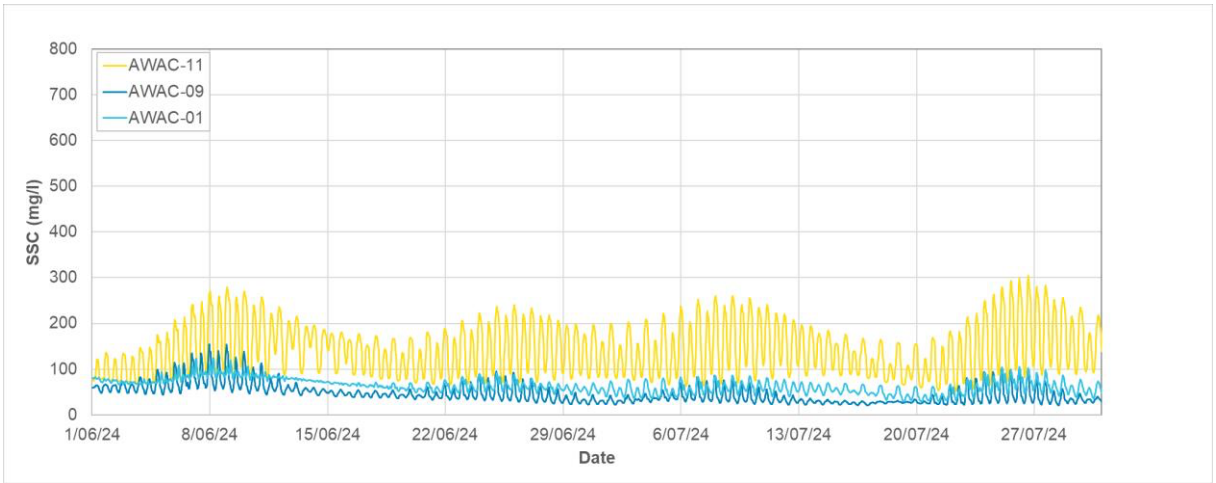


Figure 170. Modelled SSC at AWACs 01, 09 and 11 over the two-month (61 days) dry season period.

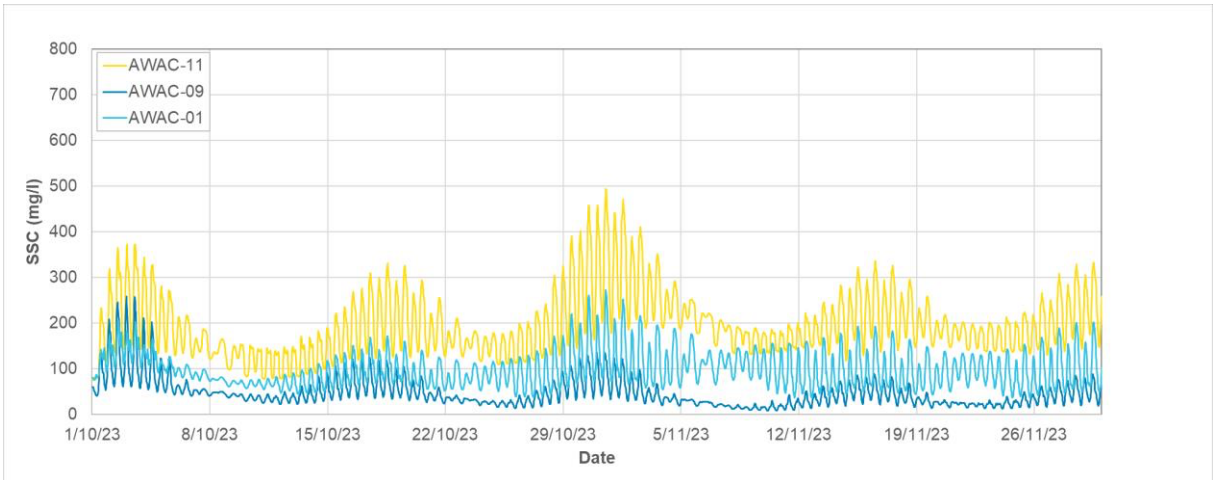


Figure 171. Modelled SSC at AWACs 01, 09 and 11 over the two-month (61 days) transitional season period.

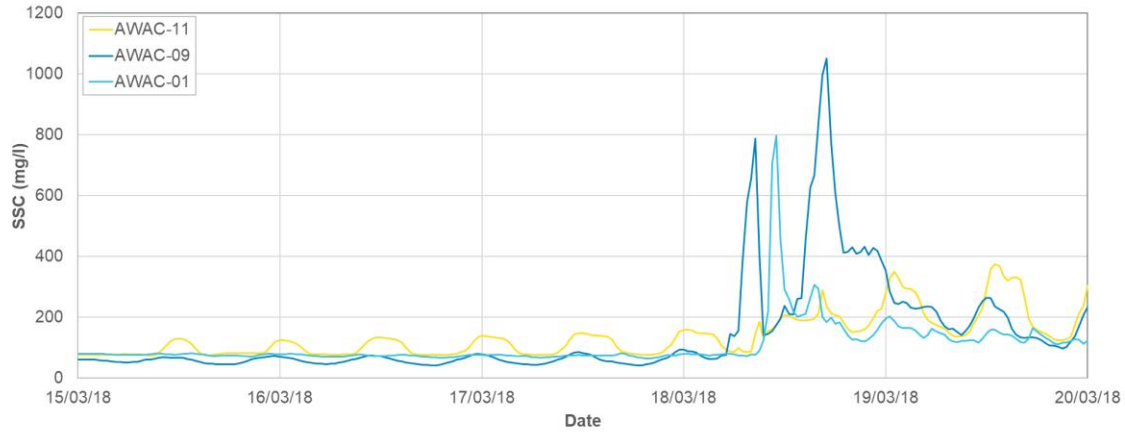


Figure 172. Modelled SSC at AWACs 01, 09 and 11 over TC Marcus.

Table 22. Statistics of the modelled existing case SSC over two months (60/61 days) of wet and dry season conditions at the 11 AWAC sites.

Site	AWAC-01	AWAC-02	AWAC-03	AWAC-04	AWAC-05	AWAC-06	AWAC-07	AWAC-08	AWAC-09	AWAC-10	AWAC-11
Wet Season SSC (mg/L)											
99th %ile	233	216	320	275	186	185	1,060	910	145	181	516
95th %ile	169	137	248	189	147	120	769	689	104	122	382
90th %ile	134	115	210	155	122	102	618	592	75	98	325
80th %ile	104	90	160	119	89	82	469	494	57	75	244
50th %ile	70	63	104	81	64	65	246	319	35	57	157
20th %ile	49	50	67	63	49	48	146	200	20	44	98
10th %ile	42	46	57	56	42	41	110	129	15	37	79
5th %ile	37	42	50	52	37	33	81	111	12	29	69
Dry Season SSC (mg/L)											
99th %ile	103	114	167	156	141	221	1,297	471	126	223	273
95th %ile	89	93	128	127	110	152	851	411	85	160	243
90th %ile	83	86	115	114	99	121	672	383	72	119	222
80th %ile	76	74	102	100	87	94	458	341	60	86	194
50th %ile	63	59	79	79	72	65	176	265	40	55	135
20th %ile	50	47	61	65	54	48	79	209	29	40	88
10th %ile	44	41	56	60	46	40	51	180	26	32	78
5th %ile	40	37	51	55	42	33	41	155	24	23	72

Table 23. Statistics of the modelled existing case SSC over two months (61 days) of the transitional season and 5 days during TC Marcus at the 11 AWAC sites.

Site	AWAC-01	AWAC-02	AWAC-03	AWAC-04	AWAC-05	AWAC-06	AWAC-07	AWAC-08	AWAC-09	AWAC-10	AWAC-11
Transitional Season SSC (mg/L)											
99th %ile	213	190	310	243	188	402	2,051	691	190	457	422
95th %ile	174	143	248	188	148	262	1,500	546	108	297	326
90th %ile	152	127	222	165	132	209	1,169	489	85	213	291
80th %ile	132	103	181	140	114	151	800	418	63	140	246
50th %ile	90	74	134	107	79	82	375	304	38	72	181
20th %ile	65	56	88	81	57	54	166	234	24	49	140
10th %ile	56	52	69	72	48	48	103	200	19	42	127
5th %ile	50	47	58	65	40	44	77	180	15	37	110
TC Marcus SSC (mg/L)											
99th %ile	602	518	627	430	679	2,106	4,849	429	929	3,553	364
95th %ile	205	222	277	294	401	938	2,172	407	448	1,818	304
90th %ile	164	176	216	236	248	555	1,469	394	372	1,377	231
80th %ile	131	145	136	178	179	437	903	332	214	846	181
50th %ile	77	75	72	88	83	76	182	172	68	73	123
20th %ile	72	68	66	80	73	68	59	143	51	57	78
10th %ile	70	64	65	76	70	66	52	134	46	52	76
5th %ile	67	62	64	74	67	63	50	130	44	47	75

5.1.2. Bedload Transport

Spatial maps of the bedload transport rate and direction at the peak flood and peak ebb stages of a spring tide in the wet and dry seasons (the transitional season is very similar to the wet season and so is not shown), around the peak in H_s of TC Marcus and during a period with high river discharge in the wet season are shown in Figure 173 to Figure 176. The plots show the following:

- The modelled bedload transport rates in CG during the peak flood and peak ebb stages of the tide ranged up to 0.4 kg/m/s, with transport rates typically higher at peak ebb than peak flood. The spatial pattern of the areas with a bedload transport rate of more than 0.1 kg/m/s within CG indicates the primary sediment transport pathway for sand, the sand being transported from upstream (south to north) via West Arm (west of Adolphus Island) into the middle of CG and the POA, then out through West Entrance (west of Lacrosse Island) to King Shoals outside of CG (Figure 177). Although the results show that bedload transport occurred both to the north (out of CG) and the south (into CG) the maps indicate that the net transport was typically in a northerly (inshore to offshore) direction out of CG.

- The highest modelled bedload transport rates were within West and East Arms, with localised areas where peak transport rates were between 0.4 and 1.5 kg/m/s. The bedload transport rates in West and East Arms were similar at peak flood and peak ebb, with a potential for flood dominance in these areas. As the plots show a single point in time it was not possible to determine the net bedload transport direction, this is further assessed based on the timeseries data below.

- During TC Marcus the plot shows that the peak flood modelled bedload transport rate was less than 0.1 kg/m/s throughout the majority of CG (i.e. lower than during peak flood on a spring tide in the wet or dry seasons), while the ebb bedload transport rate was higher than 0.2 kg/m/s throughout much of CG (i.e. higher than during peak ebb on a spring tide in the wet or dry seasons). The plots therefore indicate that during a cyclone there can be an increase in the ebb dominance of the bedload transport in CG, although this will be dependent on the characteristics of the cyclone (e.g. path, timing relative to the astronomical tide).

- During the high river discharge event in the wet season, the modelled bedload transport rate during the peak flood stage of the tide was less than 0.1 kg/m/s throughout the majority of CG, while the modelled bedload transport during the peak ebb stage of the tide was above 0.1 kg/m/s throughout the majority of CG (i.e. similar to a peak ebb stage of tide during the dry season). The results therefore indicate an ebb dominance during high river discharge events, but with the transport rates being comparable to a typical spring tide.

Timeseries plots of the water level, bedload transport rates and bedload transport directions during the wet season at sites upstream (south) of the POA (AWAC-11), within the POA (AWAC-01) and offshore of CG at King Shoals (AWAC-09) are shown in Figure 178 and at the entrance to West Arm (AWAC-08) in Figure 179. The bedload transport rates have been processed so that transport in a northerly direction is positive and transport in a southerly direction is negative. The plots show low bedload transport rates during neap tides at all sites, with the transport rates increasing as the tidal range increases towards springs. The plots indicate a northerly net transport upstream (south) of the POA, within the POA and at King Shoals. The peak bedload transport rate at the entrance to West Arm can be higher on the flood stage of the tide than on the ebb stage of the tide, but the timeseries shows an overall ebb dominance due to the bedload transport rates on the flood tide having more semi-diurnal variability than on the ebb tide. The average net bedload transport rates over the two-month (60 days) wet season simulation have been calculated at four sites:

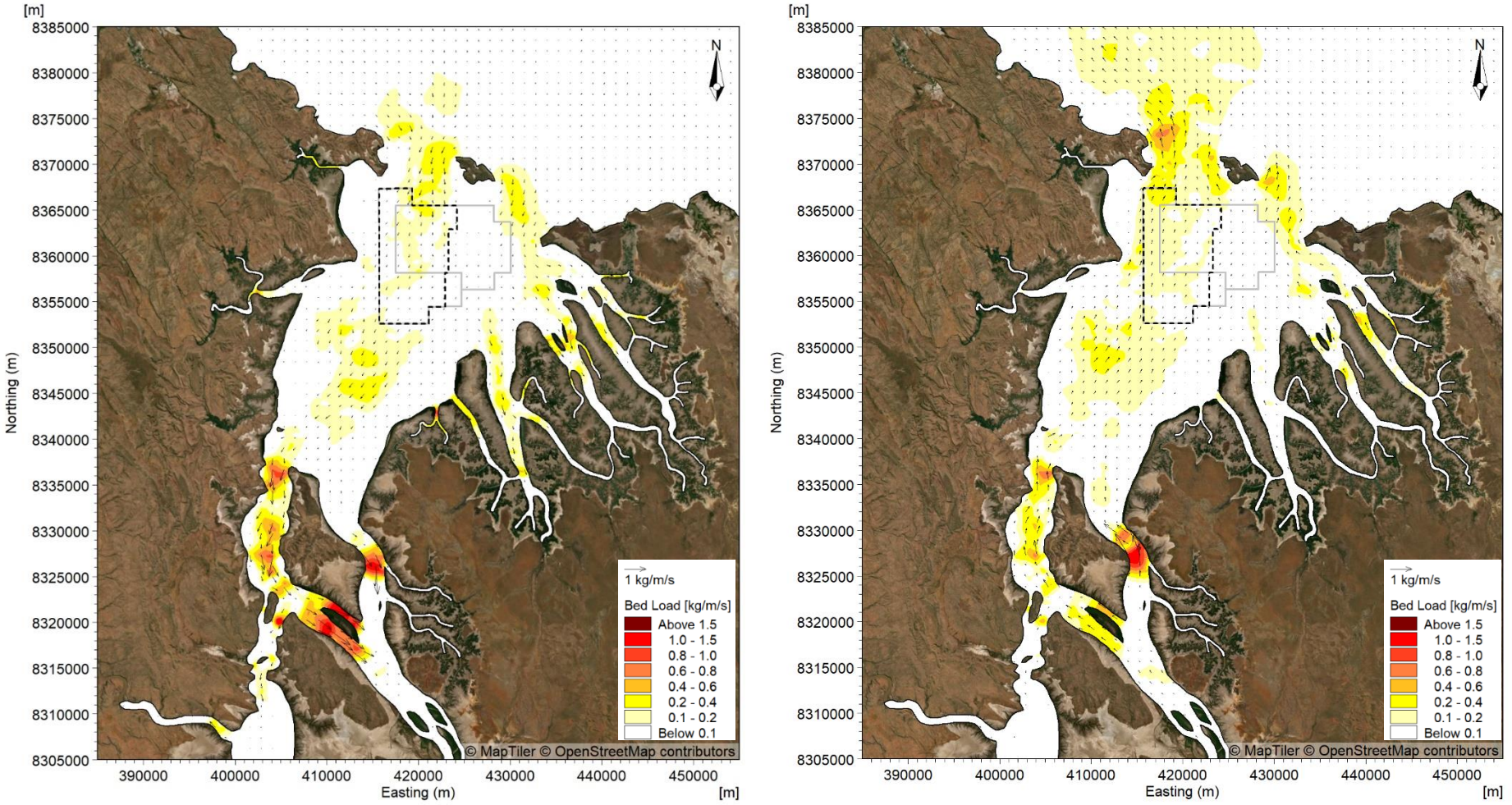
- Entrance to West Arm (AWAC-08): 0.015 kg/m/s (net northerly).
- Upstream (south) of the POA (AWAC-11): 0.012 kg/m/s (net northerly).
- Within the POA (AWAC-01): 0.0027 kg/m/s (net northerly).
- Offshore at King Shoals (AWAC-09): 0.0038 kg/m/s (net northerly).

Timeseries plots during TC Marcus of the water level, bedload transport rates and bedload transport directions at sites upstream (south) of the POA (AWAC-11), within the POA (AWAC-01) and offshore of CG at King Shoals (AWAC-09) are shown in Figure 180. The plots show a similar ebb dominance to the previous wet season plots, but with increased bedload transport in the morning on 18/03/2018, with the peak ebb bedload transport rates increasing from ~0.1 kg/m/s at the three sites to between 0.2 to

0.25 kg/m/s. The average net bedload transport rates over the 5 days of the TC Marcus simulation, which excluded any large spring tides, have been calculated at the four sites:

- Entrance to West Arm (AWAC-08): 0.006 kg/m/s (net northerly).
- Upstream (south) of the POA (AWAC-11): 0.019 kg/m/s (net northerly).
- Within the POA (AWAC-01): 0.006 kg/m/s (net northerly).
- Offshore at King Shoals (AWAC-09): 0.010 kg/m/s (net northerly).

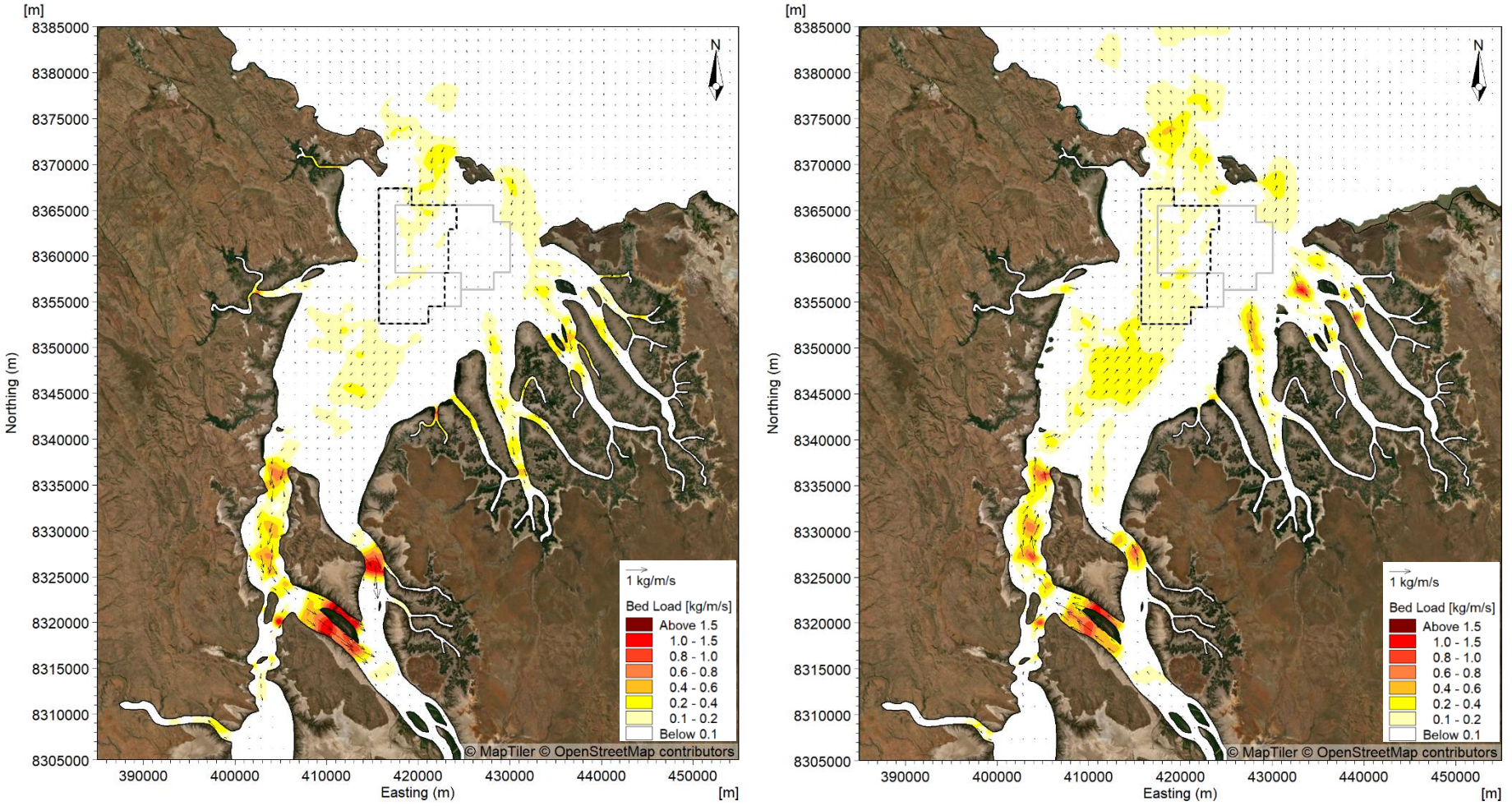
The net bedload transport rates during TC Marcus were more than double the net transport rates during typical wet season conditions within the POA and offshore of CG at King Shoals. Upstream (south) of the POA the modelled bedload transport rates were increased by around 50%, while at the entrance to West Arm the rates were 40% of the rates over a typical wet season period. The lower rates at the entrance to West Arm were due to the TC Marcus period not including large spring tides which is when the highest transport rates occur in this area.



Peak Flood

Peak Ebb

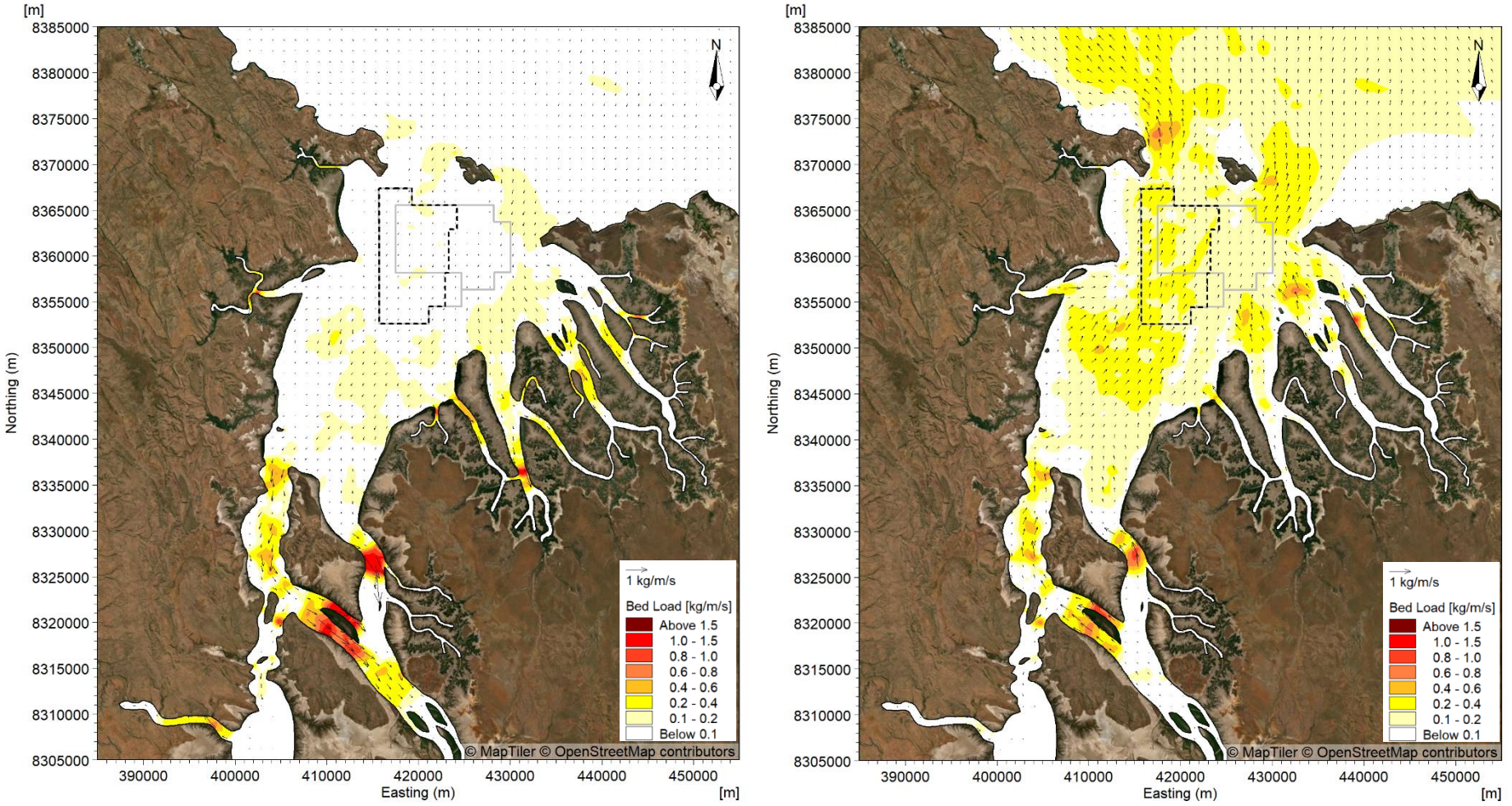
Figure 173. Modelled existing case bedload transport at peak flood and peak ebb during a spring tide in the wet season.



Peak Flood

Peak Ebb

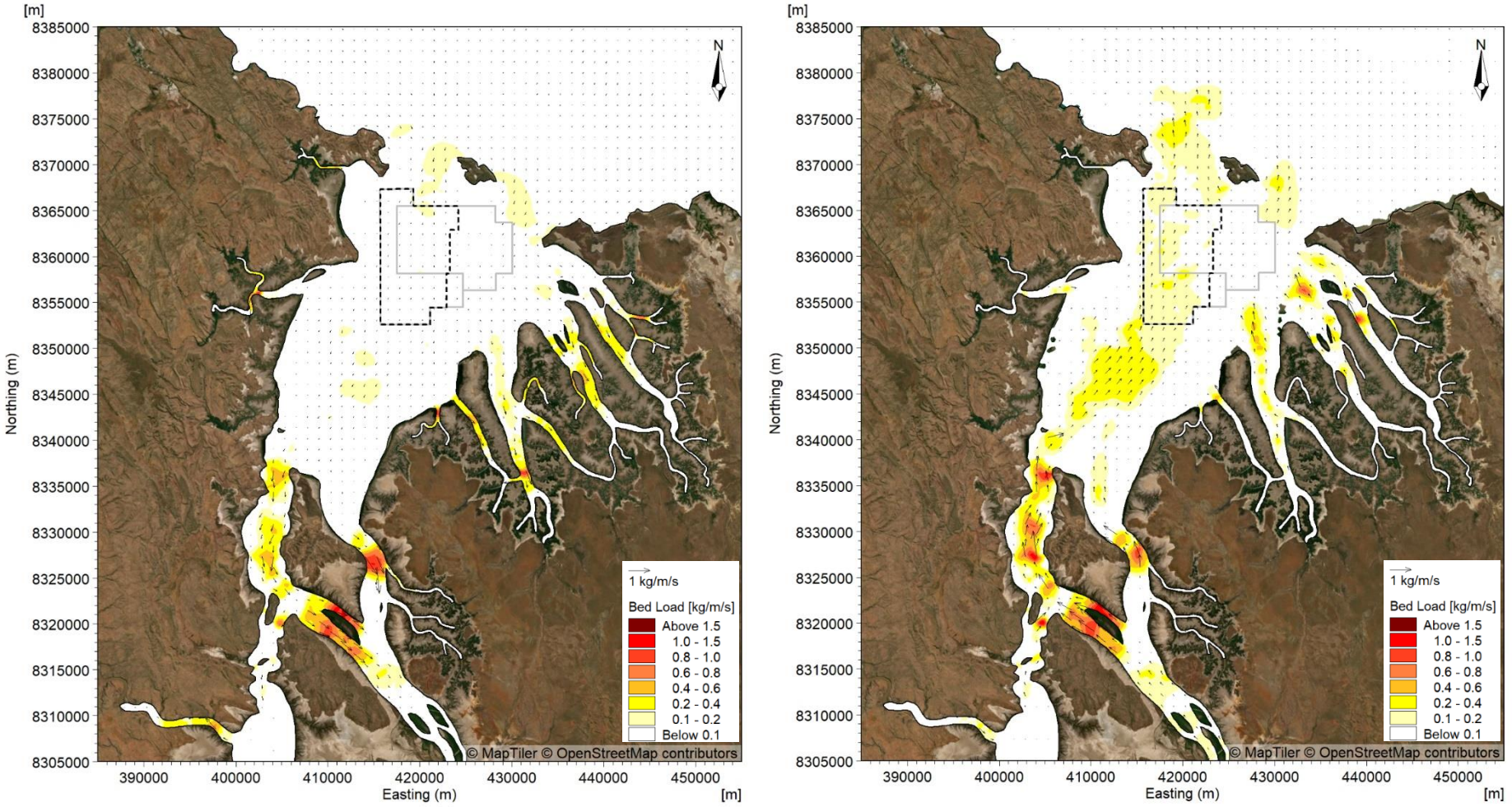
Figure 174. Modelled existing case bedload transport at peak flood and peak ebb during a spring tide in the dry season.



Peak Flood

Peak Ebb

Figure 175. Modelled existing case bedload transport at peak flood and peak ebb during TC Marcus.



Peak Flood

Peak Ebb

Figure 176. Modelled existing case bedload transport at peak flood and peak ebb during a high river discharge event in the wet season.

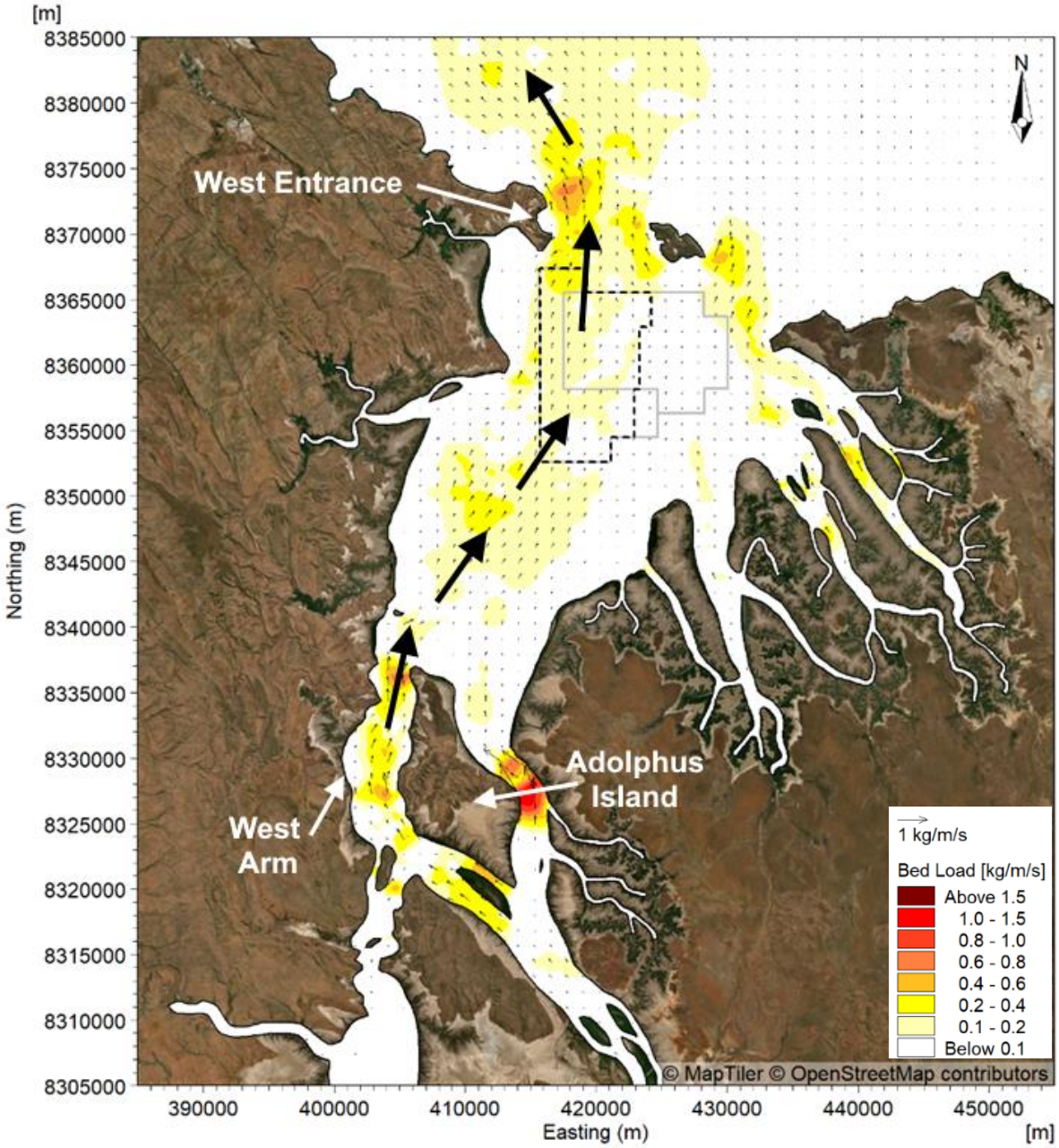


Figure 177. Annotated plot showing the primary sediment transport pathway for sand (large black arrows) on top of the bedload transport rate at peak ebb during a spring tide in the wet season.

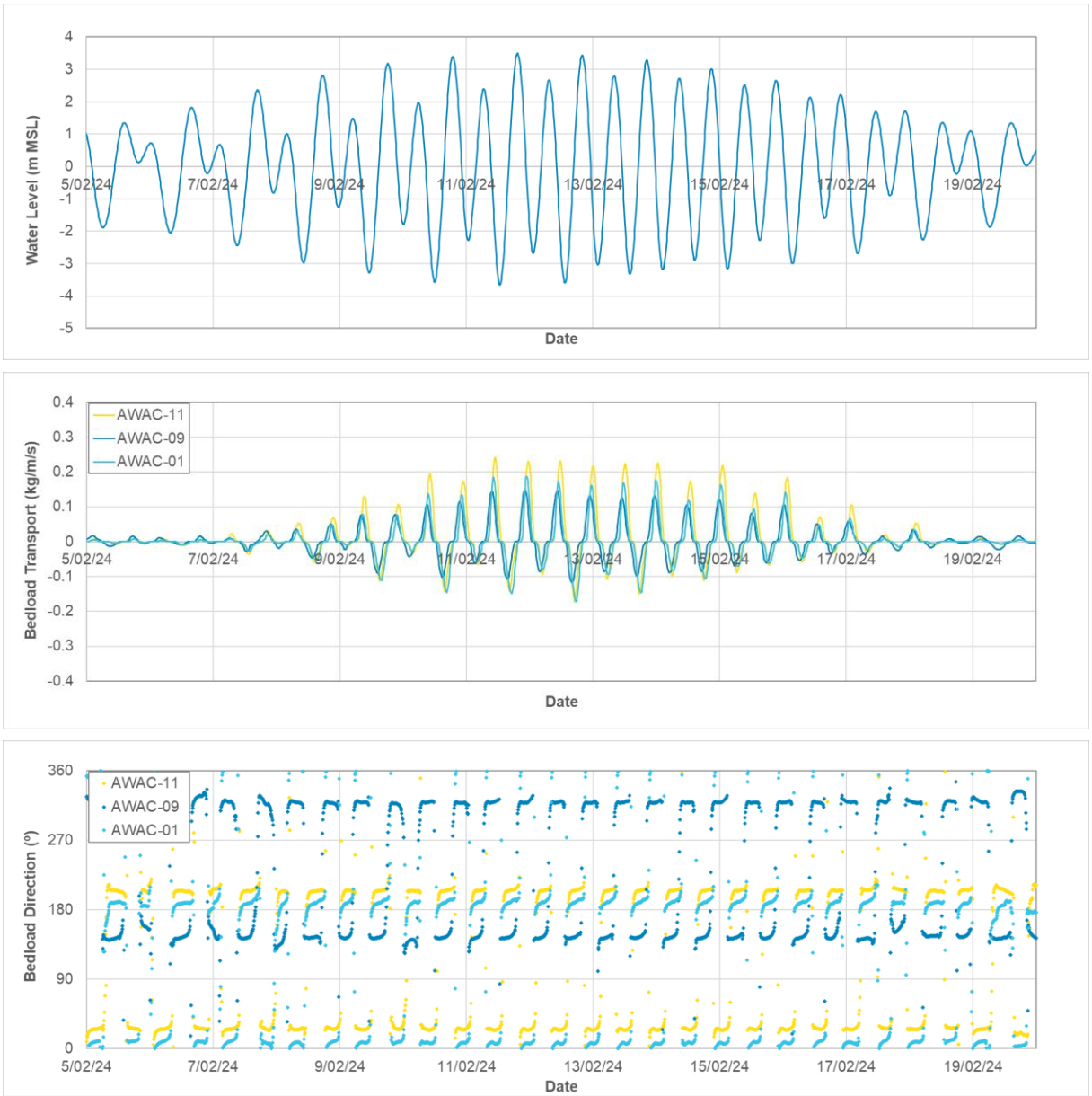


Figure 178. Modelled water level at AWAC-01 (top) and bedload transport rate (middle) and direction (bottom) at AWACs 01, 09 and 11 over a 15-day period in the wet season. *Note: positive bedload transport is to the north and negative is to the south.*

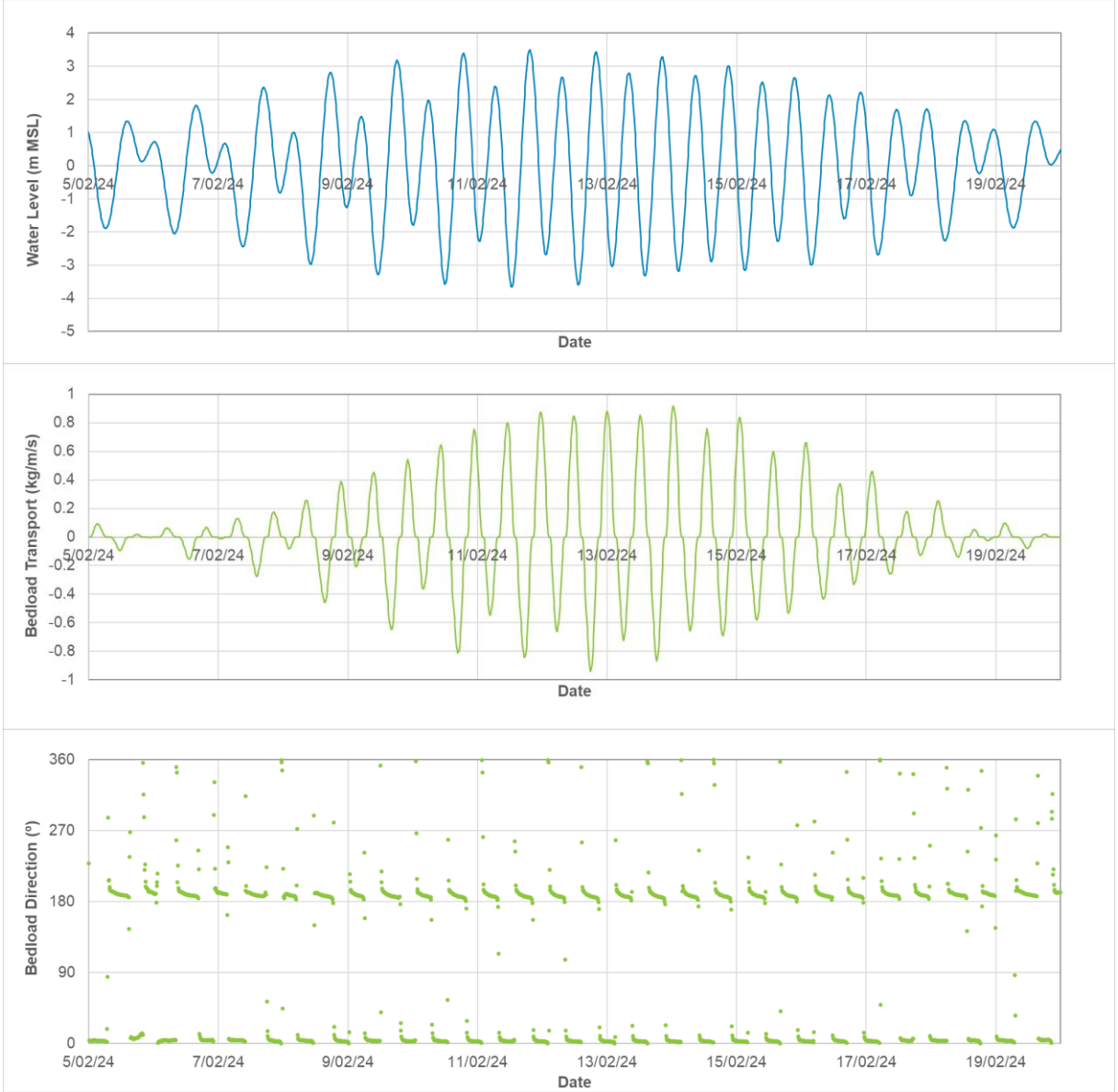


Figure 179. Modelled water level at AWAC-01 (top) and bedload transport rate (middle) and direction (bottom) at AWAC 08 over a 15-day period in the wet season. *Note: positive bedload transport is to the north and negative is to the south.*

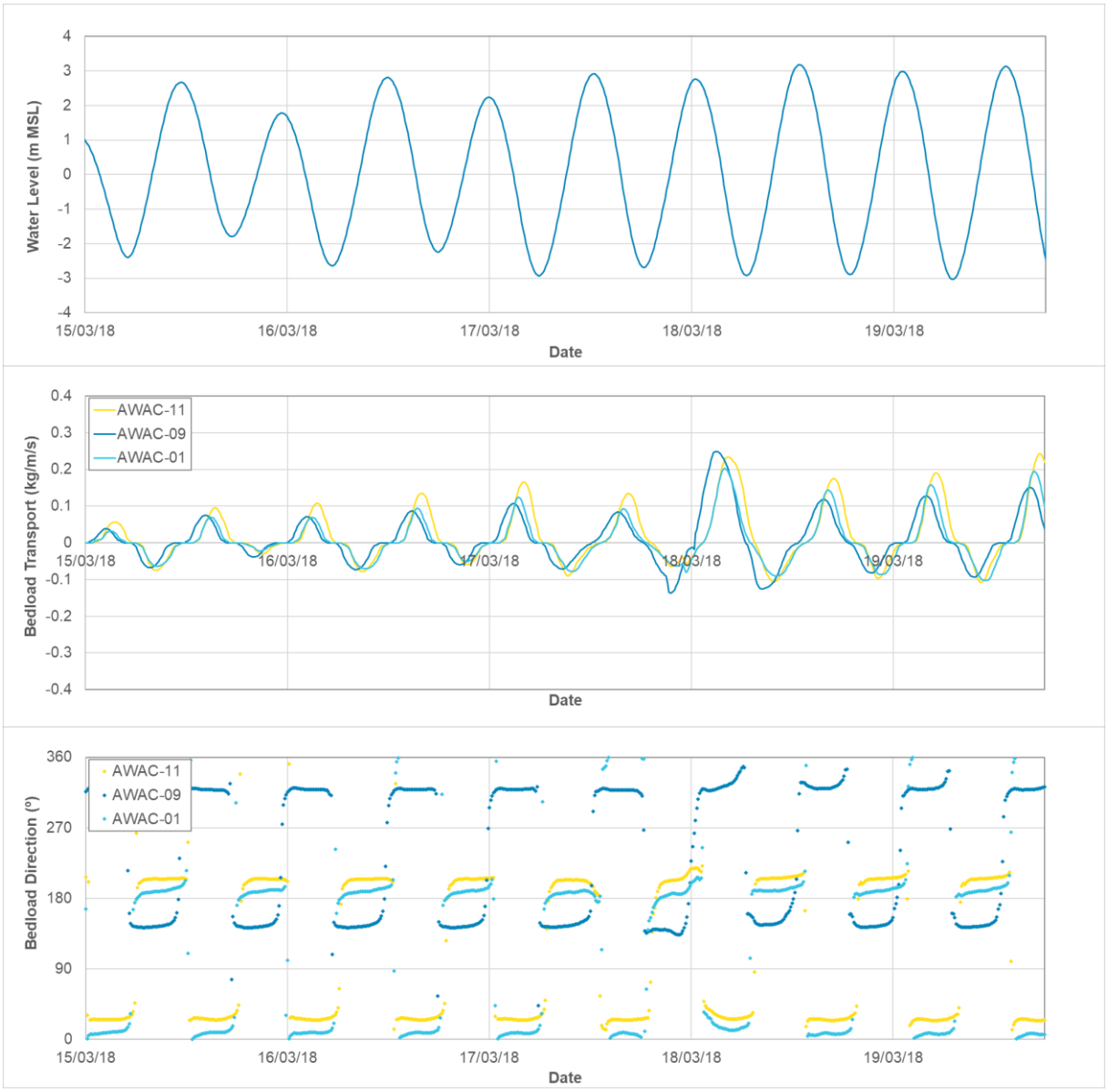
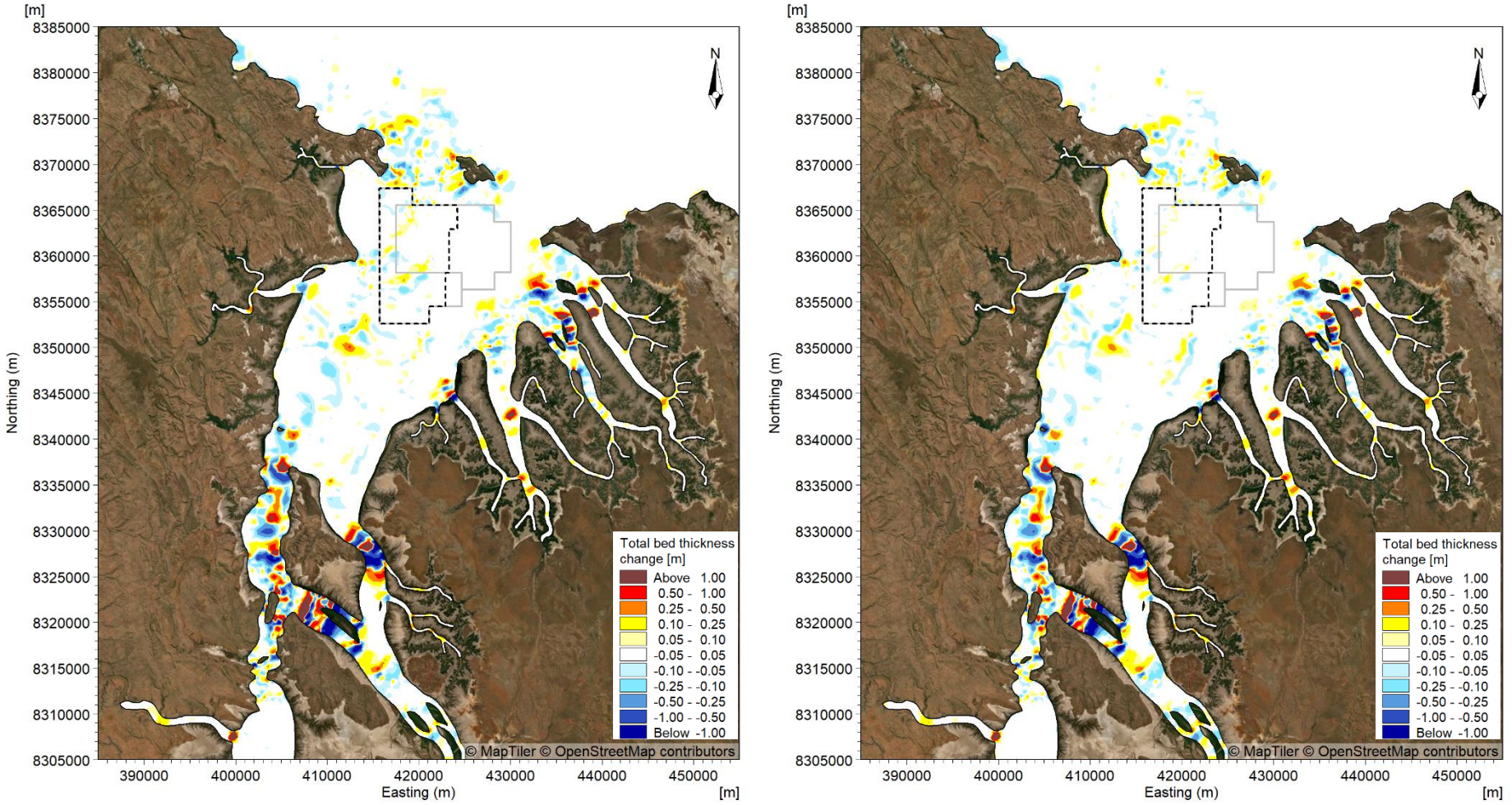


Figure 180. Modelled water level at AWAC-01 (top) and bedload transport rate (middle) and direction (bottom) at AWACs 01, 09 and 11 during TC Marcus. *Note: positive bedload transport is to the north and negative is to the south.*

5.1.3. Sedimentation

Spatial maps showing the modelled change in bed elevation over the two-month (60/61 days) wet, dry and transitional season periods and over the 5-day TC Marcus period are shown in Figure 181 and Figure 182. The plots generally show similar patterns for all the periods, but with the magnitude of the changes during the TC Marcus period being significantly smaller due to the shorter duration (5 days compared with 60/61 days). Modelled changes were slightly lower during the dry season compared with the wet and transitional seasons, while the changes during TC Marcus were higher than both the wet and transitional seasons when normalised for duration. The spatial pattern of the bed level changes shows the following:

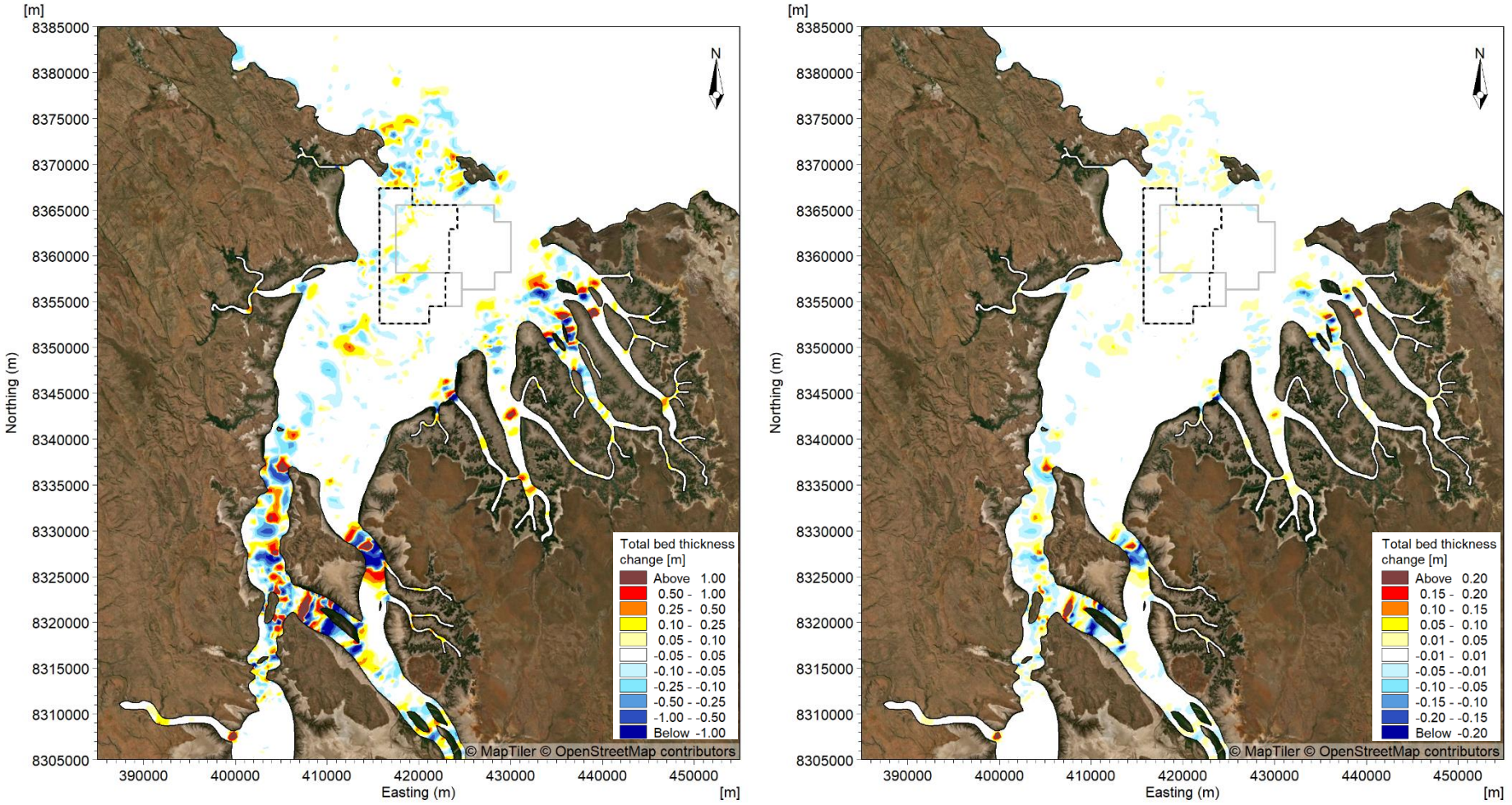
- Areas of erosion were typically adjacent to areas of accretion, indicating a potential redistribution or migration of sand rather than large areas either eroding or accreting.
- Within the POA, the modelled changes were predominantly in the southern half and along the western side, with bed level changes in the region of ± 0.25 m. The detailed multibeam survey undertaken by BKA in February 2024 (PCS 2024a) showed that large sand waves were present in these areas, and that these were subject to ongoing migration. Therefore, the modelled spatial pattern of change within the POA can be considered to be consistent with the bedforms present in the area.
- The largest changes in bed elevation were in the constrained channels of West and East Arms and in the False Mouths of the Ord, with localised changes of more than ± 1.0 m. Although changes of these magnitudes are possible, the changes could also be over-estimated due to limitations in the model in these areas, potentially relating to the bathymetry (there is relatively low confidence in the bathymetry in these areas) or due to the bed in some of the areas most likely being bedrock or gravel as opposed to sand. However, the modelled changes in these areas do not influence potential impacts due to the sand sourcing.



Wet season (2 months)

Dry season (2 months)

Figure 181. Modelled change in bed thickness due to bedload transport for the existing case over the two-month (60/61 days) wet and dry season periods.



Transitional season (2 months)

TC Marcus (5 days, different colour scale)

Figure 182. Modelled change in bed thickness due to bedload transport for the existing case over the two-month (61 days) transitional period and the 5-day TC Marcus period. *Note: the TC Marcus plot has a different colour scale.*

5.1.4. Beach Processes

As outlined in Section 1.2 and shown in Figure 2 in that section, there are three beaches located on the seaward coast outside of CG that are afforded high priority for protection, as they are important nesting sites for Flatback Turtles (*Natator depressus*). These are:

- Turtle Beach West located west of Cape Dussejour to the west of CG.
- Cape Domett Seaward Beach located east of Cape Domett to the east of CG.
- Turte Bay on the northwest coast of Lacrosse Island, in the centre of the entrance to CG.

Given the importance of these beaches as turtle nesting sites, high priority has been given to modelling any potential impacts of the proposed sand sourcing within CG on these beaches, as reported in this section.

There is also a Flatback Turtle nesting site at East Bank Point (also known as Barnett Point) inside CG, to the southeast of the POA. At this site the turtles nest on stranded sand banks (cheniers) located behind and protected by a seaward fringe of mangroves. As this site is not a proper beach, it is not amenable to beach process modelling, and is therefore not included in this section. The overall modelling of sediment transport and coastal processes reported in Section 5.2 indicates that the proposed sand sourcing will not cause measurable changes at that site.

This section presents updated results following modifications to the previous beach processes modelling presented in PCS (2024a) along with results for predicted 100 years (from today) of climate-change induced sea level rise. Overall, the updated results for the existing sea levels show the same trends and patterns compared to the results from the previous modelling, but with slightly higher longshore and cross-shore transport rates. The changes in the model results are due to changes in the modelled wave climate (the previous wave model had not been calibrated to measured wave data) along with changes in the intertidal and supratidal beach profile bathymetry which is now based on data from detailed drone-based LiDAR surveys of the beaches carried out in February 2024 (BKA 2024b - Annex 10: Aerial Drone LiDAR Report).

The locations of the cross-shore profiles adopted for the modelling are shown in Figure 183 to Figure 185. The modelled annual net potential natural longshore and cross-shore transport rates at each of the cross-shore profiles are shown in Figure 186 to Figure 187. Positive longshore transport represents transport in an easterly direction, while a negative longshore transport represents transport in a westerly direction (the exact direction varies depending on the alignment of the profile, for example at Turtle Bay positive represents transport to the north, negative represents transport to the south). For the cross-shore transport a positive transport represents net transport in a landward direction, while a negative transport represents net transport in a seaward direction. The results are discussed below for each of the three assessed turtle nesting beaches:

- Turtle Beach West: The natural longshore and cross-shore transport rates were similar, with the cross-shore transport being higher by 5,000 to 15,000 m^3/yr. The net longshore transport was modelled to be to the east at all three profiles, with similar transport rates at the western and middle profiles and lower transport at the eastern end. The modelled cross-shore transport was in a net landward direction at all three sites, indicating that sand is supplied through the cross-shore transport of sand from offshore. The potential landward transport rates at this beach were the highest out of the three beaches modelled, which is in agreement with the finding from the shoreline changes assessment presented in PCS (2024a), which showed that this beach was accreting at the highest rate.
- Cape Domett Seaward Beach: The natural cross-shore transport was modelled to vary along the length of the beach, with net landward transport at the western profile, and net offshore transport at the middle and eastern profiles. The longshore transport at the beach was consistently to the east, with rates gradually reducing from the western profile to the eastern profile. The results indicate that sand from offshore is transported landward at the western end of the beach. The sand is then transported along the beach, with accretion occurring along the length of the beach. In the middle and at the eastern end of the beach some of the sand is transported seaward by cross-shore transport. This overall understanding corresponds with shoreline changes calculated by PCS (2024a), with the western profile experiencing the highest rates of advance and the eastern profile the lowest.
- Turtle Bay, Lacrosse Island: Both the natural longshore and cross-shore transport rates at this bay were relatively low. The longshore transport rates indicate a small net southerly transport of sand at the bay, while the cross-shore transport rates indicate a small net landward transport

of sand from offshore. The modelled net onshore transport rate was slightly higher than the net southerly longshore transport rate. The relatively low transport rates at this beach correlate with the shoreline changes calculated by PCS (2024a) which showed limited change in the shoreline over time.

To show how the natural cross-shore and longshore transport varies spatially along the cross-shore profiles and how the transport rates vary over time, plots of the transport across the profile are shown over four months (121/123 days) of wet and dry season conditions and the annual transport rates from 2015 to 2019 are shown for the west profile at Turtle Bay West (TB1_WP) in Figure 188 to Figure 191. This profile was selected as both longshore and cross-shore transport rates are relatively high and it provides a typical representation as to how the transport varies along the cross-shore profile. The plots show the following:

- Cross-shore transport:
  - There was a gradual natural onshore transport of sand from the offshore end of the profile during both the wet and dry season conditions. The onshore transport occurred up to between the -2 m and -1 m AHD levels and with a potential offshore transport of sediment for the intertidal area of the profile above this elevation. The modelled cross-shore natural transport rates were significantly higher in the wet season compared to the dry season.
  - There was some annual variability in the modelled natural cross-shore sediment transport rates, with the net modelled rates varying by up to 25% of the annual average net transport rate.
- Longshore transport:
  - The model results showed that no natural longshore transport occurred along the profile below an elevation of -3 m AHD. Natural longshore transport occurred from this elevation up to the 3.5 m AHD level. The direction of the longshore transport varied between the seasons, with net transport to the east (positive) during the wet season and net transport to the west (negative) during the dry season. As with the cross-shore transport, the longshore transport rates during the wet season were significantly higher than the dry season rates.
  - There was significant annual variability in the natural longshore transport rates. The net transport to the east varied from 7,500 to 85,000 m^3, while in 2017 the net transport switched from the east to the west with a net transport of around 110,000 m^3. This indicates that Turtle Beach West is approximately aligned with the average wave direction and any variability in the mean wave direction due to large wave events can result in significant changes to the longshore transport rates.

The modelled annual net potential longshore and cross-shore transport rates at each of the cross-shore profiles assuming 0.9 m of climate-change induced sea level rise for 100 years from today are shown in Figure 192 to Figure 193. Compared with the results for the existing sea levels, the results show the potential for changes to both the longshore and cross-shore transport:

- Turtle Beach West: The model results showed a reduction in the net onshore transport at all three profiles of 5,000 to 10,000 m^3/yr. The modelled longshore transport rate was similar at the western and middle profile, while at the eastern profile it reduced from ~25,000 m^3/yr to 7,000 m^3/yr. This differential in net easterly longshore transport between the middle profile and the eastern profile would result in accretion of the beach between the two profiles.
- Cape Domett Seaward Beach: 100 years of sea level rise were modelled to result in an increase in net easterly longshore transport of 20,000 m^3/yr at the western profile, with little change in net longshore transport at the other two profiles. The modelled cross-shore transport rate was increased at all three profiles by between 2,000 and 5,000 m^3/yr.
- Turtle Bay, Lacrosse Island: The modelled longshore and cross-shore transport rates were similar to the existing sea level results.

The modelled cross-shore and longshore transport along the cross-shore profiles are shown assuming 100 years of sea level rise in Figure 194 and Figure 195. Comparison with the modelled results for the existing sea level show that due to the sea level rise, the transport occurred ~10 m further landward along the profile and up to a higher elevation. In addition, the model results showed an increase in the peak longshore transport rates (2,000 m^3/m for existing sea level compared with 2,500 m^3/m for 100

years from today) and cross-shore transport rates (165 m^3/m for existing sea level compared with 220 m^3/m for 100 years of sea level rise) for 100 years from today.

It is important to note that the simulations which assumed 100 years of sea level rise did not include any changes to the offshore bathymetry or to the beach profile in response to the sea level rise as it is not possible to reliably estimate these changes. This means that the 0.9 m of sea level rise assumed over 100 years will have resulted in a deepening of the water levels offshore of the beaches which in turn would allow increased wave energy to reach the beaches and potentially reduce wave refraction which could result in localised changes to the nearshore wave direction.

Based on this, increased longshore and cross-shore transport rates are expected when 100 years of sea level rise is included in the modelling. However, it is likely that both the offshore bathymetry and the beach profile will respond to sea level rise through morphological changes, which potentially could act to limit the wave energy which reaches the beaches. Based on this, the modelled change in longshore and cross-shore transport due to 100 years of sea level rise can be considered to be an upper estimate, with actual changes likely to be smaller.



Figure 183. Cross-shore profiles at Turtle Beach West.

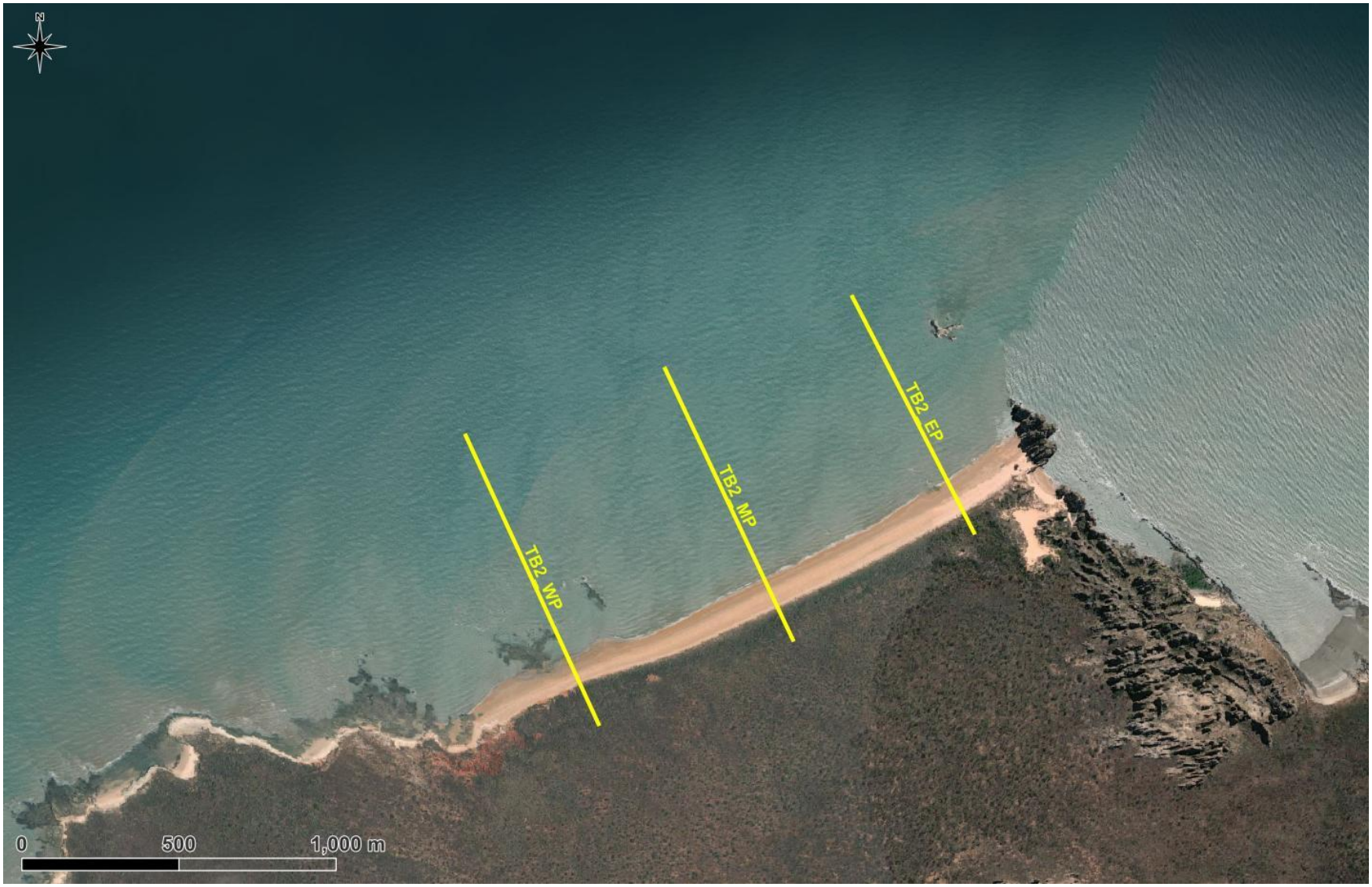


Figure 184. Cross-shore profiles at Cape Domett Seaward Beach.



Figure 185. Cross-shore profiles at Turtle Bay, Lacrosse Island.

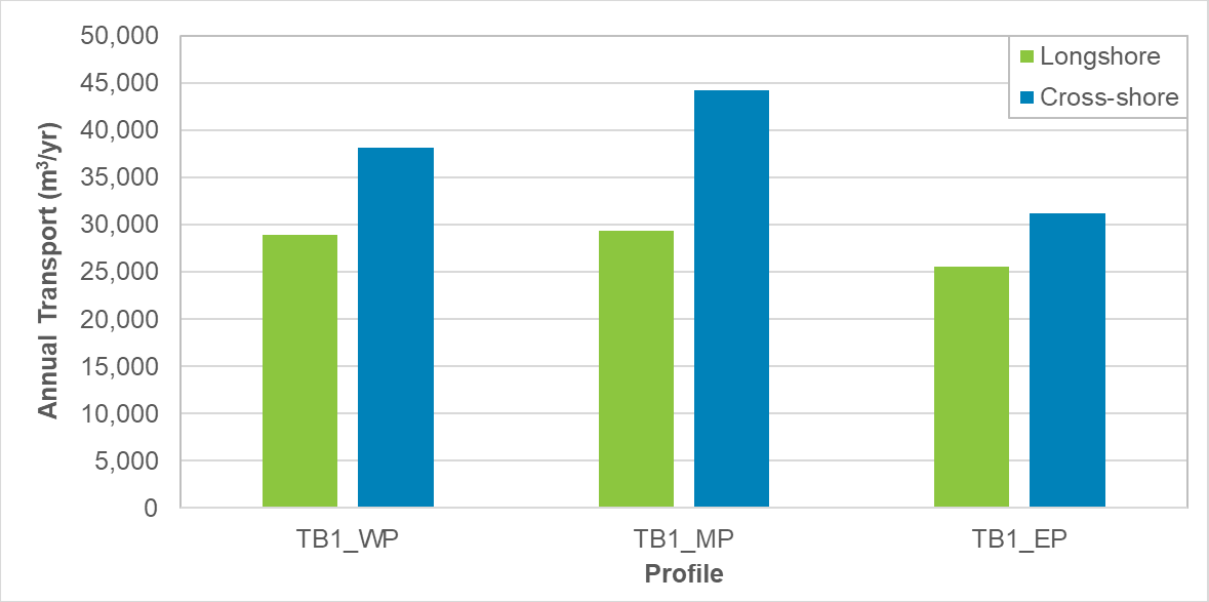


Figure 186. Modelled annual longshore and cross-shore transport at the three profiles at Turtle Beach West.

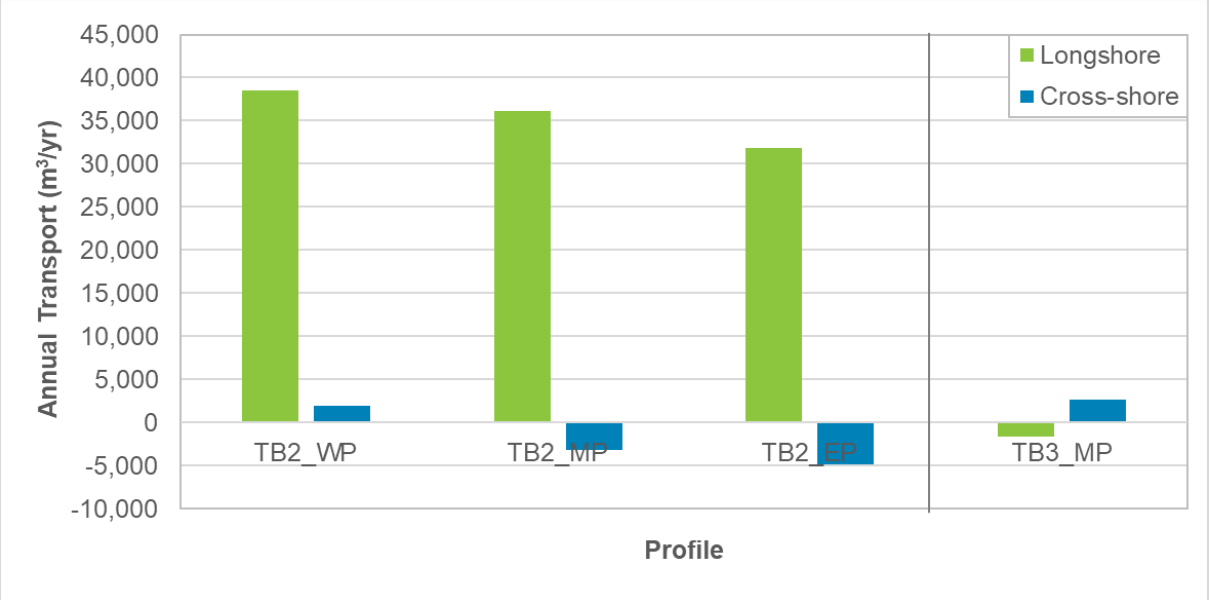


Figure 187. Modelled annual longshore and cross-shore transport at the three profiles at Cape Domett Seaward Beach and at the profile at Turtle Bay on Lacrosse Island.

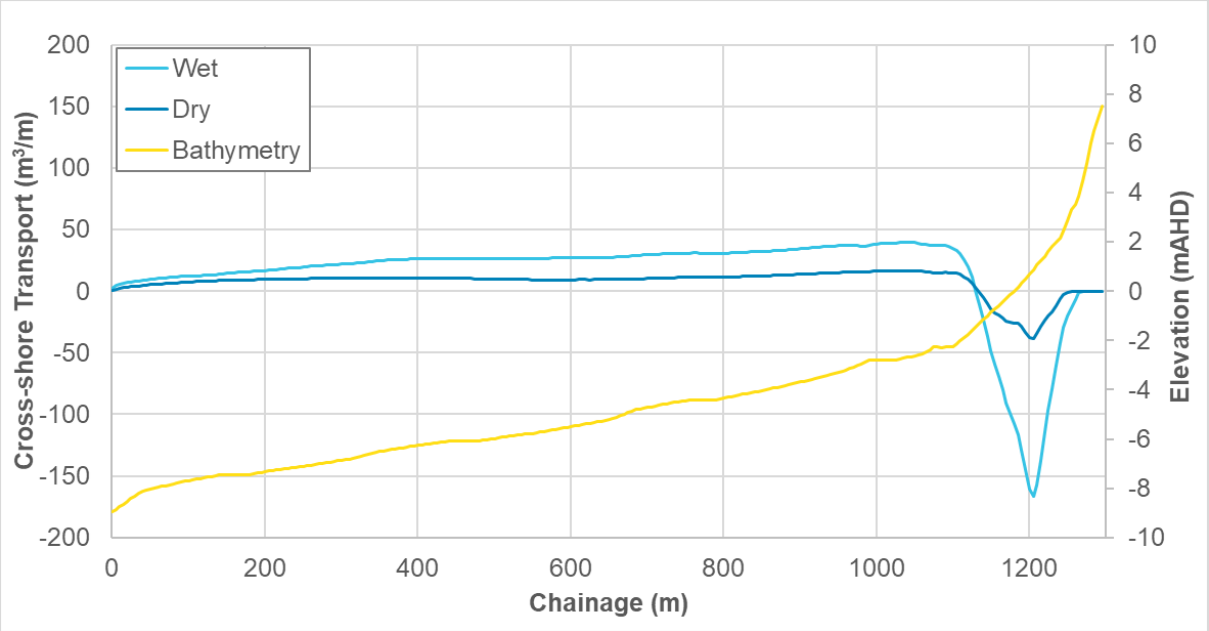


Figure 188. Spatial variation in cross-shore transport along the TB1_WP beach profile over four month (121/123 days) wet and dry season periods.

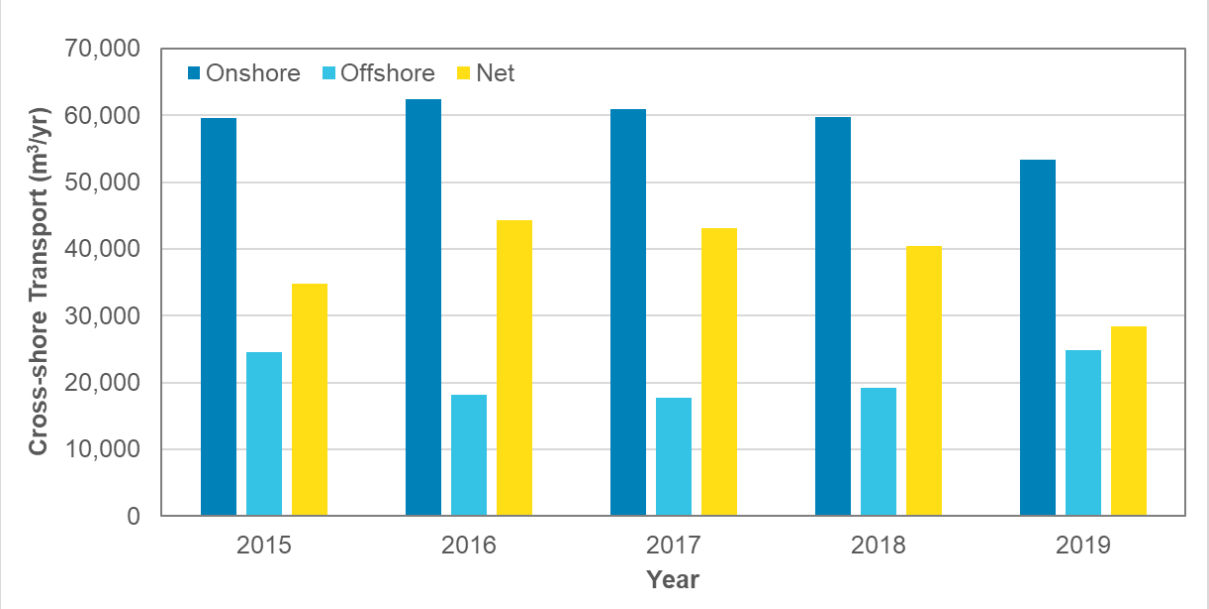


Figure 189. Annual variation in cross-shore transport at the TB1_WP beach profile from 2015 to 2019.

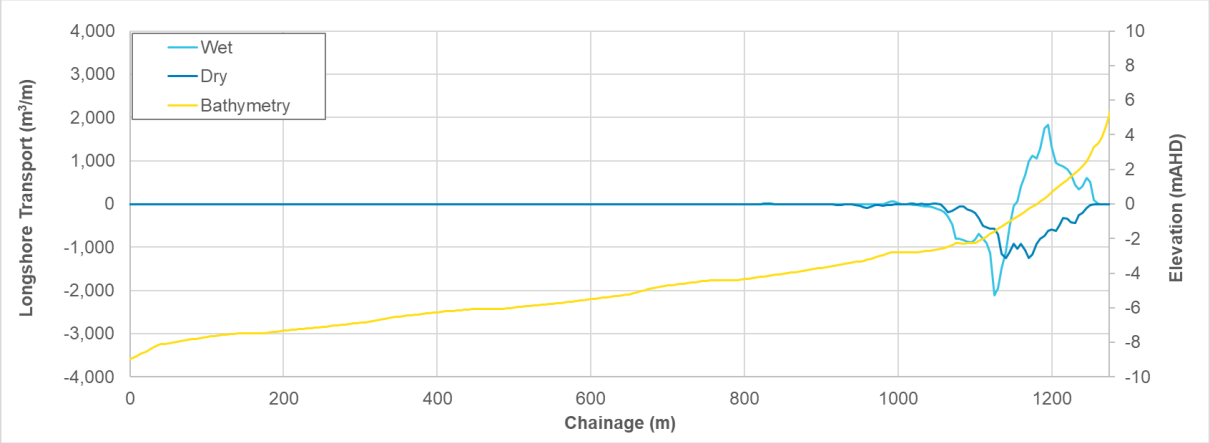


Figure 190. Spatial variation in longshore transport along the TB1_WP beach profile over four month (121/123 days) wet and dry season periods.

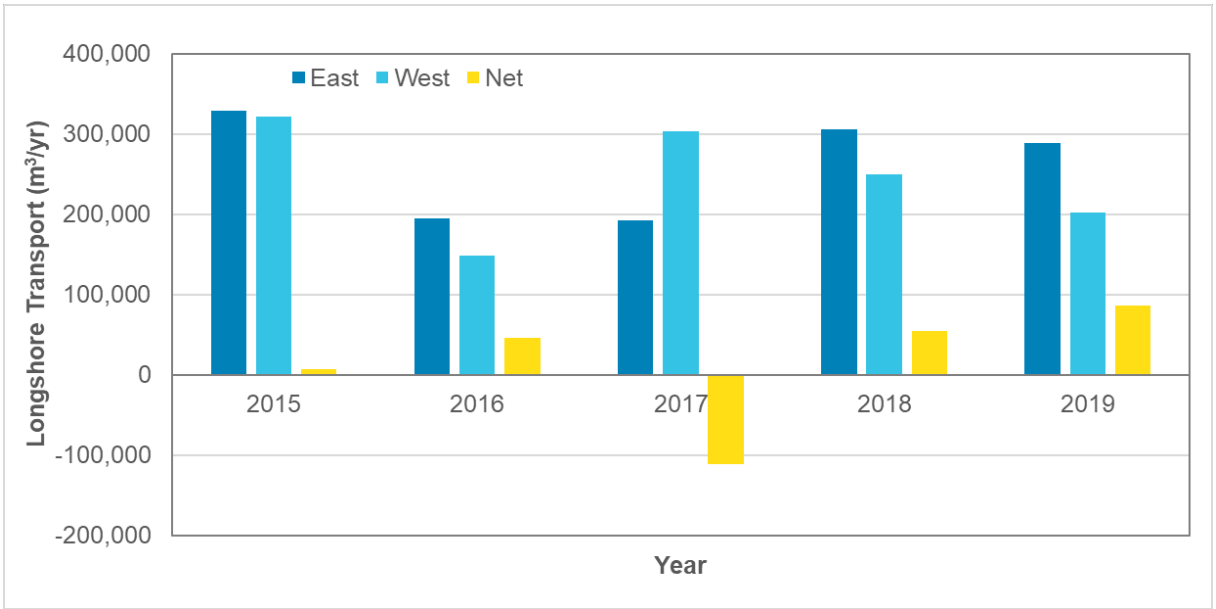


Figure 191. Annual variation in longshore transport at the TB1_WP beach profile from 2015 to 2019.

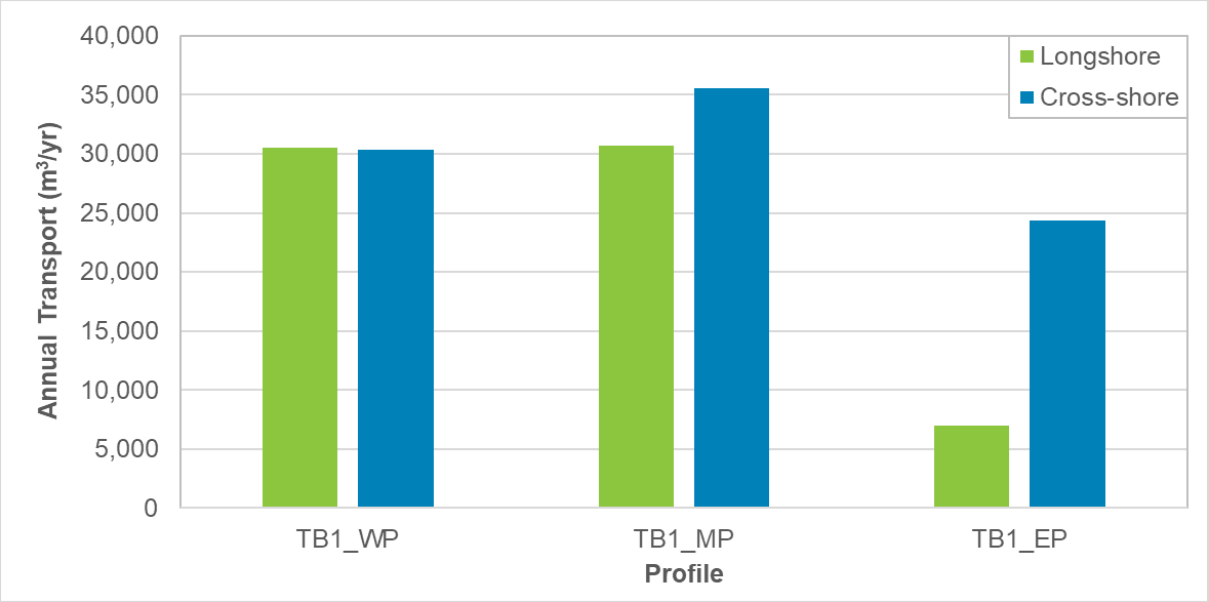


Figure 192. Modelled annual longshore and cross-shore transport assuming 0.9 m of sea level rise in 100 years at the three profiles at Turtle Beach West.

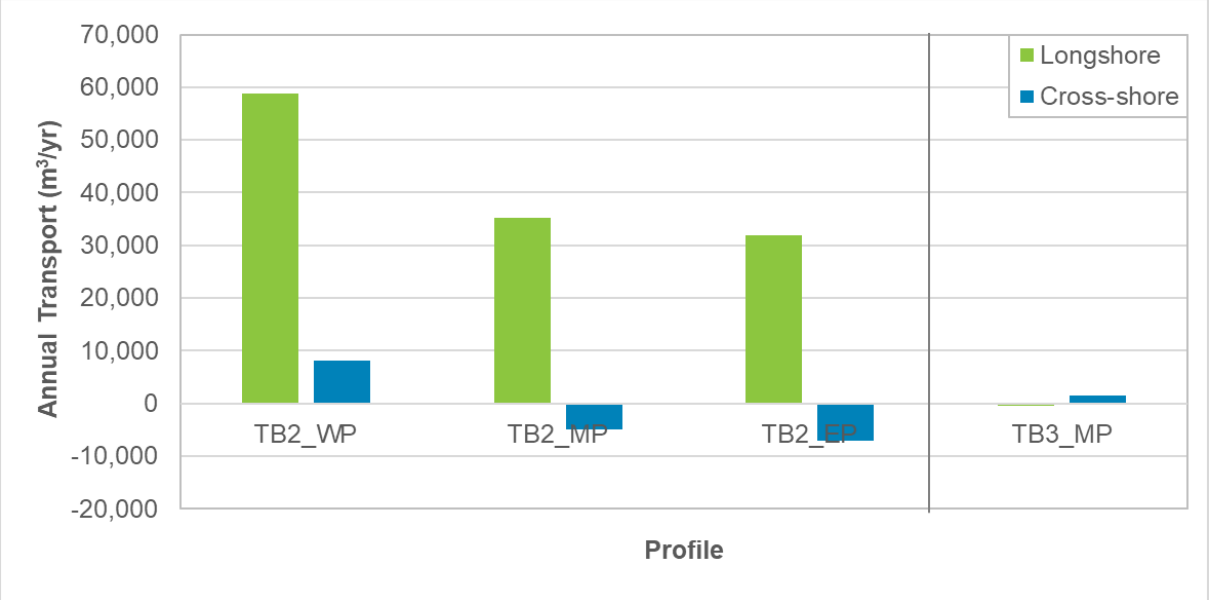


Figure 193. Modelled annual longshore and cross-shore transport assuming 0.9 m of sea level rise in 100 years at the three profiles at Cape Domett Beach and at the profile at Turtle Bay on Lacrosse Island.

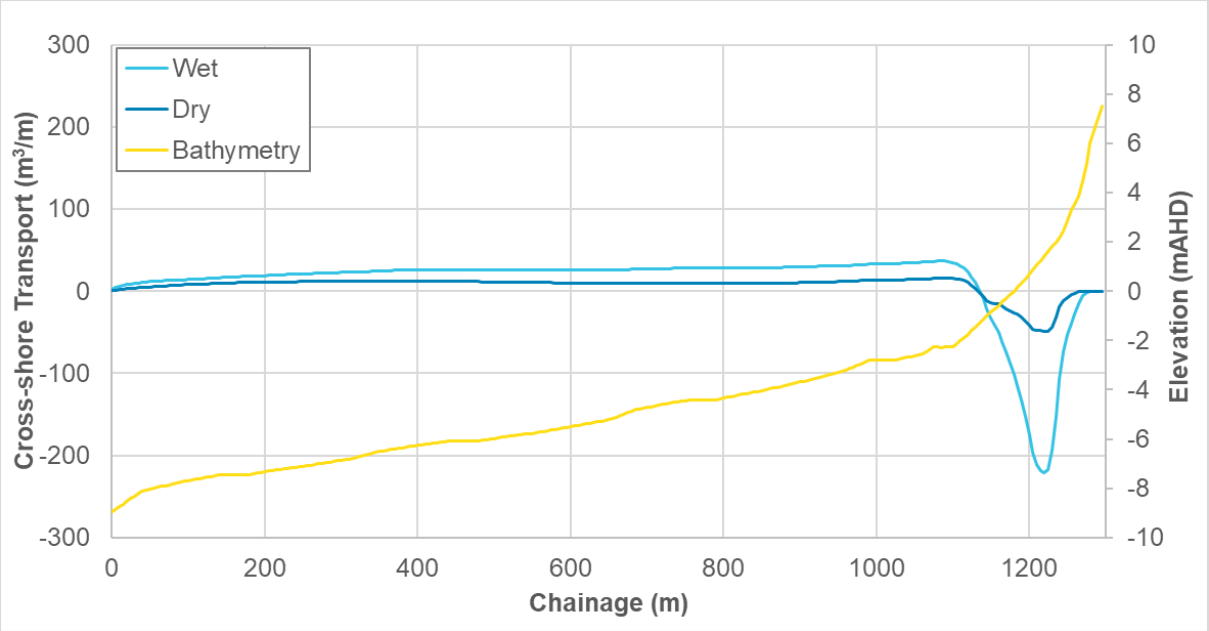


Figure 194. Spatial variation in cross-shore transport along the TB1_WP beach profile over four month (121/123 days) wet and dry season periods assuming 100 years of sea level rise.

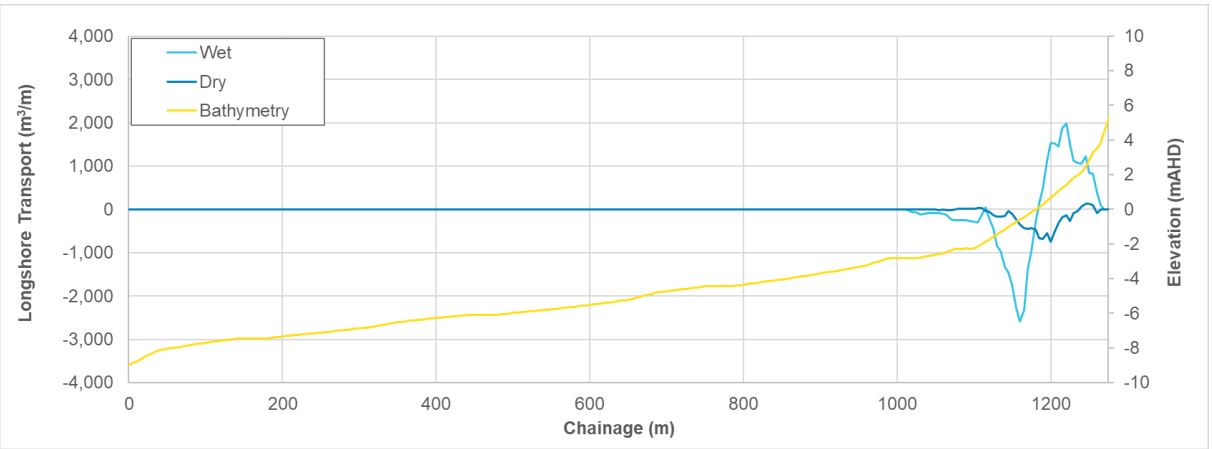


Figure 195. Spatial variation in longshore transport along the TB1_WP beach profile over four month (121/123 days) wet and dry season periods assuming 100 years of sea level rise.

5.2. Scenario Impacts

To assess potential changes since the pre-European scenario and potential future changes from 5 years (23 million m^3) of sand sourcing and 15 years (70 million m^3) of sand sourcing scenarios, results from the ST simulations for the four metocean conditions (dry season, transitional season, wet season and TC) have been compared with the existing case. In addition, results from the scenario in 100 years' time with sand sourcing have been compared with the scenario of no sand sourcing in 100 years' time to determine the potential future changes from sand sourcing.

5.2.1. Suspended Sediment

This section presents the modelled changes to SSC for specific, representative scenarios and for a range of metocean conditions. Plots of the modelled changes for all the scenarios and during all metocean conditions are provided in Appendix C.

Spatial maps of the modelled 50th and 95th percentile SSC over the two month (60 days) wet season period for the existing case, after 5 years and after 15 years of sand sourcing and for the pre-European scenario are shown in Figure 196 to Figure 201. The map plots of the 50th and 95th percentile SSC for the existing case and the sand sourcing scenarios are very similar, showing that the sand sourcing is not assessed to result in a significant change in SSC within or offshore of CG.

In contrast, the plots for the pre-European scenario show that prior to construction of the Ord River dams the SSC in CG was significantly higher during high river discharge events in the wet season. Both the 50th and 95th percentile SSC for the pre-European scenario were modelled to be significantly higher within CG compared to the existing case, being 1,000 to 2,000 mg/L in the POA compared to 100 to 500 mg/L for the existing case.

To better understand the changes in SSC due to the sand sourcing after 15 years relative to the existing case, timeseries plots of the change in SSC during the wet, dry and transitional seasons and during TC Marcus at sites from the upstream (southern) end of CG (AWAC-08) to offshore at King Shoals (AWAC-09) are shown in Figure 202 to Figure 205. In addition, a plot comparing the SSC for the existing case and with the pre-European (no dams) scenario at the same sites during the wet season is shown in Figure 206. The results show the following:

- For the existing case, natural background SSC within the main body of CG ranged from 50 mg/L to 500 mg/L for the 50th percentile and 100 mg/L to more than 3,000 mg/L for the 95th percentile.
- The 15 years (70 million m^3) of sand sourcing was modelled to result in short duration changes in SSC of up to ± 20 mg/L during the three seasons, with the magnitude of the changes varying between the sites. At most sites short duration increases and decreases in SSC were modelled during each tidal cycle, indicating that the changes were predominantly due to the small change in phase of the tide rather than an absolute change in SSC (which is why the spatial SSC percentile maps do not show any changes). Changes at the entrance to West Arm (AWAC-08) were predominantly reductions in SSC of up to 15 mg/L (except during TC Marcus when there was an increase in SSC of up to 15 mg/L), with the reduction coinciding with the lower SSC at high water. The largest (but still small) modelled changes were directly upstream (south) of the POA, where reductions in SSC occurred during the peak SSC at low water and increases in SSC occurred during the trough at high water. Within the POA the modelled changes were predominantly a reduction in the peak SSC at low water of up to 15 mg/L. The changes detailed were all considered to be very minor due to their short duration and when considered in the context of existing background SSC in CG as detailed above.
- These modelled changes to SSC caused by the sand sourcing operation were predominantly a result of the minor changes to the hydrodynamics due to the sand sourcing (see Section 4.2.1). As discussed above, the short duration changes in SSC were predominantly due to the modelled small change in the phase of the tidal propagation into CG (up to 30 seconds earlier). The other changes in SSC were likely to be a result of the small changes to current speed due to the deepening within the POA. The changes were shown to be predominantly reductions in current speed within and directly adjacent to the POA which results in a reduction in SSC at most sites.
- The modelled changes due to the 15 years of sand sourcing were larger during a tropical cyclone as modelled for TC Marcus, compared to the three seasons, with the largest change being a reduction in SSC within the POA (AWAC-01) of 200 mg/L. At the sites outside of the POA the changes during TC Marcus were up to ± 30 mg/L.
- For the pre-European scenario the results showed a very similar SSC to the existing case from the start of the simulation period up to the 7th March 2024 when there was a high river discharge event. After the high river discharge event the SSC for the pre-European scenario was significantly higher than for the existing case. The difference in SSC was greatest at the northern entrance to West Arm, with a peak SSC for the existing case of ~1,000 mg/L compared to a peak SSC for the pre-European scenario of ~4,500 mg/L. Within the POA the peak SSC for the existing case was ~300 mg/L compared to 1,700 mg/L for the pre-European scenario. The reduction in SSC in CG since European settlement was due to reduced and more controlled river discharges from the Ord River as a result of construction of the two dams in 1969 and 1971.

A statistical summary of the percent change in SSC relative to the existing case due to the 15 years of sand sourcing are provided in Table 24 and Table 25. The results show the following:

- During the three seasonal periods simulated the largest change in SSC percentiles relative to the existing case for the 15 years of sand sourcing scenario was a reduction of 8% at the sites within or directly adjacent to the POA (AWAC-01 to AWAC-04). This reduction was to the 99th percentile SSC, showing how the sand sourcing was assessed to slightly reduce peaks in SSC within the POA. Outside of the POA the modelled changes were also predominantly reductions in SSC, with changes limited to ± 3% at most sites. The only exception to this was directly upstream (south) of the POA (AWAC-11) with modelled increases in the 20th and 50th percentile SSC of 6% and 4% respectively. The timeseries plots showed that this was due to a small increase in the SSC trough at high water.

- During TC Marcus the modelled changes in SSC due to the 15 years of sand sourcing scenario were larger within the POA compared to the changes during the three seasons, with a reduction in the 99th percentile of 24% at AWAC-01. Outside of the POA both increases and decreases in SSC percentiles were modelled, with the changes predominantly within ± 3%. The only exception to this was directly upstream (south) of the POA (AWAC-11) with a modelled increase in the 95th percentile of 5%.

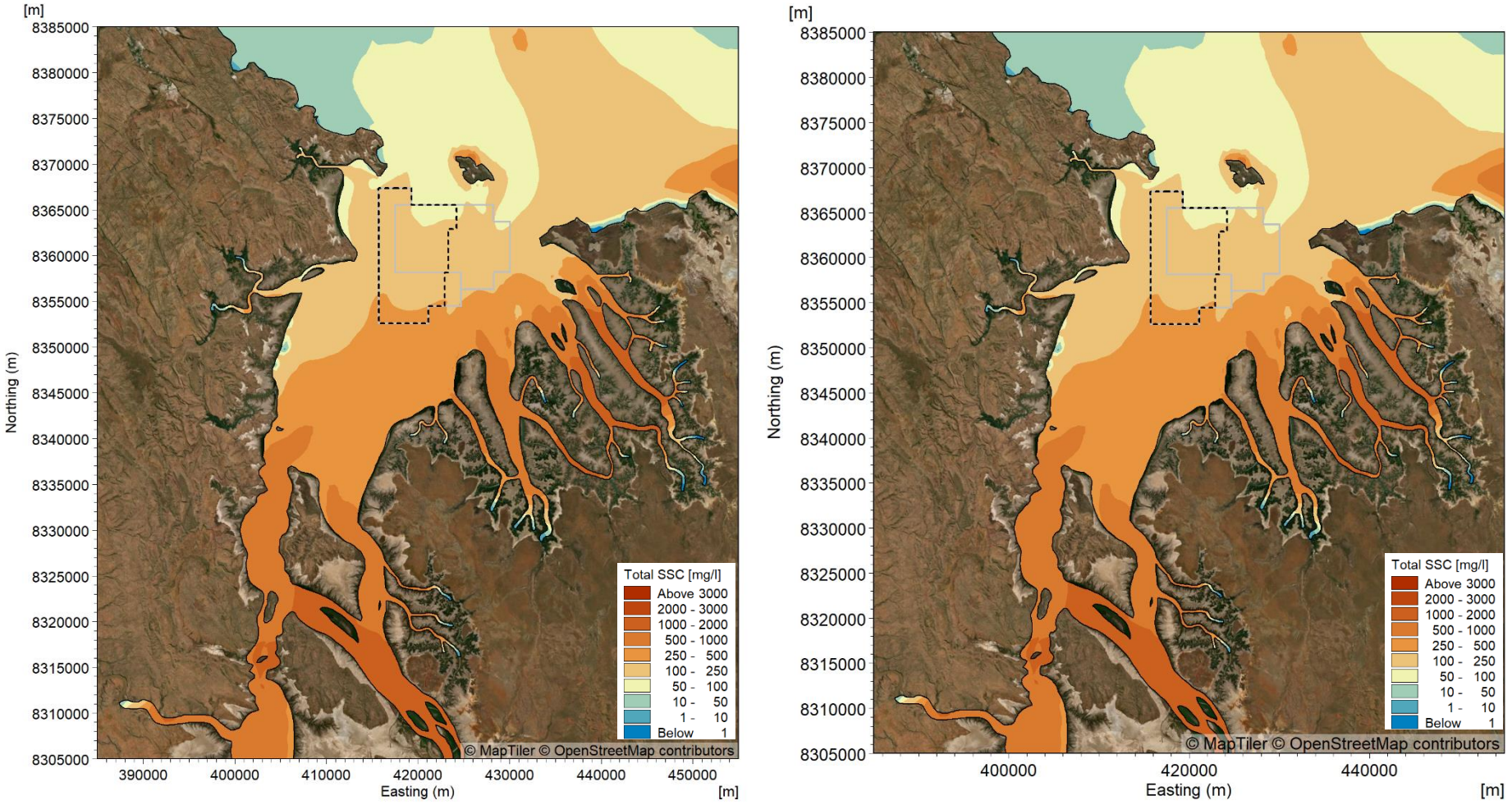
To understand the change in SSC which has occurred since European settlement (primarily due to construction of the Ord River dams) along with the modelled cumulative changes as a result of the Ord River dams and the proposed 15 years of sand sourcing, a statistical summary of the percent change in SSC is provided for the three different seasons in Table 26 to Table 28. A negative change in the tables indicates that the SSC has reduced as a result of European settlement and vice versa for a positive change. The tables show the following:

- The statistics for the pre-European scenario during the wet season indicate how much the SSC in CG has been reduced during a high river discharge event due to the construction of the Ord River dams. The results show that the 80th through to 99th percentile SSCs were assessed to have been reduced by between 56% and 87% at all sites except one (AWAC-07, located in the False Mouths of the Ord, where reductions of 5 to 16% were modelled). At these sites the 99th percentile SSC was reduced by 74% to 86%, showing how the peaks in SSC in the wet season pre-European settlement would have been significantly higher. The modelled SSC for the lower percentiles (5th to 50th) were also shown to have been higher pre-European settlement, but with reductions due to the construction of the Ord River dams assessed to be less than 30% (highest reduction was 27%).

- The SSC during the dry season was modelled to have increased by up to 16% since European settlement. This was due to the Ord River discharge in the dry season having been lower pre-European settlement, with the Ord River dams now regulating the dry season discharge to provide a constant discharge. The increases in SSC were typically above 3% at all sites, except at AWAC-07 which experienced increases in SSC of up to 2%. The largest modelled increases in SSC were at the upstream sites, namely the northern entrance to West Arm (AWAC-08) and directly upstream of the proposed operational area (AWAC-11).

- The SSC due to European settlement during the transitional season was modelled to have increased by up to 2%. The relatively small increase was due to the Ord River experiencing some river discharge at this time of year prior to the construction of the Ord River dam, meaning increases were not as large as during the dry season.

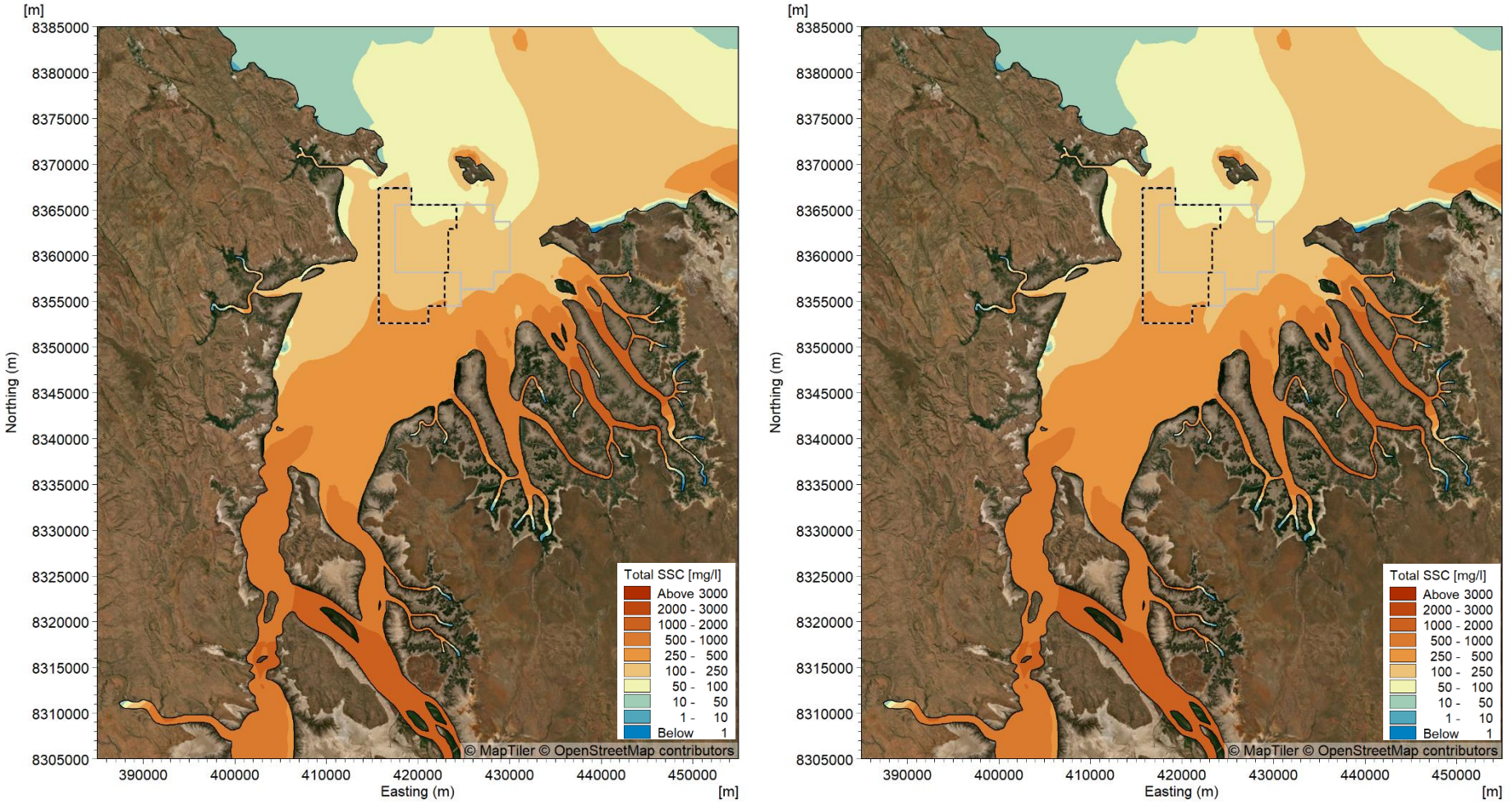
- The cumulative changes in SSC due to the Ord River dams and 15 years of sand sourcing show that during the wet season the additional change in SSC due to the sand sourcing was very small (additional changes of up to ± 3%) relative to the changes resulting from the Ord River dams. During the dry season the modelled cumulative change in SSC due to the sand sourcing and Ord River dams was typically be smaller than the change just due to the Ord River dams, meaning that the cumulative changes were less than the just Ord River dams changes. During the transitional season the cumulative change in SSC due to the sand sourcing and Ord River dams was assessed to typically either reduce the increase in SSC due to just the Ord River dams or change the increase in SSC to a reduction in SSC. Overall, the results show that the relative contribution of the sand sourcing to the cumulative changes are negligible.



Existing Case

5yr Sand Sourcing

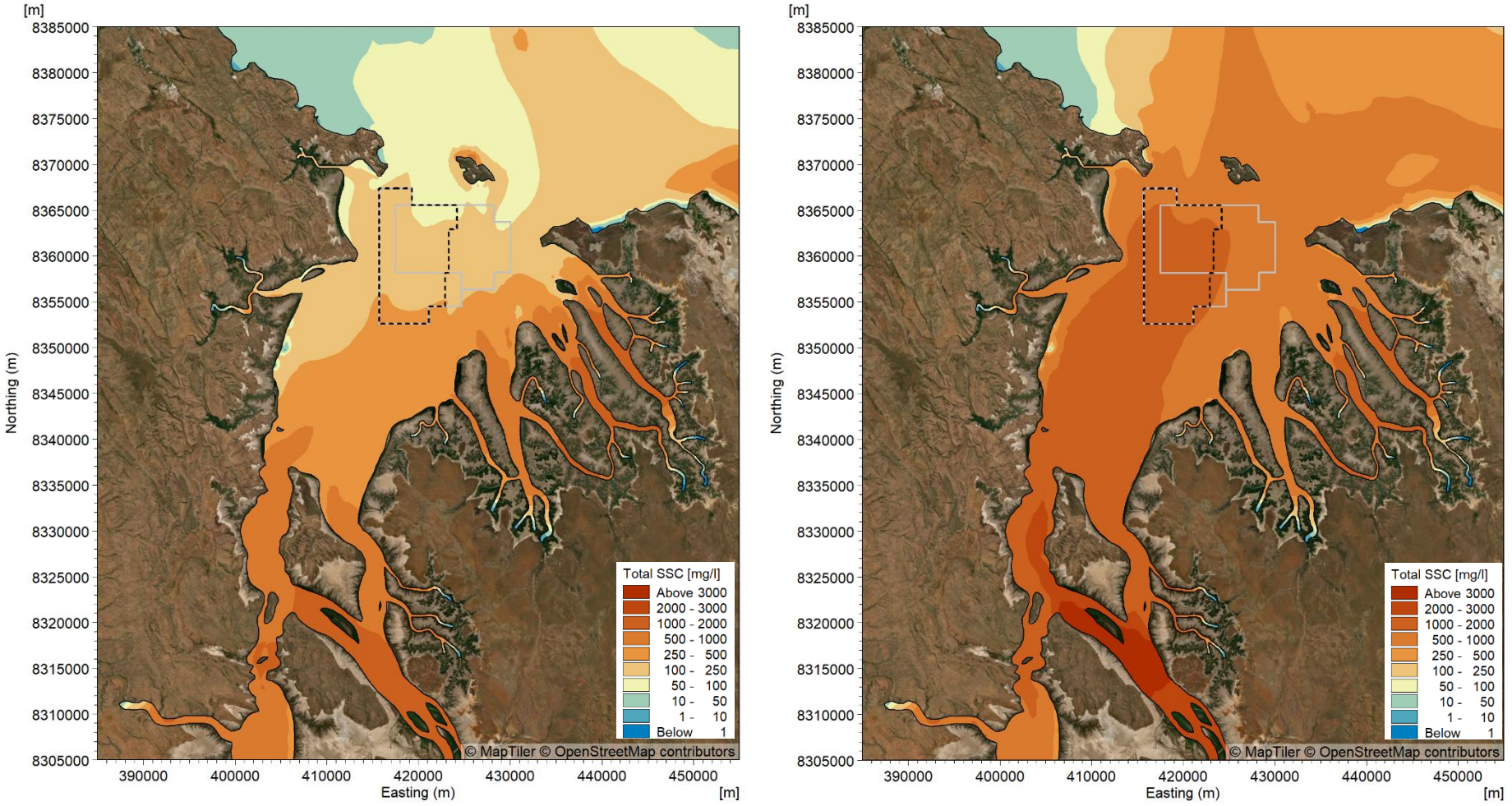
Figure 196. Modelled existing case and 5 years of sand sourcing scenario 50th percentile SSC over the two-month (60 days) wet season period.



Existing Case

15yr Sand Sourcing

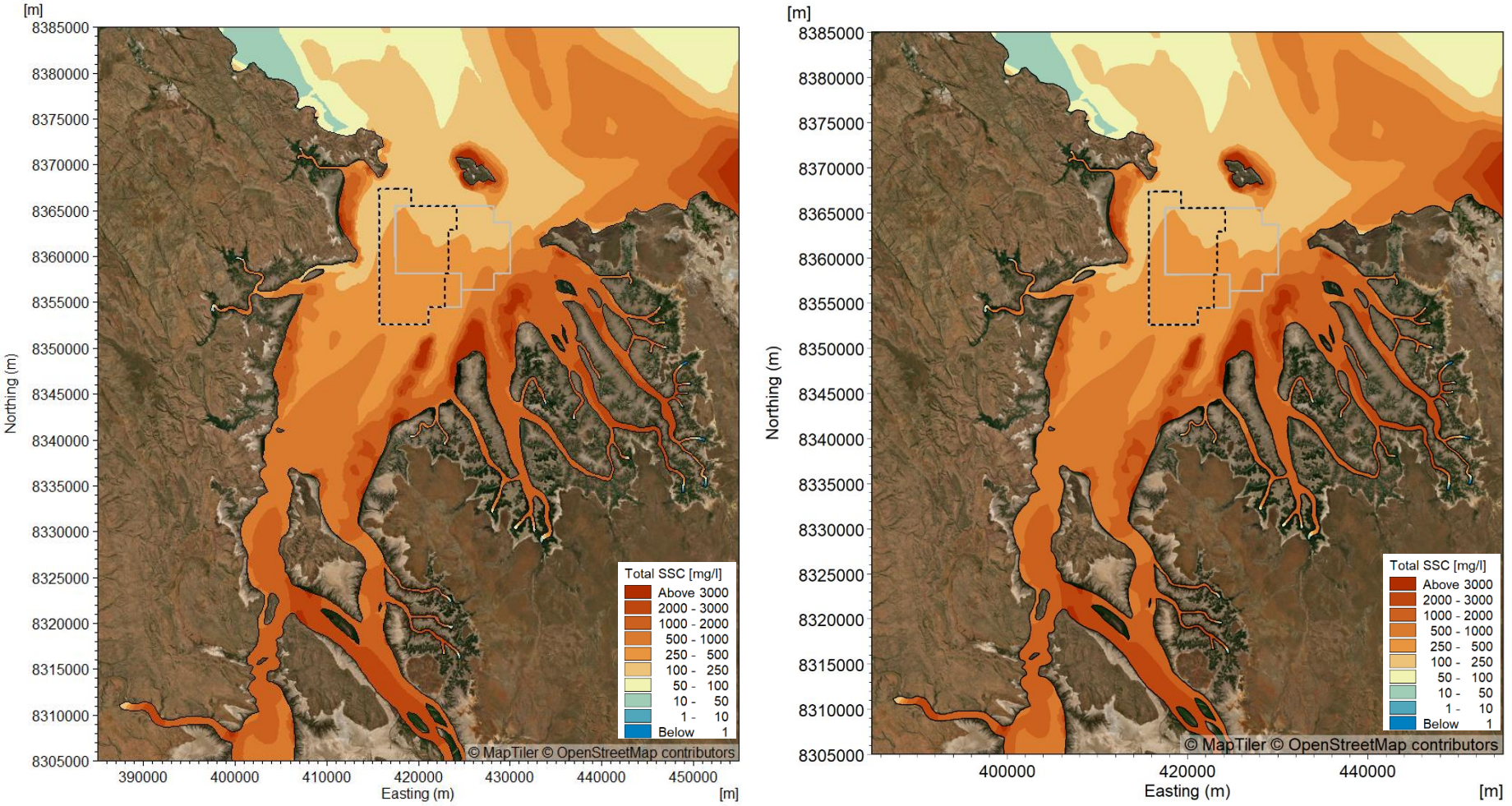
Figure 197. Modelled existing case and 15 years of sand sourcing scenario 50th percentile SSC over the two-month (60 days) wet season period.



Existing Case

Pre-European Settlement

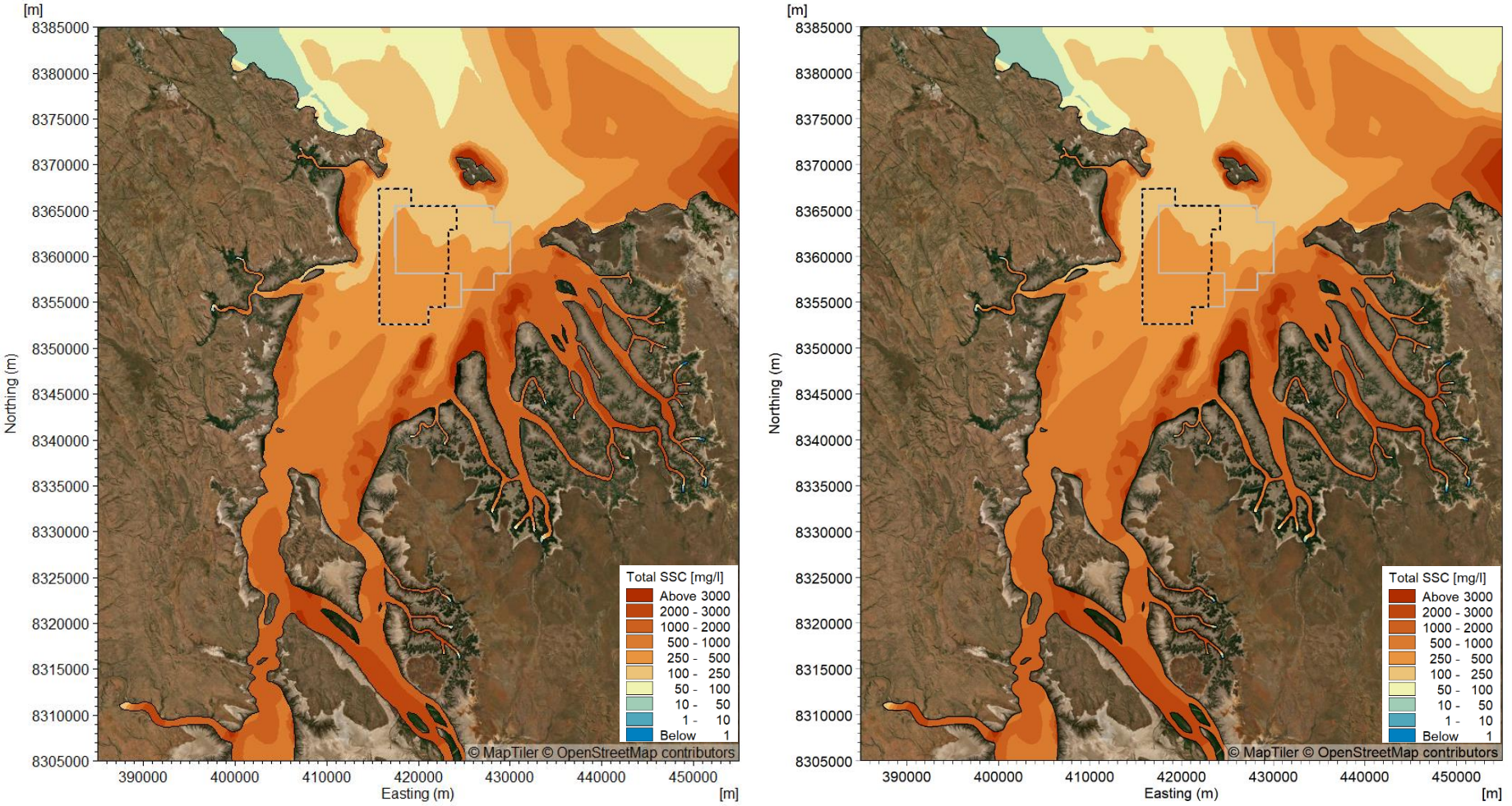
Figure 198. Modelled existing case and the pre-European settlement scenario 50th percentile SSC over the two-month (60 days) wet season period.



Existing Case

5yr Sand Sourcing

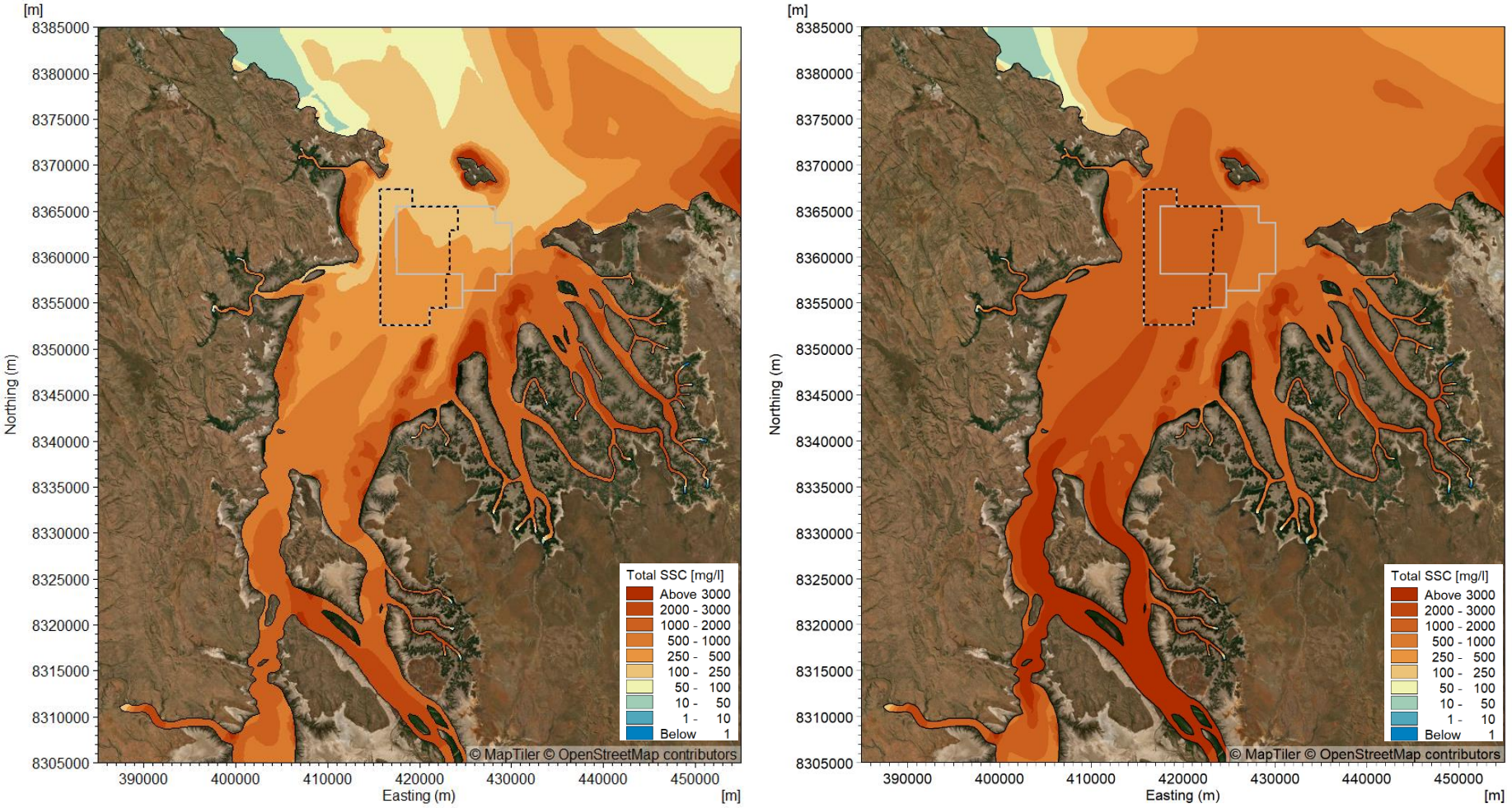
Figure 199. Modelled existing case and 5 years of sand sourcing scenario 95th percentile SSC over the two-month (60 days) wet season period.



Existing Case

15yr Sand Sourcing

Figure 200. Modelled existing case and 15 years of sand sourcing scenario 95th percentile SSC over the two-month (60 days) wet season period.



Existing Case

Pre-European Settlement

Figure 201. Modelled existing case and the pre-European settlement scenario 95th percentile SSC over the two-month (60 days) wet season period.

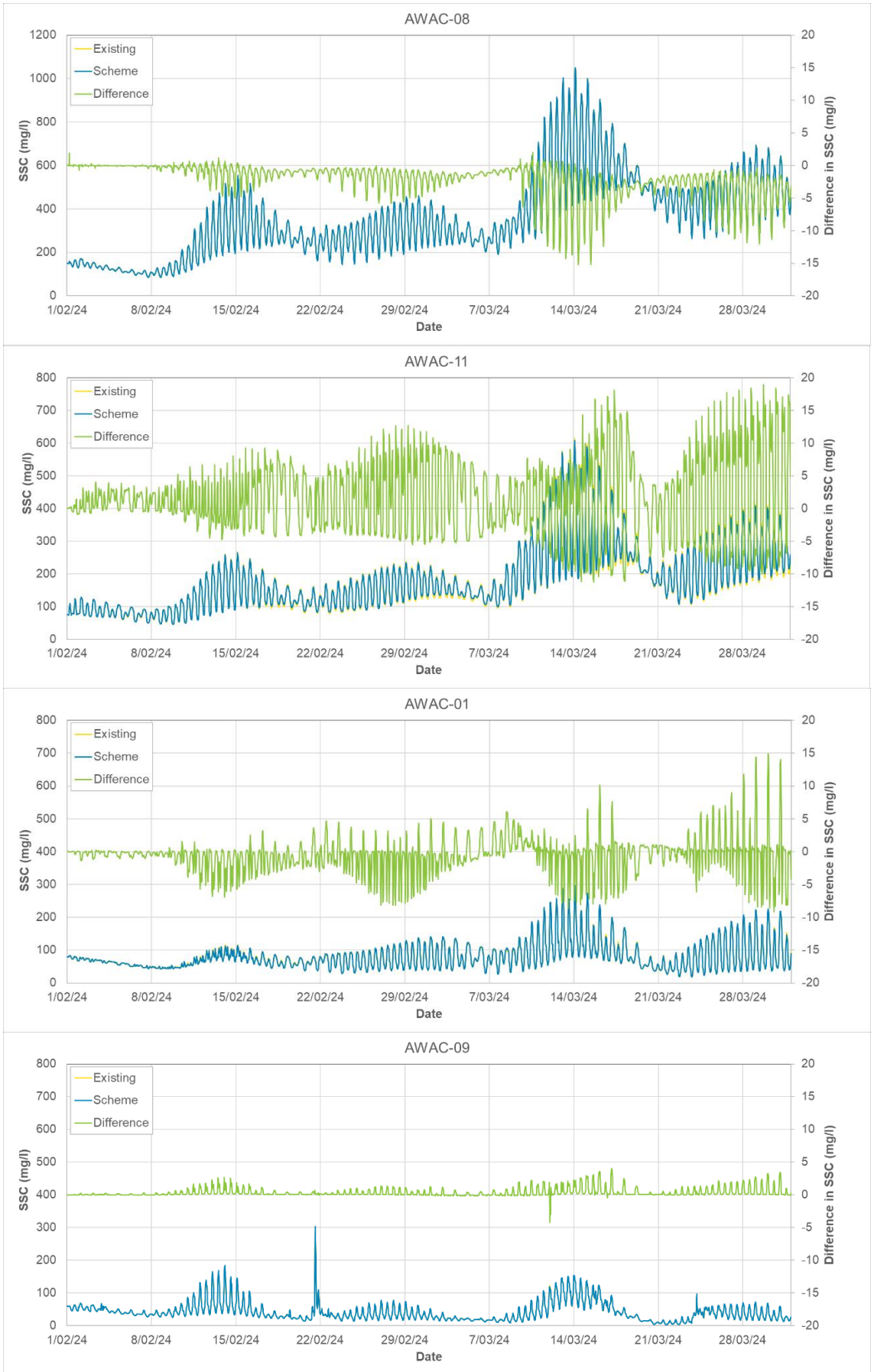


Figure 202. Timeseries showing the modelled change in SSC during the wet season due to 15 years (70 million m^3) of sand sourcing (Scheme).

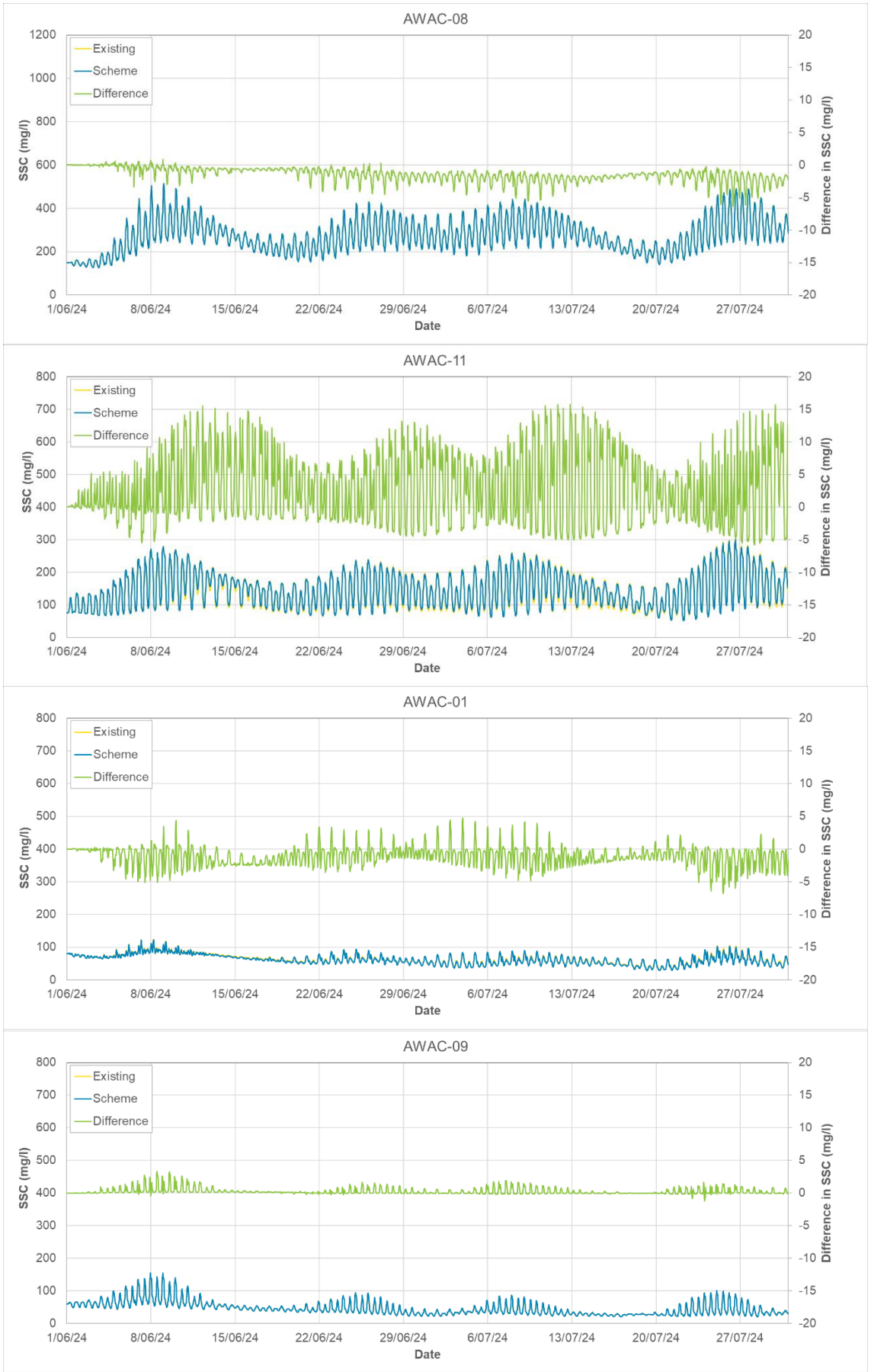


Figure 203. Timeseries showing the modelled change in SSC during the dry season due to 15 years (70 million m^3) of sand sourcing (Scheme).



Figure 204. Timeseries showing the modelled change in SSC during the transitional season due to 15 years (70 million m^3) of sand sourcing (Scheme).



Figure 205. Timeseries showing the modelled change in SSC during TC Marcus due to 15 years (70 million m^3) of sand sourcing (Scheme).

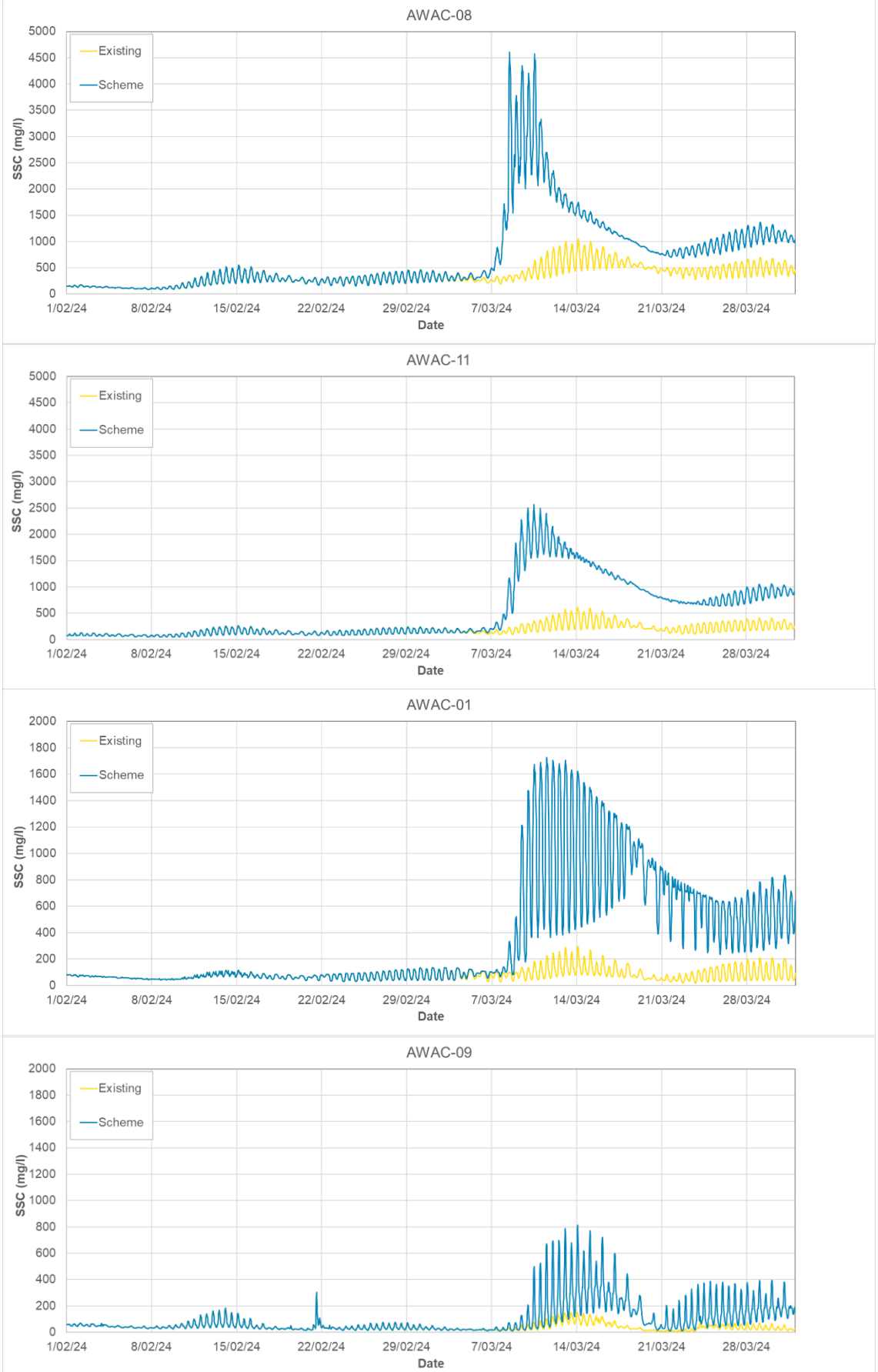


Figure 206. Timeseries showing the modelled difference in SSC during the wet season for the pre-European settlement scenario (Scheme).

Table 24. Statistics of the modelled change in SSC during the wet and dry seasons due to 15 years (70 million m^3) of sand sourcing relative to the existing case.

Statistic	AWAC01 (in POA)	AWAC02 (in POA)	AWAC03 (in POA)	AWAC04 (in POA)	AWAC05	AWAC06	AWAC07	AWAC08	AWAC09	AWAC10	AWAC11
Wet Season Change (%)											
99th %ile	2%	-8%	-2%	0%	0%	-2%	0%	0%	1%	-2%	-2%
95th %ile	0%	-7%	3%	1%	1%	-2%	0%	0%	1%	-2%	-1%
90th %ile	0%	-5%	0%	1%	2%	-2%	-1%	0%	1%	-1%	-1%
80th %ile	0%	-5%	2%	1%	1%	-2%	0%	-1%	1%	-1%	2%
50th %ile	-1%	-2%	0%	1%	1%	-1%	-1%	-1%	0%	-1%	1%
20th %ile	-1%	-2%	-3%	1%	1%	-1%	-2%	-1%	0%	-1%	3%
10th %ile	0%	-3%	-1%	0%	2%	-2%	-2%	0%	0%	-1%	3%
5th %ile	0%	-3%	-1%	0%	2%	-3%	-3%	0%	0%	-2%	2%
Dry Season Change (%)											
99th %ile	-1%	-5%	4%	-2%	0%	-1%	0%	0%	2%	-2%	-1%
95th %ile	-1%	-3%	3%	-1%	-2%	-1%	0%	0%	1%	-2%	-1%
90th %ile	-1%	-3%	4%	-1%	-2%	-2%	-1%	0%	1%	-2%	-1%
80th %ile	-1%	-2%	2%	-1%	-1%	-2%	0%	0%	1%	-2%	0%
50th %ile	-3%	-2%	-2%	-1%	-1%	-1%	-1%	-1%	0%	-1%	4%
20th %ile	-2%	-2%	-4%	-1%	0%	-1%	-2%	-1%	0%	-2%	6%
10th %ile	-2%	-3%	-4%	-1%	0%	-1%	-1%	-1%	0%	-2%	2%
5th %ile	-1%	-2%	-5%	-1%	0%	-1%	-2%	-1%	0%	-2%	1%

Note: AWAC-02 is actually located 450 m to the east of the POA, but as it is so close to the POA boundary the changes are representative of changes within the POA.

Table 25. Statistics of the modelled change in SSC during the transitional season and during TC Marcus due to 15 years (70 million m^3) of sand sourcing relative to the existing case.

Statistic	AWAC01 (in POA)	AWAC02 (in POA)	AWAC03 (in POA)	AWAC04 (in POA)	AWAC05	AWAC06	AWAC07	AWAC08	AWAC09	AWAC10	AWAC11
Transitional Season Change (%)											
99th %ile	-1%	-8%	1%	-2%	0%	-1%	0%	0%	1%	-2%	-1%
95th %ile	-4%	-5%	-1%	-1%	-2%	-2%	0%	0%	0%	-2%	0%
90th %ile	-3%	-6%	-1%	-2%	-1%	-2%	0%	0%	1%	-3%	-1%
80th %ile	-4%	-5%	-1%	-1%	-1%	-2%	-1%	-1%	0%	-3%	0%
50th %ile	-4%	-4%	-4%	0%	1%	-2%	-1%	-1%	0%	-2%	0%
20th %ile	-2%	-2%	-6%	0%	1%	-2%	-2%	-1%	0%	-3%	2%
10th %ile	-1%	-2%	-5%	0%	1%	-2%	-2%	-1%	0%	-3%	2%
5th %ile	0%	-3%	-6%	0%	2%	-2%	-3%	-1%	0%	-3%	3%
TC Marcus Change (%)											
99th %ile	-24%	0%	-15%	2%	1%	-1%	-1%	2%	0%	-1%	3%
95th %ile	-12%	-3%	0%	-4%	0%	-1%	1%	1%	1%	0%	5%
90th %ile	-5%	-1%	-4%	-1%	0%	1%	0%	1%	0%	-1%	-3%
80th %ile	-3%	-2%	-5%	-4%	-3%	-1%	-1%	1%	1%	0%	-3%
50th %ile	-1%	0%	0%	0%	-1%	0%	0%	0%	0%	-1%	-1%
20th %ile	-1%	0%	-1%	-1%	0%	0%	0%	0%	0%	0%	-1%
10th %ile	0%	0%	0%	0%	0%	0%	0%	0%	0%	0%	-1%
5th %ile	0%	-1%	-1%	0%	0%	0%	0%	0%	0%	0%	-1%

Note: AWAC-02 is actually located 450 m to the east of the POA, but as it is so close to the POA boundary the changes are representative of changes within the POA.

Table 26. Statistics of the modelled change in SSC during the wet season for the pre-European settlement scenario relative to the existing case and the cumulative change of the pre-European settlement scenario and the 15 years (70 million m^3) of sand sourcing scenario.

Statistic	AWAC01 (in POA)	AWAC02 (in POA)	AWAC03 (in POA)	AWAC04 (in POA)	AWAC05	AWAC06	AWAC07	AWAC08	AWAC09	AWAC10	AWAC11
Change since European Settlement (%)											
99th %ile	-86%	-82%	-80%	-81%	-86%	-75%	-5%	-77%	-77%	-74%	-76%
95th %ile	-87%	-86%	-82%	-85%	-86%	-82%	-7%	-70%	-70%	-80%	-78%
90th %ile	-86%	-87%	-81%	-86%	-84%	-84%	-12%	-62%	-71%	-82%	-78%
80th %ile	-85%	-86%	-80%	-83%	-85%	-83%	-16%	-56%	-63%	-82%	-74%
50th %ile	-26%	-16%	-23%	-15%	-19%	-13%	-27%	-14%	-26%	-16%	-18%
20th %ile	-16%	-6%	-2%	-8%	-12%	-8%	-5%	0%	-23%	-5%	0%
10th %ile	-12%	-8%	0%	-5%	-12%	-7%	-5%	0%	-23%	-11%	0%
5th %ile	-17%	-12%	0%	-6%	-13%	-13%	-13%	0%	-29%	-14%	0%
Cumulative Change, European Settlement and 15 years of Sand Sourcing (%)											
99th %ile	-85%	-84%	-80%	-81%	-86%	-76%	-6%	-77%	-77%	-74%	-77%
95th %ile	-87%	-87%	-81%	-85%	-86%	-83%	-8%	-70%	-70%	-81%	-78%
90th %ile	-86%	-87%	-81%	-85%	-83%	-84%	-13%	-62%	-71%	-82%	-78%
80th %ile	-85%	-87%	-79%	-83%	-84%	-83%	-17%	-56%	-62%	-82%	-74%
50th %ile	-27%	-18%	-23%	-15%	-18%	-14%	-27%	-14%	-25%	-17%	-17%
20th %ile	-17%	-8%	-5%	-7%	-11%	-9%	-7%	-2%	-23%	-6%	3%
10th %ile	-12%	-11%	-1%	-5%	-10%	-9%	-8%	0%	-23%	-12%	3%
5th %ile	-16%	-14%	-1%	-6%	-11%	-16%	-16%	0%	-29%	-16%	2%

Note: AWAC-02 is actually located 450 m to the east of the POA, but as it is so close to the POA boundary the changes are representative of changes within the POA.

Table 27. Statistics of the modelled change in SSC during the dry season for the pre-European settlement scenario relative to the existing case and the cumulative change of the pre-European settlement scenario and the 15 years (70 million m^3) of sand sourcing scenario.

Statistic	AWAC01 (in POA)	AWAC02 (in POA)	AWAC03 (in POA)	AWAC04 (in POA)	AWAC05	AWAC06	AWAC07	AWAC08	AWAC09	AWAC10	AWAC11
Change since European Settlement (%)											
99th %ile	5%	4%	9%	6%	1%	1%	0%	8%	2%	1%	7%
95th %ile	3%	2%	12%	8%	2%	1%	0%	11%	2%	1%	9%
90th %ile	3%	4%	12%	9%	2%	2%	1%	13%	2%	2%	12%
80th %ile	5%	3%	12%	8%	4%	2%	0%	14%	2%	3%	14%
50th %ile	9%	5%	11%	10%	8%	3%	1%	15%	4%	3%	14%
20th %ile	9%	7%	9%	12%	9%	4%	2%	16%	6%	5%	15%
10th %ile	9%	9%	9%	13%	9%	6%	2%	14%	6%	5%	13%
5th %ile	9%	10%	11%	14%	9%	6%	2%	7%	6%	6%	12%
Cumulative Change, European Settlement and 15 years of Sand Sourcing (%)											
99th %ile	4%	-2%	12%	4%	1%	-1%	0%	8%	4%	-1%	6%
95th %ile	2%	-1%	16%	7%	0%	0%	0%	10%	4%	-1%	8%
90th %ile	3%	1%	17%	8%	1%	-1%	0%	13%	3%	0%	11%
80th %ile	4%	1%	15%	7%	2%	0%	0%	13%	2%	0%	14%
50th %ile	6%	3%	9%	9%	7%	2%	0%	14%	4%	1%	18%
20th %ile	6%	5%	5%	11%	9%	3%	0%	15%	6%	2%	21%
10th %ile	8%	6%	5%	12%	9%	5%	0%	14%	5%	3%	16%
5th %ile	8%	7%	6%	13%	9%	5%	0%	6%	5%	4%	13%

Note: AWAC-02 is actually located 450 m to the east of the POA, but as it is so close to the POA boundary the changes are representative of changes within the POA.

Table 28. Statistics of the modelled change in SSC during the transitional season for the pre-European settlement scenario relative to the existing case and the cumulative change of the pre-European settlement scenario and the 15 years (70 million m^3) of sand sourcing scenario.

Statistic	AWAC01 (in POA)	AWAC02 (in POA)	AWAC03 (in POA)	AWAC04 (in POA)	AWAC05	AWAC06	AWAC07	AWAC08	AWAC09	AWAC10	AWAC11
Change since European Settlement (%)											
99th %ile	1%	1%	1%	1%	0%	0%	0%	2%	0%	0%	1%
95th %ile	1%	1%	1%	1%	1%	0%	0%	2%	0%	0%	1%
90th %ile	1%	0%	1%	1%	1%	0%	0%	2%	1%	0%	2%
80th %ile	1%	1%	1%	1%	1%	0%	0%	2%	0%	1%	1%
50th %ile	1%	1%	1%	1%	1%	0%	0%	2%	1%	0%	2%
20th %ile	1%	1%	1%	1%	1%	1%	0%	2%	1%	1%	1%
10th %ile	1%	1%	2%	1%	1%	1%	0%	2%	1%	1%	1%
5th %ile	2%	1%	1%	1%	1%	1%	0%	2%	1%	1%	1%
Cumulative Change, European Settlement and 15 years of Sand Sourcing (%)											
99th %ile	0%	-7%	2%	-1%	0%	-1%	0%	1%	1%	-2%	1%
95th %ile	-3%	-5%	0%	0%	-1%	-2%	0%	2%	1%	-2%	1%
90th %ile	-2%	-6%	0%	-1%	0%	-2%	0%	1%	2%	-2%	1%
80th %ile	-3%	-4%	0%	0%	0%	-2%	-1%	1%	1%	-2%	1%
50th %ile	-3%	-3%	-4%	1%	2%	-2%	-1%	1%	1%	-2%	2%
20th %ile	-1%	-1%	-5%	2%	2%	-1%	-2%	1%	1%	-2%	3%
10th %ile	0%	-1%	-4%	1%	3%	-1%	-2%	1%	1%	-2%	3%
5th %ile	1%	-2%	-4%	1%	3%	-1%	-3%	1%	0%	-1%	4%

Note: AWAC-02 is actually located 450 m to the east of the POA, but as it is so close to the POA boundary the changes are representative of changes within the POA.

5.2.2. Bedload Transport

Spatial maps of the modelled change in bedload transport rate at the peak flood and peak ebb stages of the tide due to the 5 year and 15 year sand sourcing scenarios during the wet season are shown in Figure 207 and Figure 208. Plots for the other seasons show similar changes and are included in Appendix C.

The plots show similar spatial patterns in the changes, but with the magnitude and extent of the changes being larger (but still very small) for the 15 years of sand sourcing scenario compared to the 5 years of sand sourcing. Both scenarios were modelled to result in a very minor reduction in bedload transport within the POA and adjacent to its west and east sides, and a localised very minor increase in bedload transport adjacent to the northern and southern ends of the POA. For the 5 years of sand sourcing scenario, the modelled reductions and increases were up to ± 0.005 kg/m/s (relative to existing case peak transport rates of 0.1 to 0.4 kg/m/s), while for the 15 years of sand sourcing scenario they were up to ± 0.05 kg/m/s. The areas with modelled increases in bedload transport extended up to 10 km to the north (extending through the West Entrance to CG) and south of the POA, while the modelled reductions in bedload transport extended to the entrances to the False Mouths of the Ord and towards the East Entrance to CG.

Spatial maps of the modelled change in bedload due to the 15-year sand sourcing scenario during TC Marcus are shown in Figure 209. The changes were similar in spatial pattern to the changes during the wet season, but the modelled changes were noticeably higher (but still very low) and covering a larger (but still small) spatial area at peak ebb compared with peak flood. At peak flood the modelled reductions in bedload transport within the proposed operational area were predominantly less than 0.01 kg/m/s, while during peak ebb they were between 0.01 and 0.05 kg/m/s throughout the majority of the proposed operational area.

Spatial maps of the modelled change in bedload due to the pre-European scenario at peak flood and peak ebb during a higher river discharge event in the wet season are shown in Figure 210. The plot shows the modelled bedload transport was slightly lower for the pre-European settlement scenario throughout the majority of CG by up to 0.05 kg/m/s, with localised areas of increased bedload transport within the False Mouths of the Ord. During peak ebb the modelled bedload transport was slightly higher by 0.005 to 0.05 kg/m/s through the centre of CG and within the POA, with minor reductions around the False Mouths of the Ord.

To better understand the change in bedload transport relative to the existing case due to the 15 years of sand sourcing and the pre-European settlement scenarios, timeseries plots of the change in bedload transport rate and direction during the wet season at sites from the upstream end of CG (AWAC-08) to offshore at King Shoals (AWAC-09) are shown in Figure 211 to Figure 218. The plots show the following:

- At the entrance to West Arm (AWAC-08) the 15 years of sand sourcing was modelled to result in extremely minor changes in bedload transport of up to ± 0.005 kg/m/s. The modelled changes were largest (but still extremely minor) before and after the peaks in bedload transport, with small modelled changes at the time of peak bedload transport. These modelled changes are therefore likely to be a result of the very small change in phase of the tide in the area rather than an absolute change in the peak transport rates. At the same site the pre-European scenario was assessed to have had a slightly increased peak ebb transport rate of around 0.15 kg/m/s and a slightly decreased peak flood transport rate of up to 0.4 kg/m/s compared to the existing case today.

- Directly upstream (south) of the POA (AWAC-11) the 15 years of sand sourcing was modelled to result in extremely minor increases to the peak bedload transport rates during both the flood and ebb tides. The peaks were increased by up to 0.007 kg/m/s on the ebb tide and 0.002 kg/m/s on the flood tide. These increases were due to the modelled minor increase in current speed in this area on both the flood and ebb tides. At the same site the pre-European scenario was assessed to have had a slightly increased peak ebb transport rate of around 0.025 kg/m/s and a slightly decreased peak flood transport rate of up to 0.045 kg/m/s compared to the existing case today.

- Within the POA (AWAC-01) the 15 years of sand sourcing was modelled to result in a very minor reduction in the peak bedload transport rates of up to 0.007 kg/m/s during both the flood and ebb tides. The reduction was due to the modelled minor reduction in current speed within the POA during both flood and ebb tides. At the same site the pre-European scenario was assessed to have had a slightly increased peak ebb transport rate of around 0.03 kg/m/s and a slightly decreased peak flood transport rate of up to 0.03 kg/m/s compared to the existing case today.

- At the offshore site at King Shoals (AWAC-09) the 15 years of sand sourcing was modelled to result in insignificant changes to the bedload transport rates. At the same site the pre-European scenario was assessed to have had a slightly increased peak ebb transport rate of around 0.02 kg/m/s and a slightly decreased peak flood transport rate of up to 0.01 kg/m/s compared to the existing case today.

- At all sites and for both scenarios the modelled change in bedload transport direction at the time of peak transport rates was small (less than 2º), with the plots showing that changes only occur at the times when the tide changes due to changes in the phase of the tide.

A statistical summary of the percent change in bedload transport rate relative to the existing case due to the 15 years of sand sourcing scenario are provided in Table 29 and Table 30. The results show the following:

- For the 15 years of sand sourcing during the three seasons considered the 90th to 99th percentile modelled bedload transport rates (i.e. the peaks in bedload transport rates) at the sites within the POA (AWAC-01 to AWAC-04) were all reduced relative to the existing case, with reductions ranging from 3.1% to 10.5%. Reductions in bedload transport of the lower percentiles were more variable, with the largest reduction of 31.9% being for the 20th percentile. The reductions of these lower percentiles are not considered as significant as the existing case transport rates are low (0.0002 kg/m/s).

- Outside of the POA the 90th to 99th percentile modelled bedload transport rates were increased by up to 2.6% and reduced by up to 1.8%. The changes to the lower percentiles outside of the POA ranged from increases of up to 2.4% and reductions of up to 3.0%.

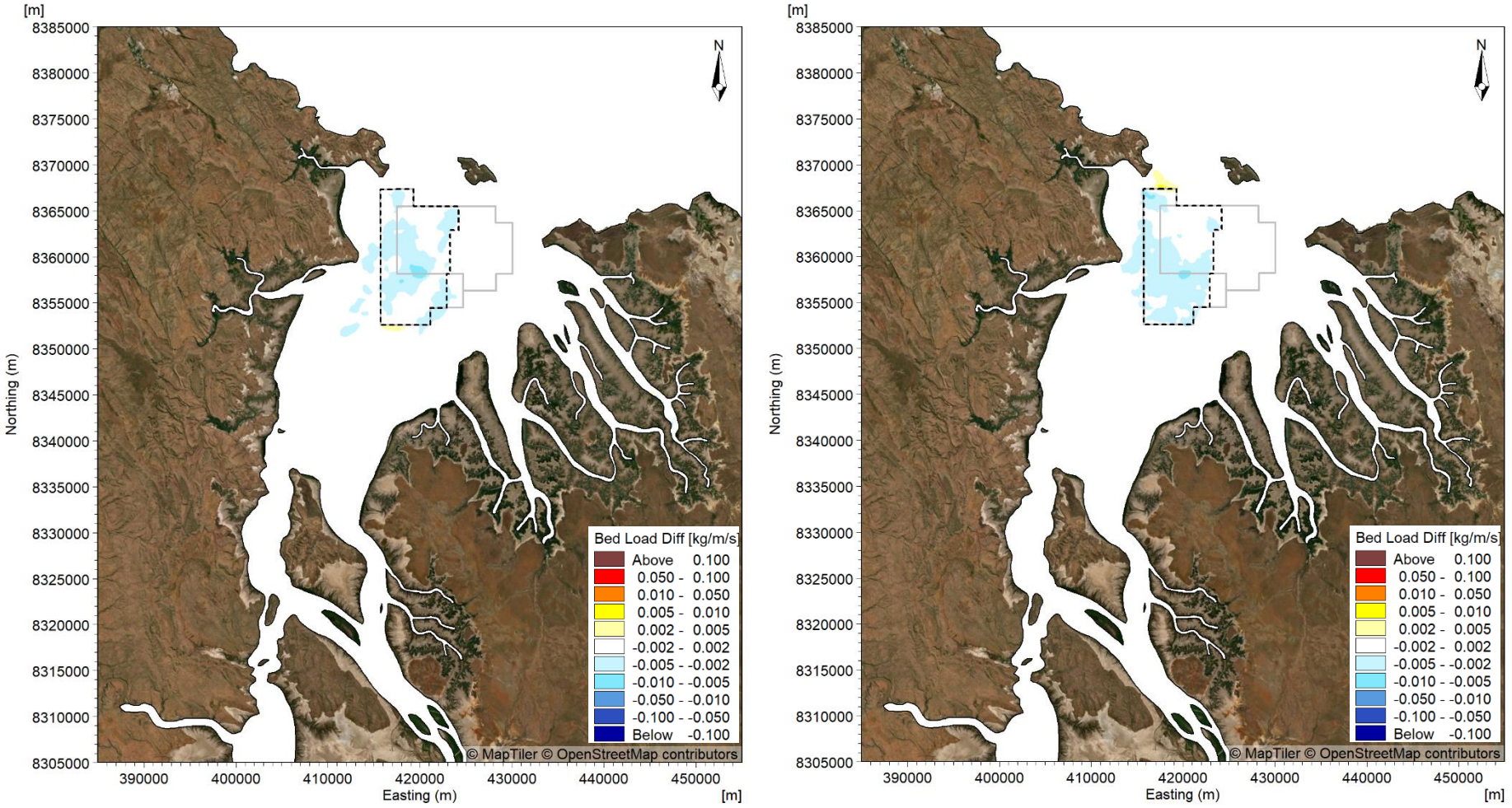
- The changes during TC Marcus were similar to the modelled changes during the three seasons, except that changes below the 90th percentile outside of the POA were slightly larger, with increases of up to 2.9% and reductions of up to 5.8%.

To understand the change in bedload transport which has occurred since European settlement (primarily due to construction of the Ord River dam) along with the cumulative changes as a result of the Ord River dams and the proposed 15 years of sand sourcing, a statistical summary of the percent change in modelled bedload transport rate is provided for the three different seasons in Table 31 to Table 33. A negative change in the tables shows that the modelled bedload transport rate has reduced since pre-European settlement conditions and vice versa for a positive change. The tables show the following:

- During the wet season at the majority of the sites the higher bedload transport rates which will occur during periods of peak transport (i.e. 95th and 99th percentiles) were modelled to have been reduced by up to 3.4% as a result of the construction of the Ord River dams. Modelled changes during the lower percentiles were more variable, with increases of up to 14.5% (although this change was for the 10th percentile which is not considered significant due to the low transport rates) along with reductions of up to 3%.

- During the dry and transitional seasons the bedload transport rates were modelled to have increased at most sites as a result of the construction of the Ord River dams. During the dry season modelled increases during periods of peak transport (i.e. 95th and 99th percentiles) were up to 1.6%, while during the transitional season the increases were lower, being up to 0.2%.

- The cumulative changes in bedload transport due to the Ord River dams and 15 years of sand sourcing consistently showed that the changes at the sites within the POA (AWAC-01 to AWAC-04) were predominantly due to the sand sourcing resulting in a localised reduction in bedload transport in this area. The modelled changes outside of the POA were more variable, with the changes due to the sand sourcing acting to reduce the impacts from the construction of the dams in some locations and increasing the changes in other locations. Over the three seasons considered, the changes in bedload transport rate outside of the POA during periods of peak transport (i.e. 95th and 99th percentiles) ranged from +2.3% to -3.9% due to the Ord River dams and from +2.9% to -3.4% for the cumulative impacts of the Ord River dams and 15 years of sand sourcing. Therefore, the cumulative assessment indicates that the sand sourcing will not significantly change the impacts in bedload transport resulting from the Ord River dams, except for locally within the POA.



Peak Flood

Peak Ebb

Figure 207. Modelled change in bedload transport rate during a spring tide at peak flood and peak ebb in the wet season due to the 5-year (23 million m^3) sand sourcing scenario.

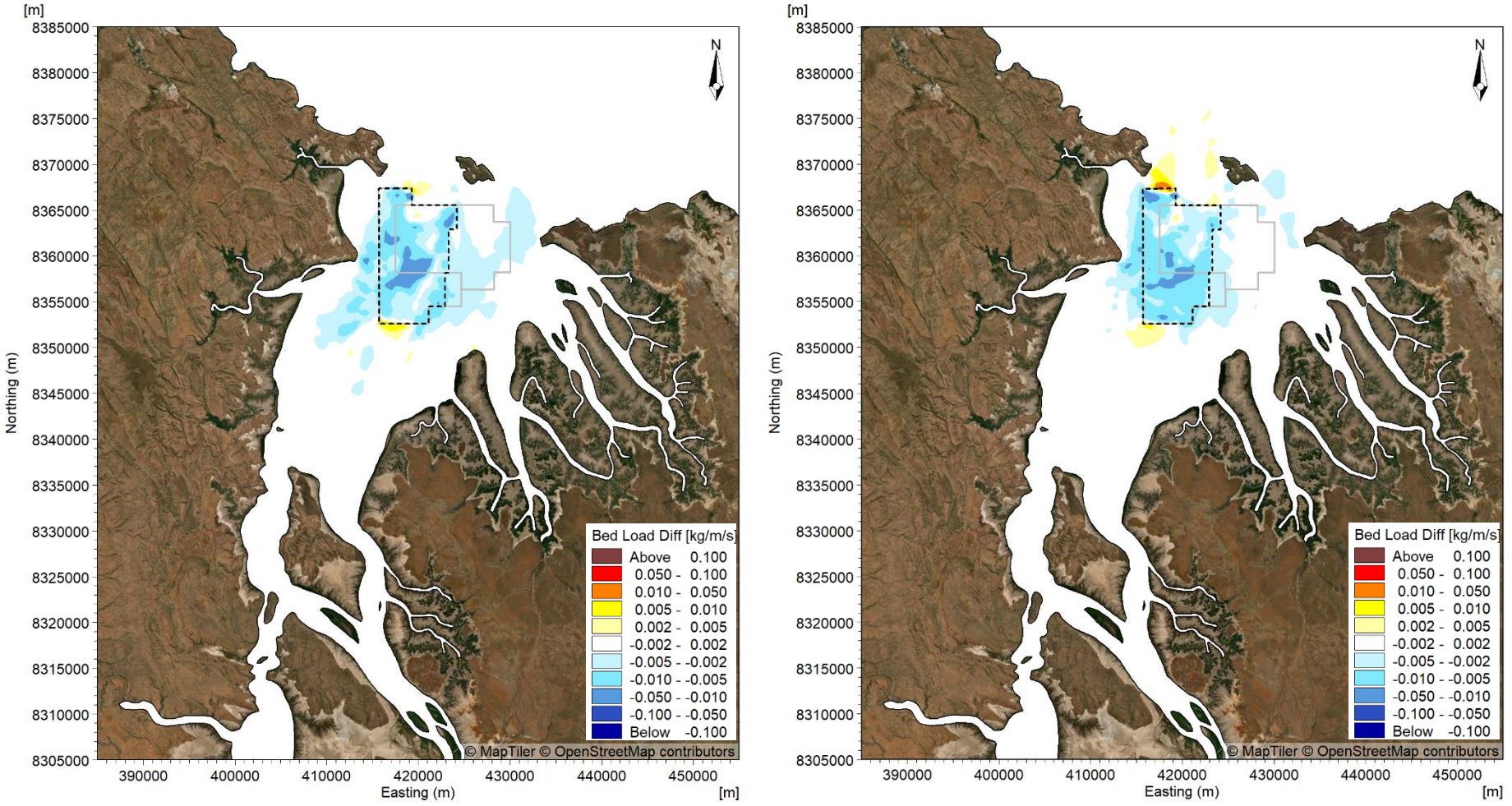
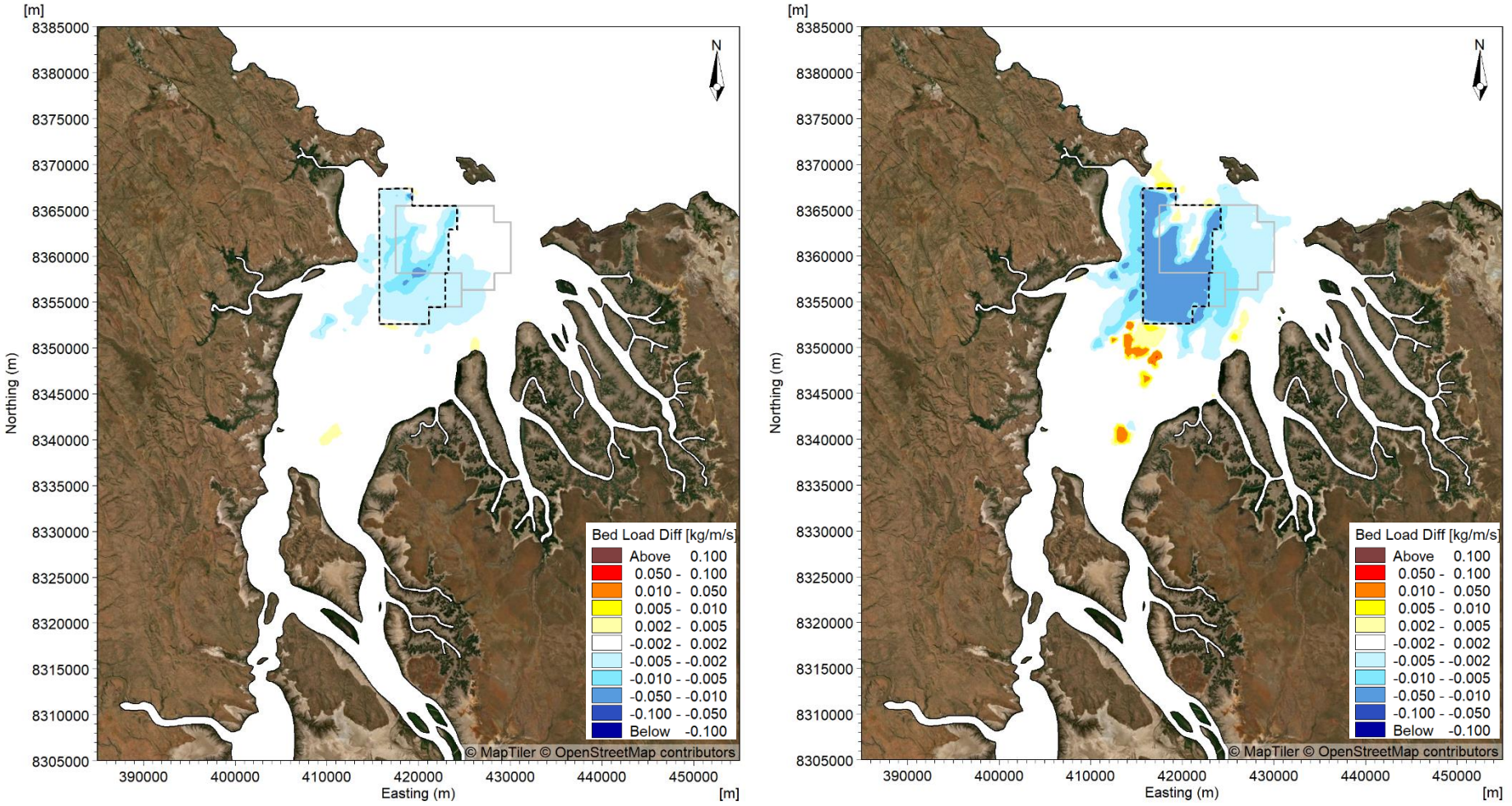


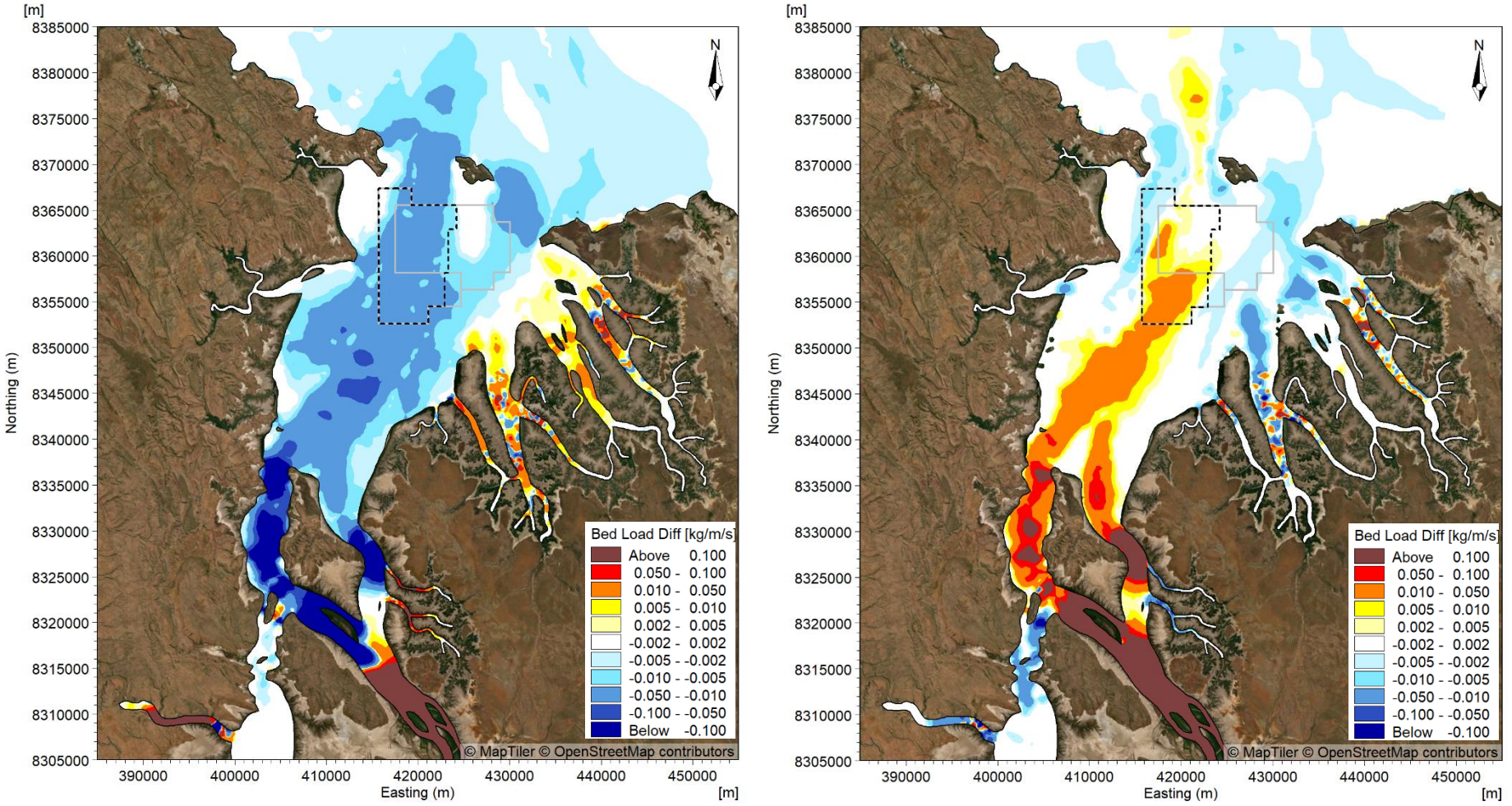
Figure 208. Modelled change in bedload transport rate during a spring tide at peak flood and peak ebb in the wet season due to the 15-year (70 million m^3) sand sourcing scenario.



Peak Flood

Peak Ebb

Figure 209. Modelled change in bedload transport rate at peak flood and peak ebb during TC Marcus due to the 15-year (70 million m^3) sand sourcing scenario.



Peak Flood

Peak Ebb

Figure 210. Modelled difference in bedload transport rate during a spring tide at peak flood and peak ebb in the wet season for the pre-European scenario compared to existing case



Figure 211. Timeseries showing the modelled change in bedload transport rate (top) and direction (bottom) at AWAC-08 during the wet season due to 15 years (70 million m^3) of sand sourcing (Scheme).

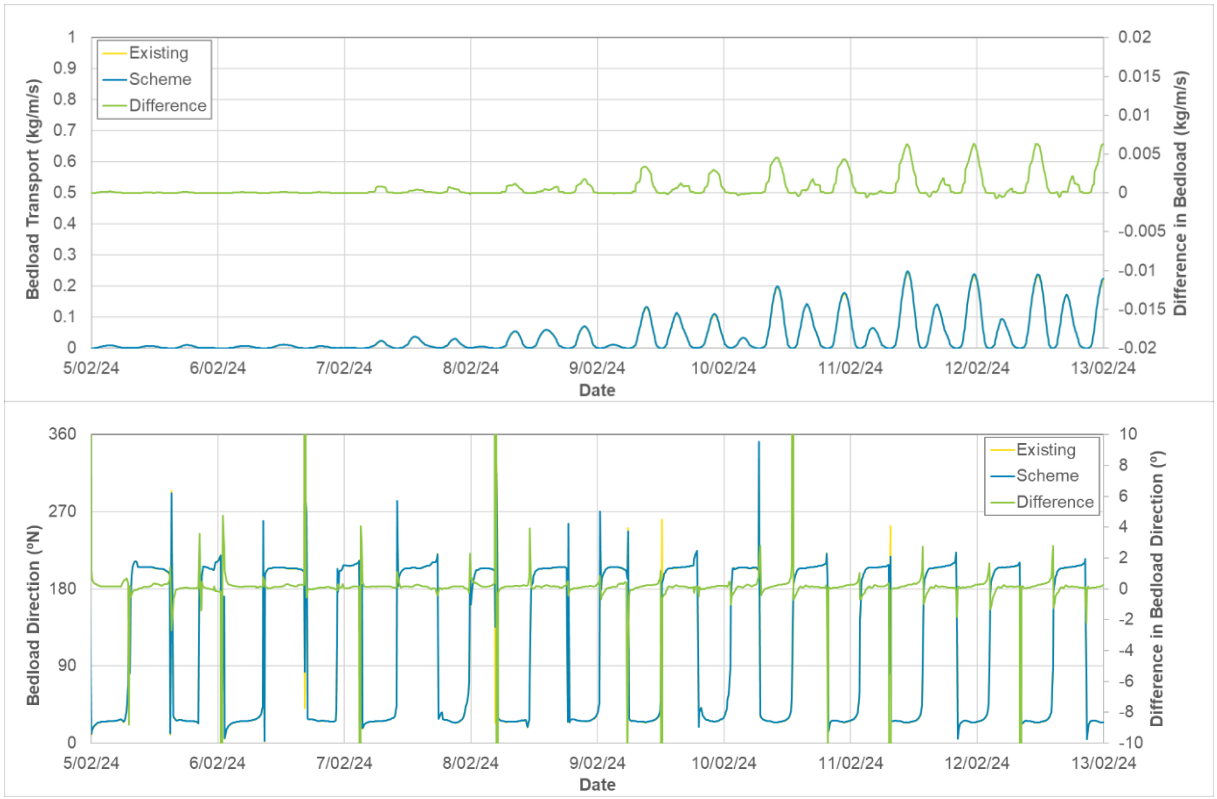


Figure 212. Timeseries showing the modelled change in bedload transport rate (top) and direction (bottom) at AWAC-11 during the wet season due to 15 years (70 million m^3) of sand sourcing (Scheme).

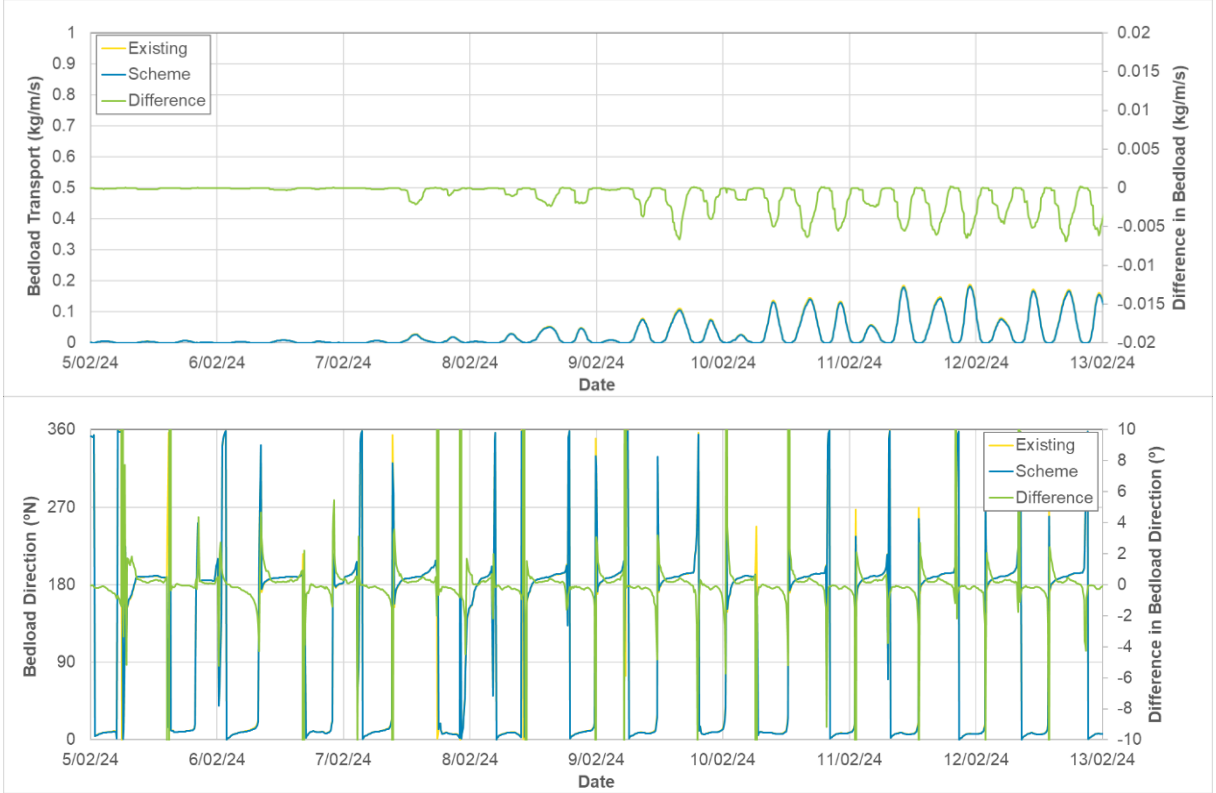


Figure 213. Timeseries showing the modelled change in bedload transport rate (top) and direction (bottom) at AWAC-01 during the wet season due to 15 years (70 million m³) of sand sourcing (Scheme).

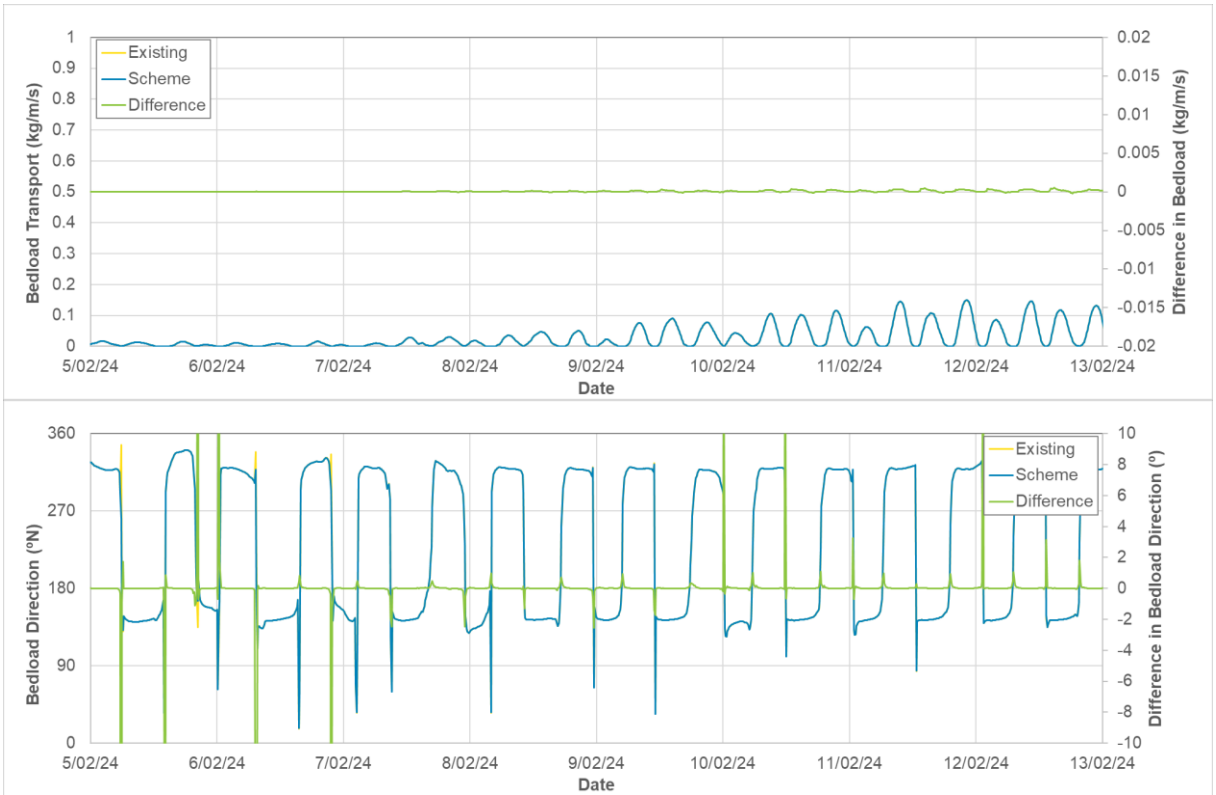


Figure 214. Timeseries showing the modelled change in bedload transport rate (top) and direction (bottom) at AWAC-09 during the wet season due to 15 years (70 million m³) of sand sourcing (Scheme).

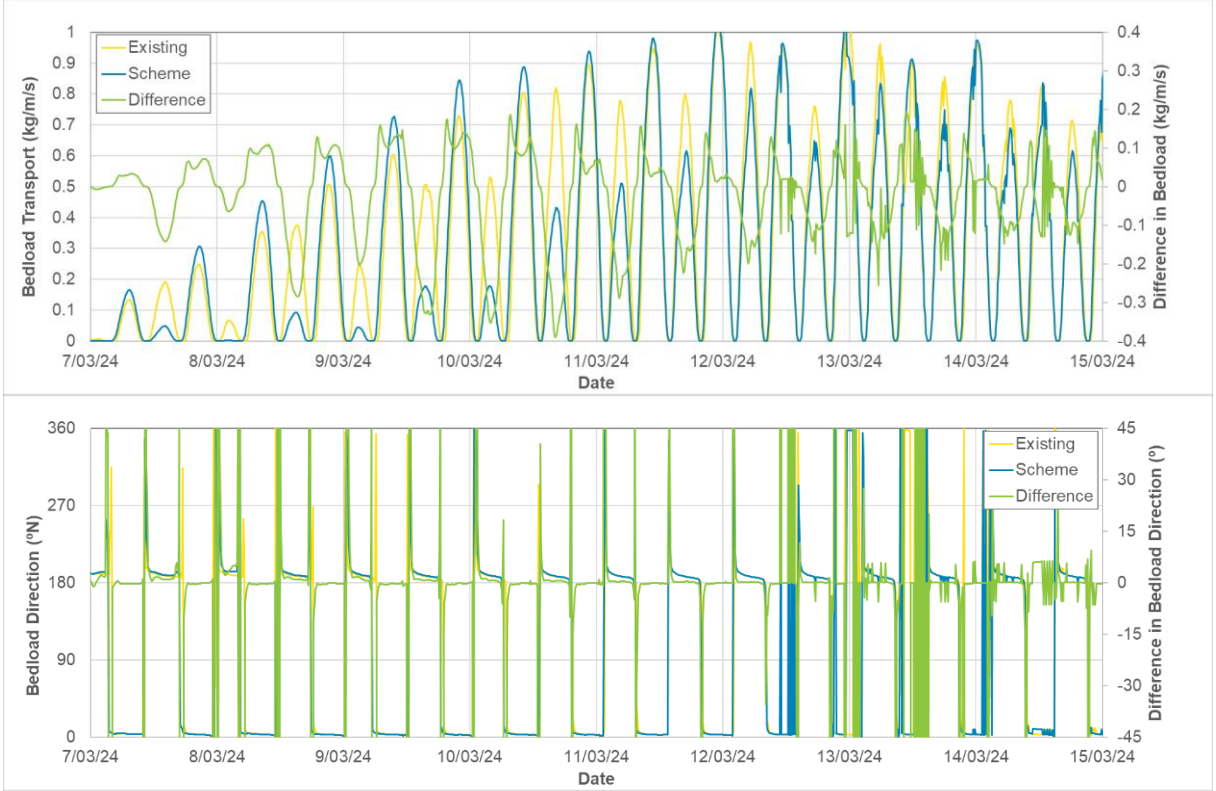


Figure 215. Timeseries showing the modelled difference in bedload transport rate (top) and direction (bottom) at AWAC-08 during a high river discharge event in the wet season in the pre-European scenario (Scheme) compared to the existing case.



Figure 216. Timeseries showing the modelled difference in bedload transport rate (top) and direction (bottom) at AWAC-11 during a high river discharge event in the wet season in the pre-European scenario (Scheme) compared to the existing case.



Figure 217. Timeseries showing the modelled difference in bedload transport rate (top) and direction (bottom) at AWAC-01 during a high river discharge event in the wet season in the pre-European scenario (Scheme) compared to the existing case.

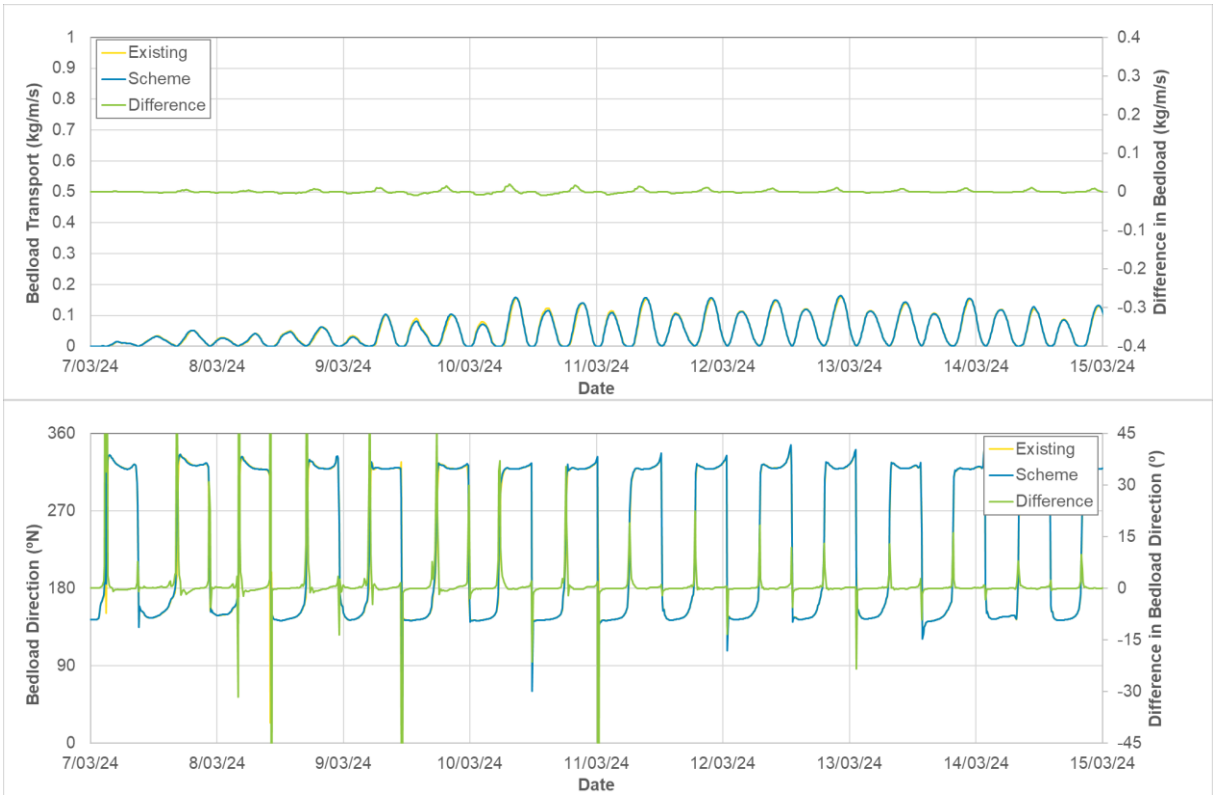


Figure 218. Timeseries showing the modelled difference in bedload transport rate (top) and direction (bottom) at AWAC-09 during a high river discharge event in the wet season in the pre-European scenario (Scheme) compared to the existing case.

Table 29. Statistics of the modelled change in bedload transport during the wet and dry seasons due to 15 years (70 million m^3) of sand sourcing relative to the existing case.

Statistic	AWAC01 (in POA)	AWAC02 (in POA)	AWAC03 (in POA)	AWAC04 (in POA)	AWAC05	AWAC06	AWAC07	AWAC08	AWAC09	AWAC10	AWAC11
Wet Season Change (%)											
99th %ile	-3.1%	-8.7%	-7.1%	-7.5%	1.1%	-1.5%	0.1%	0.1%	0.2%	-1.0%	2.5%
95th %ile	-4.1%	-6.4%	-6.3%	-9.1%	0.9%	-1.2%	0.0%	-0.2%	0.2%	-1.4%	2.2%
90th %ile	-5.2%	-6.5%	-5.7%	-10.0%	1.5%	-1.4%	0.1%	-0.2%	0.1%	-0.6%	1.4%
80th %ile	-3.6%	-7.9%	-8.9%	-8.3%	2.4%	-1.5%	0.0%	0.1%	0.1%	-0.9%	1.4%
50th %ile	-2.7%	-3.8%	-8.6%	-7.7%	-1.9%	-1.5%	0.1%	-0.3%	0.1%	-0.6%	0.4%
20th %ile	-9.8%	-4.0%	-31.9%	-7.0%	-1.5%	-0.8%	0.1%	-0.7%	0.5%	-0.8%	2.4%
10th %ile	-0.9%	-2.4%	-7.7%	-7.2%	-1.9%	-2.3%	0.3%	-3.0%	1.3%	-1.0%	0.2%
5th %ile	-2.5%	-4.1%	-12.1%	-8.7%	-0.5%	-1.4%	-0.4%	-1.3%	0.8%	-1.2%	1.2%
Dry Season Change (%)											
99th %ile	-3.6%	-7.3%	-6.1%	-8.8%	1.2%	-1.4%	0.0%	-0.2%	0.2%	-1.4%	2.4%
95th %ile	-5.0%	-4.9%	-5.9%	-10.0%	1.0%	-1.4%	-0.1%	0.3%	0.2%	-0.5%	2.2%
90th %ile	-3.7%	-6.0%	-7.2%	-8.4%	0.9%	-1.8%	0.1%	0.0%	0.1%	-0.6%	2.4%
80th %ile	-3.9%	-6.3%	-13.0%	-9.9%	1.3%	-0.9%	-0.1%	-0.1%	0.1%	-0.9%	1.2%
50th %ile	-2.6%	-4.2%	-11.3%	-8.6%	-0.7%	-1.1%	-0.3%	0.1%	0.2%	-0.5%	0.5%
20th %ile	-8.9%	-5.3%	-30.5%	-28.4%	-1.2%	-1.1%	-0.5%	-1.7%	0.2%	-0.3%	2.6%
10th %ile	-2.0%	-2.8%	-15.2%	-12.3%	-0.2%	-0.2%	-0.2%	-2.3%	-0.7%	-0.4%	0.6%
5th %ile	-3.5%	-1.9%	-19.8%	-14.9%	-0.6%	-2.3%	0.3%	0.0%	1.5%	-1.0%	1.2%

Note: AWAC-02 is actually located 450 m to the east of the POA, but as it is so close to the POA boundary the changes are representative of changes within the POA.

Table 30. Statistics of the modelled change in bedload transport during the transitional season and during TC Marcus due to 15 years (70 million m^3) of sand sourcing relative to the existing case.

Statistic	AWAC01 (in POA)	AWAC02 (in POA)	AWAC03 (in POA)	AWAC04 (in POA)	AWAC05	AWAC06	AWAC07	AWAC08	AWAC09	AWAC10	AWAC11
Transitional Season Change (%)											
99th %ile	-3.1%	-6.4%	-7.2%	-6.6%	1.2%	-1.5%	0.1%	0.2%	0.2%	-1.5%	2.6%
95th %ile	-3.5%	-6.2%	-6.0%	-8.8%	1.3%	-1.5%	-0.1%	0.8%	0.2%	-1.3%	2.2%
90th %ile	-4.3%	-6.4%	-5.6%	-10.5%	1.2%	-1.3%	0.1%	0.6%	0.2%	-0.4%	1.4%
80th %ile	-3.7%	-8.7%	-9.2%	-8.1%	1.9%	-1.8%	-0.1%	0.5%	0.2%	-1.1%	1.4%
50th %ile	-2.7%	-5.7%	-8.3%	-7.3%	-2.5%	-2.0%	0.1%	-0.3%	0.2%	-0.8%	1.0%
20th %ile	-2.2%	-2.0%	-4.7%	-5.6%	-0.8%	-2.1%	0.2%	-0.2%	0.7%	-1.6%	0.7%
10th %ile	-2.7%	-1.4%	-6.6%	-2.2%	-1.1%	-0.4%	-0.1%	0.7%	0.4%	-0.5%	0.7%
5th %ile	-1.8%	-7.5%	-9.1%	-2.5%	-1.6%	-0.4%	0.3%	-1.4%	0.4%	-0.4%	1.5%
TC Marcus Change (%)											
99th %ile	-3.2%	-4.2%	-6.8%	-6.3%	0.4%	-0.6%	0.1%	0.3%	0.1%	-0.3%	2.1%
95th %ile	-2.8%	-7.2%	-6.8%	-8.2%	1.1%	-1.7%	0.0%	0.0%	0.2%	-0.4%	2.5%
90th %ile	-3.4%	-5.4%	-7.0%	-9.9%	1.1%	-1.2%	0.1%	0.2%	0.2%	-1.1%	2.6%
80th %ile	-3.9%	-6.0%	-6.7%	-9.2%	1.2%	-1.6%	0.0%	0.0%	0.1%	-0.4%	1.6%
50th %ile	-6.3%	-5.7%	-9.0%	-14.0%	-0.9%	-1.6%	0.3%	0.0%	0.4%	1.0%	2.0%
20th %ile	-13.2%	-18.5%	-37.3%	-15.6%	2.9%	1.0%	-0.5%	2.0%	3.5%	1.1%	2.6%
10th %ile	-4.8%	-2.6%	-2.0%	-3.9%	-0.2%	-2.7%	-5.8%	-2.5%	-0.4%	-1.6%	0.6%
5th %ile	-3.7%	-1.2%	-0.3%	1.8%	-0.8%	0.8%	1.5%	2.7%	1.3%	-2.0%	0.1%

Note: AWAC-02 is actually located 450 m to the east of the POA, but as it is so close to the POA boundary the changes are representative of changes within the POA.

Table 31. Statistics of the modelled change in bedload transport during the wet season for the pre-European scenario relative to the existing case and the cumulative change of the pre-European scenario and the 15 years of sand sourcing scenario.

Statistic	AWAC01 (in POA)	AWAC02 (in POA)	AWAC03 (in POA)	AWAC04 (in POA)	AWAC05	AWAC06	AWAC07	AWAC08	AWAC09	AWAC10	AWAC11
Change since Pre-European Settlement (%)											
99th %ile	-1.2%	-0.2%	-3.4%	-0.1%	-3.9%	-0.3%	-0.3%	0.1%	-2.8%	-1.7%	-1.4%
95th %ile	0.7%	-0.9%	-1.0%	-0.7%	-2.7%	0.5%	-0.4%	2.3%	-0.2%	-2.1%	-2.5%
90th %ile	0.9%	0.2%	-0.2%	0.7%	-3.0%	0.9%	-1.1%	3.9%	-0.4%	-0.5%	1.5%
80th %ile	0.9%	0.4%	-0.8%	0.2%	-2.2%	0.6%	-1.1%	4.2%	-0.1%	0.5%	1.5%
50th %ile	0.8%	0.3%	-1.0%	0.5%	0.5%	0.8%	0.1%	7.0%	0.4%	0.1%	1.8%
20th %ile	3.1%	-0.4%	-0.5%	1.6%	0.0%	0.9%	-0.1%	11.2%	-0.1%	0.3%	-2.7%
10th %ile	1.6%	1.5%	0.1%	0.6%	0.3%	-0.6%	0.0%	14.5%	1.1%	1.0%	2.0%
5th %ile	5.4%	2.2%	-1.0%	3.3%	0.2%	-1.2%	0.1%	3.8%	0.0%	0.3%	-1.4%
Cumulative Change, Pre-European Settlement and 15 years of Sand Sourcing (%)											
99th %ile	-4.2%	-8.9%	-10.2%	-7.5%	-2.8%	-1.8%	-0.2%	0.1%	-2.6%	-2.7%	1.0%
95th %ile	-3.4%	-7.3%	-7.2%	-9.7%	-1.8%	-0.7%	-0.4%	2.1%	0.0%	-3.4%	-0.4%
90th %ile	-4.4%	-6.3%	-5.9%	-9.4%	-1.6%	-0.5%	-1.0%	3.8%	-0.3%	-1.0%	2.9%
80th %ile	-2.7%	-7.5%	-9.6%	-8.2%	0.2%	-1.0%	-1.2%	4.3%	0.0%	-0.4%	2.8%
50th %ile	-1.9%	-3.5%	-9.5%	-7.2%	-1.4%	-0.7%	0.2%	6.7%	0.6%	-0.5%	2.2%
20th %ile	-7.0%	-4.4%	-32.2%	-5.5%	-1.4%	0.1%	0.0%	10.5%	0.4%	-0.5%	-0.4%
10th %ile	0.6%	-1.0%	-7.5%	-6.6%	-1.6%	-2.9%	0.2%	11.0%	2.3%	0.1%	2.1%
5th %ile	2.8%	-2.0%	-13.0%	-5.7%	-0.2%	-2.5%	-0.4%	2.5%	0.8%	-1.0%	-0.3%

Note: AWAC-02 is actually located 450 m to the east of the POA, but as it is so close to the POA boundary the changes are representative of changes within the POA.

Table 32. Statistics of the modelled change in bedload transport during the dry season for the pre-European scenario relative to the existing case and the cumulative change of the pre-European scenario and the 15 years of sand sourcing scenario.

Statistic	AWAC01 (in POA)	AWAC02 (in POA)	AWAC03 (in POA)	AWAC04 (in POA)	AWAC05	AWAC06	AWAC07	AWAC08	AWAC09	AWAC10	AWAC11
Change since Pre-European Settlement (%)											
99th %ile	0.3%	0.6%	0.5%	0.4%	1.1%	0.9%	0.6%	1.6%	0.4%	0.8%	0.4%
95th %ile	0.7%	0.5%	0.5%	0.3%	1.2%	0.3%	0.3%	0.3%	0.2%	0.5%	0.5%
90th %ile	0.4%	0.3%	0.5%	0.6%	0.8%	0.7%	0.2%	0.7%	0.2%	0.3%	0.2%
80th %ile	0.6%	0.4%	1.0%	0.2%	0.2%	0.2%	0.1%	-0.1%	0.1%	0.1%	0.7%
50th %ile	-0.2%	0.0%	0.4%	0.1%	0.0%	0.0%	-0.2%	0.5%	0.2%	0.2%	0.4%
20th %ile	2.3%	0.0%	-0.4%	-0.7%	0.0%	0.2%	-0.3%	0.4%	0.0%	0.3%	1.2%
10th %ile	0.1%	-0.1%	0.4%	0.8%	-0.1%	-0.7%	-0.4%	0.8%	-0.3%	-0.4%	0.2%
5th %ile	-0.4%	-0.2%	-0.8%	-0.1%	-1.3%	0.8%	0.4%	-2.0%	0.2%	0.0%	-0.4%
Cumulative Change, Pre-European Settlement and 15 years of Sand Sourcing (%)											
99th %ile	-3.3%	-6.8%	-5.7%	-8.4%	2.4%	-0.5%	0.6%	1.4%	0.6%	-0.6%	2.9%
95th %ile	-4.3%	-4.5%	-5.4%	-9.7%	2.2%	-1.2%	0.1%	0.6%	0.4%	-0.1%	2.7%
90th %ile	-3.3%	-5.7%	-6.8%	-7.9%	1.7%	-1.1%	0.3%	0.6%	0.3%	-0.3%	2.6%
80th %ile	-3.3%	-6.0%	-12.1%	-9.8%	1.5%	-0.7%	0.0%	-0.2%	0.2%	-0.8%	1.8%
50th %ile	-2.7%	-4.2%	-11.0%	-8.6%	-0.7%	-1.2%	-0.5%	0.7%	0.4%	-0.3%	0.9%
20th %ile	-6.8%	-5.4%	-30.8%	-28.9%	-1.2%	-0.9%	-0.8%	-1.3%	0.2%	-0.1%	3.8%
10th %ile	-1.9%	-2.9%	-14.9%	-11.6%	-0.3%	-0.9%	-0.6%	-1.5%	-1.0%	-0.7%	0.9%
5th %ile	-4.0%	-2.1%	-20.4%	-15.0%	-1.9%	-1.6%	0.7%	-1.9%	1.7%	-0.9%	0.8%

Note: AWAC-02 is actually located 450 m to the east of the POA, but as it is so close to the POA boundary the changes are representative of changes within the POA.

Table 33. Statistics of the modelled change in bedload transport during the transitional season for the pre-European scenario relative to the existing case and the cumulative change of the pre-European scenario and the 15 years of sand sourcing scenario.

Statistic	AWAC01 (in POA)	AWAC02 (in POA)	AWAC03 (in POA)	AWAC04 (in POA)	AWAC05	AWAC06	AWAC07	AWAC08	AWAC09	AWAC10	AWAC11
Change since Pre-European Settlement (%)											
99th %ile	0.1%	0.1%	0.2%	0.2%	0.2%	0.0%	0.1%	-0.1%	0.1%	0.1%	0.1%
95th %ile	0.0%	0.1%	0.0%	0.1%	0.1%	0.1%	0.0%	-0.3%	0.1%	0.2%	0.1%
90th %ile	-0.1%	0.0%	0.1%	0.0%	0.1%	0.0%	0.1%	-0.1%	0.0%	0.0%	0.1%
80th %ile	0.0%	0.0%	0.1%	0.0%	0.2%	0.0%	-0.1%	-0.1%	0.0%	0.0%	0.1%
50th %ile	0.2%	0.0%	0.0%	0.0%	0.0%	0.1%	-0.3%	0.1%	0.0%	0.0%	0.1%
20th %ile	0.2%	-0.1%	0.0%	0.0%	0.0%	0.1%	-0.2%	-1.4%	-0.6%	0.7%	0.1%
10th %ile	0.0%	0.0%	-0.1%	0.0%	0.1%	0.0%	0.2%	-1.6%	0.0%	-0.1%	-0.2%
5th %ile	0.0%	0.0%	0.2%	0.0%	-0.1%	-0.1%	-0.1%	0.4%	-0.1%	-0.1%	0.3%
Cumulative Change, Pre-European Settlement and 15 years of Sand Sourcing (%)											
99th %ile	-3.0%	-6.2%	-7.0%	-6.4%	1.3%	-1.4%	0.1%	0.1%	0.3%	-1.3%	2.7%
95th %ile	-3.5%	-6.1%	-5.9%	-8.7%	1.4%	-1.4%	0.0%	0.5%	0.3%	-1.1%	2.3%
90th %ile	-4.3%	-6.3%	-5.5%	-10.5%	1.3%	-1.3%	0.1%	0.4%	0.1%	-0.4%	1.5%
80th %ile	-3.7%	-8.7%	-9.2%	-8.1%	2.0%	-1.9%	-0.1%	0.3%	0.3%	-1.1%	1.5%
50th %ile	-2.5%	-5.7%	-8.3%	-7.3%	-2.5%	-1.9%	-0.2%	-0.2%	0.2%	-0.8%	1.1%
20th %ile	-2.1%	-2.2%	-4.7%	-5.6%	-0.8%	-2.0%	-0.1%	-1.5%	0.1%	-0.8%	0.8%
10th %ile	-2.7%	-1.4%	-6.7%	-2.2%	-1.0%	-0.4%	0.1%	-0.9%	0.3%	-0.6%	0.5%
5th %ile	-1.8%	-7.5%	-8.9%	-2.5%	-1.7%	-0.5%	0.2%	-1.0%	0.4%	-0.5%	1.8%

Note: AWAC-02 is actually located 450 m to the east of the POA, but as it is so close to the POA boundary the changes are representative of changes within the POA.

5.2.3. Sedimentation

Spatial maps of the modelled change in bed thickness between the existing case and the 5 years and 15 years of sand sourcing scenarios over a two-month (60 days) wet season period are shown in Figure 219. The plot shows that changes were predominantly less than 0.01 m (1 cm) for the 5 years of sand sourcing, with the only modelled changes of more than this being a localised area of increased bed thickness of 0.01 to 0.05 m (1 to 5 cm) at the southwestern corner of the POA and a localised area of reduced bed thickness of 0.01 to 0.05 m (1 to 5 cm) along the northern side of the POA.

Larger (but still very small) changes were modelled for the 15 years of sand sourcing scenario, with increased bed thickness of 0.01 to 0.05 m (1 to 5 cm) along the length of the southern side of the POA. There was modelled to be a reduction in bed thickness of 0.01 to 0.05 m (1 to 5 cm) within the POA along its northern side, while there was an increase in bed thickness directly adjacent to this on the outside of the POA. There were modelled areas of both increased and reduced bed thickness of ± 0.05 m (5 cm) within the POA. The majority of the modelled changes were either within or directly adjacent to the POA, with no changes of more than ± 0.01 m (1 cm) more than 3 km from the POA boundary.

These very minor modelled changes of <5 cm due to the 15 years of sand sourcing should be considered in the context that bathymetric surveys conducted in and around the POA in February 2024 measured sand waves with heights up to 8 m and horizontal migration of up to 10 m in just 27 days (PCS 2024a), showing that the seabed sand-forms are naturally highly dynamic under the influence of tidal currents.

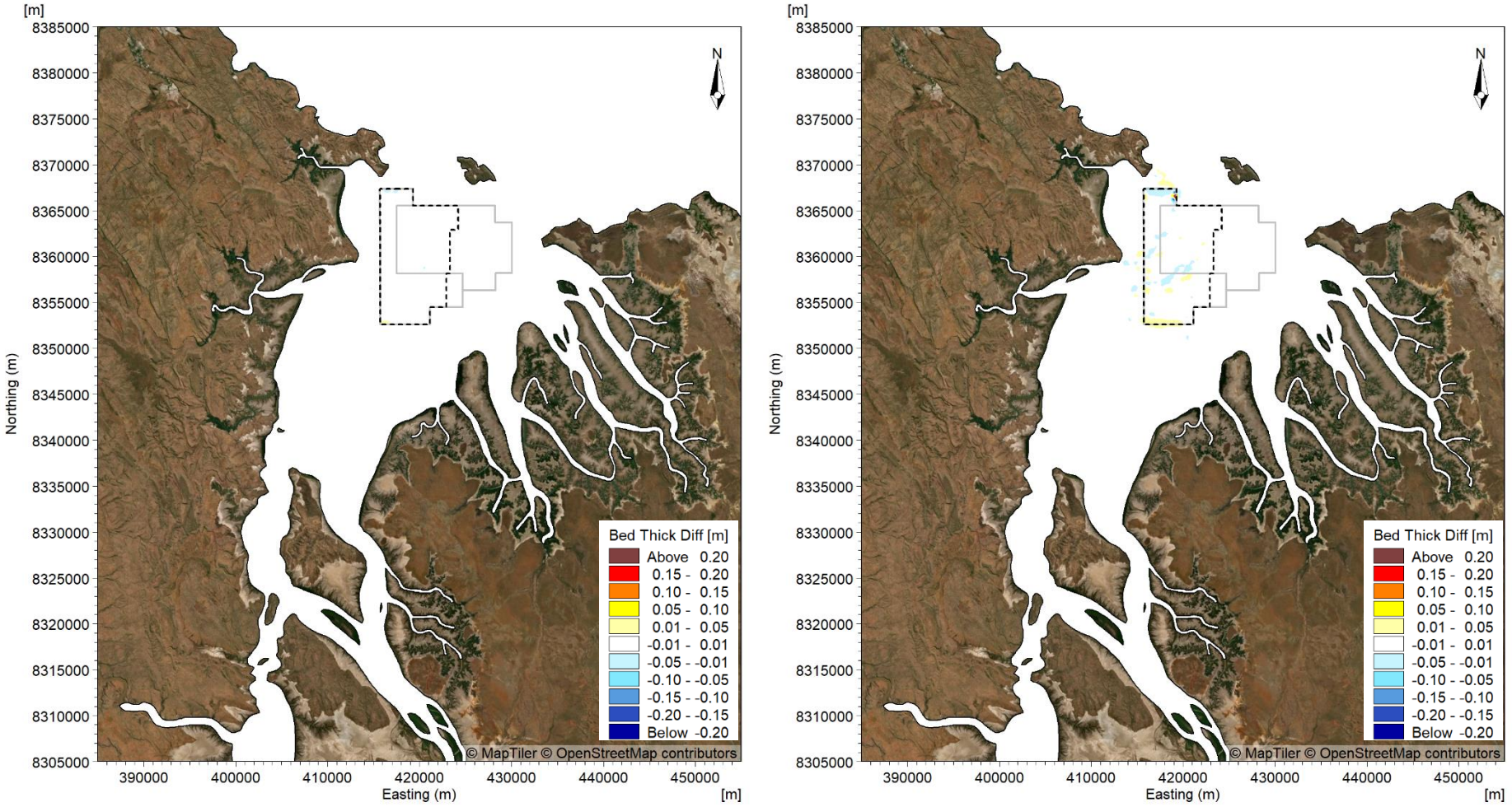
The modelled changes in bed thickness for the 5 years of sand sourcing scenario were similar for the other seasons and so plots for these are not shown. However, plots of the change in bed thickness for the 15 years of sand sourcing scenario for the dry and transitional seasons were shown in Figure 220. The plots show that the changes for the transitional season were similar to the modelled changes for the wet season. During the dry season the modelled changes were smaller, but with the same areas of increased bed thickness and reduced bed thickness along the southern and northern boundaries of the POA, respectively.

The spatial area where a modelled increase in bed thickness on the southern side of the POA occurred was calculated (~4,000 m by 300 m) for the three different seasons along with the average increase bed thickness in this area (sedimentation rates ranging from 0.02 m to 0.035 m over 2 months). Based on this, the average annual sedimentation volume for the southern end of the POA was calculated to be in the order of 200,000 m^3/yr. If the sedimentation volume is calculated based on the measured migration rate and bedform properties at the southern boundary of the POA the modelled sedimentation volume would be almost double at 375,000 m^3/yr (assuming sand waves are 5 m in height, have a 100 m wavelength and extend 1,500 m along the southern boundary and migrate at an average rate of 2 m to the north per week).

The lower sedimentation volume based on the modelling results has been used to inform the future sedimentation to be adopted in the sand sourcing after 100 years from today scenario, as a lower sedimentation volume is conservative and will have the potential to result in larger modelled changes.

The modelled change in bed thickness between the existing case and the pre-European settlement scenario over a two-month (60 days) wet season period (including a high river discharge event) and a two-month (61 days) dry season period are shown in Figure 221. During the wet season there were modelled changes in bed thickness in the West and East Arms of more than ± 0.2 m. Within CG the changes were limited to ± 0.05 m (5 cm), with the changes extending from the entrance to West Arm throughout the POA and offshore through the West Entrance to King Shoals.

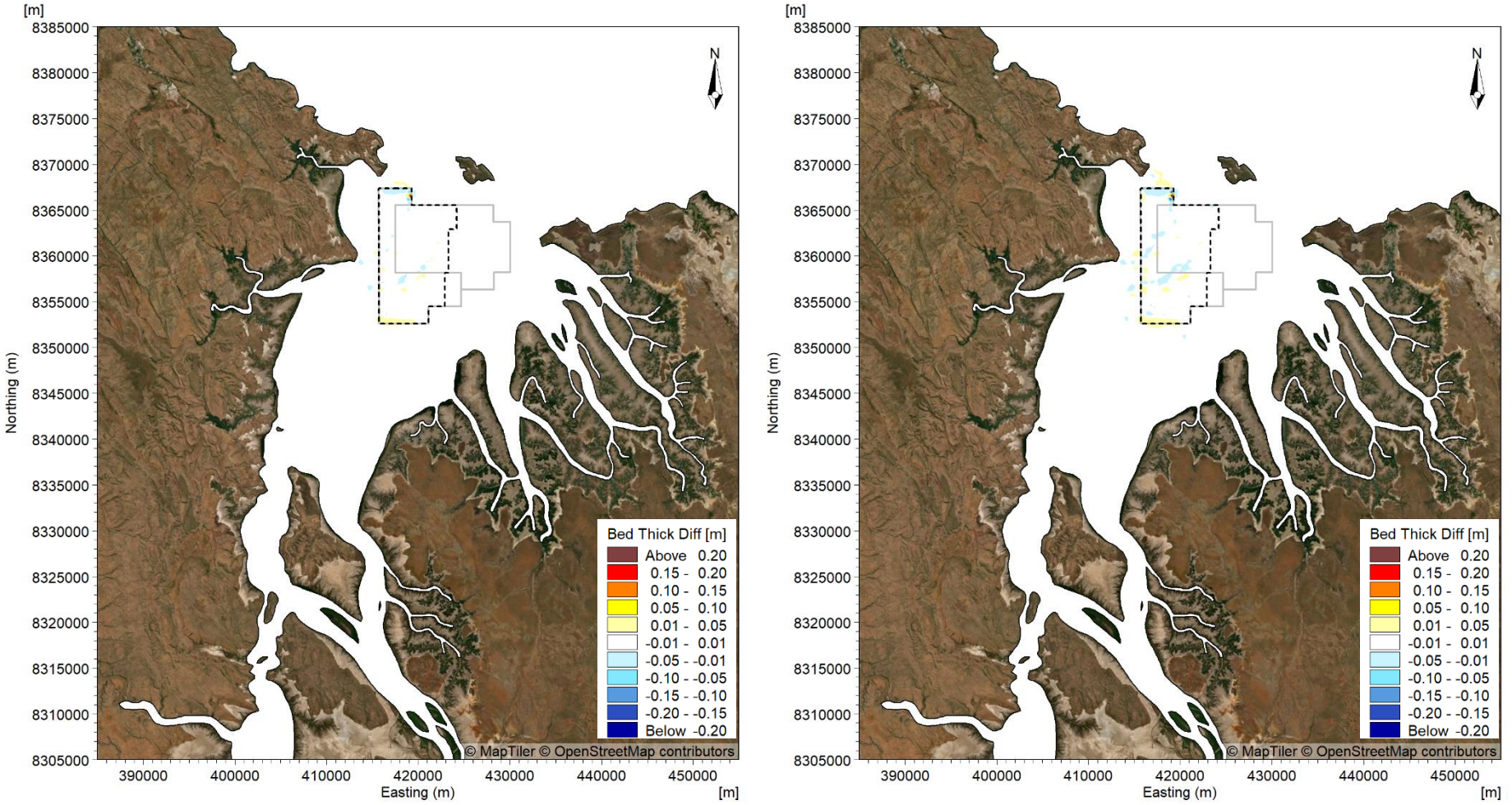
The areas of increases and decreases in the wet season typically being adjacent to each other suggests an increase in the downstream migration of sand (as the increases were typically located on the northern side of the decreases). During the dry season the modelled changes were constrained in West and East Arms and were predominantly less than ± 0.1 m (10 cm). As with the wet season, the areas of increases and decreases were typically adjacent to each other, but the decreases were located on the southern side of the increases which suggests a reduction in the downstream migration of sand as a result of the pre-European settlement scenario.



5yr Sand Sourcing

15yr Sand Sourcing

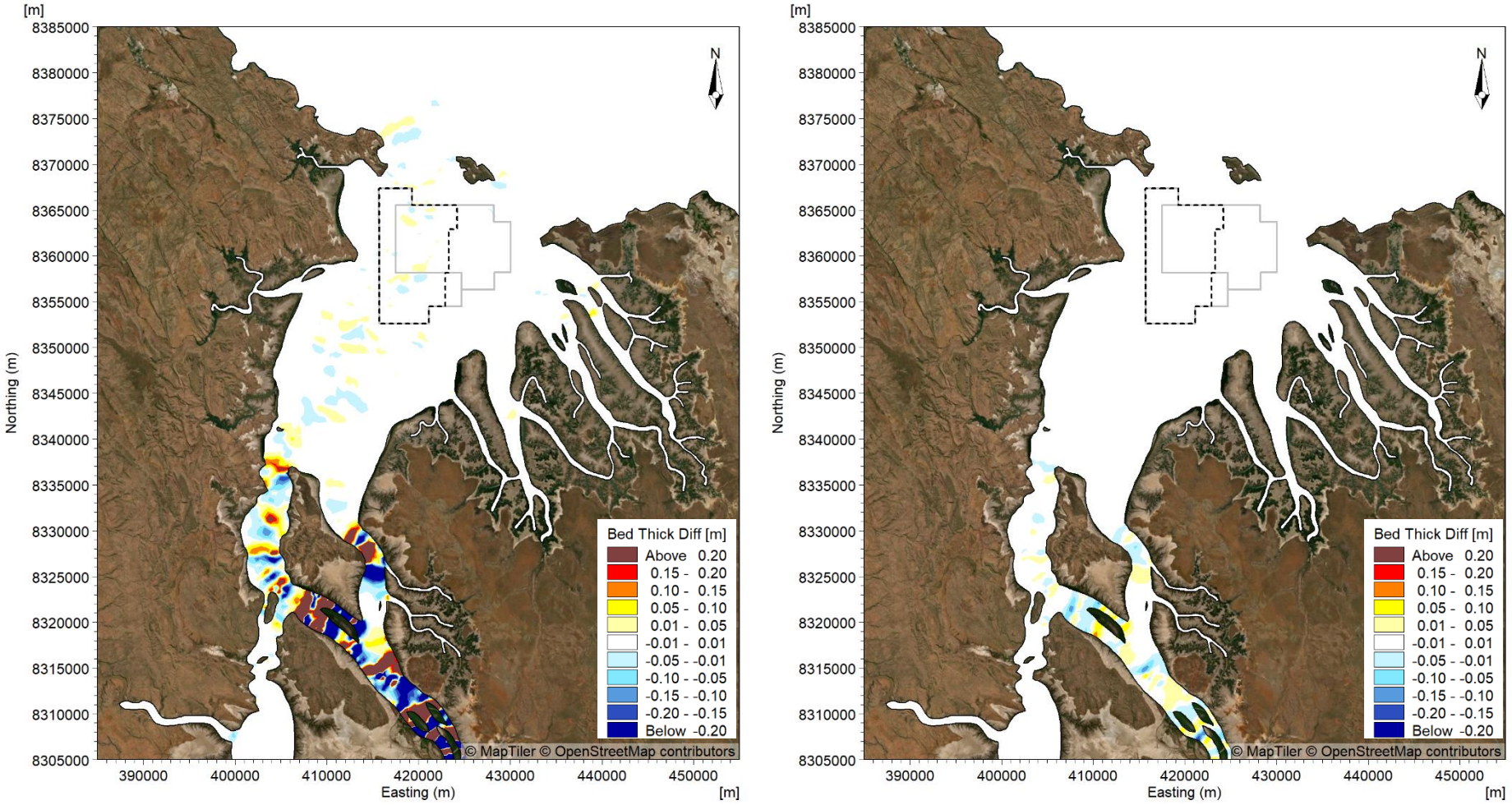
Figure 219. Modelled difference in bed thickness between the existing case and the 5 and 15 years of sand sourcing scenarios over the two-month (60 days) wet season period.



Dry Season

Transitional Season

Figure 220. Modelled difference in bed thickness between the existing case and the 15 years of sand sourcing scenario over the two-month (61 days) dry and transitional season periods.



Wet Season

Dry Season

Figure 221. Modelled difference in bed thickness between the existing case and the pre-European settlement scenario over the two-month (60/61 days) wet and dry season periods.

5.2.4. Beach Processes

As previously noted, the sand sourcing scenarios and the pre-European settlement scenario were not assessed to result in any changes to the wave conditions offshore of CG and so will not result in any direct impacts to the longshore or cross-shore sediment transport at the turtle nesting beaches.

Results from the bedload transport modelling assessed that the sand sourcing of 70 million m^3 over 15 years would only result in localised changes to the bedload transport rates within the POA extending to the West and East Entrances to CG, with no modelled reduction in bedload transport at King Shoals.

The sand sourcing will only remove some of the sand present within the POA, meaning that the areas with sand present on the seabed within the POA will still have sand present after the sand sourcing.

The modelling assessed a localised reduction in bedload transport rates within the POA (indicating ongoing sedimentation will occur there) and an increase in bedload transport rates directly to the north of the POA in the West Entrance to CG during the ebb stage of the tide. The increase adjacent to the West Entrance to CG is a response to localised increases in current speed during the peak ebb stage of the tide and the increase will ensure that the net transport of sand to the north will not be reduced due to the localised changes from the sand sourcing.

Localised reductions in bedload transport rate were modelled during both the flood and ebb stages of the tide (larger reductions during the flood stage) around the East Entrance to CG, this is a response to localised changes in current speed in the area and will only result in small, localised changes to bedload transport and is not assessed to change the supply of sand through the East Entrance to CG.

5.3. Summary Findings & Implications for the Proposal

The numerical modelling assessed the potential changes to sediment transport and beach processes from the proposed sourcing of 23 million m^3 of sand at 5 years and 70 million m^3 of sand at 15 years, as well as potential changes 100 years from today due to 70 million m^3 of sand sourcing.

The modelling also assessed the potential changes to sediment transport and beach processes that may have occurred since European settlement of the area, including from the construction two dams on the Ord River (in 1967 and 1971), as well as the potential cumulative changes due to construction of the Ord River dams and the proposed 15 years of sand sourcing.

Overall, the modelling assessed that changes to sediment transport and beach processes will mostly be negligible for the 5, 15 and 100 year scenarios, with the main modelled changes summarised below. The modelling also assessed that the cumulative changes due to construction of the Ord River dams and the proposed 15 years of sand sourcing will be negligible, with the main modelled changes summarised below.

The very small magnitude of most of the modelled changes are unlikely to cause measurable changes to the environmental resources and values of the area that are influenced by sediment transport and beach processes. These are the mangrove communities that line the coast within CG, the False Mouths of the Ord on the eastern side of CG (which are part of the Ord River Floodplain Ramsar site) and three turtle nesting beaches on the seaward coasts outside of CG and one at Barnett Point inside CG (see Section 1.2 and Figure 2 in that section).

The main modelled changes to sediment transport and beach processes are summarised as follows:

- Potential changes were similar for the different metocean conditions, as the primary driver for sediment transport in CG is the astronomical tide, although changes were generally larger (but still minor) during the wet season when larger waves occur and when the wave modelling showed the waves were most likely to be influenced by the localised deepening of the POA from the sand sourcing (noting that if 70 million m^3 of sand are sourced, the deepening will be an average of 0.94 m across the 75 km^2 of the POA where suitable sand is present over 15 years).
- The deepening of the POA due to the sand sourcing will not significantly change the SSC within CG, with short-duration changes of up to ± 20 mg/L modelled predominantly as a result of the small change in phase of the tidal propagation and very little change to the spatial pattern of the SSC. The modelling assessed a reduction in SSC within the POA of up to 8%, while at the sites outside of the POA the changes were still predominantly reductions with changes of ± 3%. These changes in SSC are not expected to change the supply of fine-grained sediment to mangroves and mudflats in the region or to measurably change the benthic light in the region.

- During a large river discharge event in the wet season the SSC was shown to have significantly reduced since pre-European settlement, with modelled reductions in peak SSC throughout CG and offshore of up to 87%. During the dry season the modelled SSC was increased by up to 16%.

- The cumulative changes in SSC due to the Ord River dams and 15 years of sand sourcing showed that during the wet season the additional changes in SSC due to the sand sourcing were small relative to the changes resulting from the Ord River dam. During the dry season the modelled cumulative changes in SSC due to the sand sourcing and Ord River dams were typically smaller than the change just due to the Ord River dams (i.e. the cumulative changes were less than just the Ord River dams changes).

- The modelled bedload transport for the existing case shows a net offshore transport of sand through CG to King Shoals. A transport pathway was assessed from upstream (south to north and inshore to offshore) via West Arm (west of Adolphus Island) into the middle of CG and the POA, then out through West Entrance (west of Lacrosse Island) to King Shoals outside of CG.

- The modelling assessed very minor changes in bedload transport due to the sand sourcing which were similar in spatial pattern to the modelled changes in current speed, and as with the changes to current speed the changes were similar on both the flood and ebb stages of the tide.

- The model results assessed minor reductions in both bedload transport and current speed within and to the west and east of the POA and minor increases directly to the north and south of the POA. The reductions in bedload transport rates around the times of peak transport were modelled to be between 3.1 and 10.5% within the POA, while outside of the POA the reductions were up to 1.8% and the increases up to 2.6%.

- As the sand sourcing will leave most of the sand (80% or more) present throughout the POA, the changes to the bedload transport were relatively small and localised and did not influence the wider sediment transport processes in CG and offshore.

- The small reductions in bedload transport within the POA will promote ongoing sedimentation in the area. The modelled increase in transport to the north of the POA and into the West Entrance to CG will ensure that the export of sand from the POA is not reduced despite the modelled small reduction in bedload transport within the POA. The localised reduction in bedload transport in the East Entrance was due to a modelled localised reduction in current speed in this area and will only result in small, localised modelled changes to bedload transport and would not change the transport of sand out through the East Entrance to CG.

- During high river discharge events in the wet season the construction of the Ord River Dams was shown to have resulted in widespread changes in bedload transport throughout CG. The modelling indicated that since construction of the Ord River dams there has been a reduction in bedload transport during the ebb stage of the tide and reduced bedload transport during the flood stage of the tide during high river discharge events.

- During the dry and transitional seasons the bedload transport rates were assessed to have increased slightly as a result of the construction of the Ord River dams. Overall, the cumulative assessment assessed that the sand sourcing would not significantly change the impacts to bedload transport resulting from the Ord River dams, except for minor changes locally within the POA.

- Modelled changes in bed thickness due to the sand sourcing showed that changes of more than 0.01 m (1 cm) over two months (60/61 days) would only occur in localised areas within and adjacent to the POA. The largest (but still minor) modelled changes within the POA over the 2-month (60/61 days) simulation period were up to ± 0.05 m (5 cm). The modelling indicated an area of sedimentation within the POA directly adjacent to its southern boundary for all metocean conditions simulated.

- The modelling also indicated an area of erosion within the POA directly adjacent to its northern boundary for all metocean conditions simulated. The erosion in this area is due to the localised increase in current speeds in the area. The erosion indicates that the area will act as a source for the supply of sand offshore to ensure that the small reduction in bedload transport within the POA due to the deepening does not change the supply of sand offshore.

- The modelling indicated that the change in sedimentation/erosion since pre-European settlement was significantly larger than for the sand sourcing, with changes assessed to extend from West and East Arms, through CG and out to King Shoals. The modelling results indicated

that the construction of the Ord River Dams reduced the transport of sand from West and East Arms, through CG to offshore.

- It is important to consider that although the sand sourcing will result in a deepening of the bathymetry within the proposed operational area, as a result of the bed already having large bedforms present and not being a flat uniform bed, the sand sourcing will be removing a relatively uniform depth of sand from both the peaks and troughs of existing bedforms, and so will not be removing the entire bedforms.

- In addition, as SPV will only be operating for 1 to 2 days every 14 days, there will be spring tides between dredge cycles, which will allow ongoing natural bedform migration to continue throughout the sand sourcing activity. Based on this it is expected that the bedforms will remain present throughout the 15 years of sand sourcing, albeit at a slightly lower elevation (<1 m on average), meaning that ongoing bedload transport and sand migration will occur through the POA.

- As noted in Section 4.2, the sand sourcing scenarios were not assessed to result in any changes to the wave conditions offshore of CG and so will not result in any direct changes to the longshore or cross-shore sediment transport at the turtle nesting beaches. Results from the hydrodynamic, wave and sediment transport modelling indicated that there will not be any direct or indirect changes from the sand sourcing on the supply or transport of sand to the three turtle nesting beaches offshore of CG or the beach at East Bank Point.

6. RESULTS: SEDIMENT PLUME MODELLING

As outlined in Section 1 the WA EPA 2021 *Technical Guidance for EIA of Marine Dredging Proposals* requires prediction of potential impacts of sediment and turbidity plumes on benthic communities and habitats (BCH), including, if applicable, definition of Zones of High Impact (ZoHI), Zones of Moderate Impact (ZoMI) and Zones of Influence (ZoI), and likely 'worst-case' and 'best-case' impacts, as defined in the guidance.

As also outlined in section 1, BKA has undertaken comprehensive surveys of BCH in CG, including at King Shoals, and no potentially sensitive BCH have been identified (see Referral Report 2 - *Setting & Existing Environment* (BKA, 2024d)). Due to extreme tidal currents (up to >5 knots on spring tides), constant seabed sediment suspension and naturally very high turbidity and lack of sunlight near the seabed, there appear to be no seagrass meadows, coral communities, sponge-beds, macro-algae communities or similar inter-tidal and sub-tidal benthic communities in CG.

Additionally, the nature of the proposed operation, using a Sand Production Vessel (SPV) similar to a Trailer Suction Hopper Dredge (TSHD), will not cause significant elevation of suspended sediments and turbidity above natural background levels. This is because the operation will only target sand and avoid areas of fine sediment, will not involve any dumping (the sand will be retained on the SPV and exported, with the SPV also being the export vessel), the SPV will only be on site for one or two days every two weeks each cycle (it will not be a continuous, turbidity-generating operation), and it will include best-practice turbidity control measures (e.g. 'green valve' on the SPV, water overflow discharge at keel etc).

Never-the-less, in order to address Objective 3 as listed in section 1, modelling of plume dispersal and changes in SSC and sedimentation above natural background levels has been carried out. However, as outlined in section 1 it has not been feasible or necessary to assess ZoHI, ZoMI and ZoI as defined in the EPA guidance, as there are no potentially sensitive benthic biota or communities to model these zones and set biological response triggers for.

This section provides details of the results from the ST modelling of the generation and dispersal of plumes of sediment, including clay, silt and very fine sand, from the SPV during sand sourcing operations. The results from the modelling are compared with the natural SSC in the area to provide context as to the relative contribution to SSC from the SPV sediment plumes as well the cumulative SSC from natural conditions and the sand sourcing operation. The modelled sedimentation from the SPV sediment plumes is also presented.

The existing SSC conditions in CG are presented in Section 5.1.1 and so are not repeated here, but plots showing percentile SSC for the existing case are presented to put the modelled SSC from the SPV plumes into context.

6.1. SPV Sediment Plumes

To assess the potential sediment plumes from the SPV sand sourcing operation, results from the two-month (60/61 days) duration ST simulations for the three seasonal metocean conditions (dry season, transitional season and wet season) have been compared with the existing case. The tropical cyclone conditions have not been included as the sand sourcing activity would not be undertaken during a tropical cyclone.

Results are presented for the two sand sourcing scenarios (repeat activity over 500 m wide area (Scenario 1) and targeted sourcing throughout the proposed operational area (Scenario 2)) and for when the sand sourcing activity coincides with either spring or neap tides. This approach provides a range of potential changes and helps to understand how the potential risk of elevated SSC or increased sedimentation rates from the sand sourcing could vary over a range of conditions.

6.1.1. Modelled SSC from SPV Plumes

Spatial maps of the 50th percentile and maximum SSC from the sand sourcing operation and the natural SSC have been calculated for the near-bed and mid-depth layers of the water column. The percentiles were calculated over a 7-day moving analysis window throughout the 2-month (60 or 61 days) model simulation durations and the maximum of all the calculated 7-day percentiles are adopted for each grid cell in the model. This approach ensures that any elevated SSC due to a single sand sourcing cycle is captured without artificially reducing the percentile SSC by calculating percentiles over a longer time period when no sand sourcing activity occurs.

Plots of the near-bed and mid-depth layers 50th percentile SSC for natural conditions and for the sand sourcing operation are shown for the wet season, neap tide release for Scenario 1 in Figure 222 and

Figure 223. The modelling results show that the 50th percentile SSC resulting from the sand sourcing operation remained below 1 mg/L for both layers, while the natural SSC ranged from 100 to 500 mg/L within CG. Results from all the simulations showed that the 50th percentile SSC from the sand sourcing operation remained below 1 mg/L throughout CG and so results for just the maximum SSC are presented for the plume resulting from the sand sourcing along with the natural SSC.

Plots of the near-bed and mid-depth layers maximum SSC for natural conditions and for the sand sourcing operation are shown for the wet season, neap tide release for Scenario 1 in Figure 224 and Figure 225. The modelling results show that the maximum SSC from the sand sourcing operation for the mid-depth layer remained below 10 mg/L in all areas, while for the near-bed layer the SSC remained below 10 mg/L within the POA, while along the west shoreline of CG there were areas with an SSC of 10 to 100 mg/L. The areas of increased SSC along the west shoreline of CG are due to some of the suspended sediment released by the sand sourcing being transported to this area and resulting in higher SSC due to the shallow water. The maximum natural SSC in the near-bed and mid-depth layers show similar magnitudes and patterns, with an SSC of 250 to 500 mg/L within the POA for both depths and an SSC of more than 3,000 mg/L along the west shoreline of CG where the sand sourcing was assessed to result in elevated SSC. As the maximum modelled SSC from the sand sourcing activity was much higher in the near-bed layer compared to the mid-depth layer, plots of just the near-bed layer are presented here, while all plots of the mid-depth layer are included in Appendix D.

The maximum SSC due to natural processes along with the maximum SSC from the sand sourcing activity are shown for the two sand sourcing scenarios, spring and neap releases and the three different seasons in Figure 224 and Figure 226 to Figure 236. The results show the following:

- For all scenarios the maximum modelled SSC resulting from the sand sourcing operation resulted in an area with an elevated SSC of between 1 and 10 mg/L within and extending to the north and south of the POA as well as other localised areas within CG (including around Lacrosse Island). The maximum natural modelled SSC in these areas ranged from 100 up to 1,000 mg/L.

- The maximum SSC resulting from the sand sourcing operation has the potential to result in elevated SSC of 1 to 100 mg/L along the west shoreline of CG and along the eastern shoreline adjacent to the entrance to East Arm (up to 250 mg/L for one scenario). The increases in these areas are due to some of the suspended sediment released by the sand sourcing being transported to these areas and resulting in higher SSC due to the shallow water. The maximum natural SSC in these areas where the sand sourcing SSC was modelled to increase above 10 mg/L were consistently very high for all seasons (above 3,000 mg/L).

- The largest plume extents were modelled to occur during the dry and the transitional seasons. However, all scenarios have shown that the maximum SSC remains below 10 mg/L throughout the majority of CG (except for adjacent to the west shoreline of CG and along the eastern shoreline adjacent to the entrance to East Arm, where increased SSC can occur due to the shallow water depths), meaning that for all scenarios the SSC from the sand sourcing would be low concentration and predominantly limited to the area within and directly to the north and south of the POA.

- Modelled results from all scenarios show that the near-bed layer maximum SSC due to the sand sourcing operation would predominantly remain within CG, with the SSC extending through the West Entrance to CG remaining below 10 mg/L. Therefore, the sand sourcing was modelled to result in a near-bed layer increase in maximum SSC of less than 10 mg/L in the King Shoals Sanctuary Zone, while the maximum near-bed layer natural SSC was between 100 and 1,000 mg/L in this area. The increase in SSC in the King Shoals Sanctuary Zone will be further assessed through time-series plots of the SSC below.

- The largest modelled plume extent and highest maximum SSC was for sand sourcing scenario 2 released during spring tides in the dry season (Figure 231). This scenario was therefore considered to represent the worst-case plume extent, while the plumes from the other simulations were considered to represent the likely normal plume extents.

- The results show that the general pattern and magnitude of sediment plumes from the sand sourcing, both within and outside of the POA, were similar regardless of whether the sand sourcing occurred during neap or spring tides. However, the results generally showed a larger area where the maximum near-bed layer SSC in the POA was above 1 mg/L when the sand sourcing occurred during spring tides compared to neap tides. This will be due to the higher tidal current speeds during spring tides resulting in increased advection of the suspended sediment released by the SPV compared to spring tides, meaning that the resultant plume has a higher SSC and takes longer to disperse.

To show the relative contribution of the modelled increase in SSC due to the sand sourcing operation, the near-bed 50th percentile and maximum SSC for the natural conditions and natural conditions plus sand sourcing are shown for the worst-case plume extent in Figure 237 and Figure 238. There are no visible differences between the natural and natural plus sand sourcing 50th percentile SSC either within CG of offshore of CG. For the maximum SSC the results were very similar for the natural and natural plus sand sourcing cases, but with a slight change to the 250 mg/L contour at the northern end of the POA due to the sand sourcing operation. The near-bed maximum SSC results do not show any changes to the contours elsewhere within CG or offshore of CG.

The spatial map plots of the near-bed maximum SSC show that the behaviour of the plume generated by the sand sourcing operation remained similar between the three seasons, with scenario 2 during the dry season (worst-case extent) resulting in the largest extent of the plume outside of the POA.

To better understand how the SSC varies temporally through the water column, depth-averaged SSC results from both the natural SSC and sand sourcing simulations at 10 locations within the POA and in the surrounding areas of CG and offshore (including King Shoals Sanctuary Zone (P10)) have been extracted (Figure 239). Timeseries plots of the SSC due to natural conditions and due to the sand sourcing activity for scenarios 1 and 2, with releases during neap tides and spring tides (neap and spring) for the dry season period are shown in Figure 240 to Figure 251 (the worst-case plume extent scenario is shown in Figure 232). The plots show the following:

- For scenario 1 the SSC resulting from the sand sourcing operation within the POA (P01 to P03) was modelled to be up to 6 mg/L for releases during spring tides and up to 2 mg/L for releases during neap tides. At these sites within the POA the natural modelled SSC ranged between 50 and 300 mg/L. The SPC-related SSC at the sites outside of the POA predominantly remained below 1 mg/L except at P06 (located in the West Entrance to CG, ~4 km north of the POA) where short duration peaks in SSC of up to 2 mg/L were modelled, although the SSC was predominantly below 1 mg/L. At P06 the natural SSC over the 2-month dry season period ranged from 30 to 100 mg/L.

- Scenario 2 was modelled to result in a lower SSC within the POA compared with scenario 1, with peaks in SSC of up to 3 mg/L. The highest modelled SSC for scenario 2 was at the southern end of the POA, this was due to the sand sourcing tracks being more focussed in this area. The modelled SSC at the sites outside of the POA remained below 1 mg/L except at P05 and P06 (located ~4 km to the south and north of the POA, respectively) where short duration peaks in modelled SSC of up to 3 mg/L occurred. At these sites the natural SSC over the 2-month dry season period ranged from 30 to 250 mg/L.

- At all sites the increase in SSC was shown to have reduced back to 0 mg/L before the subsequent sand sourcing cycle commenced 14 days later. At the sites where the modelled SSC exceeded 1 mg/L, it was modelled to return to below 1 mg/L after a maximum of 7 days from the start of the sand sourcing activity (although the SSC only exceeds 1 mg/L for a few hours at a time).

- The sites located in Medusa Bank (P09) and King Shoals Sanctuary Zone (P10) show that the SSC from the sand sourcing activity remained well below 1 mg/L for all scenarios.

A statistical summary of the depth-averaged SSC is provided for all simulations at the 10 locations within the POA and in the surrounding areas of CG and offshore in Table 34 to Table 45. The tables show the natural SSC, the SSC resulting from the sand sourcing operation and the combined natural plus sand sourcing SSC for all the different scenarios, spring and neap releases and the three metocean periods. The results show the following:

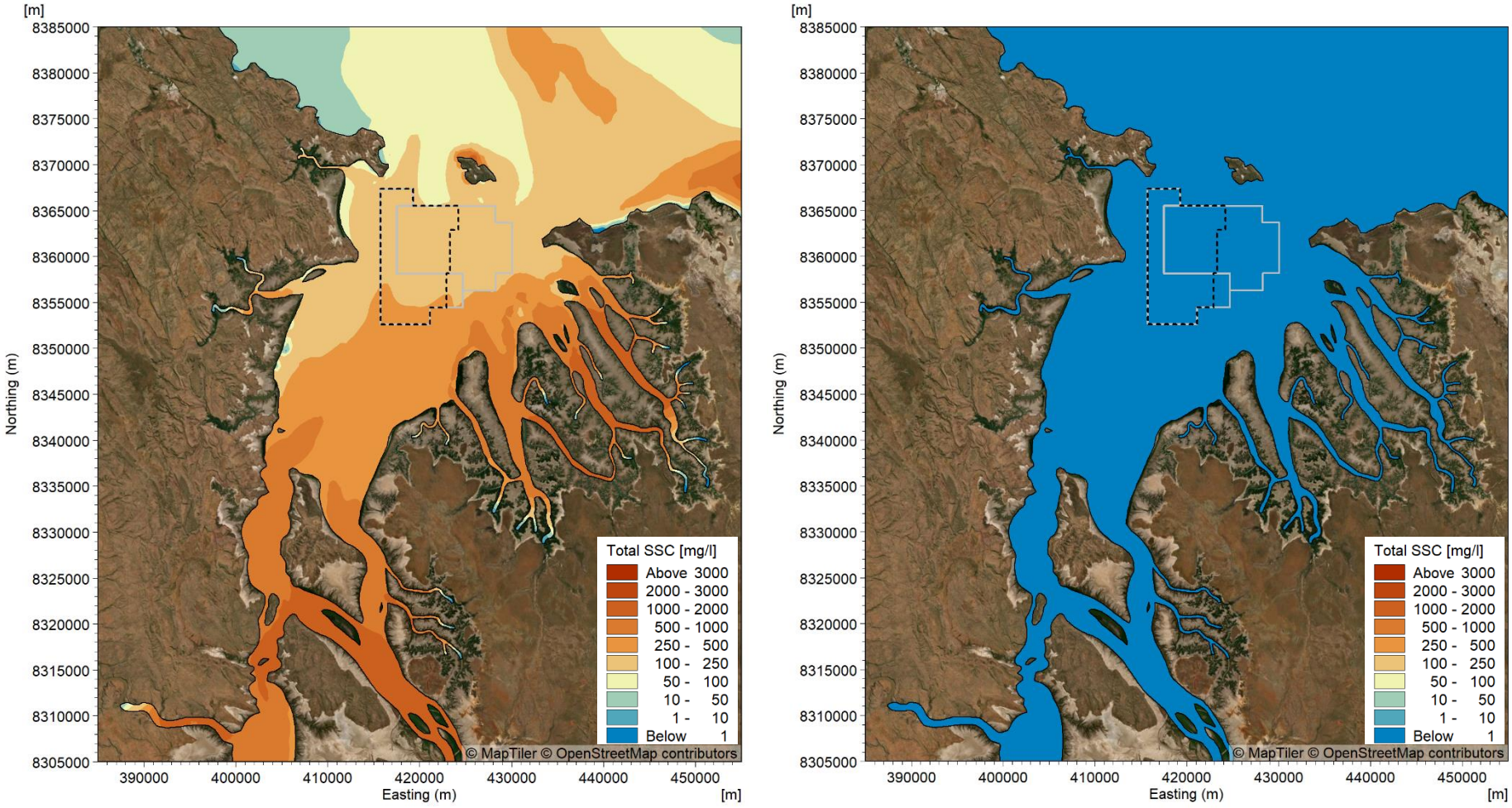
- The modelled SSC resulting from the sand sourcing operation was only above 1 mg/L for the 99th percentile, with all other percentiles having an increase of less than 1 mg/L. This demonstrates that the peaks in SSC above 1 mg/L shown in the timeseries plots only occurred for short durations.

- For sand sourcing scenario 1 the increase in modelled SSC at the sites outside of the POA (P04 to P10) for all percentiles were less than 1 mg/L.

- For sand sourcing scenario 2 the only site outside of the POA with a percentile modelled SSC increase of more than 1 mg/L was P06, where an increase of 1.8 mg/L occurred for the 99th percentile.

- The modelled SSC resulting from the sand sourcing activity at the sites located at Medusa Bank (P09) and King Shoals Sanctuary Zone (P10) only resulted in an increase in SSC of up to 0.1 mg/L (i.e. negligible increases).

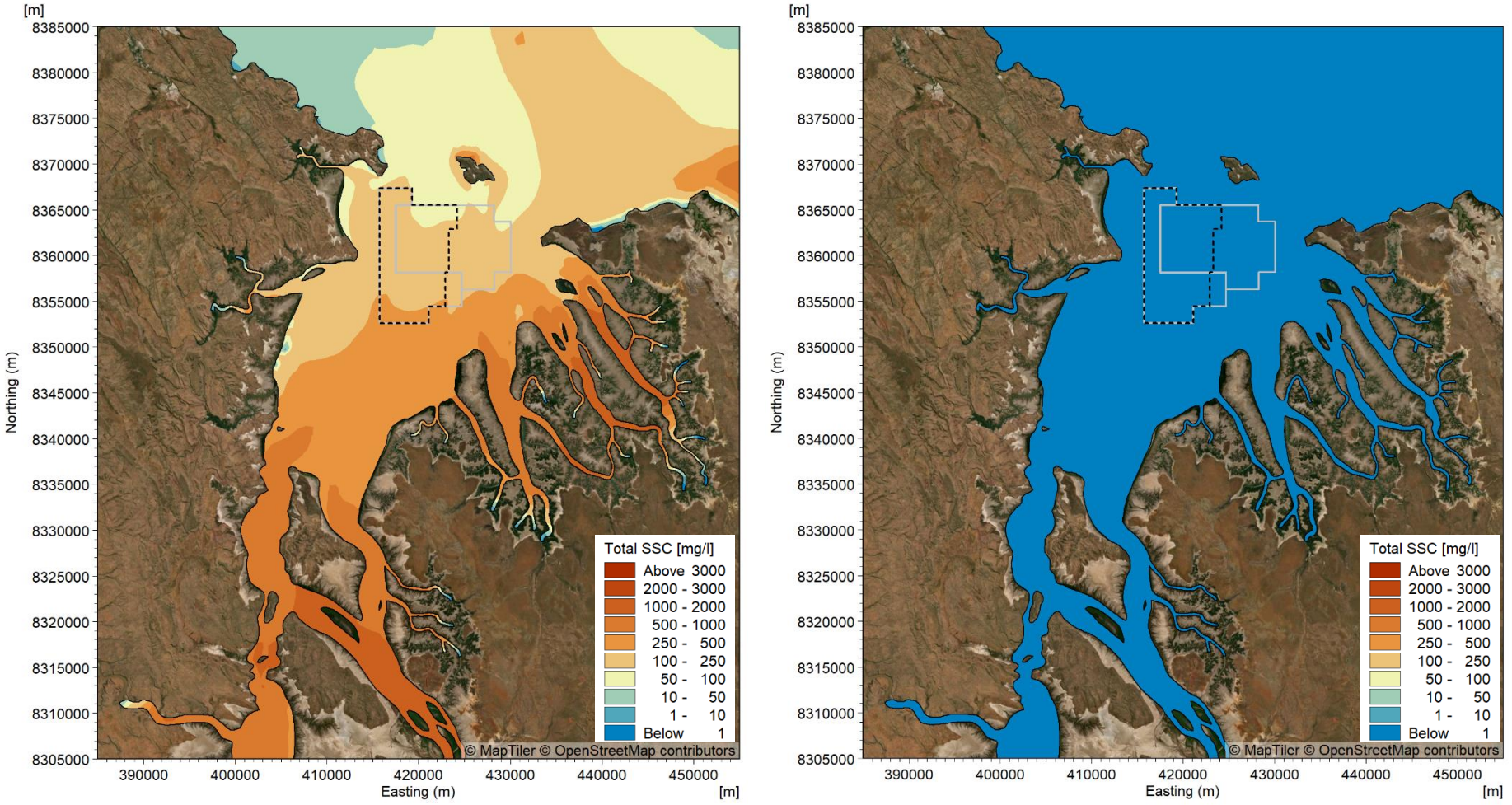
- Comparing the natural SSC percentiles with the natural plus sand sourcing SSC percentiles highlights how small the relative contribution of the sand sourcing SSC is assessed to be. The increases in SSC due to the sand sourcing were less than 1.5% of the natural SSC at all sites and for all scenarios.



Natural SSC

Sand Sourcing SSC

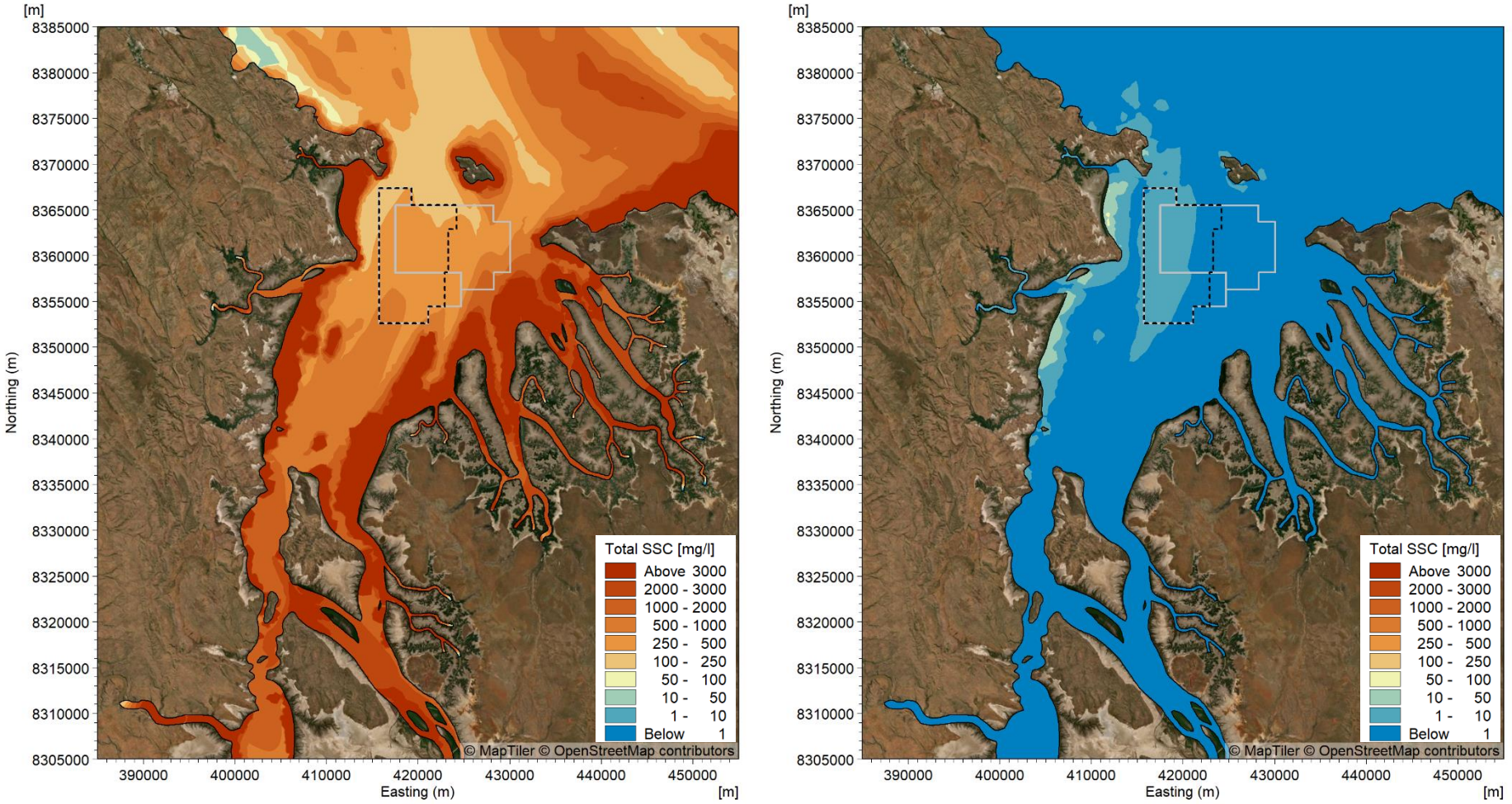
Figure 222. Modelled 50th percentile natural SSC and 50th percentile sand sourcing SSC for the near-bed layer when sand sourcing during neap tides over a two-month (60 days) period in the wet season for Scenario 1.



Natural SSC

Sand Sourcing SSC

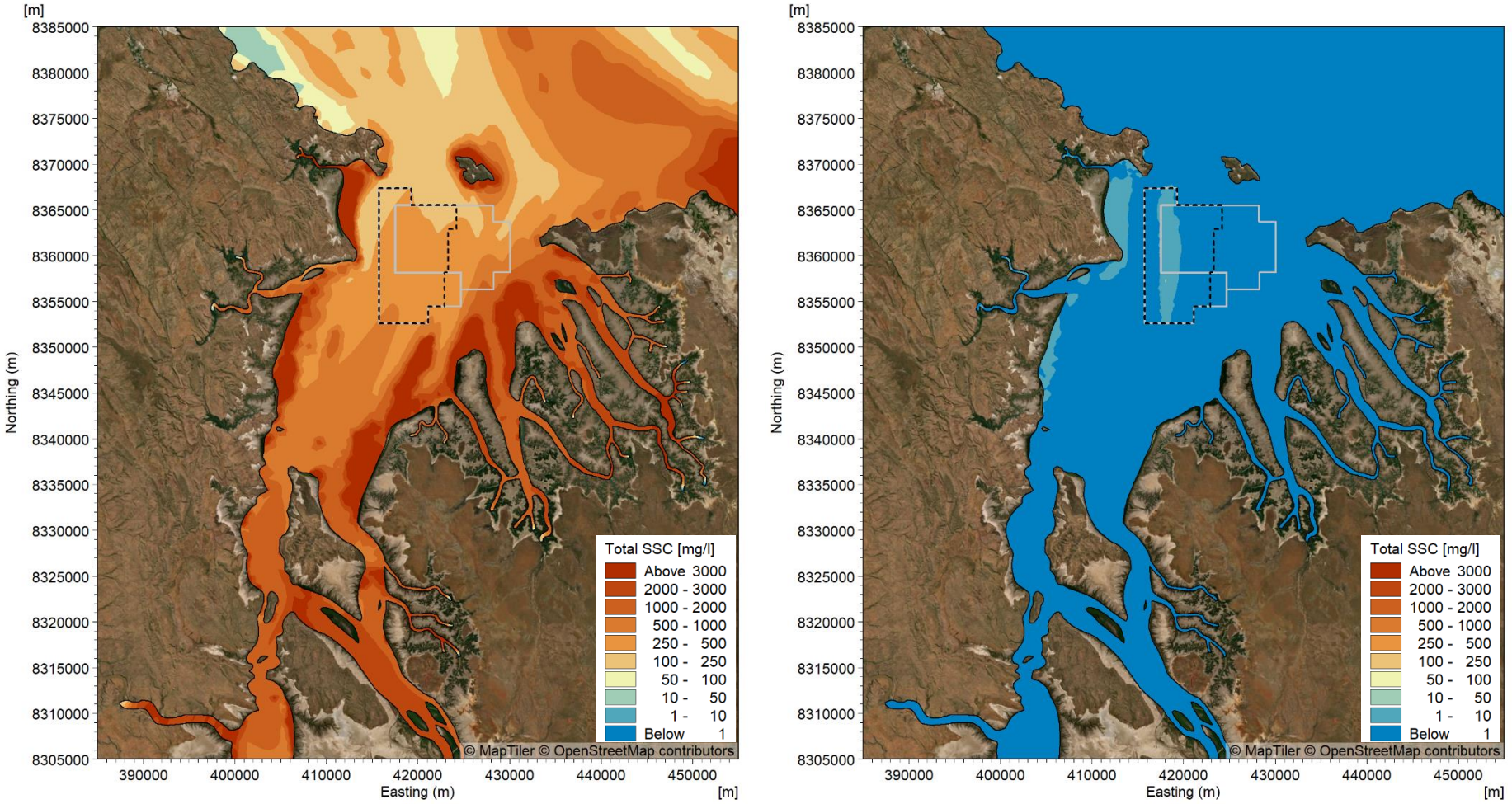
Figure 223. Modelled 50th percentile natural SSC and 50th percentile sand sourcing SSC for the mid-depth layer when sand sourcing during neap tides over a two-month (60 days) period in the wet season for Scenario 1.



Natural SSC

Sand Sourcing SSC

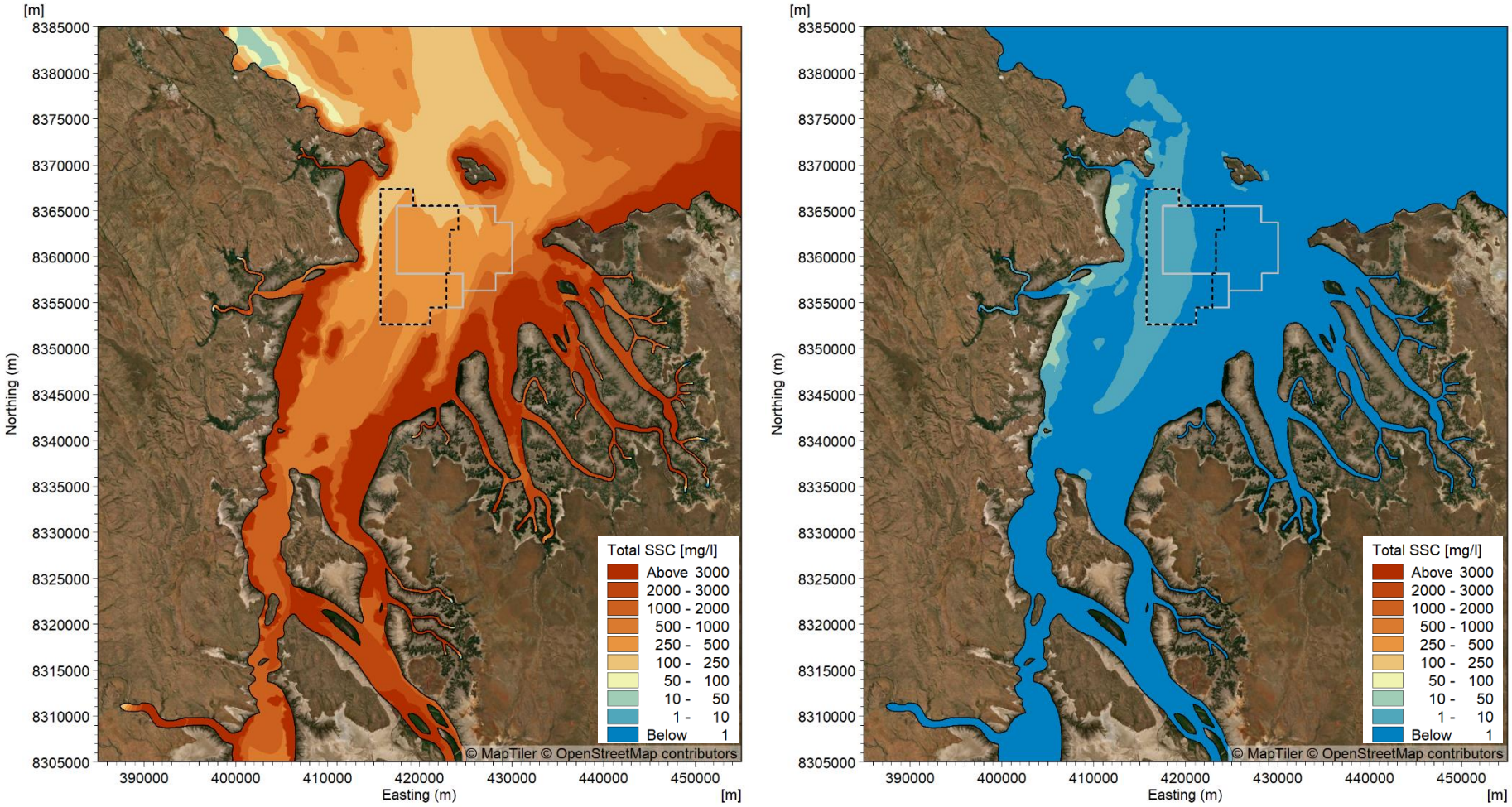
Figure 224. Modelled maximum natural SSC and maximum sand sourcing SSC for the near-bed layer when sand sourcing during neap tides over a two-month (60 days) period in the wet season for Scenario 1.



Natural SSC

Sand Sourcing SSC

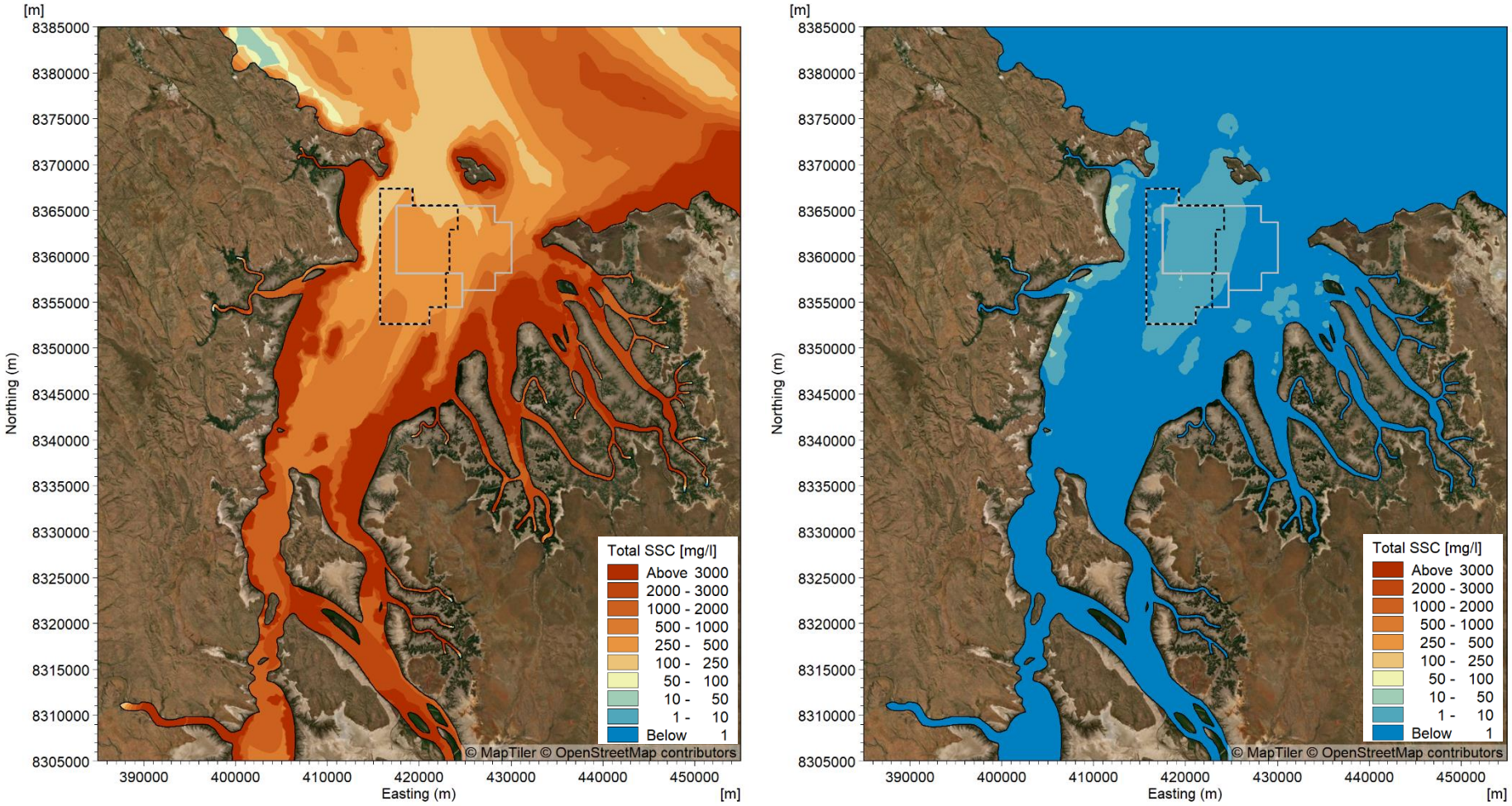
Figure 225. Modelled maximum natural SSC and maximum sand sourcing SSC for the mid-depth layer when sand sourcing during neap tides over a two-month (60 days) period in the wet season for Scenario 1.



Natural SSC

Sand Sourcing SSC

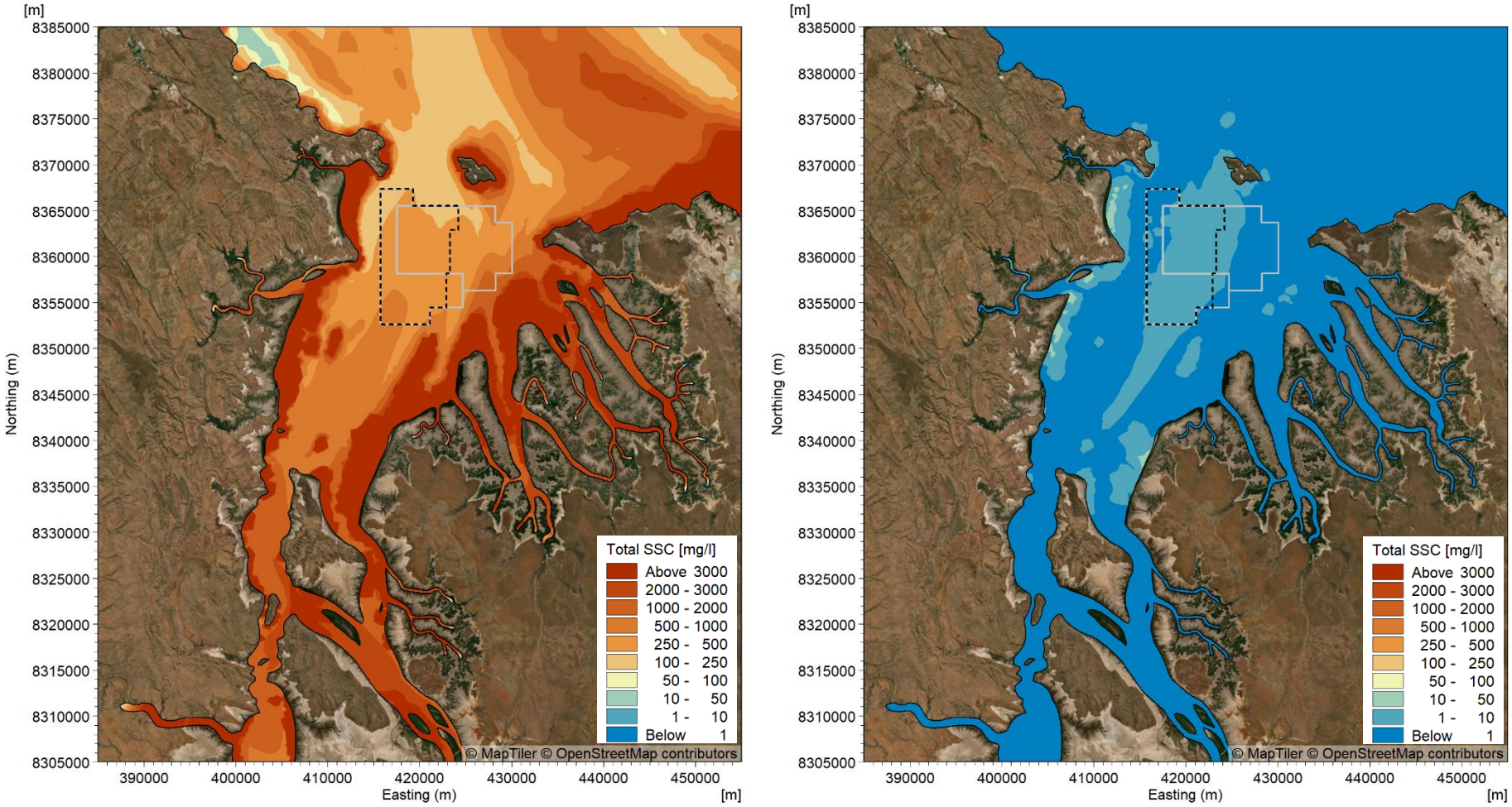
Figure 226. Modelled maximum natural SSC and maximum sand sourcing SSC for the near-bed layer when sand sourcing during spring tides over a two-month (60 days) period in the wet season for Scenario 1.



Natural SSC

Sand Sourcing SSC

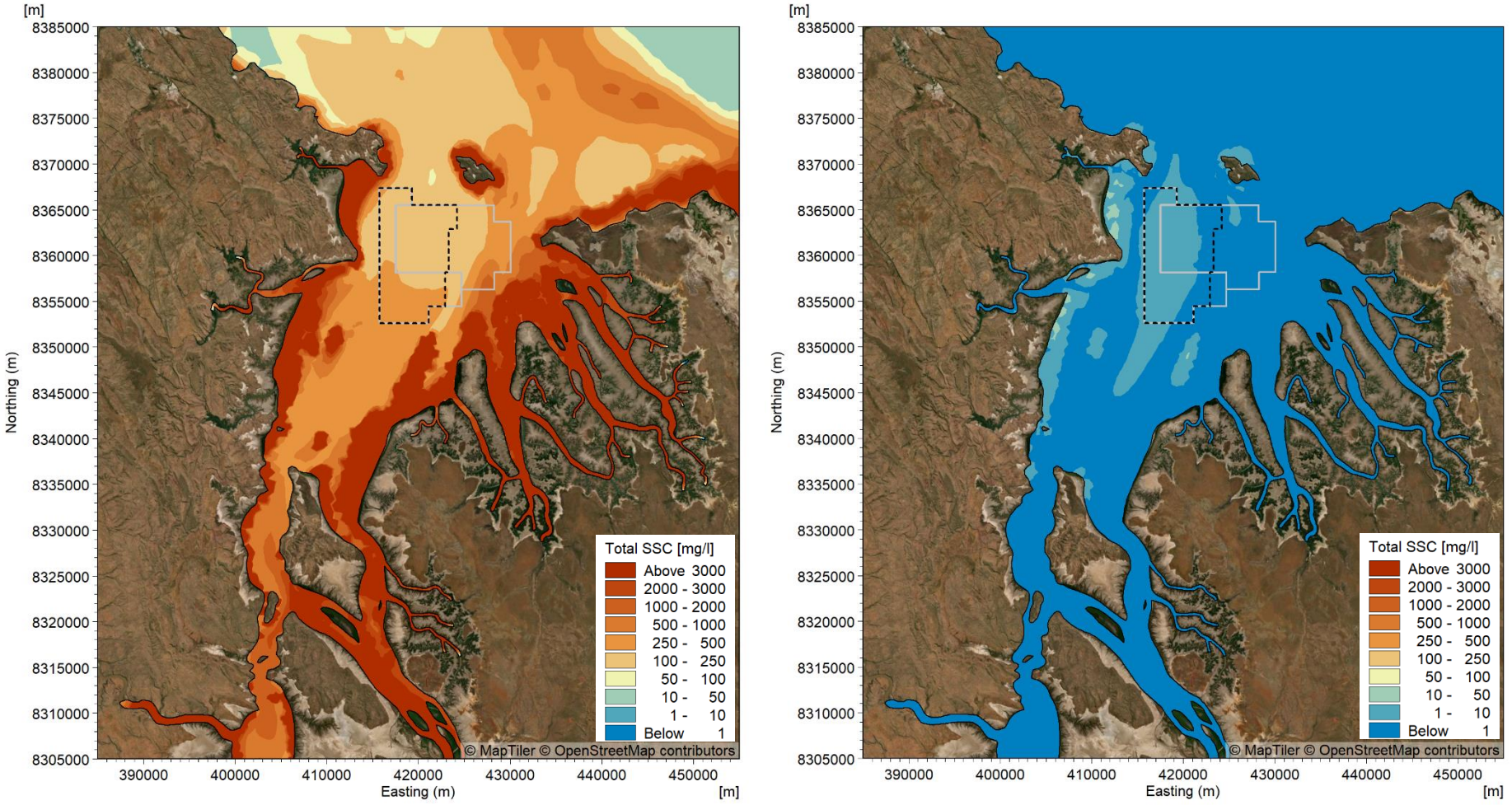
Figure 227. Modelled maximum natural SSC and maximum sand sourcing SSC for the near-bed layer when sand sourcing during neap tides over a two-month (60 days) period in the wet season for Scenario 2.



Natural SSC

Sand Sourcing SSC

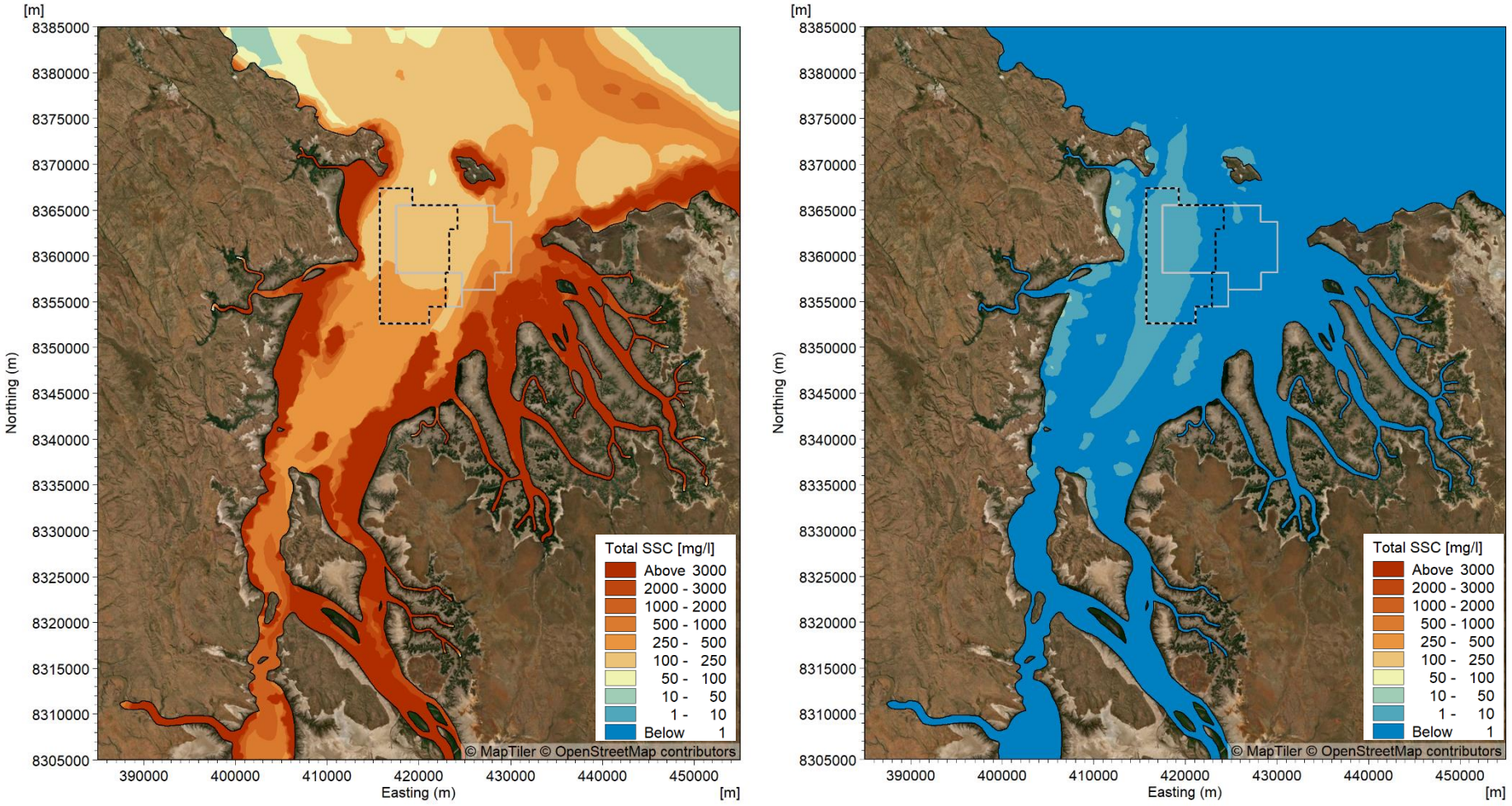
Figure 228. Modelled maximum natural SSC and maximum sand sourcing SSC for the near-bed layer when sand sourcing during spring tides over a two-month (60 days) period in the wet season for Scenario 2.



Natural SSC

Sand Sourcing SSC

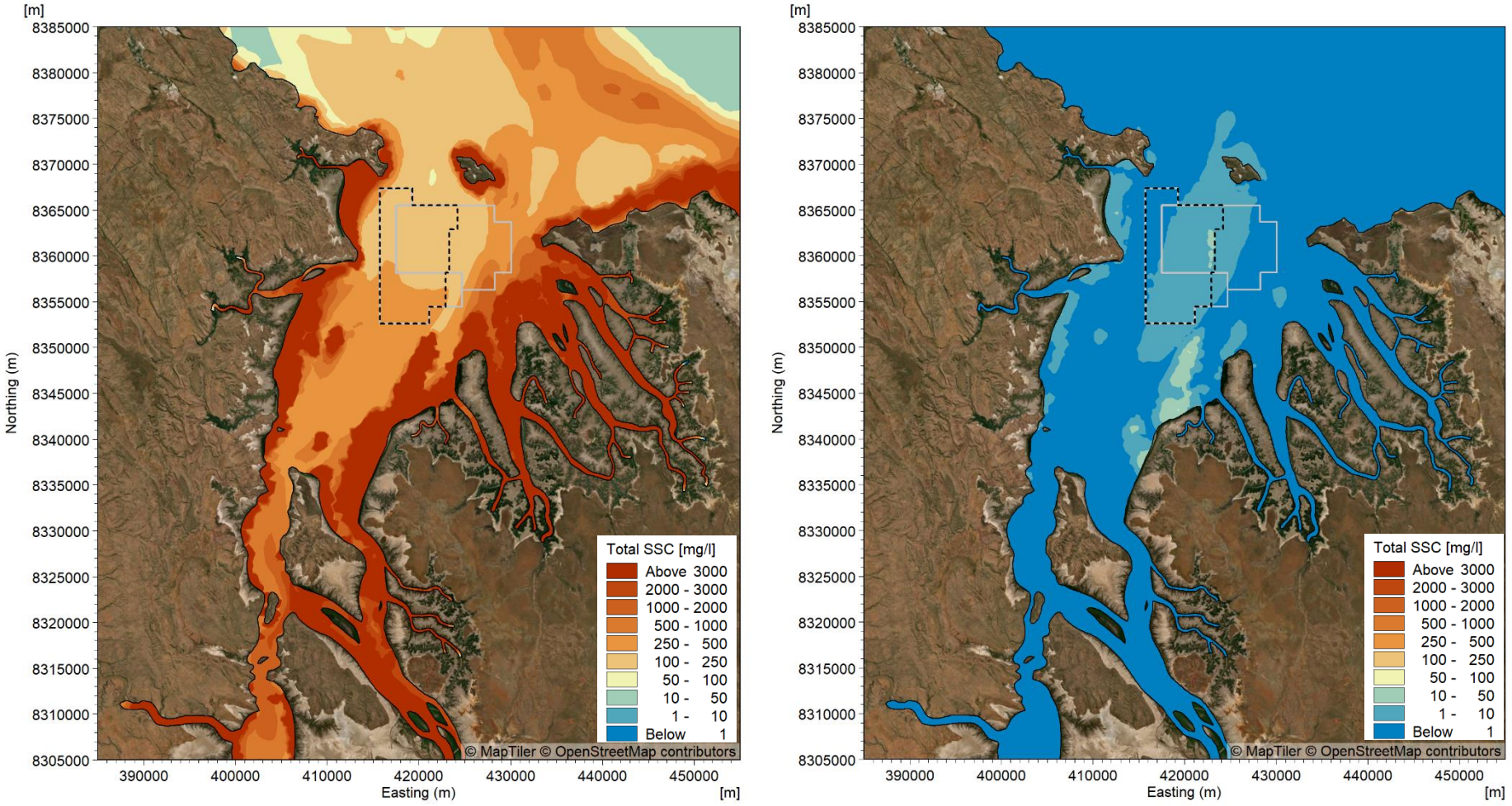
Figure 229. Modelled maximum natural SSC and maximum sand sourcing SSC for the near-bed layer when sand sourcing during neap tides over a two-month (61 days) period in the dry season for Scenario 1.



Natural SSC

Sand Sourcing SSC

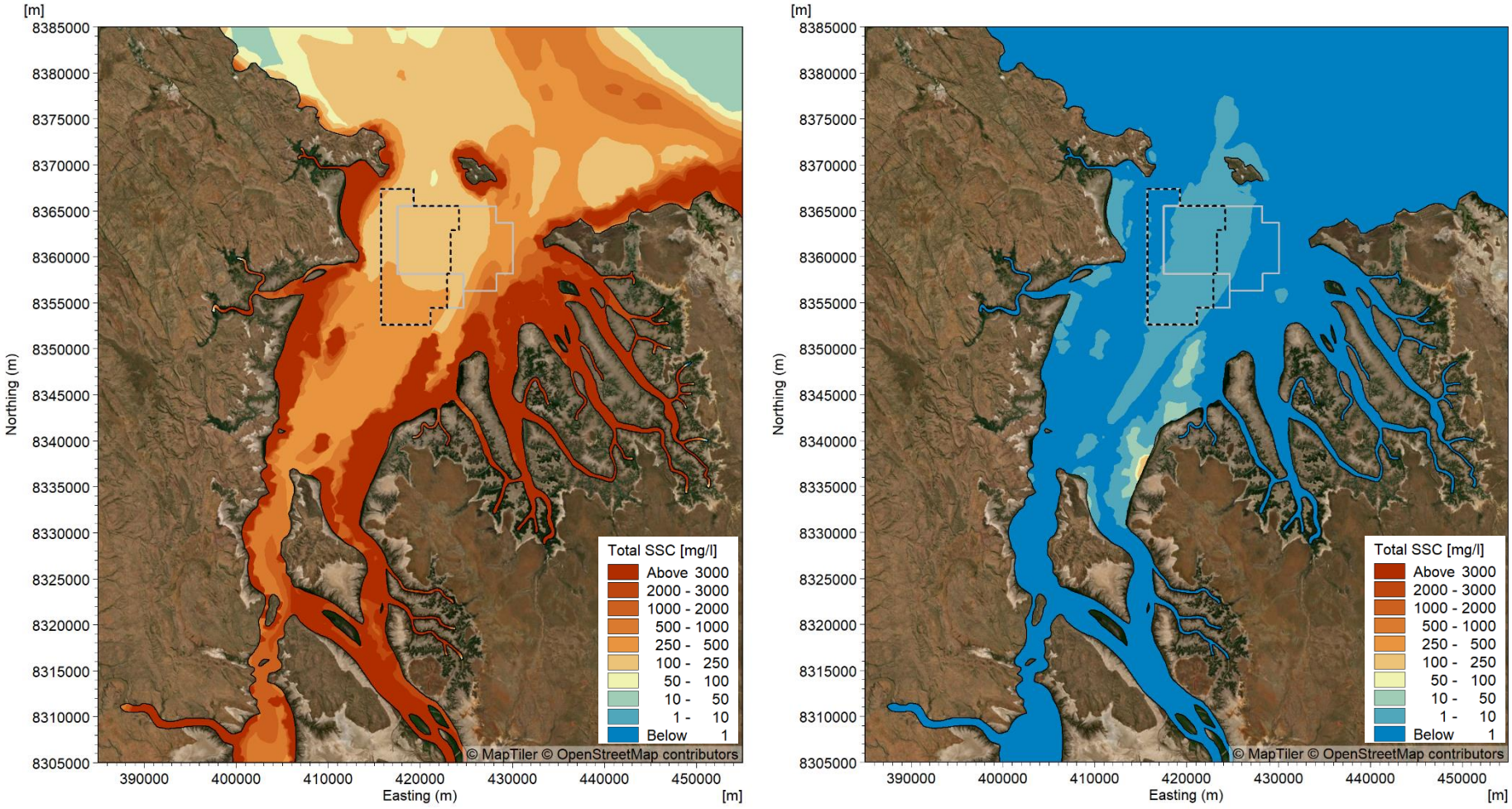
Figure 230. Modelled maximum natural SSC and maximum sand sourcing SSC for the near-bed layer when sand sourcing during spring tides over a two-month (61 days) period in the dry season for Scenario 1.



Natural SSC

Sand Sourcing SSC

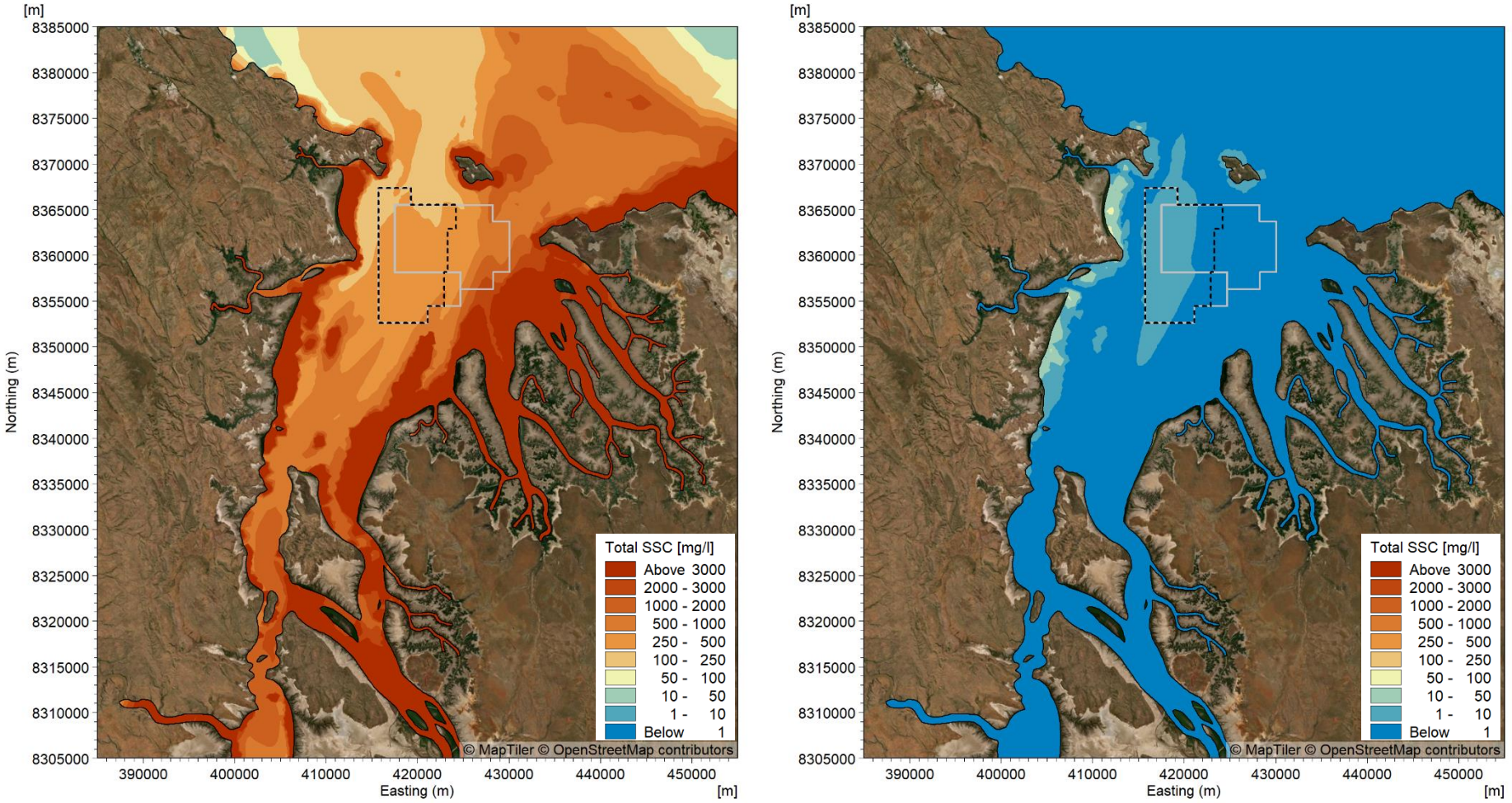
Figure 231. Modelled maximum natural SSC and maximum sand sourcing SSC for the near-bed layer when sand sourcing during neap tides over a two-month (61 days) period in the dry season for Scenario 2.



Natural SSC

Sand Sourcing SSC

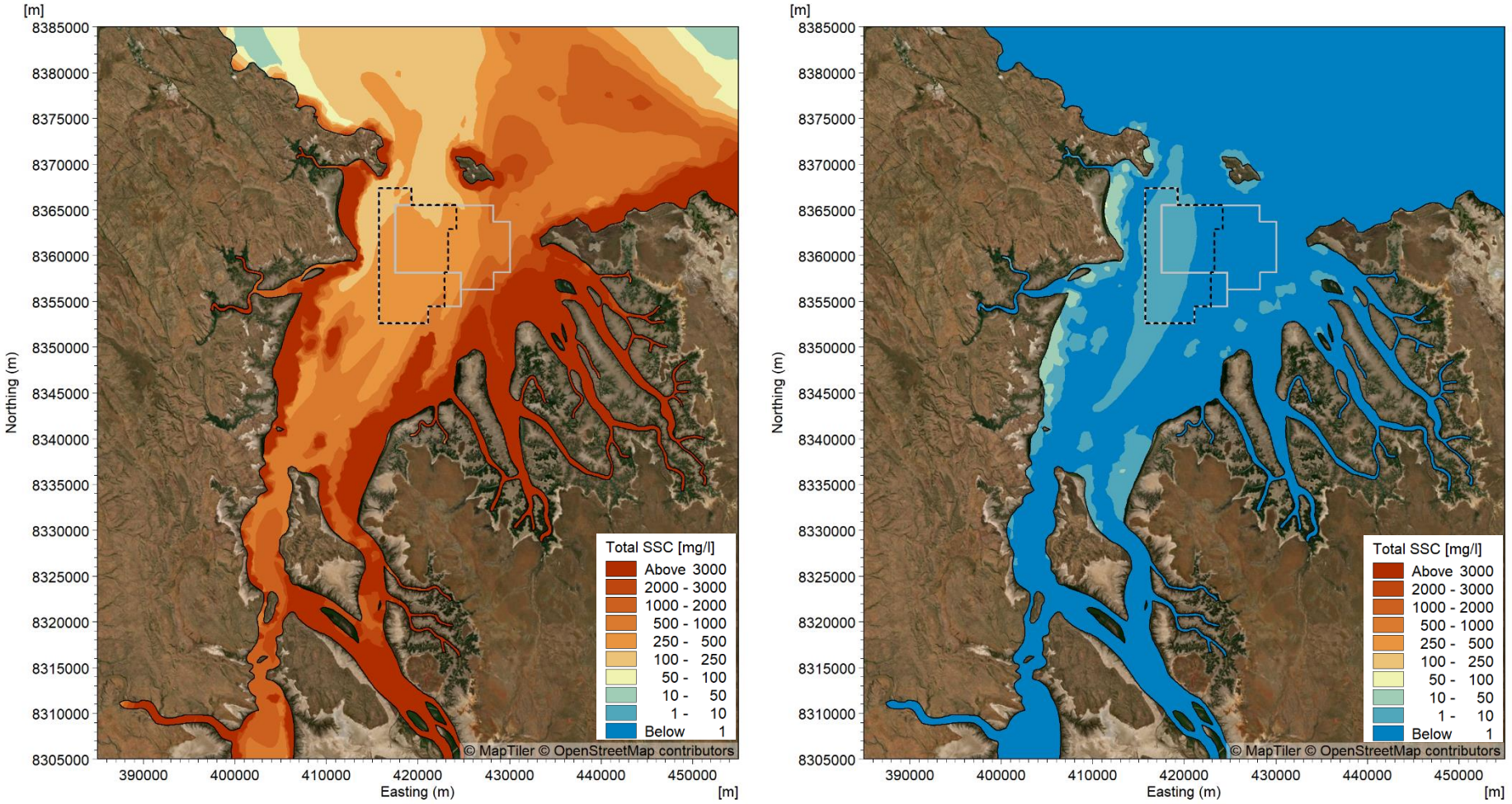
Figure 232. Modelled maximum natural SSC and maximum sand sourcing SSC for the near-bed layer when sand sourcing during spring tides over a two-month (61 days) period in the dry season for Scenario 2.



Natural SSC

Sand Sourcing SSC

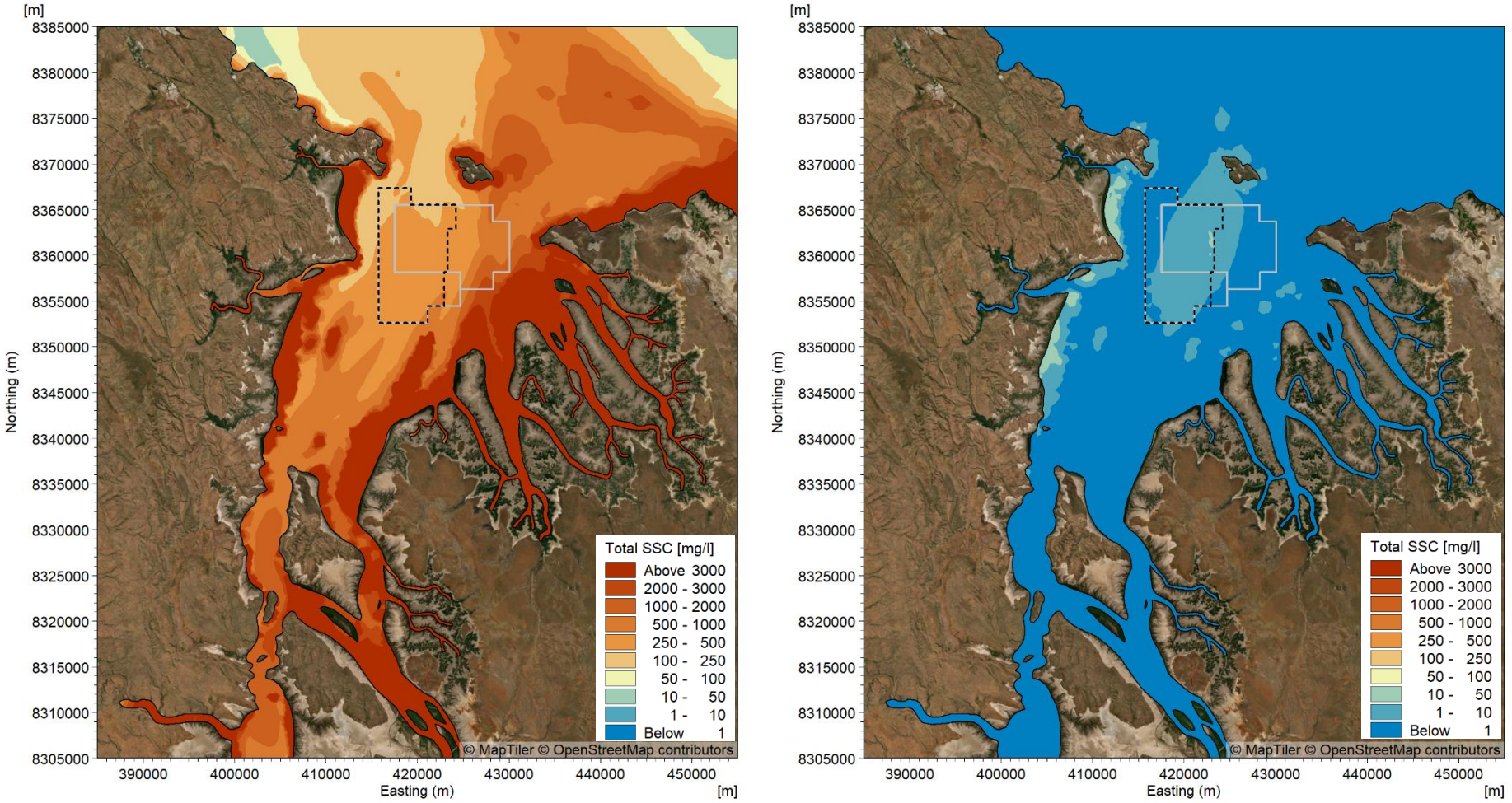
Figure 233. Modelled maximum natural SSC and maximum sand sourcing SSC for the near-bed layer when sand sourcing during neap tides over a two-month (61 days) period in the transitional season for Scenario 1.



Natural SSC

Sand Sourcing SSC

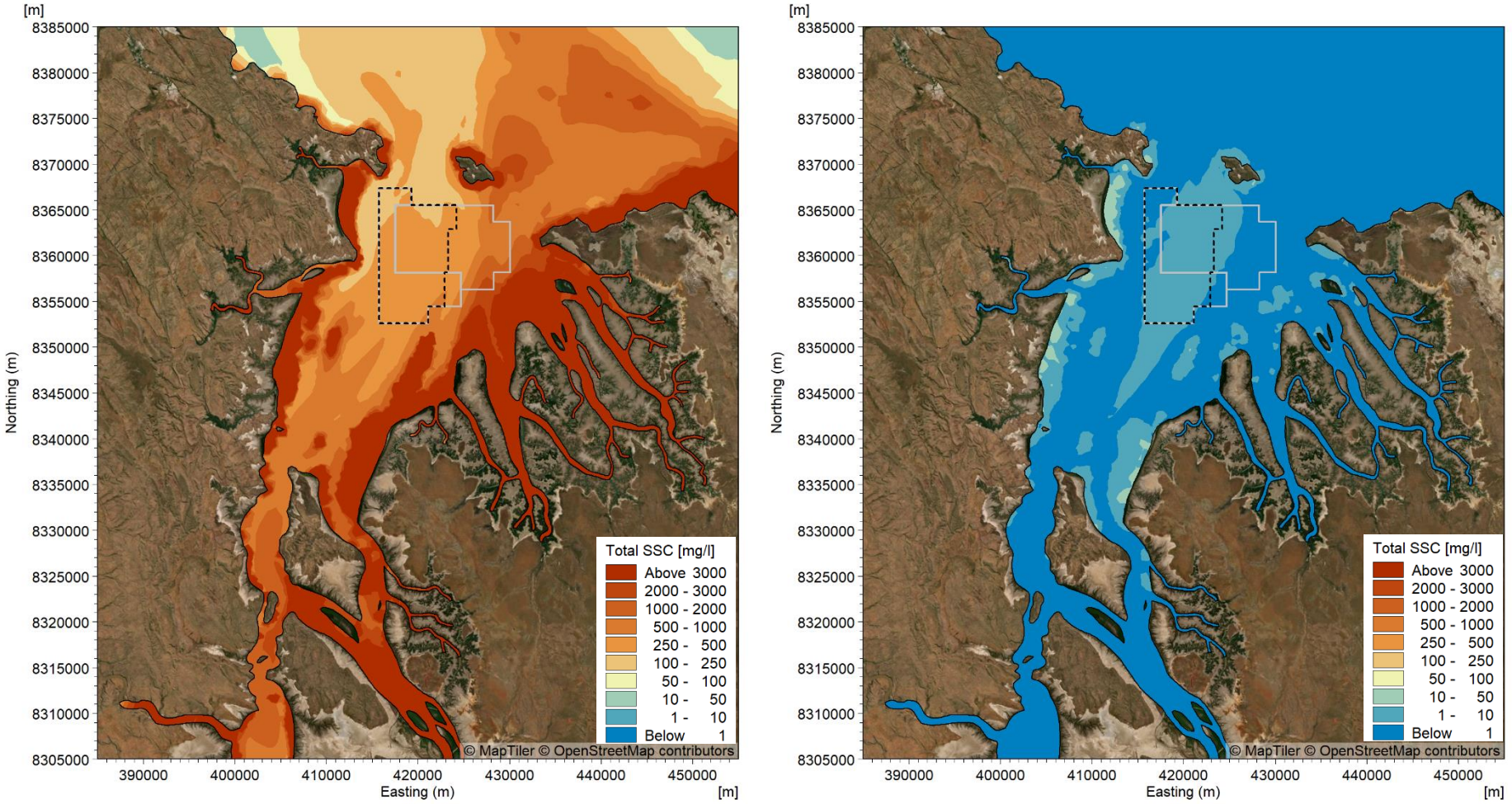
Figure 234. Modelled maximum natural SSC and maximum sand sourcing SSC for the near-bed layer when sand sourcing during spring tides over a two-month (61 days) period in the transitional season for Scenario 1.



Natural SSC

Sand Sourcing SSC

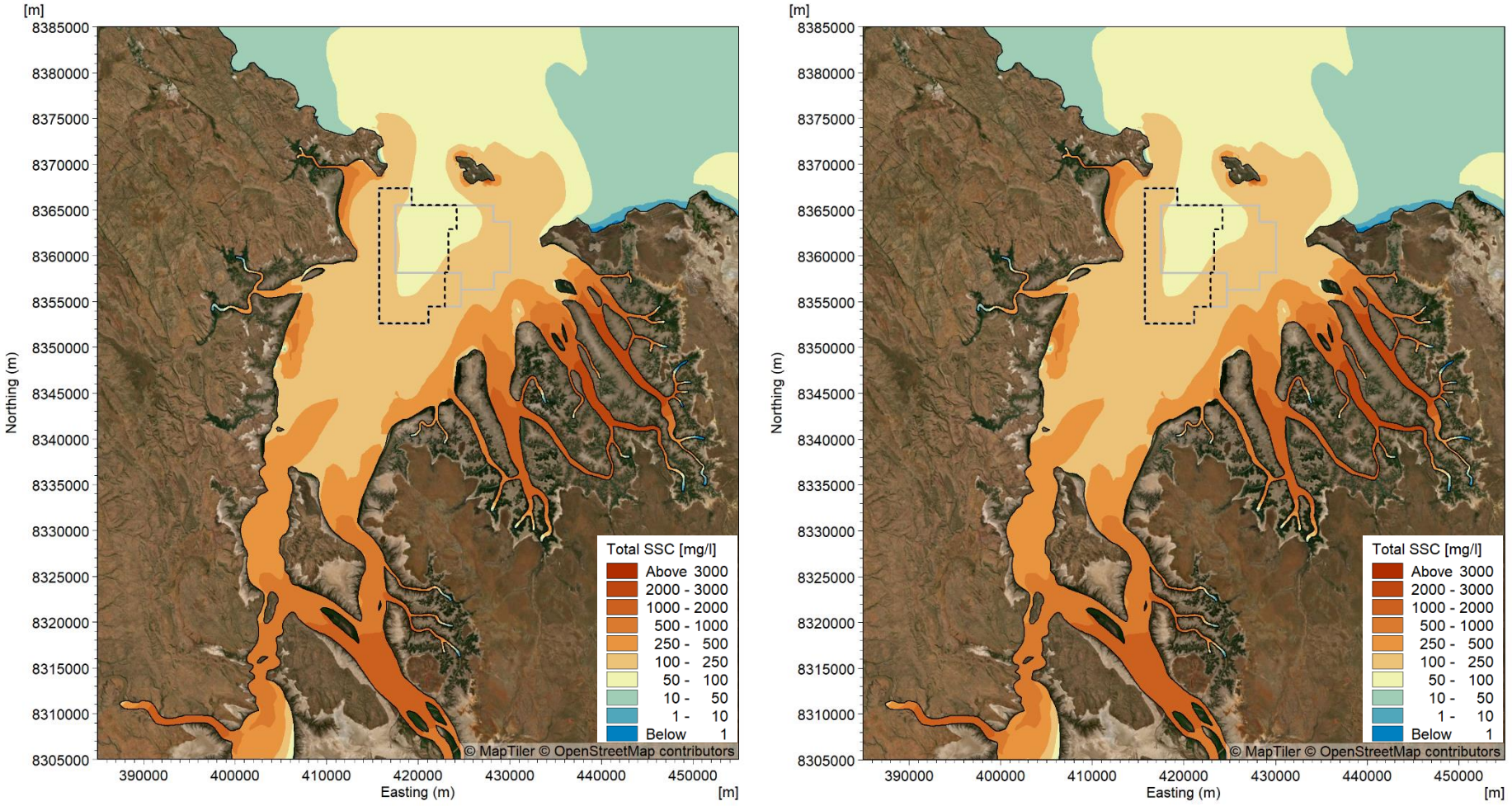
Figure 235. Modelled maximum natural SSC and maximum sand sourcing SSC for the near-bed layer when sand sourcing during neap tides over a two-month (61 days) period in the transitional season for Scenario 2.



Natural SSC

Sand Sourcing SSC

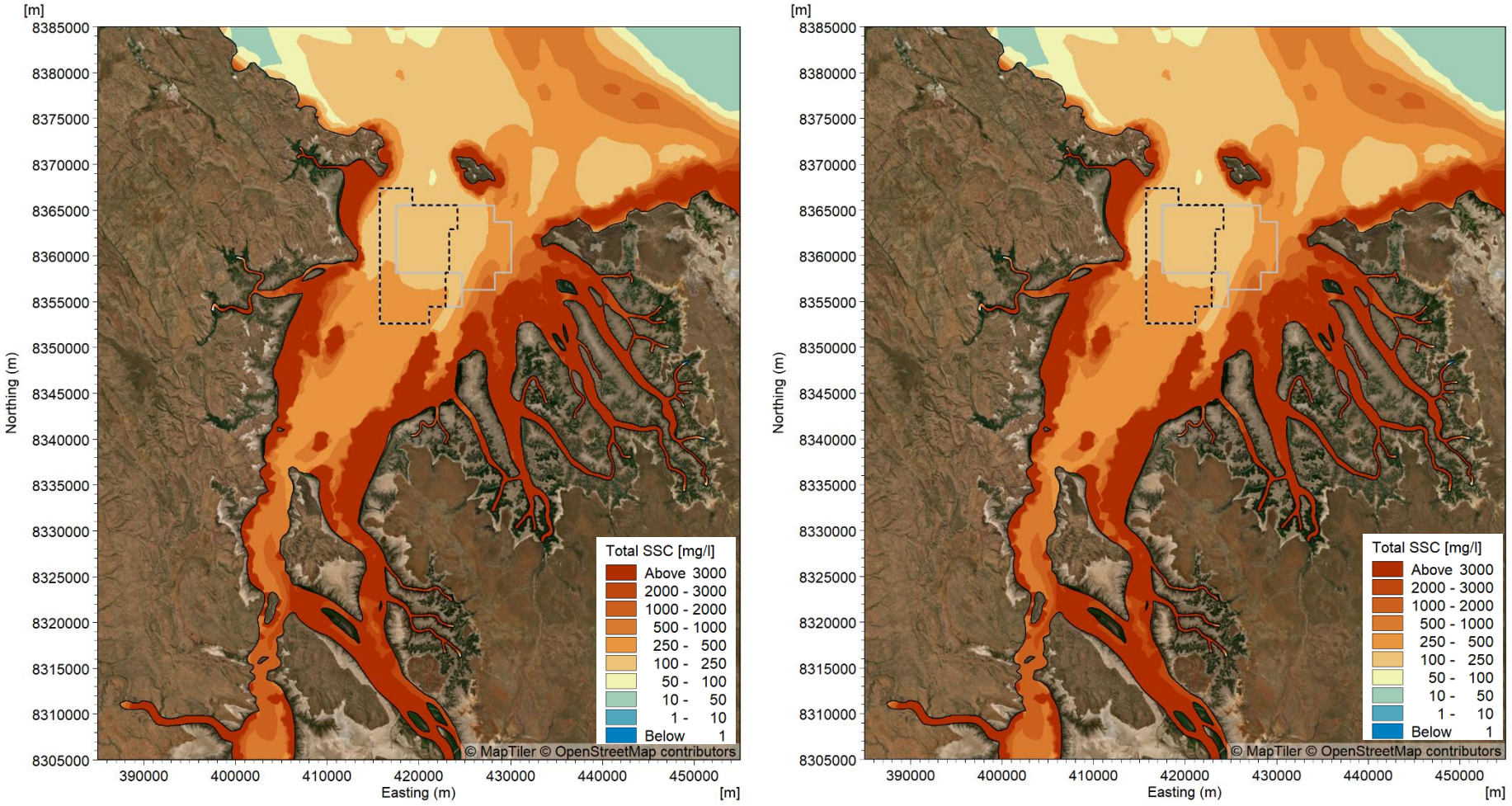
Figure 236. Modelled maximum natural SSC and maximum sand sourcing SSC for the near-bed layer when sand sourcing during spring tides over a two-month (61 days) period in the transitional season for Scenario 2.



Natural SSC

Natural + Sand Sourcing SSC

Figure 237. Modelled 50th percentile natural SSC and 50th percentile natural plus sand sourcing SSC for the near-bed layer when sand sourcing during spring tides over a two-month (61 days) period in the dry season for Scenario 2.



Natural SSC

Natural + Sand Sourcing SSC

Figure 238. Modelled maximum natural SSC and maximum natural plus sand sourcing SSC for the near-bed layer when sand sourcing during spring tides over a two-month (61 days) period in the dry season for Scenario 2.

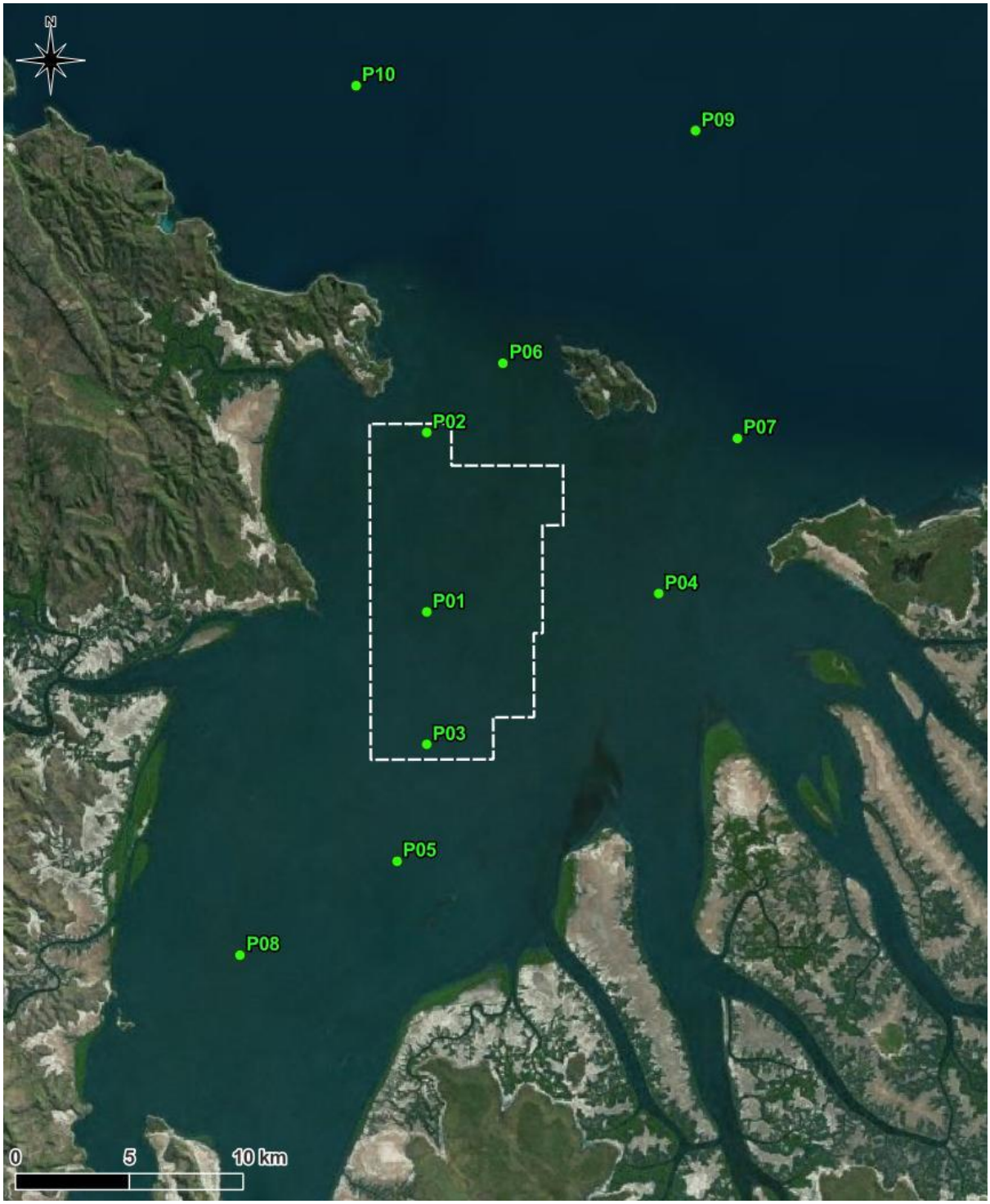


Figure 239. Locations of model output points for the SPV plume modelling along with the POA (white dashed line).

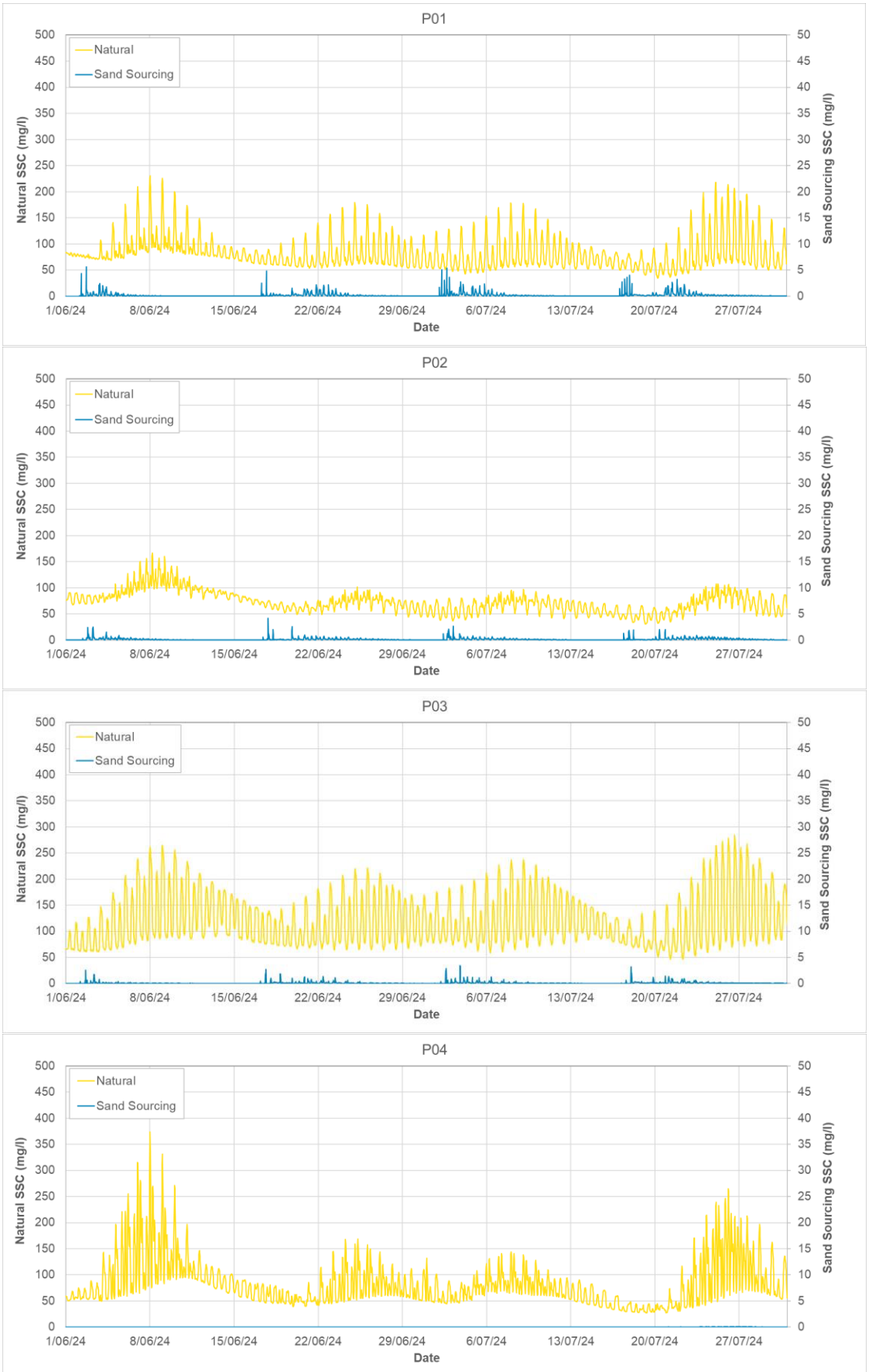


Figure 240. Timeseries showing the modelled natural SSC and sand sourcing SSC at P01 to P04 during the dry season for Scenario 1 with releases during neap tides. *Note: the sand sourcing SSC is plotted using a second y-axis with a lower SSC magnitude.*

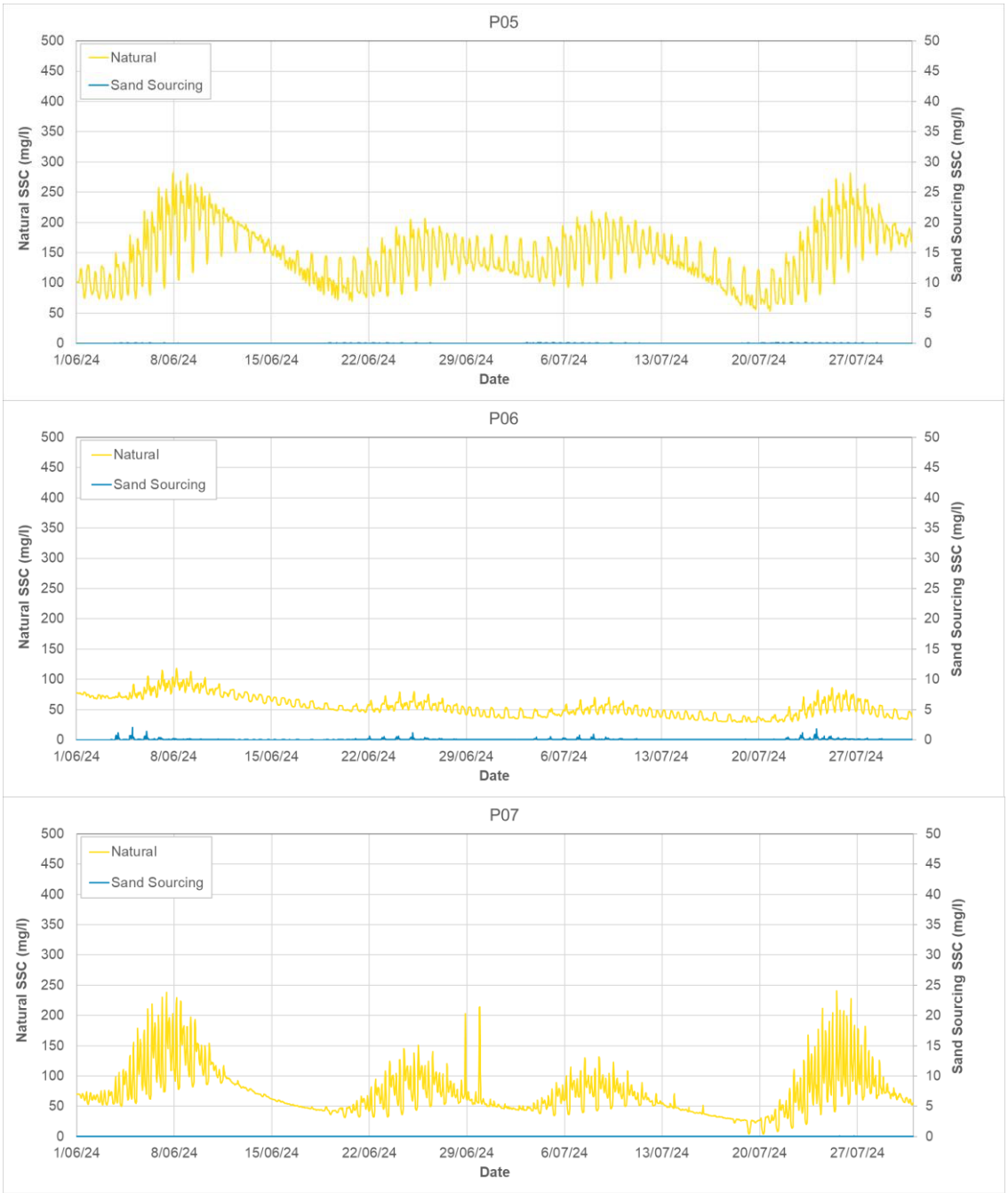


Figure 241. Timeseries showing the modelled natural SSC and sand sourcing SSC at P05 to P07 during the dry season for Scenario 1 with releases during neap tides. *Note: the sand sourcing SSC is plotted using a second y-axis with a lower SSC magnitude.*

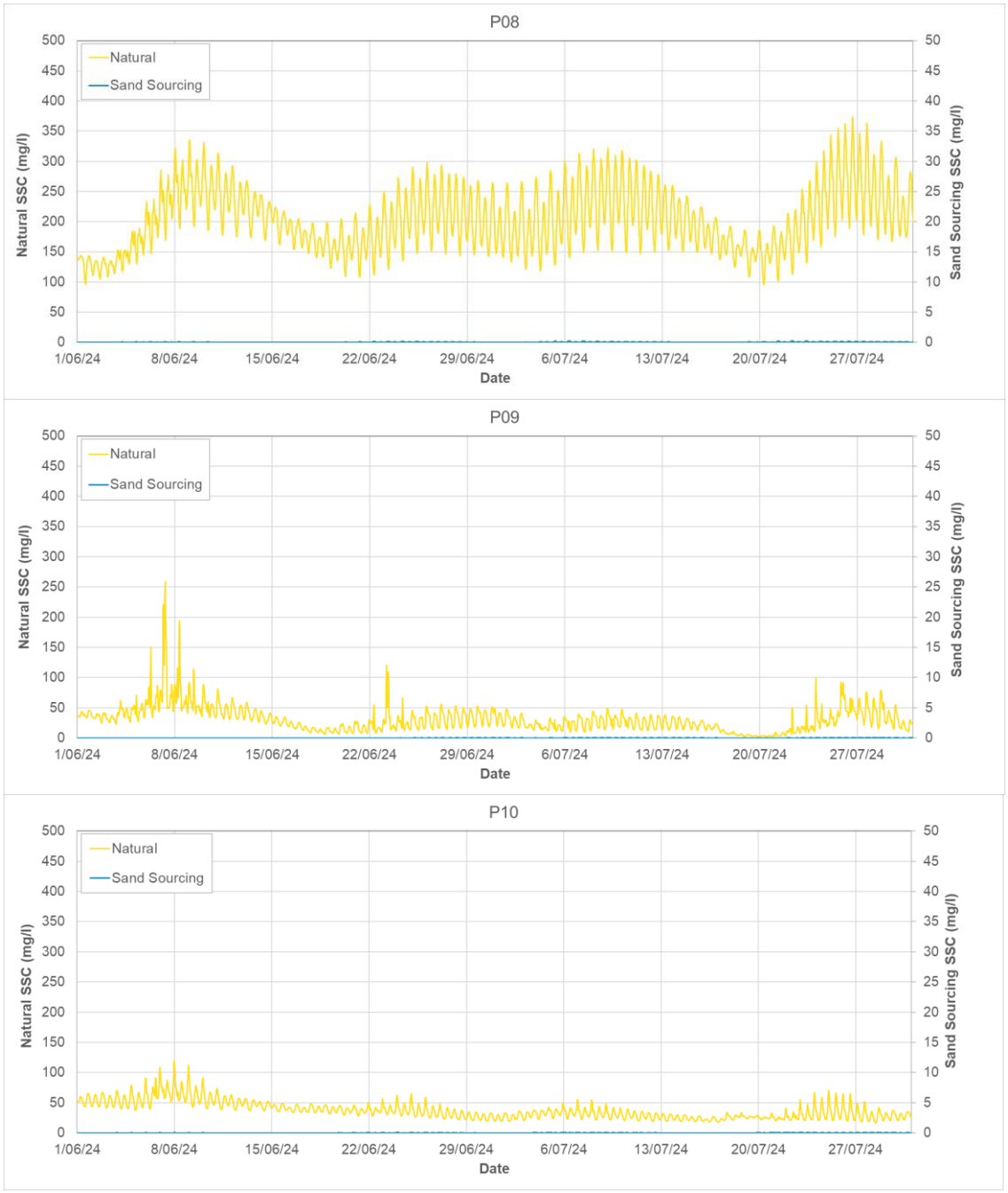


Figure 242. Timeseries showing the modelled natural SSC and sand sourcing SSC at P08 to P10 during the dry season for Scenario 1 with releases during neap tides. *Note: the sand sourcing SSC is plotted using a second y-axis with a lower SSC magnitude.*

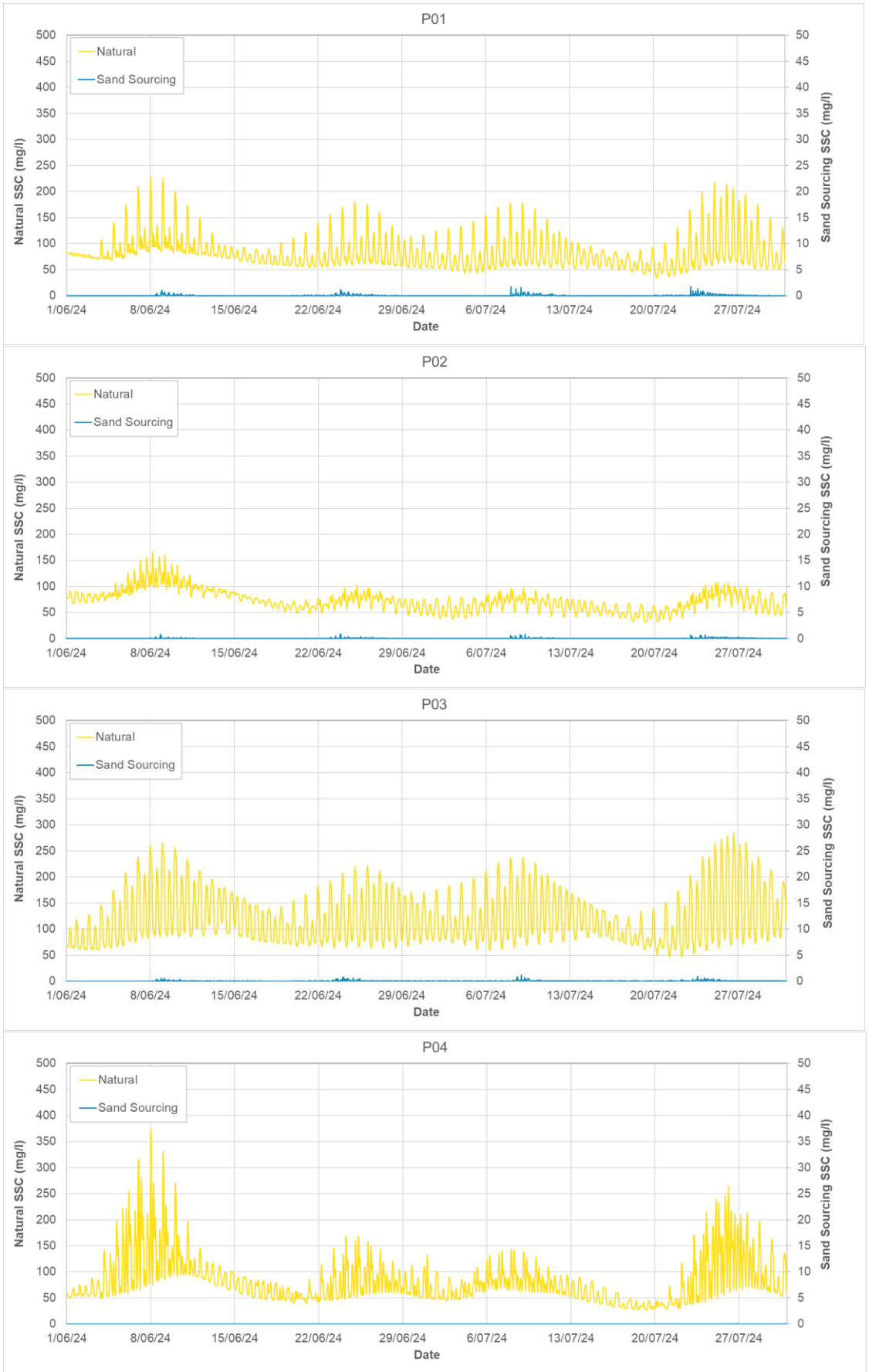


Figure 243. Timeseries showing the modelled natural SSC and sand sourcing SSC at P01 to P04 during the dry season for Scenario 1 with releases during spring tides. *Note: the sand sourcing SSC is plotted using a second y-axis with a lower SSC magnitude.*



Figure 244. Timeseries showing the modelled natural SSC and sand sourcing SSC at P05 to P07 during the dry season for Scenario 1 with releases during spring tides. *Note: the sand sourcing SSC is plotted using a second y-axis with a lower SSC magnitude.*

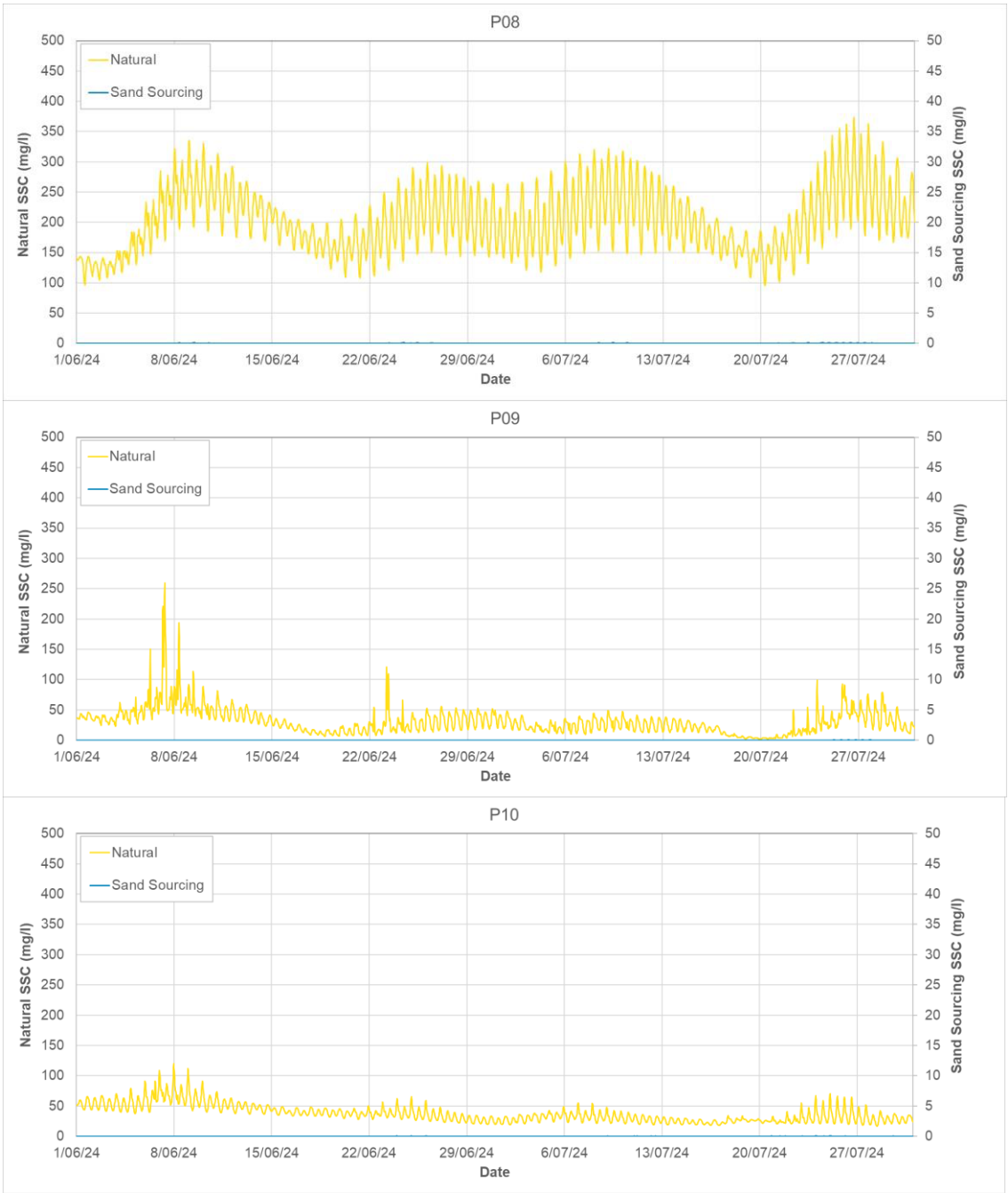


Figure 245. Timeseries showing the modelled natural SSC and sand sourcing SSC at P08 to P10 during the dry season for Scenario 1 with releases during spring tides. *Note: the sand sourcing SSC is plotted using a second y-axis with a lower SSC magnitude.*

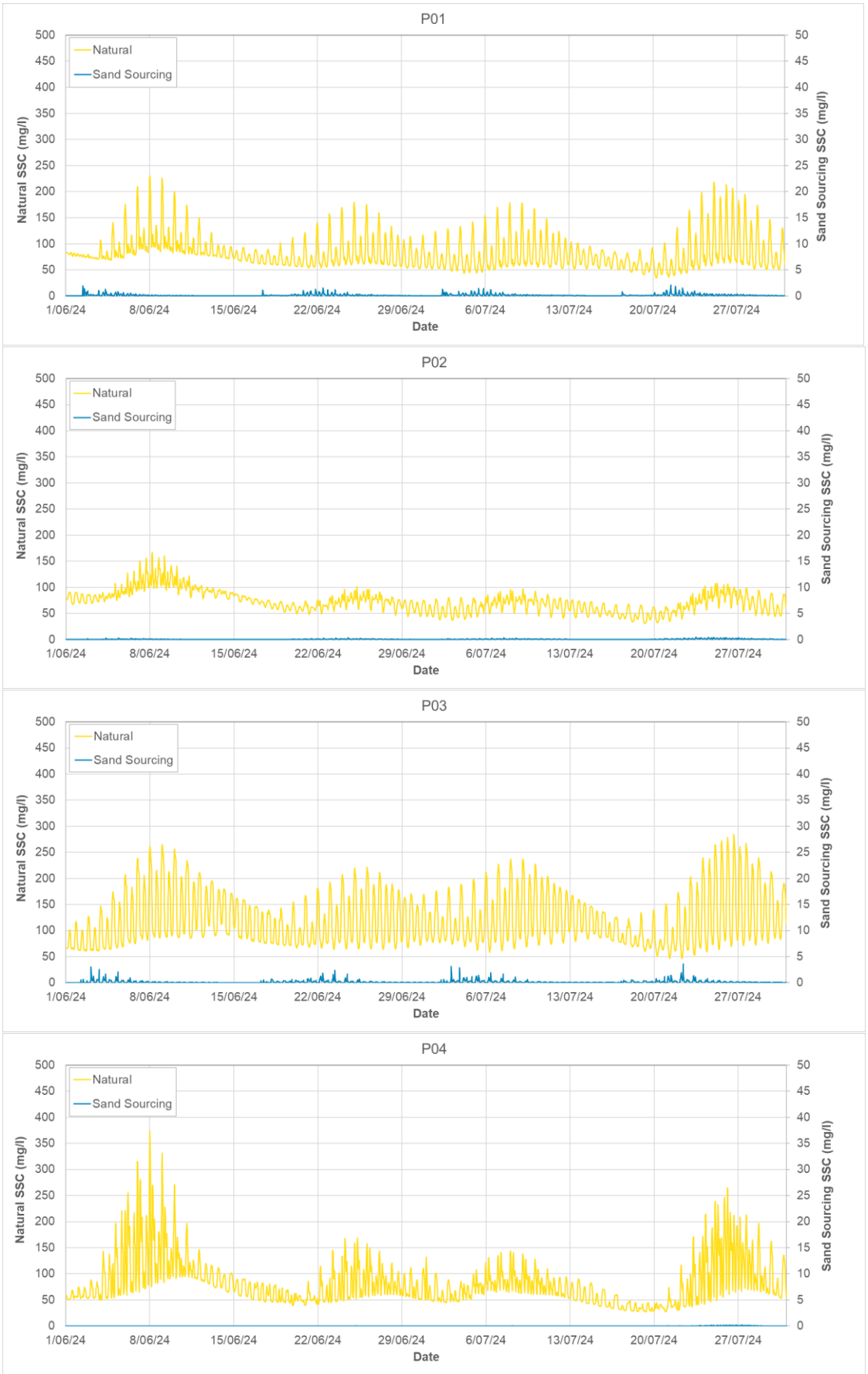


Figure 246. Timeseries showing the modelled natural SSC and sand sourcing SSC at P01 to P04 during the dry season for Scenario 2 with releases during neap tides. *Note: the sand sourcing SSC is plotted using a second y-axis with a lower SSC magnitude.*

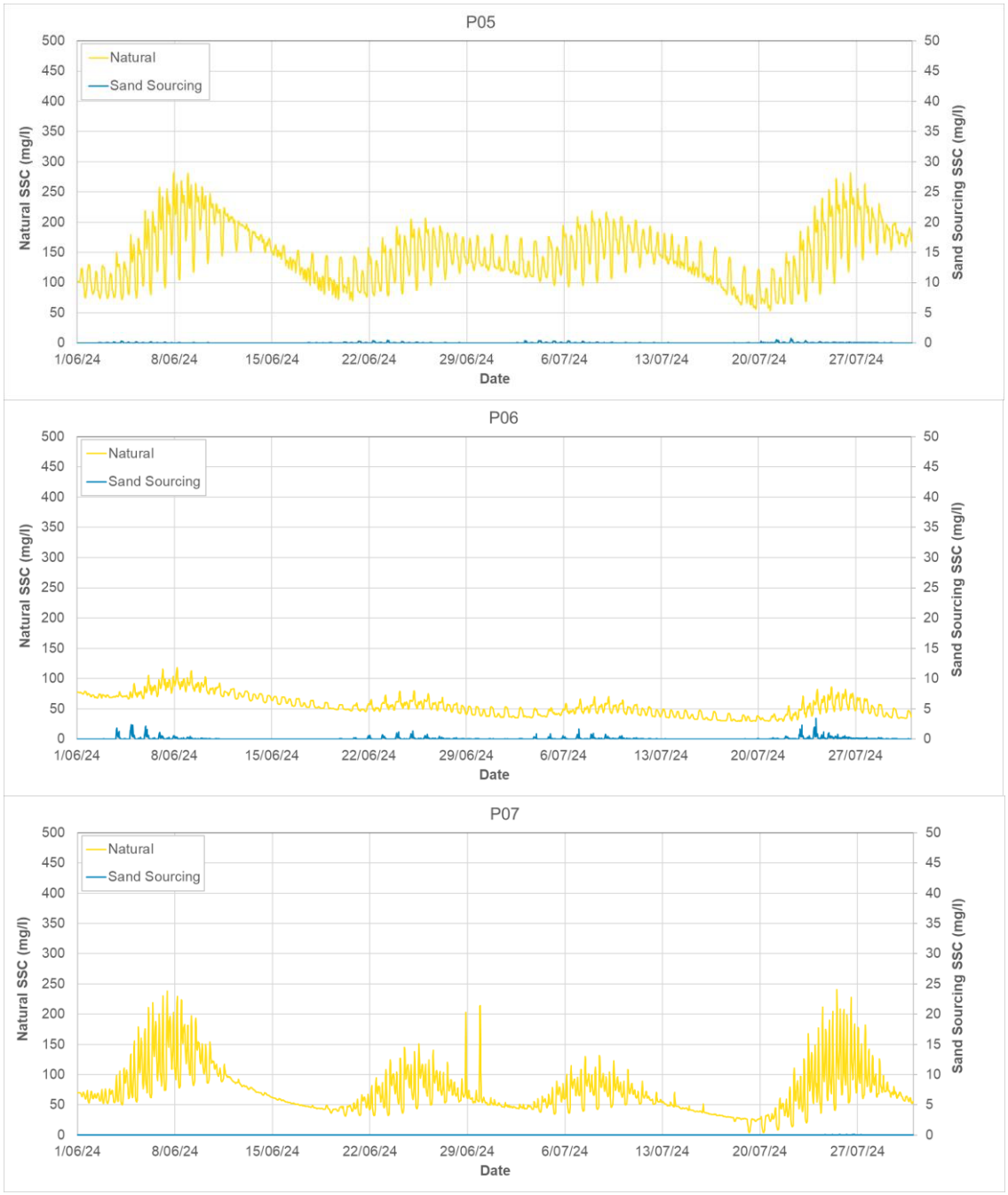


Figure 247. Timeseries showing the modelled natural SSC and sand sourcing SSC at P05 to P07 during the dry season for Scenario 2 with releases during neap tides. *Note: the sand sourcing SSC is plotted using a second y-axis with a lower SSC magnitude.*

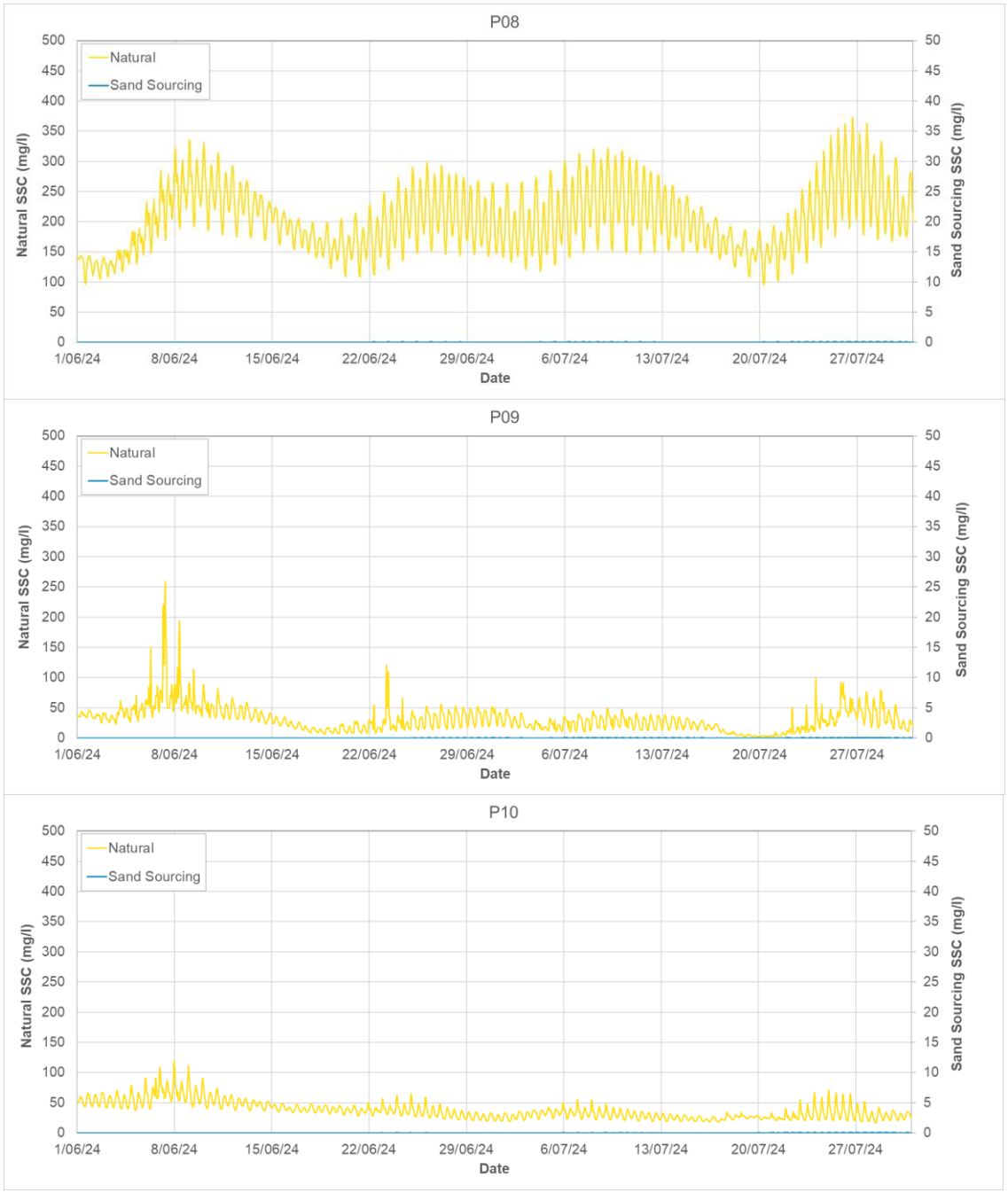


Figure 248. Timeseries showing the modelled natural SSC and sand sourcing SSC at P08 to P10 during the dry season for Scenario 2 with releases during neap tides. *Note: the sand sourcing SSC is plotted using a second y-axis with a lower SSC magnitude.*

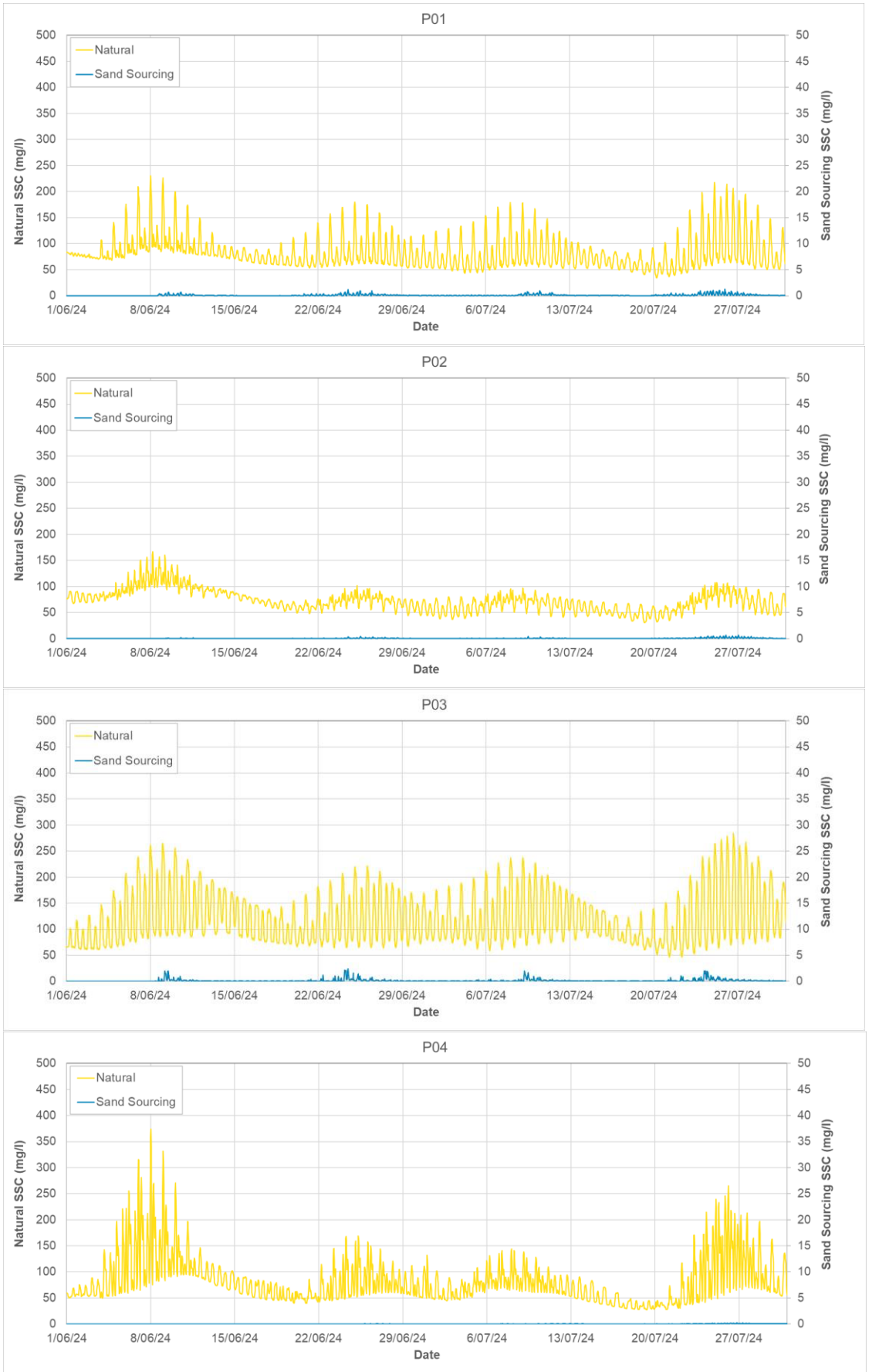


Figure 249. Timeseries showing the modelled natural SSC and sand sourcing SSC at P01 to P04 during the dry season for Scenario 2 with releases during spring tides. *Note: the sand sourcing SSC is plotted using a second y-axis with a lower SSC magnitude.*

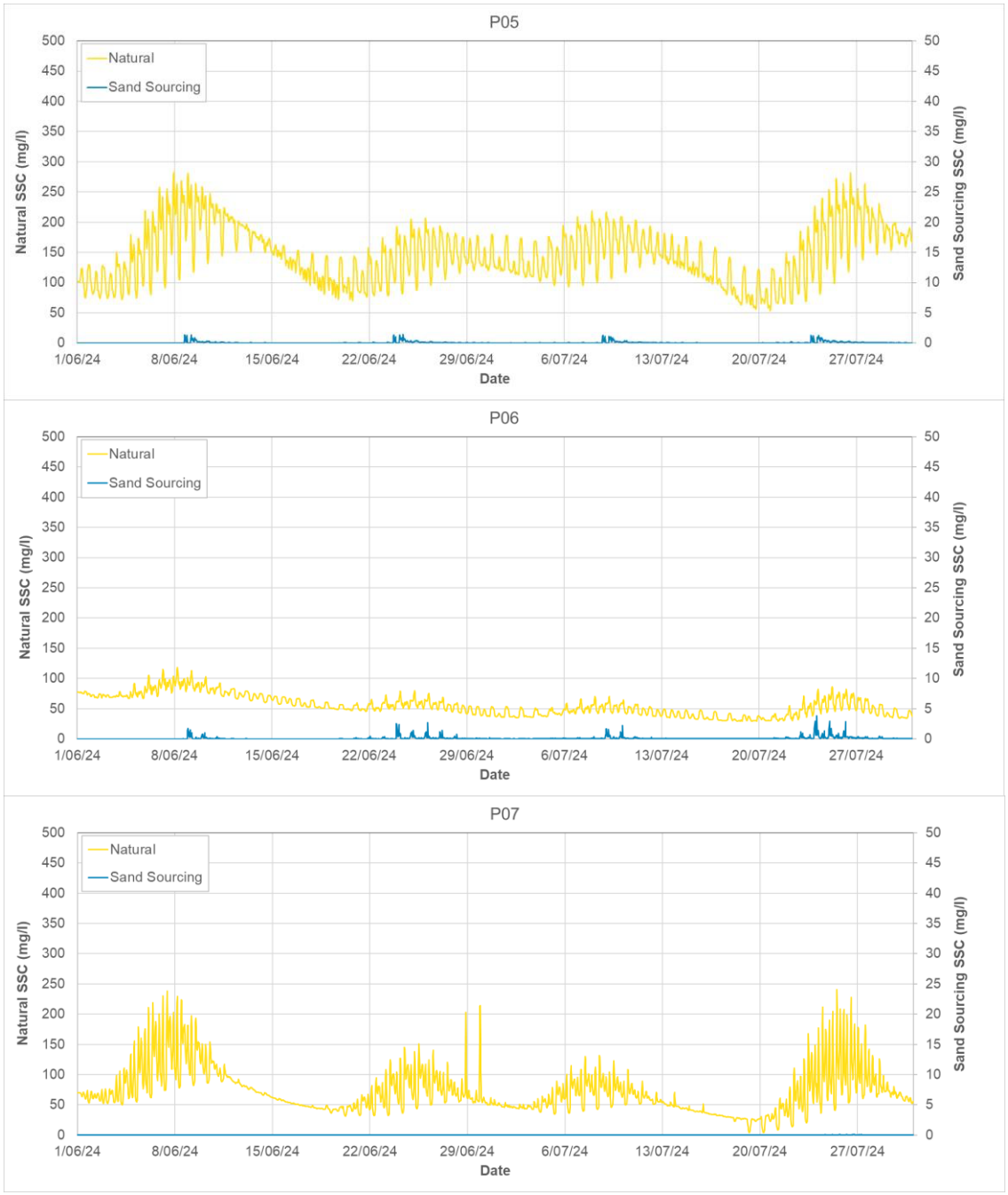


Figure 250. Timeseries showing the modelled natural SSC and sand sourcing SSC at P05 to P07 during the dry season for Scenario 2 with releases during spring tides. *Note: the sand sourcing SSC is plotted using a second y-axis with a lower SSC magnitude.*

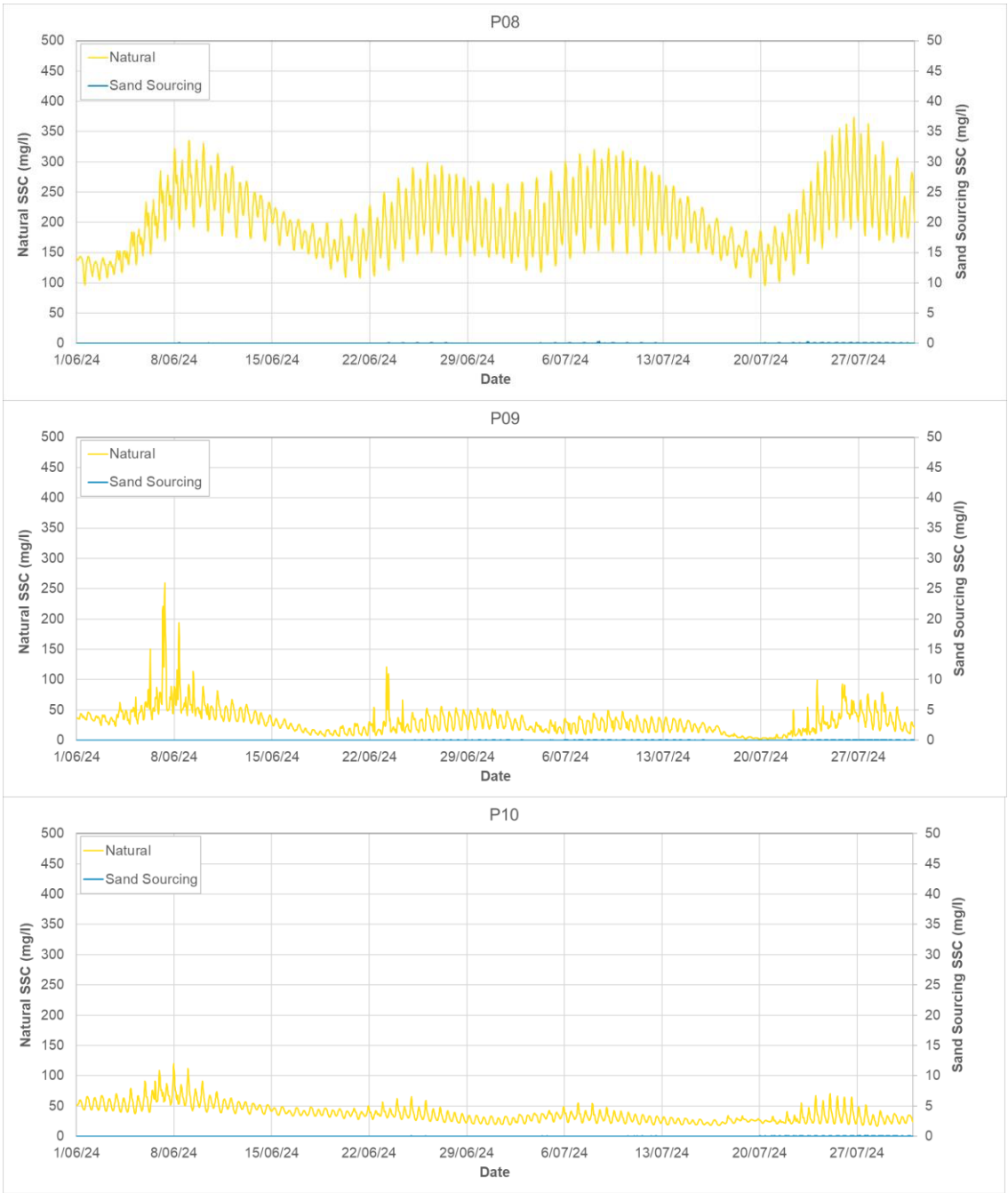


Figure 251. Timeseries showing the modelled natural SSC and sand sourcing SSC at P08 to P10 during the dry season for Scenario 2 with releases during spring tides. *Note: the sand sourcing SSC is plotted using a second y-axis with a lower SSC magnitude.*

Table 34. Statistics of the modelled natural and sand sourcing SSC during the wet season for sand sourcing scenario 1 with neap releases.

Statistic	P01 (in POA)	P02 (in POA)	P03 (in POA)	P04	P05	P06	P07	P08	P09	P10
Natural SSC (mg/L)										
99th %ile	358	200	446	336	418	128	189	686	387	119
95th %ile	255	151	350	213	363	98	127	497	215	83
90th %ile	198	127	301	175	334	86	102	429	127	62
80th %ile	142	94	222	141	287	72	81	346	79	47
50th %ile	94	66	144	76	185	50	63	216	52	28
20th %ile	66	50	92	55	125	34	47	136	40	14
10th %ile	55	44	68	47	93	29	40	106	35	10
Sand Sourcing SSC, Neap Releases (mg/L)										
99th %ile	1.9	1.3	1.0	0.1	0.0	0.5	0.1	0.1	0.0	0.1
95th %ile	0.7	0.6	0.2	0.0	0.0	0.2	0.0	0.1	0.0	0.0
90th %ile	0.4	0.4	0.1	0.0	0.0	0.1	0.0	0.0	0.0	0.0
80th %ile	0.2	0.2	0.1	0.0	0.0	0.1	0.0	0.0	0.0	0.0
50th %ile	0.1	0.1	0.0	0.0	0.0	0.0	0.0	0.0	0.0	0.0
20th %ile	0.0	0.0	0.0	0.0	0.0	0.0	0.0	0.0	0.0	0.0
10th %ile	0.0	0.0	0.0	0.0	0.0	0.0	0.0	0.0	0.0	0.0
Combined Natural + Sand Sourcing SSC, Neap Releases (mg/L)										
99th %ile	360	201	447	336	418	129	189	686	387	120
95th %ile	256	152	350	213	363	99	127	497	215	83
90th %ile	198	127	301	175	334	86	102	429	127	62
80th %ile	142	94	222	141	287	72	81	346	79	47
50th %ile	94	66	144	76	185	50	63	216	52	28
20th %ile	66	50	92	55	125	34	47	136	40	14
10th %ile	55	44	68	47	93	29	40	106	35	10

Table 35. Statistics of the modelled natural and sand sourcing SSC during the wet season for sand sourcing scenario 1 with spring releases.

Statistic	P01 (in POA)	P02 (in POA)	P03 (in POA)	P04	P05	P06	P07	P08	P09	P10
Natural SSC (mg/L)										
99th %ile	358	200	446	336	418	128	189	686	387	119
95th %ile	255	151	350	213	363	98	127	497	215	83
90th %ile	198	127	301	175	334	86	102	429	127	62
80th %ile	142	94	222	141	287	72	81	346	79	47
50th %ile	94	66	144	76	185	50	63	216	52	28
20th %ile	66	50	92	55	125	34	47	136	40	14
10th %ile	55	44	68	47	93	29	40	106	35	10
Sand Sourcing SSC, Spring Releases (mg/L)										
99th %ile	1.4	1.0	0.8	0.0	0.2	0.3	0.0	0.2	0.0	0.1
95th %ile	0.7	0.5	0.4	0.0	0.1	0.2	0.0	0.1	0.0	0.0
90th %ile	0.4	0.3	0.2	0.0	0.0	0.1	0.0	0.1	0.0	0.0
80th %ile	0.1	0.2	0.1	0.0	0.0	0.1	0.0	0.0	0.0	0.0
50th %ile	0.0	0.0	0.0	0.0	0.0	0.0	0.0	0.0	0.0	0.0
20th %ile	0.0	0.0	0.0	0.0	0.0	0.0	0.0	0.0	0.0	0.0
10th %ile	0.0	0.0	0.0	0.0	0.0	0.0	0.0	0.0	0.0	0.0
Combined Natural + Sand Sourcing SSC, Spring Releases (mg/L)										
99th %ile	360	201	447	336	418	129	189	686	387	120
95th %ile	256	152	350	213	363	99	127	497	215	83
90th %ile	198	127	302	175	334	86	102	429	127	62
80th %ile	142	94	222	141	287	72	81	346	79	47
50th %ile	94	66	144	76	185	50	63	216	52	28
20th %ile	66	50	92	55	125	34	47	136	40	14
10th %ile	55	44	68	47	93	29	40	106	35	10

Table 36. Statistics of the modelled natural and sand sourcing SSC during the wet season for sand sourcing scenario 2 with neap releases.

Statistic	P01 (in POA)	P02 (in POA)	P03 (in POA)	P04	P05	P06	P07	P08	P09	P10
Natural SSC (mg/L)										
99th %ile	358	200	446	336	418	128	189	686	387	119
95th %ile	255	151	350	213	363	98	127	497	215	83
90th %ile	198	127	301	175	334	86	102	429	127	62
80th %ile	142	94	222	141	287	72	81	346	79	47
50th %ile	94	66	144	76	185	50	63	216	52	28
20th %ile	66	50	92	55	125	34	47	136	40	14
10th %ile	55	44	68	47	93	29	40	106	35	10
Sand Sourcing SSC, Neap Releases (mg/L)										
99th %ile	0.9	0.4	0.7	0.2	0.2	1.7	0.1	0.0	0.0	0.1
95th %ile	0.5	0.3	0.3	0.1	0.1	0.5	0.1	0.0	0.0	0.1
90th %ile	0.3	0.2	0.2	0.1	0.0	0.3	0.0	0.0	0.0	0.0
80th %ile	0.2	0.1	0.1	0.0	0.0	0.2	0.0	0.0	0.0	0.0
50th %ile	0.1	0.0	0.0	0.0	0.0	0.0	0.0	0.0	0.0	0.0
20th %ile	0.0	0.0	0.0	0.0	0.0	0.0	0.0	0.0	0.0	0.0
10th %ile	0.0	0.0	0.0	0.0	0.0	0.0	0.0	0.0	0.0	0.0
Combined Natural + Sand Sourcing SSC, Neap Releases (mg/L)										
99th %ile	359	200	447	336	418	130	189	686	387	120
95th %ile	255	151	350	213	363	99	127	497	215	83
90th %ile	198	127	302	175	334	86	102	429	127	62
80th %ile	142	94	222	141	287	72	81	346	79	47
50th %ile	94	66	144	76	185	50	63	216	52	28
20th %ile	66	50	92	55	125	34	47	136	40	14
10th %ile	55	44	68	47	93	29	40	106	35	10

Table 37. Statistics of the modelled natural and sand sourcing SSC during the wet season for sand sourcing scenario 2 with spring releases.

Statistic	P01 (in POA)	P02 (in POA)	P03 (in POA)	P04	P05	P06	P07	P08	P09	P10
Natural SSC (mg/L)										
99th %ile	358	200	446	336	418	128	189	686	387	119
95th %ile	255	151	350	213	363	98	127	497	215	83
90th %ile	198	127	301	175	334	86	102	429	127	62
80th %ile	142	94	222	141	287	72	81	346	79	47
50th %ile	94	66	144	76	185	50	63	216	52	28
20th %ile	66	50	92	55	125	34	47	136	40	14
10th %ile	55	44	68	47	93	29	40	106	35	10
Sand Sourcing SSC, Spring Releases (mg/L)										
99th %ile	1.0	0.4	1.5	0.1	0.8	1.1	0.1	0.1	0.0	0.1
95th %ile	0.6	0.3	0.6	0.1	0.4	0.3	0.0	0.0	0.0	0.1
90th %ile	0.4	0.2	0.3	0.0	0.2	0.2	0.0	0.0	0.0	0.0
80th %ile	0.1	0.1	0.1	0.0	0.0	0.1	0.0	0.0	0.0	0.0
50th %ile	0.0	0.0	0.0	0.0	0.0	0.0	0.0	0.0	0.0	0.0
20th %ile	0.0	0.0	0.0	0.0	0.0	0.0	0.0	0.0	0.0	0.0
10th %ile	0.0	0.0	0.0	0.0	0.0	0.0	0.0	0.0	0.0	0.0
Combined Natural + Sand Sourcing SSC, Spring Releases (mg/L)										
99th %ile	359	200	447	336	419	129	189	686	387	120
95th %ile	256	151	350	213	363	99	127	497	215	83
90th %ile	198	127	302	175	334	86	102	429	127	62
80th %ile	142	94	222	141	287	72	81	346	79	47
50th %ile	94	66	144	76	185	50	63	216	52	28
20th %ile	66	50	92	55	125	34	47	136	40	14
10th %ile	55	44	68	47	93	29	40	106	35	10

Table 38. Statistics of the modelled natural and sand sourcing SSC during the dry season for sand sourcing scenario 1 with neap releases.

Statistic	P01 (in POA)	P02 (in POA)	P03 (in POA)	P04	P05	P06	P07	P08	P09	P10
Natural SSC (mg/L)										
99th %ile	193	134	255	246	257	99	199	332	104	85
95th %ile	149	107	216	172	227	87	148	294	64	65
90th %ile	122	97	192	138	208	78	118	275	53	58
80th %ile	98	87	166	106	186	71	93	250	44	48
50th %ile	75	72	104	72	142	52	63	197	27	34
20th %ile	60	55	78	50	105	39	45	155	15	25
10th %ile	55	48	70	42	86	35	35	141	10	22
Sand Sourcing SSC, Neap Releases (mg/L)										
99th %ile	2.0	1.1	1.1	0.1	0.1	0.5	0.0	0.2	0.0	0.1
95th %ile	0.9	0.5	0.4	0.0	0.1	0.2	0.0	0.1	0.0	0.0
90th %ile	0.4	0.3	0.2	0.0	0.0	0.1	0.0	0.1	0.0	0.0
80th %ile	0.2	0.2	0.1	0.0	0.0	0.1	0.0	0.0	0.0	0.0
50th %ile	0.1	0.1	0.0	0.0	0.0	0.0	0.0	0.0	0.0	0.0
20th %ile	0.0	0.0	0.0	0.0	0.0	0.0	0.0	0.0	0.0	0.0
10th %ile	0.0	0.0	0.0	0.0	0.0	0.0	0.0	0.0	0.0	0.0
Combined Natural + Sand Sourcing SSC, Neap Releases (mg/L)										
99th %ile	195	135	257	246	257	100	199	332	104	85
95th %ile	150	108	217	172	227	87	148	294	64	65
90th %ile	122	97	192	138	208	78	118	276	53	58
80th %ile	98	88	166	106	186	71	93	251	44	48
50th %ile	75	72	104	72	142	52	63	197	27	34
20th %ile	60	55	78	50	105	39	45	155	15	25
10th %ile	55	48	70	42	86	35	35	141	10	22

Table 39. Statistics of the modelled natural and sand sourcing SSC during the dry season for sand sourcing scenario 1 with spring releases.

Statistic	P01 (in POA)	P02 (in POA)	P03 (in POA)	P04	P05	P06	P07	P08	P09	P10
Natural SSC (mg/L)										
99th %ile	193	134	255	246	257	99	199	332	104	85
95th %ile	149	107	216	172	227	87	148	294	64	65
90th %ile	122	97	192	138	208	78	118	275	53	58
80th %ile	98	87	166	106	186	71	93	250	44	48
50th %ile	75	72	104	72	142	52	63	197	27	34
20th %ile	60	55	78	50	105	39	45	155	15	25
10th %ile	55	48	70	42	86	35	35	141	10	22
Sand Sourcing SSC, Spring Releases (mg/L)										
99th %ile	0.6	0.3	0.4	0.0	0.0	0.2	0.0	0.1	0.0	0.0
95th %ile	0.3	0.2	0.2	0.0	0.0	0.1	0.0	0.0	0.0	0.0
90th %ile	0.1	0.1	0.1	0.0	0.0	0.0	0.0	0.0	0.0	0.0
80th %ile	0.1	0.0	0.0	0.0	0.0	0.0	0.0	0.0	0.0	0.0
50th %ile	0.0	0.0	0.0	0.0	0.0	0.0	0.0	0.0	0.0	0.0
20th %ile	0.0	0.0	0.0	0.0	0.0	0.0	0.0	0.0	0.0	0.0
10th %ile	0.0	0.0	0.0	0.0	0.0	0.0	0.0	0.0	0.0	0.0
Combined Natural + Sand Sourcing SSC, Spring Releases (mg/L)										
99th %ile	193	135	256	246	257	100	199	332	104	85
95th %ile	150	107	216	172	227	87	148	294	64	65
90th %ile	122	97	192	138	208	78	118	275	53	58
80th %ile	98	87	166	106	186	71	93	250	44	48
50th %ile	75	72	104	72	142	52	63	197	27	34
20th %ile	60	55	78	50	105	39	45	155	15	25
10th %ile	55	48	70	42	86	35	35	141	10	22

Table 40. Statistics of the modelled natural and sand sourcing SSC during the dry season for sand sourcing scenario 2 with neap releases.

Statistic	P01 (in POA)	P02 (in POA)	P03 (in POA)	P04	P05	P06	P07	P08	P09	P10
Natural SSC (mg/L)										
99th %ile	193	134	255	246	257	99	199	332	104	85
95th %ile	149	107	216	172	227	87	148	294	64	65
90th %ile	122	97	192	138	208	78	118	275	53	58
80th %ile	98	87	166	106	186	71	93	250	44	48
50th %ile	75	72	104	72	142	52	63	197	27	34
20th %ile	60	55	78	50	105	39	45	155	15	25
10th %ile	55	48	70	42	86	35	35	141	10	22
Sand Sourcing SSC, Neap Releases (mg/L)										
99th %ile	1.1	0.3	1.2	0.1	0.3	1.1	0.1	0.1	0.0	0.1
95th %ile	0.6	0.2	0.6	0.0	0.2	0.4	0.0	0.1	0.0	0.0
90th %ile	0.4	0.1	0.4	0.0	0.1	0.2	0.0	0.0	0.0	0.0
80th %ile	0.2	0.1	0.2	0.0	0.0	0.1	0.0	0.0	0.0	0.0
50th %ile	0.1	0.0	0.0	0.0	0.0	0.0	0.0	0.0	0.0	0.0
20th %ile	0.0	0.0	0.0	0.0	0.0	0.0	0.0	0.0	0.0	0.0
10th %ile	0.0	0.0	0.0	0.0	0.0	0.0	0.0	0.0	0.0	0.0
Combined Natural + Sand Sourcing SSC, Neap Releases (mg/L)										
99th %ile	194	135	257	246	257	100	199	332	104	85
95th %ile	150	108	217	172	227	87	148	294	64	65
90th %ile	122	97	192	138	208	78	118	275	53	58
80th %ile	98	87	166	106	186	71	93	250	44	48
50th %ile	75	72	104	72	142	52	63	197	27	34
20th %ile	60	55	78	50	105	39	45	155	15	25
10th %ile	55	48	70	42	86	35	35	141	10	22

Table 41. Statistics of the modelled natural and sand sourcing SSC during the dry season for sand sourcing scenario 2 with spring releases.

Statistic	P01 (in POA)	P02 (in POA)	P03 (in POA)	P04	P05	P06	P07	P08	P09	P10
Natural SSC (mg/L)										
99th %ile	193	134	255	246	257	99	199	332	104	85
95th %ile	149	107	216	172	227	87	148	294	64	65
90th %ile	122	97	192	138	208	78	118	275	53	58
80th %ile	98	87	166	106	186	71	93	250	44	48
50th %ile	75	72	104	72	142	52	63	197	27	34
20th %ile	60	55	78	50	105	39	45	155	15	25
10th %ile	55	48	70	42	86	35	35	141	10	22
Sand Sourcing SSC, Spring Releases (mg/L)										
99th %ile	0.8	0.4	1.5	0.1	0.9	1.3	0.1	0.1	0.0	0.1
95th %ile	0.4	0.2	0.5	0.0	0.3	0.4	0.0	0.0	0.0	0.0
90th %ile	0.3	0.1	0.3	0.0	0.2	0.2	0.0	0.0	0.0	0.0
80th %ile	0.2	0.1	0.1	0.0	0.1	0.1	0.0	0.0	0.0	0.0
50th %ile	0.1	0.0	0.0	0.0	0.0	0.0	0.0	0.0	0.0	0.0
20th %ile	0.0	0.0	0.0	0.0	0.0	0.0	0.0	0.0	0.0	0.0
10th %ile	0.0	0.0	0.0	0.0	0.0	0.0	0.0	0.0	0.0	0.0
Combined Natural + Sand Sourcing SSC, Spring Releases (mg/L)										
99th %ile	194	135	257	246	258	101	199	332	104	85
95th %ile	150	108	217	172	227	87	148	294	64	65
90th %ile	122	97	192	138	208	78	118	275	53	58
80th %ile	98	87	166	106	186	71	93	250	44	48
50th %ile	75	72	104	72	142	52	63	197	27	34
20th %ile	60	55	78	50	105	39	45	155	15	25
10th %ile	55	48	70	42	86	35	35	141	10	22

Table 42. Statistics of the modelled natural and sand sourcing SSC during the transitional season for sand sourcing scenario 1 with neap releases.

Statistic	P01 (in POA)	P02 (in POA)	P03 (in POA)	P04	P05	P06	P07	P08	P09	P10
Natural SSC (mg/L)										
99th %ile	316	194	398	557	425	153	428	513	277	120
95th %ile	241	153	311	359	364	123	273	393	145	79
90th %ile	202	136	277	284	323	104	215	356	106	64
80th %ile	166	116	231	200	282	85	154	309	81	49
50th %ile	121	84	171	98	218	60	83	229	45	29
20th %ile	83	60	131	59	174	45	52	173	31	17
10th %ile	72	51	113	50	149	37	46	146	27	12
Sand Sourcing SSC, Neap Releases (mg/L)										
99th %ile	1.9	1.3	0.9	0.1	0.1	0.5	0.0	0.1	0.0	0.1
95th %ile	0.7	0.5	0.2	0.0	0.0	0.2	0.0	0.1	0.0	0.1
90th %ile	0.4	0.3	0.1	0.0	0.0	0.1	0.0	0.0	0.0	0.0
80th %ile	0.2	0.2	0.0	0.0	0.0	0.1	0.0	0.0	0.0	0.0
50th %ile	0.0	0.1	0.0	0.0	0.0	0.0	0.0	0.0	0.0	0.0
20th %ile	0.0	0.0	0.0	0.0	0.0	0.0	0.0	0.0	0.0	0.0
10th %ile	0.0	0.0	0.0	0.0	0.0	0.0	0.0	0.0	0.0	0.0
Combined Natural + Sand Sourcing SSC, Neap Releases (mg/L)										
99th %ile	318	196	399	557	425	153	428	513	277	120
95th %ile	241	154	311	359	364	123	273	393	145	79
90th %ile	202	137	277	285	323	104	215	356	106	64
80th %ile	166	116	231	200	282	85	154	309	81	49
50th %ile	121	84	171	98	218	60	83	229	45	29
20th %ile	83	60	131	59	174	45	52	173	31	17
10th %ile	72	51	113	50	149	37	46	146	27	12

Table 43. Statistics of the modelled natural and sand sourcing SSC during the transitional season for sand sourcing scenario 1 with spring releases.

Statistic	P01 (in POA)	P02 (in POA)	P03 (in POA)	P04	P05	P06	P07	P08	P09	P10
Natural SSC (mg/L)										
99th %ile	316	194	398	557	425	153	428	513	277	120
95th %ile	241	153	311	359	364	123	273	393	145	79
90th %ile	202	136	277	284	323	104	215	356	106	64
80th %ile	166	116	231	200	282	85	154	309	81	49
50th %ile	121	84	171	98	218	60	83	229	45	29
20th %ile	83	60	131	59	174	45	52	173	31	17
10th %ile	72	51	113	50	149	37	46	146	27	12
Sand Sourcing SSC, Spring Releases (mg/L)										
99th %ile	1.5	0.9	0.7	0.1	0.1	0.4	0.1	0.2	0.0	0.1
95th %ile	0.5	0.4	0.3	0.1	0.1	0.2	0.0	0.1	0.0	0.1
90th %ile	0.3	0.3	0.2	0.0	0.1	0.1	0.0	0.1	0.0	0.1
80th %ile	0.1	0.2	0.1	0.0	0.0	0.1	0.0	0.1	0.0	0.0
50th %ile	0.1	0.1	0.0	0.0	0.0	0.0	0.0	0.0	0.0	0.0
20th %ile	0.0	0.0	0.0	0.0	0.0	0.0	0.0	0.0	0.0	0.0
10th %ile	0.0	0.0	0.0	0.0	0.0	0.0	0.0	0.0	0.0	0.0
Combined Natural + Sand Sourcing SSC, Spring Releases (mg/L)										
99th %ile	317	195	399	557	425	153	428	513	277	120
95th %ile	241	153	311	359	364	123	273	393	145	79
90th %ile	202	137	277	285	323	104	215	356	106	64
80th %ile	166	116	231	200	283	85	154	309	81	49
50th %ile	121	84	171	98	218	60	83	229	45	29
20th %ile	83	60	131	59	174	45	52	173	31	17
10th %ile	72	51	113	50	149	37	46	146	27	12

Table 44. Statistics of the modelled natural and sand sourcing SSC during the transitional season for sand sourcing scenario 2 with neap releases.

Statistic	P01 (in POA)	P02 (in POA)	P03 (in POA)	P04	P05	P06	P07	P08	P09	P10
Natural SSC (mg/L)										
99th %ile	316	194	398	557	425	153	428	513	277	120
95th %ile	241	153	311	359	364	123	273	393	145	79
90th %ile	202	136	277	284	323	104	215	356	106	64
80th %ile	166	116	231	200	282	85	154	309	81	49
50th %ile	121	84	171	98	218	60	83	229	45	29
20th %ile	83	60	131	59	174	45	52	173	31	17
10th %ile	72	51	113	50	149	37	46	146	27	12
Sand Sourcing SSC, Neap Releases (mg/L)										
99th %ile	0.8	0.4	0.7	0.1	0.2	1.8	0.1	0.1	0.0	0.1
95th %ile	0.5	0.3	0.4	0.1	0.1	0.5	0.0	0.0	0.0	0.1
90th %ile	0.3	0.2	0.2	0.0	0.0	0.3	0.0	0.0	0.0	0.0
80th %ile	0.2	0.1	0.1	0.0	0.0	0.2	0.0	0.0	0.0	0.0
50th %ile	0.1	0.0	0.0	0.0	0.0	0.0	0.0	0.0	0.0	0.0
20th %ile	0.0	0.0	0.0	0.0	0.0	0.0	0.0	0.0	0.0	0.0
10th %ile	0.0	0.0	0.0	0.0	0.0	0.0	0.0	0.0	0.0	0.0
Combined Natural + Sand Sourcing SSC, Neap Releases (mg/L)										
99th %ile	317	195	399	557	425	155	428	513	277	120
95th %ile	241	153	312	359	364	124	273	393	145	79
90th %ile	202	137	277	285	323	104	215	356	106	64
80th %ile	166	116	231	200	282	85	154	309	81	49
50th %ile	121	84	171	98	218	60	83	229	45	29
20th %ile	83	60	131	59	174	45	52	173	31	17
10th %ile	72	51	113	50	149	37	46	146	27	12

Table 45. Statistics of the modelled natural and sand sourcing SSC during the transitional season for sand sourcing scenario 2 with spring releases.

Statistic	P01 (in POA)	P02 (in POA)	P03 (in POA)	P04	P05	P06	P07	P08	P09	P10
Natural SSC (mg/L)										
99th %ile	316	194	398	557	425	153	428	513	277	120
95th %ile	241	153	311	359	364	123	273	393	145	79
90th %ile	202	136	277	284	323	104	215	356	106	64
80th %ile	166	116	231	200	282	85	154	309	81	49
50th %ile	121	84	171	98	218	60	83	229	45	29
20th %ile	83	60	131	59	174	45	52	173	31	17
10th %ile	72	51	113	50	149	37	46	146	27	12
Sand Sourcing SSC, Spring Releases (mg/L)										
99th %ile	0.9	0.3	1.4	0.1	0.7	1.2	0.1	0.1	0.0	0.1
95th %ile	0.4	0.2	0.4	0.1	0.3	0.4	0.0	0.1	0.0	0.1
90th %ile	0.2	0.2	0.3	0.1	0.2	0.3	0.0	0.1	0.0	0.0
80th %ile	0.2	0.1	0.1	0.0	0.1	0.1	0.0	0.0	0.0	0.0
50th %ile	0.1	0.1	0.1	0.0	0.0	0.0	0.0	0.0	0.0	0.0
20th %ile	0.0	0.0	0.0	0.0	0.0	0.0	0.0	0.0	0.0	0.0
10th %ile	0.0	0.0	0.0	0.0	0.0	0.0	0.0	0.0	0.0	0.0
Combined Natural + Sand Sourcing SSC, Spring Releases (mg/L)										
99th %ile	317	195	399	557	426	154	428	513	277	120
95th %ile	241	153	312	359	365	124	273	393	145	79
90th %ile	202	137	277	285	323	104	215	356	106	64
80th %ile	166	116	231	200	283	85	154	309	81	49
50th %ile	121	84	171	98	218	60	83	229	45	29
20th %ile	83	60	131	59	174	45	52	173	31	17
10th %ile	72	51	113	50	149	37	46	146	27	12

6.1.2. Modelled Sedimentation from SPV Plumes

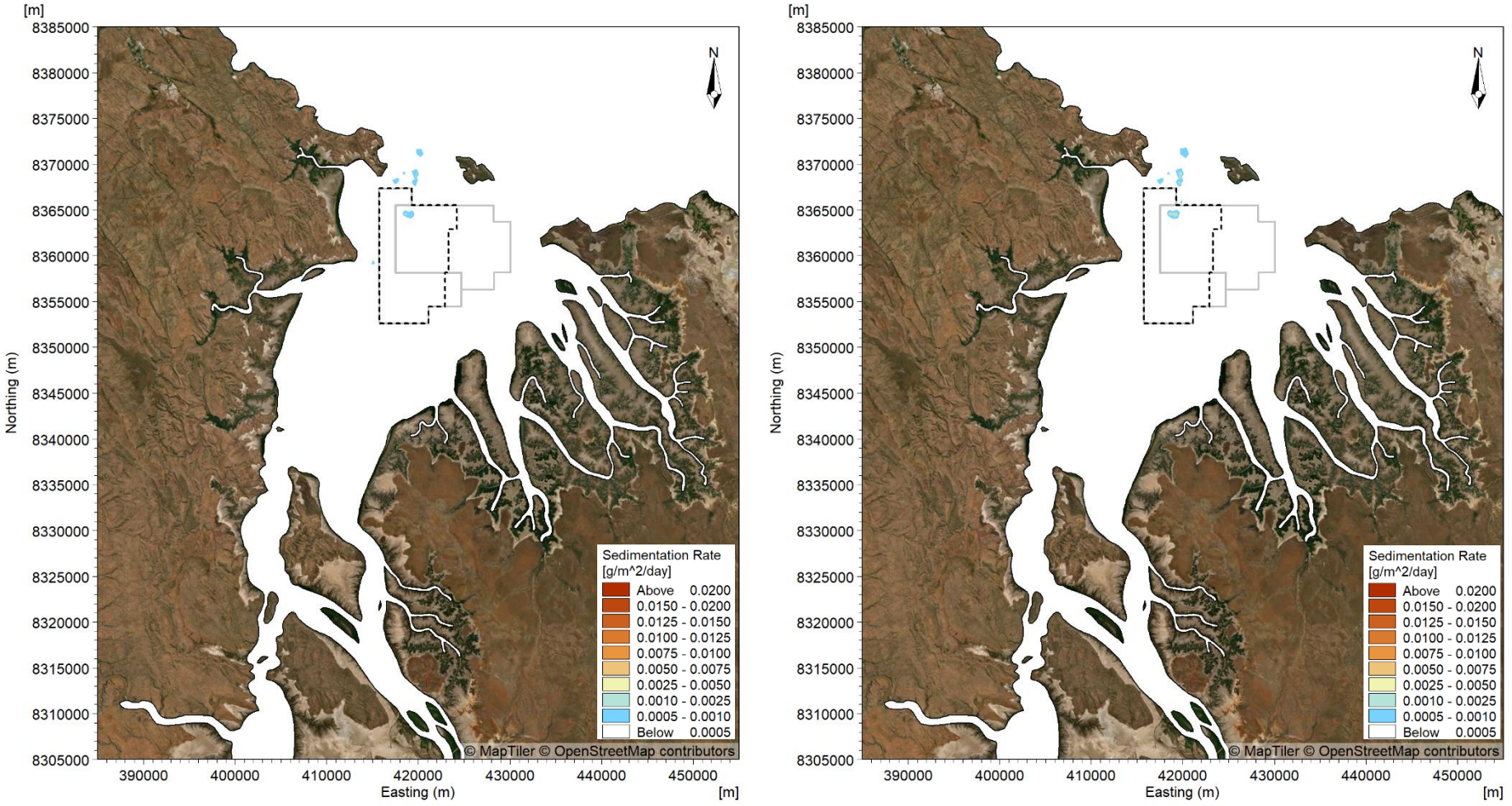
Spatial maps of the modelled sedimentation resulting from 2 months (60/61 days) of the sand sourcing operation are shown for the two scenarios in Figure 252 to Figure 257. The plots show the following:

- The sedimentation rate was modelled to be less than 0.0005 g/cm^2/day throughout the majority of CG for both sand sourcing scenarios in all seasons and when SPV releases are during spring or neap tides.

- Similar localised areas with modelled sedimentation rates of between 0.0005 and 0.0025 g/cm^2/day (less than 2.5 mm over the 60/61 days) occurred for all seasons and for SPV releases during both neap and spring tides. The areas are located within the POA at the northern end and directly to the north of the POA. The sediment modelled to be deposited in these areas was predominantly very fine sand as the silt and clay particles were modelled to be transported away from areas with such high current speeds and deposited at rates of less than 0.0005 g/cm^2/day.

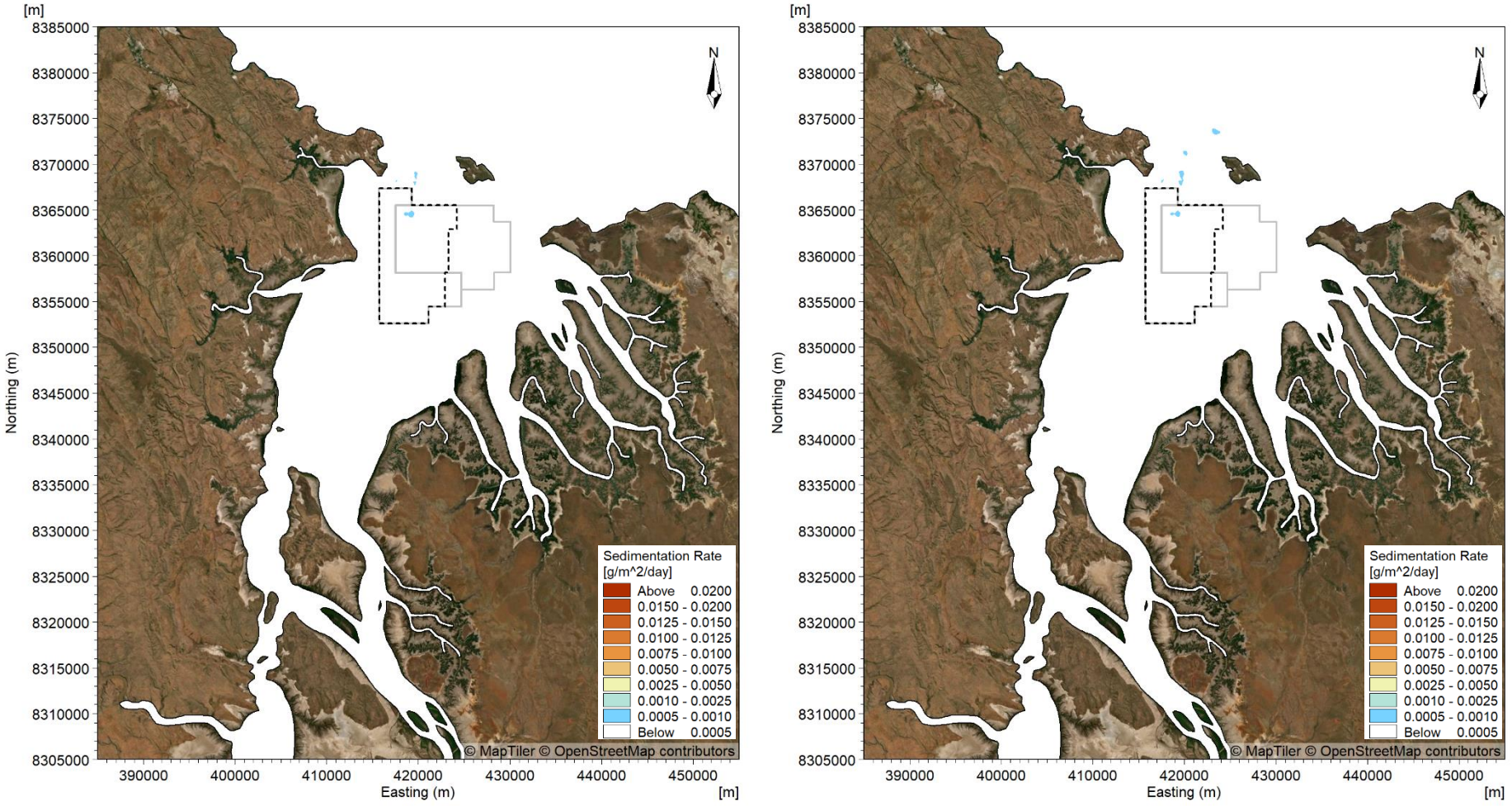
- Sedimentation rates were modelled to be slightly higher for sand sourcing Scenario 1 (up to 0.0025 g/cm^2/day) compared with sand sourcing Scenario 2 (up to 0.001 g/cm^2/day). This was due to the sand sourcing for Scenario 1 being focused in one area of the POA, while the sand sourcing for Scenario 2 was spread throughout the POA.

- The areas with modelled sedimentation rates of more than 0.0005 g/cm^2/day, due to the deposition of very fine sand suspended by the sand sourcing, were typically where the bathymetric survey undertaken by BKA in February and March 2024 showed that sand waves are present, meaning that the bed is already made up of sand in these areas (PCS 2024a). The survey also showed that extensive natural migration of these sand waves occurs (up 10 m over 27 days was measured), meaning that the natural changes in the bedforms will be much larger than the very minor sedimentation rates resulting from the SPV plumes.



Spring Neap

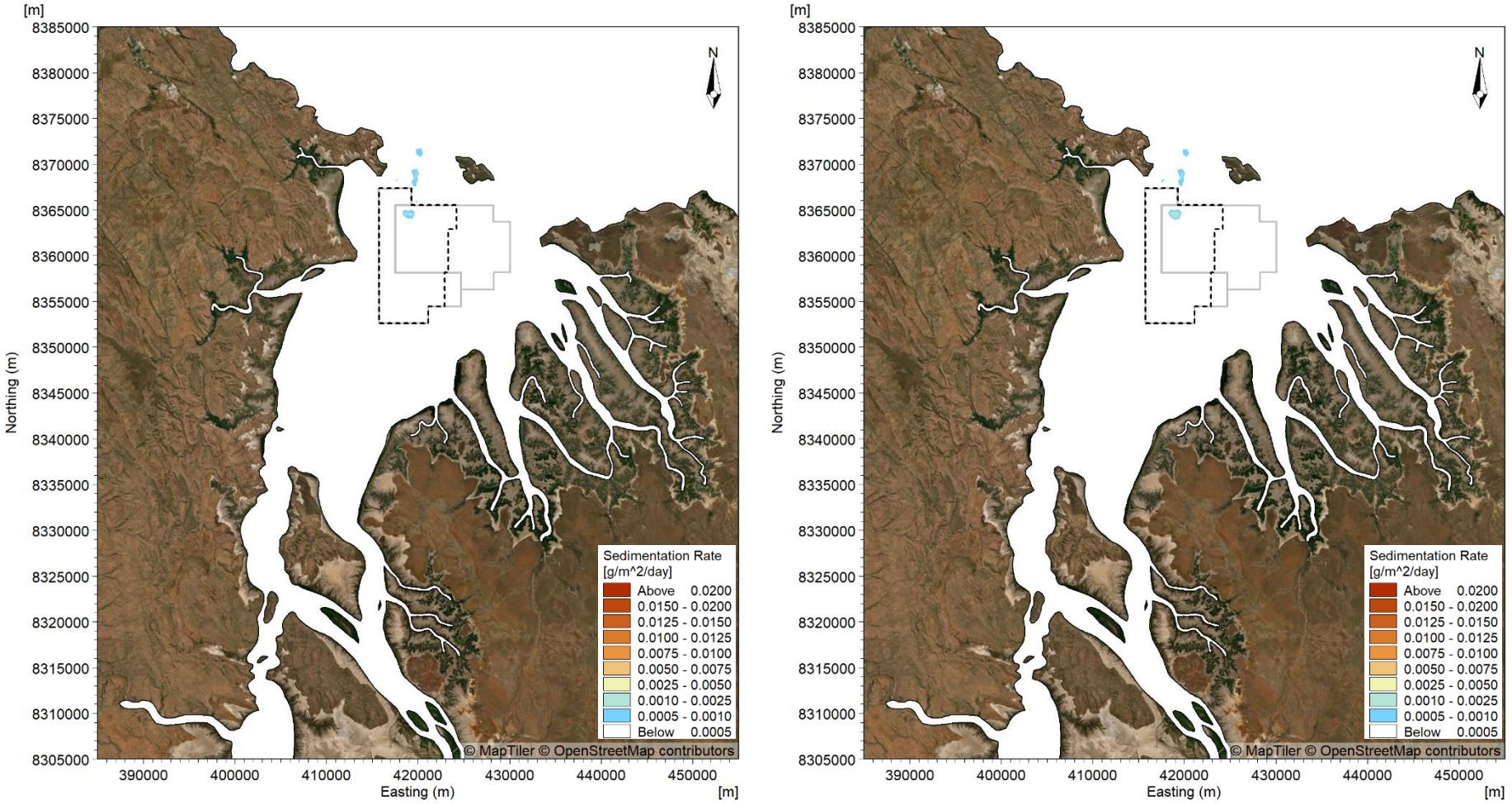
Figure 252. Modelled sedimentation resulting from 2 months (60 days) of sand sourcing in the wet season for Scenario 1 when sand sourcing activity coincided with spring (left) and neap (right) tides.



Spring

Neap

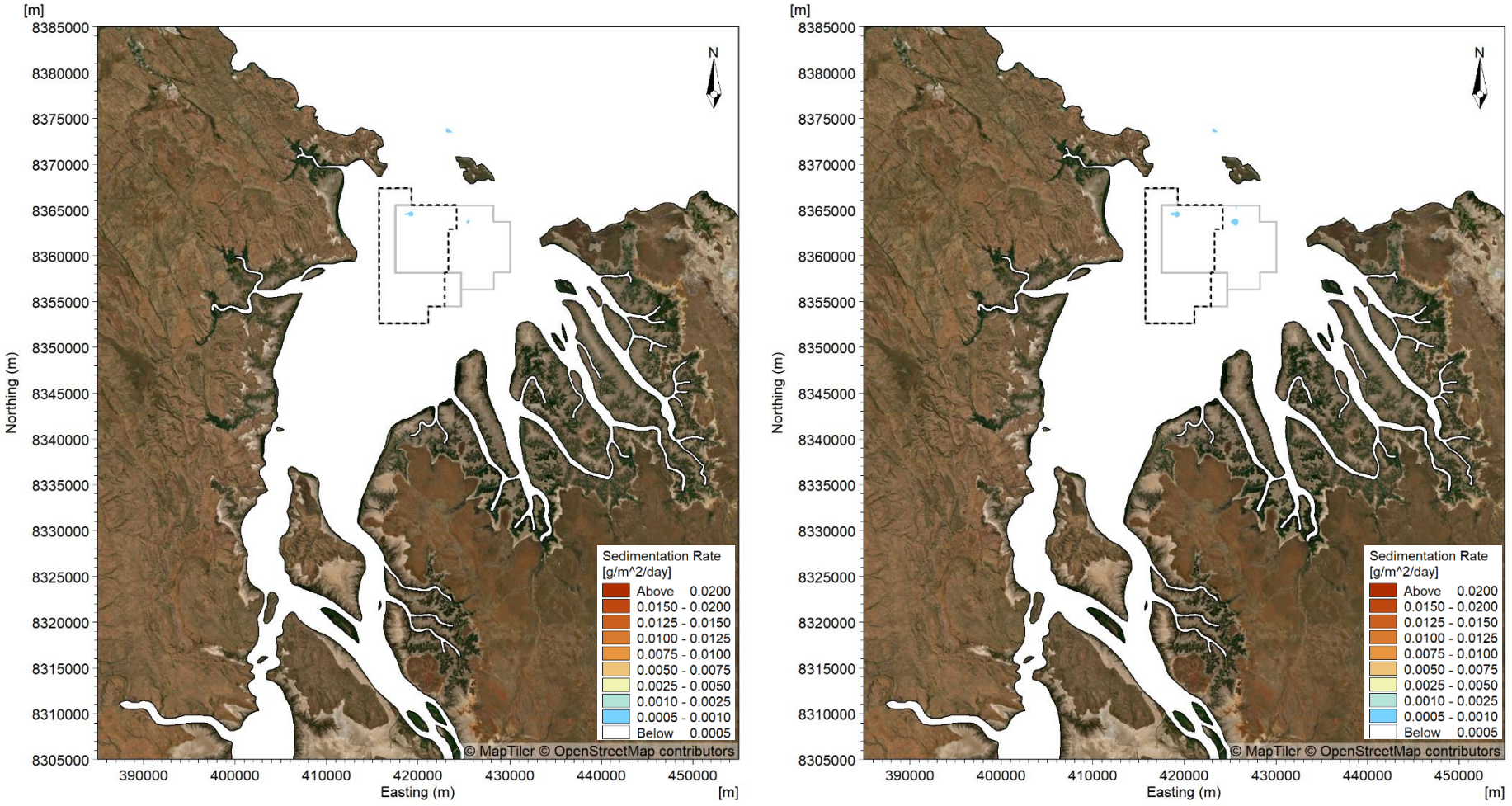
Figure 253. Modelled sedimentation resulting from 2 months (60 days) of sand sourcing in the wet season for Scenario 2 when sand sourcing activity coincided with spring (left) and neap (right) tides.



Spring

Neap

Figure 254. Modelled sedimentation resulting from 2 months (61 days) of sand sourcing in the dry season for Scenario 1 when sand sourcing activity coincided with spring (left) and neap (right) tides.



Spring Neap

Figure 255. Modelled sedimentation resulting from 2 months (61 days) of sand sourcing in the dry season for Scenario 2 when sand sourcing activity coincided with spring (left) and neap (right) tides.

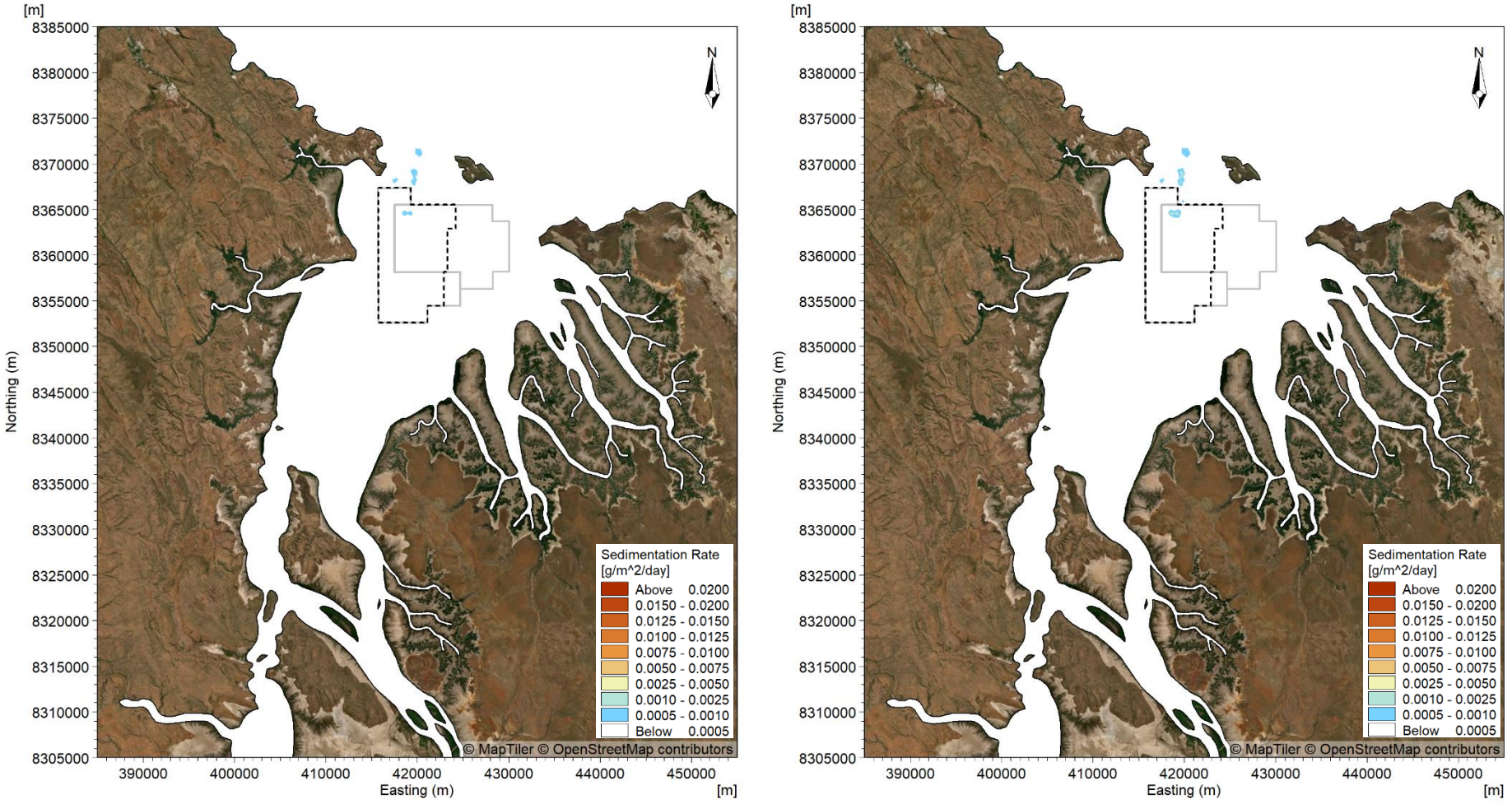
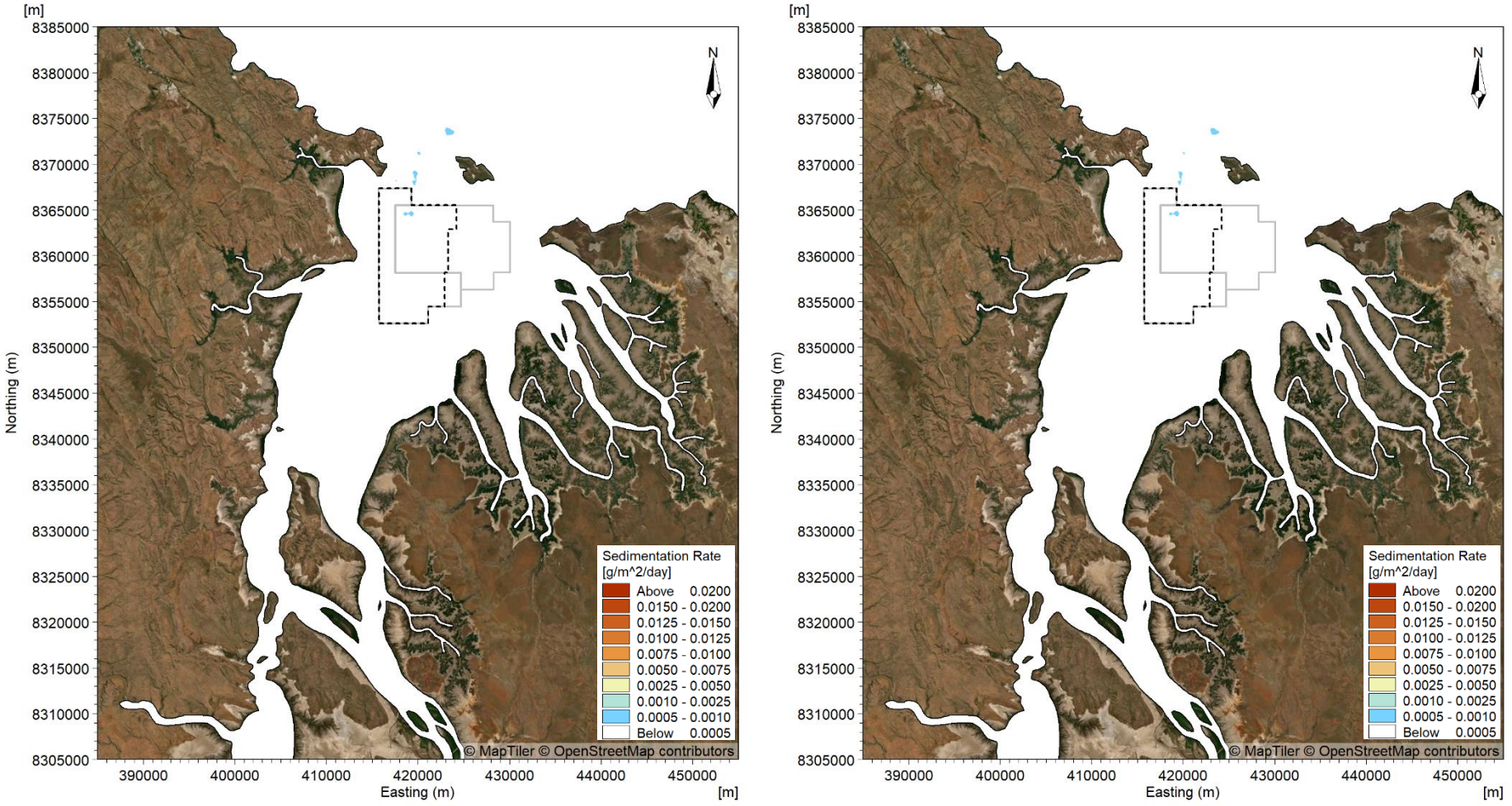


Figure 256. Modelled sedimentation resulting from 2 months (61 days) of sand sourcing in the transitional season for Scenario 1 when sand sourcing activity coincided with spring (left) and neap (right) tides.



Spring

Neap

Figure 257. Modelled sedimentation resulting from 2 months (61 days) of sand sourcing in the transitional season for Scenario 2 when sand sourcing activity coincided with spring (left) and neap (right) tides.

6.2. Summary Findings & Implications for the Proposal

The numerical modelling assessed the potential changes to SSC and seabed sedimentation from sediment plumes generated by the SPV during sand sourcing operations.

Overall, the modelling assessed that natural 50th percentile SSC in CG ranged from 50 mg/L to more than 3,000 mg/L, which are extremely high concentrations, and the increases in SSC due to the sand sourcing would be less than 1.5% of the natural SSC and that the increases in SSC would be for short durations in restricted areas.

Overall, the modelling assessed that seabed sedimentation rates from the SPV plumes would remain below 0.0005 g/cm^2/day throughout the majority of the region, with only localised areas at the northern end of the POA exceeding this, where modelled sedimentation rates of up to 0.0025 g/cm^2/day occurred over the duration of the sand sourcing operation (equivalent to less than 2.5 mm over 60 days). These modelled very minor increases in sedimentation of not more than 2.5 mm over 60 days should be considered in the context that bathymetric surveys conducted in and around the POA in February/March 2024 measured sand waves with heights up to 8 m and horizontal migration of up to 10 m in just 27 days (PCS 2024a), showing that the seabed sand waves in this area are naturally highly dynamic under the influence of tidal currents.

The extremely small magnitude of the modelled changes in SSC and sedimentation from the SPV plumes will not cause measurable changes to the environmental resources and values of the area that are influenced by SSC and sedimentation, these being BCH. It should also be noted that there are no sensitive BCH in CG that could potentially be impacted even if SSC and sedimentation was significantly elevated by the sand-sourcing operation.

The main modelled changes to SSC and seabed sedimentation from SPV plumes are summarised as follows:

- The plume modelling simulated two different sand sourcing scenarios (repeat tracks in one area and targeted tracks over entire POA), varying release times (during neap tides or spring tides) and three different seasons (wet, dry and transitional).

- The modelling results have shown that the SSC resulting from the sand sourcing activity was consistently low for all the model simulations, with only the 99th percentile depth-averaged SSC having exceeded 1 mg/L at sites both within the POA and outside of the POA. This highlights how the sand sourcing operation is only assessed to result in short duration, localised increases in SSC, as the activity only occurs for ~30 hours every 14 days, and it does not include the placement of the sediment in CG (the loaded sand will be exported).

- Comparing the modelled sand sourcing SSC with the natural SSC has shown that the relative contribution of the sand sourcing SSC was less than 1.5% of the natural SSC. Therefore, the modelling results can be considered to demonstrate that the sand sourcing activity will only result in a very small increase in SSC which, given the naturally high SSC in the region, is not expected to result in any impacts.

- The modelling indicated that sedimentation rates for the majority of CG were less than 0.0005 g/cm^2/day over the duration of the sand sourcing operation. The only area with higher sedimentation rates outside of the POA was directly to the north of the POA where sedimentation of very fine sand of up to 0.0025 g/cm^2/day was modelled (less than 2.5 mm over 60 days). Detailed bathymetric survey undertaken by BKA in 2024 showed that sand waves are present in this area and so the very fine sand from the sand sourcing activity will mix with the existing sand present in the area. In addition, the natural bedform changes in this area are likely to be significantly higher than the sedimentation resulting from the sand sourcing. Based on this, there are not expected to be any impacts from the sedimentation of the sediment suspended by the sand sourcing activity.

7. ASSESSMENT AGAINST STUDY OBJECTIVES & EPA GUIDELINES

This section provides a summary of how this report meets each of the study objectives as detailed in Section 1 as well as the requirements of each of the relevant WA EPA guidelines as also listed in Section 1.

Details of how the project objectives have been met are detailed in Table 46, while Table 47 provides details of how the WA EPA guidelines have been met. These tables are based on the data and information included in this report and in the System Understanding, Conceptual Model and Initial Modelling report (PCS, 2024a) along with the Supplementary Technical Note (PCS, 2024b).

Table 46. Summary of how this report meets the Study Objectives (as listed in Section 1)

CG = Cambridge Gulf. HD = Hydrodynamics. SPV = Sand Production Vessel. ST = Sediment transport. SW = Spectral wave. POA = Proposed operational area.

Study Objective	Summary Findings / Conclusions	Relevant sections of this report	Supporting Data Sources (references)	Assumptions, Qualifications, Limitations & Gaps
Objective 1: Hydrodynamics and Waves:				
a) Define the existing hydrodynamic conditions in the subject areas, under the seasonal range of natural conditions, including any changes since European colonisation.	The existing hydrodynamic and wave conditions have been detailed in this report based on literature, existing data and modelling results, including during wet, dry and transitional season conditions. The results have shown that CG is a tidally dominant environment, with limited influence of waves due to its relatively sheltered nature. The main changes since European colonisation are the Ord River catchment clearing (for cattle grazing and crops), which may have resulted in an increase in river water discharge and catchment sediment to the CG, and the construction of the Lower Ord and Ord River dams in 1969 and 1971, respectively. The modelling indicates that construction of the Ord River dams has caused changes to HD and ST in CG as follows: • Regulation of river flows through the dams has reduced river discharges during wet season high discharge events and increased river discharges during dry season low discharge conditions, in East Arm. • Prior to construction of the dams, during a high river discharge event the ebb tide current speeds throughout CG may have been higher by up to 0.10 m/s, while the flood tide current speeds may have been lower by up to 0.18 m/s. These are very minor differences considering that these events only occurred occasionally and for relatively short durations. • Tidal range in CG may have changed by up to 0.55% during a high river discharge event compared to pre-European settlement conditions. While this is a very minor change, it is an order of magnitude higher than the extremely minor <0.05% change modelled for the proposed sand sourcing. • SSC in CG may have been reduced by up to 86% during a large river discharge event in the wet season and increased by 8% during the dry season, compared to pre-European settlement conditions. These are an order of magnitude higher than the extremely minor changes in SSC modelled for the proposed sand sourcing. The modelling indicates that construction of the Ord River dams has not caused changes to waves in or offshore from CG.	Sections 2.1, 2.2, 4 and Appendix A	AHO (2024) BKA (2024b) BKA (2024d) PCS (2024a) PCS (2024b) PCS (2024c) PCS (2025b) This report (PCS, 2025a) Robson *et al.* (2008) Robson *et al.* (2013) Wolanski *et al.* (2001) Wolanski *et al.* (2004)	Both the hydrodynamic (HD) and spectral wave (SW) models have been calibrated and validated at multiple sites offshore and within CG during both wet and dry season conditions, based on a large volume of available measured data. This provides confidence that the models provide a realistic representation of the existing conditions within CG. To represent the change in river discharge since European settlement the peak discharge adopted for the pre-dam scenario was based on information provided by Wolanski *et al.* (2004). Although there is some uncertainty in this discharge, it is based on hydrological modelling and so it can be considered to provide a reasonable representation of the discharge from the Ord River prior to the construction of the dams.

Study Objective	Summary Findings / Conclusions	Relevant sections of this report	Supporting Data Sources (references)	Assumptions, Qualifications, Limitations & Gaps
	As these conditions have been in place for over 50 years since the dams were built, they constitute the existing conditions in CG today. They form the baseline (existing case) for assessing potential changes to hydrodynamics from the proposed sand-sourcing, as well as assessing potential cumulative changes from the proposed sand-sourcing, in addition to those caused by the dams (as required by WA EPA guidelines).			
b) Predict potential impacts of the proposed project on the hydrodynamics of the subject areas, including during the operation (5 years), at the end of the operation (approximately 15 years) and in 100 years after 15 years of sand sourcing.	Detailed modelling of potential changes to hydrodynamics and waves after five years (23 million m^3) and fifteen years (70 million m^3) of sand sourcing from the proposed operational area (POA) and 100 years from today with 70 million m^3 of sand sourcing, are provided in this report. The modelling has shown very minor and highly localised changes to both hydrodynamics and waves for all three cases, with the majority of the changes within and immediately adjacent to the POA. Overall, the modelled potential changes to hydrodynamics and waves from the proposed sand sourcing under all scenarios are so minor that there are no mechanisms whereby they could in turn cause changes to the environmental resources and values of the CG area that are influenced by hydrodynamics and waves (primally mangrove communities around the internal coasts of CG, including the Ord River Floodplain Ramsar site, and turtle nesting beaches on the seaward coasts of CG).	Section 4.2	HD and SW models along with the data used to develop and calibrate/validate the models (see Sections 3.4 and 3.5 for further details).	Both the HD and SW models have been calibrated and validated at multiple sites offshore and within CG during both wet and dry season conditions based on a large volume of available measured data. This provides confidence that the models provide a realistic representation of the existing conditions within CG. The modelling of impacts for the during operation (5 years) and at the end of operation (15 years) scenarios assumed no natural import of sand into the POA over this time. Some sedimentation will occur over this time and so the impacts can be considered to represent the worst-case scenario. For the 100 years from today scenario, sedimentation was assumed within the POA but no other morphological changes due to sea level rise were assumed. The sedimentation in the POA was based on results from the sediment transport modelling. While there will always be uncertainty with estimating sedimentation over 100 years, the results can be considered to provide an indication as to the extent and magnitude of potential changes.
c) This should include prediction of likely 'worst-case' and 'best-case' impacts and also potential 'cumulative' impacts of the proposed project on hydrodynamics (with 'worst-case' and 'best-case' being	As outlined for b) above, changes to the hydrodynamics were shown to be similar between the different metocean conditions, as the astronomical tide was the dominant process and resulted in a consistent, very minor modelled change, meaning that it is not meaningful to determine 'best-case' and 'worst-case' changes.	Section 4.2.1	HD model along with the data used to develop and calibrate/validate the model (see Section 3.4 for further details).	HD modelling results have shown comparable changes for the different metocean conditions, meaning that it has not been possible or necessary to determine

Study Objective	Summary Findings / Conclusions	Relevant sections of this report	Supporting Data Sources (references)	Assumptions, Qualifications, Limitations & Gaps
consistent with meanings in relevant WA EPA guidance as listed in section 4 (of RFP), and 'cumulative' meaning in addition to those that may have been caused by previous developments in the area, such as the Ord River dam).	The sand sourcing scenarios have been assessed relative to existing conditions (i.e. since construction of the Ord River dam) to ensure that the changes from the sand sourcing can be understood. As outlined for a) and b) above, changes resulting from the construction of the Ord River dams are also presented, which allows assessment of the potential cumulative changes from the proposed sand-sourcing, in addition to those caused by the dams. The modelled changes from the proposed sand-sourcing are negligible and an order of magnitude less than those that are assessed to have been caused by construction of the Ord River dam, and the modelled cumulative changes in addition to the changes caused by the two dams will also be negligible.			'best-case' and 'worst-case' impacts whilst still assuming realistic scenarios.
d) Provide hydrodynamics data analysis and modelling to support the other objectives below.	Results from this objective have been used to help inform the conceptual understanding, coastal processes implications and conceptual model. In addition, the HD and SW models have been used as inputs to the sediment transport, beach processes and plume modelling which are also presented in this report.	Sections 5 and 6	AHO (2024) BKA (2024b) BKA (2024d) PCS (2024a) PCS (2024b) PCS (2024c) PCS (2025b) This report - HD and SW models along with the data used to develop and calibrate/validate the models (see Sections 3.4 and 3.5 for further details).	Both the HD and SW models have been calibrated and validated at multiple sites offshore and within CG during both wet and dry season conditions based on a large volume of available measured data. This provides confidence that the models provide a realistic representation of the existing conditions within CG.
Objective 2: Sediment transport and coastal processes:				
a) Define existing sediment transport and coastal processes in the subject areas, including natural sediment sources and pathways, sediment sizes on the seabed and in transport under the seasonal range of natural conditions, and any changes since European colonization.	The existing sediment transport and coastal processes have been detailed in this report based on literature, existing data and modelling results. It has been shown that there is significant variability in the sediment transport which occurs in the region, with the tide being the dominant process which influences sediment transport in CG. Extensive sediment sampling has been undertaken throughout CG and upstream and offshore areas, as part of the Project, this has shown that there is an abundance of sediment available within CG, with a combination of sand, silt and clay all present in the region (PCS, 2024a & 2024b; BKA, 2024b). Based on data collected the sediment transport rates are higher during the wet season. Sediment transported in suspension in CG has been shown to be predominantly silt and clay sized sediment, while sand is predominantly transported as bedload.	Sections 2, 4.1 and 5.1	Wolanski *et al.* (2004) BKA (2024b) BKA (2024d) PCS (2024a) PCS (2024b) PCS (2024c) PCS (2025b) This report - ST and Beach Processes models along with the data used to develop and calibrate the models (see Section 3.6 and 3.8 for further details).	The HD, SW and ST models have been calibrated and validated at multiple sites offshore and within CG during both wet and dry season conditions based on a large volume of available measured data. This provides confidence that the models provide a realistic representation of the existing conditions within CG. To represent the change in river discharge since European settlement the peak discharge adopted for the pre-dam scenario was based on information provided by Wolanski *et al.* (2004).

Study Objective	Summary Findings / Conclusions	Relevant sections of this report	Supporting Data Sources (references)	Assumptions, Qualifications, Limitations & Gaps
	Historic shoreline changes at the turtle nesting beaches on the seaward coast of CG were determined by PCS (2024a) based on satellite imagery. The beaches east of Cape Domett and west of Cape Dussejour were shown to have advanced over the last 30 years, while the beach at Turtle Bay on Lacrosse Island was shown to have been stable. The stranded beach ridges (cheniers) at East Bank Point inside CG have migrated landward over the last 30 years. This is a common response to stranded beach ridges due to the limited supply of sand from the adjacent mudflats (that they are perched on). Data collected by previous studies in the area as well as the modelling undertaken as part of this Project have shown that the sediment transport patterns have changed since European colonisation, predominantly a result of construction of the Ord River dam in 1971. The dam was shown to have significantly reduced the sediment supply (both sand and fine-grained silt and clay) to CG from the Ord River. In addition, the dam also changed the hydrodynamics in the Ord River/East Arm. Previous studies suggested that since completion of the Ord River dam the majority of the sediment transported downstream along West Arm was subsequently imported into East Arm, with almost no fine-grained sediment being transported into CG from either West or East Arms. However, data measured at the entrance to West Arm as part of this project consistently showed higher turbidity at this location compared to the sites in CG and also showed elevated turbidity following a large river discharge event. Therefore, it can be concluded that although sedimentation has occurred in East Arm following construction of the Ord River dam, fine-grained sediment from the West and East Arms is still being transported into CG and providing an ongoing supply of fine-grained sediment for the mudflats and mangroves in the region (PCS, 2024a &2024b;BKA, 2024b). The fact that the beaches offshore of CG have advanced over the last 30 years indicates that any changes to the sediment transport processes in CG that may have been caused by the Ord River dam have not significantly reduced the supply of sand to these beaches. This finding agrees with results from elemental feature analyses undertaken by BKA detailed by PCS (2024b), which showed that the majority of the sediment at King Shoal was not from the same source as the sediment in CG, but is rather from longshore / offshore sources.			Although there is some uncertainty in this discharge, it is based on hydrological modelling and so it can be considered to provide a reasonable representation of the discharge from the Ord River prior to the construction of the dams. The SSC of the discharged water for the pre-European settlement scenario was varied depending on the discharge rate in the same way as for existing conditions. Therefore, the elevated discharge for the pre-European settlement scenario will have also resulted in higher SSC being discharged into the Ord River compared to existing conditions today.
b) Predict potential impacts of the proposed project on sediment transport and coastal processes of the subject areas, including during the operation, at the end of the operation (15 years) and in 100 years, with particular focus on:	Detailed modelling of potential changes to suspended and bedload transport after five years (23 million m^3) and fifteen years (70 million m^3) of sand sourcing from the POA and 100 years from today with 70 million m^3 of sand sourcing, are provided in this report. The summary findings are:	Section 5.2	BKA (2024b) BKA (2024d) PCS (2024a) PCS (2024b) PCS (2024c) PCS (2025b)	The HD, SW and ST models have been calibrated and validated at multiple sites offshore and within CG during both wet and dry season conditions based on a large volume of available measured data. This

Study Objective	Summary Findings / Conclusions	Relevant sections of this report	Supporting Data Sources (references)	Assumptions, Qualifications, Limitations & Gaps
	The deepening due to the sand sourcing will not significantly change the SSC within CG, with very little change to the spatial pattern of the SSC. Due to the deepening of the POA associated with the sand sourcing the modelling indicated a reduction in SSC within the POA of up to 8%, while outside of the POA the changes were still predominantly reductions with changes of ± 3%. These changes in SSC are not expected to impact the supply of fine-grained sediment to mangroves and mudflats in the region or to measurably change the benthic light in the region, which is already permanently zero to near-zero throughout CG. Changes in bedload transport due to the sand sourcing were modelled to be very minor reductions in bedload transport within and directly to the west and east of the POA and minor increases in bedload transport directly to the north and south of the POA. Reductions in peak bedload transport rates were modelled to be between 3.1% and 10.5% within the POA, while outside of the POA changes in bedload transport were between a 1.8% reduction to a 2.6% increase. As the sand sourcing will leave most of the existing sand resource present throughout the POA (the proposal will only take a maximum of 23% of the existing sand resource), the changes to the bedload transport are relatively small and localised and are not assessed to influence the wider sediment transport processes in CG and offshore. The sand sourcing is not considered to result in any changes to the wave conditions offshore of CG and so will not result in any direct impacts to the longshore or cross-shore sediment transport at the turtle nesting beaches.		This report - HD, SW, ST and Beach Processes models along with the data used to develop and calibrate/validate the models (see Section 3 for further details).	provides confidence that the models provide a realistic representation of the existing conditions within CG. The modelling of the five-year and 15-year scenarios assumed no natural import of sand into the POA over this time. Some sedimentation will occur over this time and so the modelled very minor changes can be considered to represent the worst-case scenario. For the 100 years scenario, sedimentation was assumed within the POA. This was based on results from the sediment transport modelling. While there will always be uncertainty with estimating sedimentation over 100 years, the results can be considered to provide an indication as to the extent and magnitude of potential changes.
• predicting potential for natural replenishment of sand in dredged areas of the tenements, including likely timeframes for replenishment,	The modelling has indicated ongoing sedimentation at the southern end of the POA for all metocean conditions considered. This indicates that natural replenishment of sand will occur within the area due to the natural net northerly transport of sand through CG. In addition, measured data presented by PCS (2024b) have shown that sand is imported into the POA through sandwave migration from upstream in CG. The import of sand into the POA has been estimated to be between 200,000 and 375,000 m^3/yr based on results from the numerical modelling and the bedform migration rates.	Section 5.2.1	BKA (2024b) PCS (2024b) This report - HD, SW and ST models along with the data used to develop and calibrate the models (see Section 3 for further details).	As response to Objective 2b)
• predicting potential for coastal erosion and accretion,	As outlined above the modelled potential changes to hydrodynamics are negligible as they are primarily tidally-driven and the proposed sand-sourcing will not measurably change the tidal regime of the area, so there will not be any coastal erosion or accretion due to changes in hydrodynamics. As outlined above the modelled potential changes to waves are negligible as the deepening in the POA only resulted in very small changes to the local wave conditions and so there will not be any coastal erosion or accretion due to changes in waves.	Section 5.2	BKA (2024b) BKA (2024d) PCS (2024b) This report - SW, ST and Beach Processes models along with the data used to develop and validate the models (see Section 3 for further details).	As response to Objective 2b)

Study Objective	Summary Findings / Conclusions	Relevant sections of this report	Supporting Data Sources (references)	Assumptions, Qualifications, Limitations & Gaps
	As outlined above the modelled potential changes to sediment transport are negligible as sediment transport is primarily driven by hydrodynamics, and the proposed sand-sourcing will not measurably change the hydrodynamics of the area, so there will not be any coastal erosion or accretion due to changes in sediment transport. Because the proposed operation will only source a maximum of 23% (up to 70 million m^3) of the minimum of 300 million m^3 of sand that is present in the POA, following the sand sourcing there will still be a large volume (83% or more) of sand present in the POA, and the existing bedforms will still be present. The sand-sourcing will only remove a layer of up to 40 cm of sand on each loading run. Given the highly-dynamic nature of the bedforms in the POA (migration of sand waves of up to 10 m was measured over just 27 days (PCS 2024a)), any changes to bedforms are likely to regenerate over the 14 days when there is no sand-sourcing between cycles. Ongoing transport of sand into the POA from upstream will continue to occur over the duration of the operation (15 years). Elemental feature analysis has shown that the sand located in King Shoals is predominantly from a source other than CG (i.e from longshore / offshore sources) (PCS 2024a). Therefore, any changes to sand supply from the POA either to offshore or within CG are likely to be minor and so the sand sourcing is not assessed to result in increased coastal erosion or accretion.			
• predicting potential impacts on turtle nesting beaches both inside and immediately outside Cambridge Gulf (Figure 3), including potential changes in sand grain size and beach geomorphology; and	Overall, the modelled changes to sediment transport and beach processes were shown to be negligible for the 5-, 15- and 100-year scenarios. The modelling also indicated that the cumulative changes due to construction of the Ord River dams and the proposed 15 years of sand sourcing were negligible. Sediment supply and transport at the beaches on the seaward coast of CG is controlled by the wave conditions, which will not be affected by the proposed operation. The modelling indicates that the proposed sand-sourcing will not affect sediment supply to the turtle nesting site at Barnett Point inside CG (to the SE of the POA), which comprises stranded sand banks (cheniers) located behind and protected by a seaward fringe of mangroves.	Section 5.2	BKA (2024b) BKA (2024d) PCS (2024b) This report - HD, SW, ST and Beach Processes models along with the data used to develop and calibrate/validate the models (see Section 3 for further details).	As response to Objective 2b)
• predicting potential impacts on mangroves and other coastal and intertidal communities and impacts on the Ord River Floodplain Ramsar site as a result of the sand extraction.	Overall, the modelled changes to sediment transport and coastal processes were shown to be negligible for the 5-, 15- and 100-year scenarios. The modelling also indicated that the cumulative changes due to construction of the Ord River dams and the proposed 15 years of sand sourcing were negligible.	Section 5.2	BKA (2024b) BKA (2024d) This report - HD, SW and ST models along with the data used to develop and calibrate/validate the	As response to Objective 2b)

Study Objective	Summary Findings / Conclusions	Relevant sections of this report	Supporting Data Sources (references)	Assumptions, Qualifications, Limitations & Gaps
	The modelling indicates that sediment supply and transport at the mangroves and other coastal and intertidal communities, including at the Ord River Floodplain Ramsar site, will not be affected by the proposed operation. Based on the modelling results, the sand sourcing is not expected to result in impacts to environments within CG which are dependent on a supply of fine-grained sediment or a supply of sand.		models (see Section 3 for further details).	
c) This should include prediction of likely 'worst-case' and 'best-case' impacts and also 'cumulative' impacts of the proposed project on sediment transport and coastal processes (with 'worst-case' and 'best-case' being consistent with meanings in relevant WA EPA guidance as listed in section 4, and 'cumulative' meaning in addition to those that may have been caused by previous developments in the area, such as the Ord River dam).	As previously noted in response to Object 1c) the impacts to hydrodynamics were shown to be similar between the different metocean conditions. The results for the sediment transport modelling are similar, with localised impacts for all metocean conditions and with no single metocean condition resulting in consistently larger impacts. Therefore, it is not meaningful to determine 'best-case' and 'worst-case' impacts. The sediment transport modelling has considered the cumulative impacts of the sand sourcing and the Ord River dams on both the SSC and bedload transport. The modelled cumulative changes indicated that during the wet season the additional change in SSC due to the sand sourcing was small relative to the changes as a result of the Ord River dam, while during the dry season the cumulative change in SSC due to the sand sourcing and Ord River dams was typically smaller than the change just due to the Ord River dam, meaning that the changes due to the sand sourcing (predominantly reduction in SSC) acted to reduce the changes due to the Ord River dams (predominantly increase in SSC). For bedload transport the cumulative assessment indicated that the sand sourcing would not significantly change the impacts in bedload transport resulting from the Ord River dam, except for locally within the proposed operational area where it resulted in a consistent reduction in bedload transport.	Section 5.2	BKA (2024b) BKA (2024d) This report - HD, SW and ST models along with the data used to develop and calibrate/validate the models (see Section 3 for further details).	ST modelling results have shown comparable changes for the different metocean conditions, meaning that it has not been possible to determine 'best-case' and 'worst-case' changes whilst still assuming realistic scenarios.
Objective 3: Suspended sediment and turbid plume dispersal & potential impacts on benthic habitats & communities (see note below):				
a) Define the existing suspended sediment and turbidity regime in the subject areas, under the seasonal range of natural conditions.	Measured data and numerical modelling results have been presented in this report to understand the existing suspended sediment and turbidity regime. Suspended solids concentrations (SSC) and turbidity levels in CG are extremely high in CG, with modelled 95th percentile SSC within the main body of CG ranging from 100 mg/L to more than 3,000 mg/L. There is significant spatial and temporal variability in SSC and turbidity within CG driven mainly by tidal conditions and river discharges conditions. For example, measured turbidity within the POA varies by	Sections 2.3.1 and 5.1.1	BKA (2024b) BKA (2024d) PCS (2024a) This report - ST model along with the data used to develop and calibrate the model (see Section 3.6 for further details).	The HD, SW and ST models have been calibrated and validated at multiple sites offshore and within CG during both wet and dry season conditions based on a large volume of available measured data. This provides confidence that the models provide a realistic representation of the existing conditions within CG.

Study Objective	Summary Findings / Conclusions	Relevant sections of this report	Supporting Data Sources (references)	Assumptions, Qualifications, Limitations & Gaps
	up to 70 NTU during the dry season and up to 300 NTU during the wet season and double this at the confluence between West Arm and CG. Turbidity and SSC typically increases from the seaward entrances to CG in an upstream (southern) direction to West and East Arms, where very high turbidity and SSC can occur, with measured 99th percentiles at the entrance to West Arm of 470 NTU and 1,057 mg/L. Measured data and numerical modelling results indicate that there is seasonal variability in turbidity, with higher values in the wet season compared to the dry season. The relationship between turbidity and SSC under local conditions has been established as follows: • Dry season: 1 NTU = 1.72 mg/L. • Wet season: 1 NTU = 2.77 mg/L. Numerical modelling and water quality sampling have shown that the majority of the sediment in suspension in CG is fine-grained silt and clay, with limited sand sized sediment present in suspension. Plots of the measured in-situ benthic light and turbidity at multiple sites over the full range of tidal conditions over extended deployment periods have measured a permanent near-seabed aphotic zone throughout CG. This is most likely caused by constant suspension of seabed sediments by the strong tidal currents, causing constantly high turbidity and SSC throughout CG, which is added to by wet season inputs of sediment-laden freshwater from the catchment. The permanent near-seabed aphotic zone in CG is a major inhibiter of benthic biota and communities, and as a result the benthic communities in CG are depauperate, with an absence of corals and coral reefs, seagrasses, macroalgae communities, sponge beds, oyster reefs and other significant primary-producer sub-tidal benthic communities, as reported in BKA (2024b).			It should be noted that the relationship between turbidity and SSC in an environment such as CG, where mixed sediment types can be in suspension, can be complex due to potential variability in the type and mass of suspended sediments, both spatially and temporally. In order to address this a wide range of locations and conditions were sampled and represented in the relationships. However, it is still possible that the relationships could over- or under-estimate SSC at some locations and times. Never-the-less, the relationships are considered to be suitable to allow the measured turbidity data to be converted to SSC to allow calibration and validation of the sediment transport model (Section 3.6).
b) Predict potential dispersal of sediment and turbidity plumes from the proposed operation, under the seasonal range of natural conditions, in particular towards King Shoals, which are within a State Marine Park Sanctuary Zone and therefore considered to be a high priority sensitive receptor environment.	This report presents detailed numerical modelling results of sediment plumes from the operation of the Sand Production Vessel (SPV) in CG. The modelling simulated the sand sourcing activity over two-month (60/61 days) periods in the wet, dry and transitional seasons. Two different sand sourcing scenarios were simulated (repeat tracks along set lines in the POA and targeted tracks over the entire POA, with the timing of the activity was varied between spring tides and neap tides. The modelling results indicated that the SSC resulting from the operation of the SPV was consistently very low for all the model simulations, with only the 99th percentile modelled SSC exceeding 1 mg/L at sites both within the POA and outside of the POA.	Section 6	BKA (2024b) BKA (2024d) PCS (2024a, b & c) PCS (2025b) This report - HD, SW and ST models along with the data used to develop and calibrate/validate the models (see Section 3 for further details).	The plume modelling is based on a number of assumptions relating to the SPV. These assumptions were provided by BKA and are detailed in Section 3.7.2. If the SPV specifications change then the plume modelling results would also change slightly, but it is expected that the plume SSC will remain low regardless (due to the factors listed in the 'Summary Findings / Conclusions' column).

Study Objective	Summary Findings / Conclusions	Relevant sections of this report	Supporting Data Sources (references)	Assumptions, Qualifications, Limitations & Gaps
	Comparing the SSC from the operation of the SPV with the natural SSC has shown that the relative contribution of the sand sourcing SSC is predominantly less than 1% of the natural SSC, which is considered negligible in terms of causing potential changes to marine environmental quality and impacts on benthic biota and communities. Even if SSC was significantly elevated by the sand-sourcing operation, there are no sensitive benthic communities in CG that could potentially be impacted (BKA 2024b). There are several key factors that contribute to keeping SSC from the proposed operation at low levels, in localised areas and for short durations, including the facts that: ▪ the operation will target course-sand and not fine sediments, ▪ the operation will not be continuous, as the SPV will only operate in CG for one to two days (average 30 hours) every 14 days, as, in between loading cycles, the SPV will deliver the sand to Asia and return to CG, ▪ the operation will not include any dumping of sediment in CG (as the loaded sand will be exported); and ▪ the SPV will be fitted with best-practice turbidity reduction measures, including a 'green valve' in the water overflow discharge.			

Table 47. Summary of how this report meets the relevant WA EPA Guidelines (as listed in Section 1).

CG = Cambridge Gulf. HD = Hydrodynamics. SPV = Sand Production Vessel. ST = Sediment transport. SW = Spectral wave. POA = Proposed operational area.

Guideline	Summary Findings / Conclusions	Relevant section of this report	Supporting Data Sources (references)	Assumptions, Qualifications, Limitations & Gaps
WA EPA 2021 *Technical Guidance for EIA of Marine Dredging Proposals*: • These mainly relate to impacts of sediment and turbidity plumes on benthic communities, which is not a major issue for this project (due to naturally high turbidities and lack of benthic communities). • However, Objective 3) of the RFP requires this issue to be addressed to a certain extent, and compliance with this Guideline can be addressed when addressing Objective 3).	As per the response to Objective 3. b) in Table 46 above. Potential modelled sediment plumes from the operation of the Sand Production Vessel (SPV) in Cambridge Gulf (CG) and resulting changes in suspended sediment concentrations (SSC) and seabed sedimentation have been modelled in accordance with the requirements of EPA (2021) and relevant Western Australian Marine Science Institution (WAMSI) Dredging Science Node guidelines, including Sun *et al.* (2020), Sun *et al.* (2016), Mills & Kemps (2016) and Kemps & Masini (2017). The findings are listed against Objective 3. b) in Table 46 above. EPA (2021) requires prediction of potential impacts of sediment and turbidity plumes on benthic communities and habitats (BCH), including, if applicable, definition of Zones of High Impact (ZoHI), Zones of Moderate Impact (ZoMI) and Zones of Influence (ZoI). For this project it has not been feasible or necessary to assess ZoHI, ZoMI and ZoI as defined in the EPA guidance, as there are no potentially sensitive BCH in CG to model these zones and set biological response triggers for (BKA 2024b). The lack of sensitive BCH one of the reasons that CG was selected during the alternative sites screening process (BKA 2024d).	Sections 3.7 and 6	BKA (2024b) BKA (2024d) PCS (2024a, b & c) PCS (2025b) This report - HD, SW and ST models along with the data used to develop and calibrate/validate the models (see Section 3 for further details).	The plume modelling is based on a number of assumptions relating to the SPV. These assumptions were provided by BKA and are detailed in Section 3.7.2. If the SPV specifications change then the plume modelling results would also change slightly, but it is expected that the plume SSC will remain low regardless (due to the factors listed in the 'Summary Findings / Conclusions' column).
WA EPA 2016 *Environmental Factor Guideline - Coastal Processes*: • This is the highest priority issue for this project and so all relevant elements of this Guideline need to be addressed thoroughly. • States objective is "To maintain the geophysical processes that shape coastal morphology so that the environmental values of the coast are protected".	The data analysis and numerical modelling detailed in this report is aimed at assessing potential impacts to the geophysical processes which influence coastal morphology. This is further detailed in the responses to each consideration below. A description of the geophysical processes that shape coastal morphology and the environmental values of the coast of the CG area is presented in BKA (2024b) - Referral Report No. 2 - *Setting & Existing Environment* - section 7 on Coastal Processes. An assessment of potential impacts of the proposal on geophysical processes that shape coastal morphology and the environmental values of the coast of the CG area is presented in BKA (2024d) - Referral Report No. 4 - *Impact Assessments - section* 8 on Coastal Processes.	Sections 2, 4 and 5	BKA (2024b) BKA (2024d) PCS (2024a, b & c) PCS (2025b) This report - HD, SW, ST and Beach Processes models along with the data used to develop and calibrate/validate the models (see Section 3 for further details).	The HD, SW and ST models have been calibrated and validated at multiple sites offshore and within CG during both wet and dry season conditions based on a large volume of available measured data. This provides confidence that the models provide a realistic representation of the existing conditions within CG.
• States that considerations for the EIA should include (only those directly related to PCS work are listed):	See responses to each consideration below.			

Guideline	Summary Findings / Conclusions	Relevant section of this report	Supporting Data Sources (references)	Assumptions, Qualifications, Limitations & Gaps
• Consideration 1: The predicted changes to coastal processes based on modelling and analyses to a standard consistent with recognised published guidance.	This report has presented results from detailed HD, SW, ST and beach processes modelling of potential changes to hydrodynamics, waves and sediment transport and thus coastal processes from the proposed sand sourcing. See response to Objectives 1b) and 2b) in Table 46 for further details of the impacts. The modelling was undertaken using state-of-the art 3D models that are purpose-built precisely for this type of work – being the DHI MIKE suite with flexible mesh. To ensure consistency with recognised published guidance, the modelling and analyses and the calibration and validation of the models have been undertaken in accordance with recognized international standards including Williams & Esteves (2017) and Los & Blaas (2010), and relevant Australian and Western Australian guidelines including Sun *et al.* (2020), Sun *et al.* (2016), Mills & Kemps (2016), Kemps & Masini (2017) and GBRMPA (2012).	Sections 4.2 and 5.2	BKA (2024b) BKA (2024d) PCS (2024a, b & c) PCS (2025b) This report - HD, SW, ST and Beach Processes models along with the data used to develop and calibrate/validate the models (see Section 3 for further details).	The HD, SW, ST and beach processes models have been calibrated and validated at multiple sites offshore and within CG during both wet and dry season conditions based on a large volume of available measured data. This provides confidence that the models provide a realistic representation of the existing conditions within CG.
• Consideration 2: The significance of the likely change to coastal processes as well as the environmental values affected by those changes.	A detailed assessment of the potential implications of changes to hydrodynamics, waves and sediment transport in the region is presented in this report. The potential changes have consistently been shown to be very minor relative to the natural variability of the coastal processes and they are considered unlikely to result in changes to the environmental values of the CG area that are influenced by coastal processes. A description of the coastal processes and the environmental values that are influenced by coastal processes in the CG area is presented in BKA (2024b) - Referral Report No. 2 - *Setting & Existing Environment* - section 7 on Coastal Processes. An assessment of potential impacts of the proposal on coastal processes and the environmental values that are influenced by coastal processes in the CG area is presented in BKA (2024d) - Referral Report No. 4 - *Impact Assessments* - section 8 on Coastal Processes.	Sections 4.2 and 5.2	BKA (2024b) BKA (2024d) PCS (2024a, b & c) PCS (2025b) This report - HD, SW, ST and Beach Processes models along with the data used to develop and calibrate/validate the models (see Section 3 for further details).	N/A
• Consideration 3: Impacts to coastal processes in the context of the latest climate change science and projections.	The potential impacts of the sand sourcing on HD, waves and ST, and thus coastal processes, have been simulated in 100 years from today with 70 million m^3 of sand sourcing, with the conditions assumed for this scenario based on the latest climate change science, including a predicted sea-level rise over 100 years of 0.9 m (based on Department of Transport (2010) and IPCC (2024)). The modelling shows that the proposed sand sourcing would result in negligible impacts to water levels, with a modelled change in tidal range of less than 0.05% of the existing tidal range, during a large spring tide only, which has a tidal range of ~8 m in CG. This is of no consequence in the context of a predicted 0.9 m sea level rise over 100 years from climate change.	Sections 4.2 and 5.2	WA Department of Primary Industries and Regional Development (2024) WA Department of Transport (2010) IPCC (2024)	The hydrodynamic, wave and sea level conditions adopted for the 100 years scenario were based on latest available information from the literature (WA Department of Primary Industries and Regional Development, 2024; WA Department of Transport, 2010; IPCC, 2024). For the 100 years scenario, sedimentation was assumed within the POA but no other morphological

Guideline	Summary Findings / Conclusions	Relevant section of this report	Supporting Data Sources (references)	Assumptions, Qualifications, Limitations & Gaps
				changes due to sea level rise were assumed. This was based on results from the ST modelling. While there will always be uncertainty with estimating sedimentation over 100 years, the results can be considered to provide an indication as to the extent and magnitude of potential changes.
• Consideration 4: The likely change to coastal processes and consequent risks to coastal morphology and associated environmental values.	As per response to consideration 2 above.	Sections 4.2 and 5.2	BKA (2024b) BKA (2024d) PCS (2024a, b & c) PCS (2025b) This report - HD, SW, ST and Beach Processes models along with the data used to develop and calibrate/validate the models (see Section 3 for further details).	This finding is based on the results from all of the different numerical modelling combined with a conceptual model which was developed based on all available information/data.
• States that Information required for EIA include (only those directly related to PCS work are listed):	See responses to each 'information required' below.			
• Info required 1: Characterize the coastal type and current coastal processes, including modelling of the local current and wave climate.	Results from the data analysis and HD, SW, ST and beach processes models as presented in this report and also PCS (2024a, 2024b & 2024c) have been used to provide a comprehensive characterisationcharacterization of the coastal types and current coastal processes in CG, including 3D modelling of the local currents, wave climate, sediment transport and beach processes. CG has been shown to be tidally dominated, with secondary influences from river discharges, wind and waves. Most sediment within CG is derived from the terrestrial catchment via erosion and river discharges, while sediment supply and transport at the beaches on the seaward coasts of CG is driven by waves. See also response to Objectives 1a) and 2a) in Table 46. A description of the coastal types and coastal processes and the environmental values that are influenced by coastal processes in the CG area is also presented in BKA (2024b) - Referral Report No. 2 - *Setting & Existing Environment* - section 7 on Coastal Processes.	Sections 2, 4.1 and 5.1	BKA (2024b) BKA (2024d) PCS (2024a, b & c) PCS (2025b) This report - HD, SW, ST and Beach Processes models along with the data used to develop and calibrate/validate the models (see Section 3 for further details).	The HD, SW, ST and beach processes models have been calibrated and validated at multiple sites offshore and within CG during both wet and dry season conditions based on a large volume of available measured data. This provides confidence that the models provide a realistic representation of the existing conditions within CG.

Guideline	Summary Findings / Conclusions	Relevant section of this report	Supporting Data Sources (references)	Assumptions, Qualifications, Limitations & Gaps
• Info required 2: Analysis of long-shore sediment movement and erosion and deposition patterns; beach profiling, and determination of tidal flow and exchange.	Results from the data analysis and HD, SW, ST and beach processes models as presented in this report and also PCS (2024a, b & c) have been used to provide a comprehensive analysis of long-shore sediment movement and erosion and deposition patterns; beach profiling, and determination of tidal flow and exchange in CG, including 3D modelling of the local current and wave climate and sediment transport and beach processes. The shoreline position at the turtle nesting beaches (i.e. erosion and deposition) over the last 30 years was shown by PCS (2024a) to vary from stable at Turtle Bay on Lacrosse Island, accreting at Turtle Beach West (west of Cape Dussejour) and at Cape Domett Seaward Beach, and migrating landward at the Barnett Point within CG (which is a stranded beach or 'chenier' located behind a seaward fringe of mangroves). Longshore and cross-shore sediment transport rates have been modelled at the seaward coast turtle nesting beaches, with the results showing that sand is moved onshore to the beaches through cross-shore transport. Numerical modelling results have shown that the tidal flow within CG is highly variable both spatially and temporally, while the exchange through the West Entrance is approximately three times larger than the exchange through East Entrance.	Sections 4.1, 5.1.4 and PCS (2024a)	BKA (2024b) BKA (2024d) PCS (2024a, b & c) PCS (2025b) CSIRO (2023) This report - HD, SW, ST and Beach Processes models along with the data used to develop and calibrate/validate the models (see Section 3 for further details).	The sediment properties adopted for the beach processes modelling had to be assumed due to a lack of data (it was not safe to collect sand samples from the beach due to risks from crocodiles).
• Info required 3: Predict the changes to coastal processes as a result of the proposal, taking into account the appropriate spatial and temporal scales.	Results from the data analysis and HD, SW, ST and beach processes models as presented in this report and also PCS (2024a, b & c) have been used to assess changes to coastal processes as a result of the proposal, taking into account the appropriate spatial and temporal scales, including 3D modelling of the local current and wave climate and sediment transport and beach processes. The potential changes have consistently been shown to be very minor relative to the natural variability of the coastal processes and they are considered unlikely to result in changes to coastal processes or the environmental values of the CG area that are influenced by coastal processes. The modelled changes from the proposal after 15 years (70 million m^3) of sand sourcing to factors that drive coastal processes are summarised as follows: • A small phase change of up to 30 seconds (earlier) occurred to the tidal propagation within CG – this is negligible in relation to coastal processes. • A very minor reduction in current speed of 0.05 m/s within the POA – this is negligible in relation to coastal processes.	Sections 4.2 and 5.2	BKA (2024b) BKA (2024d) PCS (2024a, b & c) PCS (2025b) This report - HD, SW, ST and Beach Processes models along with the data used to develop and calibrate/validate the models (see Section 3 for further details).	The HD, SW, ST and beach processes models have been calibrated and validated at multiple sites offshore and within CG during both wet and dry season conditions based on a large volume of available measured data. This provides confidence that the models provide a realistic representation of the existing conditions within CG.

Guideline	Summary Findings / Conclusions	Relevant section of this report	Supporting Data Sources (references)	Assumptions, Qualifications, Limitations & Gaps
	• A very minor modelled change to wave heights of ± 0.01 m occurred within CG during large wave events – this is negligible in relation to coastal processes. No modelled changes to waves outside of CG. • The sediment transport modelling indicated that the proposal will not significantly change the SSC within CG, with a general reduction in SSC of up to 3% outside of the POA – this is negligible in relation to coastal processes. • Modelled changes to the bedload transport of sand were very minor and localised within and immediately adjacent to the POA – these are not assessed to impact the supply of fine-grained silt and clay or of sand to other areas within CG or offshore. An assessment of potential impacts of the proposal on coastal processes and the environmental values that are influenced by coastal processes in the CG area is also presented in BKA (2024d) - Referral Report No. 4 - *Impact Assessments* - section 8 on Coastal Processes.			
• Info required 4: Describe the impacts resulting from the changes to coastal processes.	As outlined immediately above and in other related responses in this Table and in Table 46, the potential changes have consistently been shown to be very minor relative to the natural variability of the coastal processes, and they are considered unlikely to result in changes to coastal processes or the environmental values of the CG area that are influenced by coastal processes.	Sections 4.2 and 5.2	BKA (2024b) BKA (2024d) PCS (2024a, b & c) PCS (2025b) This report - HD, SW, ST and Beach Processes models along with the data used to develop and calibrate/validate the models (see Section 3 for further details).	The HD, SW, ST and beach processes models have been calibrated and validated at multiple sites offshore and within CG during both wet and dry season conditions based on a large volume of available measured data. This provides confidence that the models provide a realistic representation of the existing conditions within CG.
• Info required 5: Consider cumulative impacts from and to other existing and approved developments in order to determine whether the proposal, in combination with other developments, will significantly impact coastal processes and any consequential impacts to environmental values in the coastal zone.	An assessment of potential cumulative impacts of the proposal on the coastal zone is presented in BKA (2024d) - Referral Report No. 4 - *Impact Assessments* - section 16 on Cumulative & Holistic Impact Assessment. As outlined in BKA (2024d) the potential for cumulative impacts from the proposal is limited by the fact that the CG area is completely uninhabited, with no road access and no development, built facilities or infrastructure. Human activity in CG is restricted to vessel-based operations, including commercial vessels that transit through CG entering and departing the Port of Wyndham (on average 1.3 per week), small private vessels from Wyndham and Kununurra used mainly for recreational fishing along the coast and up the inlets of CG; and one commercial gillnet fisherman who is sometimes active in CG (and also along the adjacent coast outside CG). None of these other human uses of the area cause significant impacts on the environment, so do not add cumulative impacts for the BKA proposal.	Sections 4.2 and 5.2	BKA (2024b) BKA (2024d) PCS (2024a, b & c) PCS (2025b) This report - HD, SW and ST models along with the data used to develop and calibrate/validate the models (see Section 3 for further details).	The HD, SW, ST and beach processes models have been calibrated and validated at multiple sites offshore and within CG during both wet and dry season conditions based on a large volume of available measured data. This provides confidence that the models provide a realistic representation of the existing conditions within CG. To represent the change in river discharge for the pre-European settlement scenario the peak discharge adopted was based on information provided by Wolanski *et al.* (2004). Although there is some uncertainty in this discharge, it is

Guideline	Summary Findings / Conclusions	Relevant section of this report	Supporting Data Sources (references)	Assumptions, Qualifications, Limitations & Gaps
	Based on discussions held with a broad range of local and State stakeholders as part of BKA's consultation program it appears unlikely that there will be other developments in CG in the foreseeable future (see Referral Report No. 7 - *Stakeholder Consultations*). Upstream of CG, the building of two dams on the Ord River may provide a bases for triggering cumulative impacts, and the data analysis and numerical modelling presented in this report focus on assessing potential cumulative impacts of the proposed sand sourcing in relation to the Ord River dams. This included modelling HD, SW and ST conditions in CG prior to the dams under the pre-European settlement scenario, and assessing changes since European settlement due to construction of the dams. The modelling indicates that construction of the Ord River dams has caused changes to HD and ST in CG as follows: • Regulation of river flows through the dams has reduced river discharges during wet season high discharge events and increased river discharges during dry season low discharge conditions, in East Arm. • Prior to construction of the dams, during a high river discharge event the ebb tide current speeds throughout CG may have been higher by up to 0.10 m/s (or 6%), while the flood tide current speeds may have been lower by up to 0.18 m/s (or 12 %). These are very minor differences considering that these events only occurred occasionally and for relatively short durations. • Tidal range in CG may have changed by up to 0.55% during a high river discharge event compared to pre-European settlement conditions. While this is a very minor change, it is an order of magnitude higher than the extremely minor <0.05% change modelled for the proposed sand sourcing. • SSC in CG may have been reduced by up to 3,000 mg/L (or 86%) during a large river discharge event in the wet season and increased by 35 mg/L (or 8%) during the dry season, compared to pre-European settlement conditions. These are an order of magnitude higher than the extremely minor changes in SSC modelled for the proposed sand sourcing. The modelling indicates that construction of the Ord River dams has not caused changes to waves in or offshore from CG. As reported against relevant items in this table the modelled extremely minor to minor changes from the proposed sand sourcing are negligible in relation to the changes that may have occurred in CG as a result of the building of the Ord River dams. Therefore, potential cumulative impacts on coastal processes are also assessed to be negligible.			based on hydrological modelling and so it can be considered to provide a reasonable representation of the discharge from the Ord River prior to the construction of the dams. The SSC of the discharged water for the pre-European settlement scenario was varied depending on the discharge rate in the same way as for existing conditions. Therefore, the elevated discharge for the pre-European settlement scenario will have also resulted in increased SSC being discharged into the Ord River.

Guideline	Summary Findings / Conclusions	Relevant section of this report	Supporting Data Sources (references)	Assumptions, Qualifications, Limitations & Gaps
• Info required 6: Determine coastal vulnerability and the potential impacts as a result of climate change.	To account for climate change the potential impacts of the sand sourcing on HD, waves and ST have been simulated for 100 years from today with 70 million m^3 of sand sourcing, with the conditions assumed for this scenario based on the latest climate change science, including a predicted sea-level rise over 100 years of 0.9 m (Department of Transport, 2010; IPCC, 2024).). The modelling indicates that the proposed sand sourcing could result in negligible impacts to water levels, with a modelled change in tidal range of less than 0.05% of the existing tidal range, during a large spring tide only, which has a tidal range of ~8 m in CG. This is of no consequence in the context of a predicted 0.9 m sea level rise over 100 years from climate change. It is also of no consequence with respect to coastal vulnerability – a change of 0.05% during a large spring tide with a range of 8 m will not cause any impacts on the coast.	Sections 4.2 and 5.2	Department of Primary Industries and Regional Development (2024) Department of Transport (2010) IPCC (2024) BKA (2024b) BKA (2024d) This report - HD, SW and ST models along with the data used to develop and calibrate/validate the models (see Section 3 for further details).	The hydrodynamic and wave conditions adopted for the 100 years scenario were based on latest available information from the literature (Department of Primary Industries and Regional Development, 2024; Department of Transport, 2010; IPCC, 2024). For the 100 years scenario, sedimentation was assumed within the POA but no other morphological changes due to sea level rise were assumed. The sedimentation in the POA was based on results from the sediment transport modelling. While there can be uncertainty with estimating sedimentation over 100 years, the results can be considered to provide an indication as to the extent and magnitude of potential impacts in the future.
• Info required 7: Identify monitoring strategies, and management and mitigation measures	This is presented in BKA (2024d) - Referral Report No. 4 - *Impact Assessments* - Section 17 Environmental Management Plan.	N/a	This report - HD, SW, ST and Beach Processes models along with the data used to develop and calibrate/validate the models (see Section 3 for further details).	The HD, SW, ST and beach processes models have been calibrated and validated at multiple sites offshore and within CG during both wet and dry season conditions based on a large volume of available measured data. This provides confidence that the models provide a realistic representation of the existing conditions within CG.
• WA EPA 2016 *Environmental Factor Guideline - Marine Environmental Quality*: • This Guideline is relevant to the development of the Conceptual Model (but which also needs to address sediment dynamics and coastal processes – perhaps more importantly than MEQ). • Because there will not be any 'operational' discharges of pollutants from the operation, the only potential impacts of the operation on MEQ are turbid plume generation, addressed by Objective 3.	A description of the existing MEQ in the CG area is presented in BKA (2024b) - Referral Report No. 2 - *Setting & Existing Environment* - section 8 on MEQ, supported by analyses in PCS (2024a, b and c). An assessment of potential impacts of the proposal on MEQ in the CG area is presented in BKA (2024d) - Referral Report No. 4 - *Impact Assessments* - section 9 on MEQ, supported by analyses in PCS (2024a, b and c). The main potential impacts of the proposed sand sourcing on MEQ are from turbid plume generation during operation of the SPV in CG. As outlined in the response to Objective 3b) in Table 46, the modelling results indicated that the SSC resulting from the operation of the SPV was consistently very low for all the model simulations, with only the 99th percentile depth-averaged SSC exceeding 1 mg/L at sites both within the POA and outside of the POA. This is considered negligible in	Section 6	BKA (2024b) BKA (2024d) This report - HD, SW and ST models along with the data used to develop and calibrate/validate the models (see Section 3 for further details).	The plume modelling is based on a number of assumptions relating to the SPV. These assumptions were provided by BKA and are detailed in Section 3.7.2. If the SPV specifications change then the plume modelling results would also change slightly, but it is expected that the plume SSC will remain low regardless (due to the factors listed against related items above).

Guideline	Summary Findings / Conclusions	Relevant section of this report	Supporting Data Sources (references)	Assumptions, Qualifications, Limitations & Gaps
• Stated objective is "To maintain the quality of water, sediment and biota so that environmental values are protected", and defines environmental values and beneficial uses.	terms of causing potential changes to MEQ and impacts on environmental values that are influenced by MEQ (which in the case of CG is primarily ecosystem health). A conceptual understanding of the coastal processes in the CG as well as a conceptual model of possible effects of human changes in CG are presented in PCS (2024a). The conceptual model shows that the two main potential stressors from the proposed sand sourcing are an increase in suspended sediment and a reduction in sediment supply. As outlined above the modelling assessed that potential changes in these parameters is very minor to negligible.			
• States that considerations for the EIA should include (only those directly related to PCS work are listed):	See responses to each consideration below.			
• Consideration 1: The marine system that will potentially be affected and the significance of the environmental values that it supports.	The marine system is described in detail by PCS (2024a & 2024b) based on a combination of information from the literature, measured data and results from numerical modelling. This report provides further details regarding the hydrodynamics, waves and sediment transport in the area. The significant environmental values of the marine system in CG are further detailed by BKA (2024d), and these mainly comprise: • A complete lack of sensitive primary producer benthic communities, including coral communities, seagrasses, sponge beds, macroalgae communities etc, due to the extreme environmental conditions in CG. • A narrow band of mangroves around the coast and up the various inlets, creeks and rivers around CG, including the False Mouths of the Ord on the eastern side of CG, which are part of the Ord River Floodplain Ramsar wetland. • Flatback Turtle nesting beaches at three seaward sites outside of CG (Cape Domett Seaward Beach east of CG, Turtle Bay on Lacrosse Island and Turtle Beach West, west of Cape Dussejour), and ot POA), located on stranded beach (cheniers) protected behind a seaward mangrove fringe. • Habitat for Australian Snubfin Dolphins *(Orcaella heinsohni)* and Australian Humpback Dolphins *(Sousa sahulensis)*.	Sections 2, 4.1 and 5.1	BKA (2024b) BKA (2024d) PCS (2024a) PCS (2024b) This report - HD, SW, ST and Beach Processes models along with the data used to develop and calibrate/validate the models (see Section 3 for further details).	The understanding is based on a combination of literature search, dry- and wet-season field surveys, measured data and results from the numerical modelling.
• Consideration 2: Predictive modelling of the extent, duration and intensity of impacts under normal and most likely worst-case scenarios, and in combination with any other changes in MEQ caused by adjacent activities or natural events (cumulative effects).	As outlined above, the main potential impacts of the proposed sand sourcing on MEQ are from turbid plume generation during operation of the SPV in CG. As outlined in the response to Objective 3b) in Table 46, numerical modelling of sediment plumes has been undertaken – including of the extent, duration and intensity of impacts under normal and most likely worst-case scenarios, and in combination with any other changes in MEQ caused by adjacent activities (of which there are none) or natural events (cumulative effects).	Section 6	This report - HD, SW and ST models along with the data used to develop and calibrate/validate the models (see Section 3 for further details).	The plume modelling is based on a number of assumptions relating to the SPV. These assumptions were provided by BKA and are detailed in Section 3.7.2. If the SPV specifications change then the plume modelling results would also change slightly, but it is

Guideline	Summary Findings / Conclusions	Relevant section of this report	Supporting Data Sources (references)	Assumptions, Qualifications, Limitations & Gaps
	As outlined above, the modelling assessed that potential changes to MEQ and impacts on environmental values that are influenced by MEQ, including cumulative changes, were negligible.			expected that the plume SSC will remain low regardless (due to the factors listed against related items above).
• States that Information required for EIA include the following (only those directly related to PCS work are listed):	See responses to each 'information required' below.			

Info required 1: Characterisation of the local marine environment including natural background and baseline environmental quality and the pre-development EQP for the area including the environmental values to be protected.	A description of the existing MEQ in the CG area is presented in BKA (2024b) - Referral Report No. 2 - *Setting & Existing Environment* - section 8 on MEQ, supported by analyses in PCS (2024a, b and c).
	
	An assessment of potential impacts of the proposal on MEQ in the CG area is presented in BKA (2024d) - Referral Report No. 4 - *Impact Assessments* - section 9 on MEQ, supported by analyses in PCS (2024a, b and c).
	
	Section 9 of BKA (2024d) discusses a framework for Environmental Quality Management Plan (EQMP) which protects the Environmental Quality Objectives (EQOs) for each of the five environmental values stipulated by EPA, which are:
	• ecosystem health,
	• fishing and aquaculture,
	• recreation and aesthetics,
	• industrial water supply; and
	• cultural and spiritual.
	
	Section 9 of BKA (2024d) describes each of these values with regard to CG as follows:
	
	• Ecosystem health: The existing (baseline) MEQ of CG is in a natural condition and free of contaminants and pollutants, while SSC and turbidity levels are naturally very high and chlorophyll levels are relatively low. The health of the biological communities that are present in CG, and especially the mangrove communities around the coast of CG and the marine species that they support, are dependent on the maintenance of this natural, uncontaminated condition.
	
	• Fishing and aquaculture:
	  • Small private vessels from Wyndham and Kununurra use CG for recreational fishing along the coast and up the inlets of CG.
	  • One commercial gillnet fisherman is sometimes active in CG, targeting Barramundi (*Lates calcarifer*) and Threadfin Salmon (*Eleutheronema tetradactylum*). He also works the adjacent coast outside CG. Three commercial gillnet fishermen based in Broome located over 1,000 km by sea to the west are licenced to fish in CG but currently do not. The mangroves
		Section 2.3 and PCS (2024a and 2024b)	BKA (2024b)
			BKA (2024d)
			PCS (2024a)
			PCS (2024b)
				It should be noted that the relationship between turbidity and SSC in an environment such as CG, where mixed sediment types can be in suspension, can be complex due to potential variability in the type and mass of suspended sediments, both spatially and temporally. In order to address this a wide range of locations and conditions were sampled and represented in the relationships.
				
				However, it is still possible that the relationships could over- or under-estimate SSC at some locations and times. Never-the-less, the relationships are considered to be suitable to allow the measured turbidity data to be converted to SSC to allow calibration and validation of the sediment transport model (Section 3.6).

Guideline	Summary Findings / Conclusions	Relevant section of this report	Supporting Data Sources (references)	Assumptions, Qualifications, Limitations & Gaps
	around the coast of CG are important habitat for mud crabs (*Scylla spp*). • There are three commercial crab fishermen licenced to fish CG. Two are based in Broome and are not currently active in CG, and one is based in Port Headland and their licence is for sale. • The mangroves around the coast of CG are important nursery areas for Banana prawns (*Penaeus indicus* and *P. merguiensis)*, although the adults are trawled in waters over 50 to 100 km offshore from CG. • Both the recreational and commercial fishing sectors depend on the maintenance of the natural, uncontaminated condition of MEQ of CG to ensure the health of fish, crab and prawn stocks. • There is currently no aquaculture in CG and no proposals to develop aquaculture in the foreseeable future. The extreme environmental conditions of CG including strong tidal currents and naturally very high turbidity levels most likely make aquaculture non-viable in CG. • <u>Recreation and aesthetics</u>: • The only recreational activity in CG is recreational fishing as described above. There is no swimming or water sports in CG as the area is uninhabited by humans and due to the presence of crocodiles, river sharks, stinging jellyfish, strong tidal currents and naturally very high turbidity levels. • While the surrounding coast and landward backdrop of CG have high aesthetic value due to the rugged natural beauty of the area, the aesthetic value of the marine environment is very low due to naturally very high turbidity levels – the local TO groups refer to the area as 'Brown Water Country' • <u>Industrial water supply</u>: There is currently no industry that requires water supply in CG and no proposals to develop any such industry in the foreseeable future. • <u>Cultural and spiritual</u>: • BKA has consulted with the TO groups about marine-based cultural heritage and undertook an extremely comprehensive survey for potential underwater Aboriginal cultural heritage, and found no indications of such (see Referral Report No. 3 - *Traditional Owners, Native Title & Aboriginal Cultural Heritage*). As outlined above the local TO groups refer to the area as 'Brown Water Country' due to the naturally very high turbidity levels. • There are significant land-based Aboriginal cultural heritage sites on the eastern side of CG and on Lacrosse Island – which are not affected by MEQ, as they are on the land. Overall, reflecting the points above, ecosystem health is the most important environmental value that is influenced by MEQ is CG.			

Guideline	Summary Findings / Conclusions	Relevant section of this report	Supporting Data Sources (references)	Assumptions, Qualifications, Limitations & Gaps

	Section 9.6 of BKA (2024d) discusses a framework for EQMP which protects the EQOs for the environmental values listed above, and makes the following points:
	• The scope to develop a full EQMP / EQO framework for the proposed operation in CG is influenced by the following factors:
	  • the receiving environment in CG is free of contaminants and pollutants, with no significant sources of potential contamination along the immediate coastline or in the broader catchment,
	  • the overall objective should be to maintain this state,
	  • the proposed operation is unlikely to cause any changes in the level of contaminants in water, sediments or biota or any changes in the physical or chemical properties of waters and sediments relative to the natural state in CG, simplifying the ability to achieve the overall objective of maintaining the current state; and
	  • the proposal will not impact on any of the five environmental values and some of the values are not relevant to CG, as outlined in section 9.3.4 of BKA (2024d).
	• Section 9.6 of BKA (2024d) lists the five environmental values and their respective EQO options as listed in EPA 2016, *Technical Guidance - Protecting the Quality of Western Australia's Marine Environment*, and assesses how the proposal relates to each of these. This shows that:
	  • The maximum EQO for ecosystem health to *maintain ecosystem integrity at a maximum level of ecological protection* is desirable and should be possible to achieve by the proposal.
	  • The EQO for fishing that *seafood (caught or grown) is of a quality safe for eating* is desirable and should be possible to achieve by the proposal.
	  • The EQO for secondary contact recreation (fishing and boating) that *water quality is safe for secondary contact recreation* is desirable and should be possible to achieve by the proposal.
	  • The EQOs for aquaculture, primary contact recreation, aesthetics, industrial water supply and cultural and spiritual values are not relevant in CG, however the proposal would not change MEQ in any way that would affect these EQOs.
	• These factors can be used as a basis to build a more developed EQMP framework for CG, which should ideally be done in consultation with relevant agencies and stakeholders than by BKA			

Guideline	Summary Findings / Conclusions	Relevant section of this report	Supporting Data Sources (references)	Assumptions, Qualifications, Limitations & Gaps
	alone, should the project proceed toward approval and implementation.			
• Info required 2: A conceptual model of the marine system and the cause effect pathways for each threat or pressure resulting from the proposal.	As outlined above a conceptual understanding of marine environmental processes in the CG as well as a conceptual model of possible effects of human changes in CG are presented in PCS (2024a). The conceptual model shows that the two main potential stressors from the proposed sand sourcing are an increase in suspended sediment and a reduction in sediment supply. As outlined above the modelling assessed that potential changes in these parameters is very minor to negligible.	Not included in this report, see Section 5.4 in PCS (2024a).	BKA (2024b) BKA (2024d) PCS (2024a, b & c) PCS (2025b)	The conceptual model is based on the understanding of the area which is based on information from literature (Robson et al., 2008; Robson et al., 2013; Thom et al., 1975; Wolanski et al., 2001; Wolanski et al., 2004; Wright et al., 1973) along with data collected by BKA for the project and the modelling presented in this report. As outlined above the models have been calibrated and validated at multiple sites offshore and within CG during both wet and dry season conditions based on a large volume of available measured data. This provides confidence that the models provide a realistic representation of the existing conditions within CG.
• Info required 3: The criteria that will be used to predict the extent, severity and duration of any impacts and how they were derived.	The criteria used to assess the extent, severity and duration of any impacts on MEQ from sediment plumes from the SPV operation were the configuration, setup and source terms used for the 3D sediment plume model (the DHI MIKE ST model), in accordance with EPA (2021), Sun et al (2020), field data on turbidity and SSC in CG and the derived turbidity-SSC relationship, field data on the physical characteristics of the sediments present in the POA (PCS 2024a, b & c) and specifications for the SPV operation provided by BKA, as described in sections 3.7 and 6.	Sections 3.7 and 6	BKA (2024b) BKA (2024d) PCS (2024a, b & c) PCS (2025b) This report - HD, SW and ST models along with the data used to develop and calibrate/validate the models (see Section 3 for further details).	The plume modelling is based on a number of assumptions relating to the SPV. These assumptions were provided by BKA and are detailed in Section 3.7.2. If the SPV specifications change then the plume modelling results would also change slightly, but it is expected that the plume SSC will remain low regardless (due to the factors listed against related items above).
• Info required 4: A description of the extent, severity and duration of effects of the development in the context of the EQP (this is likely to involve predictive modelling).	As outlined above, the main potential impacts of the proposed sand sourcing on EQP are from turbid plume generation during operation of the SPV in CG. As outlined in the response to Objective 3b) in Table 46, numerical modelling of sediment plumes has been undertaken – including of the extent, duration and intensity of impacts under normal and most likely worst-case scenarios, and in combination with any other changes in MEQ caused by adjacent activities (of which there are none) or natural events (cumulative effects). As outlined above, the modelling assessed that potential changes to MEQ and thus impacts on EQP that are influenced by MEQ were	Section 6	BKA (2024b) BKA (2024d) PCS (2024a, b & c) PCS (2025b) This report - HD, SW and ST models along with the data used to develop and calibrate/validate the models (see Section 3 for further details).	The plume modelling is based on a number of assumptions relating to the SPV. These assumptions were provided by BKA and are detailed in Section 3.7.2. If the SPV specifications change then the plume modelling results would also change slightly, but it is expected that the plume SSC will remain low regardless (due to the

Guideline	Summary Findings / Conclusions	Relevant section of this report	Supporting Data Sources (references)	Assumptions, Qualifications, Limitations & Gaps
	negligible. The response to 'Info Required 1' above discusses EQP / EQMP / EQO.			factors listed against related items above).
• Info required 5: Consideration of the cumulative impacts of the proposal in combination with other existing and approved developments to determine if the EQP can be achieved.	As outlined above, the main potential impacts of the proposed sand sourcing on MEQ (and thus EQP) are from turbid plume generation during operation of the SPV in CG. As outlined in the response to Objective 3b) in Table 46, numerical modelling of sediment plumes has been undertaken – including of the extent, duration and intensity of impacts under normal and most likely worst-case scenarios, and in combination with any other changes in MEQ caused by adjacent activities (of which there are none) or natural events (cumulative effects). As outlined above, the modelling assessed that potential changes to MEQ (and thus EQP) and impacts on environmental values that are influenced by MEQ, including cumulative changes, were negligible.	Sections 4.2 and 5.2	BKA (2024b) BKA (2024d) PCS (2024a, b & c) PCS (2025b) This report - HD, SW and ST models along with the data used to develop and calibrate/validate the models (see Section 3 for further details).	As outlined above the models have been calibrated and validated at multiple sites offshore and within CG during both wet and dry season conditions based on a large volume of available measured data. This provides confidence that the models provide a realistic representation of the existing conditions within CG.
WA EPA 2016 *Technical Guidance - Protecting the Quality of Western Australia's Marine Environment*: • Supports the Environmental Factor Guideline (EFG).	As per response to EPA (2016b) above.	As per response to EPA (2016b) above.	As per response to EPA (2016b) above.	As per response to EPA (2016b) above.
• WAMSI/CSIRO 2020 *Guideline for Dredge Plume Modelling for EIA* (Sun et al 2020):	All numerical modelling undertaken as part of this study and presented in this report has been undertaken in accordance with relevant aspects of Sun *et al.* (2020), as well as with recognised international standards including Williams & Esteves (2017) and Los & Blaas (2010), and relevant Australian and Western Australian guidelines including Sun *et al.* (2016), Mills & Kemps (2016), Kemps & Masini (2017) and GBRMPA (2012). Details are provided in the modelling approach in Section 3.	Section 3.	BKA (2024b) BKA (2024d) PCS (2024a, b & c) PCS (2025b) This report - HD, SW, and ST models along with the data used to develop and calibrate/validate the models (see Section 3 for further details).	As outlined above the models have been calibrated and validated at multiple sites offshore and within CG during both wet and dry season conditions based on a large volume of available measured data. This provides confidence that the models provide a realistic representation of the existing conditions within CG. The plume modelling is based on a number of assumptions relating to the SPV. These assumptions were provided by BKA and are detailed in Section 3.7.2. If the SPV specifications change then the plume modelling results would also change slightly, but it is expected that the plume SSC will remain low regardless (due to the

Guideline	Summary Findings / Conclusions	Relevant section of this report	Supporting Data Sources (references)	Assumptions, Qualifications, Limitations & Gaps
				factors listed against related items above).

8. REFERENCES

Australian Hydrographic Office (AHO), 2023. AusTides (AHP114). <https://www.hydro.gov.au/prodserv/publications/ausTides/tides.htm>, viewed 7 November 2023.

Australian Hydrographic Office (AHO), 2024. Australian National Tide Tables 2024.

Becker, J., van Eekelen, E., van Wiechen, J., de Lange, W., Damsma, T., Smolders, T. and van Koningsveld, M., 2015. Estimating source terms for far field dredge plume modelling. Journal of Environmental Management 149, 282-293.

BKA, 2024b. Cambridge Gulf Marine Sand Proposal – WA EP Act s38 Referral Report No. 2: *Setting & Existing Environment*.

BKA, 2024d. Cambridge Gulf Marine Sand Proposal – WA EP Act s38 Referral Report No. 4: *Impact Assessments of Relevant Environmental Factors*.

Cilli, S., Billi, P., Schippa, L., Grottoli, E., and Ciavola, P., 2021. Bedload transport and dune bedforms characteristics in sand-bed rivers supplying a retreating beach of the northern Adriatic Sea (Italy). Journal of Hydrology: Regional Studies 37.

CSIRO, 2024. CAWCR Wave Hindcast – Aggregated Collection. < https://data.csiro.au/collection/csiro:39819>, viewed 15 August 2024.

DataWA, 2023. Web Mapping Service, Hydrographic catchments. <https://catalogue.data.wa.gov.au/dataset/hydrographic-catchments-catchments>, viewed 30 October 2023.

Department of Transport, 2010. Sea Level Change in Western Australia – Application to Coastal Planning. Discussion Paper.

National Environmental Science Programme, 2024. Earth Systems and Climate Change Hub, Wind-wave climate change along Australia's coast. https://nespclimate.com.au/wp-content/uploads/2021/04/ESCC_Wind-wave-climate-change_Factsheet.pdf, viewed 2 August 2024.

GBRMPA, 2012. Guidelines – The use of hydrodynamic numerical modelling for dredging projects in the Great Barrier Reef Marine Park. August 2012.

Geoscience Australia, 2023. High-resolution depth model for Northern Australia – 30m. <https://ecat.ga.gov.au/geonetwork/srv/api/records/1010ac13-e033-489d-b9ce-ae11fd0e11ef>, viewed 10 October 2023.

Holmes Jr., R.R., 2010. Measurement of bedload transport in sand-bed rivers: a look at two indirect sampling methods. U.S. Geological Survey Scientific Investigations Report 2010-5091.

IPCC, 2024. Sea Level projection tool, based on SSP3-7.0 for year 2120. https://sealevel.nasa.gov/ipcc-ar6-sea-level-projection-tool. Accessed 01/10/2024

Jones, R., Bessell-Browne, P., Fisher, R., Klonowski, W., and Slivkoff, M., 2016. Assessing the impacts of sediments from dredging on corals. Marine Pollution Bulletin 102, 9-29.

Kemps, H., and Masini, R., 2017. Estimating dredge source terms – a review of contemporary practice in the context of Environmental Impact Assessment in Western Australia. Report of Theme 2 – Project 2.2, prepared for the Dredging Science Node, Western Australian Marine Science Institution (WAMSI). Perth, Western Australia, 29pp.

Los, F.J. and Blaas, M., 2010. Complexity, accuracy and practical applicability of different biogeochemical model versions. Journal of Marine Systems 81, 44-74.

Maritime Safety Queensland (MSQ), 2024. Tides, Notes and Definitions. https://www.msq.qld.gov.au/tides/notes-and-definitions. Accessed 17/11/2024

Mills, D., and Kemps, H., 2016. Generation and release of sediments by hydraulic dredging: a review. Report of Theme 2 - Project 2.1 prepared for the Dredging Science Node, Western Australian Marine Science Institution, Perth, Western Australia. 97 pp.

PCS, 2024a. Cambridge Gulf Marine Sand Proposal, Metocean and Sediment Dynamics - System Understanding, Conceptual Model and Initial Modelling, P076_R01v03, July 2024.

PCS, 2024b. Cambridge Gulf Marine Sand Proposal, Metocean and Sediment Dynamics - Supplementary Technical Note, July 2024.

PCS, 2024c. Cambridge Gulf Marine Sand Proposal, Metocean and Sediment Dynamics - Factual Data Report, P076_R02v02, July 2024.

PCS, 2025a. Cambridge Gulf Marine Sand Proposal – WA EP Act s38 Referral Report No. 8: *Metocean & Sediment Dynamics – Data Analysis and Numerical Modelling Report*.

Robson, B.J., Burford, M.A., Gehrke, P.C., Revill, A.T., Webster, I.T. and Palmer, D.W., 2008. Response of the Lower Ord River and Estuary to changes in flow and sediment and nutrient loads.

Robson, B.J., Gehrke, P.C., Burford, M.A., Webster, I.T., Revill, A.T. and Palmer, D.W., 2013. The Ord River Estuary: a regulated wet-dry tropical river system. In Wolanski (ed.) Estuaries of Australia in 2050 and Beyond, Estuaries of the World.

Smith, G.A., Hemer, M., Greenslade, D., Trenham, C., Zieger, S., and Durrant, T., 2020. Global wave hindcast with Australian and Pacific Island focus: from past to present. Geoscience Data Journal, Volume 8, Issue 1, 24-33.

Sun, C., Shimizu, K., and Symonds, G., 2016. Numerical modelling of dredge plumes: a review. Report of Theme 3 - Project 3.1.3, prepared for the Dredging Science Node, Western Australian Marine Science Institution, Perth, Western Australia, 55 pp.

Sun, C., Branson, P., and Mills, D., 2020. Guideline on dredge plume modelling for environmental impact assessment. Prepared for the Dredging Science Node, Western Australian Marine Science Institution, Perth, Western Australia. 73pp.

Thom, B.G., Wright, L.D., and Coleman, J.M., 1975. Mangrove ecology and deltaic-estuarine geomorphology: Cambridge Gulf-Ord River, Western Australia. Journal of Ecology, Vol. 61, No. 1, 203 – 232.

van Rijn, L.C., 1993. Principles of sediment transport in rivers, estuaries and coastal seas. Aqua Publications, Amsterdam.

WA EPA, 2016a. Environmental Factor Guideline - Coastal Processes, December 2016.

WA EPA, 2016b. Environmental Factor Guideline - Marine Environmental Quality (MEQ), December 2016.

WA EPA, 2016c. Technical Guidance - Protecting the Quality of Western Australia's Marine Environment. Environmental Protection Authority, December 2016.

WA EPA, 2021. Technical Guidance - Environmental impact assessment of Marine Dredging Proposals. Environmental Protection Authority, September 2021.

Williams, J.J. and L.S. Esteves (2017). Guidance on setup, calibration and validation of hydrodynamic, wave and sediment models for shelf seas and estuaries. Advances in civil engineering (Volume 2017), 5251902, 25 pages.

Wolanski, E., Spagnol, S., and Pattiaratchi, C., 2001. Rapid, human-induced siltation of the macro-tidal Ord River Estuary, Western Australia. Estuarine Coastal and Shelf Science 53, 717-732.

Wolanski, E., Spagnol, S., and Williams, D., 2004. The impact of damming the Ord River on the fine sediment budget in Cambridge Gulf, Northwestern Australia. Journal of Coastal Research, 20 (3), 801-807.

Wright, L.D., Coleman, J.M., and Thom, B.G., 1973. Processes of channel development in a high tide range environment: Cambridge Gulf – Ord River Delta, Western Australia.